THE UNIVERSITY OF HULL

Preparation, type and stability of emulsions stabilised by solid particles

being a Thesis submitted for the Degree of Doctor of Philosophy in the University of Hull

by

Simon Owen Lumsdon, BSc (Hons)

November 2000

ACKNOWLEDGEMENTS

The author would like to express sincere gratitude to his supervisor, Dr. B. P. Binks, for his excellent support and encouragement throughout the three years of study.

The author would also like to thank the E.P.S.R.C. and ICI Paints (Slough, U.K.) for financial support. Dr. P. Sasada and Mr. P. S. Collins (ICI Paints) for their insight into the paint industry.

The author is grateful to Prof. R. Aveyard, Prof. P. D. I. Fletcher, Dr. J. H. Clint and Dr. V. N. Paunov for useful discussions and to all members of the Surfactant Science Group both past and present for their friendship and support.

Finally, the author is particularly grateful to his parents for their encouragement and support throughout his time at the University of Hull.

PUBLICATIONS AND PRESENTATIONS

This thesis has led to the following publications:

(1) B. P. Binks and S. O. Lumsdon, 'Stability of oil-in-water emulsions stabilised by silica particles', *Phys. Chem. Chem. Phys.*, **1**, 3007 (1999).

(2) B. P. Binks and S. O. Lumsdon, 'Catastrophic phase inversion of water-in-oil emulsions stabilised by hydrophobic silica', *Langmuir*, **16**, 2539 (2000).

(3) B. P. Binks and S. O. Lumsdon, 'Transitional phase inversion of solid-stabilised emulsions using particle mixtures', *Langmuir*, **16**, 3748 (2000).

(4) B. P. Binks and S. O. Lumsdon, 'Effects of oil type and aqueous phase composition on oil-water mixtures containing particles of intermediate hydrophobicity', *Phys. Chem. Chem. Phys.*, **2**, 2959 (2000).

(5) B. P. Binks and S. O. Lumsdon, 'Influence of particle wettability on type and stability of surfactant-free emulsions', *Langmuir*, **16**, 8622 (2000).

(6) B. P. Binks and S. O. Lumsdon, 'Emulsions stabilised by polystyrene latex particles: effects of particle size' submitted to *Phys. Chem. Chem. Phys.* 5/3/01.

The work has also been presented at the following conferences:

(1) 'Stability of oil-in-water emulsions stabilised by silica particles', 13th Conference of the European Colloid and Interface Society (ECIS), 12 – 17th September 1999, Dublin.

(2) 'Catastrophic phase inversion of water-in-oil emulsions stabilised by hydrophobic silica', The role of surfactants in wetting behaviour, Royal Society of Chemistry, Colloid and Interface Science Group, 6 – 8th September 1999, Hull.

(3) 'Effects of particle wettability on the type and stability of solid-stabilised emulsions', 10th Conference of the International Association of Colloid and Interface Science (IACIS), 23 – 28th July 2000, Bristol.

ABSTRACT

ABSTRACT

The preparation, type and stability of emulsions stabilised solely by solid silica particles has been investigated in detail using a combination of conductivity, stability, light diffraction, optical microscopy and contact angle measurements. The wettability of the particles *in situ* at the oil-water interface plays a major role in such systems.

The stability of aqueous colloidal dispersions in the presence of various electrolytes and over a range of pH is shown to be important in determining the stability of toluene-in-water emulsions formed from them. Partial flocculation of the silica dispersions enhances the emulsion stability whereas strong flocculation results in unstable emulsions. Inversion of emulsion type occurs via two mechanisms. Catastrophic inversion of water-in-oil emulsions stabilised by hydrophobic silica particles occurs upon increasing the volume fraction of water in the system. Transitional inversion of emulsions at fixed volume fraction of water has been achieved by varying the mass fraction of hydrophilic (or hydrophobic) particles in systems containing particle mixtures. Neither inversion mechanism exhibits hysteresis, in contrast to surfactant-stabilised systems.

The energy of attachment of a particle to the oil-water interface is shown to be dependent on the contact angle and the interfacial tension. The contact angle was varied by changing the hydrophobicity of the silica particles. Particles of intermediate hydrophobicity were most effective at stabilising emulsions which is thought to be due to the contact angle at the oil-water interface being close to 90°. The interfacial tension was affected by changing the nature of the oil phase or by replacing water with various polar liquids. Undecanol-water emulsions stabilised by silica particles of intermediate hydrophobicity break down via gel formation followed by coalescence.

The wettability of the silica surface was varied *in situ* by varying the pH of the aqueous phase. Increasing the pH causes dissociation of silanol groups, which increases the affinity of the particles for the aqueous phase. The type and stability of emulsions and the contact angle of an aqueous drop under toluene on hydrophobically modified glass slides were measured as a function of pH. The results are modelled using simple theory. The wettability of hydrophobic pigment surfaces is dependent on the type and concentration of added surfactant. The findings are discussed in terms of surfactant adsorption at the relevant interfaces.

CONTENTS

Appendix

CHAPTER 1

CHAPTER 1

INTRODUCTION

1.1 Industrial relevance of current research

This thesis has been partially funded by ICI Paints, Slough. Paint manufacture is a multi-million pound industry with over 100 million litres of decorative paint sold per year by ICI in the UK alone. A percentage of the companys' profits are spent on research and development in an on-going attempt to provide the customer with a high quality and broad range of products. Paint manufacture is a very complicated process involving a number of different stages and constituents. Motivation for the current research was to obtain an understanding of the pigment flushing process which involves the transfer of an aqueous-based pigment into an oil-based paint. This process is described in detail in § 1.1.2.

1.1.1 Introduction to paint

There is a wide variety of products available in the paint industry, which are designed to protect and decorate all kinds of surfaces. Different types of paint have a number of different constituents which make them suitable for their designated application. For example, the constituents of a decorative emulsion paint are vastly different to those in a paint used to coat commercial packaging (e.g. Coca-Cola cans). Therefore, it is dangerous to generalise what goes into a can of paint, but for the purpose of this introduction the following constituents are commonly found in most products:

Pigment – Pigments have both decorative and protective properties. They alter the appearance of the paint by selective absorption and/or scattering of light. The colour of the pigment is mainly dependent on its chemical structure with most pigments classified as organic or inorganic. The pigment must have chemical stability, durability, opacity and resistance to chemicals.

Binder – The binder or film-former is added to paint to hold the pigment particles to the surface. It also protects the surface by giving it a 'gloss' or sheen. The binder is a polymer when the coating has dried, but in the liquid sample it may be the monomer which reacts to form the final dry polymer. The fluidity of the paint is achieved by dissolving the binder in a solvent or by colloidal suspension of the pigment and binder in a diluent. Thus another basic ingredient of paint is a liquid.

Liquid – The binder/liquid mixture is called the vehicle for the pigment, which evaporates once applied. White spirit is often used as the liquid because it has a low odour.

Additives – A number of additives are added to paint to improve the overall quality. Driers are added in order to facilitate the evaporation of solvent. They are usually metals, for example cobalt, which act as catalysts for an auto-oxidative drying process. Thickeners, catalysts, anti-freezes, anti-foams and surfactants are all added to the formulation to get maximum performance whilst still maintaining the cost effectiveness of the paint.

1.1.2 Pigment flushing

One of the most important processes in paint manufacture is the transfer of pigment particles from an aqueous phase to an oil phase. This process is commonly referred to as pigment flushing. A comprehensive review of pigment flushing is given by Langstroth.[1] An aqueous pigment paste is agitated with a non-aqueous vehicle leading to the preferential transfer (flushing) of pigment to the non-aqueous phase. The

essentially colourless water is poured off and any residual water is vacuumed off at 50 °C. The transfer of particles is often facilitated by the use of surfactants, which affect the wettability of the particles by both phases. However, the actual mechanism of the transfer is not completely understood and further research of this process may lead to an increased flushing efficiency and ultimately to a reduction in cost. Flushed paints have a number of potential advantages over other manufacturing methods. For example, flushed colours are manufactured from pigment presscakes, which are in a deagglomerated physical form. At no stage during the process is the pigment paste dried, therefore the flushed colour retains the deagglomerated form resulting in colours that are superior in strength than those produced by a standard milling process. Flushed pigments are often high viscosity pastes that do not suffer from dry dusting which can be a problem when using dry pigment powders. Most coloured pigments can be produced in a flushed form. As a result this process can accommodate a wide selection of flushing resins and dispersants.

The mechanism of pigment flushing has been considered in terms of the wettability of individual pigment particles. It is generally understood that hydrophobic particles, such as organic pigments, are most easily flushed due to their preference for the non-aqueous phase. Hydrophilic pigments (e.g. oxides) are more difficult to flush and require careful selection of surfactants that modify their surface character. It was found by Gomm et al.[2] that the flushing process is often accompanied by considerable water-in-oil emulsification, particularly in the case when the particles were not completely wetted by the oil phase in competition with the aqueous phase.

The flushing process is highly dependent on the interfacial tensions between the solid particles and the bulk liquids.[2] The wettability of the particle also plays an important role. In order to obtain a clear understanding of pigment flushing the majority of the present work has concentrated on very simplified systems containing only particles, oil and aqueous phases. Gomm et al.[2] highlighted that the flushing process was accompanied by emulsification of water into oil. It is shown here that particles can stabilise emulsions in the absence of surfactant and that it is possible to invert from one emulsion type to the other using just one particle type. This process involves a change in the wettability of the particle from being preferentially water-wettable to being oil-wettable (or vice versa), which is akin to the particle being transferred from one phase to the other in the flushing process. The interfacial tensions in these systems have also been investigated by varying the oil type and the aqueous phase composition. An

investigation into the wettability of two common pigments in the presence of surfactant has also been carried out. It is shown that the hydrophobicity of the pigments is dependent on the type and concentration of surfactant used.

1.2 Emulsions

An emulsion may be defined as an opaque, heterogeneous system of two immiscible liquid phases ('oil' and 'water') where one of the phases is dispersed in the other as drops of microscopic or colloidal size (>1 μm). A comprehensive review of emulsion science can be found in ref. 3. There are two kinds of simple emulsion, one where oil drops are dispersed in a continuous phase of water, which are called oil-in-water (o/w) emulsions and the other where water drops are dispersed in a continuous phase of oil, which are called water-in-oil (w/o) emulsions. Agitation of two immiscible liquids leads to the formation of extremely unstable emulsions, which separate into the bulk phases immediately. However, it is possible to stabilise the emulsion by addition of a surface-active material, which protects the dispersed drops from re-coalescence. The emulsifier is usually a surfactant but it is shown in the present work that solid particles can also stabilise dispersed drops. A review of previous investigations into solid-stabilised emulsions is given in § 1.2.4. During emulsification, the interfacial area, A, becomes much larger and the surface free energy of the system ΔG, is affected by

$$\Delta G = \gamma \Delta A \tag{1.1}$$

Addition of a suitable surface-active agent reduces γ and thus considerably reduces the energy needed to obtain a particular drop size. Solid particles do not lower the surface tension (later) of a liquid due to their large diameter relative to surfactants, which results in a low surface concentration. They do stabilise emulsions however via mechanisms described later (§ 1.2.4).

1.2.1 Adsorption at liquid/liquid interfaces

The majority of work in this thesis is concerned with systems containing solid particles alone. The particles are used as a replacement for surfactant molecules which are more commonly used to stabilise emulsions. Throughout the text, comparisons between surfactant and solid-stabilised systems are made, hence a brief introduction to surfactant chemistry is required. A surfactant is a surface-active molecule which consists of both non-polar and polar parts, in other words it is amphiphilic in nature. The non-polar or hydrophobic tail is typically a straight or branched hydrocarbon or fluorocarbon chain. The hydrophilic head-group can be anionic, cationic, non-ionic or zwitterionic.[4] The schematic below is an example of a straight chain surfactant molecule.

Schematic representation of a single tailed surfactant molecule

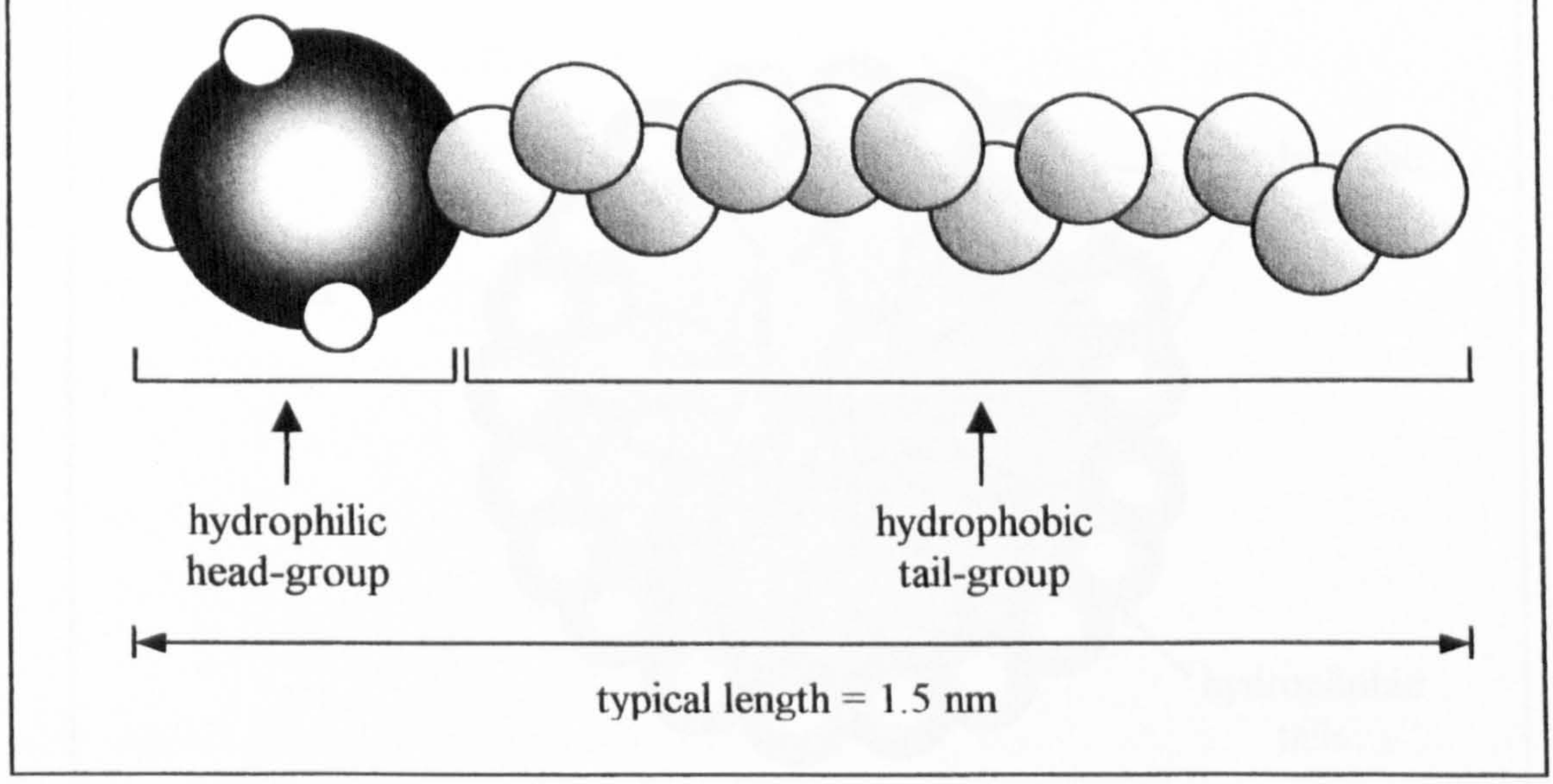

In aqueous solution attractive polar interactions occur between surfactant head-groups and water molecules. Interactions between the hydrophobic tail and surrounding water

molecules is entropically unfavourable. In order to minimise this unfavourable interaction surfactant molecules are adsorbed at the air-water (aw) interface with their tail-groups oriented out of water. This entropically driven phenomenon is known as the hydrophobic effect.[5] Adsorption of surfactant at the aw surface causes a reduction in the surface tension of water. At a critical surfactant concentration the adsorbed monolayer becomes saturated and further adsorption cannot occur as the bulk surfactant concentration is increased. Additional surfactant molecules must therefore aggregate into micelles to reduce the unfavourable chain contact with water. In normal micelles the hydrophobic tails are oriented towards the interior leaving only the hydrophilic head-groups in contact with water. A schematic representation of the cross-section of a normal spherical micelle is shown below.

Schematic representation (cross-section) of a normal spherical micelle

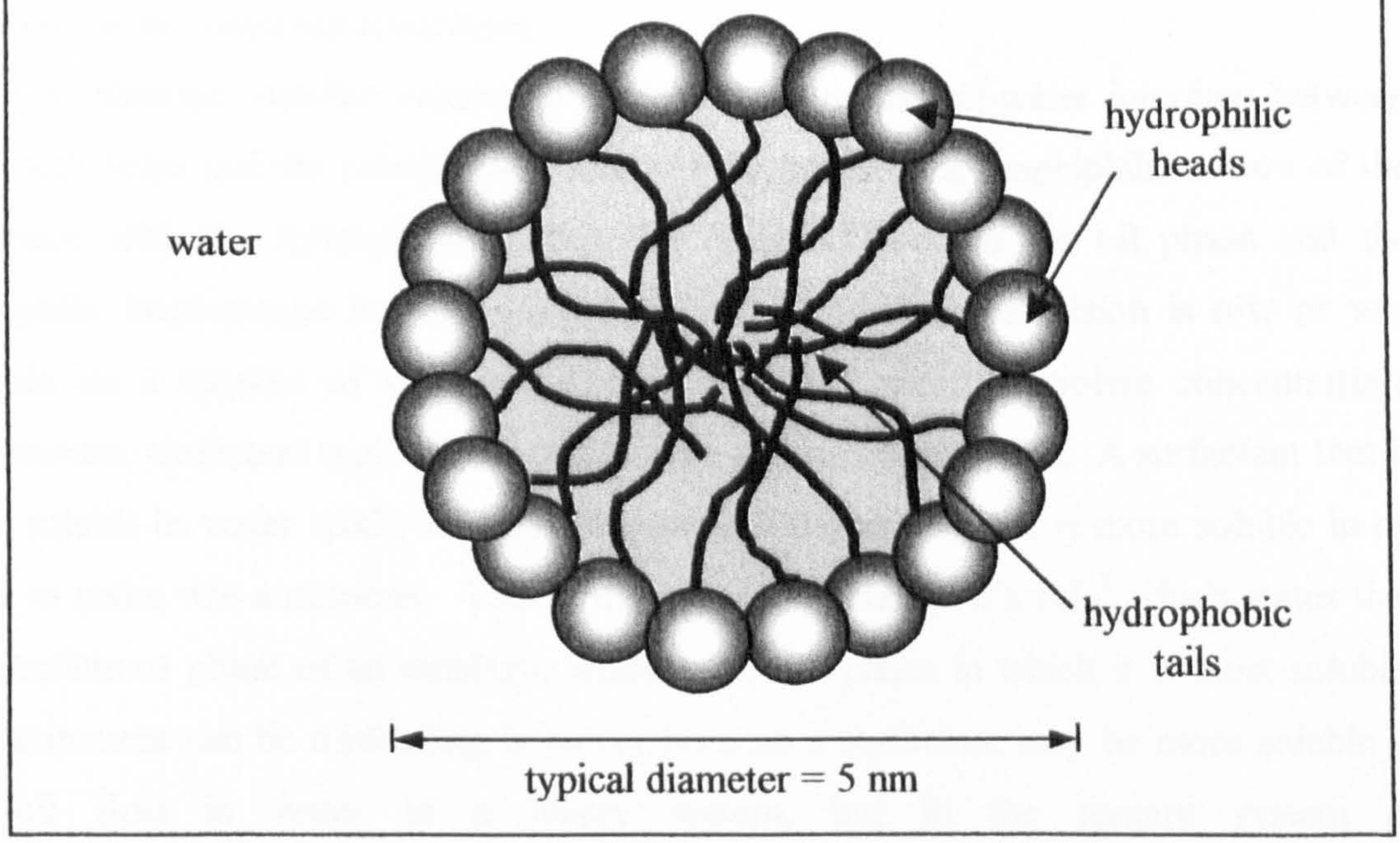

The concentration at which micelles form is known as the critical micelle concentration (c.m.c.). It can easily be determined because a number of solution properties show an abrupt change at the c.m.c., such as surface tension, conductivity and scattered light intensity.

The thermodynamic relationship between the quantity of surfactant adsorbed per unit area and the change in surface tension was first derived by Gibbs.[6] A common form of the Gibbs equation for dilute solutions of a 1:1 ionic surfactant in pure water is

$$d\gamma_{aw} = -2RT\Gamma d\ln c \qquad (1.2)$$

where $d\gamma_{aw}$ is the change in the water – vapour surface tension (mN m^{-1}), Γ is the excess surfactant concentration adsorbed at the interface (mol m^{-2}), c is the solution surfactant concentration, R is the gas constant and T is temperature. This form of the Gibbs equation assumes that the activity of the surfactant equals its concentration and is valid only for low concentrations (< 10^{-3} M). Measurement of surface tension as a function of surfactant concentration enables the determination of the surface excess concentration of surfactant in the adsorbed monolayer.

Surfactants stabilise emulsions by adsorbing at the oil-water interface between dispersed drops and the continuous phase. This satisfies the amphiphilic nature of the surfactant with the hydrophobic tail-groups being situated in the oil phase and the hydrophilic head-groups in the aqueous phase. Whether the emulsion is o/w or w/o depends on a number of variables such as oil:water ratio, electrolyte concentration, temperature, surfactant type and oil and aqueous phase composition. A surfactant that is more soluble in water tends to make o/w emulsions and one that is more soluble in oil tends to make w/o emulsions. This is the essence of Bancroft's rule[7] which states that the continuous phase of an emulsion tends to be the phase in which it is most soluble. This statement can be misleading however because a surfactant may be more soluble in say oil than in water in a binary system, but in the ternary system of oil+water+surfactant it may partition more into water.[8] As discussed in Chapter 4, the first quantitative measure of the balance between the hydrophilic and hydrophobic moieties of a surfactant was derived by Griffin who introduced the concept of the

surfactant hydrophile-lipophile balance or HLB, as a way of predicting emulsion type from surfactant molecular composition.[9] In this system the surfactant is assigned a number depending on the type of emulsion it is predicted to stabilise. For example, a hydrophilic surfactant has a large HLB number and stabilises o/w emulsions while lipophilic surfactants with a small HLB number stabilise w/o emulsions. However, the HLB number is assigned to the neat surfactant alone and does not account for the behaviour when it is adsorbed at the oil-water interface of an emulsion. The system HLB can be varied by electrolyte, temperature, oil type and co-surfactant concentration which modify the geometry of the surfactant at an interface[10] and thus change the curvature of the surfactant monolayer, which in some way affects the preferred emulsion type.[11, 12] The pigment flushing process involves adsorption of surfactant onto solid particles thus effecting their wettability. In the present work the wettability of the solid particles is affected *in situ* in the absence of surfactant but a sensible continuation of this work would be to investigate the effect of surfactant on particle wettability.

1.2.2 Emulsion inversion

Phase inversion of emulsions can occur via two mechanisms. *Catastrophic* inversion is induced by increasing the volume fraction of dispersed phase and has the characteristics of a catastrophe, meaning a sudden change in behaviour of the system as a result of gradually changing conditions. Catastrophic inversion of emulsions stabilised by solid particles of fixed hydrophobicity is discussed in detail in Chapter 4 where it is shown that inversion occurs without hysteresis in contrast to surfactant-stabilised emulsions. *Transitional* inversion is induced by changing factors which affect the HLB of the system at fixed volume fraction of water (ϕ_w). For surfactants, the HLB is affected by temperature, oil type and electrolyte concentration. Transitional inversion of solid-stabilised emulsions is discussed in detail in Chapter 5 where the system HLB is altered by varying the mass fraction of hydrophilic and hydrophobic particles at fixed ϕ_w. Inversion of emulsions has not been seen before in systems stabilised solely by solid particles.

1.2.3 Emulsion stability

Macroemulsions are not thermodynamically stable and only possess varying degrees of kinetic stability. Emulsions destabilise via a number of processes which occur simultaneously or consecutively depending on conditions. There are four main ways by which an emulsion destabilises – creaming (or sedimentation), flocculation, coalescence and Ostwald ripening, which are discussed in detail in this section and summarised schematically in Figure 1.1.

(a) *Creaming* – In an o/w emulsion, creaming is the movement of oil drops under gravity or in a centrifuge to form a concentrated layer at the top of the sample, but with no accompanying change in the drop-size distribution. Initially, a concentration gradient of drops develops in the vertical direction, often followed by the appearance of a distinct boundary between an upper cream layer and a lower depleted emulsion layer. In a w/o emulsion, the equivalent phenomenon is called *sedimentation*. Creaming arises from the action of gravity on drops of lower density than that of the continuous phase and is reversible in that gentle agitation can re-establish the original distribution of drops. In very dilute emulsions, the creaming speed, v_s, of an isolated, spherical drop of radius a moving through a fluid medium of density ρ_o and Newtonian shear viscosity η_o is given by Stokes' law[13]

$$v_s = 2a^2(\rho_o - \rho)g/9\eta_o \qquad (1.3)$$

where g is the acceleration due to gravity and ρ is the density of the dispersed phase. In the absence of flocculation, Stokes' law indicates that creaming in a dilute emulsion can be inhibited by reducing the average drop size, reducing the density difference between the phases or by increasing the viscosity of the continuous phase. In emulsions stabilised by solid particles, the phase in which the particles are dispersed becomes more viscous as the particle concentration increases. However, this may lead to non-Newtonian character of the phase and hence a complication in applying equation 1.3.

Figure 1.1

Schematic illustration of different types of emulsion destabilisation, shown for an o/w emulsion.

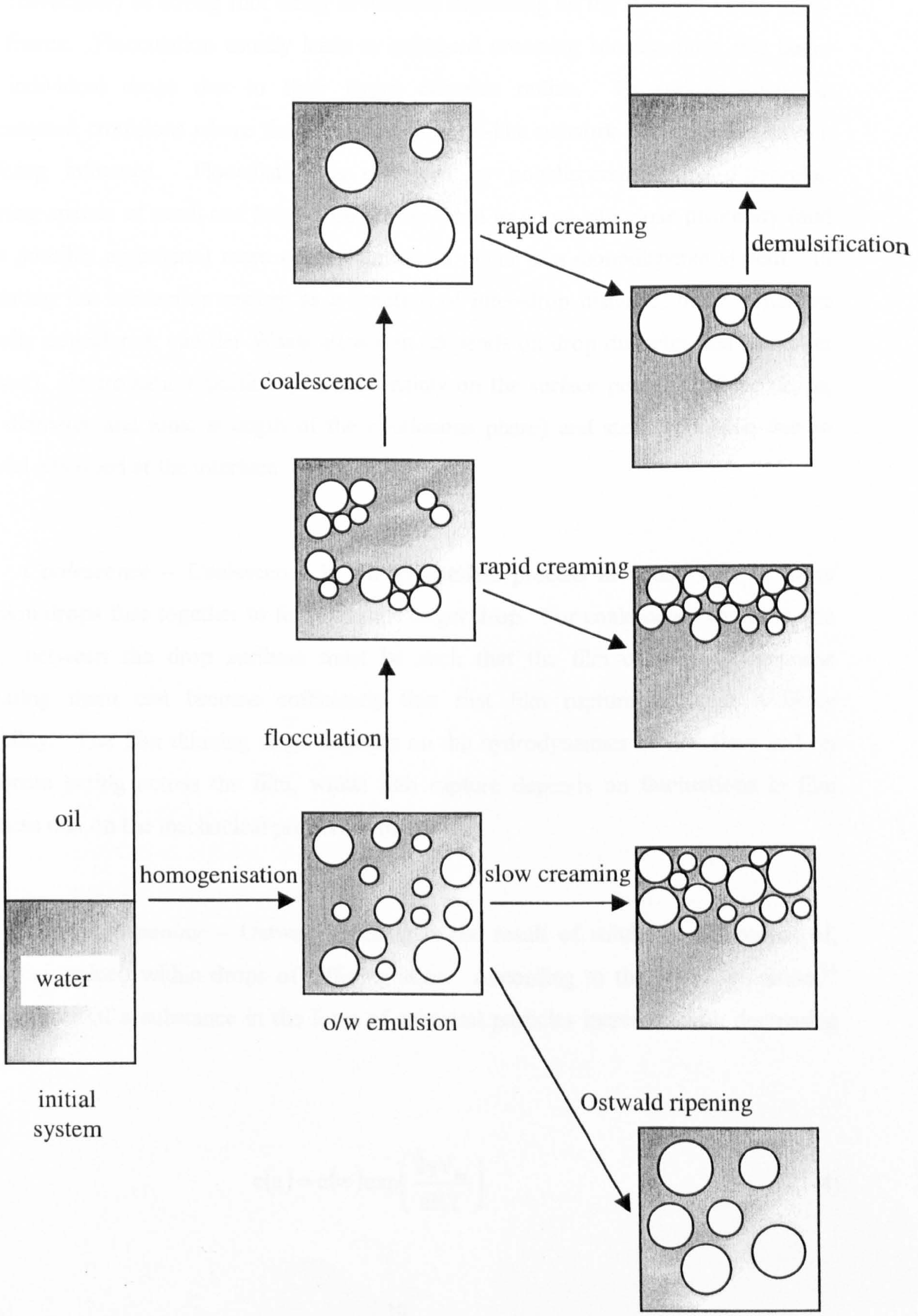

(b) *Flocculation* – Flocculation is the process in which emulsion drops aggregate, without rupture of the stabilising layers at the interfaces, if the pair interaction free energy between drops becomes appreciably negative at a certain separation. It may be weak (reversible) or strong (not easily reversible) depending on the strength of the inter-drop forces. Flocculation usually leads to enhanced creaming because flocs rise faster than individual drops due to their larger effective radius. Exceptions occur in concentrated emulsions where the formation of a gel-like network structure can have a stabilising influence. Flocculation is enhanced by polydispersity since differential creaming speeds of small and large drops cause them to come into close proximity (and hence possibly aggregate) more often than would occur in a monodisperse system. In calculating the interaction energy as a function of inter-drop distance, three terms are normally considered; van der Waals attraction (depends on drop diameter and Hamaker constant), electrostatic repulsion (depends mainly on the surface potential of the drops, drop diameter and ionic strength of the continuous phase) and steric repulsion due to material adsorbed at the interface.

(c) *Coalescence* – Coalescence is the irreversible process in which two or more emulsion drops fuse together to form a single larger drop. For coalescence to occur, the forces between the drop surfaces must be such that the film of continuous phase separating them can become sufficiently thin that film rupture becomes a likely possibility. The film thinning stage depends on the hydrodynamics of film flow and on the forces acting across the film, whilst film rupture depends on fluctuations in film thickness and on the mechanical properties of the film.

(d) *Ostwald ripening* – Ostwald ripening is the result of solubility differences of, say, oil contained within drops of differing sizes. According to the Kelvin equation,[14] the solubility of a substance in the form of spherical particles increases with decreasing size:

$$c(a) = c(\infty)\exp\left(\frac{2\gamma V_m}{aRT}\right) \qquad (1.4)$$

where c(a) is the aqueous phase solubility (m^3 m^{-3}) of oil contained within a drop of radius a, c(∞) is the solubility in a system with only a planar interface, γ is the interfacial tension between the two phases and V_m is the molar volume of the oil (m^3 mol^{-1}). As a consequence of its increased solubility, material contained within the smaller drops tends to dissolve and diffuse through the aqueous phase, recondensing onto the larger drops. It is proposed in Chapter 3.2 that emulsions of toluene-in-water stabilised by hydrophilic silica particles exhibit Ostwald ripening until the silica particles surrounding the small drops becomes close-packed, preventing further destabilisation. Ostwald ripening results in an overall increase in the size of the emulsion drops and an accompanying decrease in the interfacial area. This provides the driving force for growth of the drops. Theoretically, the process of Ostwald ripening should be completed by merging all the drops into one, but this does not occur in practice owing to a considerable decrease in the rate of the process as the average size of the drops increases.

1.2.4 Solid-stabilised emulsions

The majority of investigations describing the preparation, stability and properties of macroemulsions involve the use of low molecular weight or polymeric surfactants.[15] Very few studies have dealt with emulsions whose interfaces are stabilised by solid particles,[16 - 37] and most of these involve particle-surfactant combinations. Investigations into emulsions prepared from oil, water and solid alone are in the minority.[16 – 18, 34, 37] Many formulations in a range of industries contain emulsions stabilised by particle-surfactant mixtures, e.g. drilling fluids in crude oil recovery, various foodstuffs and of course the pigment flushing process in the paint industry. However, the precise role of the solid particles in such systems is difficult to ascertain in the presence of the other adsorbing species. In order to obtain a clear understanding of the role of solid particles the majority of the present work has concentrated on surfactant-free systems.

In the early 1900's Pickering[16] recognised the role of finely divided solid particles in stabilising emulsions, but it was not until the work of Finkle et al.[19] that the relationship between the type of solid and emulsion type (o/w or w/o) was recognised.

These authors stated that in an emulsion containing solid particles, one of the liquids will probably wet the solid more than the other liquid, with the more poorly wetting liquid becoming the dispersed phase, which is similar to Bancroft's rule for surfactants. The importance of the wettability of the particles at the oil-water interface, quantified by the contact angle θ that the particle makes with it, was thus noted. If θ (measured through the aqueous phase) is less than 90° the particles will be held at the interface and tend to stabilise o/w emulsions.

Schematic representation of hydrophobic and hydrophilic particles at the oil-water interface of solid-stabilised emulsions

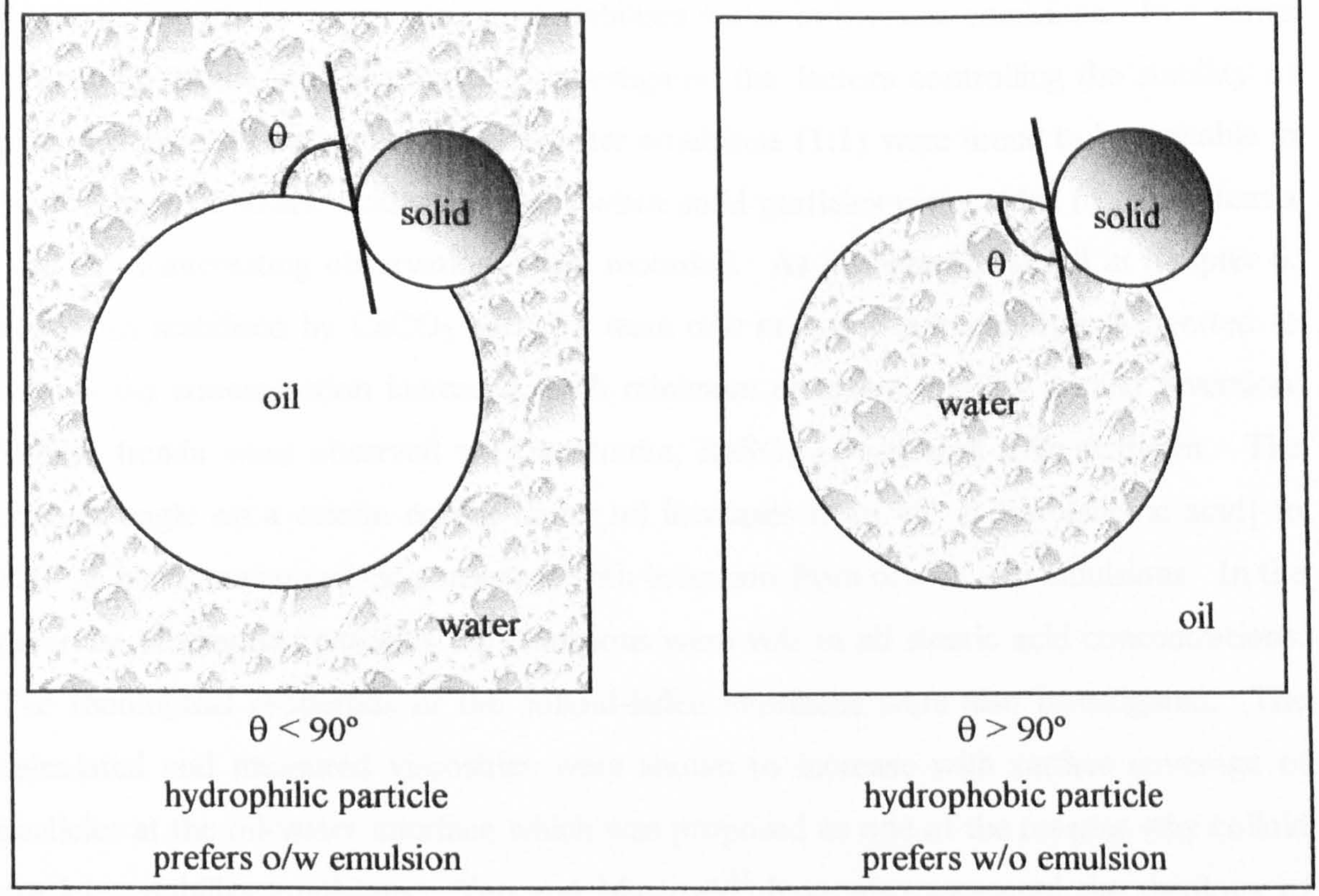

$\theta < 90°$	$\theta > 90°$
hydrophilic particle	hydrophobic particle
prefers o/w emulsion	prefers w/o emulsion

If the particle is preferentially wetted by the oil phase, the contact angle will be greater than 90°, and will now stabilise w/o emulsions. It is shown in Chapter 6 that the ability of particles to stabilise emulsions is highly dependent on θ with unstable emulsions formed if the particle is too hydrophilic (low θ) or too hydrophobic (high θ).

A number of authors have investigated the effect of surfactant adsorption on the wettability of solid particles, and the subsequent effect on the ability of these particles to stabilise emulsions.[20, 22 – 24, 26, 28 32, 34, 37] Schulman and Leja,[20] for example, investigated the wettability of $BaSO_4$ crystals in the presence of various surfactants. They showed that the stability of emulsions is highly dependent on the wettability of the particle in the presence of the surfactant. The contact angle of a water drop on a $BaSO_4$ crystal under benzene is 120° in the presence of 1×10^{-4} M sodium dodecyl sulphate (SDS) surfactant. Under these conditions the solid powder stabilises w/o emulsions, but in the absence of solid the emulsion is o/w. In the presence of oleic acid, the particles stabilise o/w emulsions and the contact angle of an aqueous drop on the surface is now 60°. In the absence of solid, however, oleic acid stabilises water-in-benzene emulsions. In a series of papers, Tambe and Sharma[28 - 32] investigated the factors controlling the stability of colloid-stabilised emulsions. Decane-water emulsions (1:1) were found to be unstable in the presence of stearic acid. However, when solid particles were added to the system a number of interesting observations were recorded. As discussed in detail in Chapter 6, emulsions stabilised by $CaCO_3$ particles were o/w at low [stearic acid] and inverted to w/o as the concentration increased, with minimum emulsion stability around inversion. Similar trends were observed with bentonite, $BaSO_4$ or silica as solid particles. The contact angle on a calcite crystal under oil increases from 40° at low [stearic acid] to 120° at high concentrations consistent with inversion from o/w to w/o emulsions. In the presence of graphite particles the emulsions were w/o at all stearic acid concentrations. The rheological properties of the colloid-laden interfaces were also investigated. The calculated and measured viscosities were shown to increase with surface coverage of particles at the oil-water interface which was proposed as one of the reasons why colloid particles stabilise emulsions. Yan and Masliyah[33] have also measured the rheology of oil-in-water emulsions with added solids. The presence of solid particles increased both the viscosity and the non-Newtonian behaviour, resulting in a reduction of the creaming of the emulsions and in the sedimentation of the solids.

Adsorption of surfactant can also have a detrimental effect on the stability of emulsions stabilised by solid particles. Gelot et al.[24] observed stable w/o emulsions in the presence of carbon black but the stability decreased upon addition of dodecyltrimethylammonium bromide (DoTAB) and no emulsion was formed in the presence of SDS. They also observed inversion of o/w emulsions stabilised by calcium bentonite to w/o on addition of DoTAB. Levine et al.[25, 27] have derived a theoretical model of emulsion stabilisation by fine powders and carried out some experiments to support their findings. They conclude that almost all of the solid particles are adsorbed at the oil-water interface which explains why the emulsion drop size decreases with an increase in the concentration of solid particles.

A number of authors propose that the solid particles must be flocculated in order to stabilise emulsions. Hassander et al.[26] have used a neutral polymer polyvinylpyrrolidone (PVP) and a cationic surfactant to cause aggregation of silica particles. They suggest the silica particles must be flocculated before they adsorb at the oil-water interface and hence the drops are stabilised by multilayers of silica particles. Midmore has shown that hydrophilic silica particles flocculated by hydroxypropylcellulose (HPC) stabilise paraffin oil-in-water emulsions,[35] whereas hydrophobic silica stabilises water-in-paraffin oil emulsions in the presence of HPC but are flocculated only at extremes of pH.[36] It has been claimed that emulsion stability is due to adsorption of the flocs at the oil-water interface but this could be misleading because presumably the polymer is also surface-active and may contribute to the emulsion stability. The effect of electrolytes on the ability of hydrous ferric oxide to stabilise benzene-water emulsions was investigated by Briggs.[18] In the absence of electrolyte no stable emulsions were formed with the liquids separating into their bulk phases immediately. When NaCl was added to the aqueous ferric oxide suspension, the colloid was flocculated and the stability of the subsequent emulsion with benzene was greatly enhanced. Addition of NaCl, a weak flocculating agent, decreases the affinity of ferric oxide for the aqueous phase and hence increases the likelihood that it will enter the oil-water interface which is necessary for it to stabilise emulsions. However, when Na_2SO_4, a strong flocculating agent, was added to ferric oxide, no emulsions were produced. The large flocs were too coarse in size to stabilise the emulsion drops as they didn't reside evenly at the oil-water interface. Partial flocculation of particles was also shown to be necessary for efficient emulsion stabilisation by Lucassen-Reynders and van den Tempel.[21] These authors described the effect of added surfactant on the stability of

water-in-paraffin oil emulsions containing glycerol tristearate crystals. The crystals formed a strong network in oil in the absence of surfactant which was not capable of stabilising emulsions. Addition of surfactant (such as sodium bis-(2-ethylhexyl) sulphosuccinate (Aerosol OT, AOT)) decreases the interaction between the crystals resulting in partial flocculation. In this state the crystals were found to be more efficient at stabilising emulsions.

In conclusion, a wide variety of solid materials have been used as stabilisers of either o/w or w/o emulsions including iron oxides, hydroxides, metal sulphates, silica, clays and carbon. The effectiveness of the solid in stabilising emulsions depends on particle size and shape, particle concentration, particle wettability and the interactions between particles. The wettability of solid particles can be affected by adsorption of a suitable surfactant,[20, 22 – 24, 26, 28 – 32] in some cases leading to inversion of the preferred emulsion type.[20, 22, 24, 28] In addition, several studies conclude that stable emulsions can only be formed if the particles are flocculated to some extent.[18, 21, 26, 35, 38] Depending on the exact system, there at least two mechanisms by which colloidal particles stabilise emulsions. In the first, the particles are required to adsorb at the oil-water interface and remain there forming a dense film (monolayer or multilayer) around the *dispersed* drops impeding coalescence. In the second, additional stabilisation arises when the particle-particle interactions are such that a three-dimensional network of particles forms in the *continuous* phase surrounding drops. This has been invoked particularly in clay-containing systems in which the emulsion oil drops become captured and largely immobilised in the array of clay platelets in water.[34, 37] The enhanced viscosity of the continuous phase reduces the rate and extent of creaming.

1.3 Colloids

A colloid is defined as a dispersion of one material (within the size range 1 nm to approximately 1 μm) in another. An emulsion is actually one type of colloid where both the materials are liquids. In this section however we will discuss the properties of sols, which are colloidal dispersions of a solid in a liquid. Aqueous or non-aqueous sols are prepared prior to formation of solid–stabilised emulsions by dispersing silica in water or

oil depending on the hydrophobicity of the particle. It is therefore appropriate to give a general introduction to aqueous and non-aqueous colloid chemistry in this section with a more comprehensive description of the anomalous behaviour of silica dispersions given in Chapter 3.

1.3.1 Aqueous colloids

Colloidal particles undergo Brownian motion and as a result will be continually colliding with one another. They will only remain as individual particles if the collisions do not result in permanent associations. However, the lowest free energy state for lyophobic colloids is when they are all condensed together into one large aggregate. Such systems only remain as individual particles if some mechanism prevents aggregation during a collision. There are two ways by which that can be done:

(i) the particles can be given an electrical charge (either positive or negative) and if all have the same charge they will repel one another on approach.

(ii) the particles can be coated with an adsorbed layer of some material (say a polymer), which itself prevents their close approach.

Mechanism (i) is referred to as *electrostatic stabilisation* and mechanism (ii) as *steric stabilisation*, where the term stability refers to the aggregation behaviour of the dispersion. Electrostatic stabilisation is the mechanism that prevents aggregation of the silica particles discussed in Chapter 3 so it is this that will be described in detail.

Most substances acquire a surface electric charge when brought into contact with a polar (e.g. aqueous) medium. This can occur by *ionisation* of surface groups which is highly dependent on pH, or via *ion adsorption* of oppositely charged ions in solution. Ionic substances can also acquire a surface charge by virtue of unequal *dissolution* of the oppositely charged ions of which they are composed. For example, hydrogen and hydroxyl ions are potential determining for hydrous metal oxide sols:

$$\text{-M} - \text{OH} + \text{H}^+ = \text{-M} - \text{OH}_2^+$$

$$\text{-M} - \text{OH} + \text{OH}^- = \text{-M} - \text{O}^- + \text{H}_2\text{0}$$

The surface charge influences the distribution of nearby ions in the polar medium. Ions of opposite charge (counter-ions) are attracted towards the surface and ions of like charge (co-ions) are repelled away from the surface. However, they are also subject to thermal motion, which tends to distribute them uniformly through the surrounding medium. This charge arrangement is referred to as the *diffuse electrical double layer* around the particle. The double layer can be regarded as consisting of two regions; an inner region consisting of adsorbed ions and a diffuse region where ions are distributed in the bulk.

Schematic representation of a diffuse electric double layer

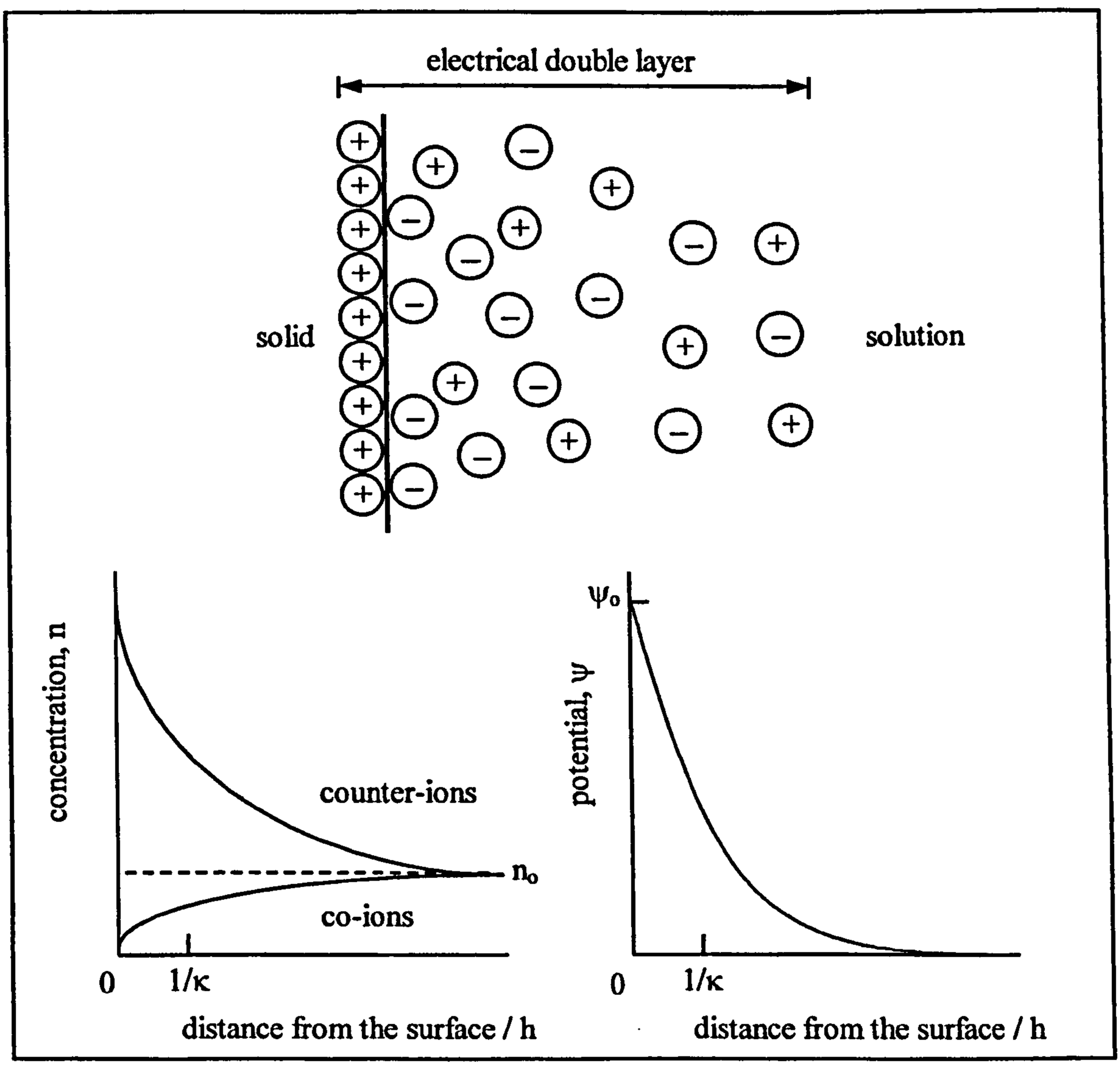

Gouy[38] and Chapman[39] derived a quantitative treatment of the diffuse part of the electrical double layer. In their model, the surface is assumed to be flat, of infinite extent, uniformly charged and the ions are assumed to be point charges distributed according to Boltzmann's distribution. For a positively charged surface of electrical potential (ψ_o), the distribution of ions in solution can be determined by applying the Boltzmann distribution,

$$n_+ = n_o \exp\left[\frac{-ze\psi}{kT}\right] \tag{1.5}$$

and

$$n_- = n_o \exp\left[\frac{+ze\psi}{kT}\right] \tag{1.6}$$

where n_+ and n_- are the respective numbers of positive and negative ions per unit volume at points where the potential is ψ (i.e. where the electric potential energy is $ze\psi$ and $-ze\psi$ respectively), and n_o is the corresponding bulk concentration of each ionic species. The surface potential, ψ_o, is dependent on the surface charge density and on the ionic compression of the medium. If the double layer is compressed then either the surface charge density must increase or the surface potential must decrease or both. The size of the double layer depends on the electrolyte concentration in solution. Increasing the electrolyte concentration causes the diffuse double layer to shrink so that the electrostatic potential decreases more quickly with distance. The variation in electrical potential with distance, h, from the surface is obtained by solving Poisson's equation,

$$\frac{d^2\psi}{dh^2} = -\frac{\rho_e}{\varepsilon_r \varepsilon_o} \tag{1.7}$$

where ρ_c is the charge density (measured in C m^{-3}), ε_r is the relative dielectric constant and ε_o is the permittivity of free space.

In 1924 Stern[40] proposed a model to describe the inner region of the electrical double layer. In this model the double layer is divided into two parts separated by a plane (the Stern plane) located at approximately a hydrated ion radius (δ) from the surface. He described the existence of specifically adsorbed ions which are attached (albeit temporarily) to the surface by van der Waals and/or electrostatic forces strongly enough to overcome thermal agitation. The centres of the adsorbed ions are located in the Stern layer which is located between the surface and the Stern plane. Ions located outside the Stern plane form the diffuse part of the double layer as described previously by Gouy and Chapman. The potential changes from ψ_o at the surface to ψ_d (the Stern potential) in the Stern layer.

Schematic representation of the structure of the electrical double layer according to Stern's theory

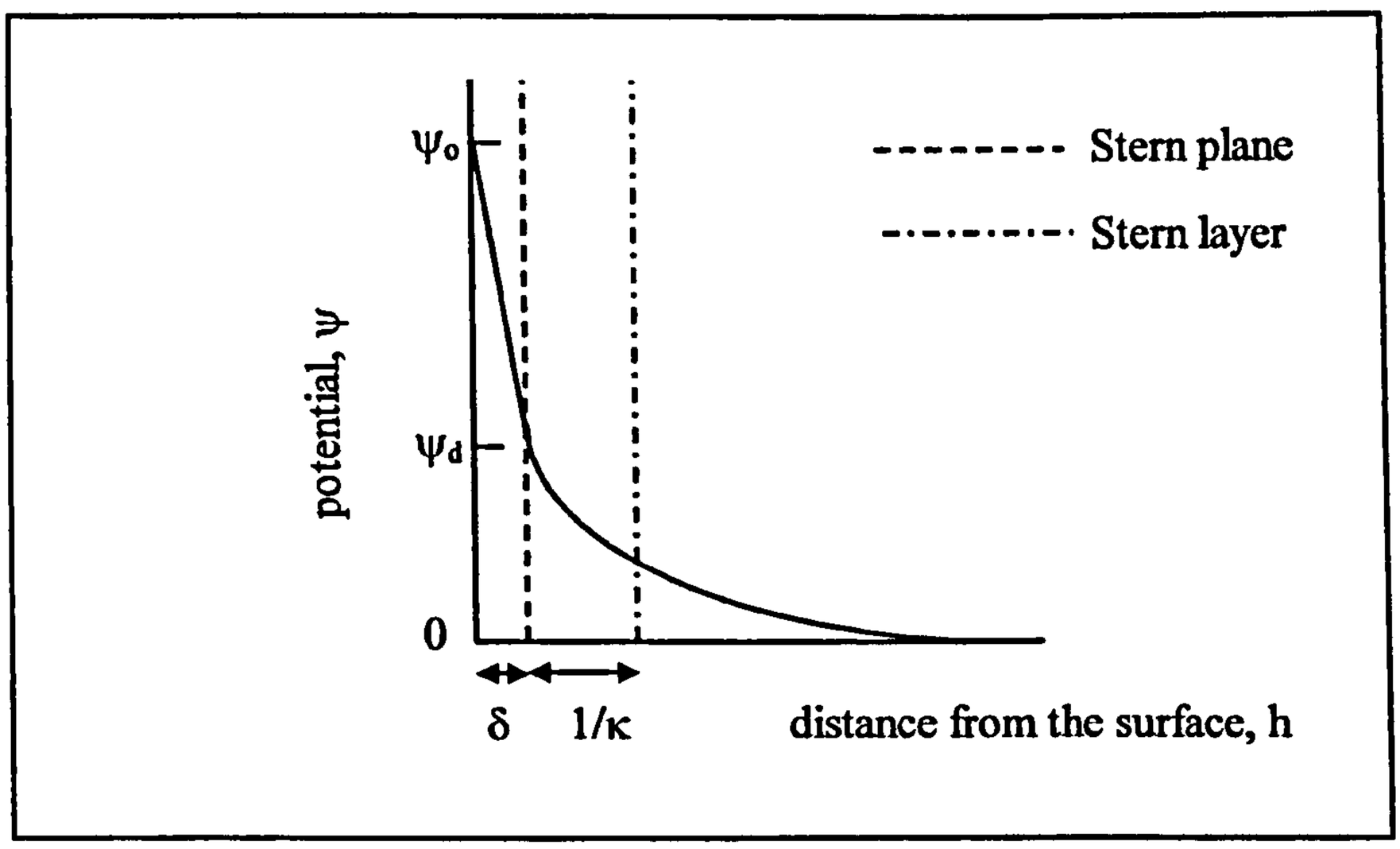

ψ_d can be estimated from zeta potential (ζ) or electrokinetic measurements. The zeta potential is the potential measured at the surface of shear between the charged surface and the electrolyte solution. The shear plane is usually located at a small distance further out from the surface than the Stern plane and as a result the zeta potential is usually marginally smaller than ψ_d. However, they are assumed to be identical in most experimental investigations. It is possible for reversal of charge within the Stern layer to take place if surface-active co-ions adsorb onto the surface resulting in ψ_o and ψ_d having opposite signs.

1.3.2 Colloid stability

The stability of aqueous colloidal dispersions is dependent on the interaction between particles in a sol or droplets in an emulsion.[41] Derjaguin and Landau[42] and Verwey and Overbeek[43] independently developed a quantitative theory which describes the features of colloidal interactions, especially in relation to added electrolyte. The theory involves estimations of the energy due to the overlap of electric double layers (usually repulsive) and the London-van der Waals energy (usually attractive) in terms of inter-particle distance. Repulsive interactions arise from overlapping of the diffuse parts of the electric double layers around two spherical particles (as described by Gouy-Chapman). It is an approximately exponential function of the distance between particles with a range of the order of the thickness of the double layer ($1/\kappa$). Attractive interactions can be one of three types;

(i) orientation of two molecules with permanent dipoles in such a way that attraction results,

(ii) dipolar molecules induce dipoles in other molecules so that attraction results,

(iii) the existence of dispersion forces between two non-polar molecules due to the polarisation of one molecule by fluctuations in the charge distribution in a second molecule, and vice versa.

Dispersion forces account for nearly all of the van der Waal interactions between two molecules. These interactions decrease as the inverse power of the distance between the particles. The total interaction potential V_t between two approaching particles is

$$V_t = V_d + V_e \tag{1.8}$$

where V_d and V_e are the van der Waals dispersion energy and repulsive electrostatic energy respectively. Depending on the relative magnitude of the attractive and repulsive terms the particles will remain dispersed or will flocculate at a given separation. The schematic below shows a typical plot of the total interaction potential as a function of the inter-particle distance H. The attractive term dominates when H is very large or very small resulting in a negative V_t and hence flocculation.

Schematic representation of the interaction potential energy versus distance curve between two particles

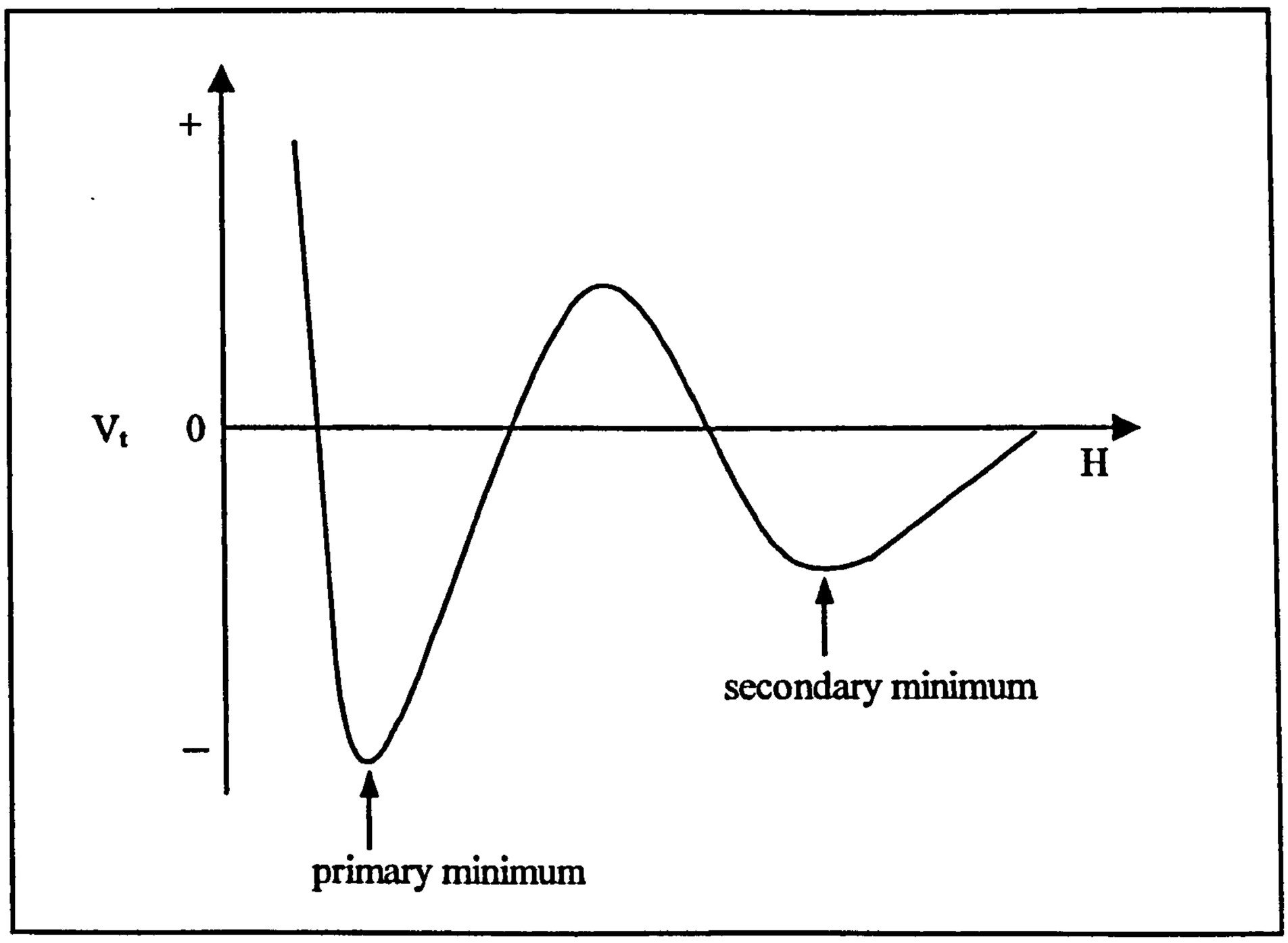

The secondary minimum at large separation will give rise to a loose, easily reversible flocculation if it is moderately deep compared to kT. For small particles (radius < 10^{-8} m) the secondary minimum is never deep enough for flocculation to occur. The primary minimum is normally so deep that when the total interaction energy has this value particle aggregation becomes irreversible. At intermediate separations the repulsive double layer force dominates and gives rise to a potential energy barrier to flocculation. If the potential energy maximum is large compared with the thermal energy kT of the particles the system should be stable. The height of the barrier to flocculation depends on the magnitude of ψ_d (and ζ) which itself is dependent on the concentration of electrolyte in solution. The barrier to flocculation is thus decreased in the presence of electrolyte resulting in an unstable colloidal dispersion.

1.3.3 Non-aqueous colloids

In the present work hydrophilic silica particles were modified to varying extents with dimethyldichlorosilane groups. These particles were dispersed in oil using an ultrasonic probe and then homogenised with an aqueous phase to form a solid-stabilised emulsion. The stability of these non-aqueous dispersions was not examined in detail; observations of viscosity and general appearance were recorded only.

In contrast to aqueous colloids, van der Waals dispersion forces and steric forces are dominant in non-aqueous dispersions. Electrostatic repulsive forces are minimal due to the non-polar continuous phase. Dispersion forces between particles are dependent on the nature of the continuous phase in which they are dispersed. In a 'good' solvent the dispersion forces are negligible and the colloid remains dispersed. In a 'poor' solvent the particles tend to flocculate because attractive inter-particle interactions are strong. Cyclohexane is shown to be a good solvent for silica particles coated with octadecyl chains whereas ethanol is a poor solvent for the same particle type.[44] Changing the temperature of the system can also result in destabilisation of the non-aqueous dispersion. Jansen et al.[45] show that attraction between silica particles coated with octadecyl chains increases with decreasing temperature. Below a certain temperature

(which is dependent on the solvent) the particles are irreversibly flocculated. Small chained solvents (6 carbons) have lower instability temperatures (4 °C) than long chain solvents (16 carbons, 29 °C). In similar work Edwards et al.[46] report both upper and lower temperature-induced flocculation boundaries. These silica particles, also coated with octadecyl chains, are dispersed in various alkanes and their turbidity is measured as a function of temperature. The upper flocculation boundary is attributed to an increase in van der Waals attractions between particles as the density of the intervening liquid decreases. Steric stabilisation of non-aqueous colloids has been observed by a number of authors[47 - 49] for dispersions of silica in toluene. The silica particles are grafted with polystyrene or polydimethylsiloxane chains to which different types of free polymer chains are added. The interaction between the chains determines the stability of the colloid.

Flocculation of aqueous silica colloids is shown to increase the stability of o/w emulsions (Chapter 3). However, there is no evidence to suggest the non-aqueous colloids are flocculated prior to emulsification. It is more likely that the stability arises from the contact angle of the particles at the oil-water interface being closer to 90°.

1.4 Presentation of thesis

The main aim of this research was to prepare emulsions stabilised solely by solid particles and investigate their type and stability in a number of different systems. This was achieved by carrying out a systematic study beginning with toluene-water emulsions stabilised by hydrophilic silica particles in the absence and presence of various types of electrolyte (Chapter 3). An attempt was made to relate the stability of the aqueous colloid to the stability of the solid-stabilised emulsion. A second type of silica particle, with hydrophobic groups on its surface, was shown to stabilise w/o emulsions at a volume fraction of water equal to 0.5 (Chapter 4). When the volume fraction of water was increased in this system, the emulsion type catastrophically inverted to o/w. Transitional phase inversion of emulsions was achieved by varying the mass fraction of hydrophilic and hydrophobic particles in systems of fixed volume fraction of oil and water (Chapter 5).

A range of silica particles with varying degrees of hydrophobic modification were used to stabilise emulsions (Chapter 6). The emulsions catastrophically inverted from one emulsion type to the other with the volume fraction of water at inversion dependent on the particle hydrophobicity. Particles of intermediate hydrophobicity were found to be the most efficient at stabilising emulsions due to their high energy of attachment to the oil-water interface. The energy of attachment is dependent on the contact angle of the particle at the oil-water interface and the interfacial tension between the liquids. The interfacial tension and contact angle were investigated further by varying the type and composition of oil and aqueous phases (Chapter 7).

An increase in the aqueous phase pH causes dissociation of silanol groups on silica particles which renders them more hydrophilic (Chapter 8). Particles initially located in the oil phase transferred to the aqueous phase with increasing pH. In contrast to these systems where the hydrophobicity is changed *in situ*, the hydrophobicity of pigment particles has been affected by adsorption of surfactant (Chapter 9). The hydrophobicity can be controlled by adsorption of different surfactants at different concentrations.

CHAPTER 2

CHAPTER 2

EXPERIMENTAL

This chapter contains a detailed description of the materials used along with a comprehensive review of all experimental methods.

2.1 Materials

2.1.1 Water

Water was passed through an Elgastat Prima reverse osmosis system and then through a Milli-Q reagent water system. Water treated in this way had a surface tension of 71.9 mN m^{-1} at 25 °C (measured using a du Noüy ring), in excellent agreement with good literature values.[50, 51]

2.1.2 Oil and polar phases

Table 2.1 lists the various oils used along with their suppliers and purities. All oils were columned twice through chromatographic alumina (Aldrich, activated basic, ~ 150 mesh) in order to remove polar impurities. The structures of the perfume oils, eugenol (2-methoxy-4-[2-propenyl]phenol) and cineole (eucalyptol) are given below.

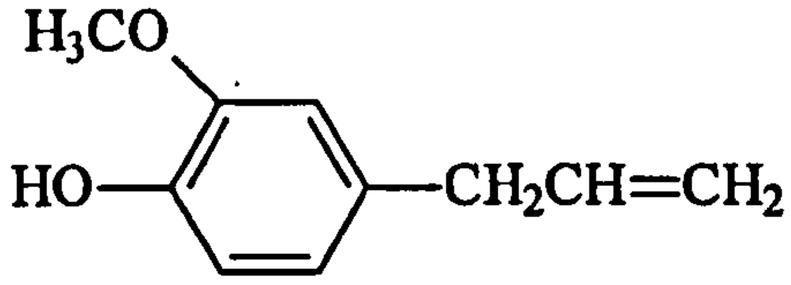

eugenol

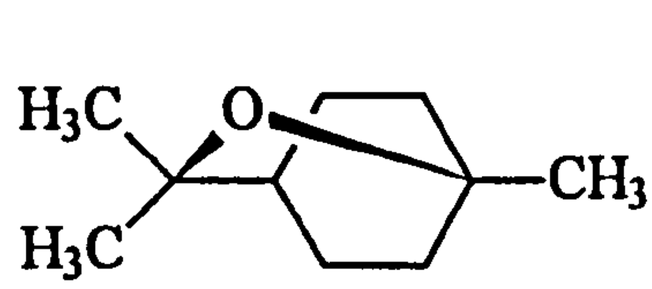

cineole

Table 2.1 Source and purity of oils used

Oil phase	Supplier	Purity
toluene	Fisher Scientific	> 99.97 %
n-heptane	Fisher Scientific	> 99 %
n-dodecane	Avocado	> 99 %
n-tetradecane	Sigma	99 %
cyclohexane	Fisher Scientific	> 99 %
squalane	Aldrich	99 %
polydimethylsiloxane (PDMS), 0.65, 20 and 50cS	Dow Corning	Unknown
1-undecanol	Aldrich	99 %
perfluorohexane	Fluorochem	99 %
perfluoroheptane	Fluorochem	99 %
diiodomethane	Lancaster	99 %
methyl myristate	Fluka	99 %
isopropyl myristate	Fluka	99 %
eugenol (above)	Fluka	99 %
cineole (above)	Fluka	99 %

Table 2.2 lists the polar phases used, their suppliers and purities. All of these liquids were used as received.

Table 2.2 Source and purity of polar phases used

Polar phase	Suppliers	Purity
ethylene glycol	Fisher Scientific	> 99 %
glycerol	Lancaster	99 %
formamide	Acros	99.5 %

2.1.3 Other chemicals

Table 2.3 lists the purity and suppliers of the other chemicals used in the experimental work. All of these chemicals were used as received.

Table 2.3 Source and purity of other chemicals used

Chemical	Supplier	Purity
sodium chloride	Prolabo Normapur	99.5 %
lanthanum chloride	Vickers Laboratories	98 %
tetraethylammonium bromide (TEAB)	Acros Organics	99+ %
sodium hydroxide	Prolabo Normapur	98 %
potassium hydroxide	BDH	Analar Grade
hydrochloric acid	May & Baker	
nitric acid	Fisher Scientific	
methanol	Fisher Scientific	99 %
chloroform	Sigma	> 99.5 %
dimethyldichlorosilane (DMDCS)	Fluka	> 99.5 %

2.1.4 Solid particles

(a) Silica

Two main types of silica particles have been used to stabilise oil-water emulsions. Precipitated silica (Ludox HS-40, purchased from Aldrich) is prepared by nucleation of silica particles and grown by alkaline hydrolysis of sodium silicate solutions. Ludox HS-40 is supplied as a 40 wt.% dispersion in water of pH 9.7, with a quoted diameter of 15 nm and a surface area of 200 m^2 g^{-1}. The surface of these particles consists mainly of SiOH and $Si(OH)_2$ groups.[52] The majority of work has investigated emulsions stabilised by fumed/pyrogenic silica, both with and without

hydrophobic modification. The source and properties of the fumed silica particles used are given in Table 2.4. All samples were gifts from the respective companies and were used as received. All had a primary particle diameter of between 5 and 30 nm, which can aggregate into larger units of 100 nm in diameter due to the formation of hydrogen bonds between the silanol groups on adjacent particles.[53] These aggregates form three-dimensional agglomerates when dispersed in liquids resulting in an increased viscosity. Silica particles are used in a number of industrial processes as thickening agents, the viscosity of the liquid dependant on the concentration of particles and the dispersion procedure. The hydrophilic silica (Aerosil 200 and HDK N20) is prepared by flame hydrolysis of silicon tetrachloride in an hydrogen/oxygen flame.

$$SiCl_4 + 2H_2 + O_2 \rightarrow SiO_2 + 4HCl \qquad (2.1)$$

The silica is hydrophilic due to the silanol groups (SiOH) present on its surface. The surface also contains siloxane bridges (Si-O-Si) as shown in Figure 2.1. Fuji et al.[54] describe silica as hydrophilic when surface modification is less than 20 %. Hence, all the silica particles listed in Table 2.4 that do not have 100 % SiOH surface coating will be referred to as partially hydrophobic. Hydrophobic silica is prepared by reacting hydrophilic silica with dimethyldichlorosilane reagent to varying extents in the presence of water followed by drying at 300 °C for 2 hours.[55]

$$-SiOH + SiCl_2(CH_3)_2 \rightarrow -Si\text{-}(OSiCl(CH_3)_2) \qquad (2.2)$$

This reaction produces covalent siloxane bonds between the silica atoms of the organosilane molecules and the silica atoms of the solid surface. However, it is possible for the remaining chlorine molecule to react with an adjacent silanol group or another dimethyldichlorosilane group to form doubly bound bidentate siloxane bridges and polymerised coatings respectively[56, 57] (see Figure 2.2). The silanol content remaining on the silica surface was determined by titration with aqueous NaOH, while the carbon content was measured using a carbon analyser. There are approximately 2 SiOH groups / nm^2 on the hydrophilic silica which falls progressively to 1 SiOH group / nm^2 for the most hydrophobic silica (H18).

Figure 2.1
Schematic of hydrophilic silica

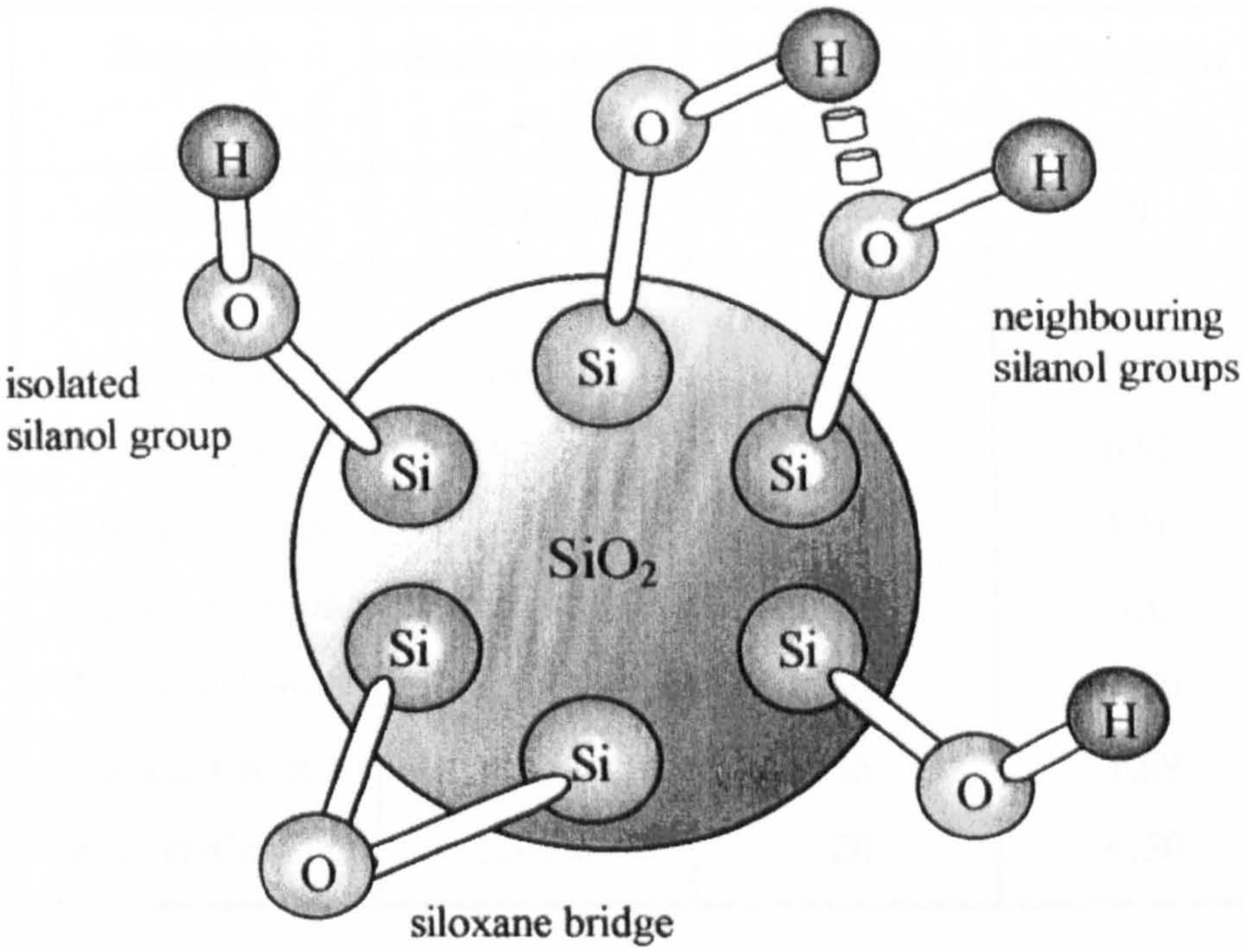

Figure 2.2
Schematic of hydrophobic silica

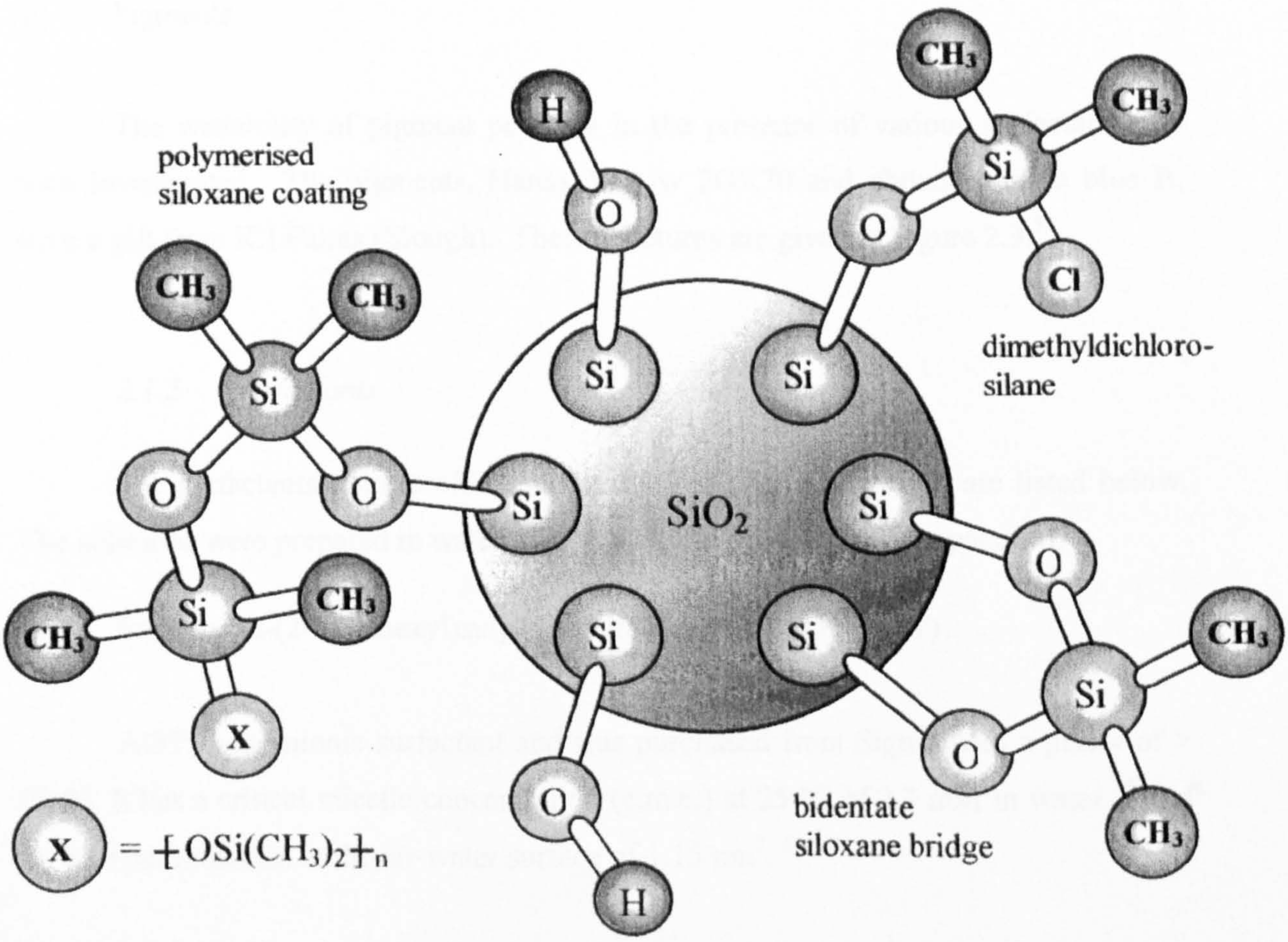

Table 2.4 Suppliers and specifications of silica particles

Code name	Supplier	Surface area[3] ($m^2 g^{-1}$)	SiOH content (wt. %)	C content (wt. %)
Aerosil 200	Degussa[1]	200±25	100	0
HDK N20	Wacker-Chemie[2]	200±30	100	0
SLM 078	Wacker-Chemie	300±30	79	0.68
SLM 079	Wacker-Chemie	300±30	76	0.83
SLM 081	Wacker-Chemie	300±30	67	1.10
SLM 957	Wacker-Chemie	200±20	57	1.0
HDK H30	Wacker-Chemie	300±30	50	1.80
SLM 091	Wacker-Chemie	200±20	36	1.69
HDK H18	Wacker-Chemie	200±40	20	4.50

1 Particles supplied by Degussa were synthesised in Hanau, Germany.

2 Particles supplied by Wacker-Chemie were prepared in Berghausen, Germany.

3 Surface areas quoted refer to the bare silica particles prior to modification.

(b) Pigments

The wettability of pigment powders in the presence of various surfactants has been investigated. The pigments, Hansa Yellow 2GX70 and phthalocyanine blue B, were a gift from ICI Paints (Slough). Their structures are given in Figure 2.3.[58]

2.1.5 Surfactants

The surfactants used to affect the wettability of pigment discs are listed below. The solutions were prepared in water and used within three days of preparation.

(a) Sodium bis-(2-ethylhexyl)sulphosuccinate (Aerosol OT, AOT)

AOT is an anionic surfactant and was purchased from Sigma with a purity of > 99 %. It has a critical micelle concentration (c.m.c.) at 25 °C of 2.3 mM in water [59] and an area per molecule at the air-water surface of 1.15 nm^2. [60, 61]

Figure 2.3

Structure of pigments

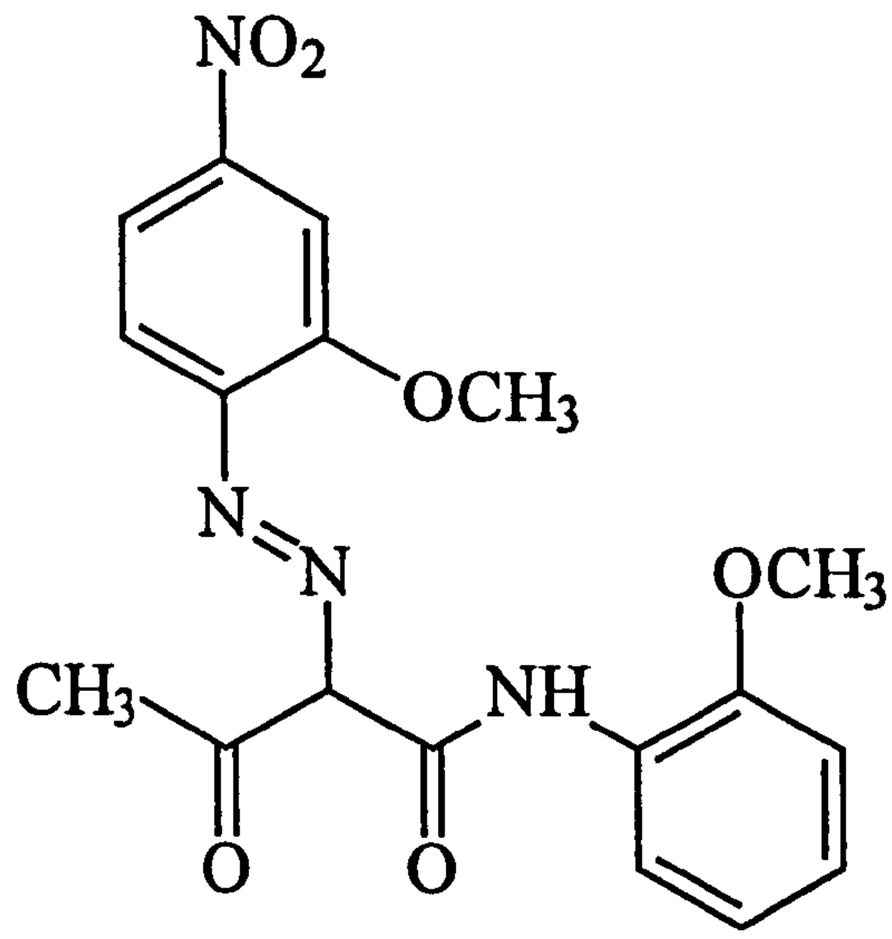

Hansa Yellow 2GX70

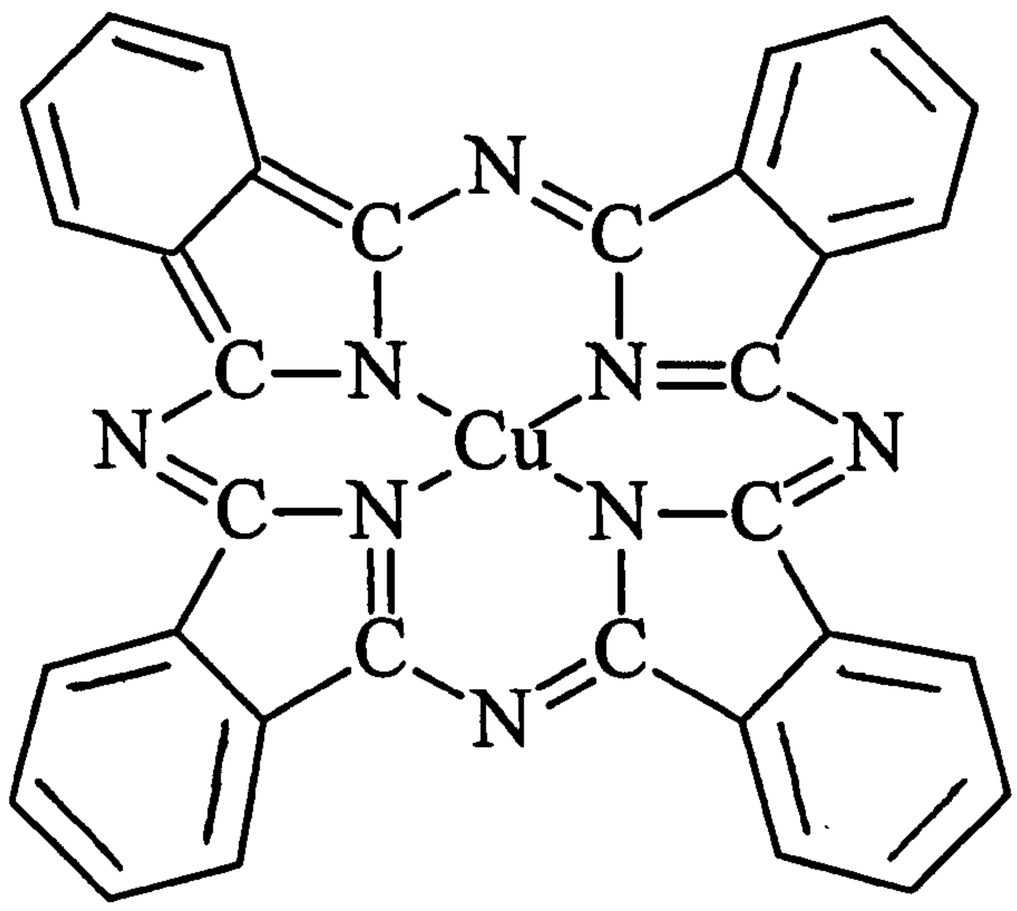

Phthalocyanine blue B

(b) Cetyltrimethylammonium bromide (CTAB)

CTAB is a cationic surfactant and was purchased from Acros Organics with a purity of 99+%. It has a c.m.c. at 25 °C of 0.97 mM in water[59] and an area per molecule at the air-water surface of 0.61 nm^2.[62]

(c) Sodium dodecylsulphate (SDS)

SDS is an anionic surfactant and was purchased from Lancaster with a purity of 99 %. It has a c.m.c. at 25 °C of 8.0 mM in water.[59]

(d) Dodecyl pentaoxyethyleneglycol ether ($C_{12}E_5$)

$C_{12}E_5$ is a nonionic surfactant and was purchased from Nikkol (Japan) with a purity of 99 %. It has a c.m.c. at 25 °C of 4.5×10^{-5} M in water.[63]

(e) Silwet copolymer L-77

L-77 is a nonionic silicone surfactant of approximate formula Me_3SiO $[Si(CH_2)_3(OCH_2CH_2)_{7.5}OMe]$ OSi Me_3 with a c.m.c. at 25 °C of 1.2×10^{-4} M in water.[64] It was a gift from OSi Specialties.

2.1.6 Glassware

Great care was taken to ensure glassware was not contaminated by surfactant. All glassware was first cleaned with alcoholic KOH then rinsed with copious amounts of Milli-Q water and finally dried in a laboratory oven at 60 °C.

2.2 Methods

2.2.1 Preparation and characterisation of colloidal dispersions

(a) Ultrasonic dispersion

Dispersions of solid particles in water or oil were prepared by dispersing a known mass of powder in the solvent (no more than 25 cm^3) using a high intensity ultrasonic vibracell processor[65] (Sonics & Materials, tip diameter 3 mm), operating at 20 kHz and up to 10 W for 2 minutes. During sonication, the dispersion was cooled in an ice-bath.

(b) Measurement of pH

In systems where the pH and electrolyte concentrations of the aqueous colloid were varied, the electrolyte was always added before pH adjustment. The pH was measured using a Jenway PHM 6 meter with a saturated KCl electrode. The meter was calibrated before use with buffer solutions of pH = 4, 7 and 10. The pH of the aqueous colloid was varied by addition of hydrochloric acid or sodium hydroxide.

(c) Transmission Electron Microscopy (TEM)

TEM of aqueous dispersions of hydrophilic silica were performed using a Jeol 100c 80kV electron microscope. The aqueous colloids were prepared in the usual way and diluted to 0.125 wt.% using water of the same pH value as the colloid. 10 µl of the colloid was placed onto a copper grid containing a very thin layer of carbon, which acts as a support to the solution. Two methods of drying were investigated, air drying and freeze drying.[66] The colloids that were allowed to air dry tended to clump (Figure 2.4 (a)) but more defined images with visible primary particles joined into aggregates were obtained with the freeze drying technique (Figure 2.4 (b)). This involved the grid being immersed in liquid nitrogen for two minutes. Most of the liquid nitrogen was then removed and the cell was loaded into an Edwards freeze drier under vacuum for three hours to ensure complete drying before being observed under the microscope.

Figure 2.4

TEM images of 0.125 wt.% Aerosil 200 at pH 2 prepared by air drying (a) and freeze drying techniques (b). Scale bar equals 100 nm.

(a)

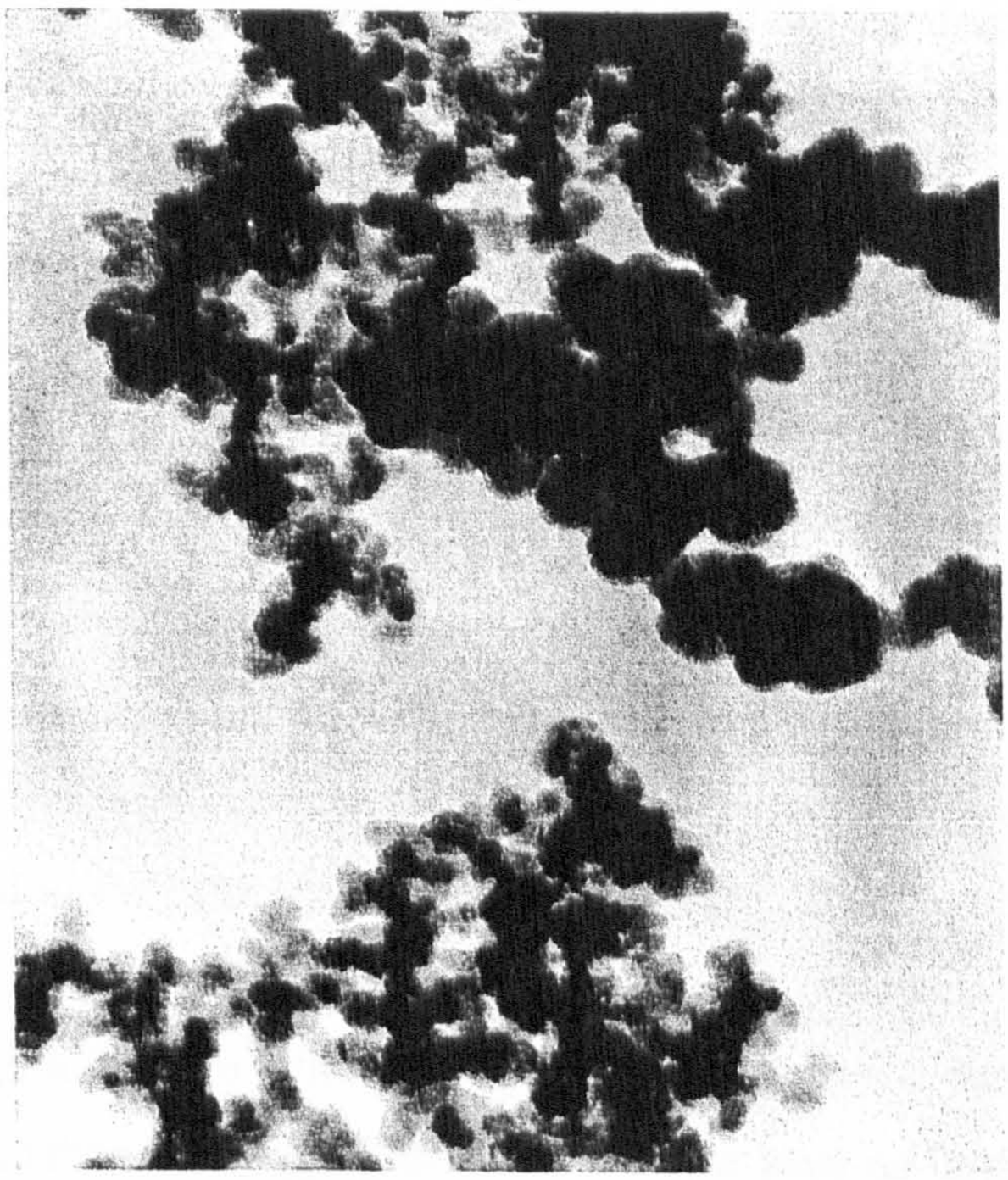

(b)

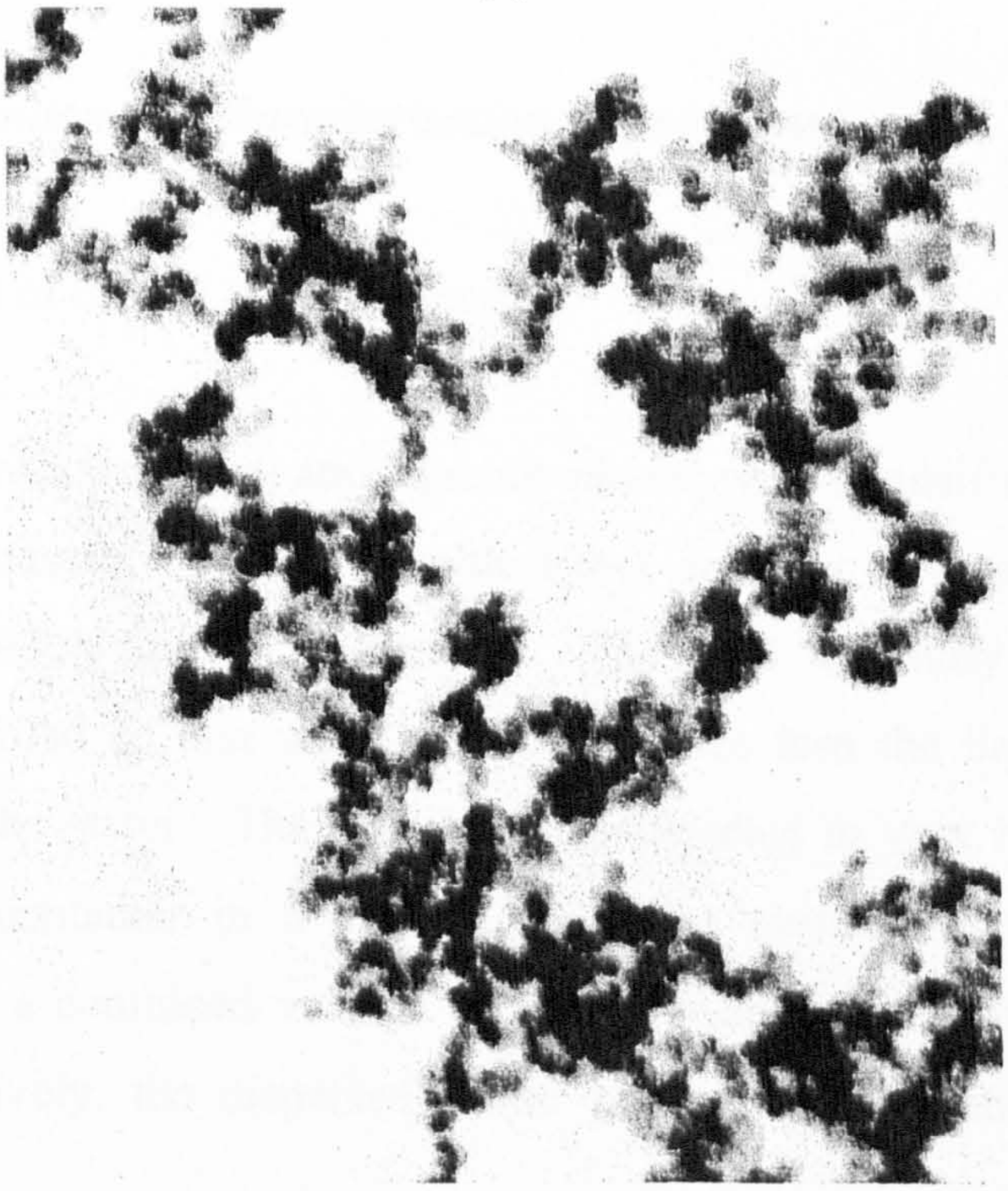

(d) Turbidity of aqueous dispersions

The turbidity of the aqueous colloids was measured on a Hach Analytical Nephelometer (Model 2424) at room temperature (~ 20 °C). 25 cm^3 of the solution was placed in glass vessels (25 x 100 mm) and a photomultiplier tube detects the intensity of light scattered at 90° to the incident beam at a height of 10 mm from the base of the cell. The instrument records the turbidity in empirical Nephelometric Turbidity Units (NTU) based on the amount of light scattered by particles of a reference standard Formazin.

(e) Photon Correlation Spectroscopy (PCS)

The apparent size of hydrophobic HDK H30 silica particles in toluene was measured by photon correlation spectroscopy. Light scattering from solutions containing between 0.01 and 1 wt.% particles indicated the presence of particle aggregates as opposed to the primary particles themselves. Sample times were in excess of 100 μs before slight correlations in the scattering were observed. Filtering the 0.05 wt.% solution through a 200 nm Whatman Anotop 10 membrane resulted in no change to the scattering, indicating that aggregate sizes were at least as large as this value. A detailed description of PCS can be found in ref. 61.

2.2.2 Preparation and characterisation of emulsions

(a) Emulsification of oil and aqueous phases

The required volumes of oil and aqueous phases were emulsified with a Janke & Kunkel T25 homogeniser (rotor-stator) with either an 8 or 18 mm shaft operating between 8000 and 24000 rpm for 2 minutes. The head was fully immersed in the material to be emulsified so that when the rotor blades turn the liquids were forced between the slits in the stator. The liquids were subjected to very high shear and by slowly moving the container in a vertical motion a uniform homogenisation was achieved. Typically, a combined volume of 10 cm^3 was used for direct formation of emulsions. Alternatively, the dispersed phase was added sequentially to 5 cm^3 of

continuous phase with 1 minute emulsification between each addition. Coarser emulsions were formed when mixtures were hand-shaken vigorously for 30 seconds.

(b) Conductivity and type of emulsions

The conductivity of emulsions was determined immediately after homogenisation using a PTI-58 digital conductivity meter with Pt/Pt black electrode at room temperature. The meter was calibrated with 0.1 M KCl solution. In some cases when the emulsion was unstable the conductivity was measured *in situ* during homogenisation. Emulsion type was also inferred by observing what happened when a drop of emulsion was added to a volume of either pure oil or pure water. Water continuous (oil continuous) emulsions dispersed in water (oil) and remained as drops in oil (water).

(c) Emulsion stability

The emulsions were transferred into stoppered, graduated glass vessels of i.d. 1.3 cm and length 10 cm which were thermostatted in a glass tank using a Grant LT D6G water-heater. The stability of o/w emulsions to creaming was assessed by monitoring the increase with time of the position of the clear water (serum) / emulsion interface. Stability to coalescence was measured by monitoring the height of the oil / emulsion interface. For w/o emulsions, the downward movement of the oil-emulsion interface was used as a measure of the stability to sedimentation, and the position of the water-emulsion interface was used as a measure of coalescence. Photographs of the vessels containing emulsions were taken with a Kodak DC 290 digital camera and downloaded into a PC.

(d) Measurement of emulsion drop size distributions

Emulsion drop size distributions were determined using a Malvern MS20 laser diffractometer. By use of three different lenses, the instrument covers the range from 0.1 to 600 μm and was calibrated using a monodisperse sample of latex of quoted diameter 5.0 μm. Figure 2.5 shows a typical calibration plot. The drop diameter (in μm)

Figure 2.5

Calibration plot for Malvern MS20 laser diffractometer. The monodisperse latex in water has a quoted diameter = 5.0 μm. The drop diameter is shown as a function of the percentage oversize distribution (left-hand ordinate – line) and the frequency distribution (right-hand ordinate – bars).

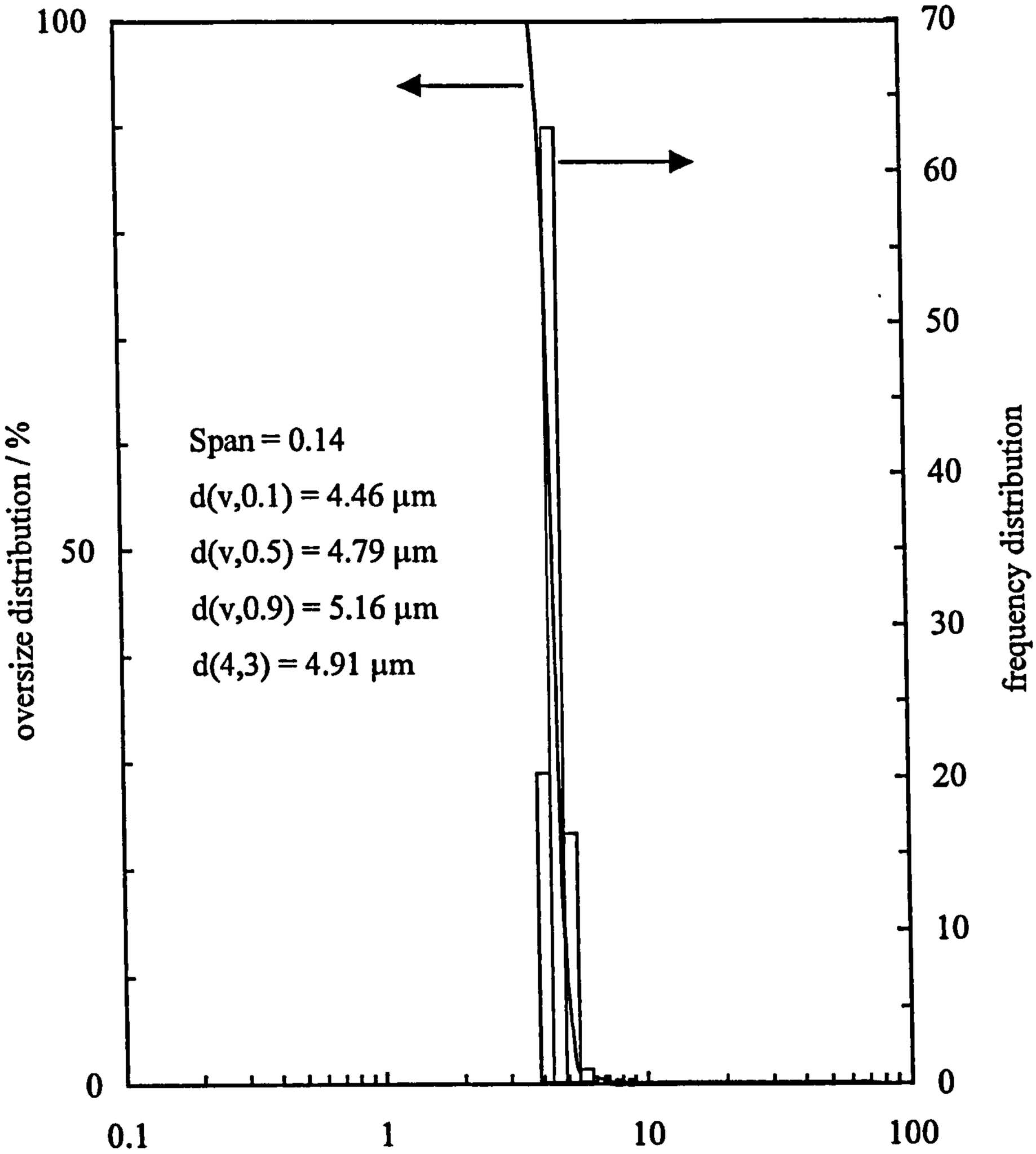

is plotted as a function of the percentage volume oversize distribution (left-hand ordinate - line) and the frequency distribution (right hand ordinate – bar). The span (= 0.14) is very small for the monodisperse latex sample and is defined as

$$\text{span} = d(v,0.9) - d(v,0.1)/d(v,0.5) \qquad (2.3)$$

where d(v,0.9) equals the volume distribution of drops of diameter below which 90 % exist, d(v,0.1) is the diameter below which 10 % of the drops exist and d(v,0.5) equals the diameter below which 50 % of the drops exist, also called the median diameter. The arithmetic mean (d(4,3)) is also included on the printout.

Figure 2.6 shows the basic configuration of the instrument. The light from a low power Helium – Neon laser is used to form a collimated and monochromatic beam of light, typically 18 mm in diameter. This beam is called the analyser beam and drops passing through it in the sample presentation cell will scatter the laser light. Large drops scatter at small angles and small drops at large angles. The scattered light is incident on the receiver lens. This operates as a Fourier Transform lens forming the far field diffraction pattern of the scattered light at its focal plane. The receiver lens has a special configuration, which means that regardless of the position or movement of the drops its diffraction pattern is stationary and focuses onto the multi-element photo-electric detector plane.

The presentation cell used to introduce the sample into the beam was cleaned between measurements by rinsing in isopropyl alcohol followed by copious amounts of the continuous phase. Measurements were taken by sampling approximately 0.5 cm^3 of emulsion from the centre of the emulsion phase, and diluting to 50 cm^3 with its own continuous phase. For o/w emulsions the diluting solution consisted of the aqueous colloid at the respective pH and salt concentration and for w/o emulsions either the colloid or the pure solvent were used (discussed further in Chapter 4.2).

Prior to measurement, a number of experimental parameters must be entered on the software used to run the instrument. The focal length of the lens determines the effective drop size range to be used. For example, the 45 mm lens can only be used for drops between 0.1 and 80 μm. The presentation code is dependent on the type of emulsion to be studied and is calculated from the refractive indices of the two liquids. In earlier models of the instrument, the presentation code was ignored and a systematic

Figure 2.6

Schematic of Malvern MS20 laser diffractometer

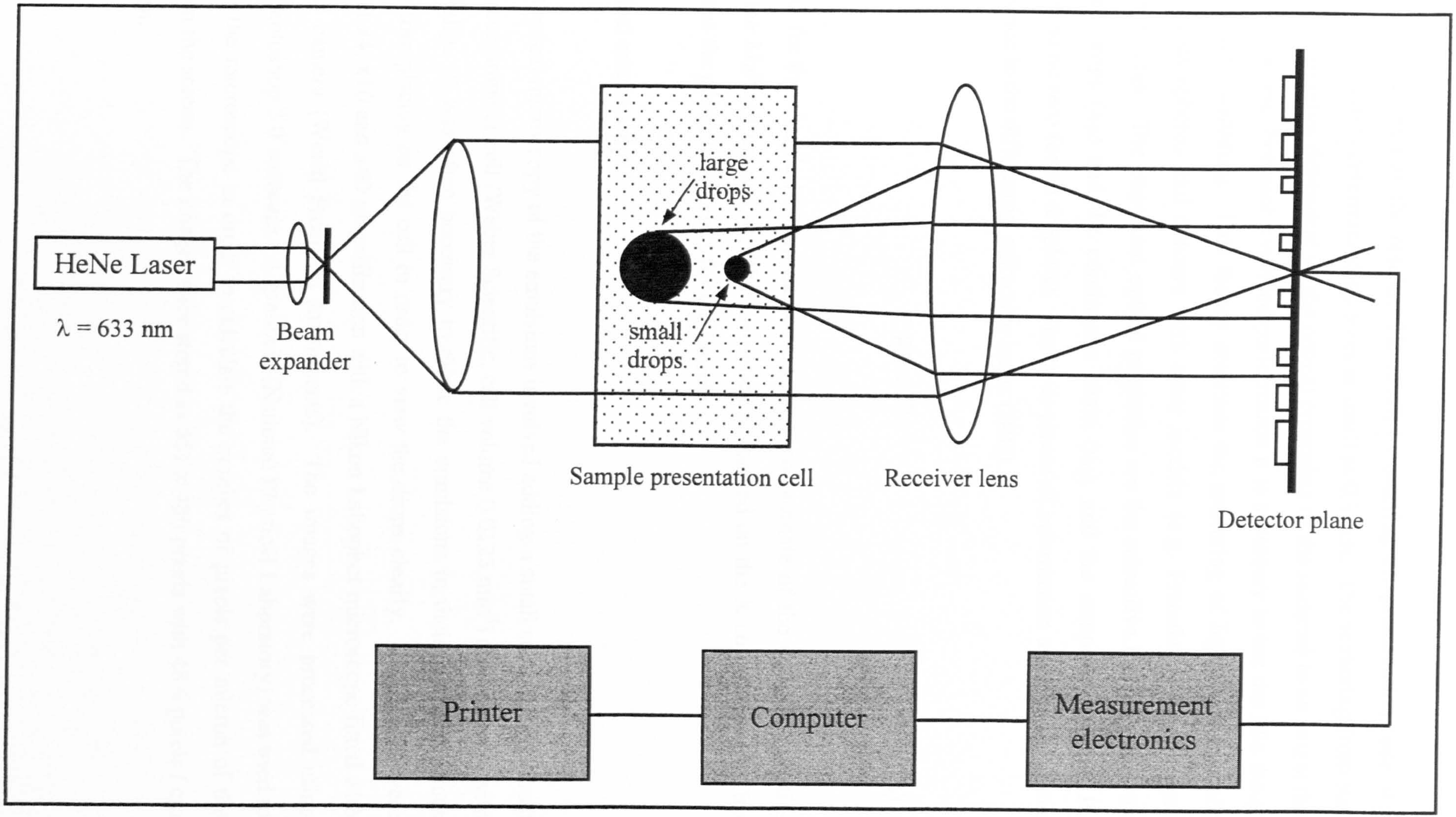

error was introduced into the results. However, by entering the presentation code, it is possible to accurately determine drop sizes as small as 0.1 μm. The scattering from such small drops becomes dependent on the optical properties of the material to an extent that cannot be ignored. For such extended performance it is necessary to use the Mie theory model of light scattering. This theory describes the scattering of light from optically homogeneous spheres and concurs with other models (e.g. Fraunhofer) within their applicable range. The important optical properties are the refractive index of both the dispersed drops (n_D) and the continuous phase (n_C), and the sample absorption R_A (assumed to be zero for all droplets). The three pieces of information are reduced to two by reference to the differential refractive index (DRI).

$$DRI = \frac{n_D}{n_C} \tag{2.4}$$

The DRI for the sample is then marked on the Y co-ordinate of the optical properties grid in the Malvern manual and the absorption is marked on the X co-ordinate.[67] This constitutes the presentation code for the sample.

(c) Optical microscopy

Optical microscopy of the emulsions involved adding a small sample (2-3 drops) to a haemocytometer cell (Weber Scientific, cell volume 0.0125 mm^3) and covering with a cover slip. It was often necessary to dilute the emulsions in their own continuous phase before placing on the cell in order to view the drops clearly. The images were viewed at x4, x10 and x40 magnification with a Nikon Labophot microscope fitted with a DIC-U camera (World Precision Instruments). The images were processed using Adobe Photoshop 3.0 software. A graticule (National Physical Laboratory) was used to calibrate the microscope in order to calculate the number of pixels per micron of the images on the screen. The images were stored as 651 x 486 pixels with 48.6 pixels / cm resolution.

(f) Ultracentrifugation

The stability of w/o emulsions in an ultracentrifugal field was investigated using a Beckman L8-M ultracentrifuge thermostatted at 25 ± 1 °C. Beckman thin-walled polyallomer centrifuge tubes (25 x 89 mm, Lot No. P80409) of volume 38.5 cm^3 were filled ¾ full with the emulsion before being sealed with a titanium cap assembly. The tubes were tapped lightly on the bench to ensure there were no air bubbles in the emulsion. The tube and cap assembly are shown in Figure 2.7. The stem was pushed

Figure 2.7

Tube and cap assembly for ultracentrifuge

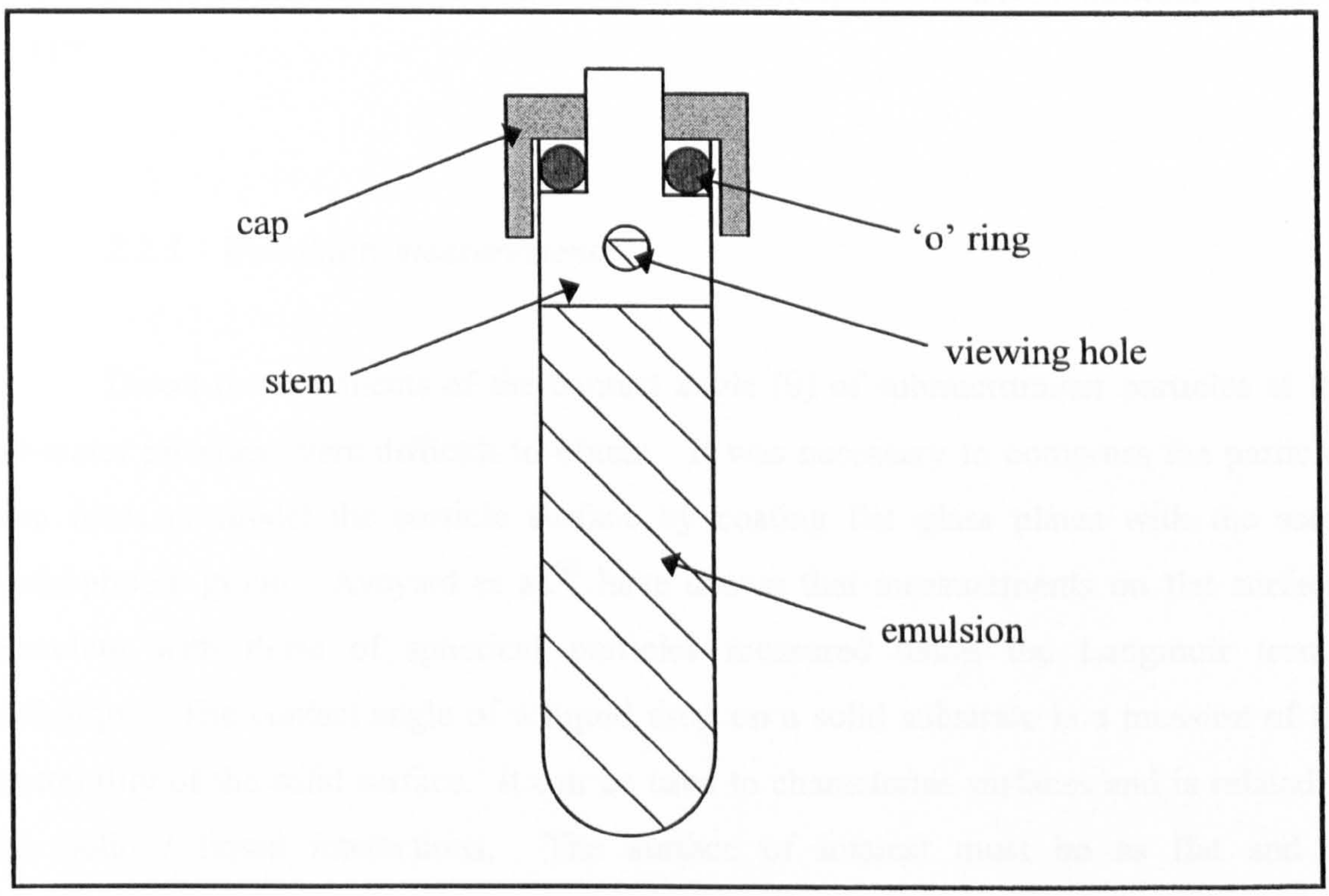

into the tube so that the 'o' ring was below the rim. The cap was then hand-fastened using the nut and the remaining emulsion was injected through a hole in the stem. A grub screw was then inserted into the hole and the tube was weighed. The mass of the tubes had to be within 0.05 g of each other so that the rotor was properly balanced. The tube was then clamped in a vice and a torque wrench was used to tighten the cap to 100-120 inch pounds. The tube was then loaded into a fixed angle (24°) Beckman type 50.2 Ti rotor, ensuring an even number of tubes are used so that the rotor was balanced. The

speed, temperature and time parameters were then set. The time required for acceleration to constant speed varied from 20 seconds at 1000 rpm to 5 minutes at 30000 rpm. Freshly prepared emulsions were used immediately for each experiment and the tubes were only used once. The relative centrifugal field, RCF, is equal to the ratio of the centrifugal acceleration at a specified radius (r) of 8.12 cm and angular velocity (ω) to the standard acceleration due to gravity (g) according to

$$RCF = \frac{r\omega^2}{g} = 1.118\times10^{-5}\, r(rpm)^2 \qquad (2.5)$$

where r is the distance (in cm) from the centre of rotation to the centre of the tube. The rpm was varied between 1000 and 24000, which corresponds to a RCF between 90.8 and 52317.

2.2.3 Wettability measurements

Direct measurements of the contact angle (θ) of submicrometer particles at the oil-water interface were difficult to obtain. It was necessary to compress the particles into discs or model the particle surface by coating flat glass plates with the same hydrophobic group. Aveyard et al.[68] have shown that measurements on flat surfaces correlate with those of spherical particles measured using the Langmuir trough technique. The contact angle of a liquid drop on a solid substrate is a measure of the wettability of the solid surface. It can be used to characterise surfaces and is related to the solid / liquid interactions. The surface of interest must be as flat and as homogeneous as possible.

2.2.3.1 Preparation of solid surfaces

(a) Pigment discs

In order to measure contact angles relevant to pigment powders, the pigments were compressed into discs of diameter 16 mm. This was achieved using a Perkin Elmer

KBr press using a stainless steel die. 10 tonnes of pressure was applied to Hansa yellow powder and 6.5 tonnes to phthalocyanine blue B powder. Two Teflon discs were used to 'sandwich' the phthalocyanine blue B powder to prevent the disc adhering to the die.

(a) Hydrophobically modified glass slides

All glass slides used for contact angle measurements were cleaned thoroughly before modification.[69] The Pyrex borosilicate glass slides were immersed in hot nitric acid for 30 minutes, rinsed with Milli-Q water and then immersed in warm 0.3 M KOH for 10 minutes. They were then rinsed thoroughly with Milli-Q water and stored in a laboratory oven at 110 °C for 1 hour. All slides cleaned in this way had a contact angle at the air / liquid / solid interface of less than 5°. Silanisation of the slides was carried out in an atmosphere of dry nitrogen in a glove bag (Aldrich) which contained open dishes of P_2O_5 (BDH) as a drying agent. Chlorine atoms on the silane molecules readily hydrolyse under the influence of atmospheric humidity and may then form undefined polymerised material. Dimethyldichlorosilane (DMDCS) was diluted in cyclohexane and the plates were immersed in 50 cm^3 of the solution for 30 minutes with continuous stirring. The concentration of DMDCS was varied between 1×10^{-5} and 0.05 M in order to obtain surfaces of varying hydrophobicity. On removal from the liquid the plates were immediately immersed and agitated in a beaker of pure cyclohexane before being transferred to a beaker of chloroform for 10 minutes, which removes unadsorbed DMDCS. Finally, the plates were immersed in fresh chloroform and dried in an oven at 110 °C overnight. The silanised plates were stored in a desiccator and used within 24 hours.

2.2.3.2 Contact angle measurements

Contact angle measurements on the solid surfaces were carried out using the sessile drop method on a Krüss G1 microscope fitted with a goniometer scale eyepiece at ambient temperature. The drop was placed on the horizontal surface and observed in cross section through the goniometer eyepiece on the microscope (see Figure 2.8). The angle of vision is just off horizontal so the edge of the drop and its reflected image are both visible. This allows the tangent to be determined precisely at the point of contact between the drop and the surface. The vertical marker was aligned to the edge of the

drop at the three phase line of contact (tplc) and rotated until it formed a tangent through the contact line drawn from the base of the drop. The angle measured through the aqueous phase was then read from the goniometer scale. Measurements were repeated at least three times on different parts of the same surface and a mean contact angle was recorded. The reproducibility of this technique is ± 2-3°.

Figure 2.8

Schematic representation of the goniometer used for measuring contact angles

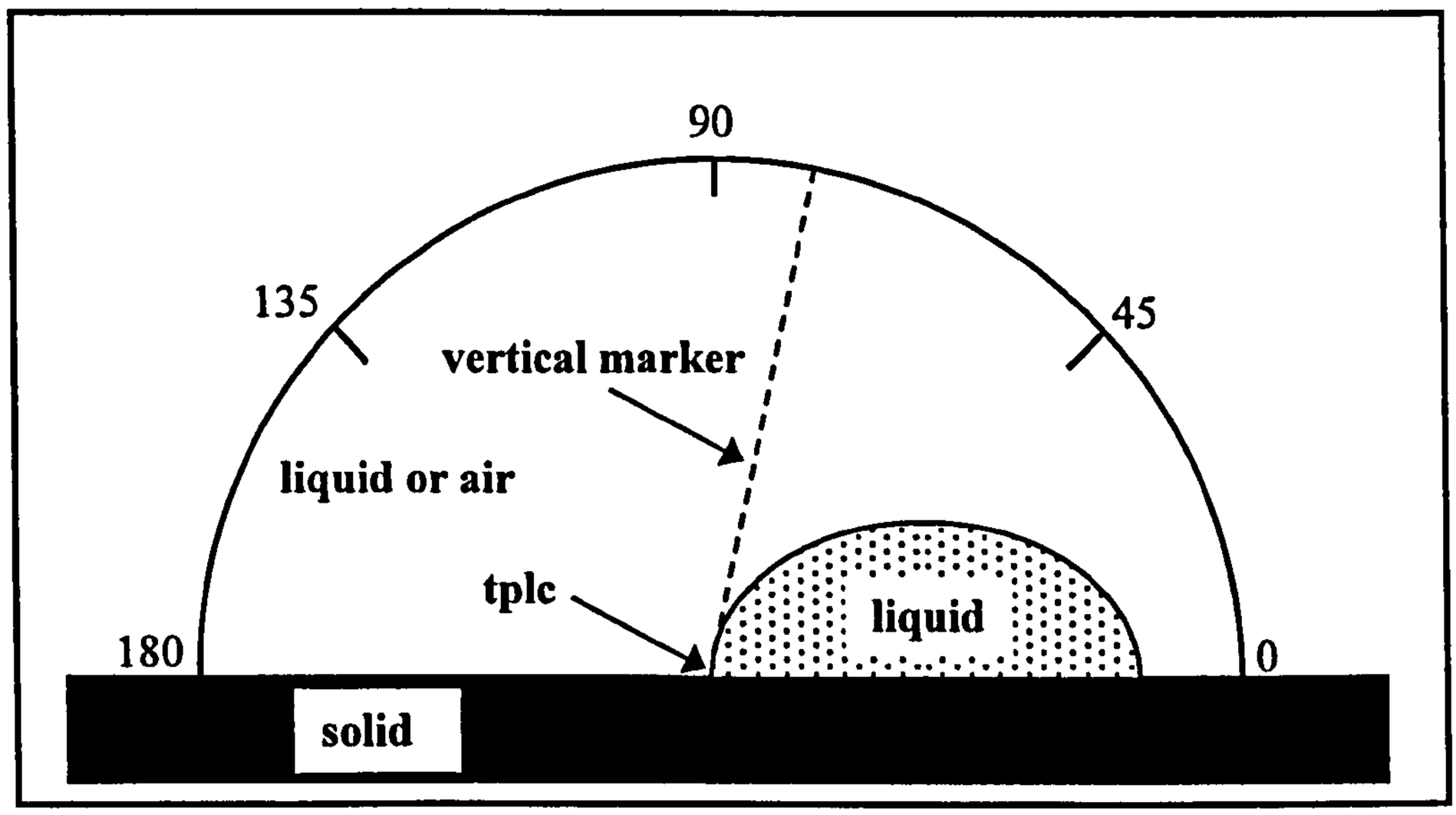

(a) Air/liquid/solid interfaces

Contact angle measurements under air were carried out in two ways. Method 1 involved measurement in an open atmosphere and Method 2 was measured in a closed cell with a saturated vapour environment in order to prevent evaporation. In both cases the drop was positioned on the solid using an SGE micro-syringe. Initially, a 10 µl drop was applied and then an additional 10 µl was added to swell the drop to give a static advancing contact angle (θ_{aw}^{adv}). These measurements were taken 10 minutes after application to ensure equilibrium values were obtained. The static receding contact angle (θ_{aw}^{rec}) was measured by slowly removing 10 µl of liquid from the drop so that the tplc was seen to contract (recede) over the surface previously covered by the liquid phase. Measurements were taken 5 minutes after liquid withdrawal from the drop. The

receding angle gives an indication of the surface heterogeneity via the contact angle hysteresis.

(a) Liquid/liquid/solid interfaces

In these systems the air was replaced by various liquids and so the solid substrate was placed in a small glass vessel. Two methods were used to measure these angles. In Method 1, the bulk liquid is layered onto the solid and the liquid drop is injected through it close to the solid surface. In Method 2, the liquid drop is injected onto the solid in air and then the second liquid is layered on top. The values of θ vary considerably depending on which method is used. The procedure for static advancing and receding angle measurements is the same as for air/liquid/solid systems.

2.2.4 Surface and interfacial tension measurements

2.2.4.1 du Noüy ring method

(a) Theory

The du Noüy ring method is commonly used for the determination of surface and interfacial tensions. This method enables a high degree of accuracy to be attained from a relatively simple experimental procedure. A platinum/iridium ring is raised from the surface of the test liquid and the maximum force required to pull the meniscus from the surface is related to the surface tension of the liquid. Harkins and Jordan[70] showed that the surface tension, γ, of a solution is given by

$$\gamma = \frac{mgF}{4\pi R} = \frac{\Delta\rho VgF}{4\pi R} \qquad (2.6)$$

where R is the radius of the ring (Figure 2.9), g is the acceleration due to gravity and m is the mass of the solution raised by the ring. The correction factor, F, is a function of R^3/V and R/r, where V is the volume of liquid pulled from the surface by the maximum pull of the ring and r is the radius of the wire from which the ring is made. The

correction factors are applied by measuring the radii of the ring and the wire, and the density difference between the fluids $\Delta\rho$. A value of R^3/V is calculated for each determination and the correction factor is obtained from the tables according to the value of R/r. The accuracy of these table has been shown to be within 0.25 % of those obtained from theoretical variations in meniscus shapes by Freud and Freud.[71] The data of Harkins and Jordan has been extended by Zuidema and Waters[72] to include the measurement of interfacial tensions below 25 mN m^{-1}.

Figure 2.9

Schematic cross-section of the du Noüy ring

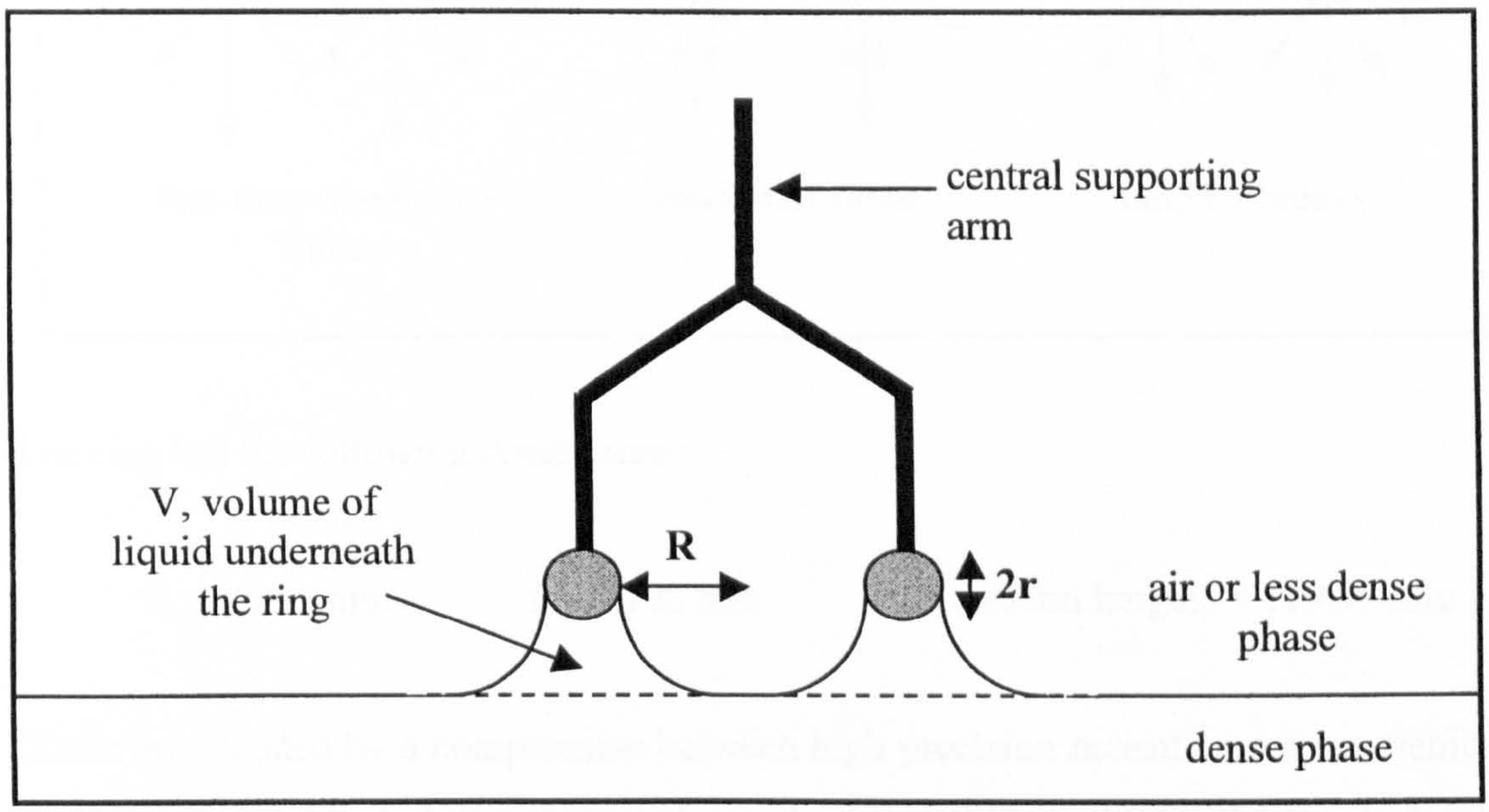

(b) Digital tensiometer

The majority of surface and interfacial tension measurements were carried out using the du Noüy ring method on a Krüss K10 Digital Tensiometer. The ring is placed on a sensitive torsion balance and lowered into the sample liquids. The liquids are contained in a glass vessel, which is housed within a thermostatting cell, and are left to equilibrate for 15 minutes. Provided that the wire is completely wetted, a meniscus begins to form as the ring is pulled from the surface. The three stages of withdrawal are shown in Figure 2.10. The force reaches a maximum as soon as the tangent at the point

of wetting is vertical to the surface. Any additional force causes rupture of the lamellae. However, the tensiometer is programmed to stop once the maximum force is reached.

Figure 2.10

Cross-sectional view of the du Noüy ring showing the different stages of measurement

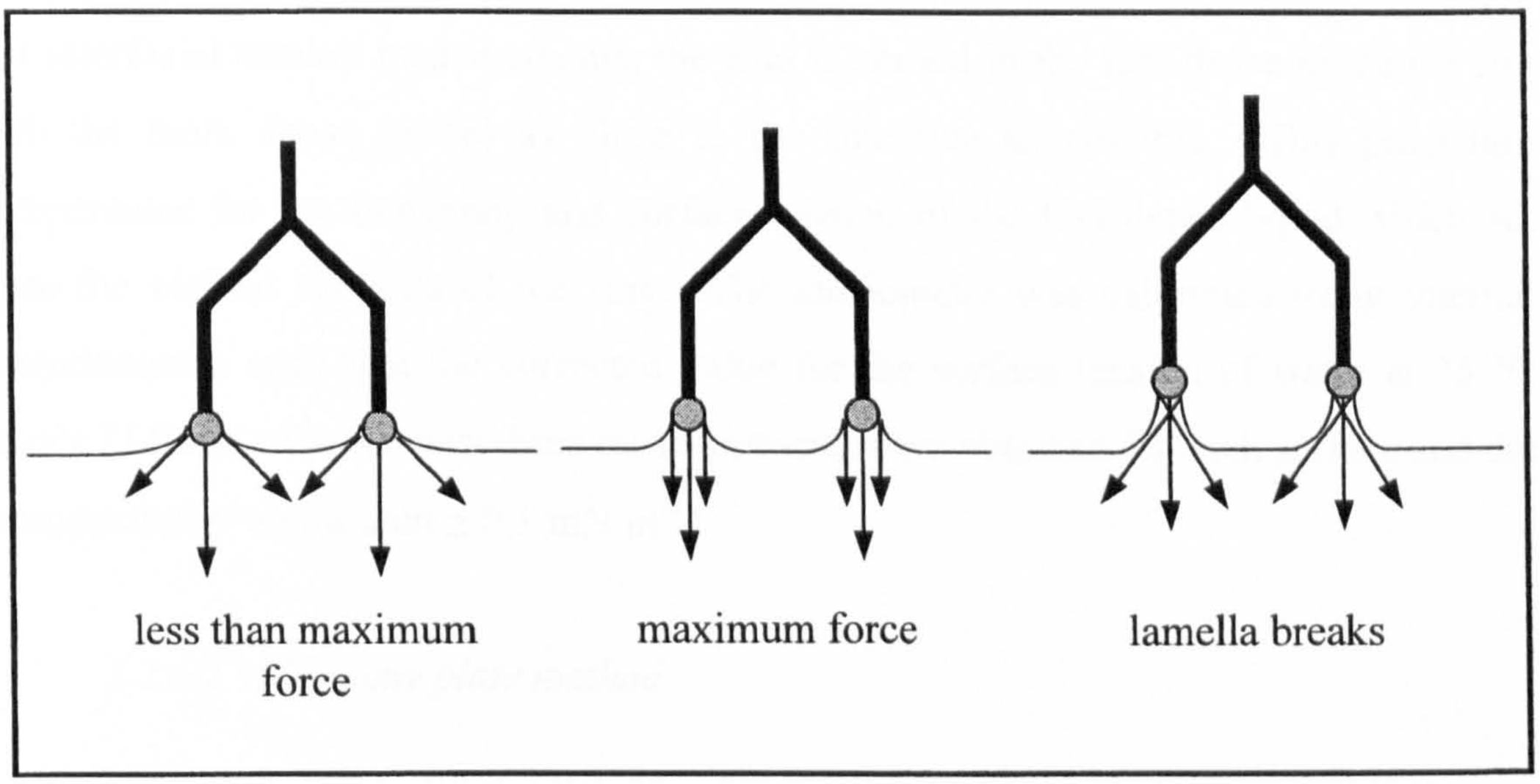

The ring has the following dimensions:

R = 9.545 mm r = 0.185 mm L (wetted length) = 119.95 mm

These are dictated by a compromise between high precision measurement, convenience, mechanical stability and a minimum of sample material. In order for the ring to function correctly and in a reproducible manner the following criteria must be met:

(i) that the wire of the ring lie in one plane,

(ii) that the plane of the ring be horizontal,

(iii) that the vessel containing the liquid (s) be large enough so that any curvature of the surface of the liquid would not be great enough to affect the shape of the liquid raised by the ring,

(iv) that there be no motion of the ring except a slow upward movement,

(v) that the ring be circular.

Before use, the ring was rinsed in alcoholic KOH and then Milli-Q water and briefly heated to glowing by holding in a blue bunsen flame. The glass vessel was cleaned in

chromic acid, thoroughly rinsed in Milli-Q water and dried in a laboratory oven at 110 °C.

For surface tension measurements, the torsion balance is first zeroed with the ring suspended in air close to the surface of the liquid. The ring is then immersed in the liquid by manually raising the vessel and allowed to equilibrate for 5 minutes. The servo-motors in the tensiometer lower the vessel until the maximum force is measured. For interfacial tension measurements, the ring is zeroed in the less dense phase (*in situ* with the more dense phase) as close to the interface as possible. This procedure compensates for the buoyancy and surface tension of the less dense liquid which act upon the vertical supports of the ring. The tensiometer was calibrated using internal potentiometers such that the corrected value for the surface tension of water at 25 °C equals 71.9 mN m^{-1}. At least three measurements were obtained for each surface and the reproducibility was within ± 0.1 mN m^{-1}.

2.2.4.2 Wilhelmy plate method

(a) Theory

In 1863 Wilhelmy[73] stated that the surface tension of a liquid could be determined from the force required to pull a glass plate from the surface of that liquid. Dognon and Abribat[74] later modified Wilhelmy's method to enable tension measurements without detaching the plate from the surface.

The tension is calculated from the following equation

$$\gamma = \frac{F}{L\cos\theta} \qquad (2.7)$$

where F is the force measured when the bottom of the plate is perfectly level with the surface of the liquid, as shown in Figure 2.11. In this position there is no effect from the buoyancy of the plate. The wetted perimeter L is given in equation 2.8 and shown in Figure 2.12. If it is assumed that the plate is perfectly wetted, i.e. the contact angle θ = 0, the tensiometer can be calibrated to give a direct reading of γ.

$$L = (2l + 2b) \qquad (2.8)$$

Figure 2.11

Cross-section of the Wilhelmy plate

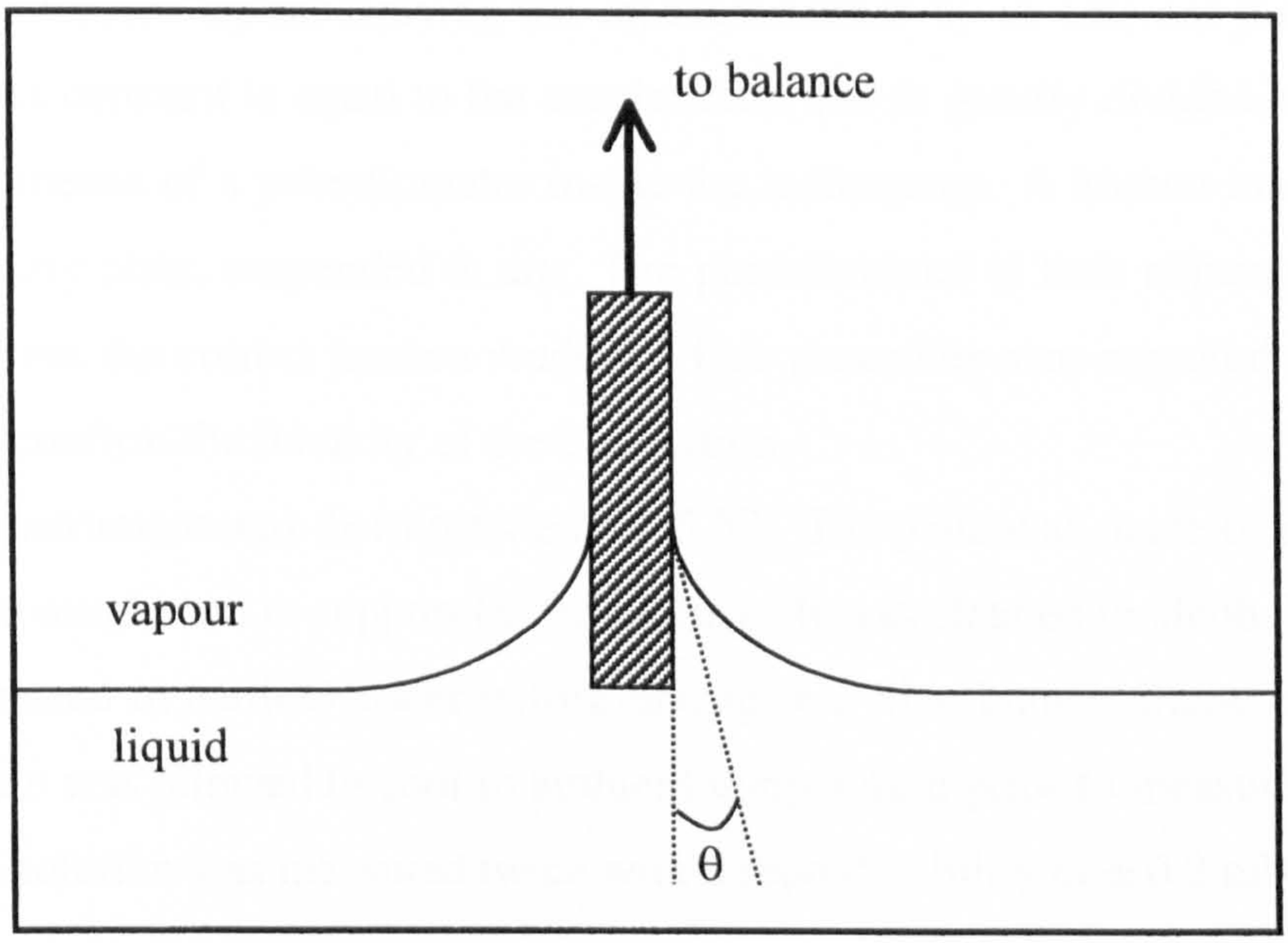

Figure 2.12

Wetted perimeter of Wilhelmy plate

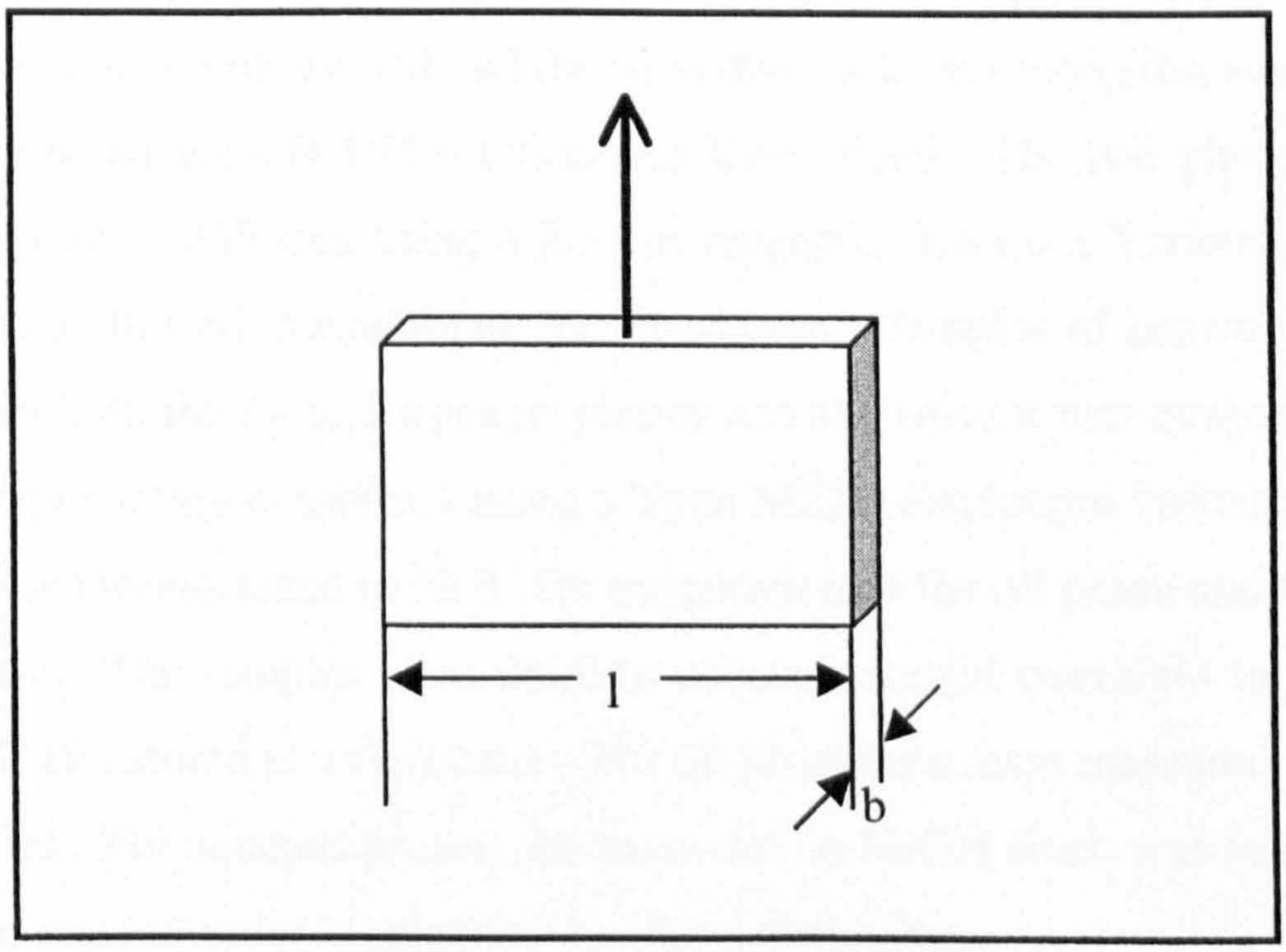

(b) Digital tensiometer

The Krüss K10 Digital Tensiometer was used to measure the variation in surface tension of Aerosil 200 silica dispersed in water at pH = 2 and 10. The instrument calculates the tension by multiplying the measured mass by an internal proportionality constant. This constant is equal to the acceleration due to gravity divided by L and can be varied by means of a potentiometer inside the instrument. A known mass is applied to the Wilhelmy plate, suspended in air. The potentiometer is then adjusted so that the instrument gives the correct tension reading. This procedure was repeated with a range of masses to confirm the linearity of the calibration.

The instrument was thermostatted at 25 °C. The plate was made of platinum and had been fine roughened to support better wetting. It was cleaned in alcoholic KOH and thoroughly rinsed in Milli-Q water before drying in a blue bunsen flame until glowing red. The plate was allowed to cool to ambient temperature prior to measurements being made. Each solution was measured twice with a reproducibility of $\pm$ 0.2 mN m^{-1}.

2.2.5 Partitioning of particles between oil and aqueous phases

The partitioning of silica particles between equal volumes of oil and water as a function of the aqueous phase pH was determined as follows. A known mass (0.30 g) of silica particles was dispersed in a known mass of toluene in a glass vessel of dimensions 42 mm x 75 mm using ultrasound and the total mass was recorded after sonication. An equal volume of aqueous NaOH solution was then added. The two phases were then stirred for 1 hour at 250 rpm using a 2.5 cm magnetic flea on a Variomag multipoint stirrer, and then allowed to equilibrate for 30 minutes. Samples of known volume were removed from both the oil and aqueous phases and the solvent was evaporated using a Buchi Rotavapor rotary evaporator using a Type MZ2C diaphragm vacuum pump. The water-bath was thermostatted to 50 °C for evaporation of the oil phase and 60 °C for the aqueous phase. The samples were dried to constant weight overnight in a laboratory oven at 60 °C and stored in a desiccator. For oil phases the mass measured refers to that of the particles. For aqueous phases, the mass due to NaOH alone was subtracted from the measured mass in order to calculate the true partitioning.

2.2.6 Foamability of aqueous surfactant solutions

Partially hydrophobic silica particles are often used as antifoams in a number of industrial processes but often do not work in extremes of pH. It is proposed here that this is due to a change in wettability of the particles towards water at high pH. The foamability of aqueous solutions of 0.01 M SDS was determined by measuring the initial foam volume (with and without 30 mg of SLM 081 silica) formed from 10 cm^3 of solution contained in 100 cm^3 measuring cylinders. Foams were formed by vigorously hand-shaking the mixtures for 5 seconds. These crude 'shake-test' experiments give remarkably reproducible results if performed according to a set protocol. A minimum of three runs were made for each system studied which resulted in an error of ± 4 cm^3. The silica particles were sprinkled onto the aqueous solution and gently swirled into the bulk liquid before foam formation. As a result the particle size in solution is likely to be large (maybe 50 μm or so).

2.2.7 Powder immersion measurements

In order to obtain a qualitative measure of the wettability of the range of silica particles the time taken for a fixed mass of solid to completely immerse in a mixture of methanol and water was measured. 50 mg of the powder was placed carefully and evenly on the surface of 20 cm^3 of a given water/methanol mixture contained in a tube of diameter 2.3 cm at room temperature. The time taken for all the powder to disappear from the liquid surface was measured and is equated with the immersion time.[75] Water-methanol mixtures were chosen for these experiments because the most hydrophilic and most hydrophobic powders can ultimately enter the liquid depending on the volume fraction of each. The dielectric constants of the liquids are sufficiently close (78.5 and 32.6 at 25 °C, for water and methanol respectively) for the above condition to apply.

2.2.8 Other experimental techniques

(a) Density measurements

Densities of various liquids were measured at 25 °C using a Paar DMA 55 densimeter. Thermostatting was by means of a Haake F3-C water thermostat.

(b) Refractive index measurements

An Abbé refractometer and sodium lamp were used to measure the refractive indices of some liquids and aqueous colloids. Measurements were made to ± 0.0001.

CHAPTER 3

CHAPTER 3

OIL-IN-WATER EMULSIONS STABILISED BY HYDROPHILIC SILICA PARTICLES

3.1 Introduction: Anomalous DLVO behaviour of aqueous silica dispersions

Mixtures of oil and water are thermodynamically and kinetically unstable and separate to their bulk phases immediately. An emulsifier is required to give kinetic stability to oil drops dispersed in water (o/w emulsion) or water drops dispersed in oil (w/o emulsion). The emulsifier is usually a surfactant, which has an amphiphilic structure where part of the molecule prefers to be in oil and the other part prefers to be in water. However, it is shown here and by work described in Chapter 1, that it is possible to stabilise emulsions using solid particles alone. Solid particles do not have an amphiphilic structure but stabilise emulsions by accumulating at the oil-water interface. Silica particles, for example, have been used to stabilise emulsions. However previous investigations[26, 35, 36] have been in the presence of another adsorbing species such as a surfactant or polymer. Hassander et al.[26] described the mechanism of paraffin oil-in-water emulsion stabilisation by precipitated silica (Ludox) in the presence of various costabilisers. Stable o/w emulsions were formed in the presence of CTAB surfactant or polyvinylpyrrolidone (a neutral polymer) which caused agglomeration of the silica particles. The agglomerates then adsorbed at the oil-water interface and stabilised the emulsion. Midmore[35, 36] has described the preparation of precipitated silica and hydrophobic silica stabilised emulsions in the presence of hydroxypropylcellulose (HPC). At a high volume fraction of water (> 0.8) oil-in-water emulsions[35] are stabilised by precipitated silica when the particles have been flocculated by HPC. The flocs adsorb at the oil-water interface where they are thought to form a two-dimensional gel structure. As a result, stabilisation is achieved when the interface is coated with the equivalent of only 29 % of close-packed spheres. Thus, complete coverage of the oil drops with a rigid crust of silica particles is unnecessary. Water-in-oil emulsions[36] are stabilised by silica coated with hydrophobic trimethyl silanyl groups. Addition of HPC

to the aqueous phase results in highly stable, relatively monodisperse, silica stabilised emulsions. These emulsions were flocculated at extremes of pH due to acid or alkali catalysed cleavage of surface siloxane groups. The acidic reaction proceeded via protonation of the oxygen on the siloxane group followed by nucleophilic attack by water at one of the silicon atoms. The alkali reaction involved nucleophilic attack by the hydroxyl ion. Both reactions resulted in an increase in the density of surface silanol groups which results in hydrogen bonding between neighbouring silica particles and therefore a greater degree of flocculation. In summary, all of the previous investigations involving emulsions stabilised by silica particles have been complicated by addition of another adsorbing species, such as a surfactant or polymer. It is therefore dangerous to attribute the stability of the emulsions to the silica particles alone. In the present work however, only silica particles were added to the oil-water system, therefore any stability can confidently be assigned to the solid alone.

Prior to emulsification, the particles are dispersed in one of the phases to form a colloidal suspension, the properties of .which have an important influence on the behaviour of the subsequent emulsion. This chapter describes the properties of oil-in-water emulsions stabilised by hydrophilic silica particles (Aerosil 200 and Ludox HS-40) dispersed in water. The charge on the particles and the extent of flocculation in the dispersion was modified by pH control and addition of simple electrolyte respectively. The salts chosen were NaCl (1:1), $LaCl_3$ (3:1) and the organic electrolyte tetraethylammonium bromide (TEAB). The stability of emulsions stabilised by the cationic surfactant, cetyltrimethylammonium bromide (CTAB), in the presence of silica was also investigated because of its similar structure to TEAB.

The chemistry of colloidal silica in water has been widely investigated and a comprehensive review was compiled by Iler in 1979.[52] There are two main types of silica particles, precipitated and pyrogenic / fumed silica, the syntheses of which are described in the Experimental chapter. When initially dispersed in water, there appears to be a significant difference in the two particle types, which manifests itself in the sensitivity of the aqueous colloidal dispersion to flocculation by electrolyte. The surface of precipitated silica (e.g. Ludox HS-40) consists solely of very hydrophilic groups such as SiOH and $Si(OH)_2$. Fumed silica (e.g. Aerosil 200) however, contains silanol groups as well as more hydrophobic siloxane bridges (Si-O-Si). Colloidal dispersions of silica in water have been the subject of much discussion due to the "anomalous" behaviour with respect to pH and electrolyte addition observed by a number of authors.[76-82] The

critical coagulation concentration (c.c.c.) of salt required to flocculate most oxide and latex colloids is very low around the isoelectric point (i.e.p.) and *increases* progressively above it as the repulsion between charged particles increases. This can be accounted for in terms of the classical DLVO theory,[42, 43] which takes into account the electrostatic energy of repulsion and the attractive van der Waals energy between charged particles as they approach each other. This behaviour has been observed for silica particles by a number of authors who suggest the behaviour is dependent on the preparation procedure of the dispersion or the nature of the silica itself.[65, 83, 84] However, Iler[52] noted that silica sols were remarkably stable to electrolyte around their i.e.p. and in the presence of high concentrations of salt at around neutral pH, contrary to the predictions above. The first definitive study of the anomalous behaviour of silica sols was by Allen and Matijevic[76] who looked at precipitated Ludox HS silica of diameter equal to 15 nm. With NaCl as electrolyte, the sols remained dispersed (hence stable) up to the solubility limit of NaCl (around 5 M) at pH values between 2 and at least 5. Above pH 6, the c.c.c. *decreased* with increasing pH. These authors also investigated the stability of silica in the presence of other electrolytes.[77] The stability in the presence of LiCl and KCl was similar to NaCl but a minimum in the stability at intermediate pH was observed in the presence of CsCl. The results were discussed in terms of an ion exchange mechanism, described below. Depasse and Watillon[78] observed the same trends in the presence of Na^+ ions for 120 nm diameter silica particles prepared by polymerisation of silicic acid in alkaline solution. Very similar effects were reported by Rubio and Goldfarb[79] for fumed Aerosil 200 silica particles of 12 nm diameter. Thus this anomalous behaviour is not restricted to precipitated silicas, and as Harding[80] showed, is rather confined to silicas having primary particles below a certain size.

The zeta potential of silica sols, like other oxide sols, becomes increasingly negative with increasing pH above the i.e.p. Scales et al.[85] measured the streaming potential at the vitreous silica-water interface and found that it varies from zero at pH 2 to –115 mV at pH 7.5 in 1 x 10^{-4} M KCl. The zeta potential, ζ, is related to the streaming potential, ΔE_s, by the following equation,[86]

$$\zeta = \left(\frac{\eta \kappa_c}{D\varepsilon_o}\right)\left(\frac{\Delta E_s}{\Delta P_c}\right) \qquad (3.1)$$

where η is the viscosity of the fluid, κ_c is the conductivity of the capillary, D is the permittivity of the medium, ε_o is the permittivity of a vacuum and ΔP_c is the applied pressure gradient across the capillary. The magnitude of the zeta potential decreases uniformly at each pH as the salt concentration is increased (Figure 3.1). The usual result of such variation in zeta potential with pH and 1:1 electrolyte concentration is that the c.c.c. increases with pH as calculated by the DLVO theory. Thus, the opposite trend measured experimentally for silica sols has another origin not accounted for in DLVO theory. A number of reasons for the enhanced stability of silica at low pH have been postulated. Allen and Matijevic[76, 77] proposed that the stability of silica in acidic conditions is caused by particle hydration, with the silanol groups being capable of hydrogen bonding with water, such that silica behaves more like a lyophilic than a lyophobic colloid. Substitution of silanol protons by cations (M^{n+}) of the electrolyte as the pH increases leads to destabilisation of the sol by eliminating sites for hydrogen bonding (dehydration).

$$\begin{array}{c} | \\ -Si- \\ | \end{array} OH + M^{n+} \leftrightarrow \begin{array}{c} | \\ -Si- \\ | \end{array} OM^{(n-1)+} + H^{+} \qquad (3.2)$$

Due to the low Hamaker constant for silica of 1.2×10^{-20} J,[87] the dispersion forces are very low and it appears that one monolayer of water is quite enough to screen dispersion forces between particles preventing coagulation. Below pH 10, the ability of the cations to exchange and hence destabilise the sol follows the order $Cs^+ > K^+ > Na^+ > Li^+$. However, why ion exchange should render the silanol surface less stable is open to speculation. By contrast, direct inter-particle bridging was suggested by Depasse and Watillon[78] as a mechanism for the coagulation of silica. At pH > 6 and at the respective c.c.c., coagulation occurs because the particles become linked by acid-base bonds formed by silanol groups on one particle and dissociated $Si\text{-}O^-$ groups on another. Very quickly these bonds are transformed into siloxane bonds (Si-O-Si).

$$\begin{array}{c} | \\ -Si- \\ | \end{array} OH + {}^{-}O \begin{array}{c} | \\ -Si- \\ | \end{array} \rightarrow \begin{array}{c} | \\ -Si- \\ | \end{array} O \begin{array}{c} | \\ -Si- \\ | \end{array} + OH^{-} \qquad (3.3)$$

Of course at low pH near the i.e.p. no dissociated silanol groups are present on the surface so no acid-base bonds can be formed. At high pH (> 11) the sols are only coagulated in the presence of acidic cations from the electrolyte. There is a transition

Figure 3.1

Zeta potential of a fused silica capillary versus pH in aqueous solutions of KCl as determined by the flat-plate streaming potential technique. The concentrations of KCl (in M) are given in the figure. Redrawn from ref. 85.

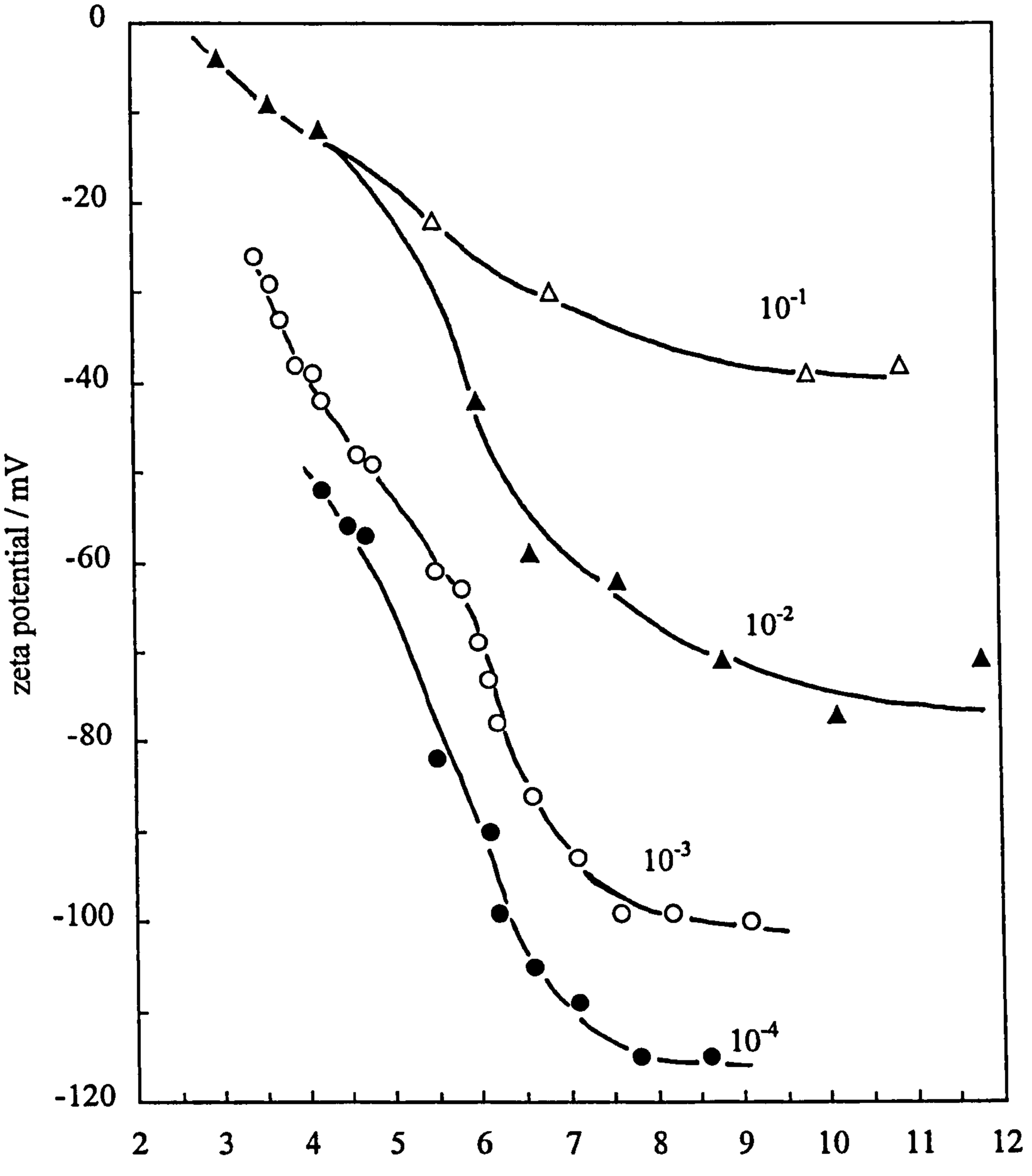

from silanol-dissociated silanol bonds to dissociated silanol-acidic cation bonds as the number of undissociated silanol groups decreases. Recently, Depasse[88] has argued in favour of the latter hypothesis in the light of new experimental data. A third explanation of the high stability of silica in terms of steric stabilisation effects has been given by Healy[89] and requires that oligomeric or polymeric silicate species are present at the silica / water interface and that steric repulsion results during the overlap of such layers causing electrostatic interactions to be severely diminished.

These explanations suggest that silica is subjected to a repulsive force not considered in the classical DLVO theory. This force is exponentially repulsive between hydrophilic surfaces and is commonly referred to as the hydration or structural force. However the origin of the force is open to debate.[90] In surfactant systems, the hydration force is attributed to steric interactions between headgroups of surfactant monolayers across soap films.[91] In the case of colloidal particles however, the DLVO theory often fails because the water separating the particles has been treated as a structureless continuum. This is applicable at large separation distances but strongly H-bonding surface groups (SiOH in the case of silica) cause an ordering of water surrounding the particles giving it a discrete structure which is significantly different to that of the bulk.[92] As the particles approach one another, overlap of the ordered layers creates a repulsive force. Repulsive hydration forces have been measured between flat silica surfaces where they have been found to decay exponentially with decay length of ~ 1 nm but effective range of 3 – 5 nm.[93, 94] The existence of this force allows an extended form of the classical DLVO theory to be written[95]

$$V_t = V_d + V_e + V_h \qquad (3.4)$$

where V_t is the net potential energy for the interaction between two colloidal particles. The van der Waals dispersion energy, V_d, between two spherical particles of radius a is given by

$$V_d = -\frac{aA_{131}}{12H} \qquad (3.5)$$

where A_{131} is the Hamaker constant for the system particle-water-particle and H is the surface-to-surface separation between particles. The Hamaker constant A_{131} for a solid particle in water can be calculated from the approximate expression:

$$A_{131} \cong \left(\sqrt{A_{11}} - \sqrt{A_{33}}\right)^2 \tag{3.6}$$

in which A_{11} is the Hamaker constant of a solid in vacuo and A_{33} is that for water. The repulsive electrostatic energy, V_e, for the case of constant potential is given by

$$V_e = 32\pi\varepsilon akT\left[\tanh\left(\frac{e\psi_o}{4kT}\right)\right]^2 e^{-2}\exp(-\kappa H) \tag{3.7}$$

where ε is the permittivity of water (equal to its relative permittivity multiplied by the permittivity of a vacuum ε_o), ψ_o is the surface potential (often substituted by the zeta potential ζ), e is the elementary charge and κ is the inverse Debye length (or the reciprocal of the double layer thickness) given by

$$\kappa = \left(\frac{2e^2 N_A c_{el} z^2}{\varepsilon kT}\right)^{1/2} \tag{3.8}$$

where N_A is Avogadro's number, c_{el} is the bulk concentration of electrolyte of valency z, k is Boltzmann's constant and T is the temperature. For a 1:1 electrolyte, the double layer thickness is about 1 nm for a 0.1 M solution and about 10 nm for a 0.001 M solution. Equation 3.7 is valid when $\kappa H > 1$ assuming the range of interaction and the separation H is much less than the radii of the particles.

Since the abnormal stabilisation mechanism of silica depends on salt concentration, the structural force should depend on it in the same way. Assuming that the hydration energy, V_h, is directly proportional to salt concentration, c_{el}, Molina-Bolivar et al.[96] have proposed the following expression for V_h,

$$V_h = \pi a N_A C_h c_{el} \lambda_d^2 \exp(-H/\lambda) \tag{3.9}$$

where C_h is the hydration constant (in J) and λ_d is the decay length. Figure 3.2a shows the results of calculations of the separate terms V_d and V_e along with V_t versus the particle separation H using the classical DLVO theory (where $V_t = V_d + V_e$), for the interaction of two spherical particles of radius 0.1 μm. The conditions chosen are 0.2 M of 1:1 electrolyte, an experimentally determined zeta potential for silica at this concentration of –5 mV (corresponding to a pH of 2)[85] and the Hamaker constant is the average of theoretical and experimental values for silica.[95] As seen, the overall energy is attractive and the electrostatic contribution is virtually zero. Thus DLVO theory would predict flocculation of the colloid whereas it is found to be extremely stable. Figure 3.2b shows the calculations using the extended DLVO theory ($V_t = V_d + V_e + V_h$) for the same system. The hydration-repulsion term dominates over the dispersion-attraction one leading to a total energy which is positive and hence repulsive. The value of λ taken is 1 nm (as determined directly for glass surfaces[94]) and the hydration constant C_h has been varied until the secondary minimum in the total energy just disappears, as it should since no flocculation occurs.

It is shown in this chapter that aqueous dispersions of fumed Aerosil 200 silica particles exhibit anomalous DLVO behaviour in the presence of NaCl electrolyte. The dispersions are also stable (dispersed) at low pH and unstable (flocculated) at high pH in the presence of low concentrations of the trivalent electrolyte $LaCl_3$. In the presence of TEAB electrolyte, the dispersions are stable at low and high pH but exhibit an interesting restabilisation phenomenon at intermediate pH. The behaviour of the aqueous colloids is shown to be important in dictating the stability of subsequent emulsions formed with toluene.

3.2 Systems containing NaCl electrolyte

(a) Aerosil 200 silica

The magnitude of the hydration force in silica dispersions is dependent on the presence of a monovalent electrolyte such as NaCl. As the concentration of electrolyte is increased the hydration force will decrease at any pH. In order to investigate if the proposed anomalous behaviour exists, the effect of pH and NaCl concentration on the

Figure 3.2

Interaction energies V versus distance H between two spherical particles of radius 0.1 μm calculated using (a) classical DLVO theory, and (b) extended DLVO theory with $C_h = 3 \times 10^{-19}$ J and $\lambda = 1 \times 10^{-9}$ m. The values of $\psi_o = -5$ mV, $c_{el} = 0.2$ M, $A_{131} = 1.2 \times 10^{-20}$ J are taken in both cases.

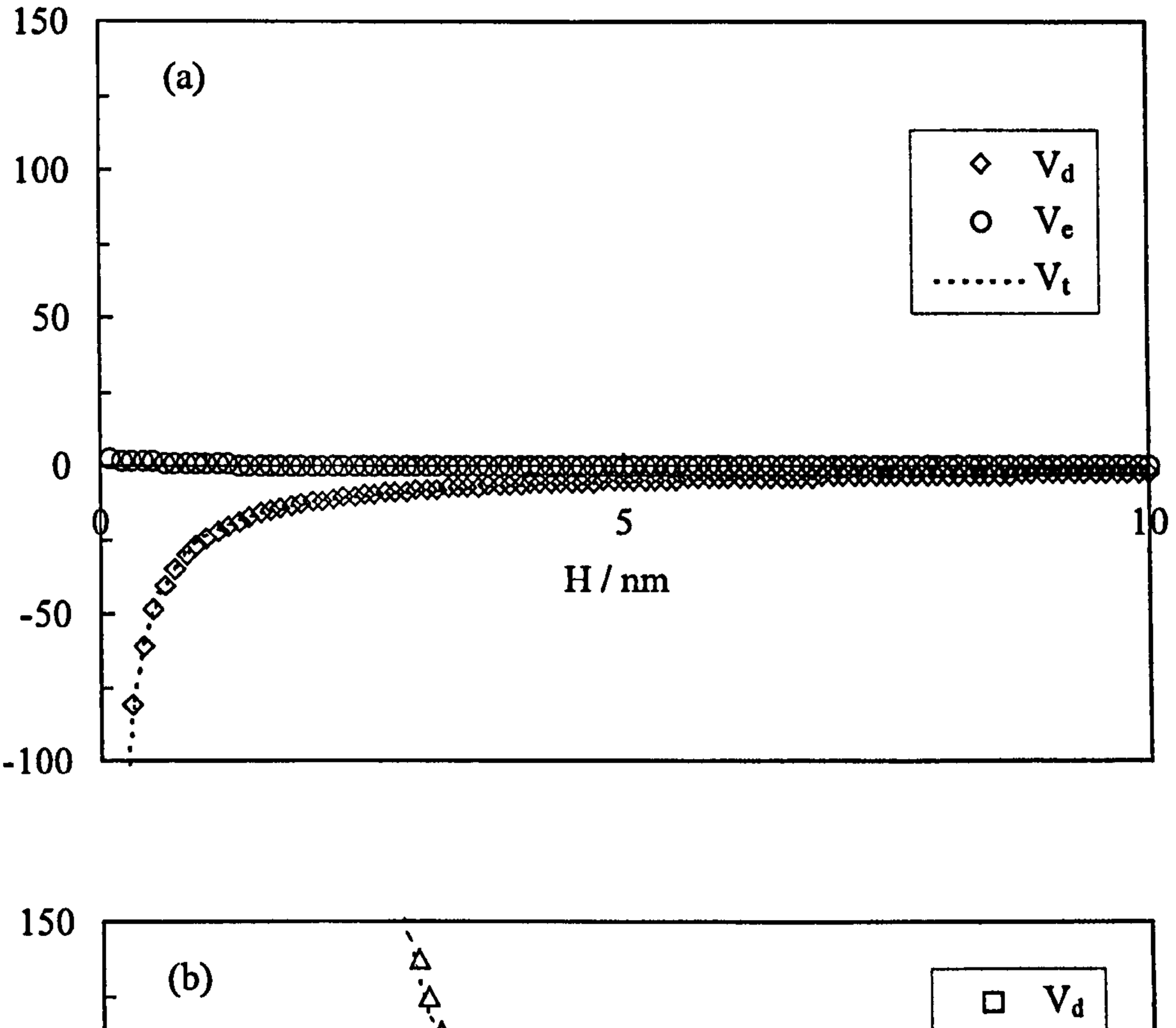

stability to flocculation of aqueous dispersions of Aerosil 200 silica particles has been investigated. The extent of flocculation was determined by measuring the turbidity of 25 mls of dispersion. Figure 3.3 shows the turbidity of 0.5 wt.% dispersions as a function of NaCl concentration at pH 2 (i.e. at the i.e.p.), immediately after preparation and after 24 hours. No visible change in the appearance of the pale blue colloids on addition of salt or as a function of time was observed i.e. no flocculation occurred. The decrease in the measured turbidity is due to a change in the refractive index of the aqueous salt solution with increasing concentration. The turbidity, τ, of a dispersion of non-interacting particles of dimension much less than the wavelength of light is related to the refractive index by[97]

$$\tau = \frac{24\pi^3 P^2 N V_p^2}{\lambda^4} \qquad (3.10)$$

where λ is the wavelength, N is the number of particles per unit volume, V_p is the volume of one particle and

$$P = \frac{n_p^2 - n_w^2}{n_p^2 + 2n_w^2} \qquad (3.11)$$

with n_p and n_w being the refractive indices of the particle and water solvent respectively. The observed decrease in the turbidity is due to a decrease in the magnitude of P due to an increase in n_w from 1.3330 in pure water to 1.3758 in 4.85 M NaCl. Constraining the turbidity for no added salt to equal the measured value of 310 NTU, the full line in Figure 3.3 is the calculated variation of τ with [NaCl] taking n_p equal to that for fused quartz (1.458 at 18 °C and 589 nm) and values of n_w from ref. 50.

Noting that the product NV_p (in equation 3.10) is equal to the volume fraction of the particles, it is clear that the turbidity of the dispersion is proportional to the average particle volume. An increase in τ should then be due to an increase in V_p i.e. due to flocculation, over and above the decrease in N. Figure 3.4 shows the turbidity of 0.5 wt.% Aerosil 200 as a function of NaCl concentration at pH 10 (i.e. well above the i.e.p.). The initial turbidity decreases with [NaCl] as at pH 2. However, after 24 hours the turbidity shows a marked increase above 0.4 M NaCl due to separation of the

Figure 3.3

Turbidity of 0.5 wt.% Aerosil 200 dispersions in water at pH 2 as a function of NaCl concentration. Circles - immediately after adding NaCl; diamonds - 24 hours later. The line is a fit as described in the text.

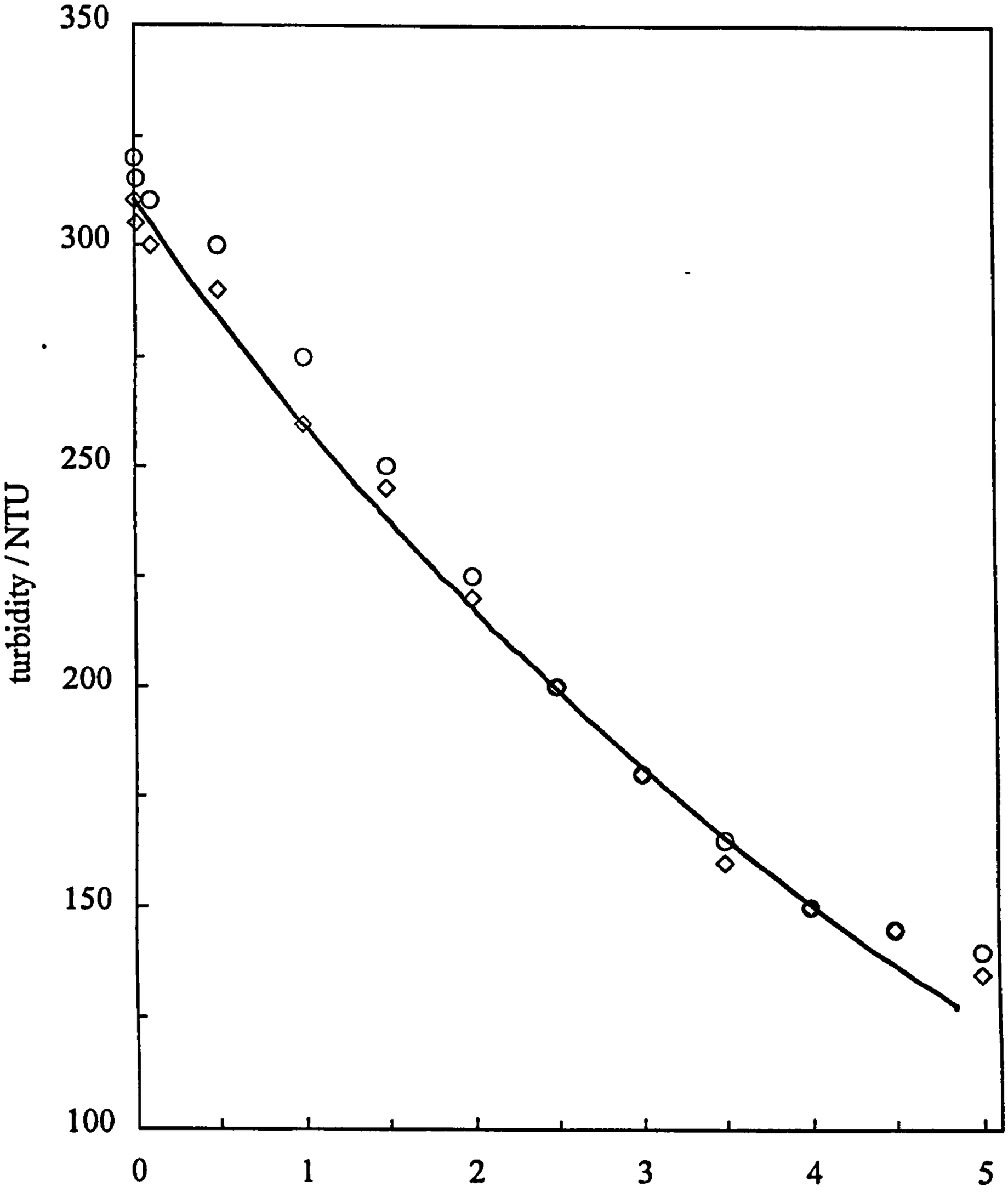

Figure 3.4

Turbidity of 0.5 wt.% Aerosil 200 dispersions in water at pH 10 as a function of NaCl concentration. Circles - immediately after adding NaCl; diamonds - 24 hours later.

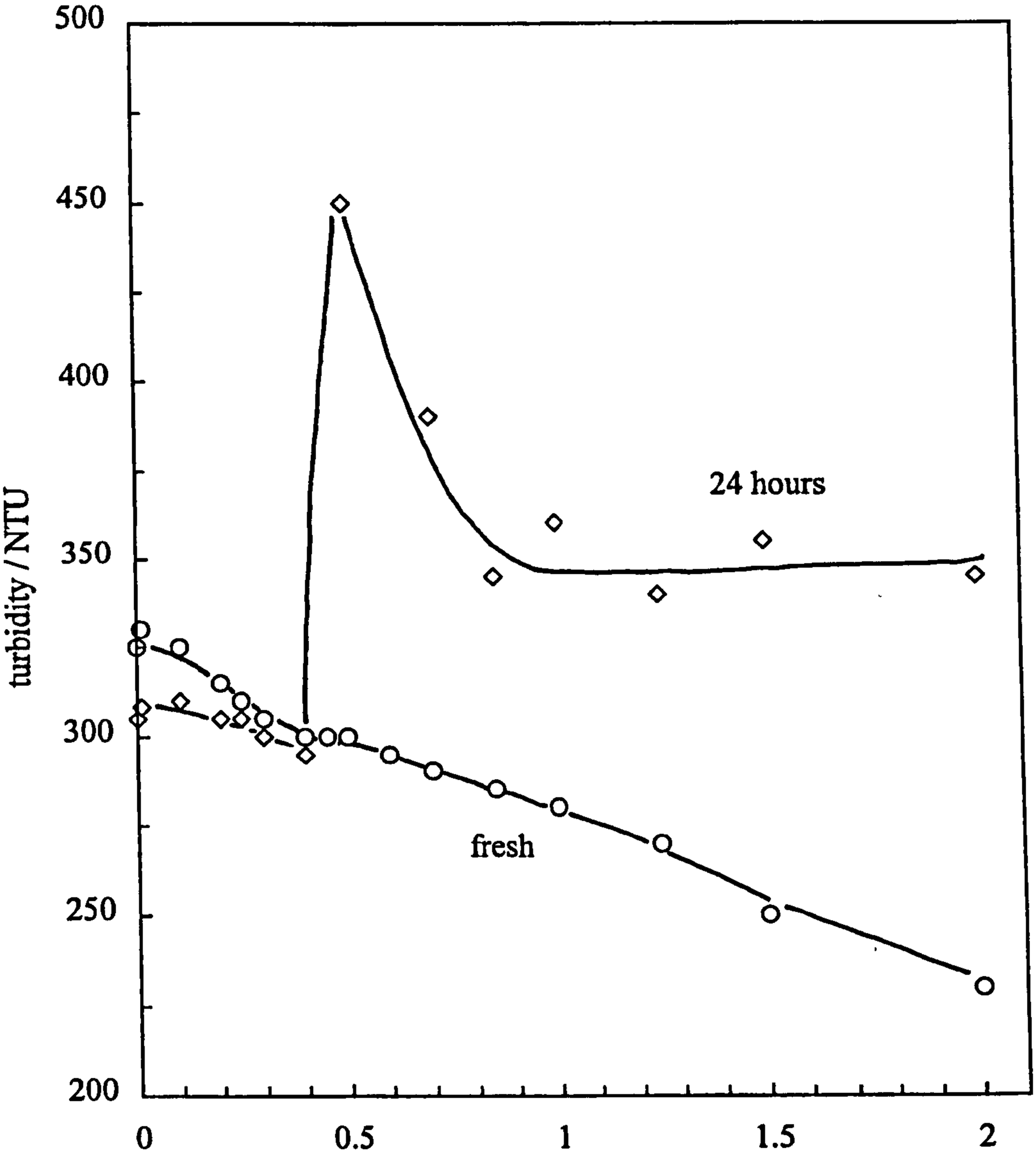

aqueous colloid into a clear upper phase (of low volume) and a turbid lower phase containing visible flocculated particles. The diamond points in the figure refer to systems which have not been shaken. The time dependence of the turbidity of unshaken colloids in 1.5 and 2 M NaCl at pH 10 is shown in Figure 3.5. The onset of the turbidity increase (around 2 hours) coincides with the first appearance of the clear upper layer. Figure 3.6 shows the turbidity-salt concentration curves for unshaken colloids measured 24 hours after preparation for various pH values. At pH 2, 4 and 5 there is no flocculation and the turbidity decreases with increasing refractive index of the aqueous salt solution. At pH 6 and above, flocculation is accompanied by a sharp increase in turbidity. The concentration of salt at the onset of flocculation decreases with an increase in pH, whereas the maximum turbidity increases with pH possibly indicating a large floc size (hence V_p) which forms when the negative charge on particles is screened by electrolyte. The c.c.c. of NaCl required to flocculate the Aerosil 200 dispersions is plotted in Figure 3.7 as a function of pH. Data from the literature for Aerosil 200[79] and Ludox HS-40[76] silica particles are included for comparison. Below the points the colloid is stable and dispersed whereas above them it is unstable and flocculated. The anomalous DLVO behaviour is evident in all cases.

In order to investigate the surface activity of silica particles the surface tension of the aqueous dispersions was measured as a function of silica concentration at pH 2 and 10 using the Wilhelmy plate method (Figure 3.8). Surfactants tend to lower the tension by adsorbing at the oil-water and air-water interface. In order for particles to stabilise emulsions they must exhibit a certain degree of surface activity. The aqueous colloid (5 wt.%) was diluted to the required concentration using water of the same pH as the colloid. The surface tension is shown to be virtually independent of particle concentration and equal to that of pure water at both pH because the particles are large (~15 nm diameter) and hence the surface excess concentration Γ is low. This is in contrast to surfactant systems where the typical head-group area is < 0.5 nm^2 therefore the surface tension is dependent on surfactant concentration. It is possible to prove the independence of the surface tension γ on particle concentration c by rearranging the Gibbs adsorption isotherm to give

$$-\frac{d\gamma}{d\ln c} = \Gamma RT \qquad (3.12)$$

Figure 3.5

Change in turbidity with time of 0.5 wt.% Aerosil 200 dispersions in water at pH 10 in the presence of NaCl of given molarity.

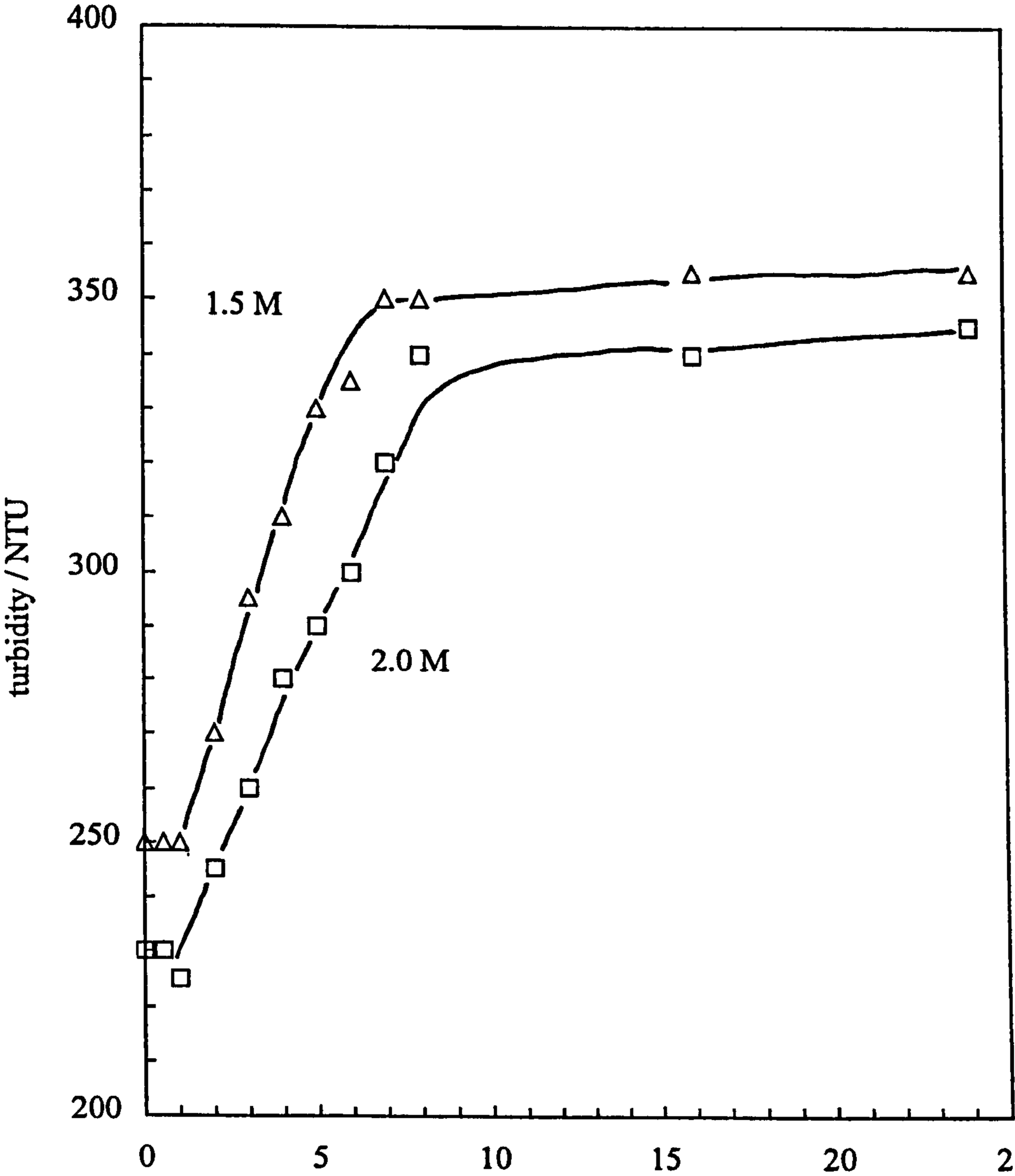

Figure 3.6

Turbidity of 0.5 wt.% Aerosil 200 dispersions in water 24 hours after adding NaCl. The pH values are 2 (open circles), 4 (filled diamonds), 5 (open squares), 6 (open triangles), 7 (crosses) and 10 (filled triangles).

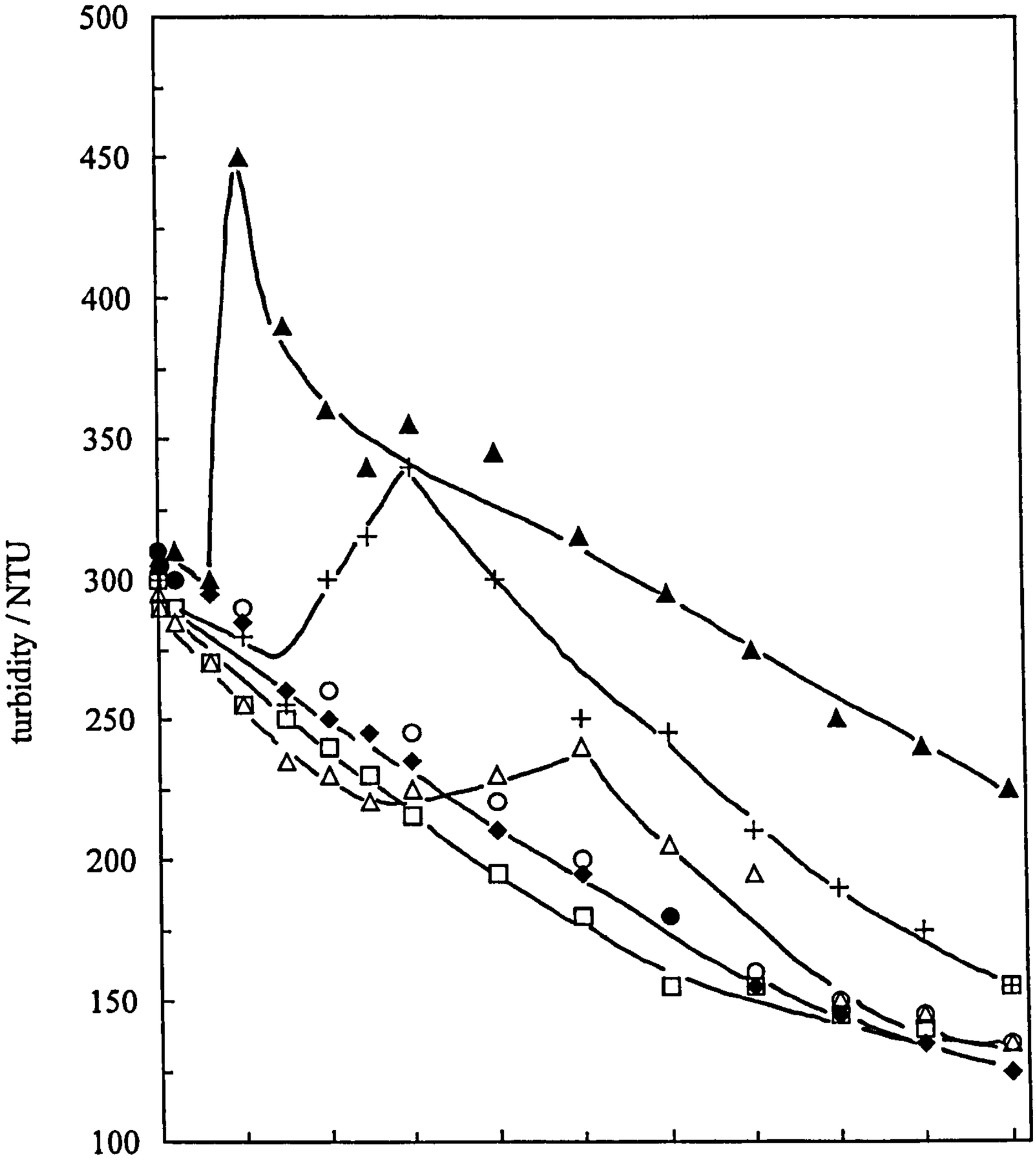

Figure 3.7

Critical coagulation concentration of NaCl for silica dispersions in water as a function of pH, 24 hours after mixing. Triangles are from ref. 76 with 0.2 wt.% Ludox HS silica, circles are present data with 0.5 wt.% Aerosil 200 and squares are from ref. 79 with 0.2 wt.% Aerosil 200 silica.

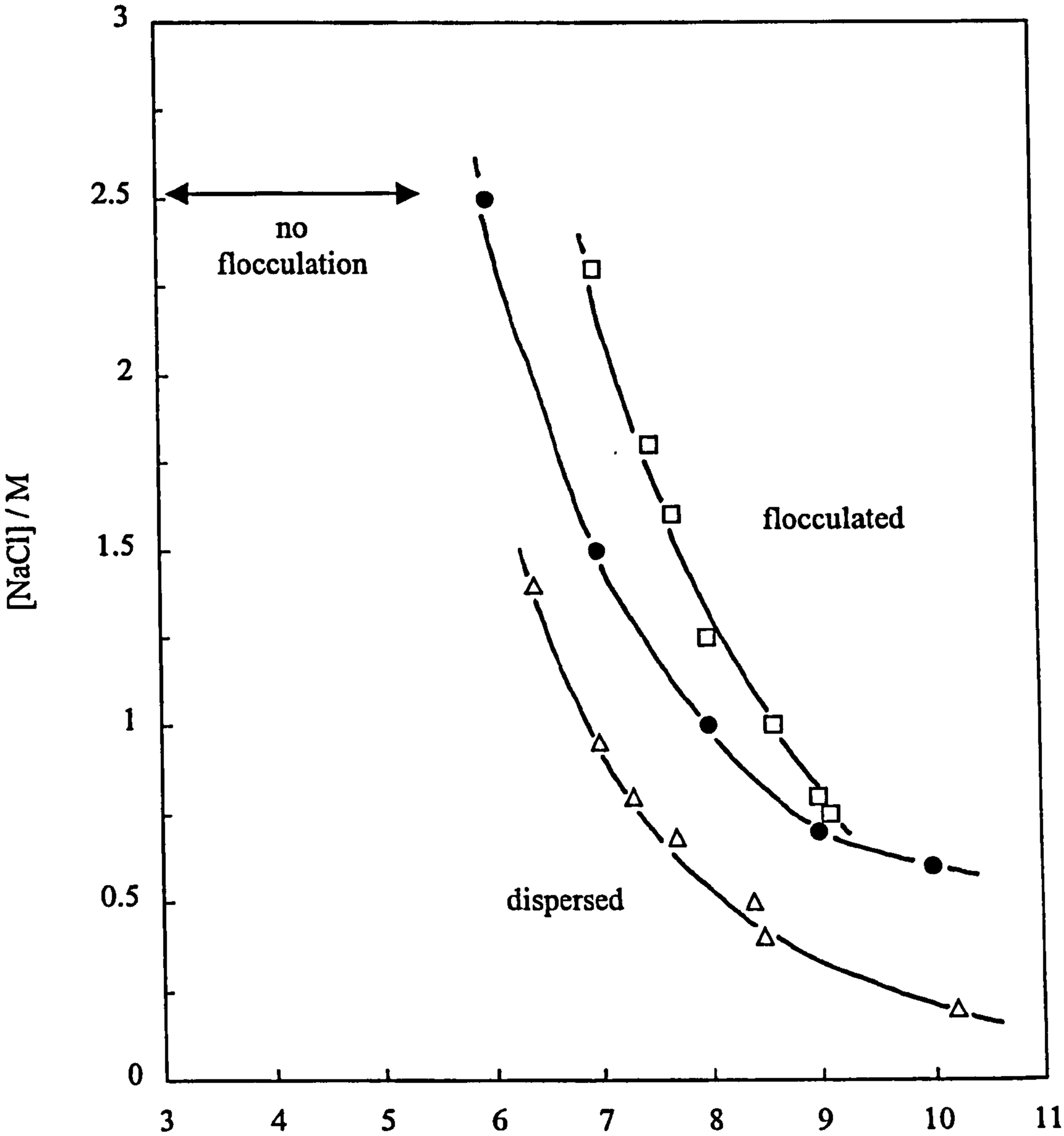

Figure 3.8

Surface tensions of Aerosil 200 dispersions in water at pH 2 (diamonds) and 10 (squares) at 25 °C as a function of particle concentration measured using the Wilhelmy plate method.

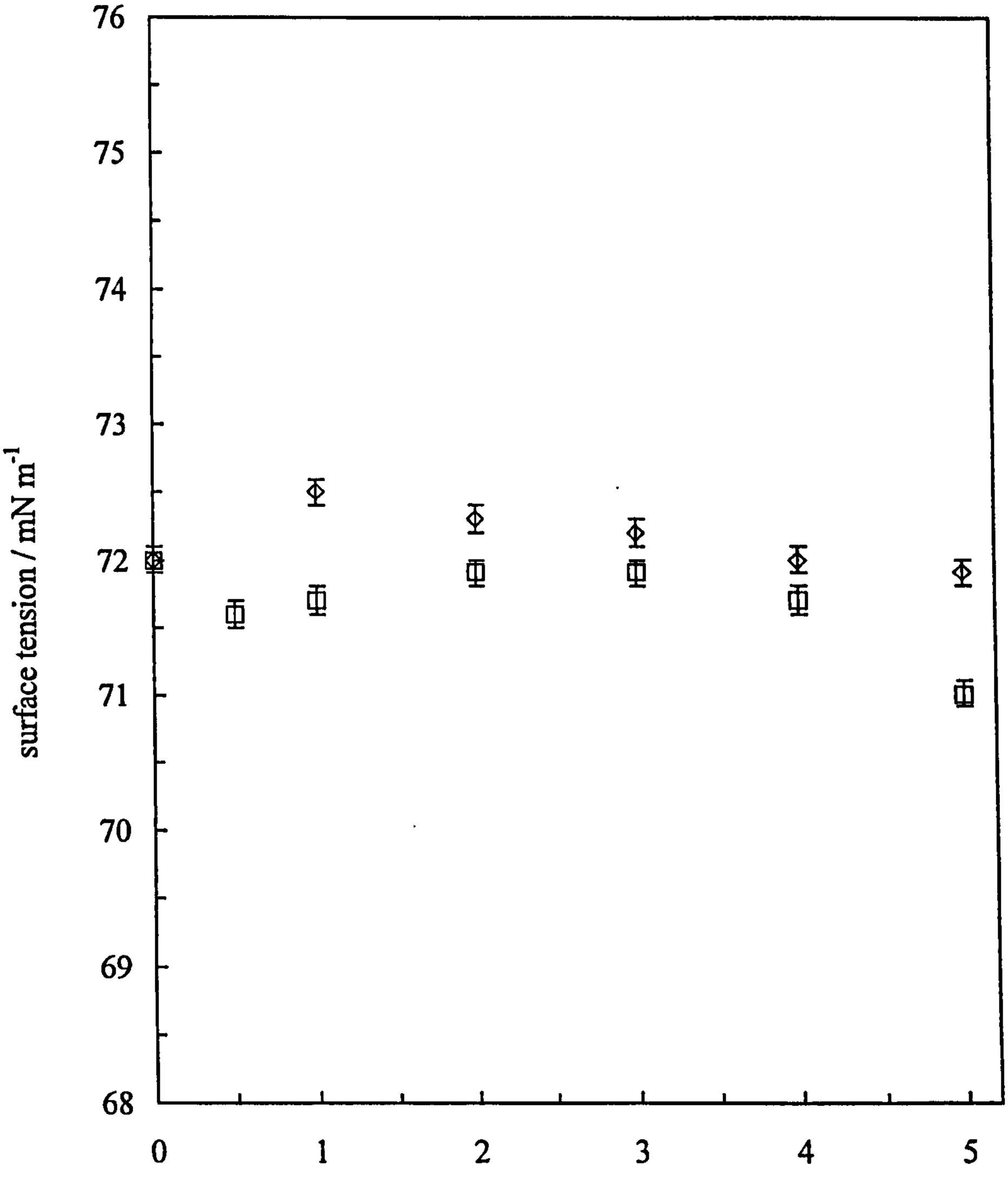

where R is the gas constant and T is the temperature. When the particle concentration is increased from 1 to 5 wt.% the gradient ($d\gamma$ / dlnc) only changes by 1.75 % hence adsorption at the air-water surface is minimal. The actual lowering of tension for particles of radius (a) equal to 6 nm can be calculated assuming a close packed monolayer on the surface.

The area (A) per particle equals

$$A = \pi a^2 \tag{3.13}$$

The number of particles (N_p) in 1 m^2 is

$$N_p = 1 / \pi a^2 \tag{3.14}$$

The number of moles of particles (N_m) in 1 m^2 is

$$N_m = 1 / N_A \pi a^2 = \Gamma \text{ (moles } m^{-2}) \tag{3.15}$$

where the surface excess concentration, Γ equals

$$\Gamma = -\frac{1}{RT}\frac{d\gamma}{d\ln c} \tag{3.16}$$

The maximum value of ($d\gamma$ / dlnc) equals

$$\frac{d\gamma}{d\ln c} = -\frac{RT}{N_A \pi a^2} = -\frac{kT}{\pi a^2} \tag{3.17}$$

Differentiating results in,

$$\frac{d\gamma}{dc} = -\frac{1}{c}\frac{kT}{\pi a^2} = -\frac{1}{5}\frac{400\text{x}10^{-23}}{\pi\, 36\text{x}10^{-18}} = -0.7\text{x}10^{-5}\ \text{J m}^{-2}\ \text{wt.\%}^{-1} \tag{3.18}$$

Comparing this value with the maximum experimental value from Figure 3.8 of -0.1 mN m^{-1} wt.%$^{-1}$ (equal to -1x10^{-4} J m^{-2} wt.%$^{-1}$) it is clear that particles of this size do not affect the surface tension to a notable extent. However it is shown in this chapter that particles are able to stabilise emulsions and hence must adsorb at the oil-water interface.

Before investigating the effect of electrolyte on the stability of emulsions, it was important to determine the minimum concentration of particles required to form stable emulsions in toluene-water systems. In order to stabilise the emulsion there must be enough particles to coat (with at least a monolayer) the surface of the spherical drops of the dispersed phase. The transmission electron micrographs shown in Figure 2.4 prove that ultrasonic dispersion of the silica powder breaks the agglomerates down into their primary particles of diameter approximately 12 nm. For an oil:water volume ratio of 1:4, an average emulsion drop radius (R_{oil}) of 20 μm (later) and an average particle radius (r_p) of 6 nm it is possible to calculate the mass of particles required to cover all drops of an oil-in-water emulsion with a monolayer assuming an hexagonal close packing (HCP) arrangement of spherical silica particles.

The volume of one oil drop (V_{oil}) equals

$$V_{oil} = \frac{4}{3}\pi R_{oil}^{3} = 3.35\text{x}10^{-14}\,\text{m}^3 \qquad (3.19)$$

The number of oil drops (N_{oil}) in 2 cm^3 of oil is

$$N_{oil} = \frac{2\text{x}10^{-6}\,\text{m}^3}{3.35\text{x}10^{-14}\,\text{m}^3} = 5.97\text{x}10^{7} \qquad (3.20)$$

The surface area of one oil drop (S_{oil}) equals

$$S_{oil} = 4\pi R_{oil}^{2} = 5.03\text{x}10^{-9}\,\text{m}^2 \qquad (3.21)$$

The total surface area (S.A.) of all oil drops is

$$\text{S.A.} = N_{oil}\,4\pi R_{oil}^{2} = 0.30\,\text{m}^2 \qquad (3.22)$$

and the volume ($V_{part.}$) of one silica particle is

$$V_{part.} = \frac{4}{3}\pi r_p^{\ 3} = 9.0x10^{-25} m^3 \qquad (3.23)$$

The area occupied by one silica particle at the oil-water interface ($S.A._{.part.}$) assuming HCP equals

$$S.A._{.part.} = 2\sqrt{3}r_p^2 = 1.24x10^{-16} m^2 \qquad (3.24)$$

The number of particles ($N_{part.}$) required to cover all oil drops with a monolayer equals

$$N_{part.} = \frac{S.A.}{S.A._{.part.}} = \frac{0.30\ m^2}{1.24x10^{-16} m^2} = 2.4x10^{15} \qquad (3.25)$$

The mass ($M_{part.}$) of one silica particle equals

$$M_{part.} = V_{part.}\rho_{part.} = 9.0x10^{-25} m^3 \text{ x } 0.05x10^6 g\ m^{-3} = 4.5x10^{-20} g \qquad (3.26)$$

where $\rho_{part.}$ equals the particle density. Therefore the mass of particles (M_{total}) required to cover all oil drops is

$$M_{total} = M_{part.}N_{part.} = 4.5x10^{-20} g \text{ x } 2.4x10^{15} = 1.08x10^{-4} g \qquad (3.27)$$

In 8 cm^3 of 0.5 wt.% Aerosil 200 in water there are $4x10^{-3}$ g of particles, i.e. nearly 40 times as many particles as is required to cover the oil drops with a monolayer. The mass of particles required increases to $2.72 \text{ x } 10^{-4}$ g at an oil:water ratio of 1:1 and to $4.34 \text{ x } 10^{-4}$ g at a ratio of 4:1. However, the mass of particles in a 0.5 wt.% dispersion is still greater than the mass required to cover the oil drops even at a ratio of 4:1 where there are $1 \text{ x } 10^{-3}$ g of particles in $2cm^3$ of the dispersion.

The emulsion stability was measured in graduated vessels, which were stored in a thermostatted glass tank. The stability of o/w emulsions to creaming and coalescence were calculated using equations 3.28 and 3.29 respectively.

Calculation of emulsion stability to coalescence and gravity-induced separation

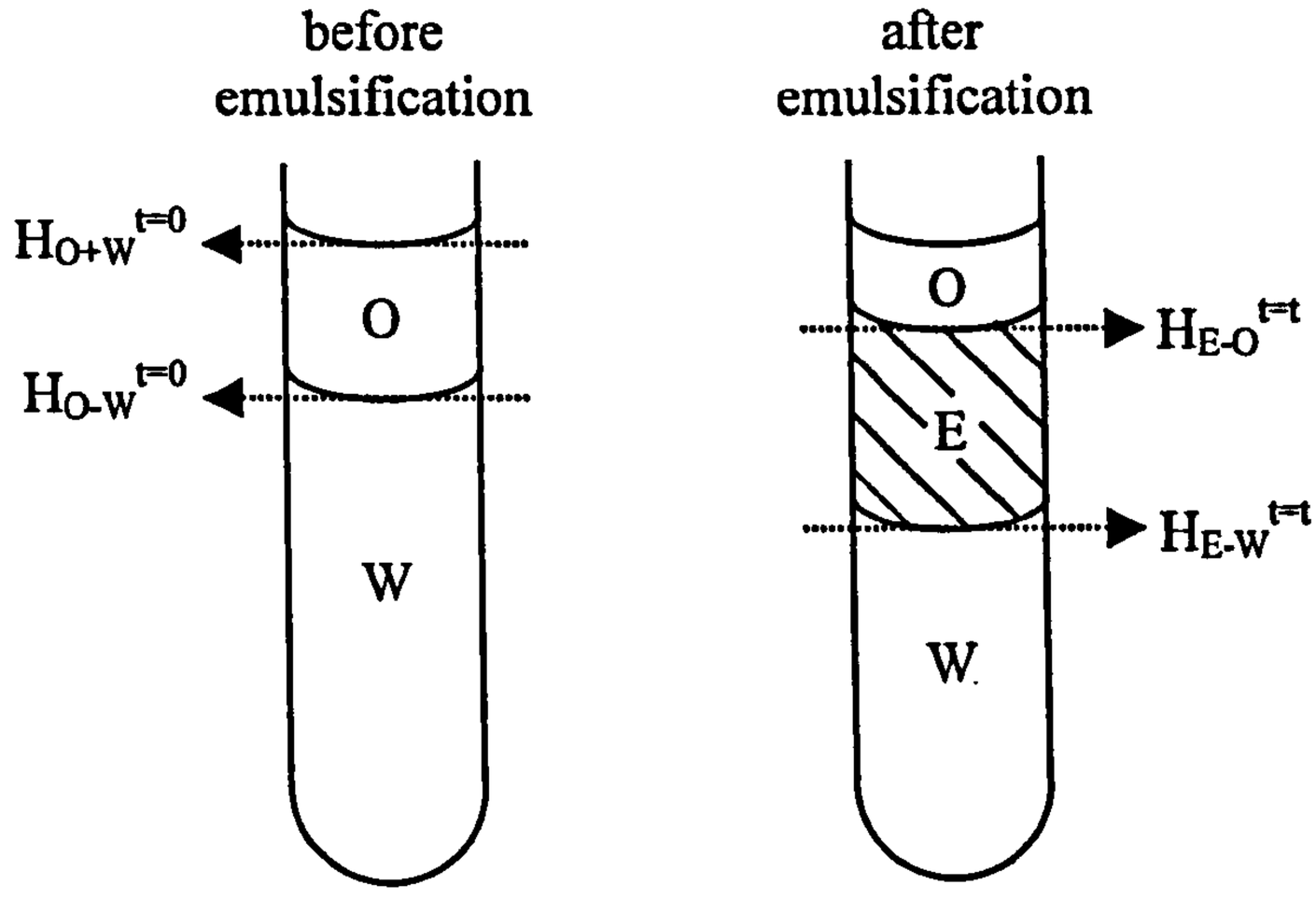

$$\text{stability to creaming} = \left(\frac{H_{E-W}^{t=t}}{H_{O-W}^{t=0}}\right)\left(\frac{H_{O-W}^{t=0}}{H_{O+W}^{t=0}}\right) \tag{3.28}$$

$$\text{stability to coalescence} = \left(\frac{\left(H_{O+W}^{t=0} - H_{O-W}^{t=0}\right) - \left(H_{E-O}^{t=t} - H_{O-W}^{t=0}\right)}{H_{O+W}^{t=0} - H_{O-W}^{t=0}}\right)\left(\frac{H_{O-W}^{t=0}}{H_{O+W}^{t=0}}\right) \tag{3.29}$$

where: $H_{O-W}^{t=0}$ = height of oil-water interface prior to emulsification

$H_{O+W}^{t=0}$ = total height of oil + water prior to emulsification

$H_{E-W}^{t=t}$ = height of emulsion-water interface t minutes after emulsification

$H_{E-O}^{t=t}$ = height of emulsion-oil interface t minutes after emulsification

Figure 3.9 shows the effect of particle concentration on the stability of 20 vol% toluene emulsions in the absence of added salt at pH 4. All emulsions are o/w, with the stability to creaming plotted on the left-hand ordinate as the fraction of emulsion which forms a

Figure 3.9

Stability to creaming (open points, left hand ordinate) and coalescence (filled points, right hand ordinate) of 20 vol% toluene-in-water (no salt) emulsions stabilised by Aerosil 200 at pH 4. Wt.% values of silica in water are 0.2 (diamonds), 0.5 (squares) and 1.0 (triangles).

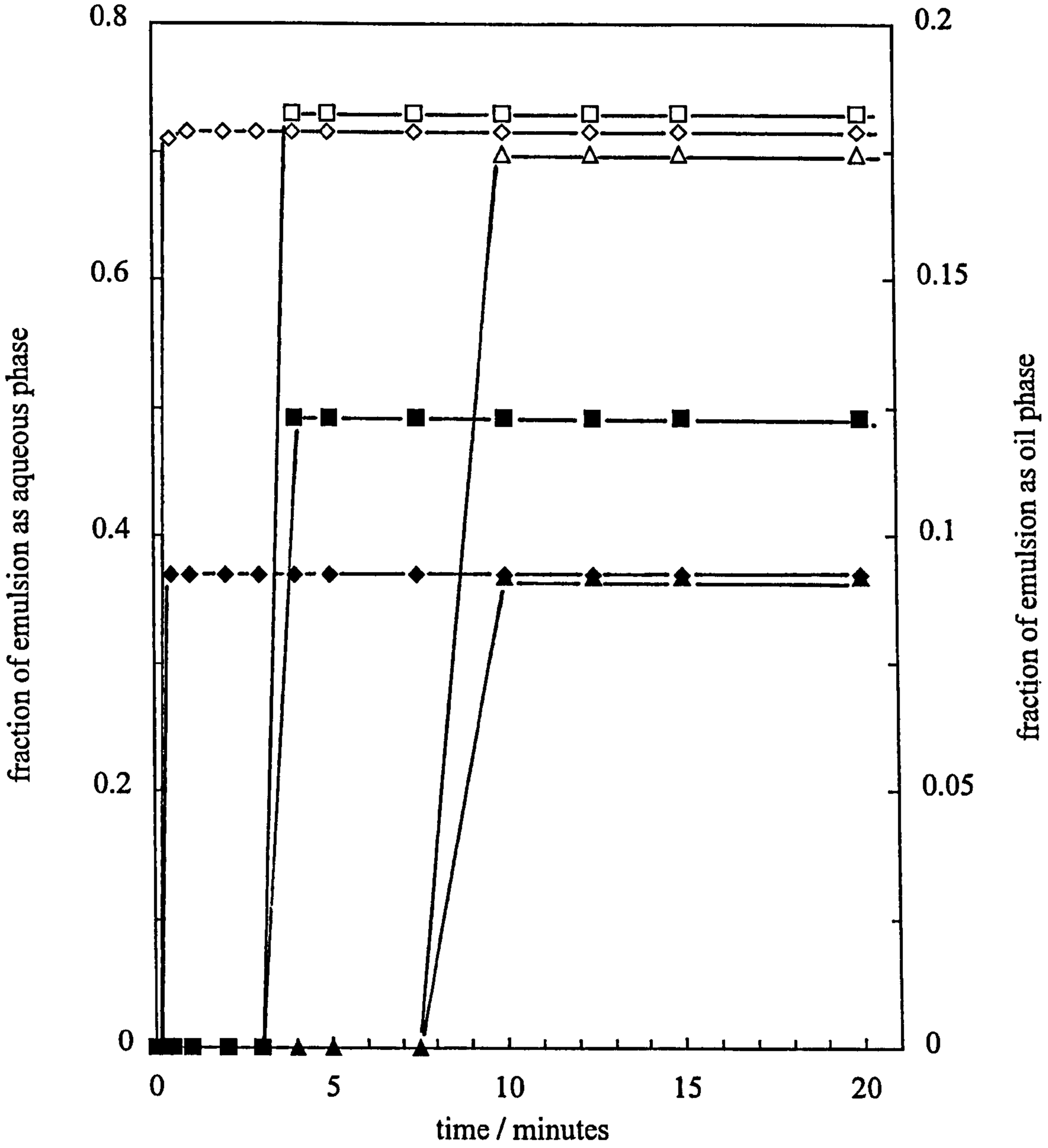

clear aqueous phase (0 = stable, 0.8 = unstable) and the stability to coalescence on the right-hand ordinate as the fraction of emulsion appearing as a separated oil phase. The two types of instability are initiated simultaneously at pH 4 (the natural pH of the silica colloids) and the induction times for each increase with particle concentration. By 20 minutes, most of the emulsion has creamed and around 50 % of oil has coalesced. The remaining cream is a high volume fraction o/w emulsion which is very stable. At pH 10, Figure 3.10 shows that creaming and coalescence occur immediately and to a similar extent for all particle concentrations. However, the emulsions broke completely within 2 hours. Particle concentration has a minimal effect on emulsion stability within the concentration and time range studied here. A concentration of 0.5 wt.% Aerosil 200 silica in water was used for the subsequent experiments. At this concentration, in the absence of electrolyte and at natural pH, the aqueous colloid is clear blue with a viscosity similar to that of pure water. It may be possible that the emulsions coarsen to some extent by Ostwald ripening, which has been observed for toluene-in-water emulsions stabilised by surfactant.[98] Toluene is slightly soluble in water (= 0.0334 vol%)[99] which is necessary for Ostwald ripening to occur. The Kelvin equation[14] (equation 3.30) predicts that the solubility of a substance in the form of spherical drops increases with decreasing size,

$$c(a) = c(\infty)\exp\left(\frac{2\gamma V_m}{aRT}\right) \qquad (3.30)$$

where c(a) is the aqueous phase solubility of oil in a drop of radius a, c(∞) is the solubility in a system with only a planar interface, γ is the interfacial tension between the two phases and V_m is the molar volume of the oil. Immediately after emulsification the oil drops will be small, and hence more soluble in the continuous phase. This may result in the growth of some drops at the expense of others. The resultant large drops are unstable due to a less dense covering of silica at the interface (see diagram below). Figures 3.9 and 3.10 show growth occurs to a certain extent and then stops. Ostwald ripening of the small drops will stop once the silica becomes close packed and held very strongly to the oil-water interface. The remaining cream is very stable probably consisting of particle-laden interfaces. This is in contrast to surfactant systems where Ostwald ripening continues until the emulsion is completely destabilised due to

Figure 3.10

Stability to creaming (open points, left hand ordinate) and coalescence (filled points, right hand ordinate) of 20 vol% toluene-in-water (no salt) emulsions stabilised by Aerosil 200 at pH 10. Wt.% values of silica in water are 0.2 (diamonds), 0.5 (squares) and 1.0 (triangles).

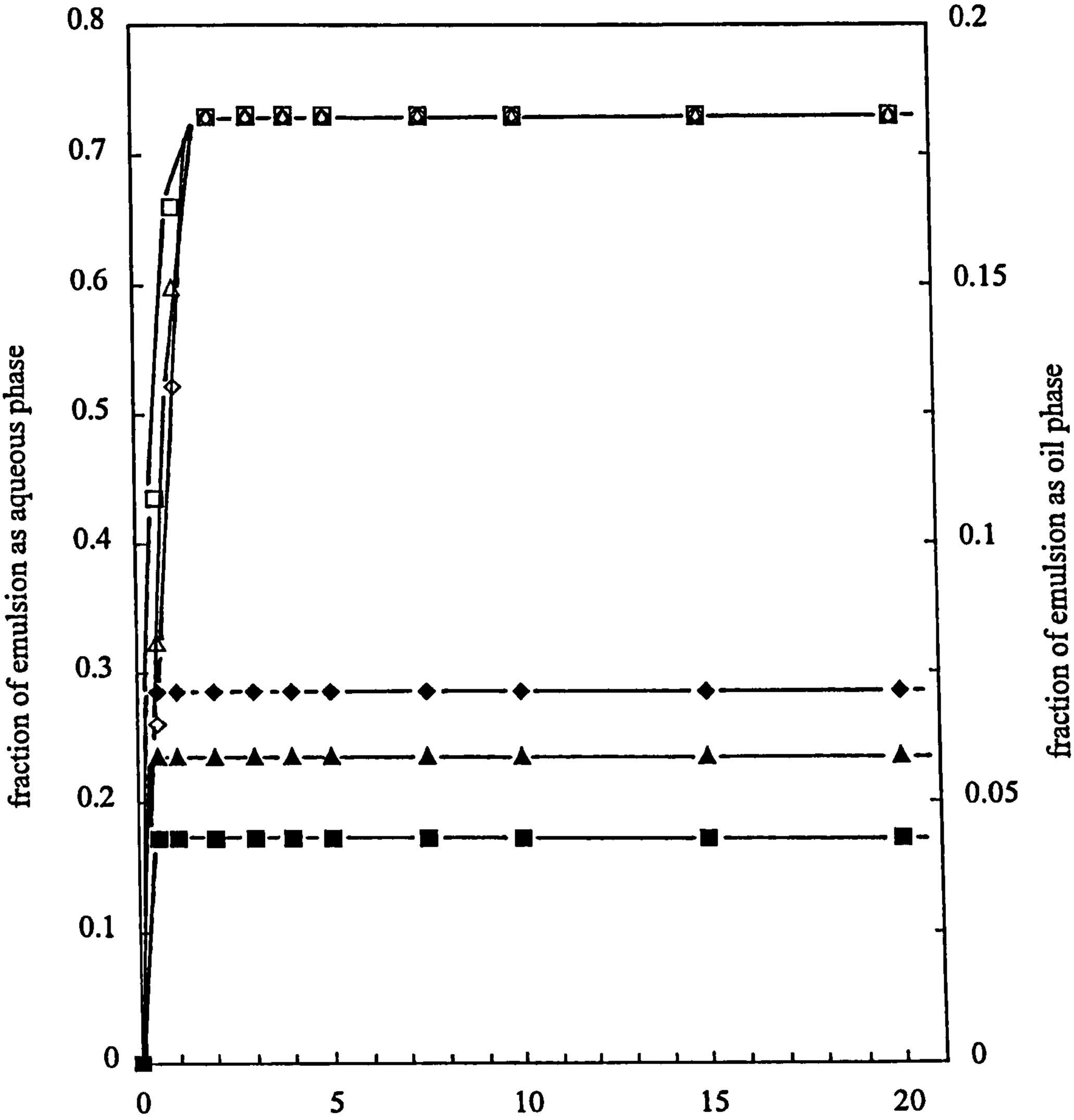

reversible adsorption of surfactant to the interface.[100] It is hypothesised here that the Laplace pressure ($2\gamma/r$), which is the driving force for Ostwald ripening, becomes constant for all drop sizes when ripening ceases. The diagram below shows how the small drops decrease in size until the oil-water interface is coated in irreversibly bound particles. A decrease in the drop radius results in an increase in γ. The large drops grow and may or may not adsorb more particles and hence γ will either increase or remain constant. Ripening will cease at a critical point when γ/r is the same for both drops.

Schematic representation of Ostwald ripening in solid-stabilised emulsions

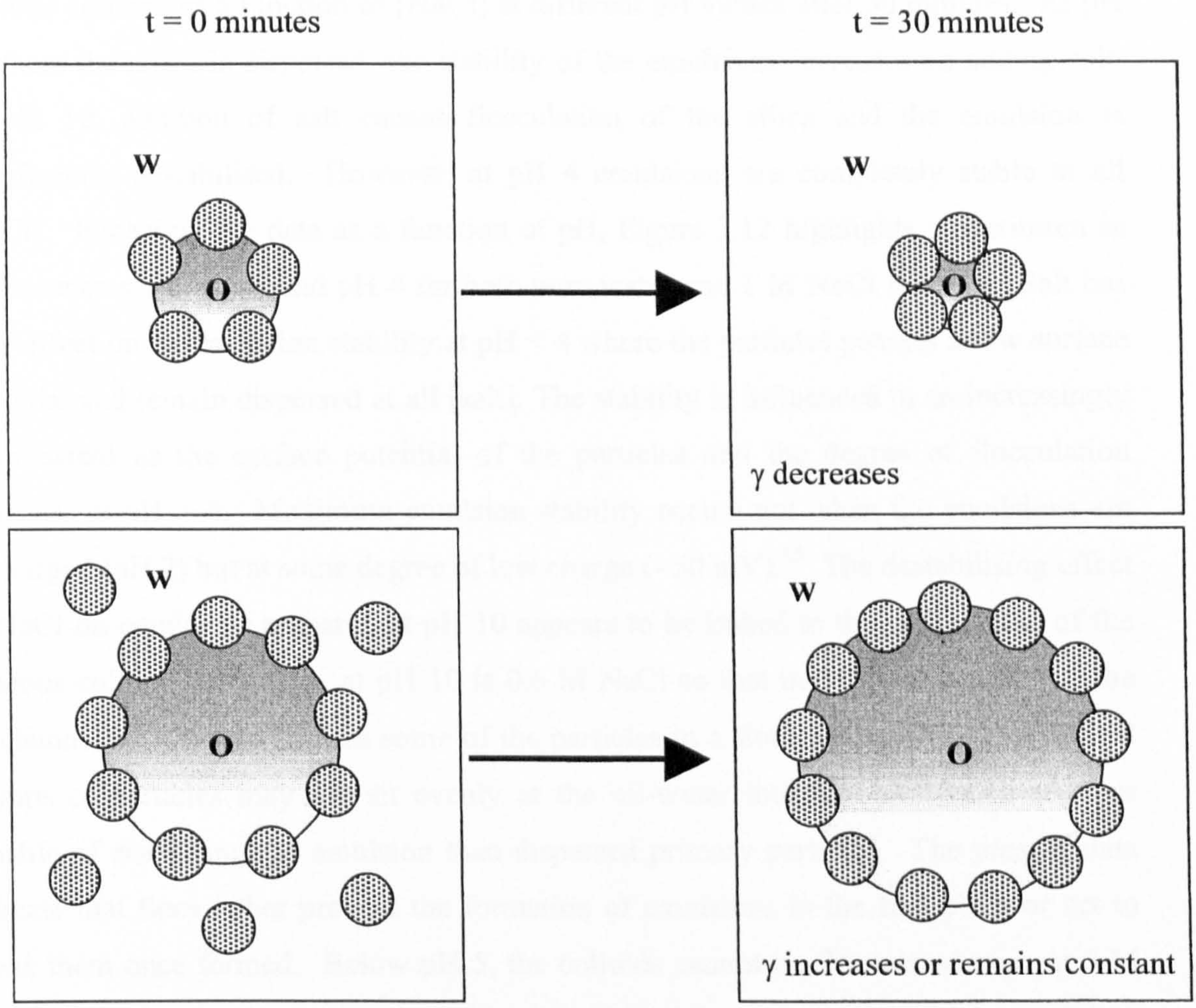

Aqueous Aerosil 200 silica dispersions were shown to exhibit anomalous DLVO behaviour in the presence of NaCl i.e. they remain dispersed at low pH when the surface has no charge but flocculate at high pH when the surface is negatively charged.

Flocculation, when it occurred, was found to be time dependent. Emulsions, formed immediately after addition of electrolyte to the aqueous colloid, exhibited the same behaviour as emulsions formed 24 hours after addition of electrolyte where the colloid was given time to flocculate. This suggests the process of homogenisation accelerates flocculation of the colloid in some way. Hence, all measurements of emulsion stability were carried out immediately after preparation of the colloid. At all pH values between 2 and 10 and [NaCl] between 0 and 2 M, emulsions were unstable to creaming such that after 30 minutes more than 90 % of the aqueous phase was resolved. However, coalescence of the emulsions is dependent on the pH and salt concentration. Figure 3.11 shows the stability to coalescence of 20 vol% toluene emulsions formed from the aqueous colloids as a function of [NaCl] at different pH values after 30 minutes. At pH 2, where the silica is dispersed, the stability of the emulsions increases on adding salt. At pH 10, addition of salt causes flocculation of the silica and the emulsion is significantly destabilised. However, at pH 4 emulsions are completely stable at all [NaCl]. Recasting the data as a function of pH, Figure 3.12 highlights a maximum in coalescence stability around pH 4 for both pure water and 1 M NaCl systems. Salt has little effect on the emulsion stability at pH < 4 where the particles possess a low surface potential and remain dispersed at all [salt]. The stability is influenced to an increasingly large extent as the surface potential of the particles and the degree of flocculation increases at pH > 4. Maximum emulsion stability occurs not when the emulsions are uncharged (pH 2) but at some degree of low charge (- 50 mV).[85] The destabilising effect of NaCl on emulsions prepared at pH 10 appears to be linked to the flocculation of the aqueous colloid. The c.c.c. at pH 10 is 0.6 M NaCl so that in 1.0 M salt solution, the emulsions are likely to contain some of the particles in a flocculated state. Flocculated clumps of particles may not sit evenly at the oil-water interface and hence are less capable of stabilising the emulsion than dispersed primary particles. The present data indicate that flocs either prevent the formation of emulsions in the first place or act to *break* them once formed. Below pH 5, the colloids cannot be flocculated even at 5 M NaCl, which is most likely the reason for the minor effect of salt on emulsion stability. The conductivity of equal volume oil and water emulsions stabilised by 0.5 wt.% Aerosil 200 is given in Figure 3.13. In all cases the conductivity remains high indicating emulsions are o/w with no inversion to w/o at high concentrations of salt. The surface of Aerosil silica is coated with hydrophilic silanol groups and hence prefers to stabilise o/w emulsions even in the presence of electrolytes which cause it to flocculate (i.e. lower its

Figure 3.11

Stability to coalescence after 30 minutes of 20 vol% toluene-in-water emulsions stabilised by 0.5 wt.% Aerosil 200 as a function of NaCl concentration at three pH values.

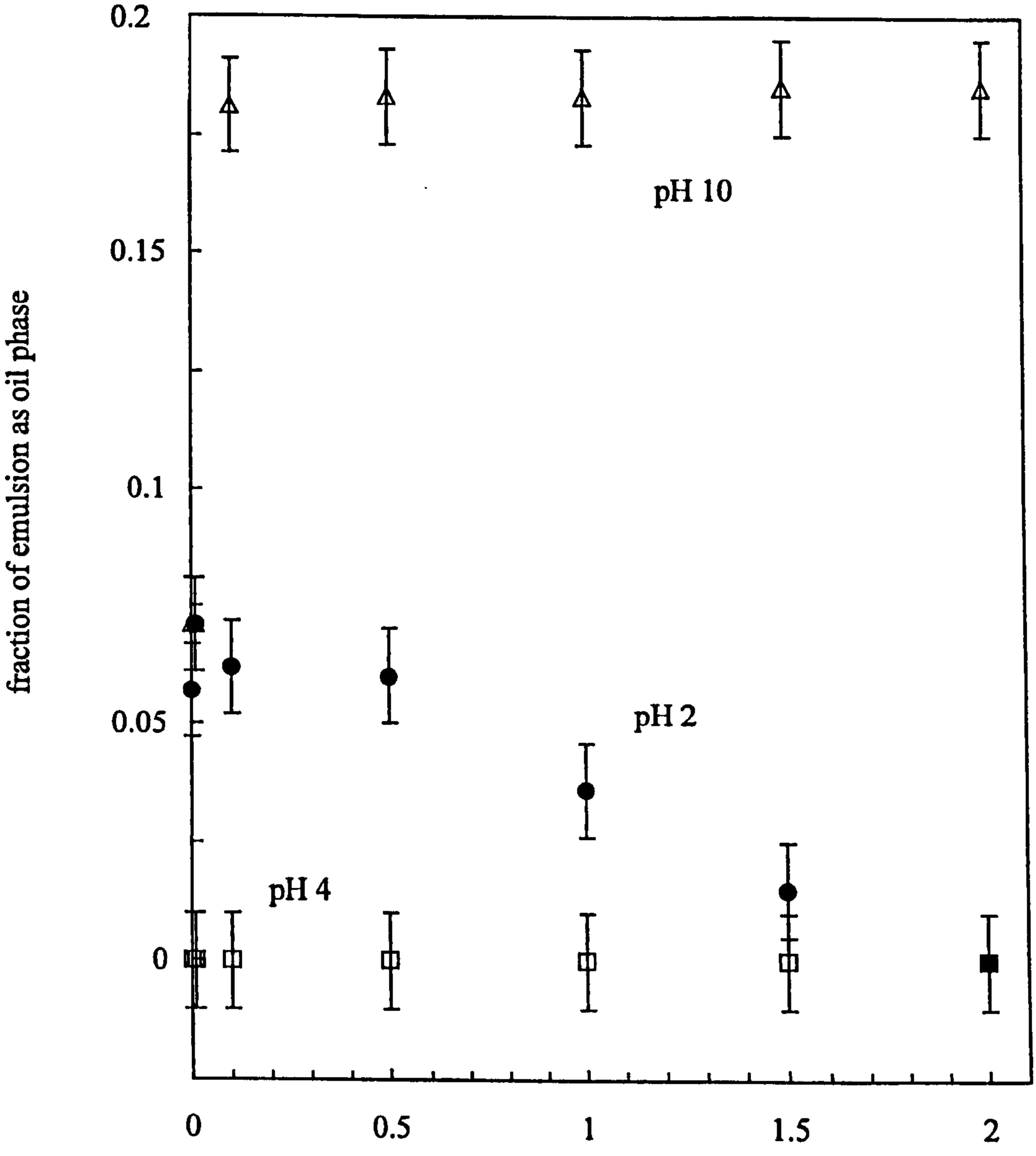

Figure 3.12

Stability to coalescence after 30 minutes of 20 vol% toluene-in-water emulsions stabilised by 0.5 wt.% Aerosil 200 as a function of pH at two NaCl concentrations, given.

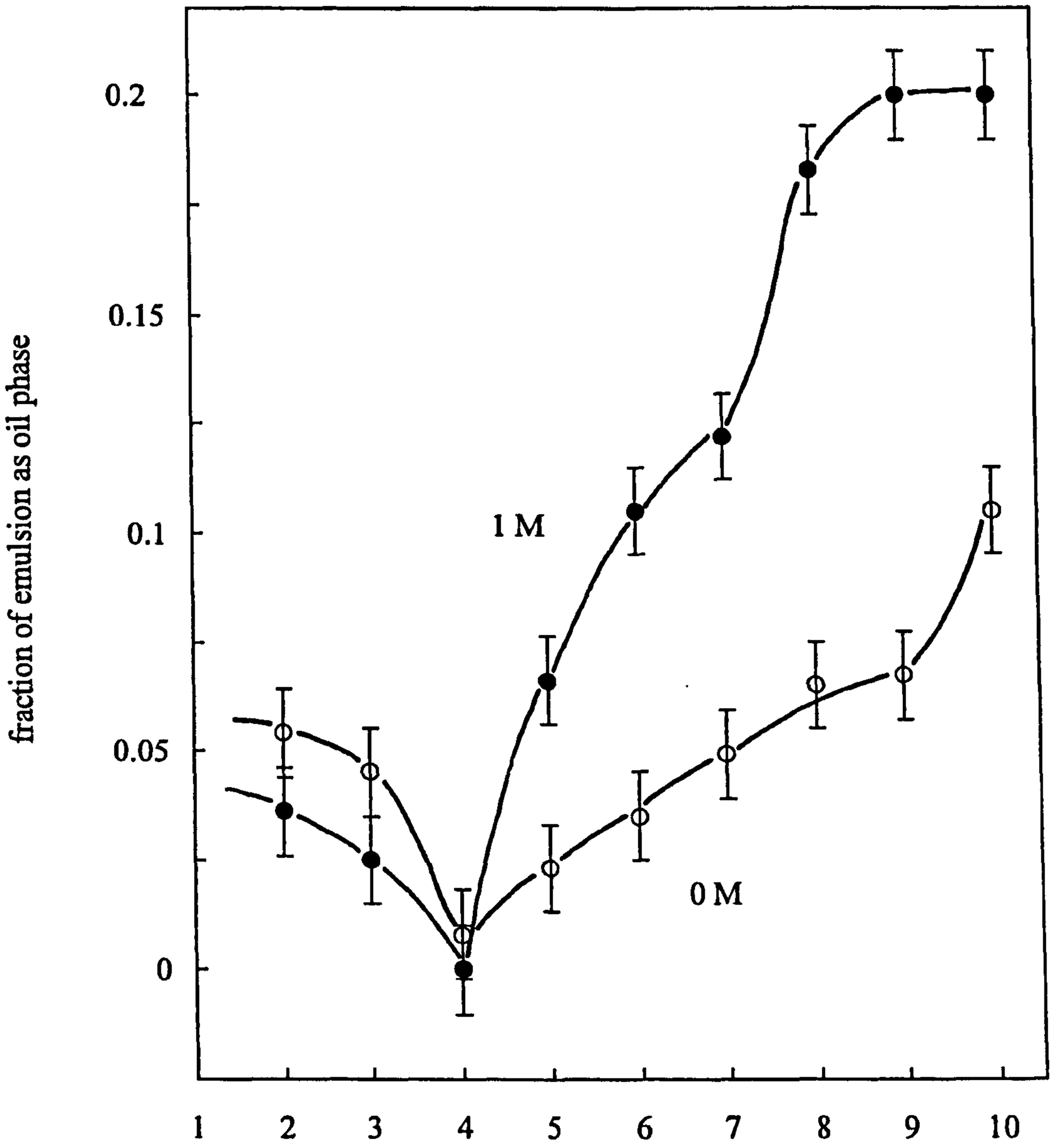

Figure 3.13

Conductivity of toluene-in-water emulsions stabilised by 0.5 wt.% Aerosil 200 as a function of NaCl at pH 2 (diamonds), 5 (squares) and 10 (triangles).

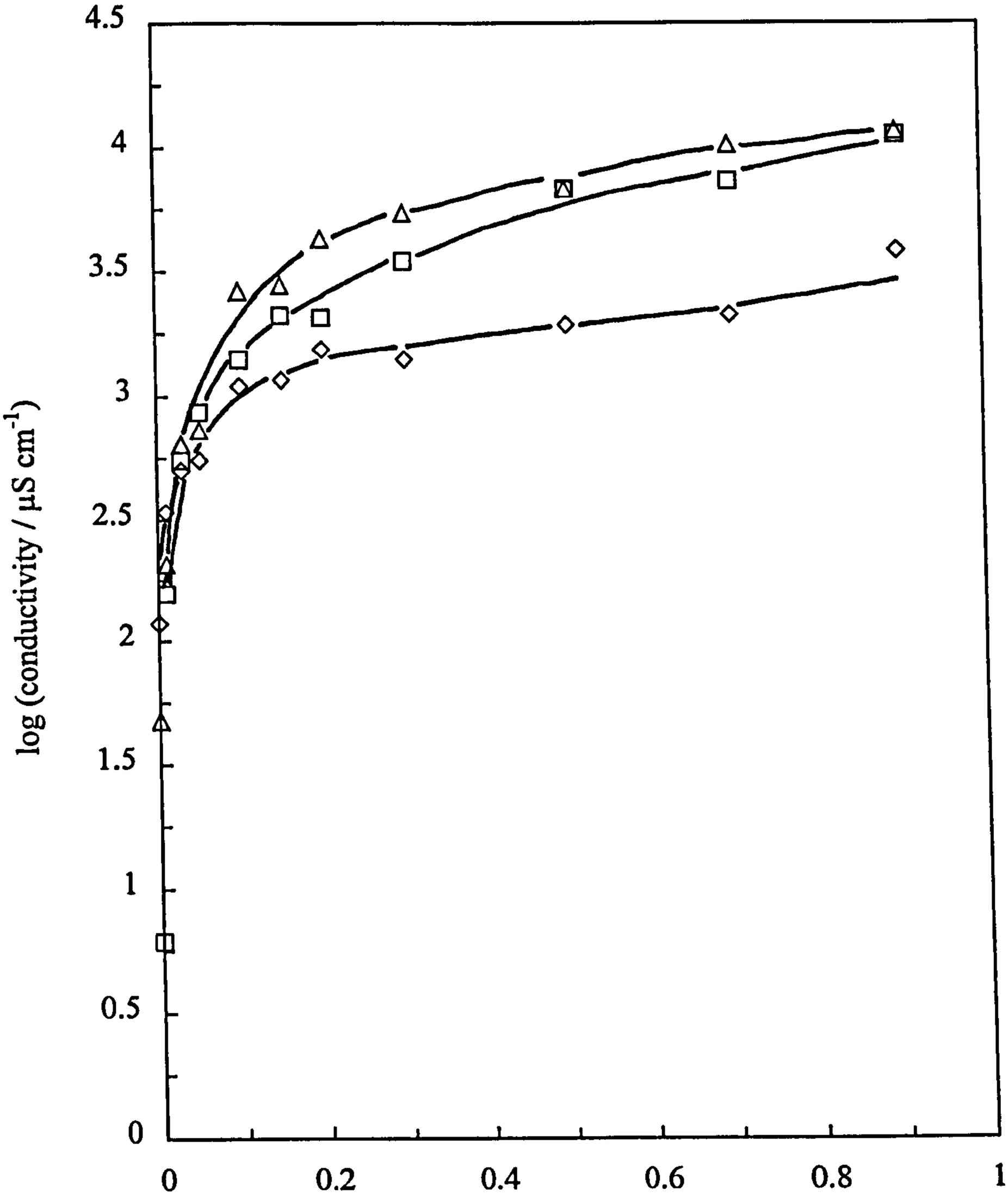

affinity for water). The association between particle wettability (whether it is hydrophobic or hydrophilic) and the preferred emulsion type is discussed later. By comparison, when very hydrophilic surfactants are used as stabilisers, e.g. single chain sulphates or large ethylene-oxy nonionics, w/o emulsions cannot be formed on adding NaCl.[64]

(b) Ludox HS-40 silica

The effect of particle concentration on the stability of toluene-water emulsions stabilised by precipitated Ludox HS-40 silica at pH 2 (i.e.p.) is given in Figure 3.14. Creaming of the emulsion occurs to greater than 90 % completion within 3 minutes for all particle concentrations between 0.5 and 5 wt.% (0.5 and 3.5 wt.% are shown). Stability to coalescence is higher than pyrogenic Aerosil 200 silica with only 20 % of the oil resolved after 30 minutes. At pH 10, where the particles are highly charged, the stability to creaming is similar in extent and rate to that seen at pH 2, but coalescence is more extensive (Figure 3.15). There is no real systematic dependence on particle concentration. In order to eliminate effects on creaming due to the density difference between toluene and water of 0.13 g cm^{-3}, emulsions containing 17 vol% carbon tetrachloride in toluene have been prepared. The density difference between the phases in these systems is approximately zero. Figure 3.16 shows that at pH 2 creaming is delayed until over one hour and no coalescence occurs within 4 hours. For pH 10, both creaming and coalescence are inhibited compared with the pure toluene case.

In the presence of NaCl at pH 2, the onset of creaming is delayed from 1 minute in 0.1 M NaCl, 4 minutes in 0.3 M NaCl and 10 minutes in 0.7 M NaCl for toluene-water emulsions stabilised by 0.5 wt.% Ludox HS-40 (Figure 3.17). However, the extent of creaming is > 90 % after 20 minutes in all cases and the resolved aqueous phase is clear blue suggesting the aqueous colloid is dispersed. The stability to coalescence is similar to that seen in the absence of NaCl. At pH 9, emulsions are very unstable to both creaming and coalescence with the majority of emulsion breaking within the first 2 minutes (Figure 3.18). The resolved aqueous phase is cloudy and eventually separates into clear upper phase and a cloudy, slightly viscous lower phase consistent with having flocculated silica particles. Emulsions stabilised by Ludox HS-40 indicate that if the proposed anomalous behaviour exists,[76] then the presence of flocculated particles is detrimental to emulsion stability. Ludox HS-40 was not

Figure 3.14

Stability to creaming (open points, left hand ordinate) and coalescence (filled points, right hand ordinate) of 20 vol% toluene-in-water (no salt) emulsions stabilised by Ludox HS-40 at pH 2. Wt.% values of silica in water are 0.5 (diamonds) and 3.5 (triangles).

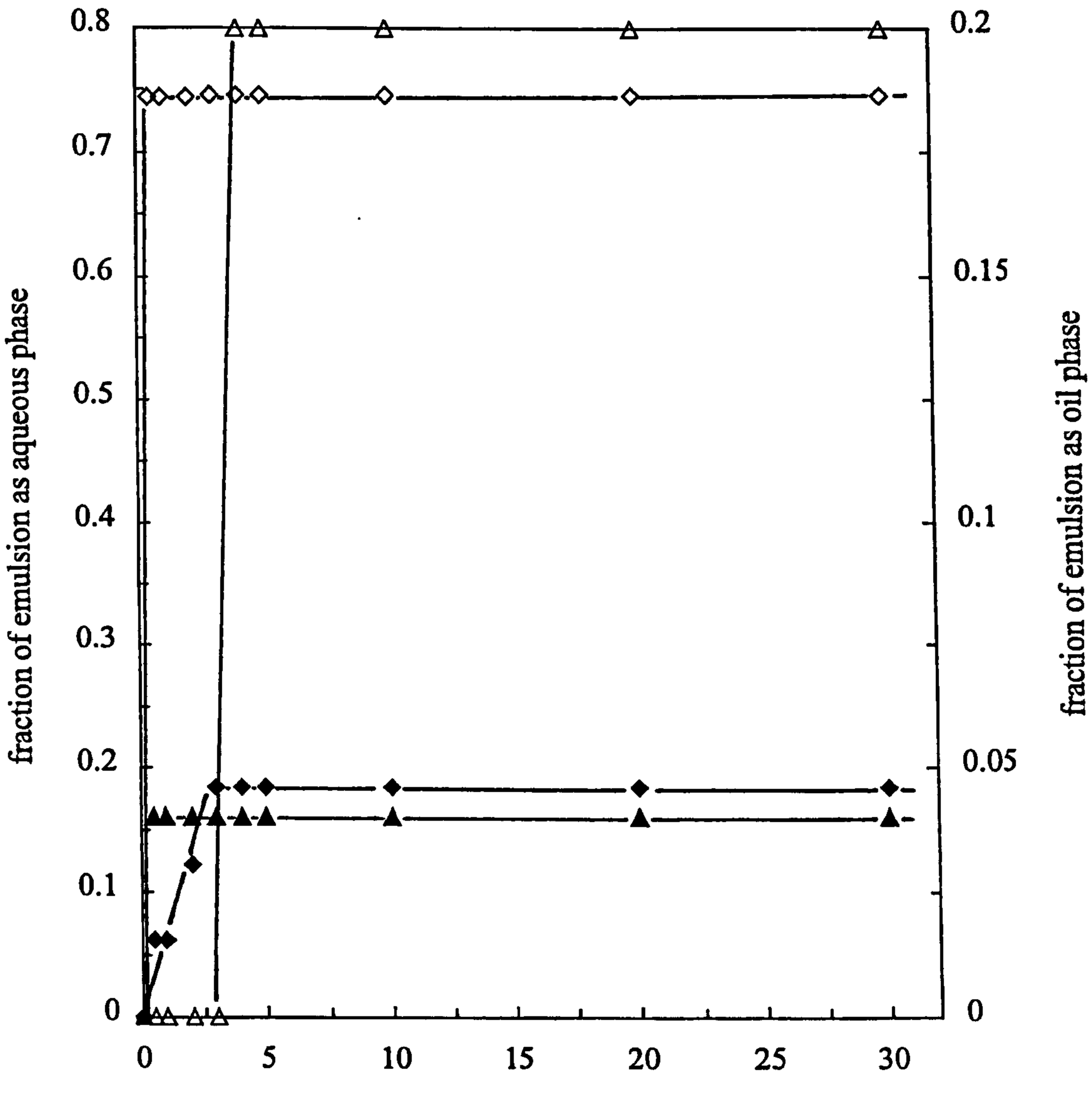

Figure 3.15

Stability to creaming (open points, left hand ordinate) and coalescence (filled points, right hand ordinate) of 20 vol% toluene-in-water (no salt) emulsions stabilised by Ludox HS-40 at pH 10. Wt.% values of silica in water are 1.0 (diamonds), 2.0 (squares) and 5.0 (triangles).

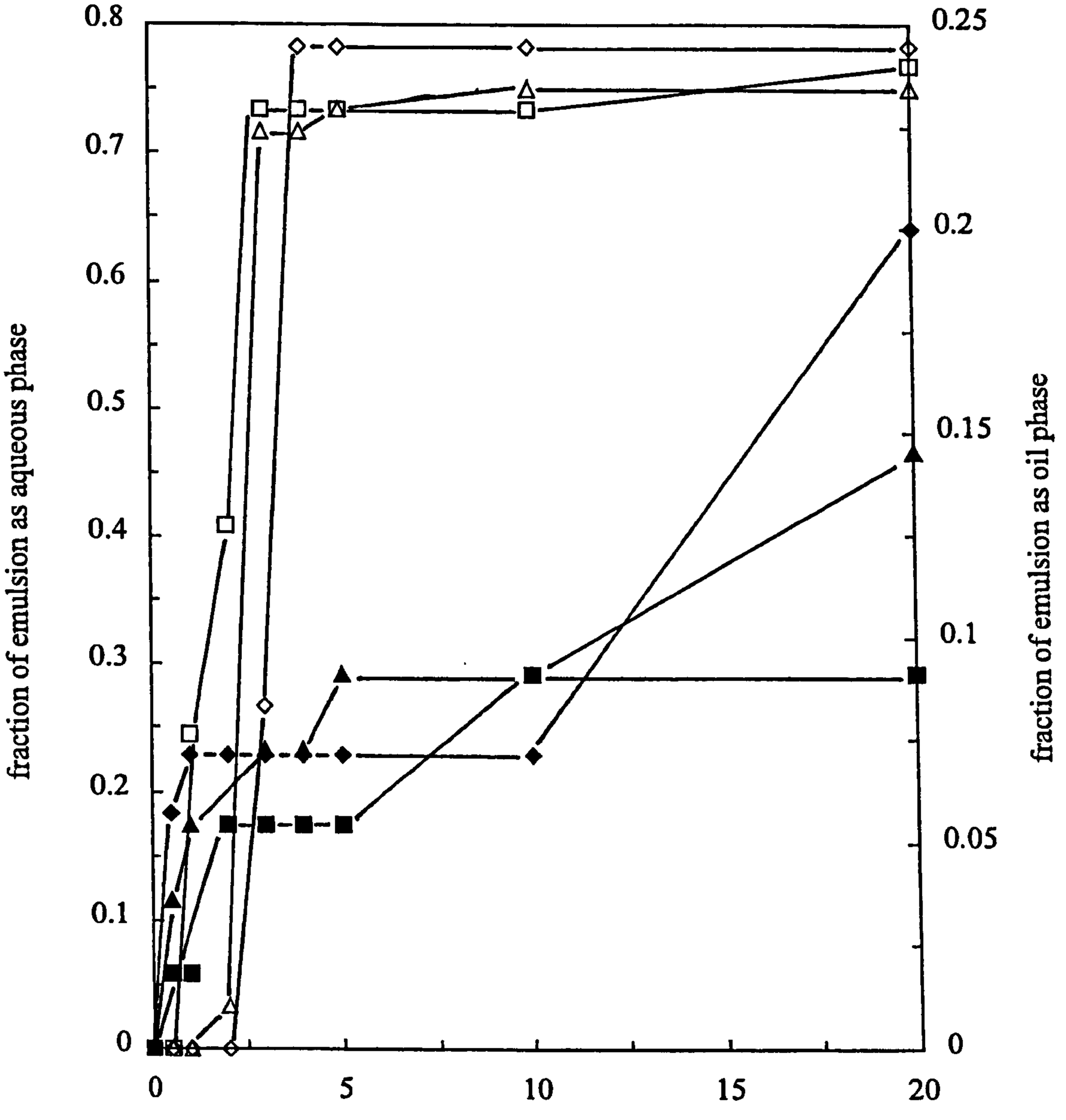

Figure 3.16

Stability to creaming (open points, left hand ordinate) and coalescence (filled points, right hand ordinate) of 20 vol% toluene/CCl_4-in-water emulsions stabilised by 0.5 wt.% Ludox HS-40 at pH 2 (diamonds) and pH 10 (squares).

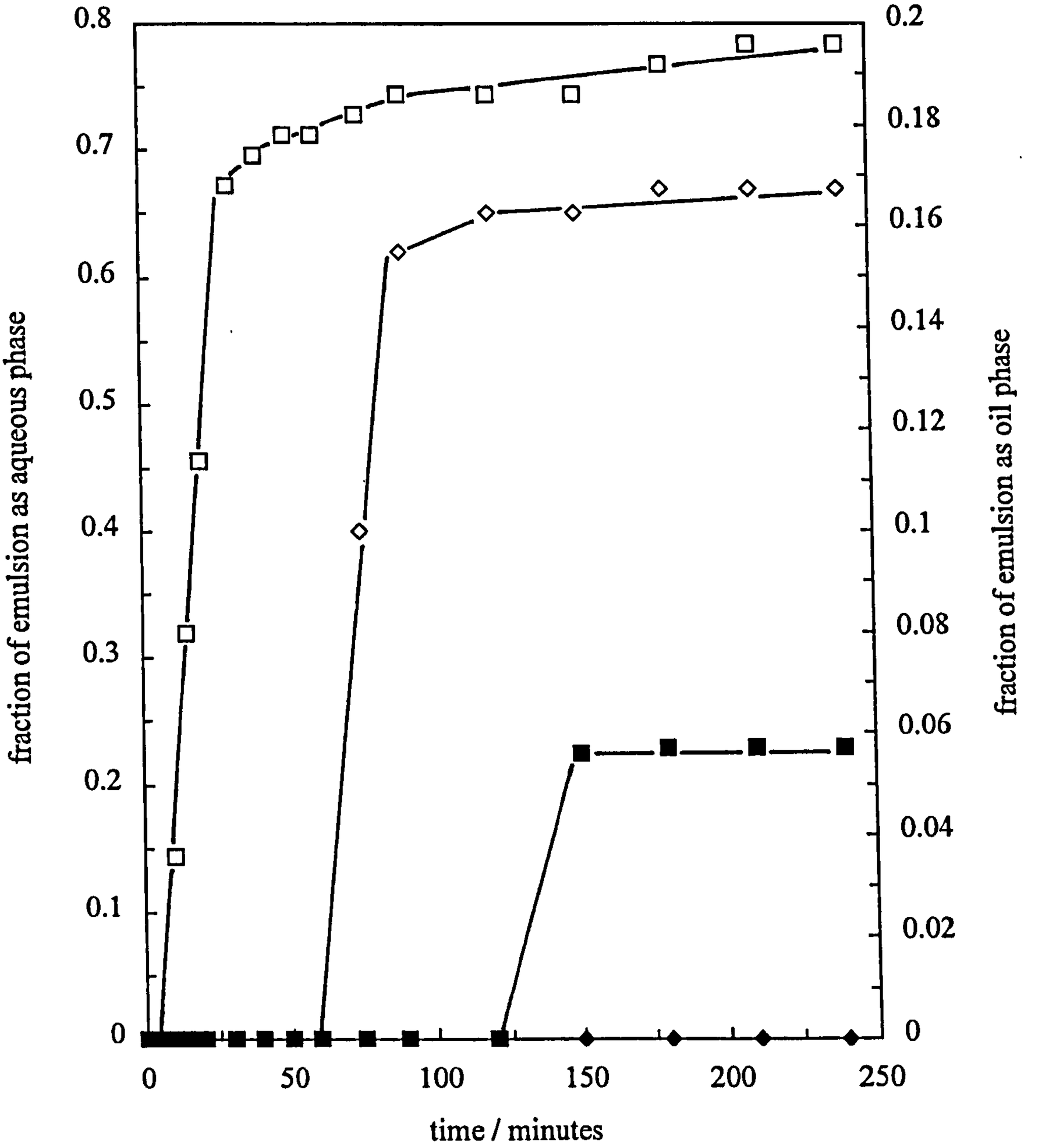

Figure 3.17

Stability to creaming (open points, left hand ordinate) and coalescence (filled points, right hand ordinate) of 20 vol% toluene-in-water emulsions stabilised by 0.5 wt.% Ludox HS-40 at pH 2. NaCl concentrations are 0.1 M (diamonds), 0.3 M (squares) and 1.0 M (triangles).

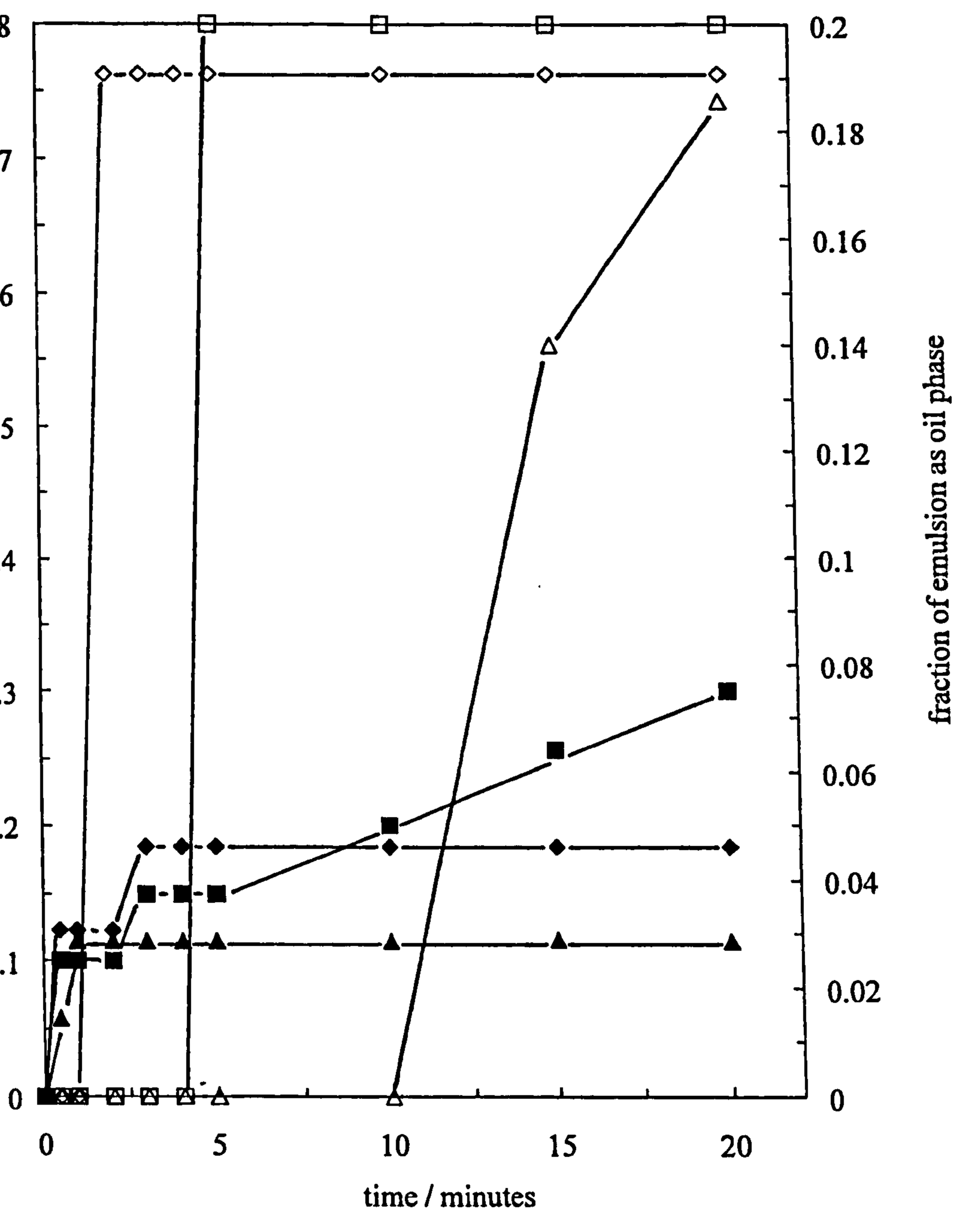

Figure 3.18

Stability to creaming (open points, left hand ordinate) and coalescence (filled points, right hand ordinate) of 20 vol% toluene-in-water emulsions stabilised by 0.5 wt.% Ludox HS-40 at pH 9. NaCl concentrations are 0.1 M (diamonds), 0.3 M (squares) and 0.7 M (triangles).

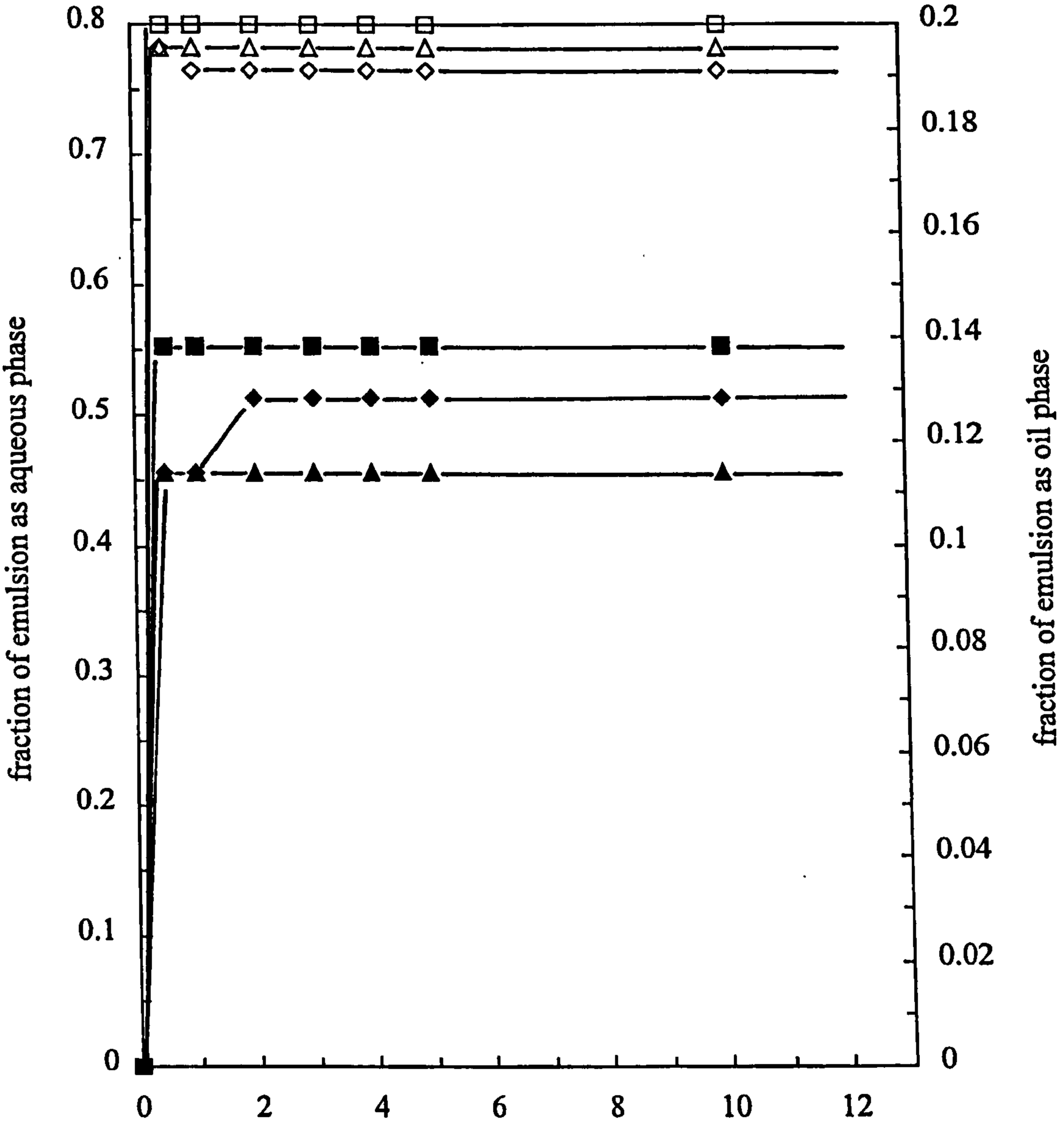

investigated further because of the possibility of surfactant being present in the liquid dispersion.

In summary, both types of silica particles exhibit anomalous DLVO behaviour in the presence of NaCl electrolyte and flocculated particles were found to be detrimental to emulsion stability.

3.3 Systems containing $LaCl_3$ electrolyte

Given the relationship between the properties of the aqueous colloid and the subsequent emulsion stability, it is of interest to vary the nature of the flocculating cation in these silica systems. The Schülze-Hardy[101, 102] rule for lyophobic colloids predicts that the critical concentration of salt required to flocculate a given colloid will be much less for a trivalent ion than a monovalent one. Addition of electrolyte causes a compression of the diffuse parts of the double layers around the particles thus reducing the double-layer repulsive interactions sufficiently to allow van der Waals forces to predominate. The concentration *c* of electrolyte required to cause flocculation of the colloid is related to the valency *z* of the electrolyte by[103]

$$c = \frac{\text{constant}}{z^6} \tag{3.31}$$

This is a simplified form of the Schulze-Hardy rule which assumes the surface potential of the particles is high. This is not strictly true as coagulation usually occurs between low potential surfaces, but this commonly used form of the equation highlights the difference between the critical flocculation concentrations of monovalent and trivalent electrolytes.

The interactions between two particles dispersed in a liquid can simply be regarded as the sum of electrostatic and van der Waals interactions as a function of particle separation (H) as described earlier in the classical DLVO treatment. A third term was added to this equation to account for the anomalous behaviour of silica particles in the presence of electrolyte. In this section, however, a different term is added to the DLVO theory to account for the electron acceptor/electron donor (or Lewis acid/base (AB)) interactions between particles dispersed in a polar medium. These

energies, whether repulsive or attractive, are commonly as much as 100 times greater than van der Waals energies and 10 times greater than electrostatic energies at short separation distances (1-5 nm).[104] The net potential energy of interaction between two colloidal particles as a function of H can now be written as

$$V_t = V_d + V_e + V_{AB} \tag{3.32}$$

where V_{AB} is the energy due to Lewis acid/base interactions. The van der Waals dispersion energy V_d, is often described as the apolar component (γ_s^d) of the surface free energy (γ_s) for a solid particle (s). The surface free energy however is the sum of the apolar component and the polar acid-base component (γ_s^{AB}).

$$\gamma_s = \gamma_s^d + \gamma_s^{AB} \tag{3.33}$$

The polar surface component (γ_s^{AB}) consists of two non-additive parameters, one for the hydrogen acceptor (γ_s^-) and one for the hydrogen donor (γ_s^+). Wu et al.[105] have obtained values for these parameters by measuring the contact angles of various liquids on a glass surface (similar to the silica used here). By analysis of the surface tension components, the energies of interaction and zeta potential measurements, these authors ascribe the stability of silica dispersions in the absence of electrolyte to acid-base repulsive interactions. This is a direct result of a large hydrogen acceptor component (γ_s^-) of the surface energy reflecting the oxygen-rich surface of silica. In the presence of the trivalent electrolyte $LaCl_3$ however, the silica particles flocculate due to an increase in the hydrophobicity of the solid surface. For example, the zeta potential of glass particles falls from –52.7 mV in pure water of pH 7.5 to –16.4 mV in the presence of 0.47 mM $LaCl_3$, whilst the contact angle at the solid/liquid/vapour interface increases from 49.4 to 65.9°. It is argued that the main effect of the La^{3+} ion is not in the screening of the negative charge on the solid but the neutralisation of the Lewis base sites on the surface, thus lowering the hydrogen acceptor value (γ_s^-) of the acid-base surface tension component. As a result attractive acid-base interactions predominate causing flocculation of the particles. Allen and Matijevic[77] have investigated the stability of Ludox HS silica in the presence of $La(NO_3)_3$ as a function of pH. The colloid remains stable (dispersed) at all electrolyte concentrations below pH 6. Above pH 6 the c.c.c.

decreases rapidly from 0.7 M $La(NO_3)_3$ to 2 x 10^{-4} M at pH 7 whereupon it remains constant.

In order to examine whether the proposed anomalous behaviour exists in the presence of $LaCl_3$ the critical coagulation concentration of Aerosil 200 silica at various pH has been investigated. The turbidities of 0.5 wt.% Aerosil 200 colloids at pH 2 and 10 are given in Figure 3.19 as a function of [$LaCl_3$] both initially and 24 hours after addition of electrolyte. The colloids were shaken prior to measurement in all cases. There is no change in turbidity at pH 2 up to 20 mM $LaCl_3$ and no phase separation was observed. This independence is due to the fact that the refractive index of the salt solution is changed by < 0.075 % in this concentration range. At pH 10, however, the turbidity increases by nearly a factor of three on addition of 20 mM $LaCl_3$ due to flocculation which occurs immediately. Concomitant with this the colloids separated into a clear, upper layer and a turbid lower layer for [$LaCl_3$] ≥ 1 mM after 24 hours. Figure 3.20 shows the turbidity changes for various pH values. No phase separation occurs between pH 2 and 4 where the turbidity remains constant. The turbidity begins to depend on [$LaCl_3$] for pH > 4 with phase separation occurring at progressively lower salt concentrations. A marked effect occurs between pH 6 and 8 similar to that seen in the presence of $La(NO_3)_3$ in ref. 77.

The effect of low concentrations of $LaCl_3$ (≤ 20 mM) on the stability of emulsions at pH 2 and 10 has been investigated. Figure 3.21 shows the stability to creaming (fraction of emulsion as aqueous phase) and coalescence (as oil phase) after 30 minutes of 20 vol% toluene-water emulsions stabilised by 0.5 wt.% Aerosil 200 at pH 2. At all [$LaCl_3$], creaming is more or less complete and coalescence is over 50 %. The resolved aqueous phase is clear blue as it was before addition of oil indicating the presence of the silica particles. At this pH (the i.e.p.) little effect of salt is anticipated in line with the findings. In contrast to low pH, the emulsion stability is highly sensitive to [$LaCl_3$] once the particles are charged. The stability to both coalescence and creaming at pH 10 shows a marked maximum at intermediate concentrations around 2-5 mM (Figure 3.22). These emulsions remained at this stability for up to 6 months. The small volume of aqueous phase resolved is colourless, implying the particles originally dispersed in the water have transferred elsewhere either into the dispersed oil phase or to the oil-water interface around the drops. Below 2 mM, rapid creaming occurs in which the resolved aqueous phase is clear blue. Above 6 mM, the resolved aqueous phase is viscous and

Figure 3.19

Turbidity of 0.5 wt.% Aerosil 200 dispersions in water at two pH values as a function of $LaCl_3$ concentration. Squares - immediately after adding $LaCl_3$; circles - 24 hours later.

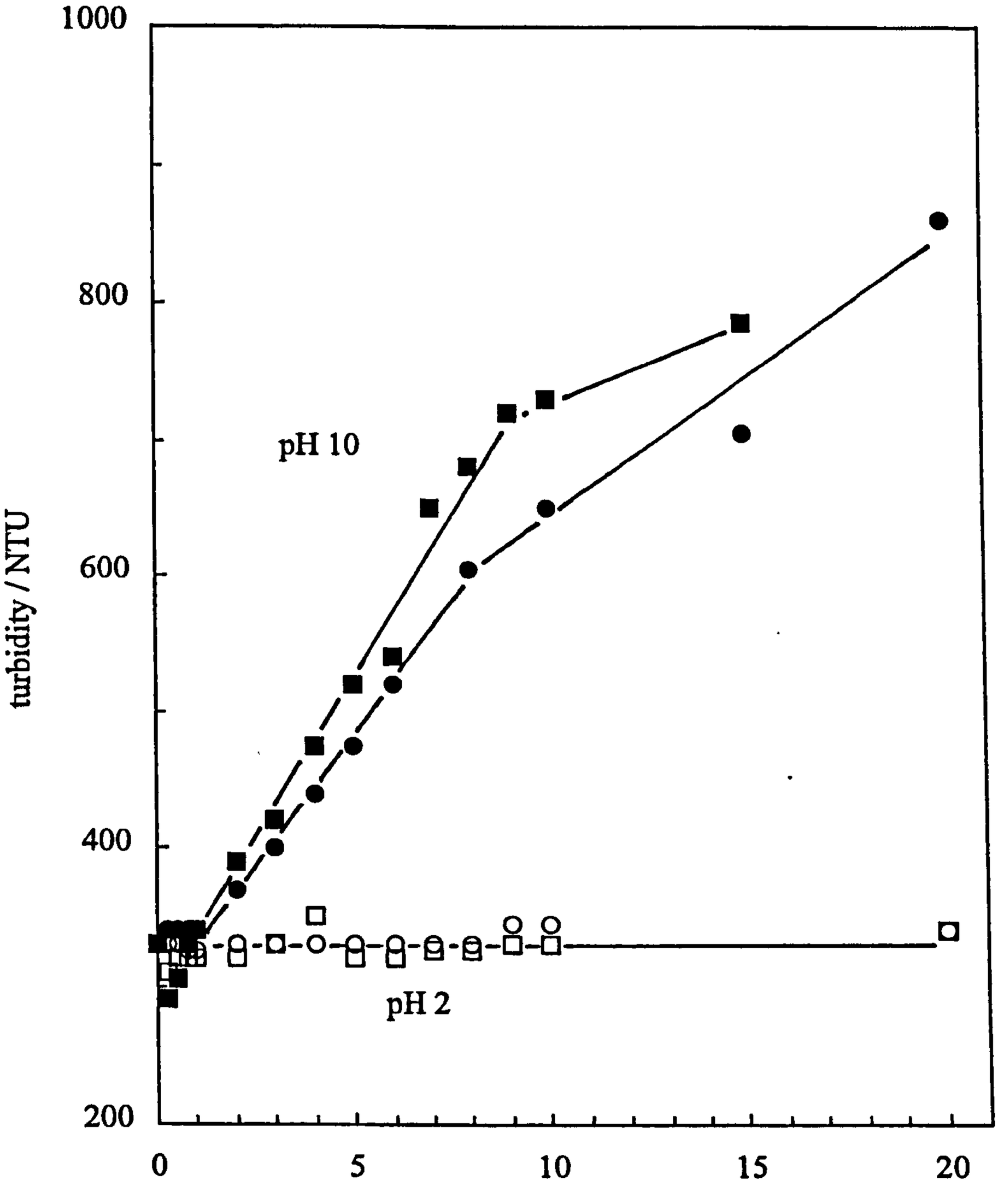

Figure 3.20

Turbidity of 0.5 wt.% Aerosil 200 dispersions in water 24 hours after adding $LaCl_3$. The pH values are 2 (open circles), 4 (open triangles), 4.5 (diamonds), 5 (filled triangles), 6 (asterisks), 8 (filled circles) and 10 (squares).

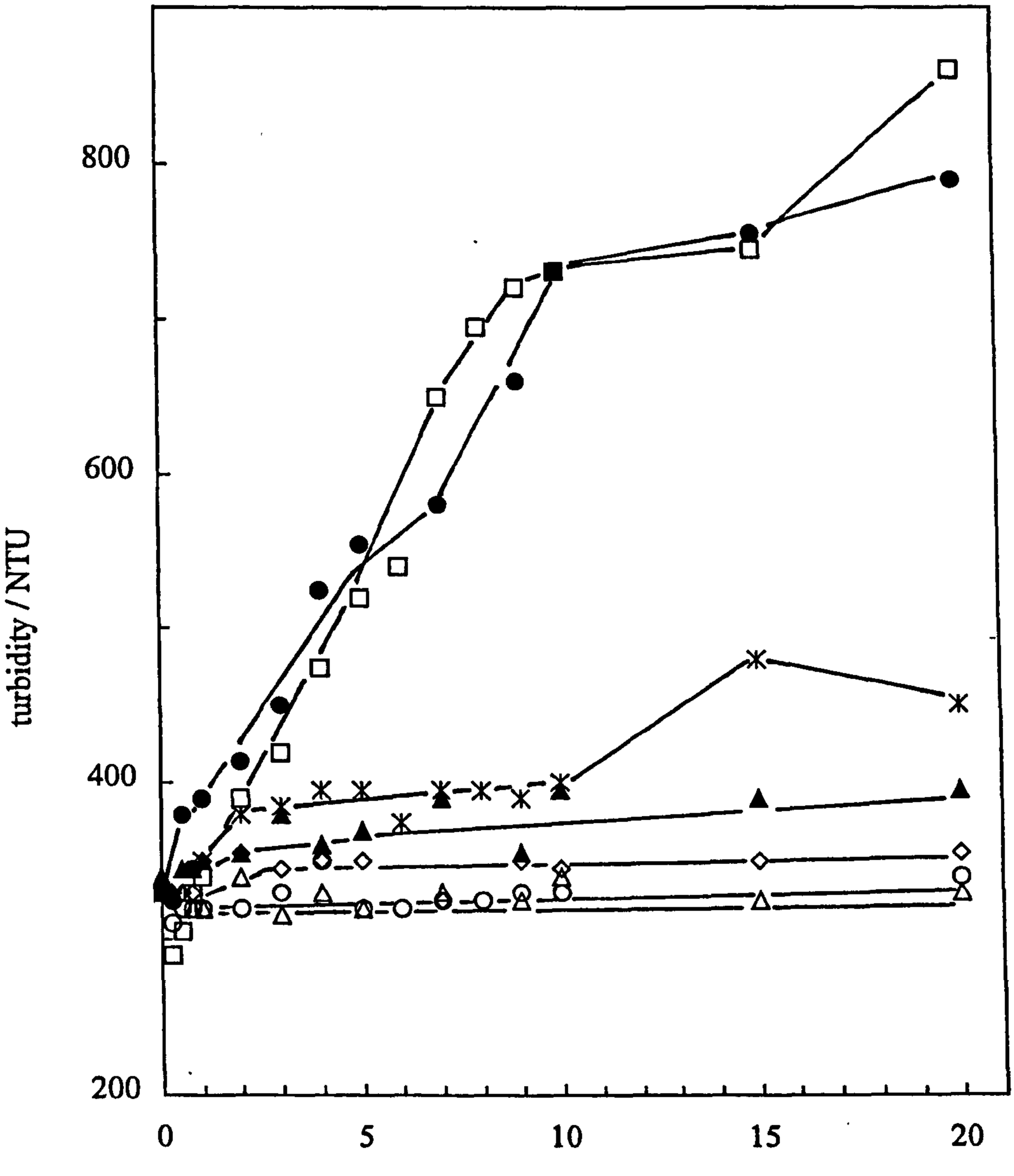

Figure 3.21

Stability to creaming (open points, left hand ordinate) and coalescence (filled points, right hand ordinate) after 30 minutes of 20 vol% toluene-in-water emulsions stabilised by 0.5 wt.% Aerosil 200 as a function of $LaCl_3$ concentration at pH 2.

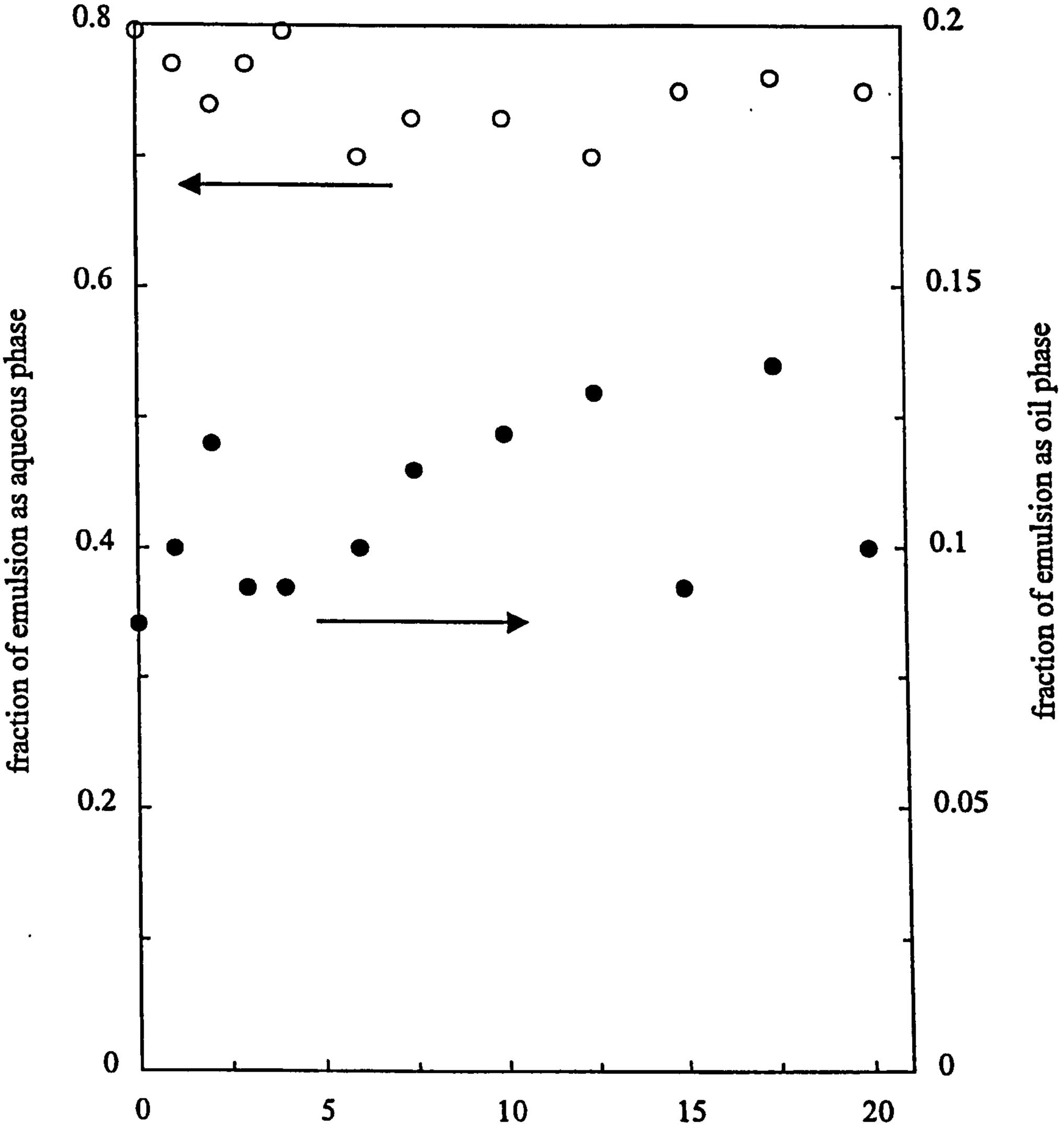

Figure 3.22

Stability to creaming (open points, left hand ordinate) and coalescence (filled points, right hand ordinate) after 30 minutes of 20 vol% toluene-in-water emulsions stabilised by 0.5 wt.% Aerosil 200 as a function of $LaCl_3$ concentration at pH 10.

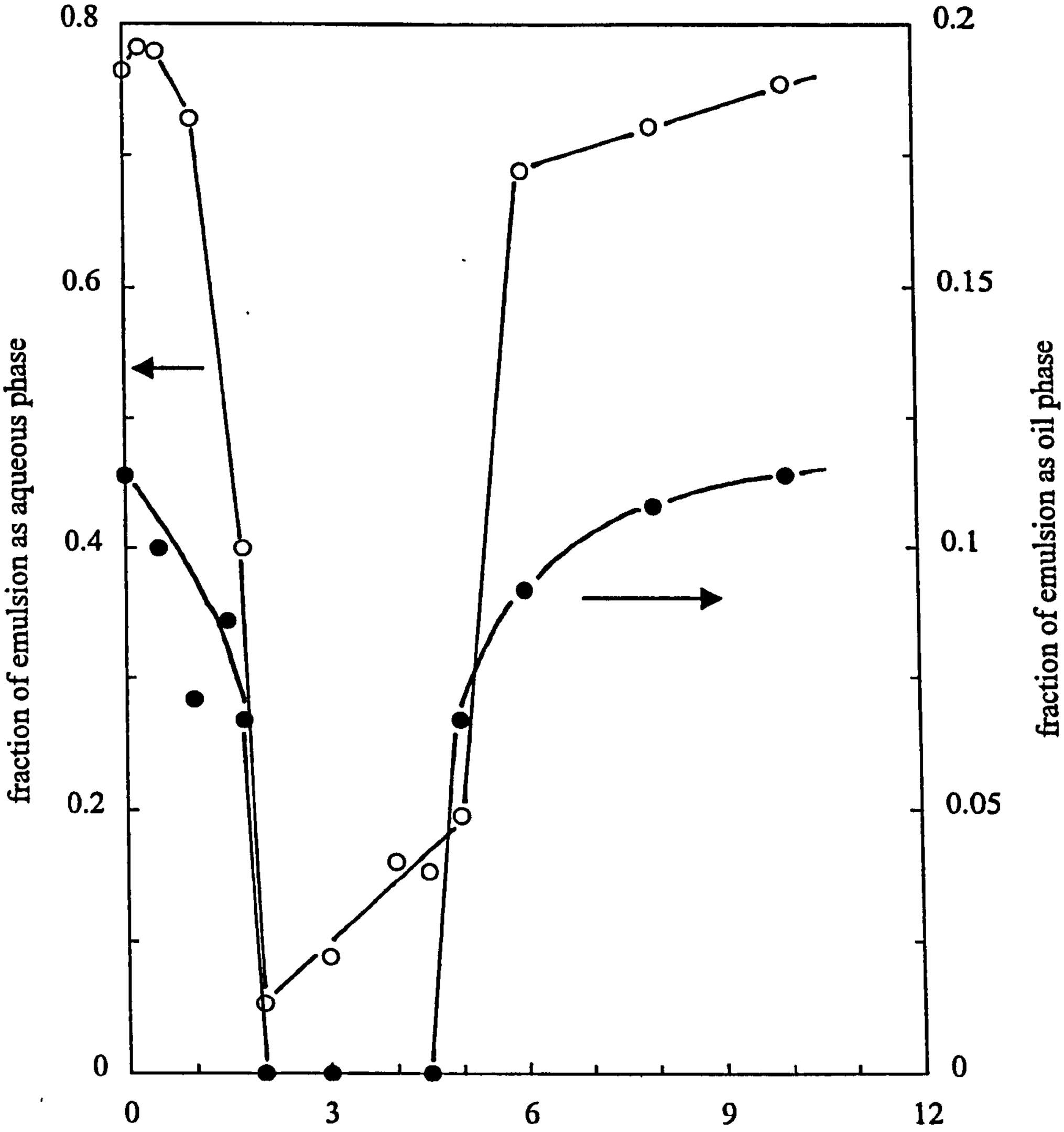

turbid and most likely contains flocculated particles. The effect of increasing pH on emulsion stability at fixed [$LaCl_3$] is shown in Figures 3.23 and 3.24. In the presence of 5 mM $LaCl_3$ (3.23), emulsions formed at pH $\leq$ 5 are unstable to creaming with more than 90 % of blue aqueous phase resolved. For pH $\geq$ 6 the low volume of aqueous phase resolved is colourless. Stability to coalescence increases progressively with pH. For 10 mM $LaCl_3$ (3.24), maximum stability to both creaming and coalescence is observed at intermediate pH (~ 6) and the sequence of observations is similar to that described earlier for increasing [$LaCl_3$] at pH 10 (Figure 3.22).

As with NaCl as electrolyte, the state of the initial aqueous colloid in the presence of $LaCl_3$ is important in dictating the final stability of emulsions. At low pH where the colloid remains dispersed the emulsions are very unstable. At pH 10, a marked increase in turbidity of the colloids occurs between 1 and 2 mM $LaCl_3$ marking the onset of flocculation. This is exactly where the stability of emulsions begins to increase markedly. Unlike with NaCl however, the appearance of flocculated particles in $LaCl_3$ containing systems initially *enhances* the emulsion stability. Further increase in the concentration of $LaCl_3$ results in *destabilisation*. It may be hypothesised that small flocs formed at low [$LaCl_3$] adsorb more readily to interfaces than dispersed particles due to their decreased affinity for the continuous phase, resulting in stabilisation, whereas at higher [$LaCl_3$] the floc size and extent may be larger and adsorption is reduced. The stabilising effect of partially flocculated silica, i.e. moderately prevalent attraction between the solid particles, agrees with the conclusions of other authors.[21, 18] Lucassen-Reynders and van den Tempel[21] described the effect of added surfactant on the stability of water-in-paraffin oil emulsions containing glycerol tristearate crystals. The crystals form a 3-D network in oil in the absence of surfactant and so do not accumulate at the oil-water interface, and hence do not stabilise emulsions. Addition of surfactant (such as AOT) decreases the interaction between the crystals resulting in partial flocculation. In this state the crystals were found to be more efficient at stabilising emulsions. Briggs[18] described the effect of flocculating agents (electrolytes) on benzene/water emulsions stabilised by hydrous ferric oxide. In the presence of NaCl, a weak flocculating agent, the particles entered the oil-water interface and hence stabilised emulsions. As the concentration of NaCl was increased the emulsion stability increased. However, in the presence of sodium sulphate, which was described as a strong flocculating agent, no emulsions were formed and large flocs of

Figure 3.23

Stability to creaming (open points, left hand ordinate) and coalescence (filled points, right hand ordinate) after 30 minutes of 20 vol% toluene-in-water emulsions stabilised by 0.5 wt.% Aerosil 200 in 5 mM $LaCl_3$ as a function of pH.

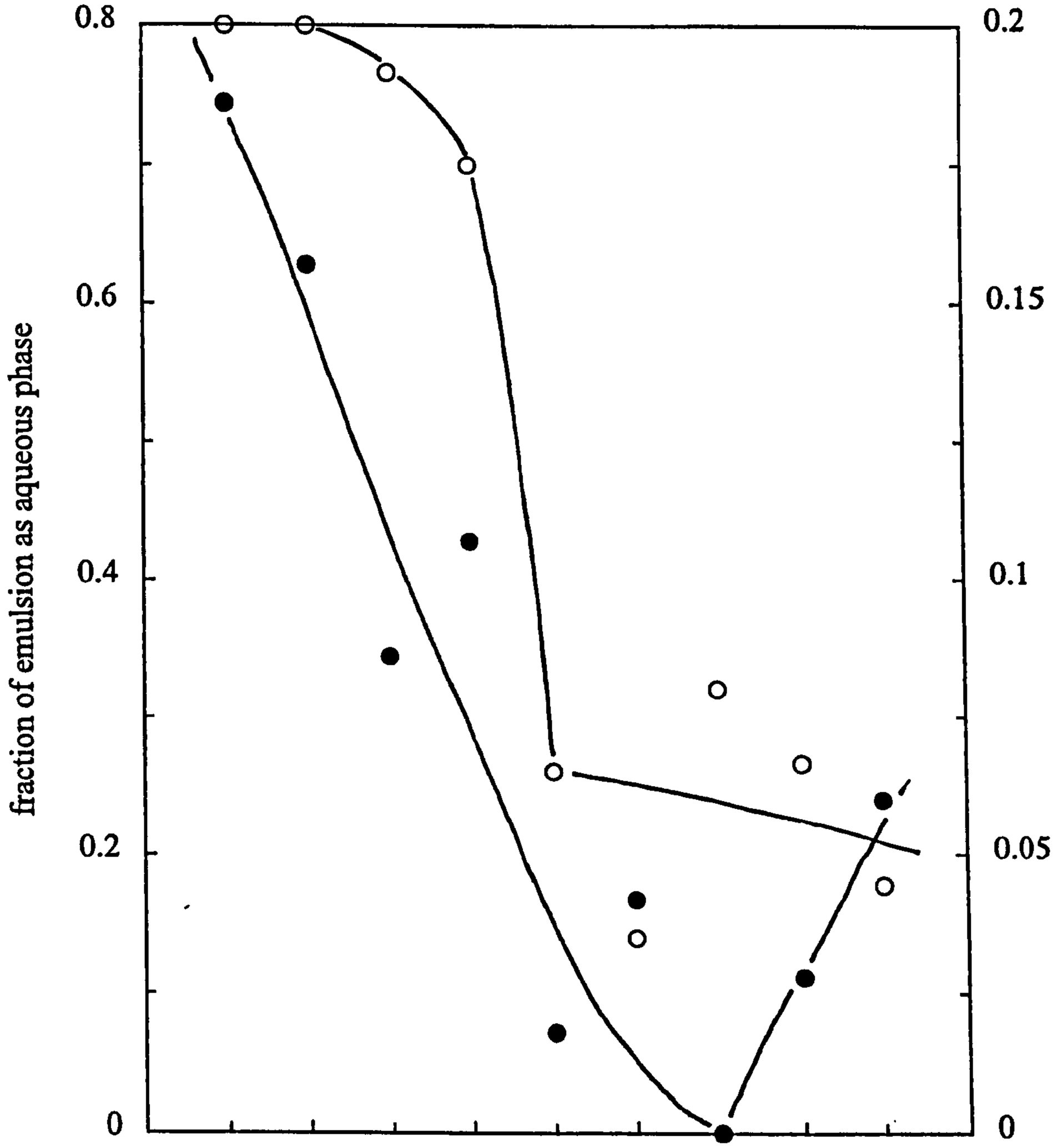

Figure 3.24

Stability to creaming (open points, left hand ordinate) and coalescence (filled points, right hand ordinate) after 30 minutes of 20 vol% toluene-in-water emulsions stabilised by 0.5 wt.% Aerosil 200 in 10 mM $LaCl_3$ as a function of pH.

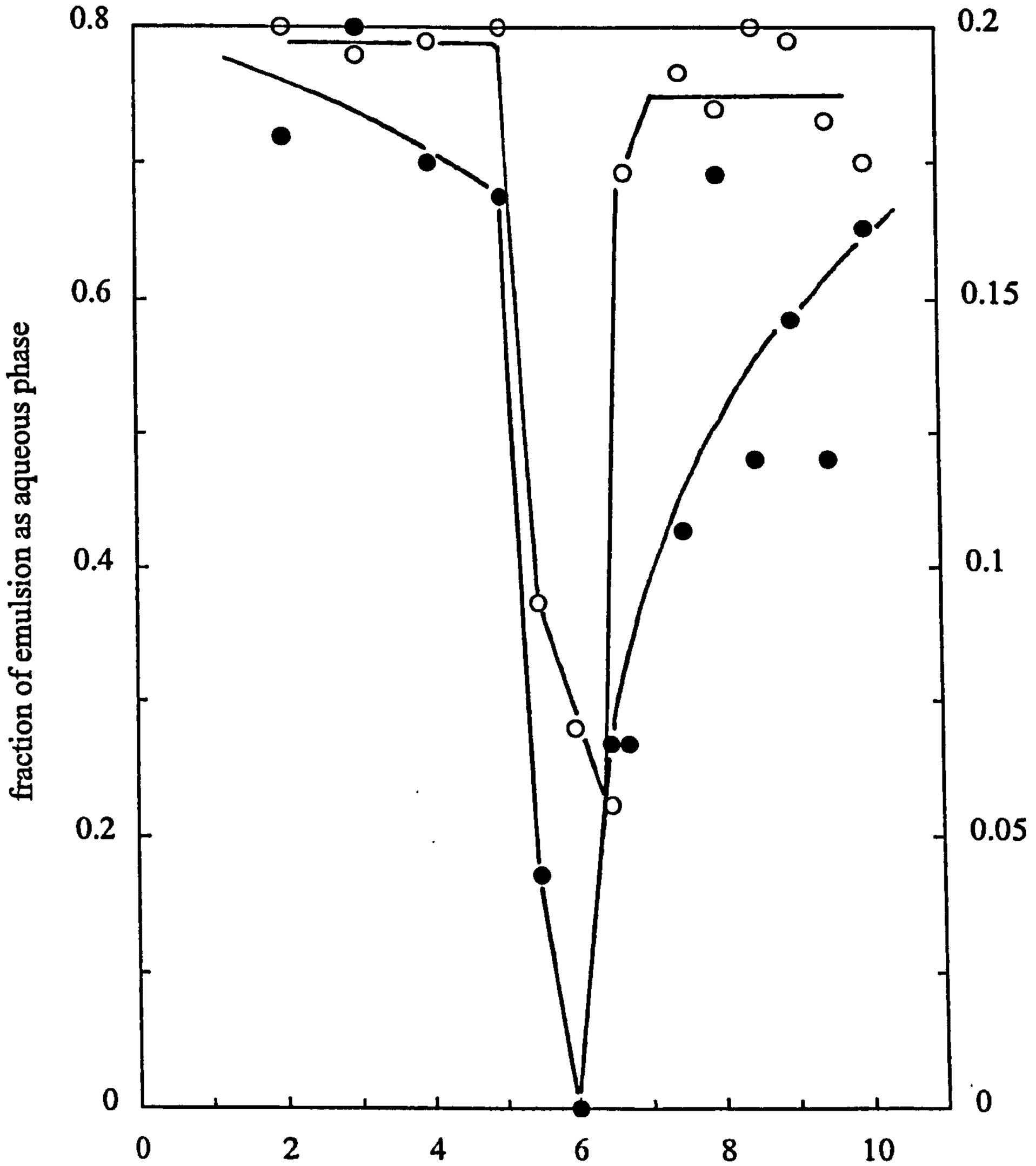

ferric oxide were observed in the aqueous phase. In the work described in this chapter the c.c.c. decreases with pH, hence inducing flocculation by either an increase in [$LaCl_3$] at fixed pH or an increase in pH at fixed [$LaCl_3$] has the same effect.

Figure 3.25 shows the initial emulsion drop diameters as a function of [$LaCl_3$] at pH 2 and 10. The median diameter, d(v,0.5), of 78 μm is reasonably large and independent of salt concentration at pH 2. As shown earlier, these large drops cream rapidly at a rate also independent of salt concentration (Figure 3.21). The polydispersity of these emulsions is fairly high, with a span of 0.75 seen visually in the optical microscopy images at 1, 5 and 10 mM $LaCl_3$ (Figure 3.26) taken immediately after homogenisation. At pH 10 however, the median drop diameters are considerably smaller and pass through a minimum value of 42 μm between 2 and 3 mM $LaCl_3$, increasing by a factor two at higher salt concentrations. The minimum position corresponds closely to that for which emulsions are most stable (Figure 3.27). The optical microscopy images in Figure 3.26 at pH 10 indicate some degree of flocculation of emulsion drops at 5 mM $LaCl_3$. This may enhance the stability by forming a network of drops enclosing the continuous phase. Since the velocity of creaming depends on the square of the drop radius[3] the rate of creaming is reduced for these smaller sized emulsions. Figure 3.28 shows the conductivity of the aqueous colloids and emulsions as a function of [$LaCl_3$]. The conductivity of the aqueous colloid remains approximately two times that of the emulsion at all [$LaCl_3$]. It is clear that the emulsions remain water continuous at all [$LaCl_3$] at pH 6 despite the fact that the particles appear to leave the aqueous phase and the suggestion by Wu et al.[105] that $LaCl_3$ causes the solid to become more hydrophobic.

3.4 Systems containing TEAB electrolyte

In previous sections, non-adsorbing, indifferent electrolytes, which reduce the Debye length and the potential of the surface without changing the surface charge, have been used to coagulate silica particles. The relationship between the flocculation of the aqueous colloid and emulsion stability has been investigated further with tetraethylammonium bromide (TEAB) as electrolyte. In contrast to the previous systems, one of the ions in TEAB may preferentially adsorb at the particle surface altering both the surface charge and potential. Such ions are potential determining ions

Figure 3.25

Effect of $LaCl_3$ concentration on the initial volume average diameter of 20 vol% toluene-in-water emulsions stabilised by 0.5 wt.% Aerosil 200 at pH 2 (open points) and 10 (filled points).

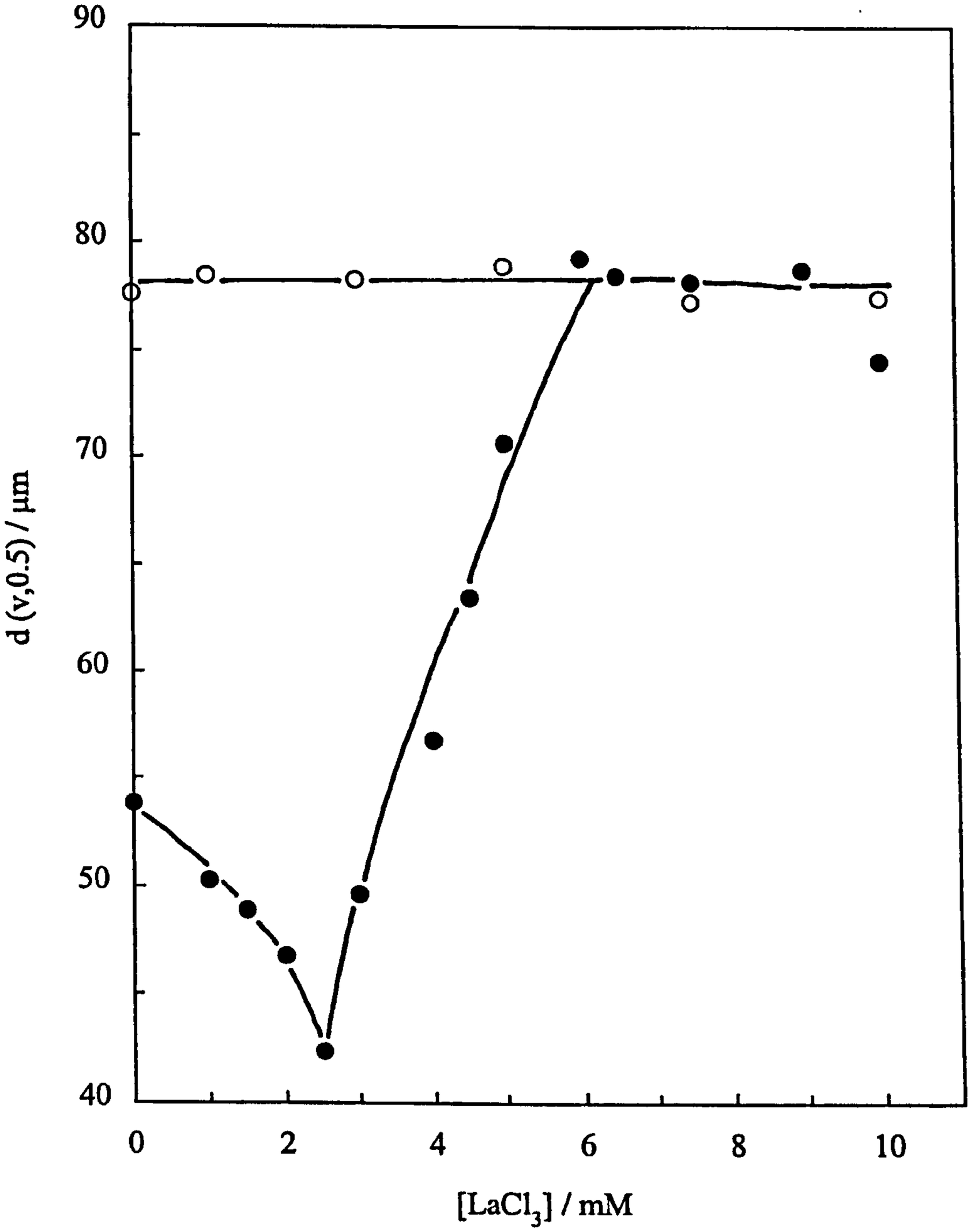

Figure 3.26

Optical microscopy images of 20 vol% toluene-in-water emulsions stabilised by 0.5 wt.% Aerosil 200 at pH 2 and 10 as a function of $LaCl_3$. Scale bar equals 200 μm.

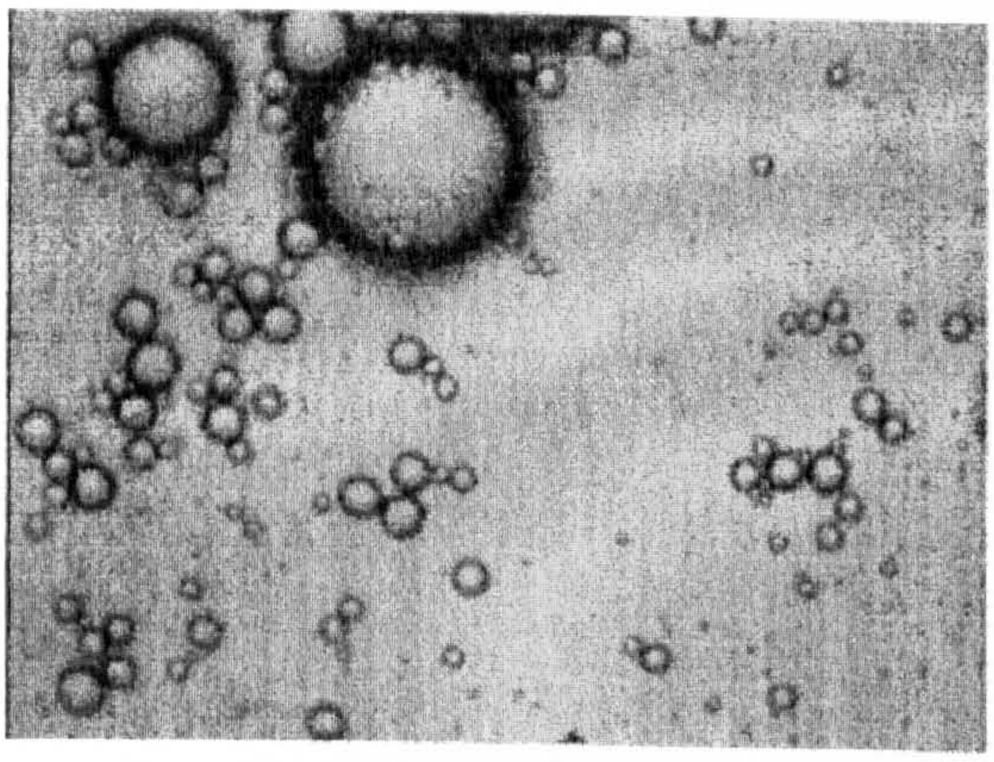

pH 2, 1 mM $LaCl_3$

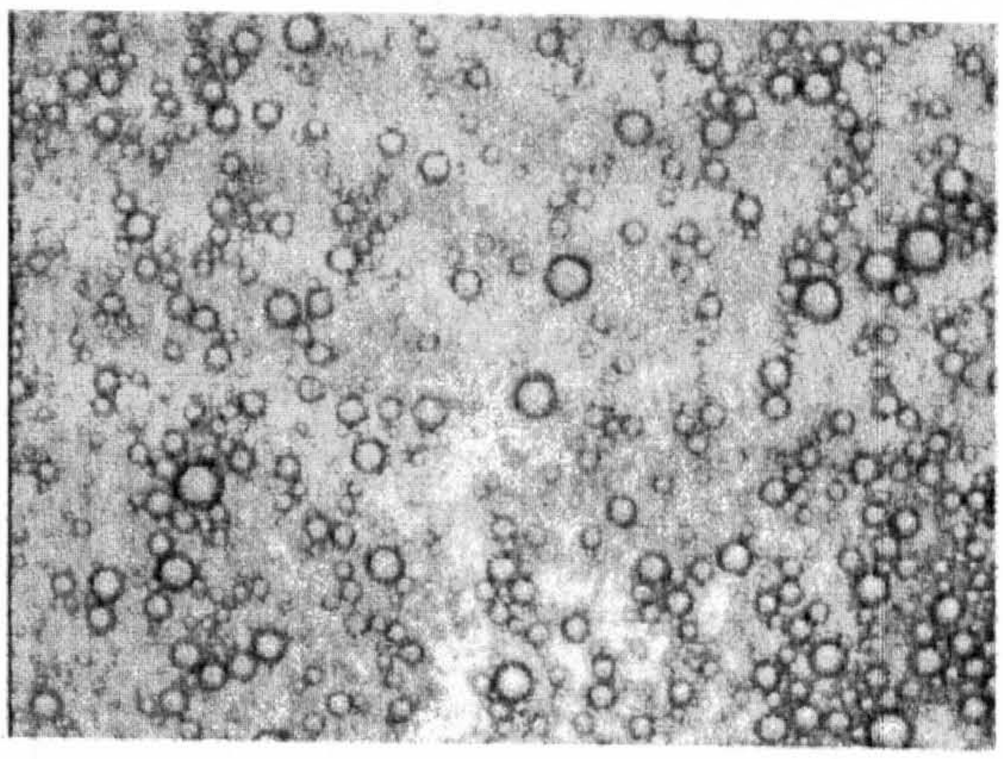

pH 10, 1 mM $LaCl_3$

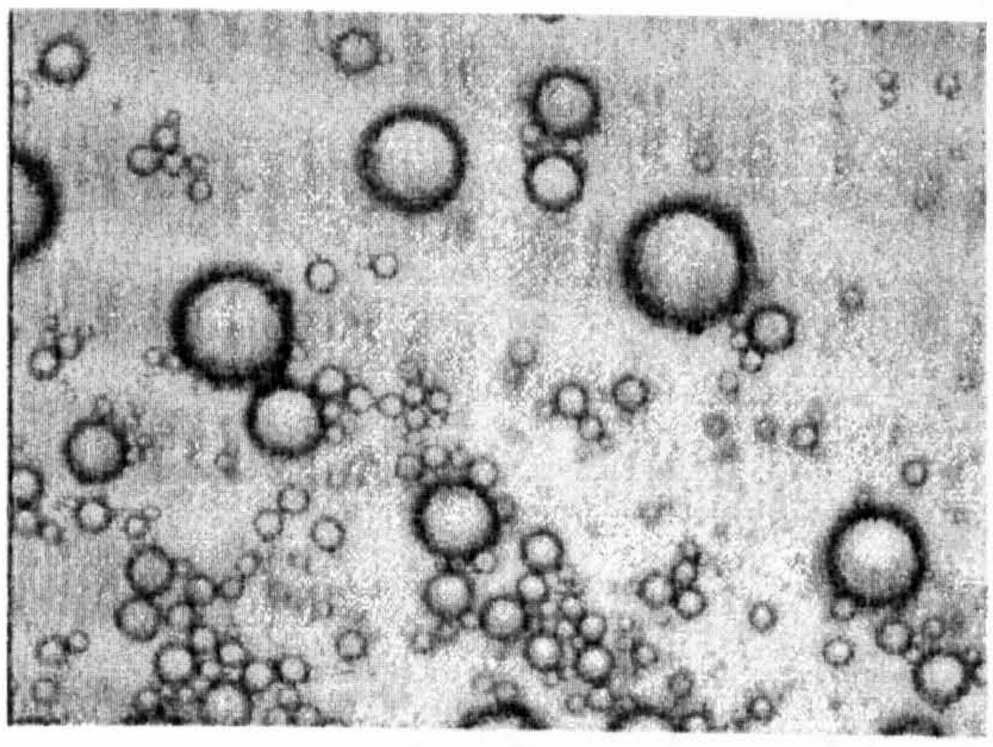

pH 2, 5 mM $LaCl_3$

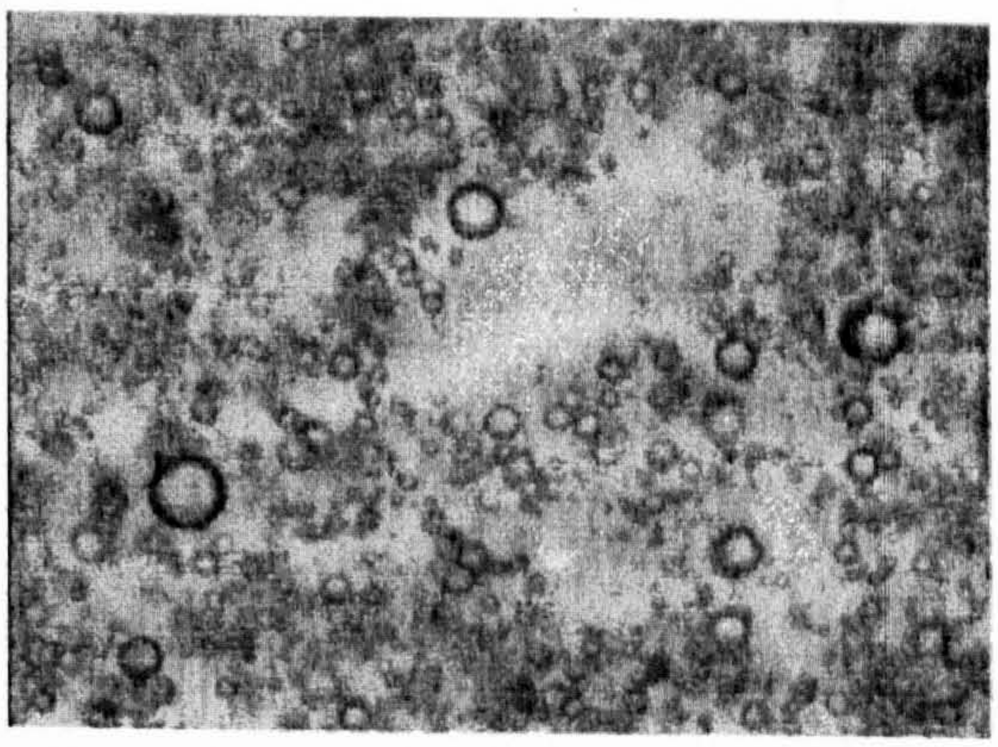

pH 10, 5 mM $LaCl_3$

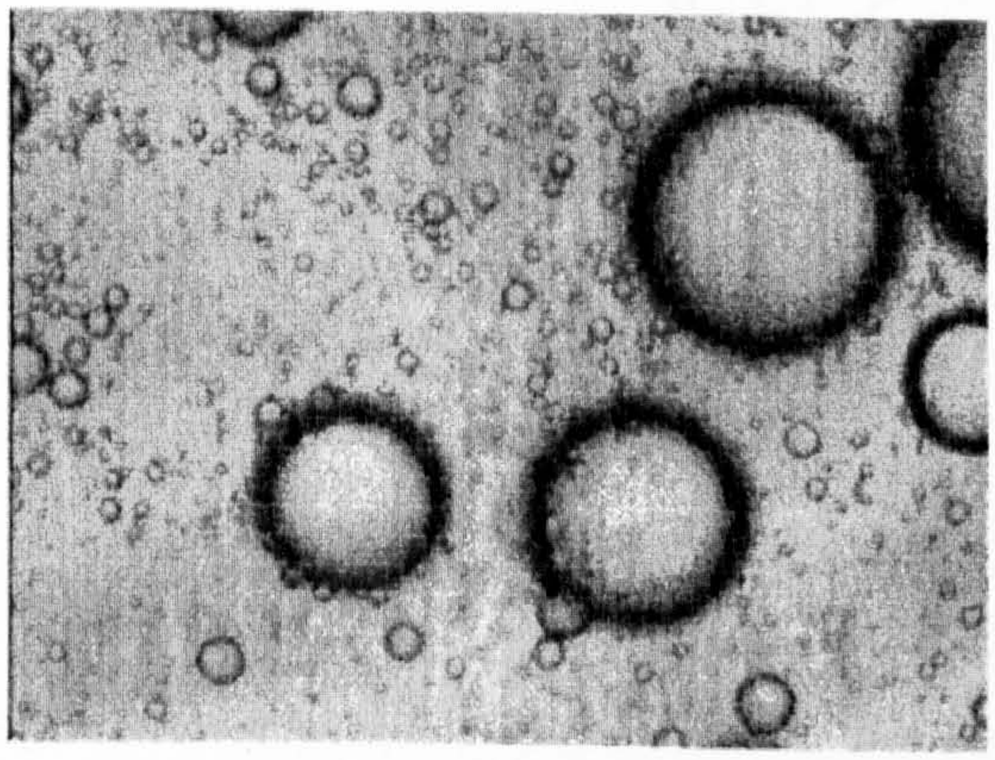

pH 2, 10 mM $LaCl_3$

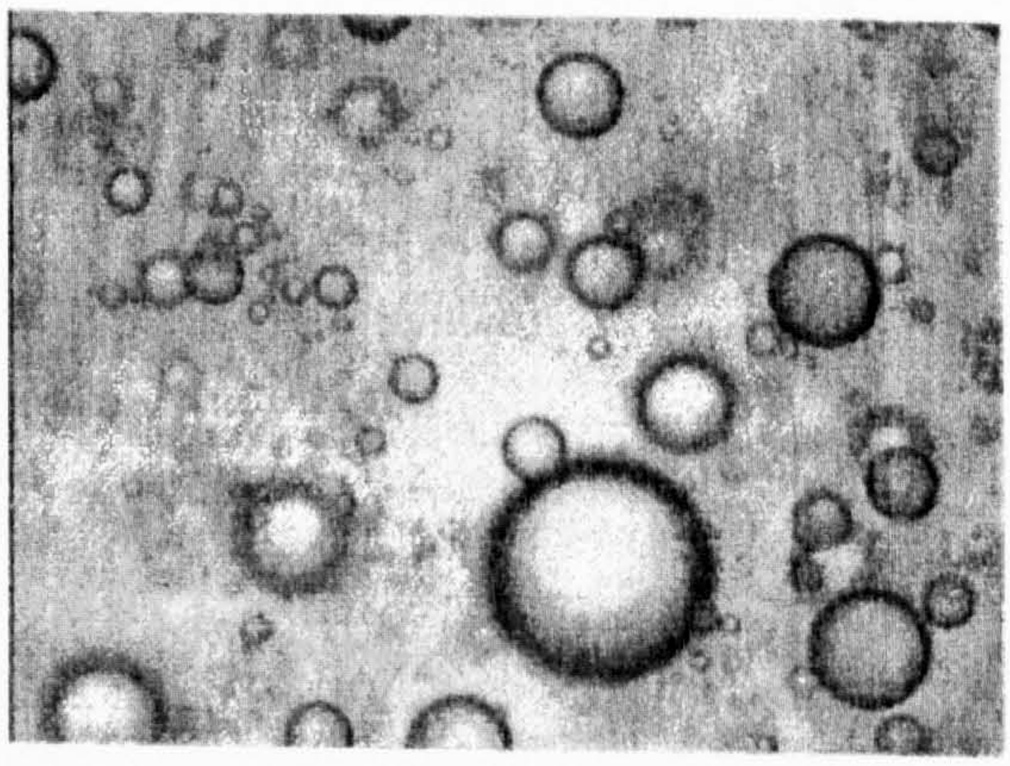

pH 10, 10 mM $LaCl_3$

Figure 3.27

Effect of $LaCl_3$ concentration on the initial volume average diameter (filled points, left hand ordinate) and stability to creaming (open points, right hand ordinate) of 20 vol% toluene-in-water emulsions stabilised by 0.5 wt.% Aerosil 200 at pH 10.

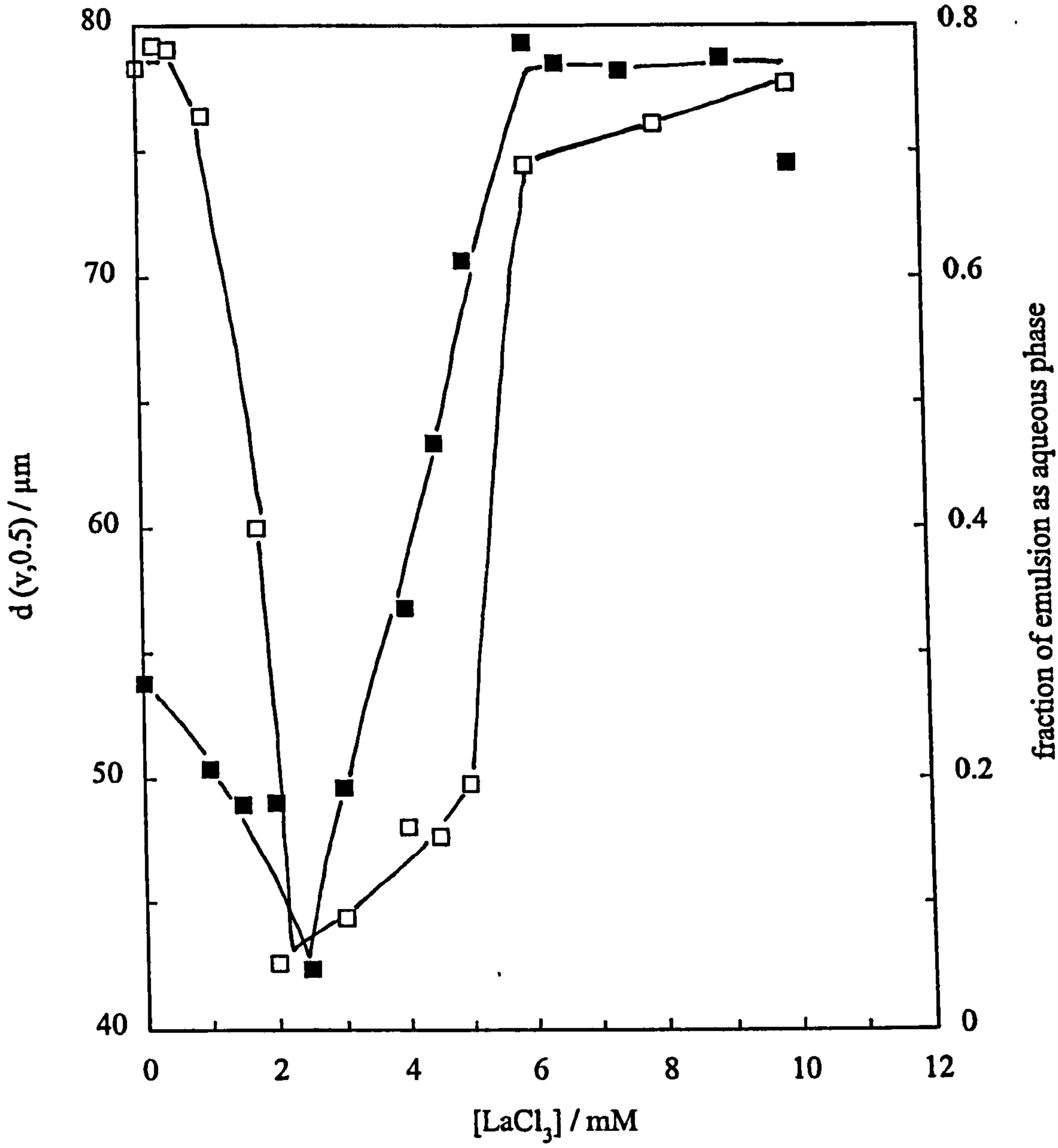

Figure 3.28

Conductivity of 0.5 wt.% Aerosil 200 dispersions in water (diamonds) and 50 vol% toluene-in-water emulsions stabilised by 0.5 wt.% Aerosil 200 (squares) at pH 6 as a function of $LaCl_3$ concentration.

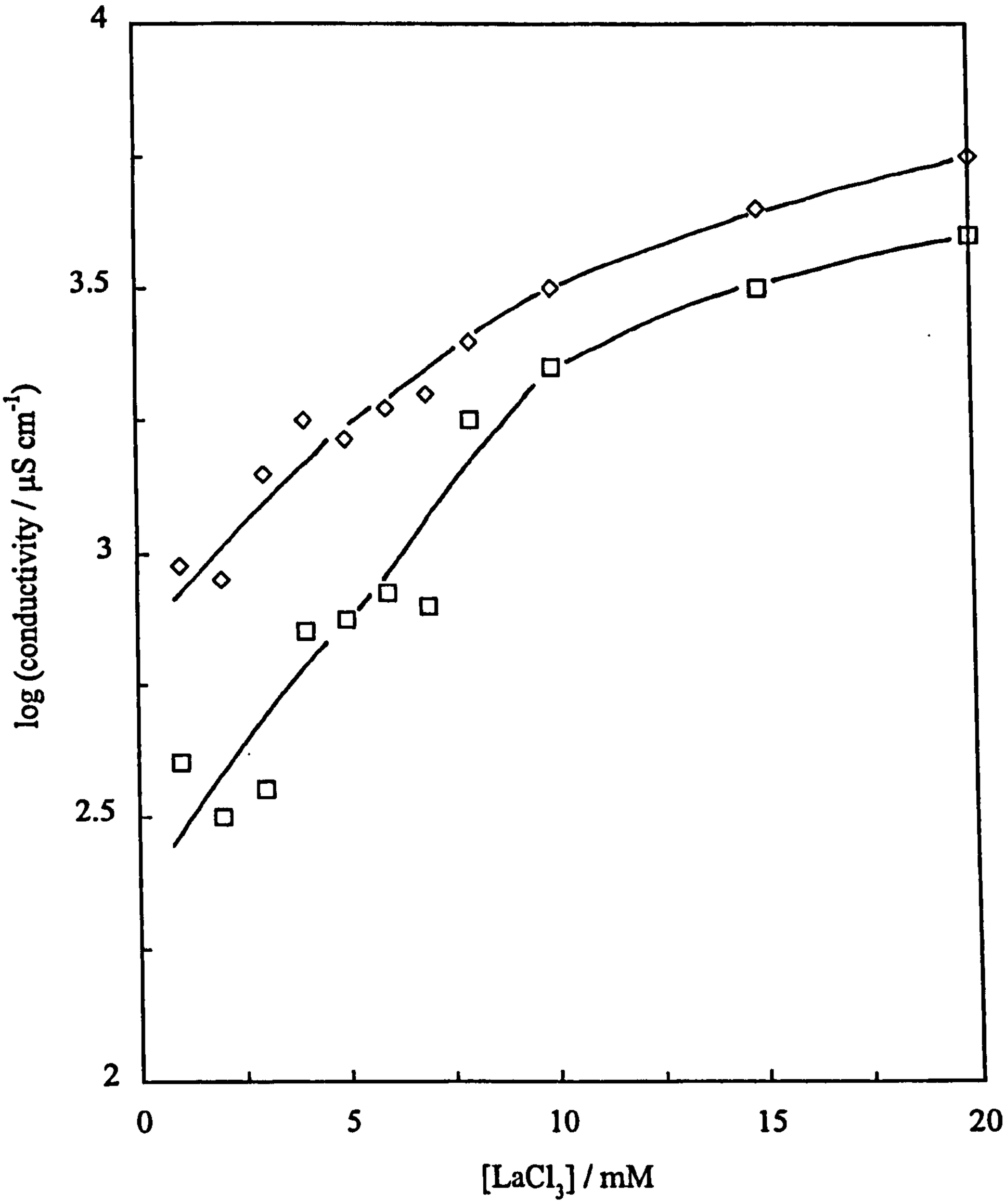

when they alter the i.e.p. of a colloid. The i.e.p. of Aerosil silica has been shown to increase to pH 5 in the presence of 0.01 M TEAB.[106] Short chain symmetrical quaternary ammonium salts like TEAB cause charged silica to flocculate when added at low concentrations but restabilise the colloid at high concentrations.[79] These authors attribute the restabilisation phenomena to the formation of a bilayer of TEAB. The electrolyte adsorbs onto the surface via the N^+ cation rendering the particle partially hydrophobic due to the exposed alkyl chains. Flocculation takes place due to hydrophobic bonding between alkyl chains. The silica is redispersed by adsorption of a second layer of TEAB with the cation (N^+) now exposed to water causing repulsion between particles. However, Claesson et al.[107] have shown that only one layer of symmetrical quaternary ions can adsorb onto a mica surface which suggests that the formation of a bilayer is unlikely. A more plausible explanation was proposed by Rutland and Pashley,[66] who investigated the zeta potentials of monodisperse colloidal silica as a function of pH and as a function of the concentration of various symmetrical quaternary ammonium ions in aqueous solution. These authors describe a site-binding model to explain the dispersion-flocculation-redispersion behaviour of silica in the presence of TEAB. Due to their hydrophobic character, TEA^+ ions can adsorb onto neutral, undissociated silanol groups without displacing hydrated protons in addition to adsorbing directly onto negative, dissociated sites in competition with protons. At low concentrations of TEAB, 'hydrophobic' adsorption is greater than direct adsorption resulting in a slight decrease in the surface charge density (σ_c). As the concentration increases, σ_c remains constant since adsorbed TEA^+ ions begin to displace protons. Eventually the surface becomes covered with TEA^+ ions and thereafter the effect of increasing [TEAB] is equivalent to increasing the concentration of indifferent electrolyte, i.e. σ_c increases with concentration leading to restabilisation of the dispersion.

(a) Aqueous colloids and emulsions at pH 2 and 10

Figure 3.29 shows the turbidity of aqueous silica dispersions as a function of [TEAB] at pH 2 and 10. The turbidity remains constant up to 0.3 M TEAB for both pH values. It then begins to decrease at higher salt, which can be attributed to an increase in the refractive index of the solution as described earlier for NaCl solutions. The

Figure 3.29

Turbidity of 0.5 wt.% Aerosil 200 dispersions in water 24 hours after adding TEAB. The pH values are 2 (circles) and 10 (triangles).

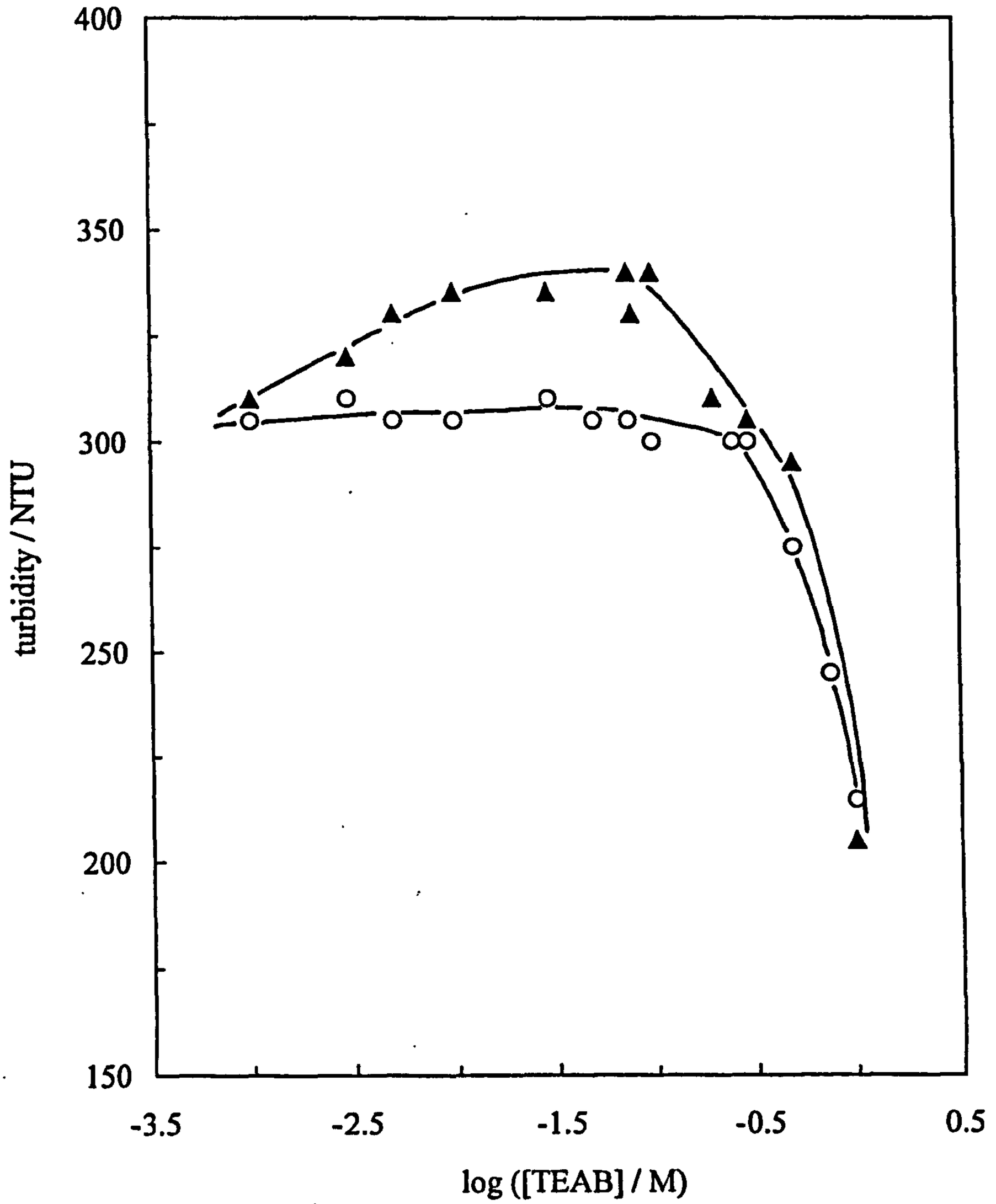

dispersions remain clear blue at both pH up to 1 M TEAB and hence no flocculation is observed. Figure 3.30 shows the stability of o/w emulsions prepared from the stable silica dispersions at pH 2 and 10. Emulsions were unstable to creaming at all [TEAB] at pH 2 with the resolved aqueous phase resembling the initial blue colloid. The remaining cream was stable to coalescence and large (mm) oil drops were visible. The instability of these emulsions is due to the lack of adsorption of TEA^+ ions onto silica at this pH, consistent with an increase in the i.e.p. of silica to around pH 5 in 0.01 M TEAB rendering the surface positively charged.[106] At pH 10, the emulsions are extremely unstable to creaming and coalescence with no emulsion phase remaining after 5 minutes at all concentrations. Here, adsorption of TEA^+ occurs on the high negatively charged silica as a monolayer and the reason for the instability is possibly due to the van der Waals attraction between alkyl chains coating the outer surface of the drops, leading ultimately to coalescence. Optical microscopy images of emulsion drops in the presence of TEAB at pH 2 are shown in Figure 3.31. The drops are dispersed and are of relatively large size, ranging from 50 – 100 μm in diameter. In summary, at both pH 2 and 10, the dispersed silica forms emulsions which are unstable to creaming in the presence of TEAB.

(b) Aqueous colloids and emulsions at pH 6

According to Rubio and Goldfarb,[79] aqueous silica dispersions are flocculated at intermediate pH in the presence of TEAB electrolyte due to hydrophobic bonding between alkyl chains. Figure 3.32 shows the variation in turbidity as a function of [TEAB] at pH 6. The turbidity increases by a factor 1.5 at ~0.003 M TEAB, remains constant to 0.07 M and then decreases to values at high salt recorded at pH 2 and 10. Visual observations of the dispersions across the salt concentration range studied are shown in Figure 3.32. The silica has a clear blue appearance at low [TEAB] where it is dispersed. Phase separation occurs between 0.003 and 0.6 M when the silica is flocculated and a colourless aqueous phase is present above the turbid white silica. Above 0.7 M TEAB, the silica is re-dispersed and the clear blue appearance is recovered. The extent of phase separation is shown in Figure 3.33 alongside the turbidity of the dispersions. The height of colourless aqueous phase resolved is zero when the silica is dispersed at low and high concentrations of TEAB but increases to a maximum of 2.5 cm when the silica is highly flocculated. The critical concentrations of

Figure 3.30

Stability to creaming after 30 minutes of 20 vol% toluene-in-water emulsions stabilised by 0.5 wt.% Aerosil 200 as a function of TEAB concentration. The pH values are 2 (circles) and 10 (triangles).

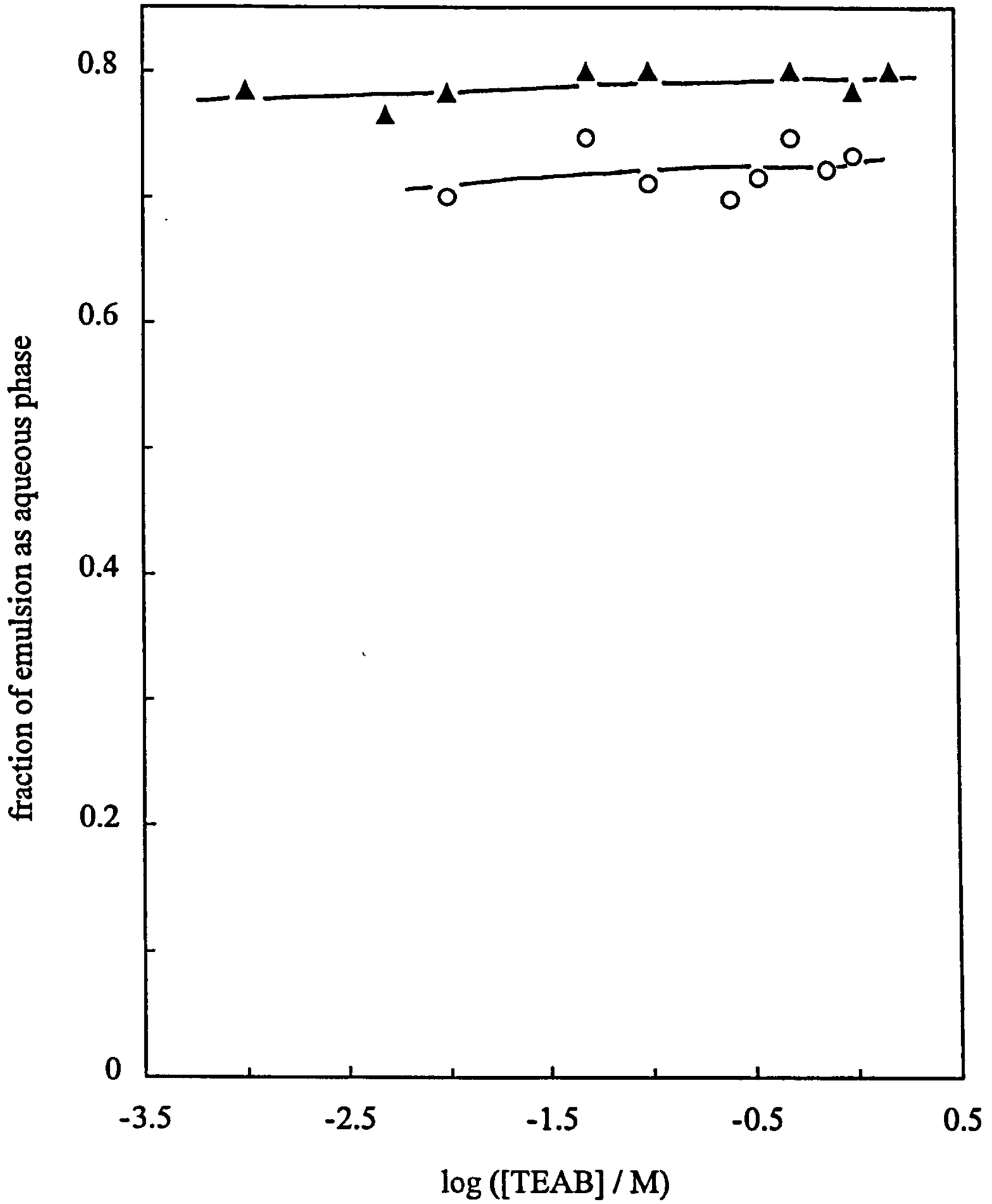

Figure 3.31

Optical microscopy images of 20 vol% toluene-in-water emulsions stabilised by 0.5 wt.% Aerosil 200 as a function of TEAB concentration at pH 2. Scale bar equals 500 μm.

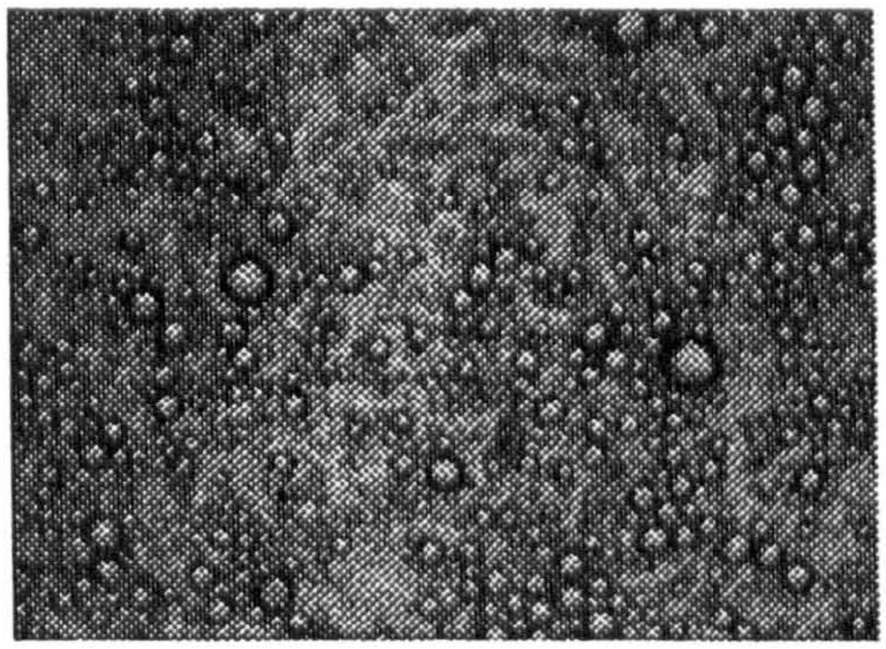

0.01 M TEAB

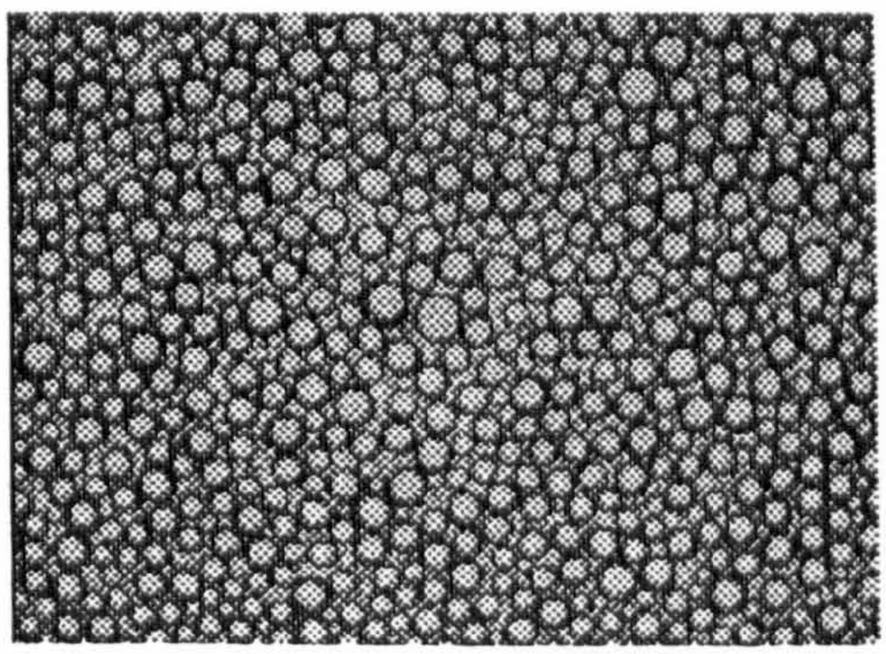

0.05 M TEAB

Figure 3.32

Turbidity of 0.5 wt.% Aerosil 200 dispersions in water 24 hours after adding TEAB at pH 6. The tubes show the visual appearance of the colloids.

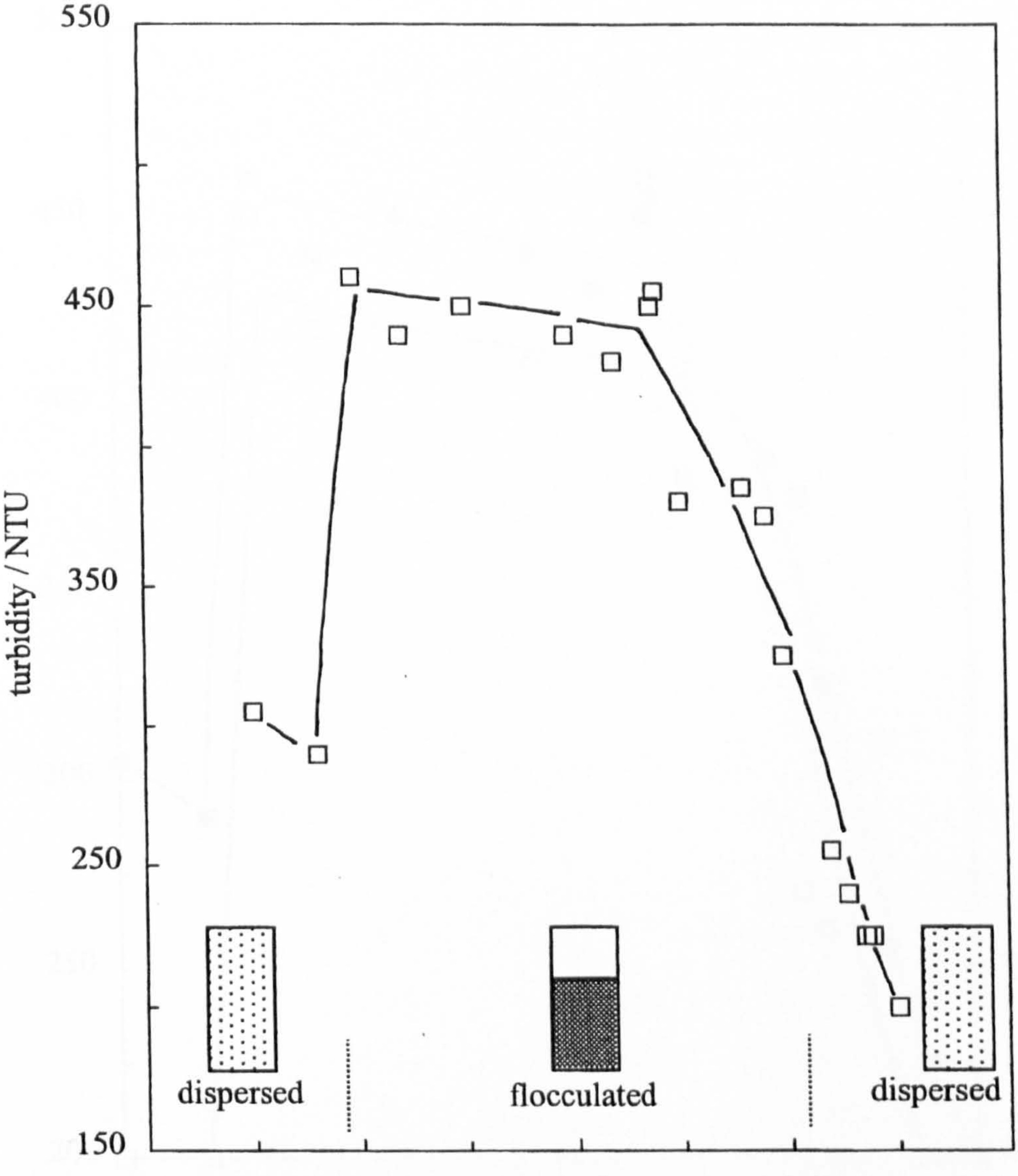

Figure 3.33

Turbidity (filled points, left hand ordinate) and height of resolved aqueous phase (open points, right hand ordinate) of 0.5 wt.% Aerosil 200 dispersions in water 24 hours after adding TEAB at pH 6.

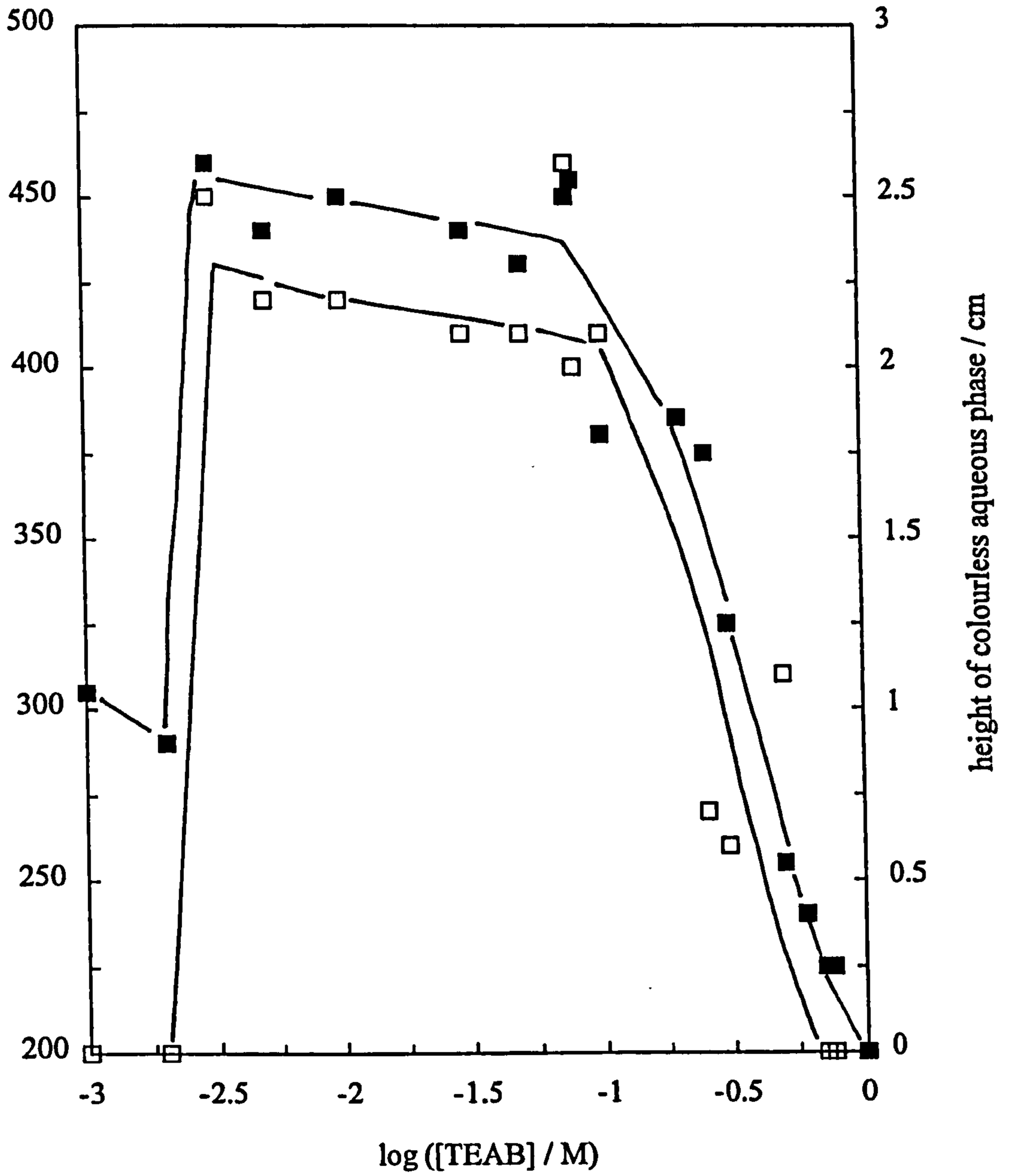

TEAB where flocculation occurs are in good agreement with those of Rubio and Goldfarb.[79]

It is of interest to investigate silica-stabilised emulsions in the presence of TEAB at pH 6 too see how the interesting colloidal behaviour affects the stability. All the emulsions were completely stable to coalescence but Figure 3.34 shows how the stability to creaming is highly dependent on [TEAB]. At 0.001 M TEAB, almost 90 % of the blue aqueous phase is resolved within 30 minutes. The volume of aqueous phase resolved decreases as the concentration increases to 0.005 M, and remains very low (i.e. stable emulsion) up to 0.5 M TEAB. The small amount of aqueous phase resolved is colourless in this range indicating that the flocculated particles are incorporated in the creamy white emulsion. Remarkably, emulsions at this TEAB are completely stable for at least 3 months. The stability decreases at higher [TEAB] and above 0.3 M the resolved aqueous phase is viscous and turbid. By 1.0 M, the aqueous phase is clear blue again. Figure 3.35 shows how flocculation of the aqueous colloid occurs in the same salt concentration range as the maximum stability of the emulsions. As the colloid becomes more flocculated the emulsion becomes less stable. This is similar to the behaviour seen in $LaCl_3$ systems. The dispersed colloid at low and high [TEAB] is again poor at stabilising emulsions as it was at low and high pH.

The variation in average emulsion drop diameter at pH 6 is shown in Figure 3.36. A marked minimum in the drop size is seen at intermediate salt concentrations, which parallels the increase in the stability to creaming although the curve is shifted to slightly higher salt concentrations. The optical microscopy images in Figure 3.37 reveal some changes in the structure of the emulsions not evident from the drop size measurements. At low (0.002 M) and high ($\geq$ 0.3 M) salt concentrations, emulsion drops are dispersed as individual entities and of relatively large size. Drop flocculation takes place from 0.005 M, with its degree increasing to 0.05 M and then decreasing again. The highly flocculated emulsion is very stable and flocs can be seen separated by areas of drop-free continuous phase, resembling the situation seen for surfactant-stabilised emulsions depletion flocculated by non-adsorbing micelles.[108] The conductivity of the aqueous colloids and emulsions shown in Figure 3.38 again indicates that the emulsions remain of the o/w type at all [TEAB] at pH 6.

Figure 3.34

Stability to creaming after 30 minutes of 20 vol% toluene-in-water emulsions stabilised by 0.5 wt.% Aerosil 200 as a function of TEAB concentration at pH 6. The dotted lines mark the onset and limit of the flocculated colloid region at pH 6.

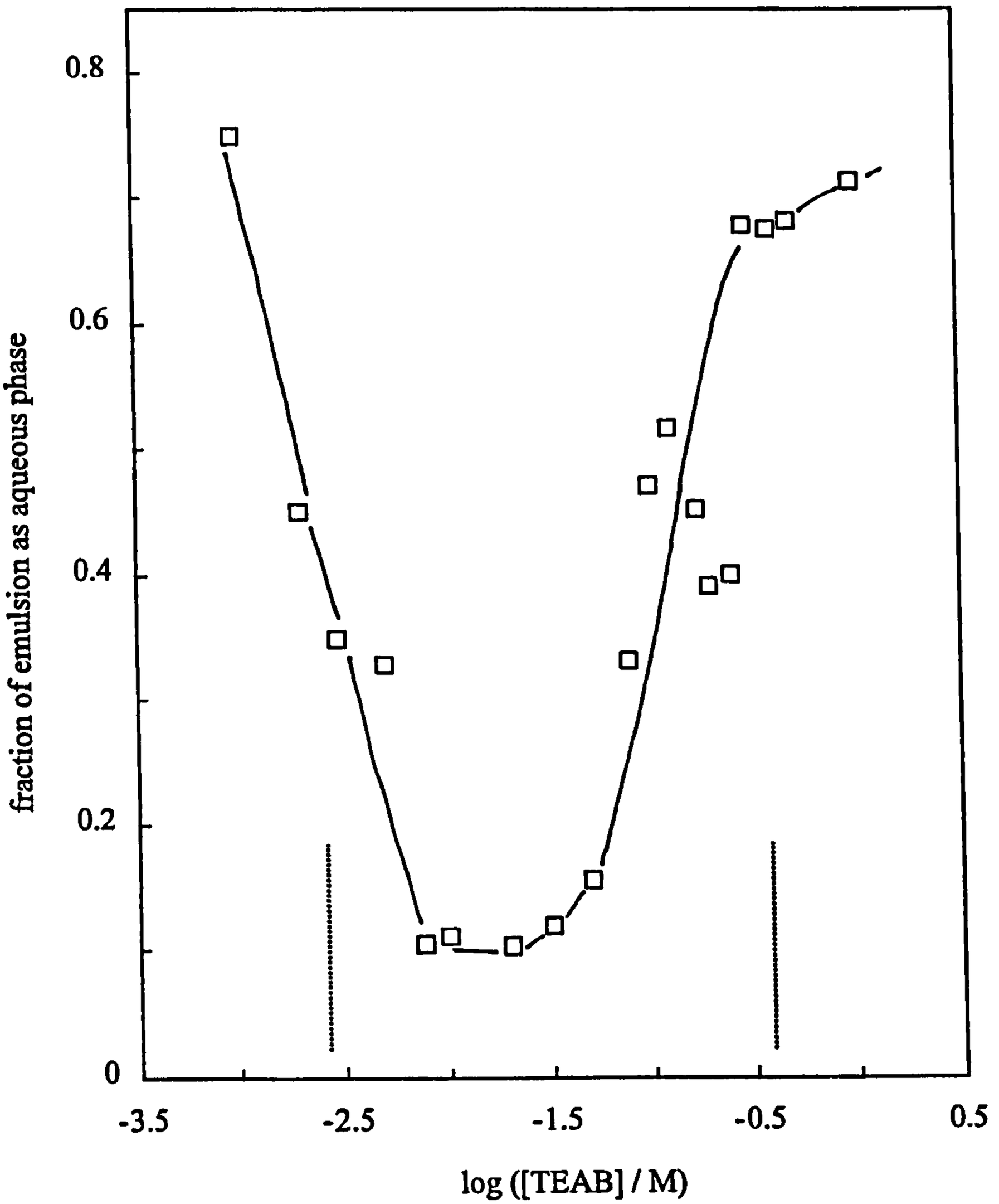

Figure 3.35

Turbidity of 0.5 wt.% Aerosil 200 dispersions in water 24 hours after addition of TEAB (filled points, left hand ordinate) and stability to creaming after 30 minutes of 20 vol% toluene emulsions stabilised by 0.5 wt.% Aerosil 200 (open points, right hand ordinate) at pH 6 as a function of TEAB concentration.

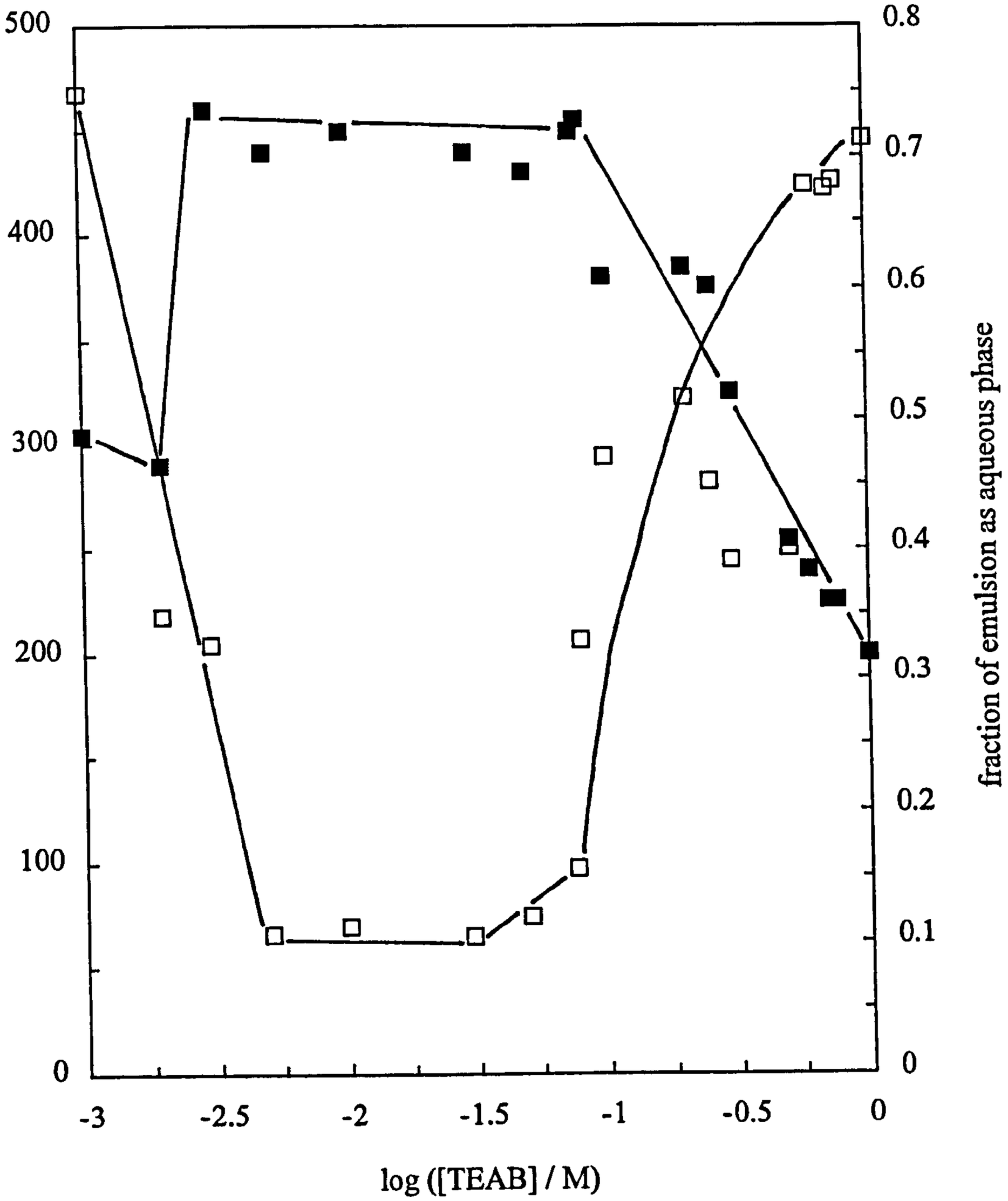

Figure 3.36

Initial volume average diameter of 20 vol% toluene-in-water emulsions stabilised by 0.5 wt.% Aerosil 200 as a function of TEAB concentration at pH 6.

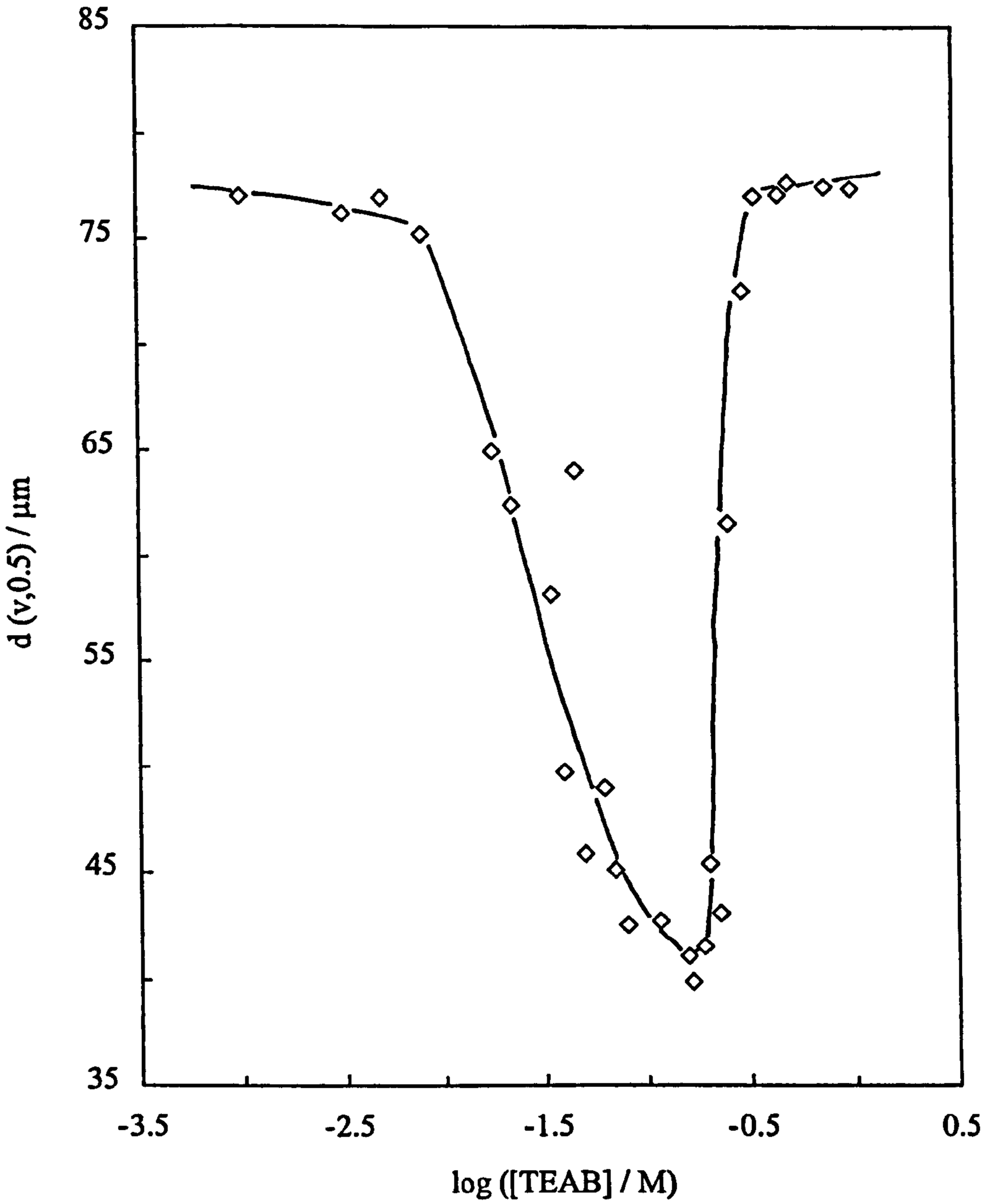

Figure 3.37

Optical microscopy images of 20 vol% toluene-in-water emulsions stabilised by 0.5 wt.% Aerosil 200 as a function of TEAB concentration at pH 6. Scale bar equals 500 μm.

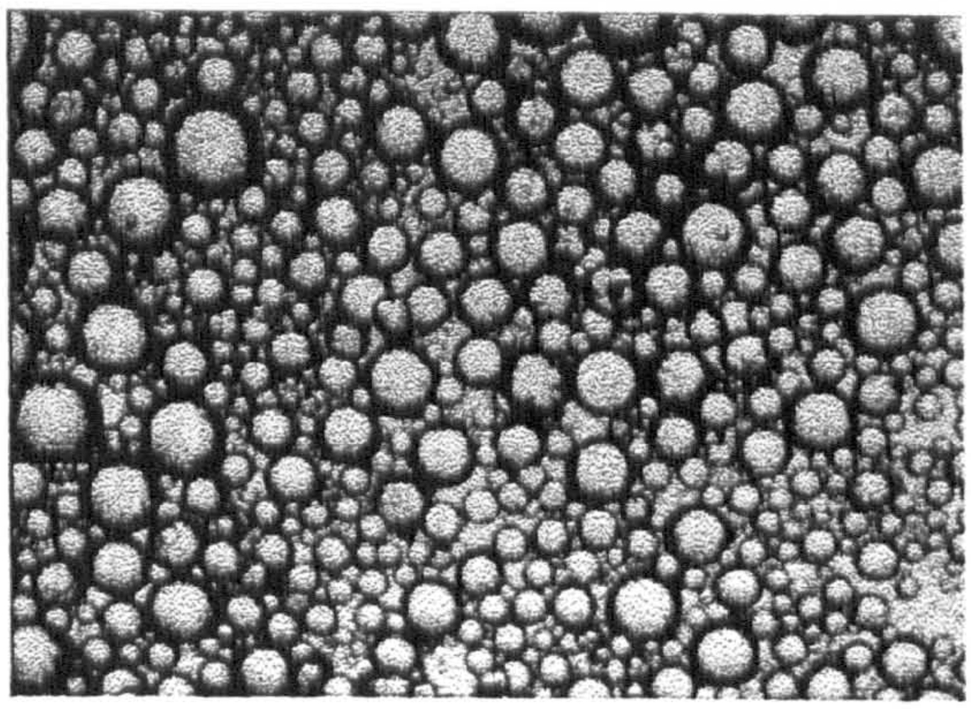

0.002 M TEAB

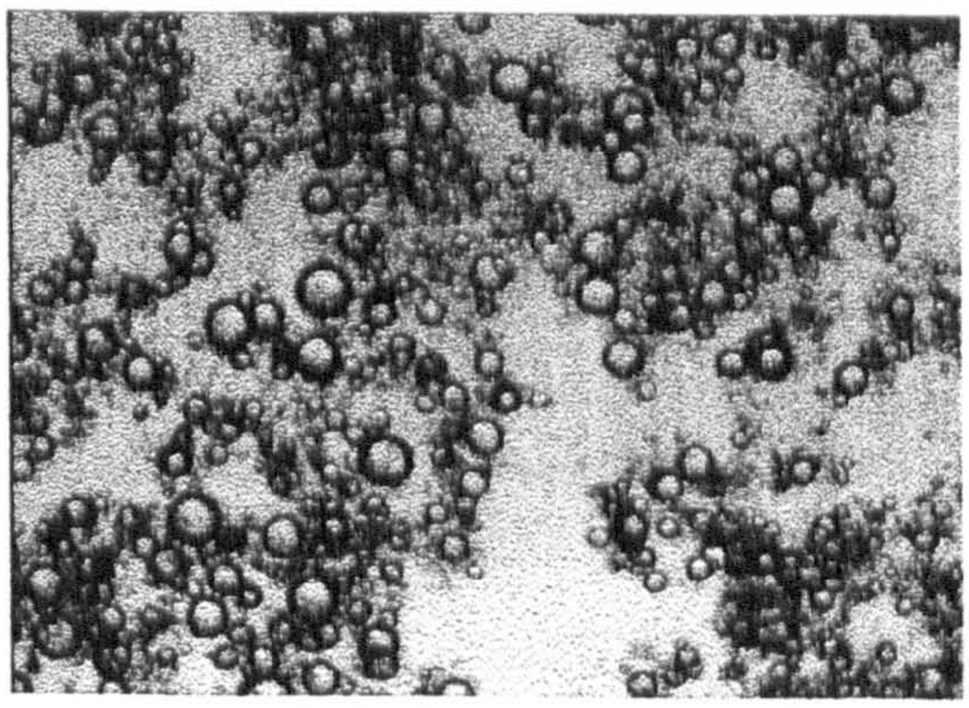

0.005 M TEAB

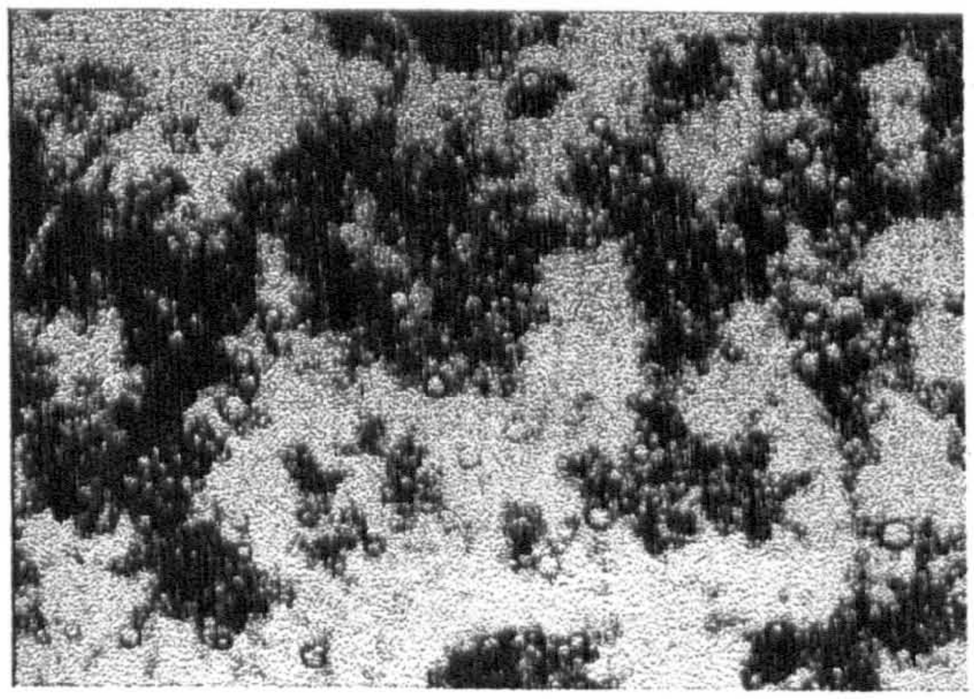

0.01 M TEAB

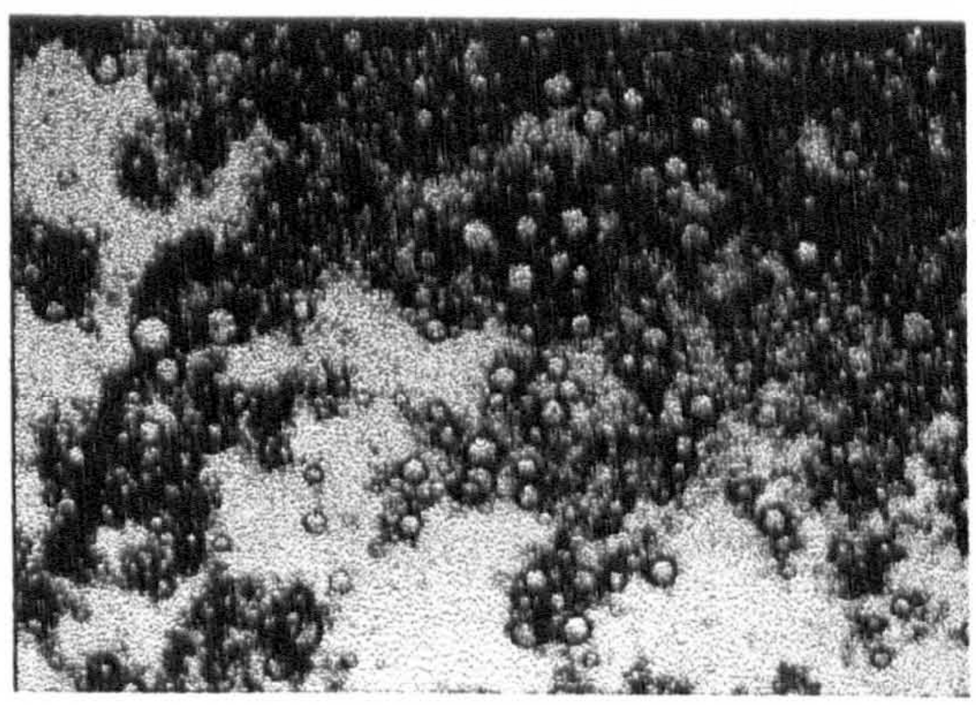

0.03 M TEAB

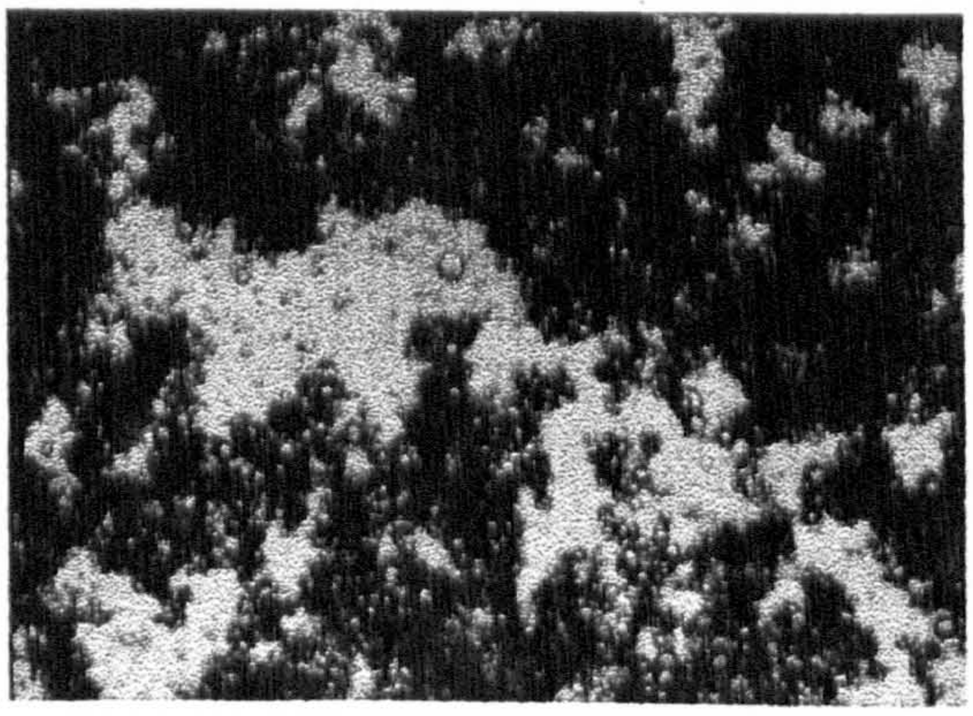

0.04 M TEAB

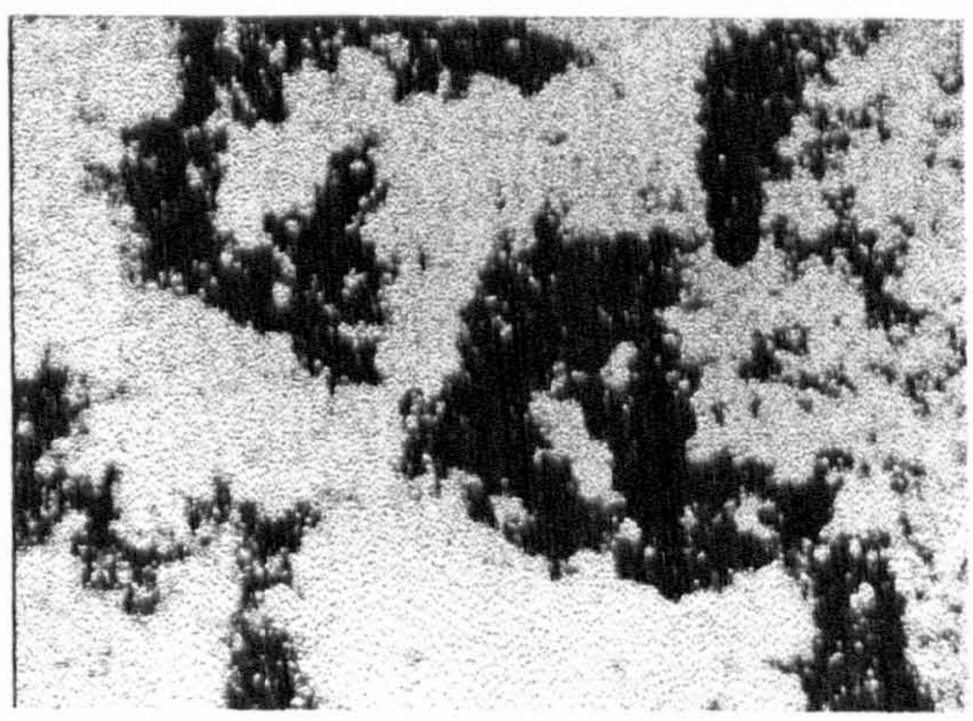

0.05 M TEAB

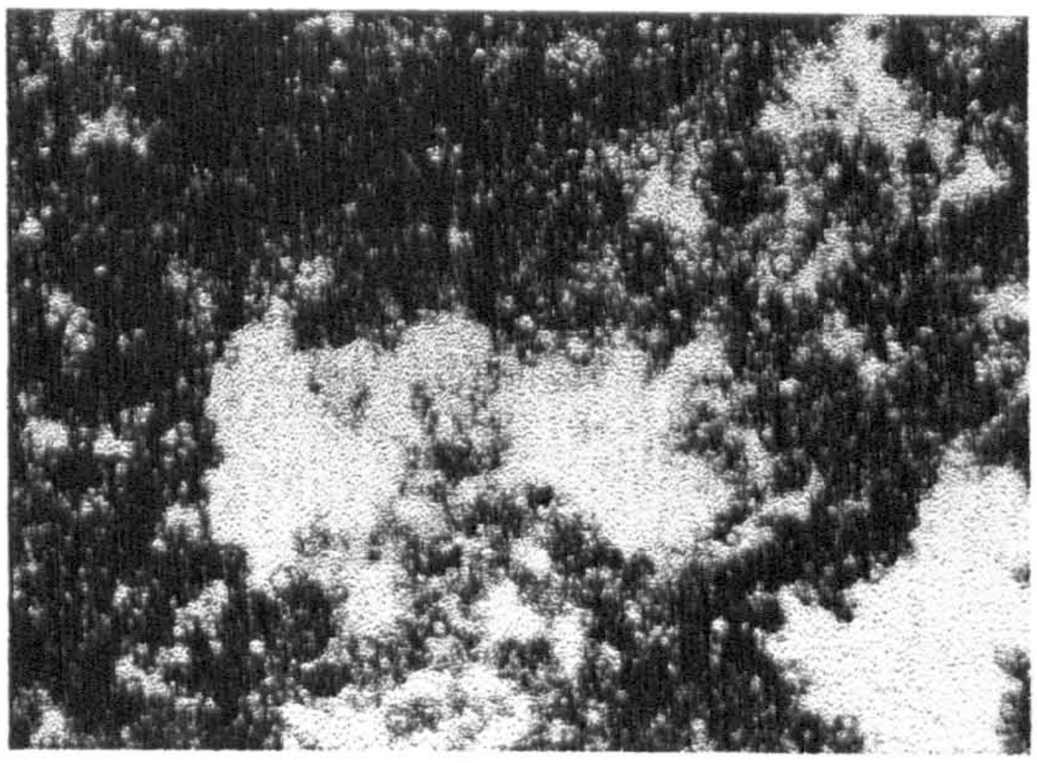

0.06 M TEAB

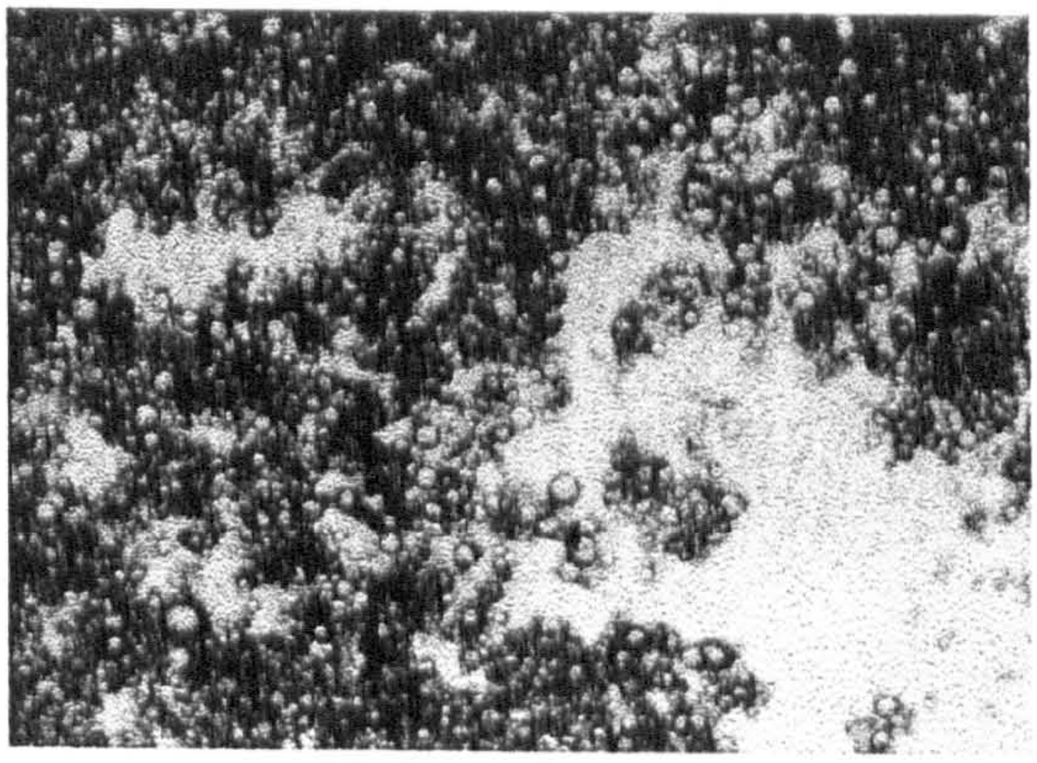

0.07 M TEAB

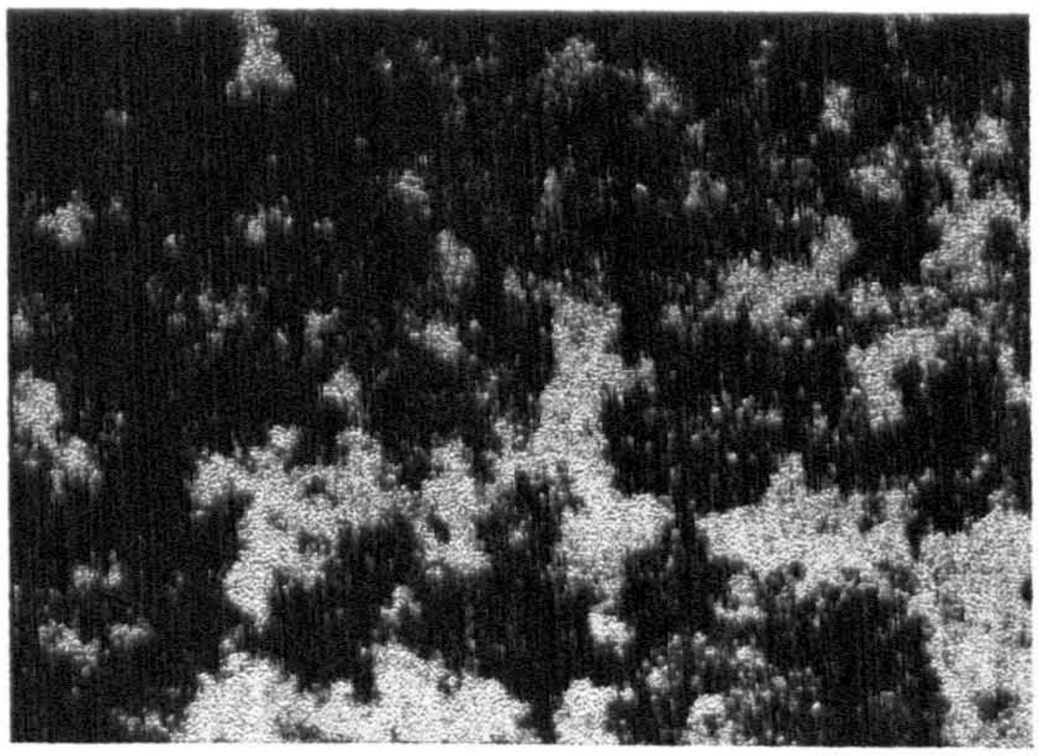

0.1 M TEAB

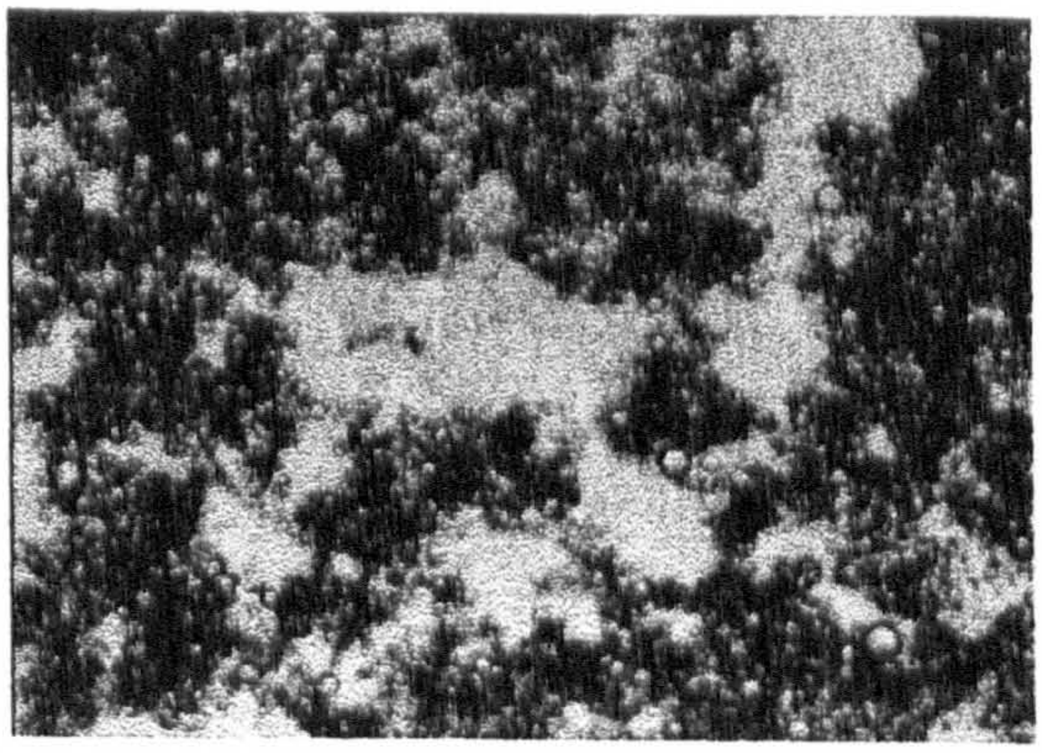

0.2 M TEAB

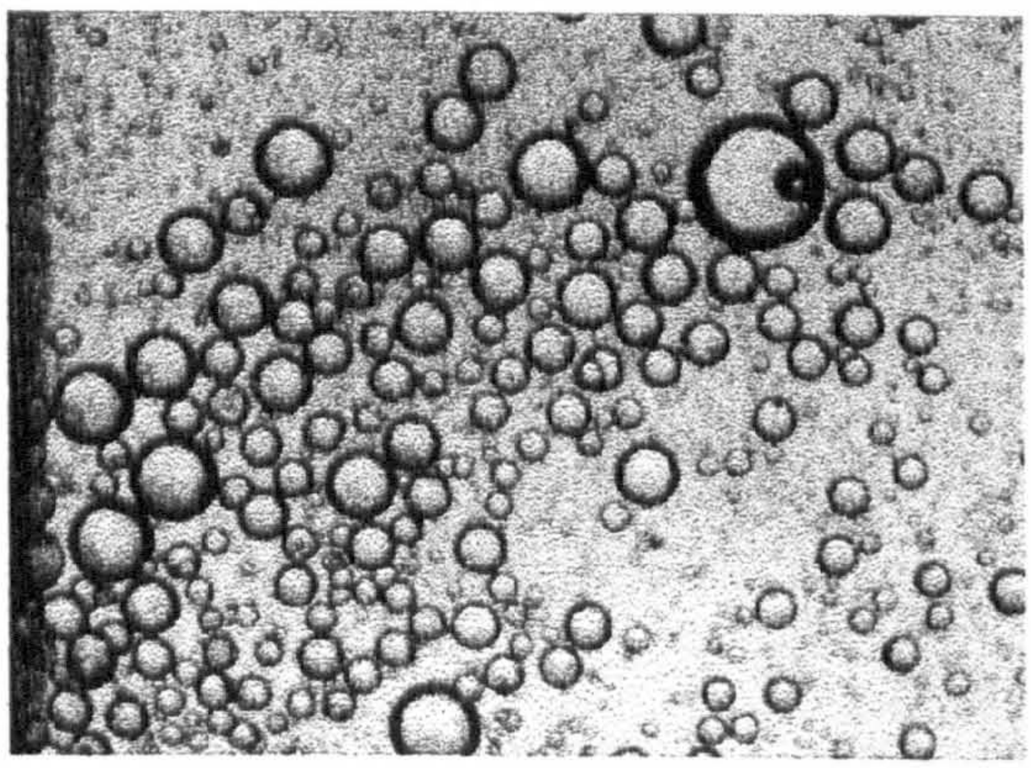

0.3 M TEAB

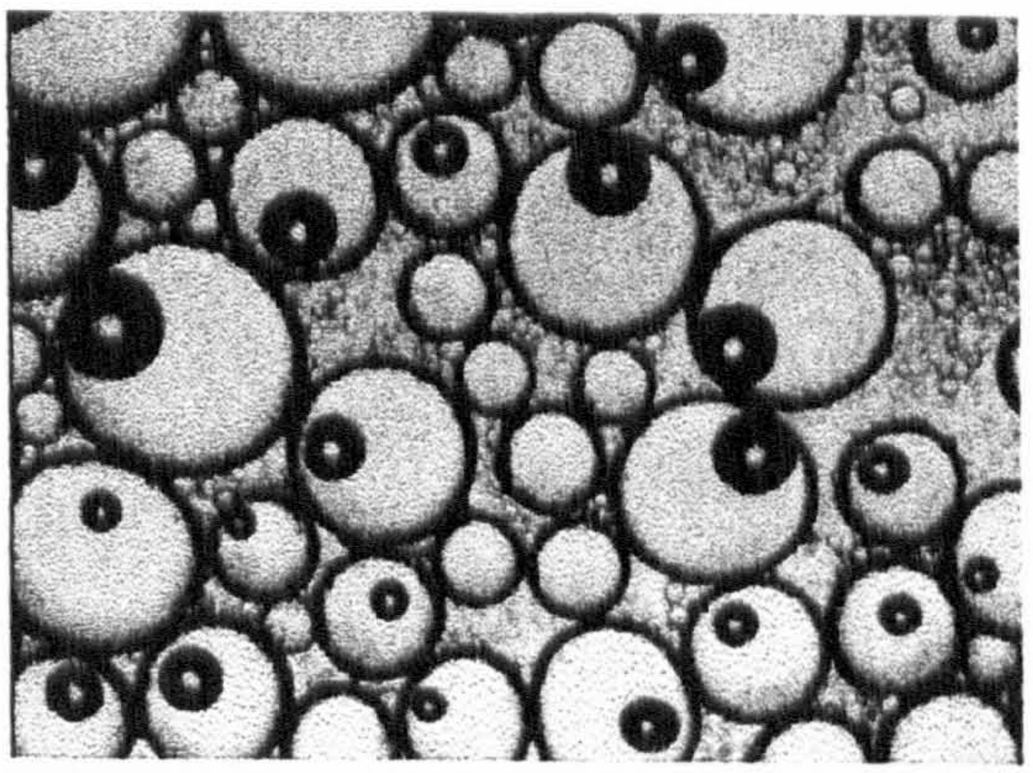

0.5 M TEAB

Figure 3.38

Conductivity of 0.5 wt.% Aerosil 200 dispersions in water (diamonds) and 50 vol% toluene-in-water emulsions stabilised by 0.5 wt.% Aerosil 200 (squares) at pH 6 as a function of TEAB concentration.

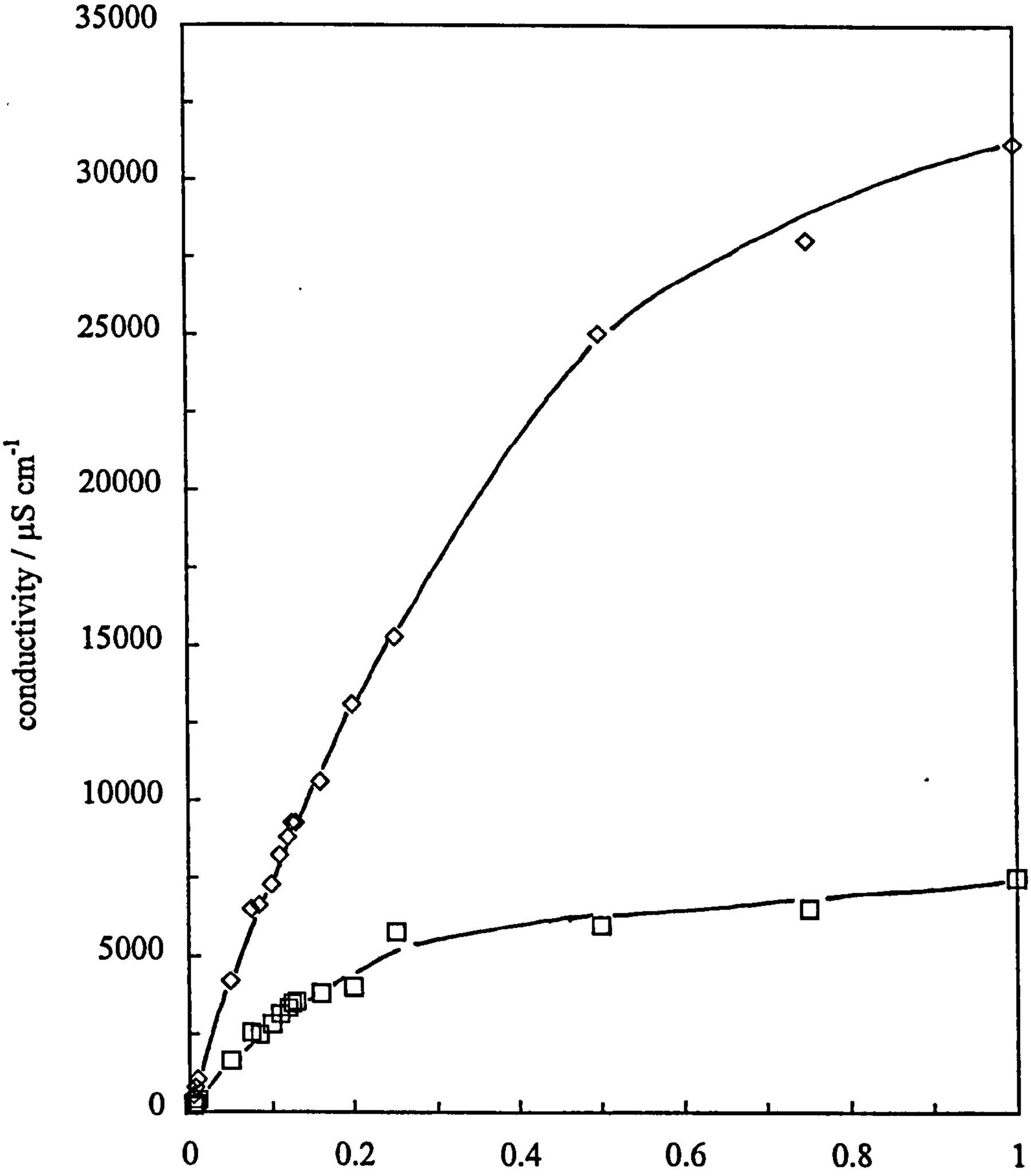

3.5 Systems containing CTAB surfactant

Symmetrical quaternary ammonium salts like TEAB are similar to surfactants in that they have ionic and hydrophobic moieties and they adsorb onto the silica surface. TEAB is not amphiphilic however, because the ionic site is surrounded by a hydrophobic cage which screens the charge of the cation. It does however lower the surface tension of water but not to the same extent as the cationic surfactant cetyltrimethylammonium bromide (CTAB) which has a similar structure to TEAB and also readily adsorbs onto silica particles.[109] In an attempt to invert emulsions from o/w to w/o, CTAB has been used to stabilise emulsions containing hydrophilic Aerosil 200 silica particles. In order to stabilise w/o emulsions the silica particles must become hydrophobic, i.e. have a contact angle at the oil-water interface of > 90° (see later in Chapter 6). CTAB adsorbs onto silica via the cationic head-group thus exposing the hydrophobic tail. Static advancing contact angle measurements of an aqueous CTAB drop on a clean glass slide under dodecane were carried out in an attempt to model the behaviour of a silica particle at the oil-water interface. Dodecane was used as the oil phase because it provided more reproducible results than toluene. At natural pH (~6), Figure 3.39 shows how the contact angle increases to a maximum of 130° around the critical micelle concentration (c.m.c.) of 9×10^{-4} M. Above the c.m.c. the contact angle decreases presumably due to a bilayer of CTAB forming on the glass surface thus exposing the hydrophilic head-groups. These contact angle measurements confirm that the silica surface does become hydrophobic in the presence of CTAB and suggests that they may now stabilise w/o emulsions.

The effect of [CTAB] on the stability to creaming and coalescence of 20 vol% dodecane-water emulsions at pH 2, 6 and 10 in the presence of 0.5 wt.% Aerosil 200 is given in Figure 3.40. The required concentration of CTAB was added to a known mass of Aerosil 200 in water which was then dispersed using ultrasound. The pH was then adjusted using HCl or NaOH before homogenisation with the required volume of dodecane. At pH 2 and 6 the emulsions are very stable to coalescence at all [CTAB] whereas at pH 10 the stability decreases considerably below 3×10^{-6} M CTAB. Stability to creaming is maximum around the c.m.c. for pH 6 and 10 but the stability continues to increase above the c.m.c. for pH 2. In general, emulsions stabilised by CTAB alone were found to be more stable to creaming than those stabilised by CTAB + silica particles. However, emulsions stabilised by CTAB + silica were more stable to

Figure 3.39

Static advancing contact angle of a drop of aqueous CTAB solution (pH 6) on a hydrophilic glass plate under dodecane measured 30 minutes after addition of oil.

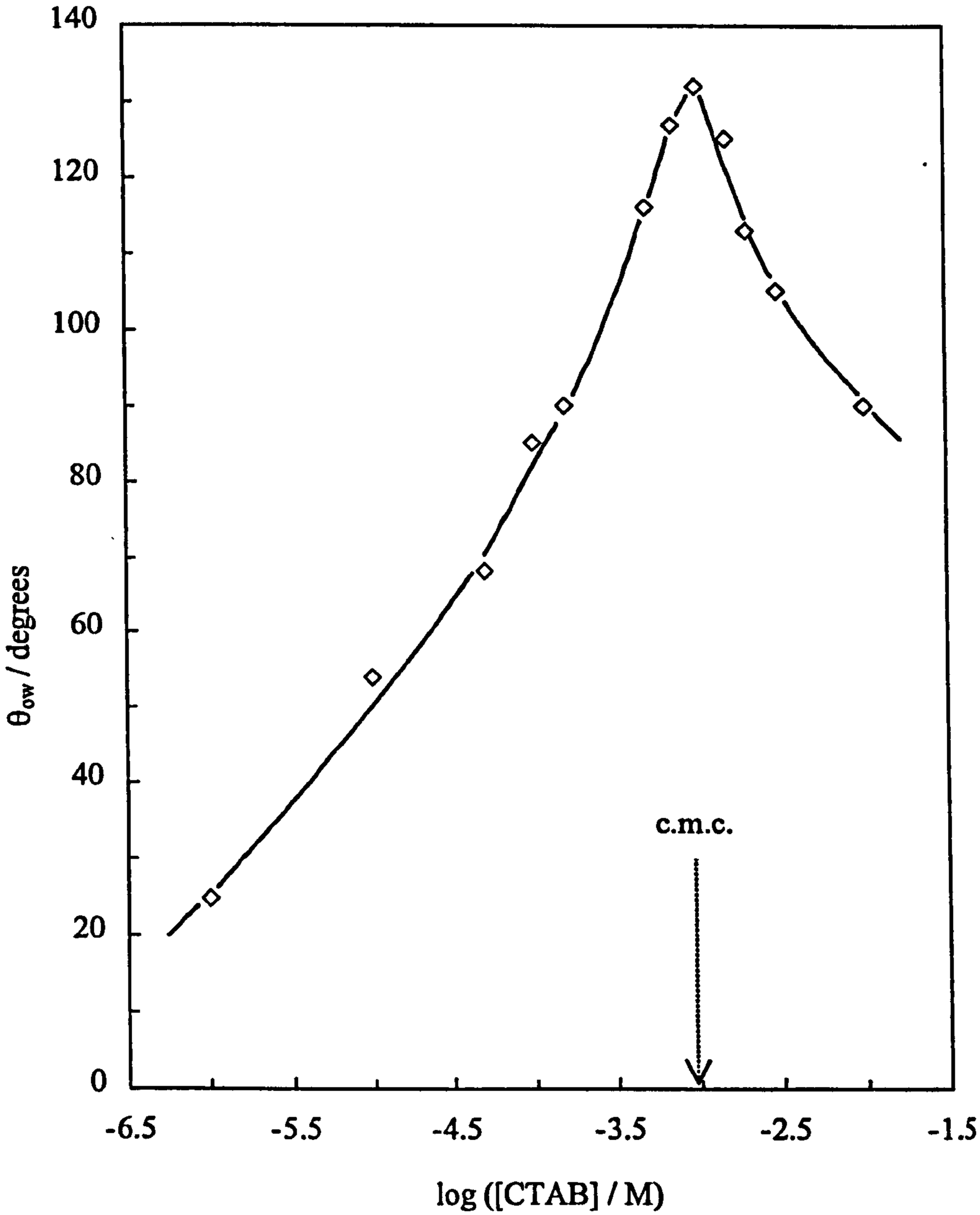

Figure 3.40

Stability to creaming (filled points, left hand ordinate) and coalescence (open points, right hand ordinate) of 20 vol% dodecane-in-water emulsions stabilised by 0.5 wt.% Aerosil 200 as a function of CTAB concentration. The pH values are 2 (diamonds), 6 (triangles) and 10 (circles).

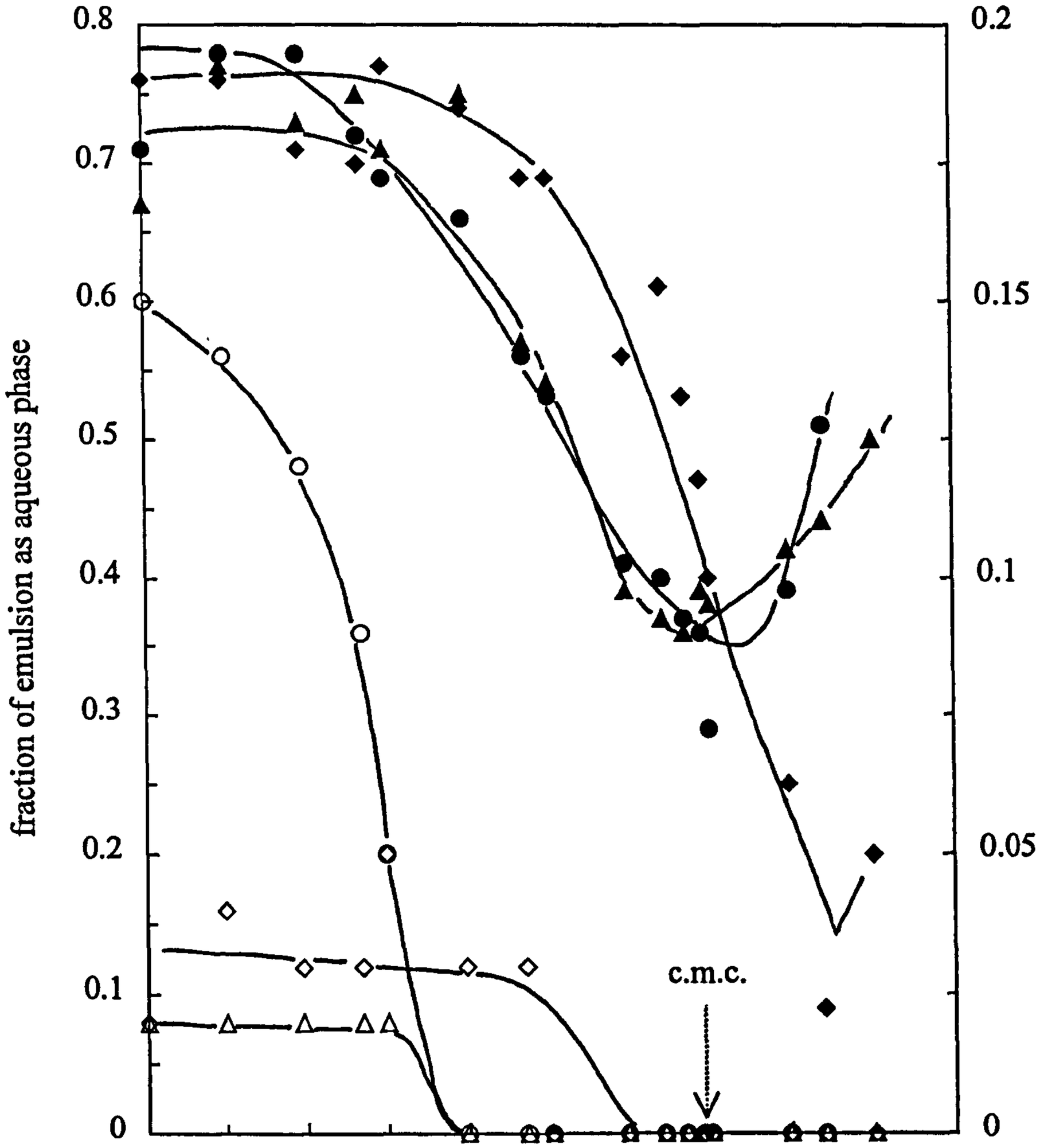

coalescence than those stabilised by CTAB alone. This could be due to the reversible adsorption of CTAB at the oil-water interface compared with silica, which once adsorbed tends to remain at the interface preventing coalescence. The type of emulsion formed was detected by measuring the conductivity as a function of [CTAB] at pH 2, 6 and 10 of 50 vol% dodecane-water emulsions in the presence of 0.5 wt.% Aerosil 200 (Figure 3.41). Also plotted is the conductivity of the aqueous colloid prior to emulsification. The decrease in conductivity of the emulsion compared to the aqueous colloid is due to two effects of the oil drops on the conductivity of ions present in the aqueous phase. The first is that the drops cause a dilution of the continuous phase (with respect to the total system volume) by a factor of 0.5 in this case (equal to 1 minus the volume fraction of oil in the emulsion, ϕ_o). The second is that the non-conducting drops obstruct the conduction by the small ions. As discussed previously,[110] the latter effect reduces the diffusivity of small species by an additional factor of $1/(1+\phi_o/2)$. The ratio of the emulsion conductivity, κ_{em}, to the conductivity of the continuous phase, $\kappa_{cont.}$, is given by,

$$\frac{\kappa_{em}}{\kappa_{cont.}} = \frac{1-\phi_o}{(1+0.5\phi_o)} \qquad (3.34)$$

For a $\phi_o = 0.5$, the equation predicts the emulsion conductivity will be a factor 0.4 less than the aqueous colloid continuous phase. At pH 2, the conductivity of the aqueous colloid is independent of [CTAB] with a value of ~10000 $\mu S\ cm^{-1}$. The high conductivity can be attributed to the H^+ ions in solution following addition of HCl to the aqueous dispersion (cf. the conductivity of water at pH 2 = 7760 $\mu S\ cm^{-1}$). The conductivity of the subsequent emulsion is also independent of [CTAB] at a value of ~4000 $\mu S\ cm^{-1}$ indicative of oil-in-water emulsions even above the c.m.c. For a CTAB concentration of 5×10^{-6} M at pH 2 for example, the conductivity of the emulsion is 4200 $\mu S\ cm^{-1}$ and the aqueous colloid equals 10700 $\mu S\ cm^{-1}$, hence the experimental ratio ($\kappa_{em}/\kappa_{cont.}$) equals 0.39 very similar to the prediction. At pH 6, the conductivity of the aqueous colloid is much lower due to the absence of ions in solution. Above the c.m.c. however, the conductivity increases as the concentration of surfactant in solution increases. The emulsion conductivities follow the same trend but with values consistently lower than those for the aqueous colloid but greater than values expected for

Figure 3.41

Conductivity of 0.5 wt.% Aerosil 200 dispersions in water (diamonds) and 50 vol% dodecane–water emulsions stabilised by 0.5 wt.% Aerosil 200 (squares) at pH 2, 6 and 10 as a function of CTAB concentration.

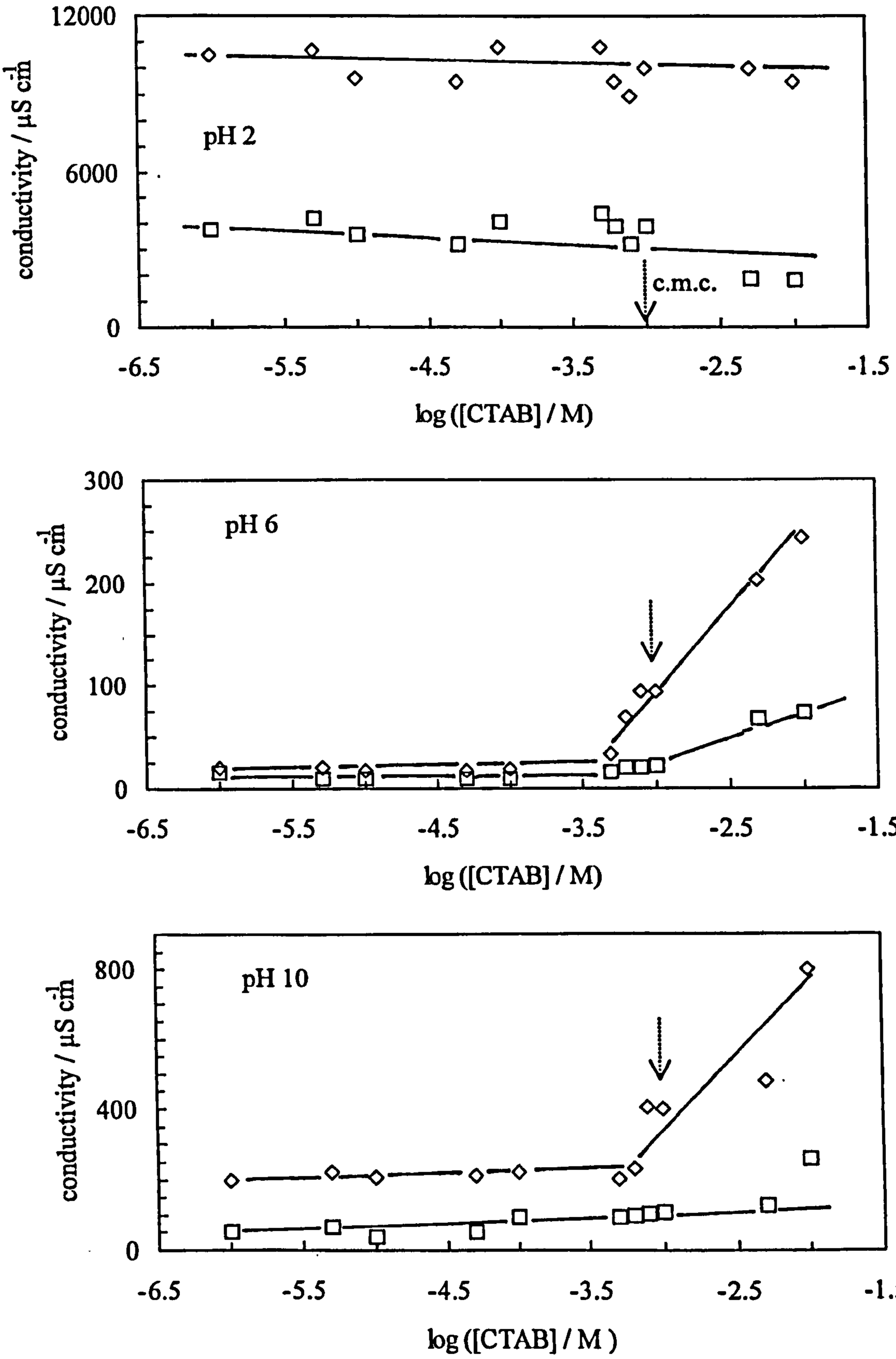

w/o emulsions which are typically less than 1 μS cm^{-1}. At pH 10, the conductivity again increases after the c.m.c. for both the colloid and the emulsion. The conductivity is low in comparison to the aqueous colloids and emulsions at pH 2 due to the low conductivity of water at pH 10 (= 19.56 μS cm^{-1}). The emulsions at all pH and [CTAB] were confirmed to be o/w by adding a drop of emulsion to dodecane or water. In all cases the drop dispersed in water but remained on the surface of oil.

These results highlight an important difference between the behaviour of silica particles in a dynamic emulsion system and the silica surface in static contact angle measurements. The contact angle was 130° at the c.m.c. suggesting the silica surface becomes hydrophobic; however emulsions remained o/w in all cases. In the dynamic system there is no reason why CTAB cannot compete with silica for adsorption at the interface, which is not the case in the static contact angle measurements where CTAB alone adsorbs on the silica surface. It is important to note that phase inversion has been reported for similar systems when an oil soluble surfactant has been used.[28] In this case, n-decane/water emulsions stabilised by silica dispersed in water inverted to water/n-decane emulsions on addition of stearic acid surfactant to the oil and an increase in the aqueous phase pH above 8. At this pH the silica surface is negatively charged and the carboxyl group on stearic acid is dissociated into $-COO^-$. Unfortunately, no explanation is proposed as to how the negatively charged surfactant adsorbs onto negatively charged silica.

3.6 Conclusions

Aqueous silica dispersions have been shown to be very sensitive to addition of electrolyte and changes in pH. The stabilities of the subsequent emulsions with toluene were also dependent on the type of electrolyte and the extent of flocculation of the particles. In summary, the following conclusions can be drawn:

- Aerosil 200 dispersions in water exhibit anomalous DLVO behaviour **in the presence of NaCl**. Emulsions formed from these colloids are unstable to creaming at all salt concentrations (0 – 5 M) at pH values between 2 and 10. Stability to coalescence passes through a maximum around pH 4 where the particles have a low, negative zeta potential. Flocculation of the colloid at high pH results in

destabilisation of the emulsions. Emulsions stabilised by precipitated Ludox HS-40 silica are more stable to coalescence at low pH than at high pH with the addition of NaCl delaying the onset of creaming at low pH.

- **In the presence of $LaCl_3$,** emulsions are unstable when the Aerosil silica is dispersed at low pH. At high pH, emulsion stability passes through a pronounced maximum between 2 and 5 mM salt corresponding to the onset of flocculation of the aqueous colloid. These emulsions remain stable to both creaming and coalescence for over 3 months, even though relatively large (40 μm diameter) drops are formed. Extensive flocculation at higher [$LaCl_3$] results in destabilisation of the emulsions.
- **In the presence of TEAB,** emulsions are relatively unstable at both high and low pH corresponding to conditions where the aqueous colloid is dispersed. At intermediate pH, emulsions are stable to coalescence but exhibit maximum stability to creaming around salt concentrations corresponding to the onset of colloid flocculation. Emulsion drops themselves are highly flocculated too. Further flocculation of the colloid de-flocculates the emulsion leading to destabilisation.
- **In the presence of CTAB surfactant,** emulsions remain o/w at all pH and [CTAB] despite the static advancing contact angle on a glass slide increasing to 130° around the c.m.c.

The author would like to acknowledge Mr. I. Kolev, a visiting TEMPUS student from the University of Sofia, for his work on silica in the presence of CTAB surfactant.

CHAPTER 4

CHAPTER 4

CATASTROPHIC PHASE INVERSION OF WATER-IN-OIL EMULSIONS STABILISED BY HYDROPHOBIC SILICA

4.1 Introduction

It was shown in Chapter 3 that hydrophilic silica particles can stabilise o/w emulsions in the absence of any other adsorbing species. Flocculation of the particles by addition of various electrolytes and charging through changes in pH only affects the subsequent stability and not the type of emulsion formed. These particles are readily dispersed in water to high concentrations but are not easily dispersed in toluene due to the silanol groups on the surface. However, in order to stabilise emulsions, the particles must enter the oil-water interface and hence become wetted by the oil phase. The particles do enter the interface due to the favourable energy gain obtained from displacing an area of high energy interface as described by Aveyard et al.[111] but are expected to reside more in the aqueous phase than the oil due to their hydrophilic nature. Finkle et al.[19] observed that particles in an emulsion will probably be wetted by one phase more than the other and suggested that the more poorly wetting liquid will become the dispersed phase. The wettability of the particle by both phases is therefore an important parameter in determining the preferred emulsion type. The wettability is quantified by the contact angle, θ, (measured through the aqueous phase) that the particle makes at the oil-water interface. Hydrophilic particles are preferentially wetted by the aqueous phase with $\theta < 90°$, whereas hydrophobic particles are preferentially wetted by oil with $\theta > 90°$. The relationship between particle wettability and the energy of attachment of a particle at the oil-water interface is directly related to the type and stability of the emulsions; this is discussed in more detail in Chapter 6. In this chapter the type and stability of emulsions stabilised by hydrophobic silica particles is

investigated. It is shown that at a volume fraction of water, ϕ_w, equal to 0.5 the preferred emulsion type is w/o as expected.

In surfactant systems, Bancroft's rule states that the preferred emulsion type is dependent on the solubility of the surfactant in each phase with the external phase of the emulsion being the one that contains most surfactant.[7] Griffin first defined the affinity of a nonionic surfactant for oil and water phases in terms of an empirical quantity, the hydrophile-lipophile balance (HLB) number.[9] In general, lipophilic surfactants are assigned with a low HLB number and hydrophilic surfactants with a high HLB number. In order to stabilise an emulsion the [surfactant] must be greater than the c.m.c. in one of the phases prior to emulsification. At equilibrium, multiphases of oil, water and surfactant coexist which can be of several types.[8] Winsor I systems arise when the surfactant is more soluble in water than oil resulting in an o/w microemulsion plus an excess oil phase. Emulsification of a Winsor I system results in an o/w emulsion. Winsor II systems arise when the surfactant is more soluble in the oil than water resulting in a w/o microemulsion plus excess water phase. Emulsification of this system forms a w/o emulsion. Three phase, Winsor III systems arise when the surfactant has equal affinity for the oil and water phases. In this case excess oil and water phases are separated by a third surfactant-rich phase possibly of bicontinuous structure containing co-solubilised oil and water. Emulsification of this system tends to form emulsions that are unstable.

There are a number of ways of changing the affinity of a surfactant for oil and water and hence change the preferred emulsion type formed. The HLB of the surfactant can be altered by changing the type of oil, the temperature of the system, by addition of electrolyte and by using a co-surfactant.[112, 113] However, it is also possible to invert the emulsion type by changing the oil:water volume ratio without affecting the system HLB. At ϕ_w equal to 0.5 the emulsion type favoured by the surfactant is formed. For example, a w/o emulsion is formed from a low HLB surfactant in equal volumes of oil and water. If however, the volume fraction of water is increased a sudden change in behaviour of the system can occur as the water drops coalesce and the original oil continuous phase becomes the dispersed phase. This phenomenon is known as *catastrophic phase inversion* of the emulsion. Catastrophe theory[114], a mathematical framework used to describe catastrophes, has been successfully applied by Vaessen and Stein[115] to

reproduce the qualitative features of catastrophic phase inversion first described by Dickinson.[116] A catastrophe in this sense means a sudden change in behaviour of a system, as a result of gradually changing conditions. Dickinson's[116] application was based on the fact that phase inversion induced by increasing the volume fraction of the dispersed phase displays the qualitative characteristics of the cusp catastrophe.[117] There are a number of universal features that are pertinent to a theoretical understanding of this phenomenon.

(i) The emulsion exhibits *bimodality* – a system containing roughly similar amounts of oil and water can exist in one of two stable states (o/w or w/o).

(ii) Phase inversion occurs with a *sudden jump* in the microscopic structure of the system as indicated by radical changes in the physical properties of the emulsion (e.g. viscosity and conductivity).

(iii) Most importantly, the emulsion type depends on its previous history, i.e. repeated inversion exhibits *hysteresis*.

The cusp catastrophe is characterised by a single behaviour parameter (S), which indicates the macroscopic structure of the system (i.e. whether it is o/w or w/o) and hence is related to the curvature of the oil-water interface. At equal volumes of oil and water ($\phi_w = 0.5$) the emulsion behaves as if the o/w and w/o states are separated by a large free energy barrier (Figure 4.1). The system is said to be at equilibrium if it lies in a local free energy minimum. In order to invert from one emulsion type to the other it is therefore necessary to do mechanical work on the system. This is achieved by giving the system enough energy to cross the barrier (by heating, increasing the intensity of agitation or rate of liquid addition) or by adjusting the composition gradually so that the height of the barrier is reduced to zero (i.e. by catastrophic inversion). In the latter case for systems stabilised by hydrophilic surfactant, inversion occurs at a volume fraction of oil, $\phi_{o,} \approx 0.74$ as the oil droplets become close packed and begin to distort from spherical symmetry[119] forcing the emulsion to invert to w/o. Re-inversion requires a gradual reduction in ϕ_o from ~ 0.74 to 0.26 whereupon the same inversion mechanism occurs in reverse. Hence catastrophic inversion exhibits considerable hysteresis as depicted by the ball-in-hole analogy given in Figure 4.2. As the volume fraction of water is increased

Figure 4.1

Schematic representation of inversion from o/w to w/o emulsions. The free energy G is plotted as a function of the behaviour parameter S. The filled line A represents the inversion process when the system is given energy and the dashed line B represents inversion when the composition of the system is gradually changed (i.e. by catastrophic inversion). Redrawn from ref. 118.

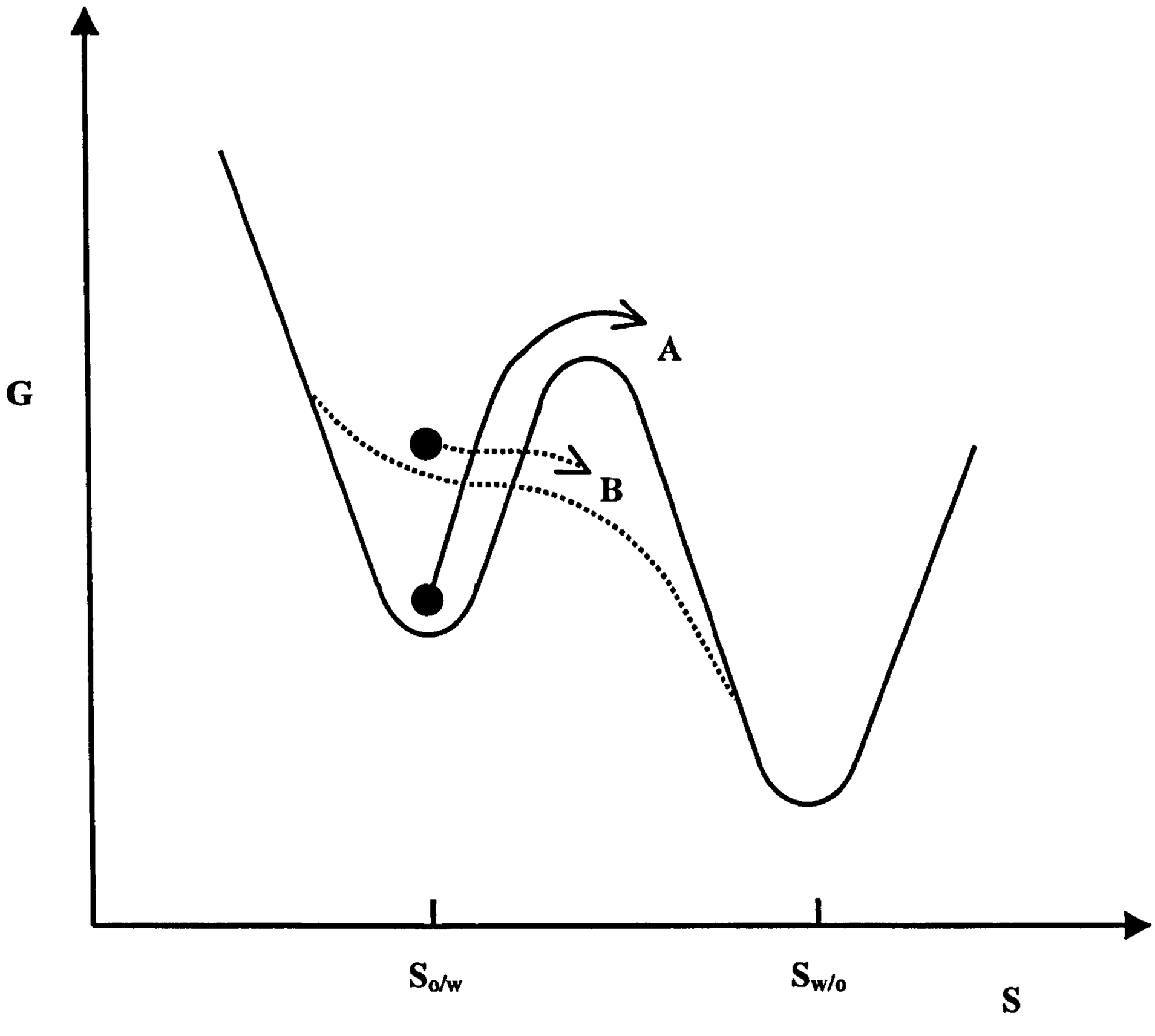

Figure 4.2

The ball-in-hole analogy to depict the hysteresis which occurs upon catastrophic inversion of a surfactant-stabilised emulsion. The volume fraction of water in the system increases from A to E. The figure has been copied from ref. 112.

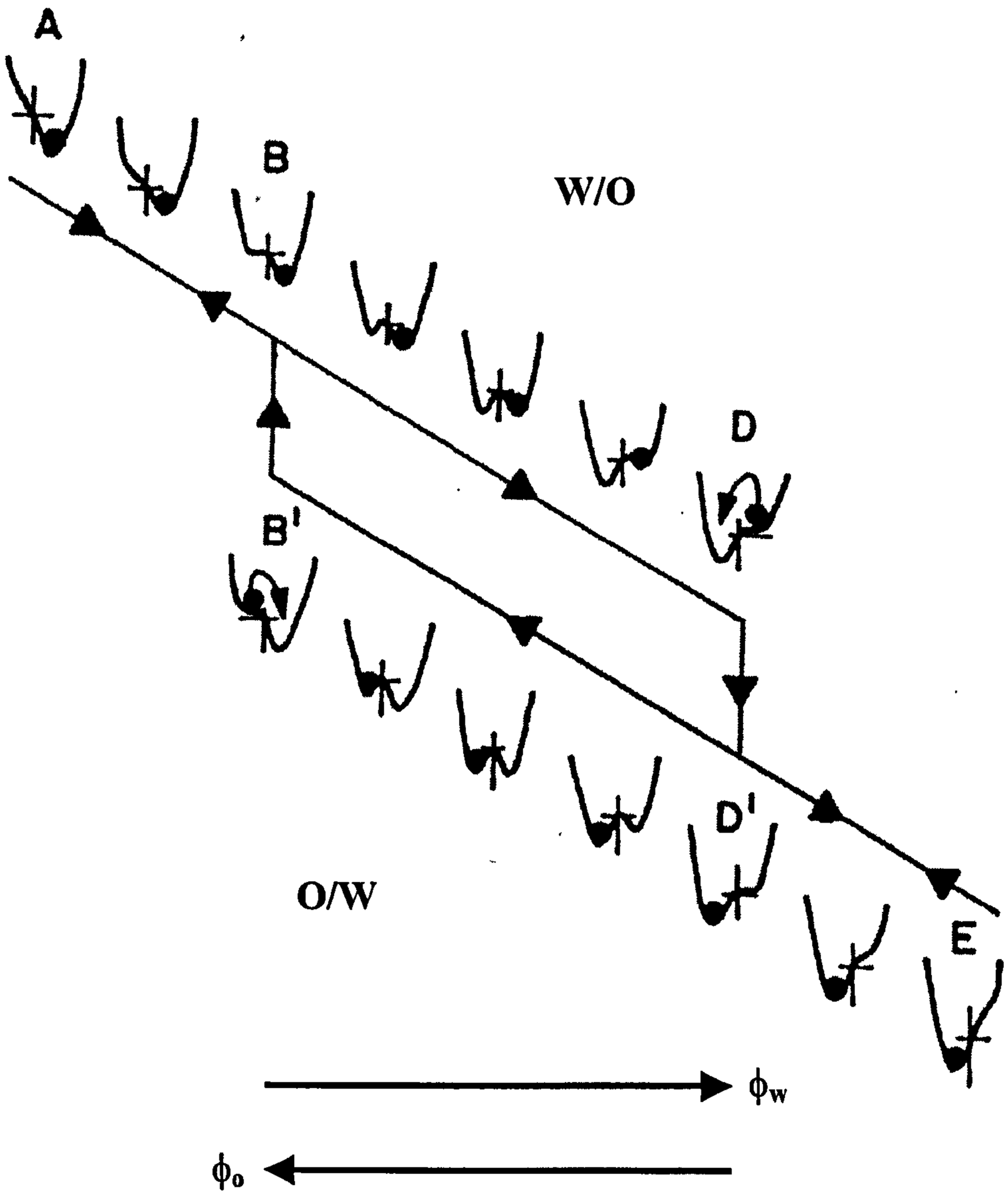

from A to D the energy barrier to inversion falls and eventually the 'ball' drops into the adjacent energy minimum as the emulsion inverts (D to D'). As the volume fraction of oil is increased from E to B' the emulsion remains w/o until the water drops are close-packed forcing the 'ball' to drop back into the original energy minimum. The section D' to B' corresponds to the hysteresis zone for this system. In practical situations the hysteresis zone is smaller due to perturbations in the system (e.g. intensity of agitation and the rate of liquid addition to the emulsion[120]) although the point of inversion can still differ by up to 0.3 in volume fraction depending on the history of the emulsion.

Catastrophic phase inversion of emulsions is shown schematically in Figure 4.3 where the system HLB and type of Winsor system are plotted as a function of ϕ_w.[121] The thick black line represents the inversion locus between the two emulsion types. Catastrophic inversion occurs from o/w to w/o at $\phi_w \approx 0.3$ for high HLB systems (B' to A') on decreasing ϕ_w and from w/o to o/w at $\phi_w \approx 0.7$ for low HLB systems (B to A) on increasing ϕ_w. Both occur when the volume fraction of dispersed phase reaches the close-packed condition for spheres of around 0.74 as modelled by Ostwald.[119] The preferred emulsion type ($\phi_w = 0.5$) is o/w for high HLB systems and w/o for low HLB systems. The bold dashed line shows the inversion hysteresis that occurs in surfactant systems on repeating the experiment by increasing ϕ_w at high HLB and decreasing ϕ_w at low HLB. The degree of hysteresis is seen to increase as the magnitude of the HLB increases. The emulsion stability increases at intermediate volume fraction but then decreases to a minimum at inversion;[120] emulsions in regions B and B' are also unstable. The emulsions in region A and A' are described as anomalous because the amount of oil (low ϕ_w) or water (high ϕ_w) is too low to make it the external phase and hence the opposite type of emulsion is formed. These emulsions tend to be unstable or can be multiple emulsions,[122] e.g. emulsions in region A may be water-in-oil-in-water (w/o/w) which is a way for the system to satisfy Bancroft's rule.[7]

For solid-stabilised emulsions it is proposed in this chapter that the system HLB which determines the preferred emulsion type may be varied by changing the wettability of the particles. It is hypothesised that hydrophobic particles give rise to low HLB systems and hydrophilic particles give rise to high HLB systems. In addition, in one and the same system, it may be possible to phase invert the emulsion via catastrophic inversion without altering the particle type. In this way, both types of emulsion may be

Figure 4.3

Schematic representation of catastrophic phase inversion of emulsions (by changing ϕ_w) and, in the case of surfactant-containing systems, the transitions between Winsor systems with system HLB. The bold dashed line represents the inversion hysteresis which occurs in surfactant systems. For solid-stabilised emulsions, path B to A upon increasing ϕ_w is followed for hydrophobic silica, and path B' to A' upon decreasing ϕ_w is followed for hydrophilic silica.

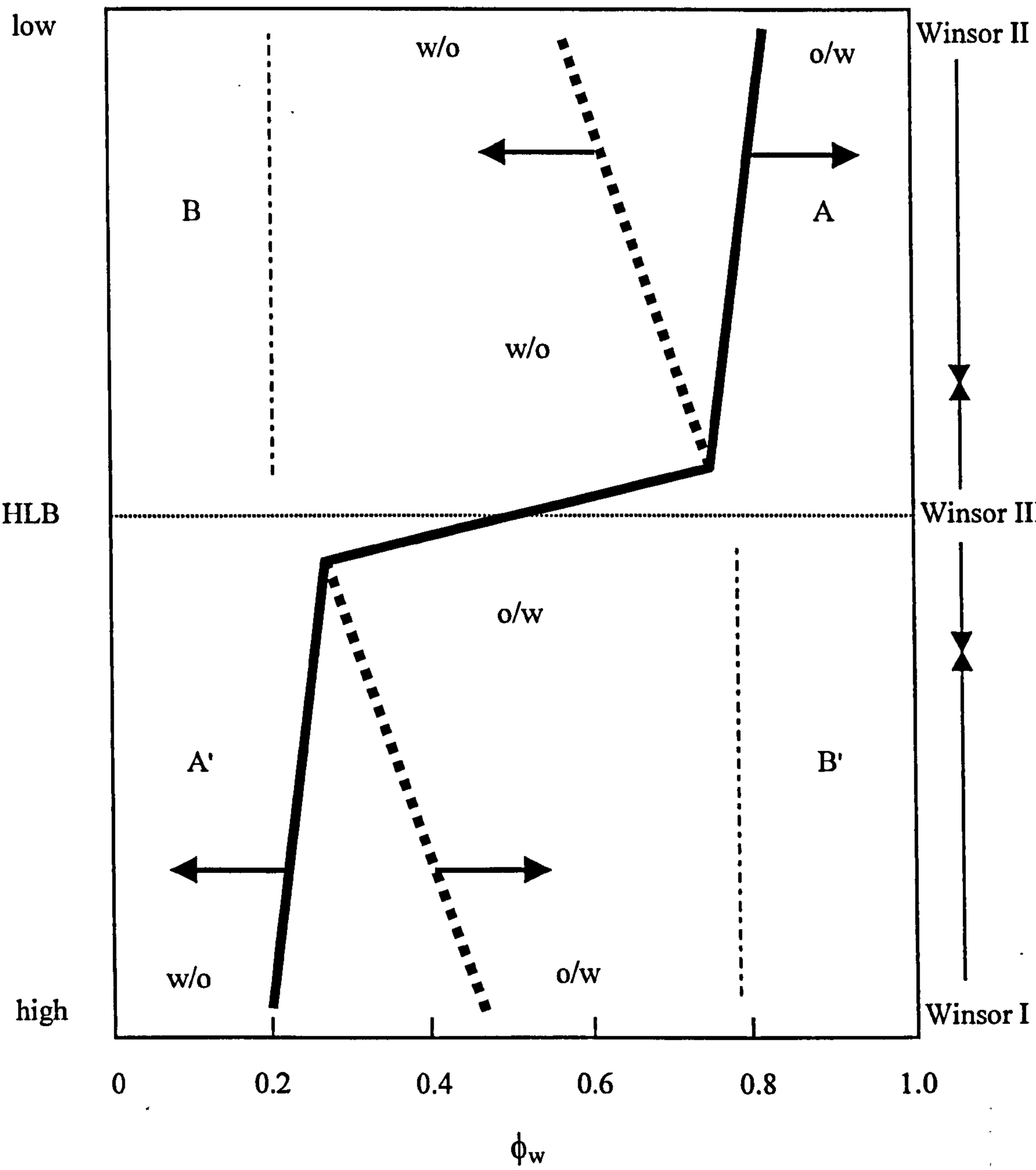

prepared from one kind of solid. In this chapter, the effect of particle concentration and homogenisation speed on the stability and size of emulsions stabilised by hydrophobic silica particles (H30) are investigated. Catastrophic phase inversion of the emulsions, from w/o to o/w for hydrophobic silica and from o/w to w/o for hydrophilic silica, occurs on increasing the volume fraction of dispersed phase. The dramatic changes in the system around inversion are investigated via drop size and stability measurements.

4.2 Effect of particle concentration and homogenisation speed on the stability and drop size of w/o emulsions stabilised by hydrophobic silica

One of the main industrial applications of silica particles is to provide thixotropic behaviour to a variety of fluids. Aggregation of particles in dispersions greatly increases the viscosity of the medium. The aggregates, of between 100 and 500 nm diameter, then form agglomerates (≈ 10 μm diameter) as the concentration of particles is increased further until a three dimensional network is formed. For hydrophilic N20, the interactions between the particles are due to hydrogen bonds between silanol groups on the surfaces of adjacent particles. Additional attractive interactions occur between the silylated surfaces of hydrophobic H30 particles. The behaviour of hydrophobic H30 dispersions in toluene, as observed in the present study, is summarised in Table 4.1.

Table 4.1 Effect of particle concentration on the appearance of H30 silica in toluene

wt.% in toluene	Appearance
0.1	colourless, flows like toluene
0.5	colourless, flows like toluene
1.0	pale blue, flows like toluene
2.0	clear blue, slightly more viscous
3.0	clear blue, reasonably viscous
4.0	clear blue, viscous
5.0	clear blue, viscous, flows slowly
5.5	clear blue, very viscous, flows slowly
5.75	clear blue, very viscous, barely flows
6.0	clear blue, very viscous, no flow

It is very difficult to disperse H30 in toluene at concentrations greater than 6 wt.% because the toluene does not wet all the particles. TEM of H30 particles in toluene (Figure 4.4) confirms the existence of particle networks even at low concentrations. Light scattering from solutions containing between 0.1 and 1 wt.% particles also indicated the presence of aggregates of particles as opposed to the primary particles themselves (see § 2.2.1e).

Emulsions stabilised by hydrophobic H30 silica particles dispersed in toluene are water-in-oil (w/o) at a ϕ_w equal to 0.5. This suggests that the particles accumulate at the oil-water interface but sit more in the oil than the water. This is in contrast to the previous chapter where the hydrophilic particles stabilised o/w emulsions at $\phi_w = 0.5$. Figure 4.5 shows how the emulsion stability varies with initial H30 particle concentration in toluene 30 minutes after preparation. The stabilities are expressed in terms of the parameters defined in equations 3.28 and 3.29. The emulsions are completely stable to coalescence (fraction of emulsion as aqueous phase) above 0.25 wt.% particles in oil. The stability to sedimentation (fraction of emulsion as oil phase) increases progressively with particle concentration such that by 3 wt.% no oil is released. The sedimentation velocity depends on the emulsion drop size and the continuous (oil) phase viscosity. The average drop size is shown to be virtually constant (shown later) so the increase in stability is most likely the result of the increase in viscosity of the oil phase described in Table 4.1. The emulsions stabilised by greater than or equal to 3 wt.% particles remained completely stable for at least 12 months.

In order to measure the drop size distributions the emulsion must be diluted to low dispersed phase volume fractions. In surfactant-containing systems, the diluting phase should be of the same composition as the continuous phase of the emulsion so that desorption of surfactant from the emulsion drop interface does not occur. If, for o/w emulsions, pure water is used as diluent instead of aqueous surfactant solution then drop growth via coalescence can occur since surfactant molecules are very labile species. To obtain a protocol for diluting emulsions containing solid particles, the effect of changing the composition of the diluting phase on the subsequent size distributions has been investigated. The drop diameter distributions for water-in-toluene emulsions stabilised by 2 wt.% H30 particles initially in oil are given in Figure 4.6. Within experimental error, the distributions remain unchanged whether diluting with pure toluene (0 wt.%) or with 0.5 to 2 wt.% H30 in toluene and thus pure toluene was used for all subsequent

Figure 4.4

Transmission Electron Microscopy image of 0.1 wt.% H30 particles in toluene. Scale bar equals 100 nm.

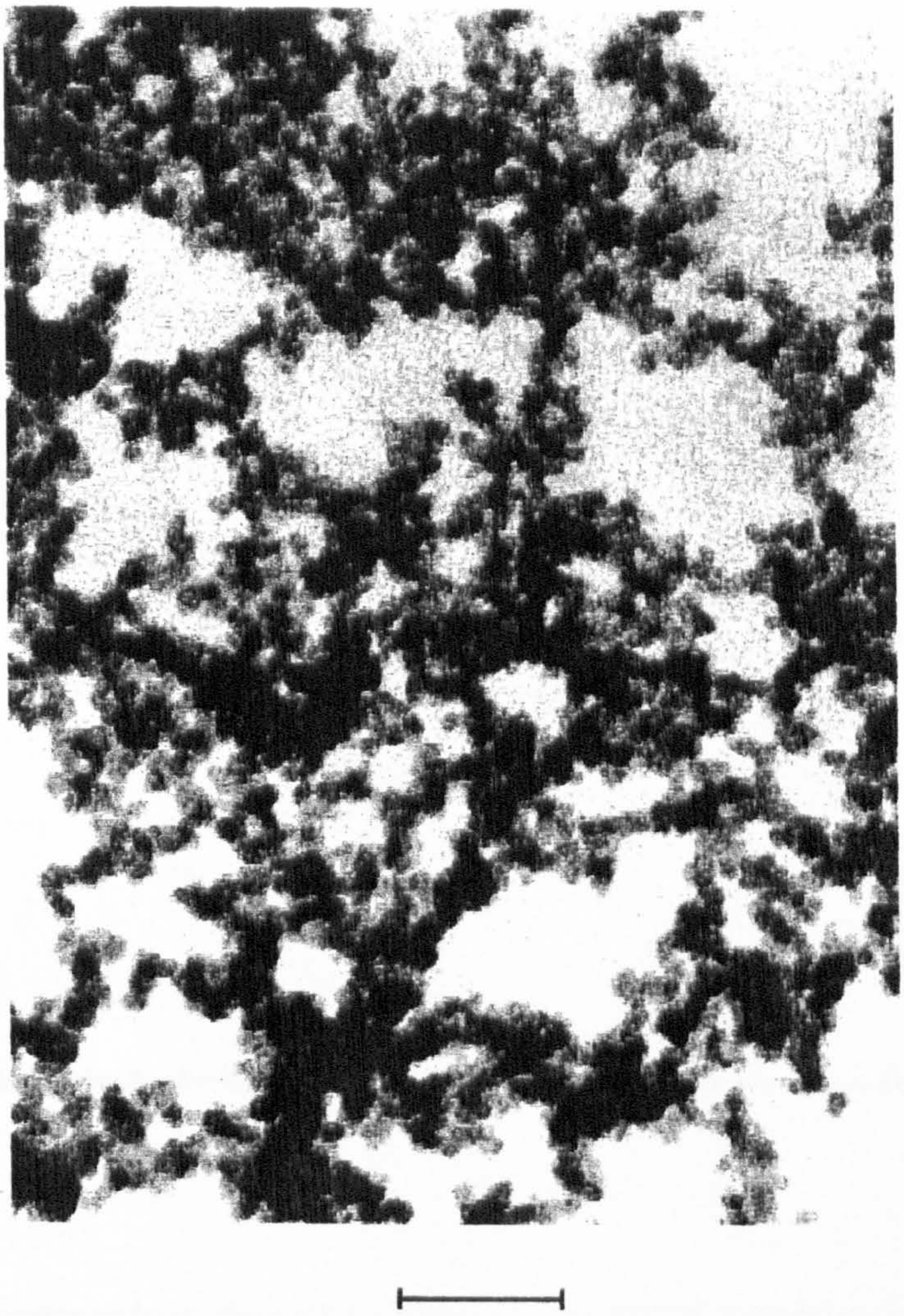

Figure 4.5

Stability to coalescence (filled points, left hand ordinate) and sedimentation (open points, right hand ordinate) after 30 minutes of 50 vol% water-in-toluene emulsions stabilised by H30 particles as a function of initial concentration of particles in oil.

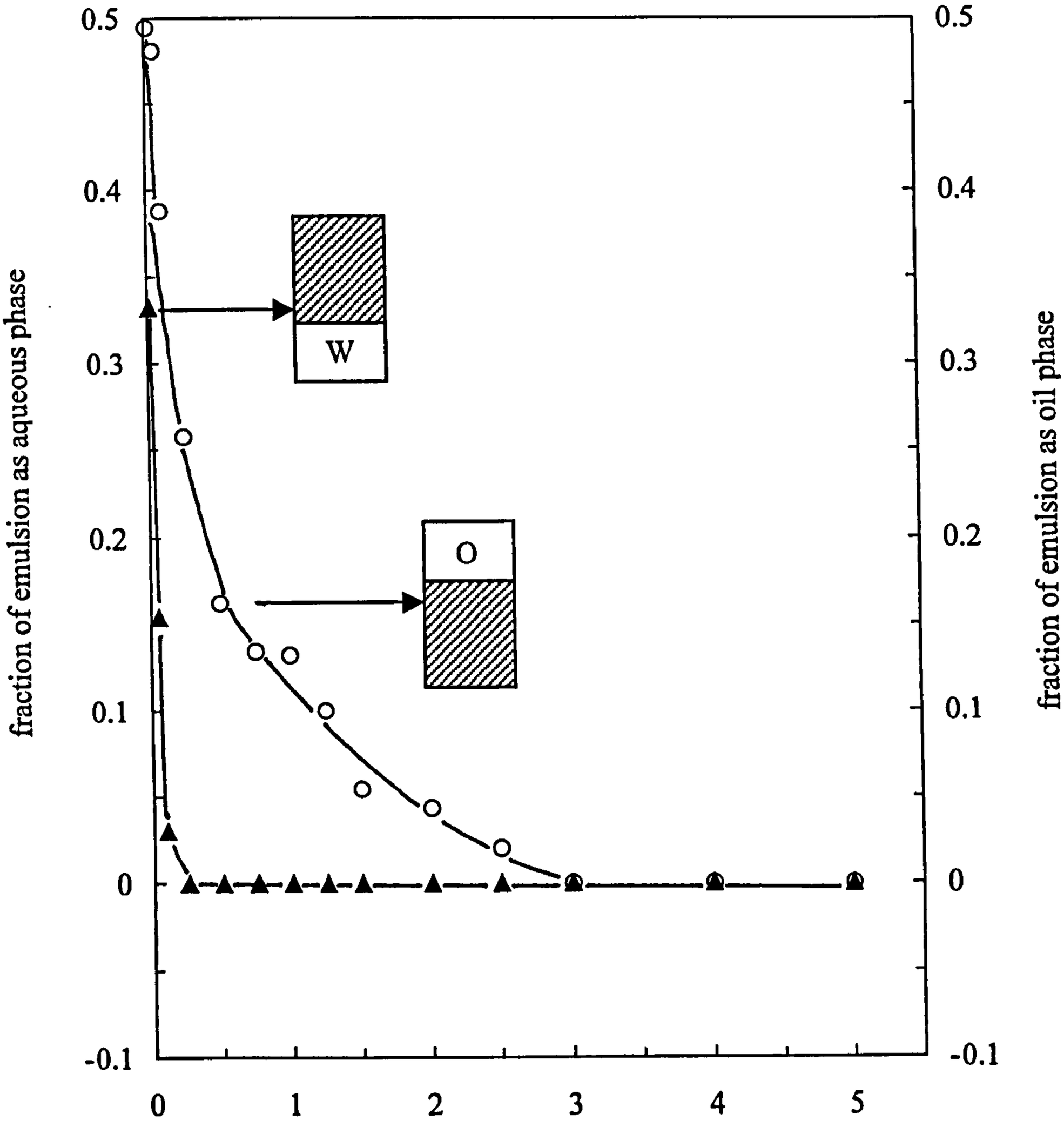

Figure 4.6

Drop diameter volume distributions for water-in-toluene emulsions (ϕ_w = 0.5) stabilised by 2 wt.% H30 for various concentrations (given) of particles in toluene as the diluting phase.

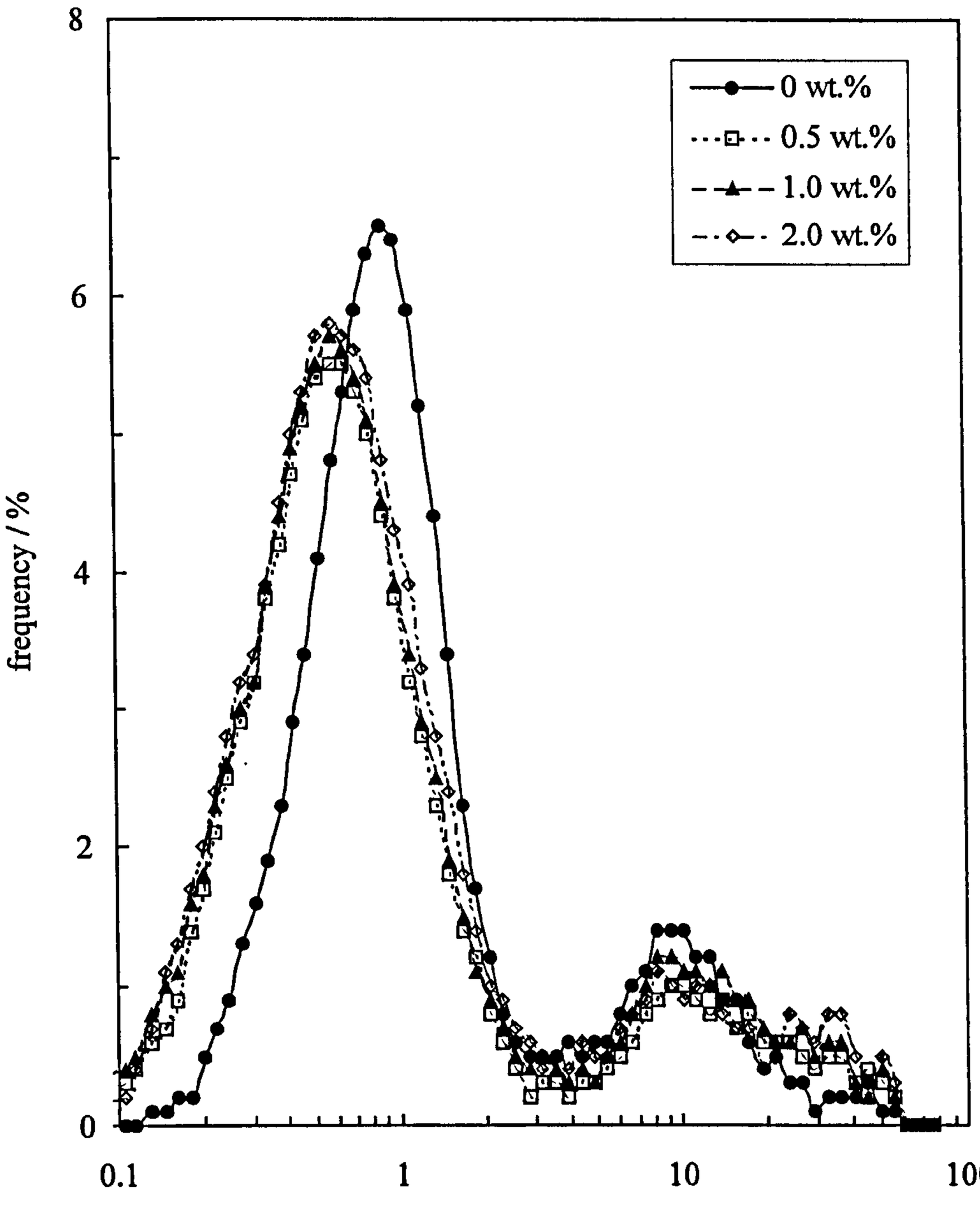

determinations. This independence on continuous phase composition can be attributed to the high stability of these emulsions to coalescence, suggesting the particles once adsorbed at the oil-water interface are held strongly. The emulsion drop size distributions as a function of initial particle concentration are given in Figure 4.7. At low concentrations two drop populations are present centered at 0.6 and 50 μm, with over 80 % of the drops in the range of diameters between 0.1 and 1 μm. For this modest energy input during homogenisation the fact that these stable emulsions can be prepared implies that such solid particles are both good emulsifiers and stabilisers compared with conventional surfactants. On increasing particle concentration the population of larger drops disappears and the two populations merge into one. The improved emulsification efficiency at higher particle concentration is in line with the increase in emulsion stability shown in Figure 4.5. Optical microscopy images of the emulsions as a function of particle concentration are shown in Figure 4.8. Above 1 wt.% the drop size remains virtually constant, consistent with the stability and drop size measurements.

During emulsification, an increase of the energy consumption by the mixture invariably leads to a reduction in the average drop diameter for surfactant-stabilised systems.[123] The data in Figure 4.9 shows that this is not the case for w/o emulsions stabilised by H30 particles. The average drop diameter and the span of the distribution (see Experimental) do not vary significantly between 8000 and 24000 rpm of the Ultra Turrax. Even at the lowest speed, emulsification is very effective in reducing the drop size which reaches a limit for this particular system.

4.3 Effect of dispersed phase volume fraction on emulsion type and stability

As described earlier it may be possible to invert an emulsion stabilised by particles of fixed hydrophobicity by increasing the volume fraction of dispersed phase. Hydrophobic particles give rise to low HLB systems and as shown previously stabilise w/o emulsions at $\phi_w = 0.5$. Figures 4.10 and 4.11 show the variation in emulsion conductivity with ϕ_w and, in agreement with the predictions, the conductivity is shown to increase by four orders of magnitude as the emulsion inverts to o/w at $\phi_w \approx 0.7$. The experiment was carried out in four different ways in order to investigate if these emulsions show any hysteresis on inversion. Figure 4.10 shows the conductivity of

Figure 4.7

Drop diameter volume distributions (right-hand ordinate) for water-in-toluene emulsions (ϕ_w = 0.5) stabilised by H30 for different initial concentrations of particles (in wt.%, given) in toluene. The solid curves show the cumulative volume distribution (left-hand ordinate).

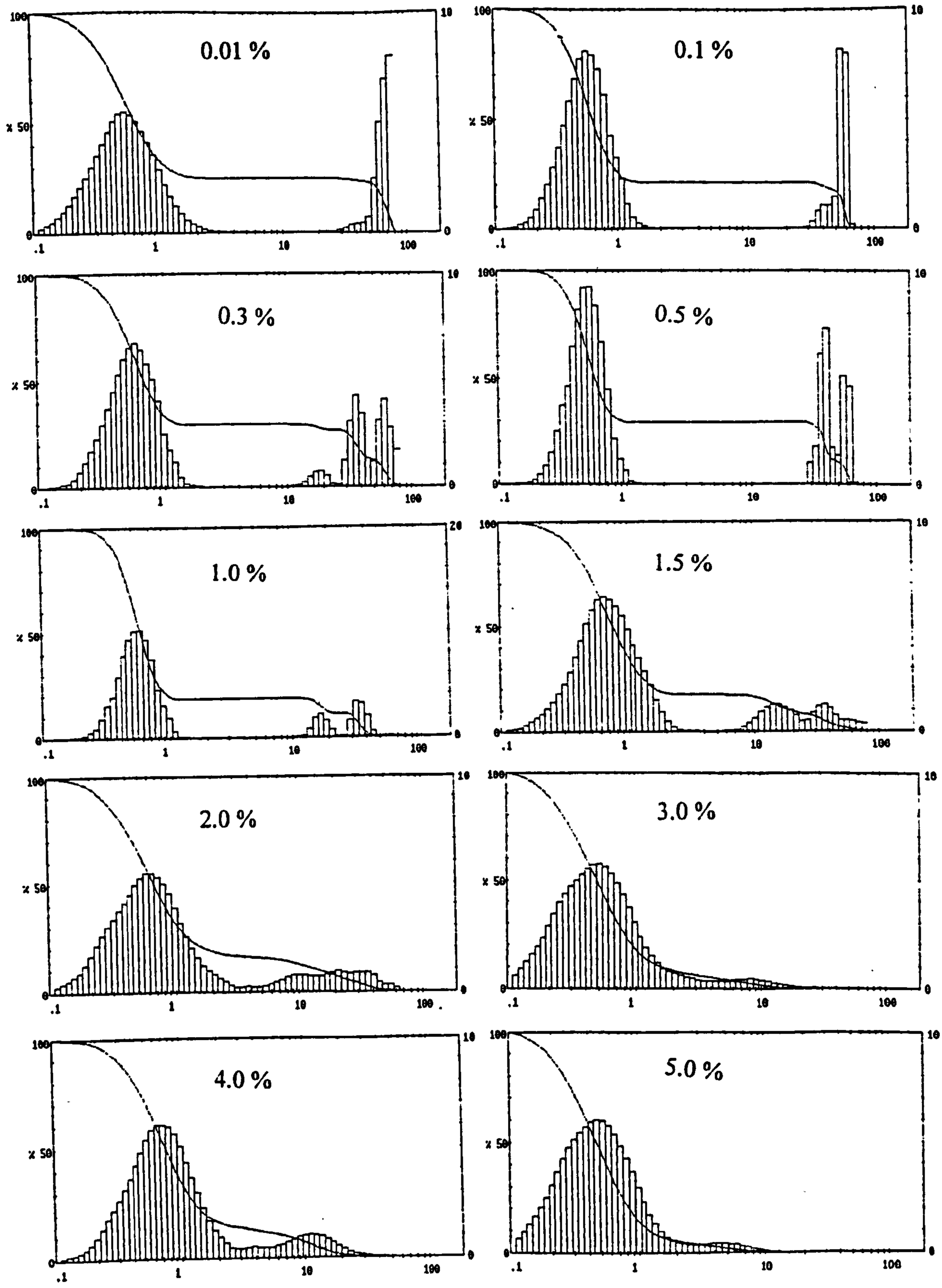

Figure 4.8

Optical microscopy images of water-in-toluene emulsion ($\phi_w = 0.5$) stabilised by H30 particles as a function of initial concentration of particles in oil (given). Scale bar equals 100 μm.

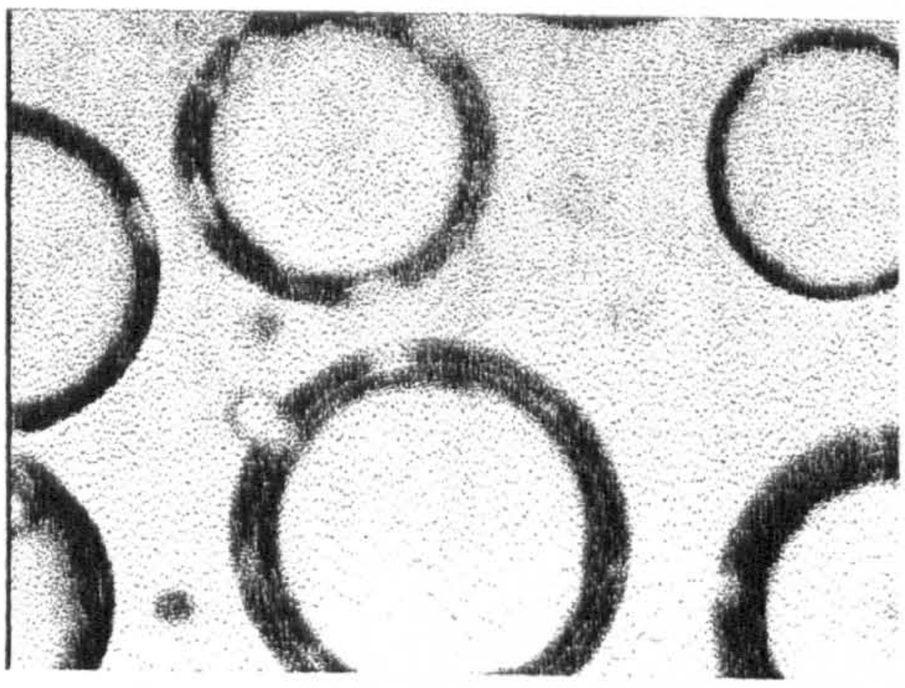

0.1 wt.%

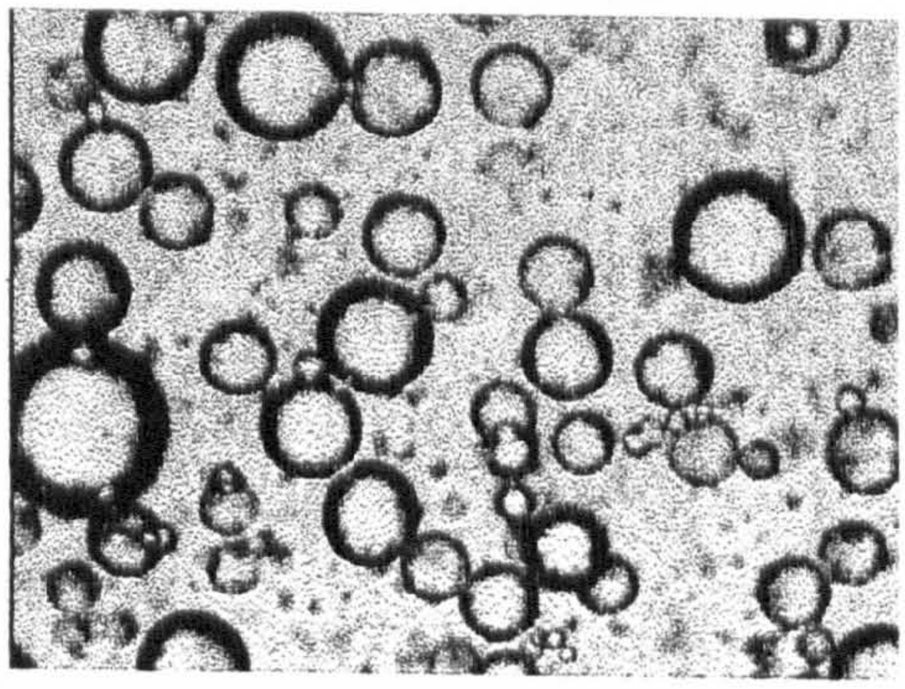

0.5 wt.%

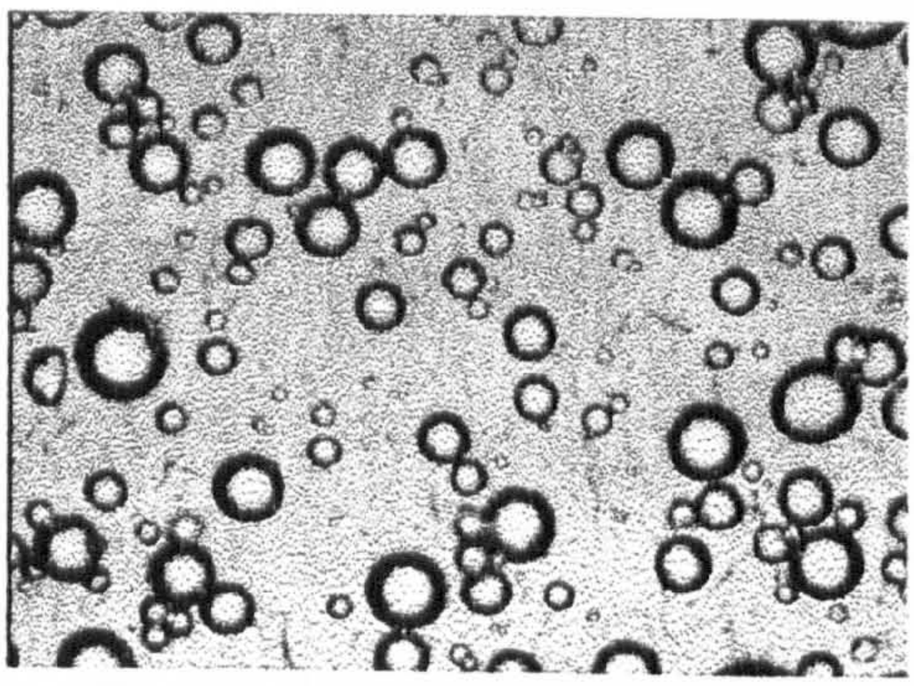

1.0 wt.%

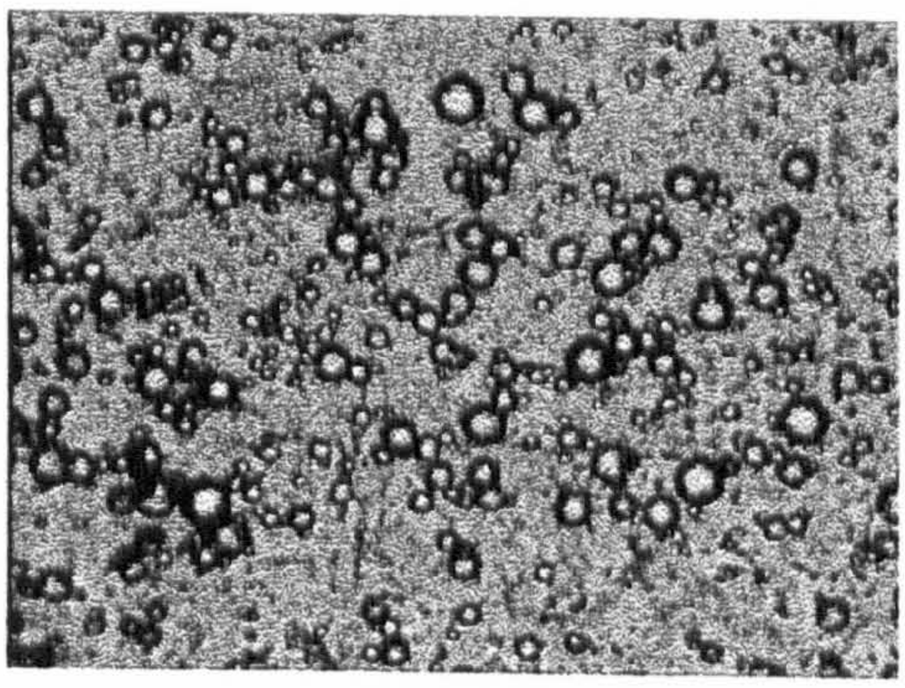

2.0 wt.%

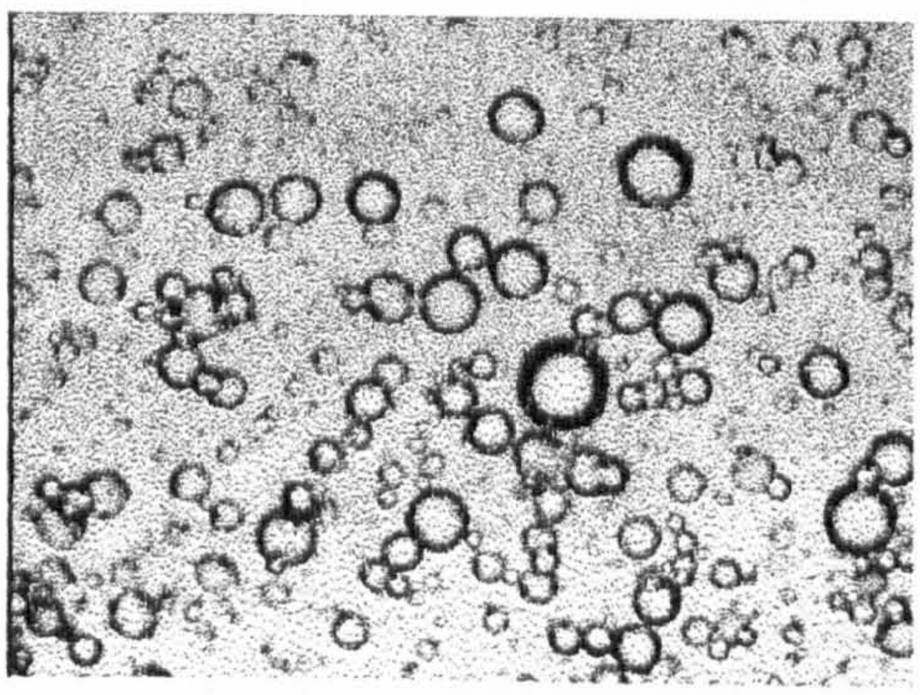

2.5 wt.%

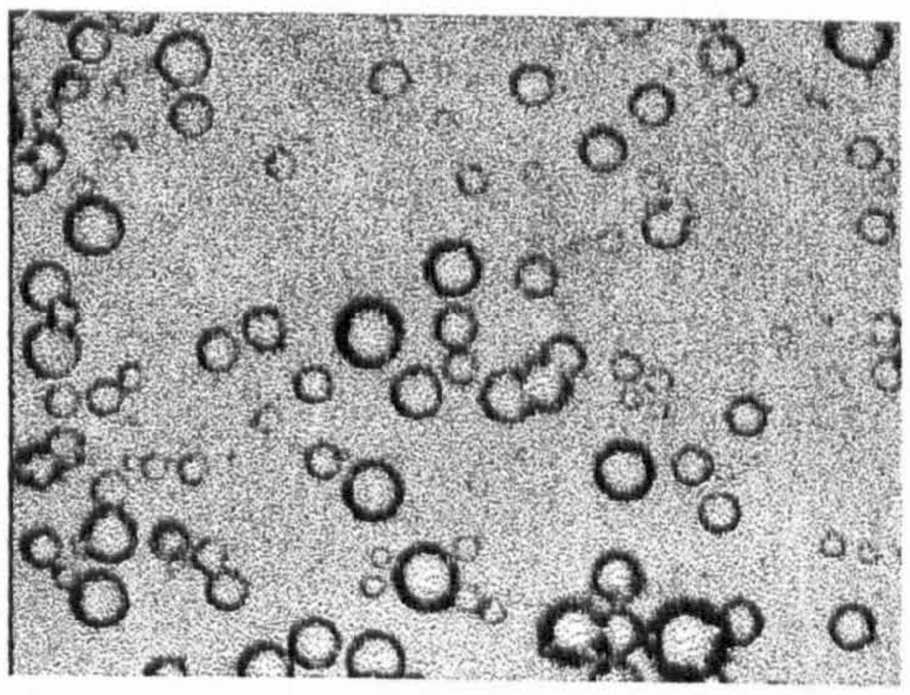

3.0 wt.%

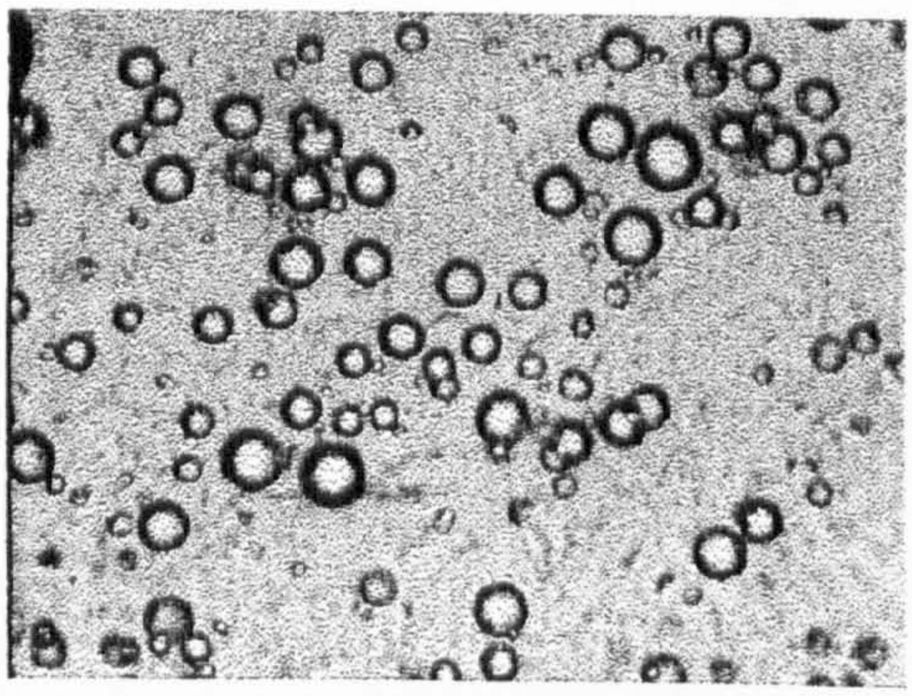

4.0 wt.%

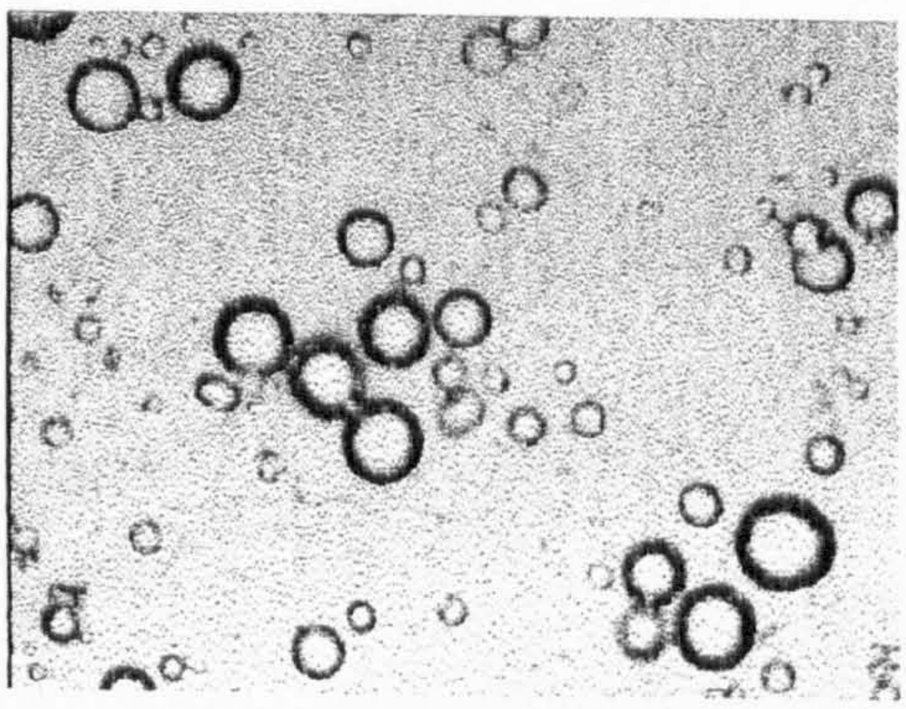

5.0 wt.%

Figure 4.9

Effect of homogenisation speed for 2 minutes on the various volume drop diameters for water-in-toluene emulsions (ϕ_w = 0.1) stabilised by 2 wt.% H30. v(x) is the drop diameter below which 100x % of the drops are present.

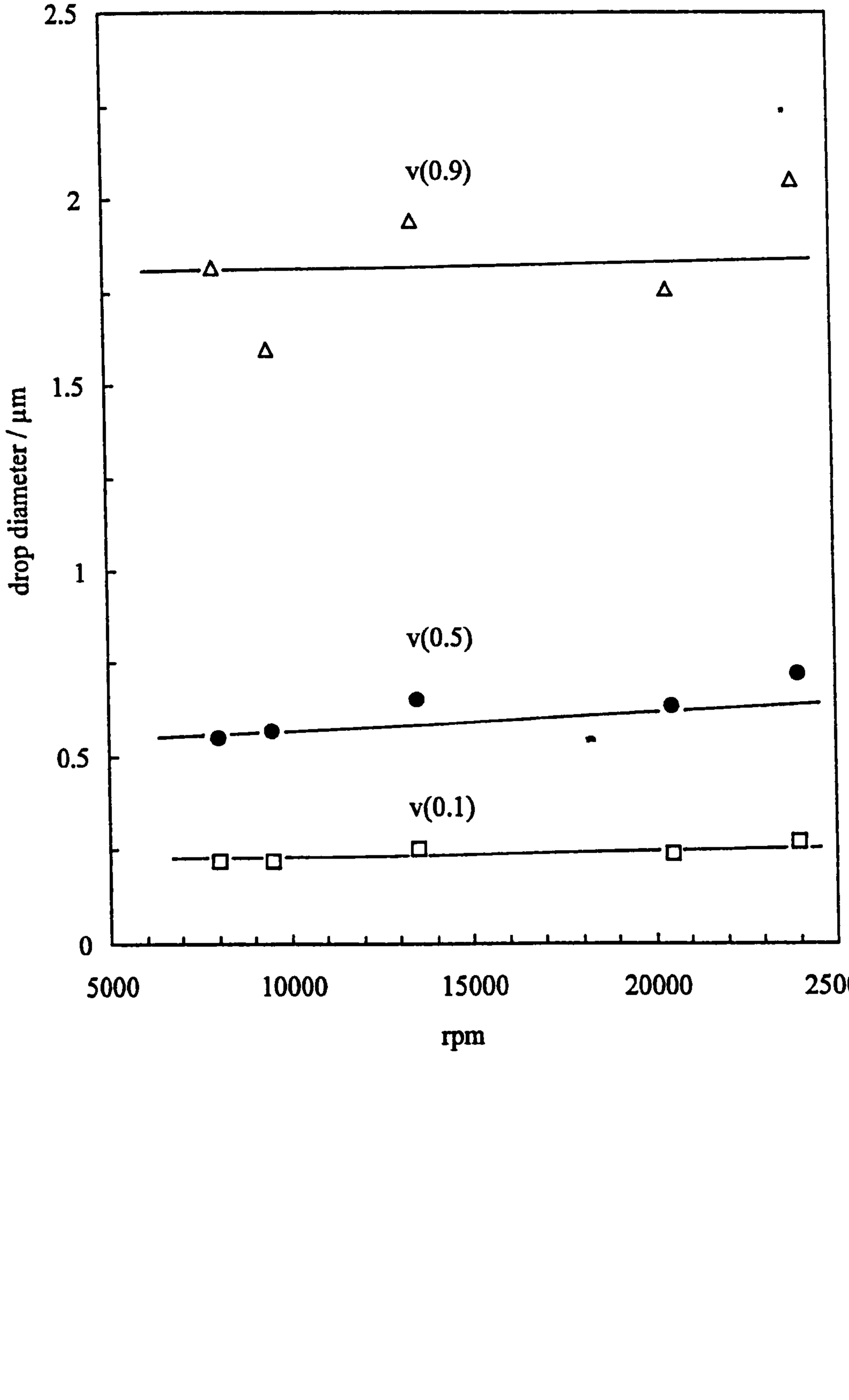

Figure 4.10

Conductivity of water-toluene emulsions stabilised by 2 wt.% H30 particles in oil as a function of the volume fraction of water. Water added sequentially to oil (open points) or oil added sequentially to water (filled points).

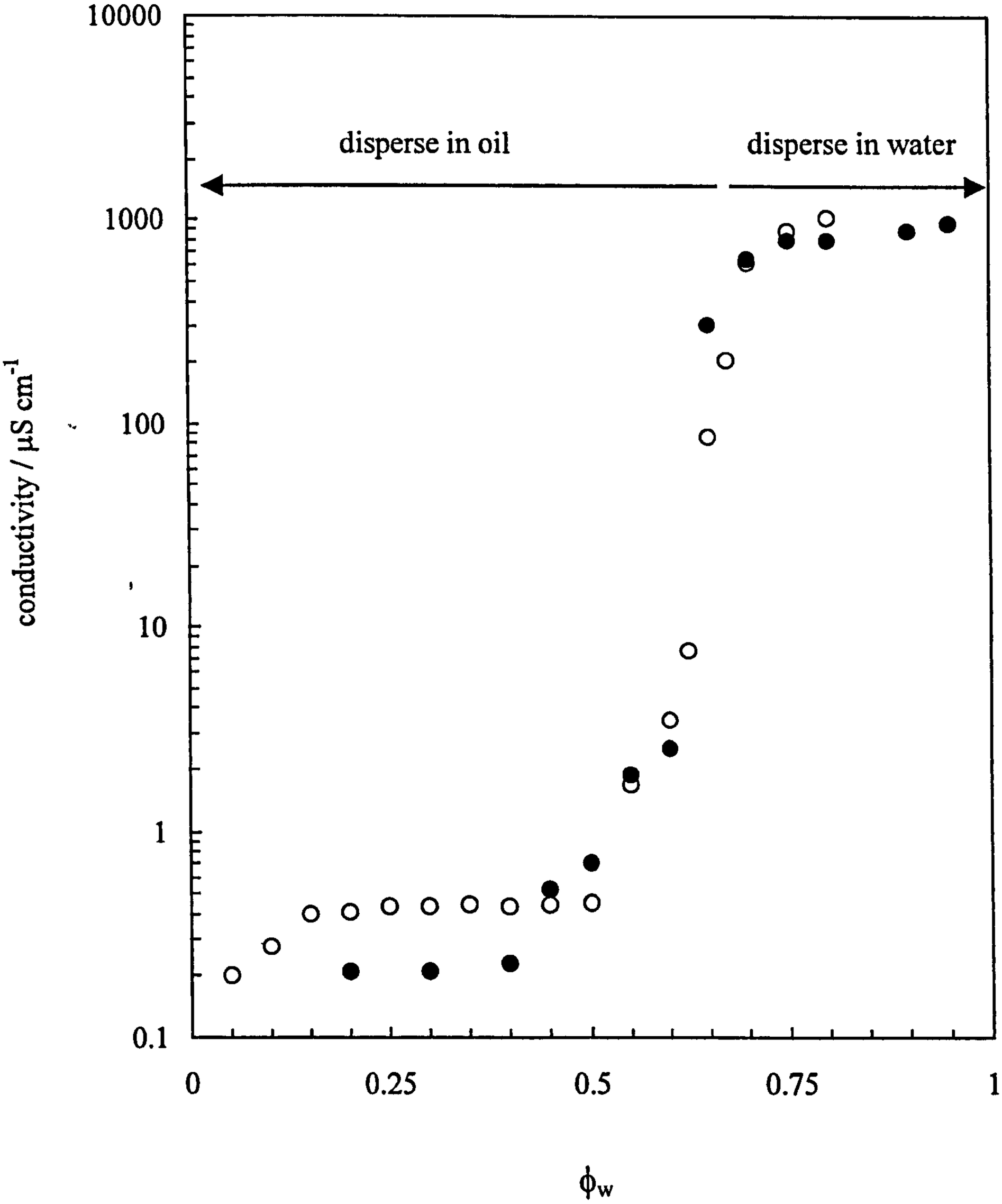

emulsions prepared by sequential addition of water to toluene (open points) or by sequential addition of toluene to water (filled points), the oil containing 2 wt.% particles in both cases. The conductivity is low, similar to that of pure toluene (0.1 $\mu S\ cm^{-1}$), at low ϕ_w and increases by four orders of magnitude at high ϕ_w. Below $\phi_w = 0.7$ the emulsions dispersed in toluene but not in water (indicative of w/o), whereas above this value they dispersed in water and not in toluene (indicative of o/w). Remarkably, phase inversion occurs without hysteresis in contrast to surfactant-stabilised emulsions where the two curves may be separated by as much as 0.3 in volume fraction.[124 - 126] Hysteresis is linked with the irreversible instability phenomena sometimes referred to as catastrophes as described earlier. In Figure 4.11, emulsions were prepared separately at each ϕ_w by direct mixing of components. The data sets refer to a fixed concentration of particles in oil ([particles] varies in emulsions) and a constant particle concentration in all emulsions ([particles] varies in oil). Again the two routes invert at $\phi_w \approx 0.7$, which confirms that irrespective of route or particle concentration, emulsion phase inversion can be achieved without altering the particle wettability. It was also observed that the emulsion viscosity passes through a maximum around the inversion condition as seen previously by other authors.[127, 128] The absence of hysteresis is unique to solid-stabilised emulsions and is in direct contrast to the mathematical predictions of catastrophe theory. The desire for the solid particles to form the preferred emulsion type is so great that the mode of preparation is irrelevant in these systems.

The stability of the previous emulsions is very sensitive to the volume fraction of water. However, all emulsions whether w/o or o/w are completely stable to coalescence at all ϕ_w for up to 6 months. This is in marked contrast to surfactant systems where coalescence is appreciable around phase inversion.[129] The time dependence of sedimentation of w/o emulsions below $\phi_w = 0.7$ and creaming of o/w emulsions above $\phi_w = 0.7$ is given in Figures 4.12 and 4.13 respectively. The ordinates indicate the fraction of continuous phase resolved calculated using equations 3.28 and 3.29 without including the term in the second bracket so that these values are independent of volume fraction. For w/o emulsions (Figure 4.12), stability increases with ϕ_w, with a noticeable increase between 0.2 and 0.3 (cf. vertical dotted line in Figure 4.3). For o/w emulsions (Figure 4.13), stability decreases with ϕ_w with creaming virtually complete after 1 hour. Both data sets are summarised in Figure 4.14 where the stability of toluene-water emulsions after 1 hour is plotted as a function of ϕ_w. A stability maximum is clearly

Figure 4.11

Conductivity of water-toluene emulsions stabilised by H30 silica particles as a function of the volume fraction of water. Emulsions prepared at each ϕ_w by direct mixing of components. Open points: 1 wt.% particles in emulsion. Filled points: 2 wt.% particles in oil initially.

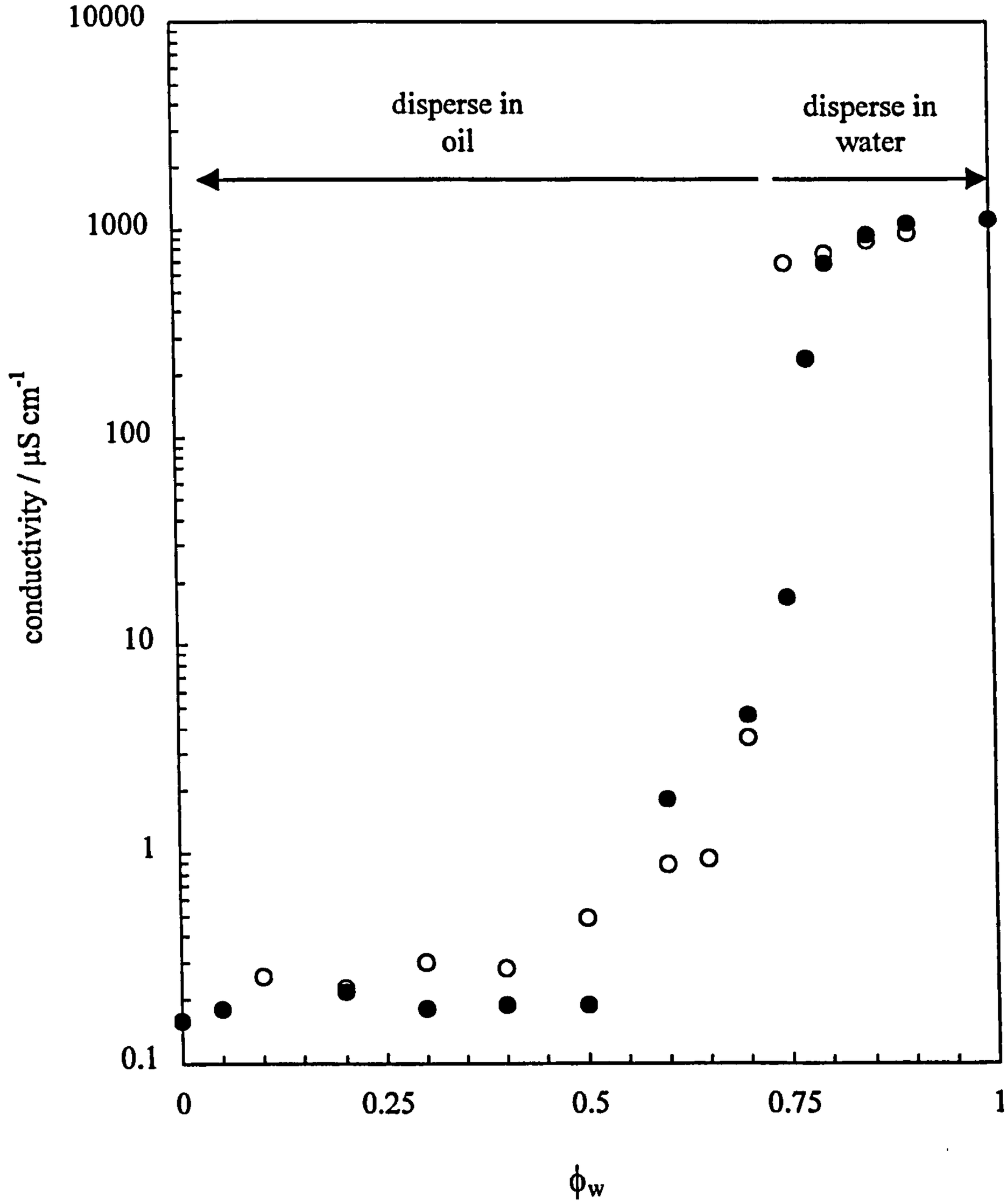

Figure 4.13

Fraction of aqueous phase resolved versus time for toluene-in-water emulsions stabilised by 2 wt.% H30 particles in oil for different ϕ_w given.

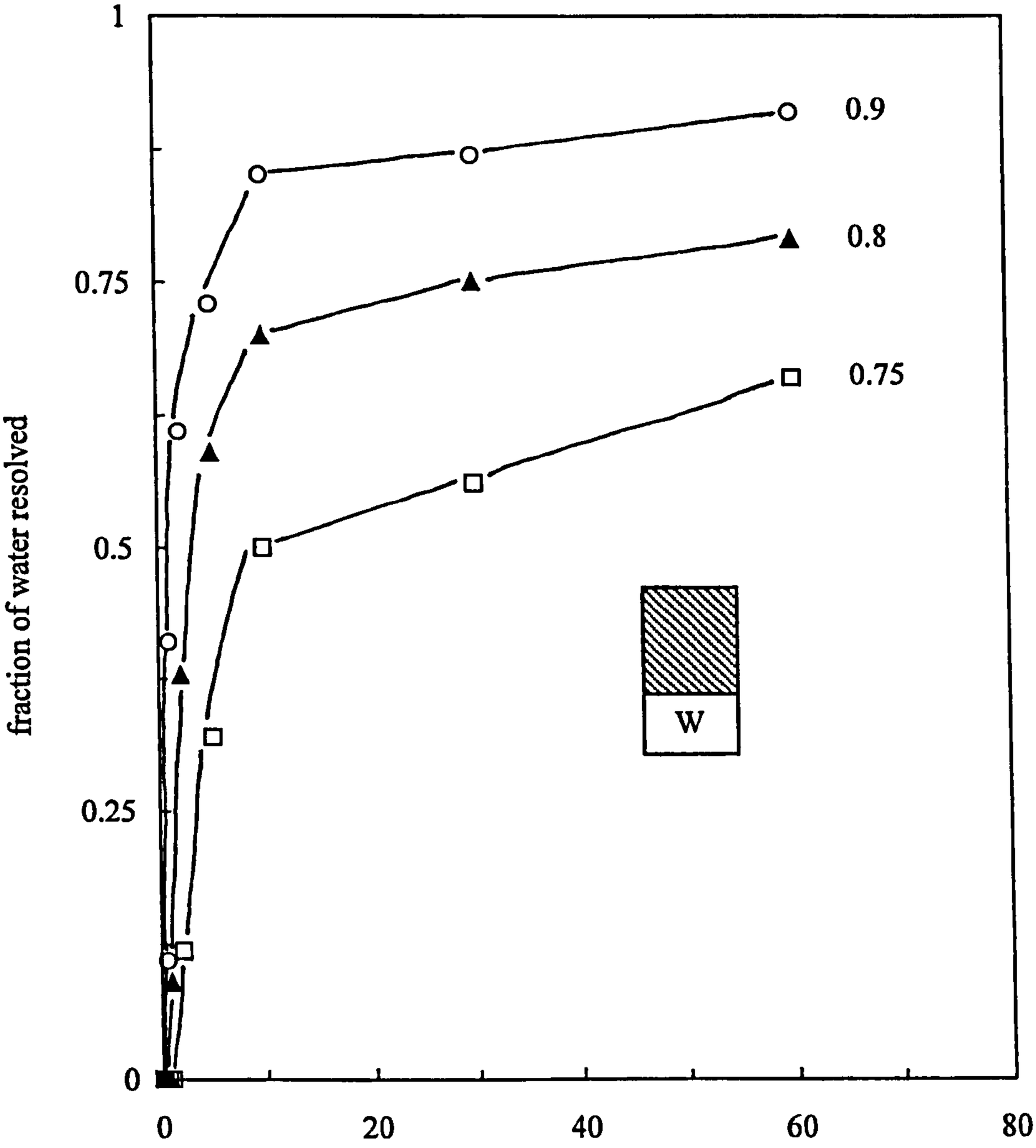

Figure 4.14

Stability after 1 hour of toluene-water emulsions stabilised by 2 wt.% H30 particles in oil as a function of ϕ_w. Triangles refer to coalescence; circles refer to sedimentation for w/o and creaming for o/w emulsions.

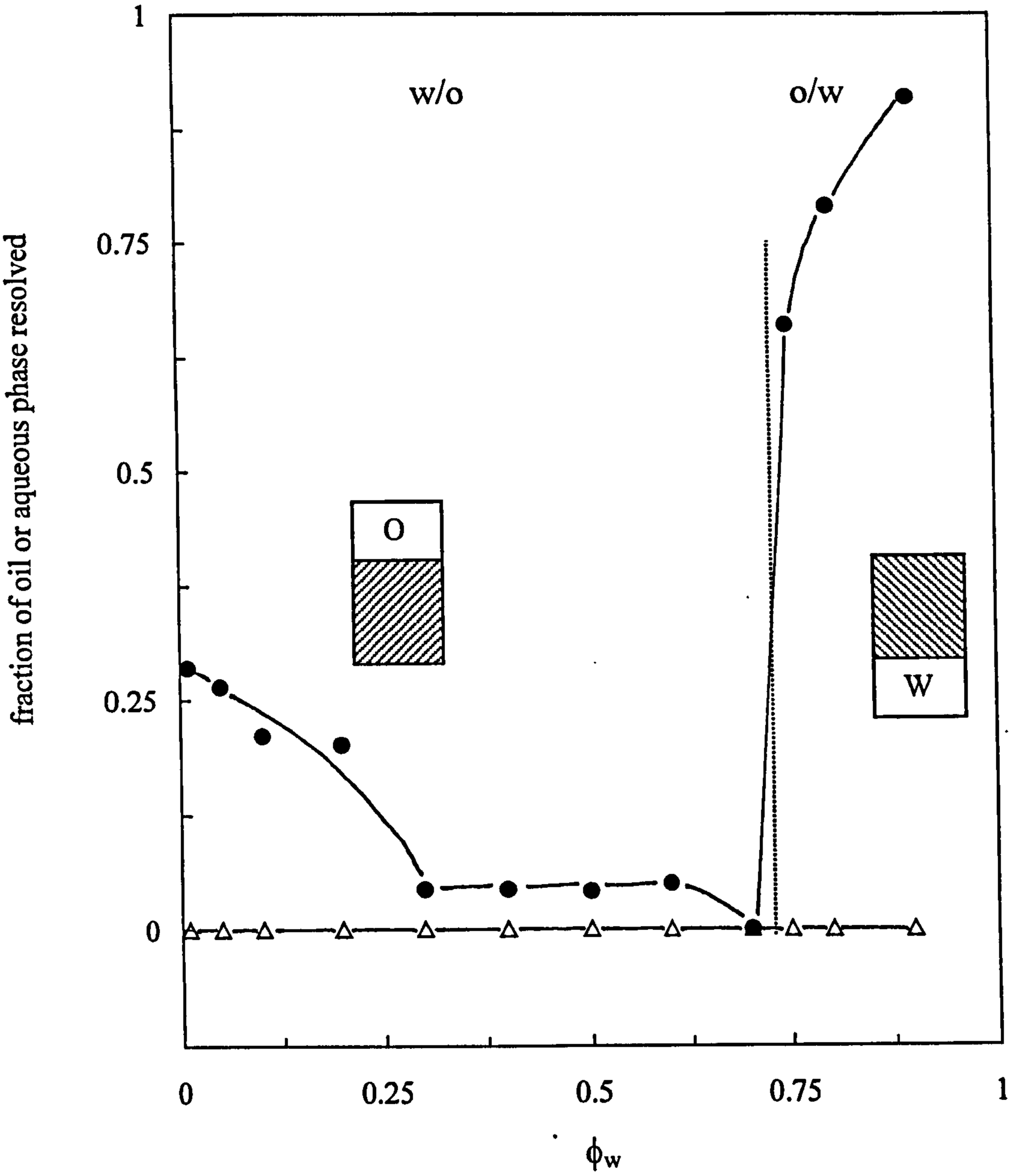

visible around phase inversion. The most stable emulsions are w/o just below inversion and the stabilities of the o/w emulsions are significantly lower than any of the w/o emulsions. The difference in the relative stabilities is due in part to the very different drop sizes presented below.

Figure 4.15 shows the drop diameter distributions of emulsions stabilised by a constant initial particle concentration in oil of 2 wt.% at nine values of ϕ_w. The emulsions were prepared by sequential addition of water to oil. The w/o emulsions up to $\phi_w = 0.6$ change from a single log-normal distribution at low volume fraction to a bimodal distribution at higher ϕ_w but the majority of drops are less than 1 μm in both cases. Since the particle concentration in the system falls progressively, it appears that some of the additional water added creates a new interface which may not be covered sufficiently by adsorbed particles, so that drop growth by coalescence becomes possible during emulsification. The o/w emulsions at $\phi_w \geq 0.7$ show a single log-normal distribution at much larger diameters (around 100 μm) with a concomitant reduction in interface area. The drop size distributions are summarised in Figure 4.16 where the arithmetic mean (d(4,3)) and the median diameter (d(v,0.5)) are plotted as a function of ϕ_w. The mean diameter, which is more representative of the whole distribution due to the bi-modality in some cases, increases progressively to 10 μm up to inversion whereupon it increases by a factor of 10 once the o/w emulsions are formed. The median diameter is more biased to the small size drop fraction and a discontinuous change occurs between w/o and o/w emulsions. Figure 4.16 also shows the sizes of emulsions prepared separately at each ϕ_w by direct mixing (diamonds). The two data sets are virtually identical confirming that phase inversion does not depend on the previous history of the emulsion.

At the phase inversion volume fraction a dramatic change in the system occurs as water (or oil) drops coalesce and the original continuous oil (or water) phase forms the dispersed phase. The volume fraction of dispersed phase at inversion is either 0.7 upon increasing the water content or 0.3 upon increasing the oil content (Figures 4.10 and 4.11), hence the mechanism of inversion is presumably different in the two cases. Inversion occurs from a state of close packed, small drops to a more dilute state of large drops or vice versa. At a water volume fraction of 0.7 the water drops are near to the limit of close-packing for spherical drops, implying that coalescence of w/o emulsions is initiated as soon as the drops begin to deform. Above inversion the o/w emulsions

Figure 4.15

Effect of ϕ_w (given) on the drop diameter volume distributions (right-hand ordinate) for water-toluene emulsions stabilised by H30 particles prepared by sequential addition of water to oil (containing 2 wt.% particles). Emulsions are w/o for $\phi_w \leq 0.65$ and o/w above this. The solid curves show the cumulative volume distributions (left-hand ordinate).

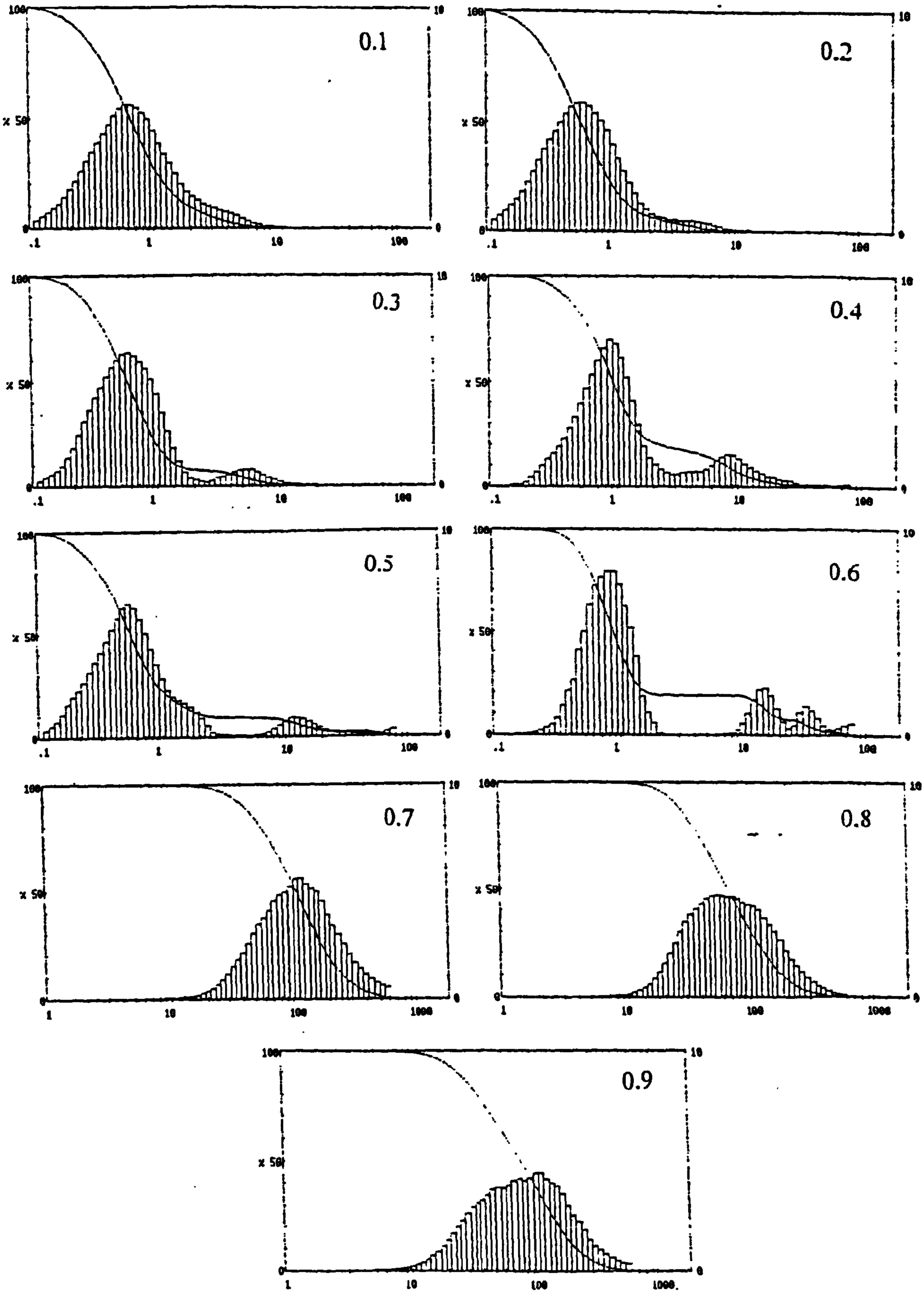

Figure 4.16

Drop diameters versus ϕ_w for toluene-water emulsions stabilised by 2 wt.% H30 particles. d(4,3) is the arithmetic mean diameter (filled points), d(v,0.5) is the initial volume average diameter (open points). Circles are emulsions prepared by sequential addition; diamonds are emulsions prepared by direct addition.

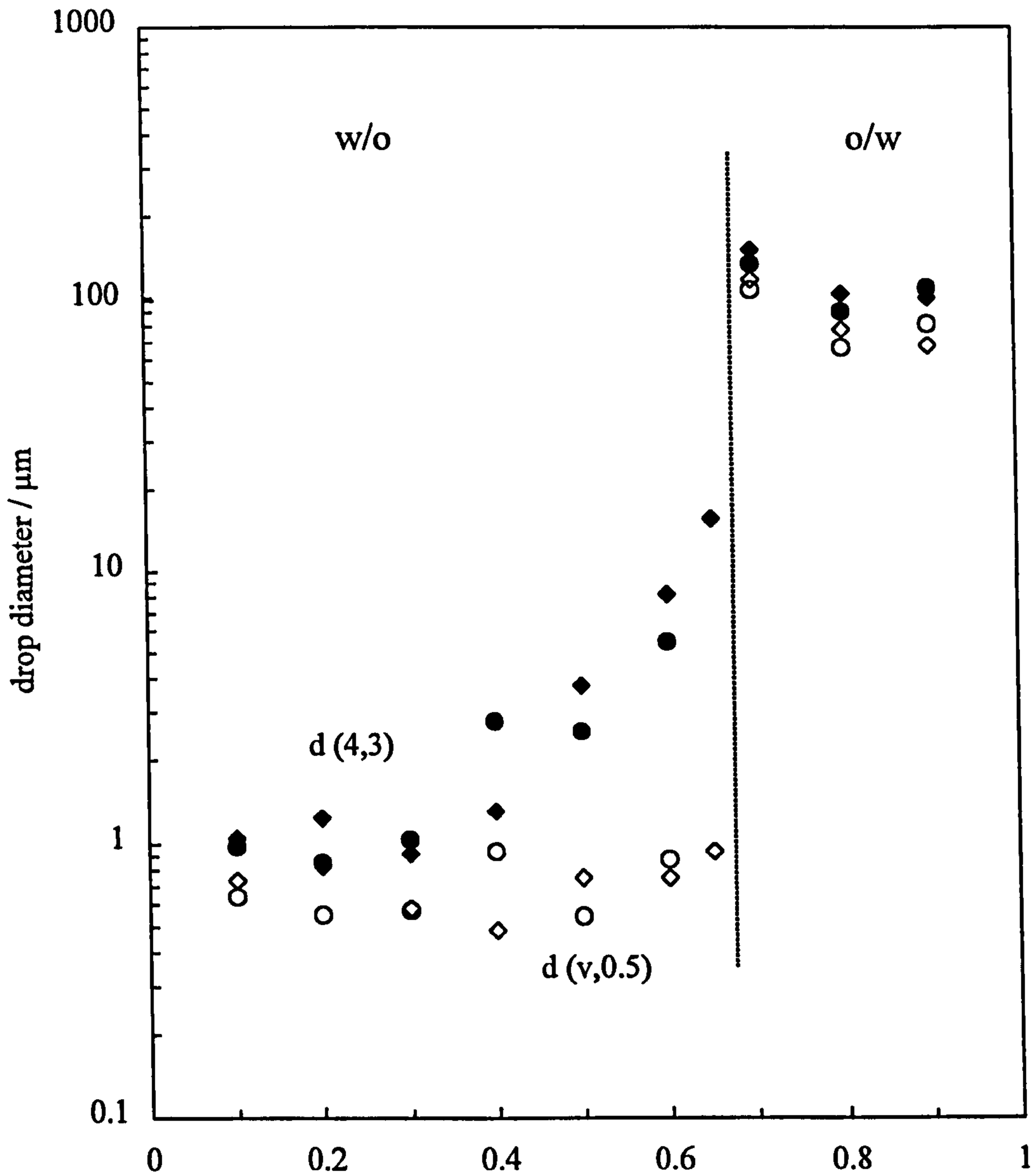

cream to an extent which depends on the initial ϕ_w. The continuous phase of the cream has been confirmed to be water and Figure 4.17(a) shows how the volume fraction of oil in the cream varies with the initial ϕ_w. During creaming, ϕ_o in the remaining emulsion increases with a larger change occurring at higher ϕ_w. It is worth noting that even for the most concentrated cream (at $\phi_w = 0.95$), the value of ϕ_o is, within error, just less than that at the critical inversion condition (≈ 0.75) and hence it itself does not invert but remains o/w. During creaming, there is a fractionation in size of the drops as the larger ones rise first. Figures 4.17(b) and (c) shows optical microscopy images of the emulsion sampled from the bottom and top of the cream respectively. At the bottom of the cream, the majority of the drops are spherical, relatively small and slightly flocculated. The larger drops at the top of the cream are non-spherical exhibiting peculiar shapes which move slowly across the field of view. When the oil drops collide coalescence does not occur but the interfaces are seen to deform followed by drop separation. Unlike surfactant systems, there is little evidence of multiple w/o/w drops.

In contrast to hydrophobic particles, high HLB systems are thought to arise from hydrophilic particles at $\phi_w = 0.5$. The conductivity of emulsions stabilised by hydrophilic particles as a function of ϕ_w is given in Figure 4.18. The conductivity is high at $\phi_w = 0.5$ indicative of o/w emulsions. The conductivity of these o/w emulsions decreases slightly with decreasing ϕ_w since the oil drops formed act as obstructing entities in the conduction of the aqueous phase. As the volume fraction of water is decreased further the emulsions invert to w/o at a $\phi_w = 0.3$. This is the same value of dispersed phase as was seen in hydrophobic silica-stabilised emulsions. The w/o emulsions formed are very unstable but catastrophic inversion of the emulsion is definitely apparent. Again, no hysteresis is observed as a result of the mode of addition (filled and open points). In contrast to w/o emulsions stabilised by hydrophobic particles, o/w emulsions stabilised by hydrophilic N20 are of average diameter around 150 μm (Figure 4.19) and therefore cream rapidly. Since the N20 particles are very hydrophilic this lowers the tendency for them to leave the bulk aqueous phase and enter the oil-water interface. In contrast, the H30 particles are only partially hydrophobic and more readily adsorb at the interface.

Figure 4.17

Toluene-in-water emulsions stabilised by H30 particles. (a) Volume fraction of oil in creamed emulsion versus initial volume fraction of water. Micrographs of o/w emulsion from initial $\phi_w = 0.85$ sampled from bottom of cream (b) and top of cream (c). Scale bar equals 50 μm.

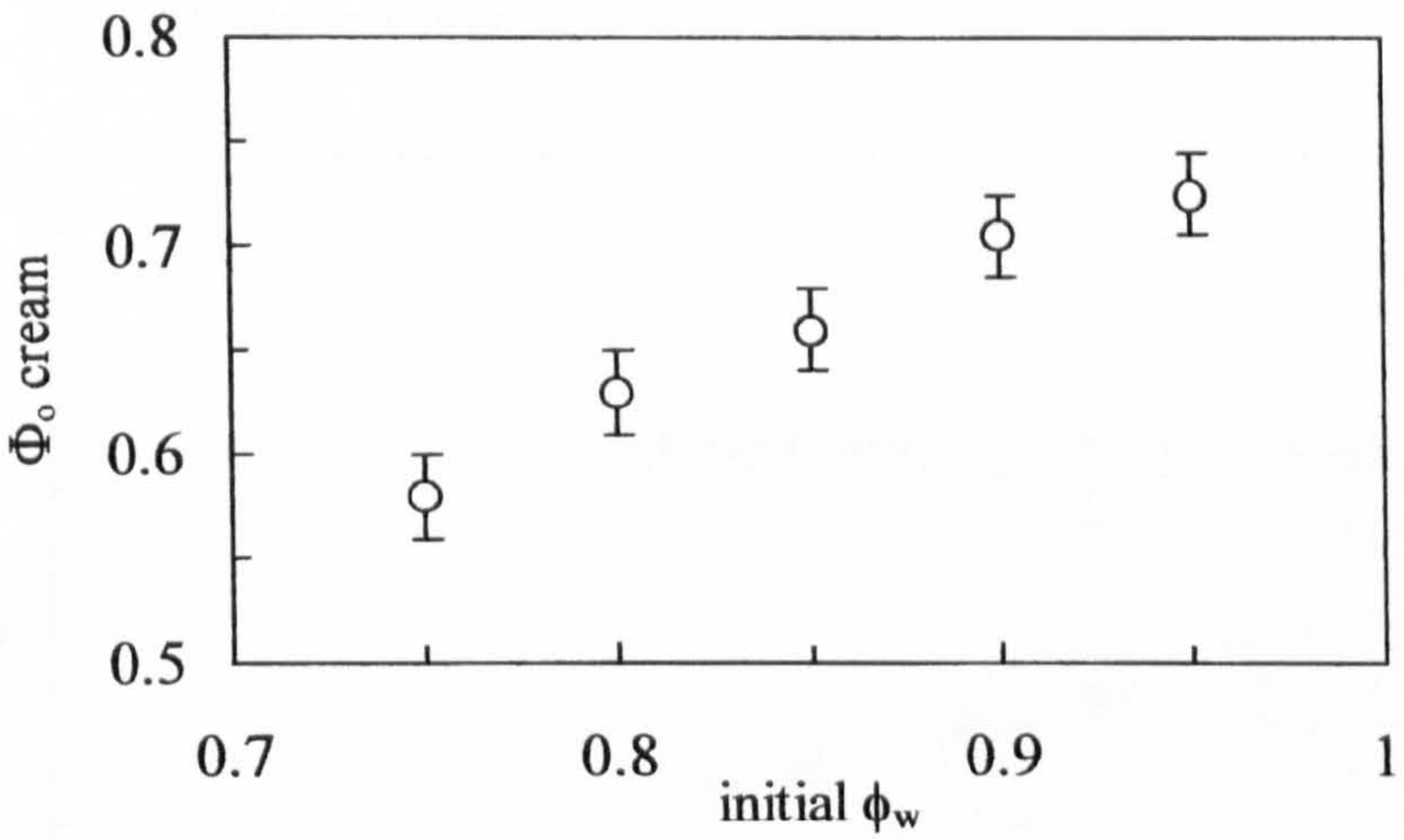

(a)

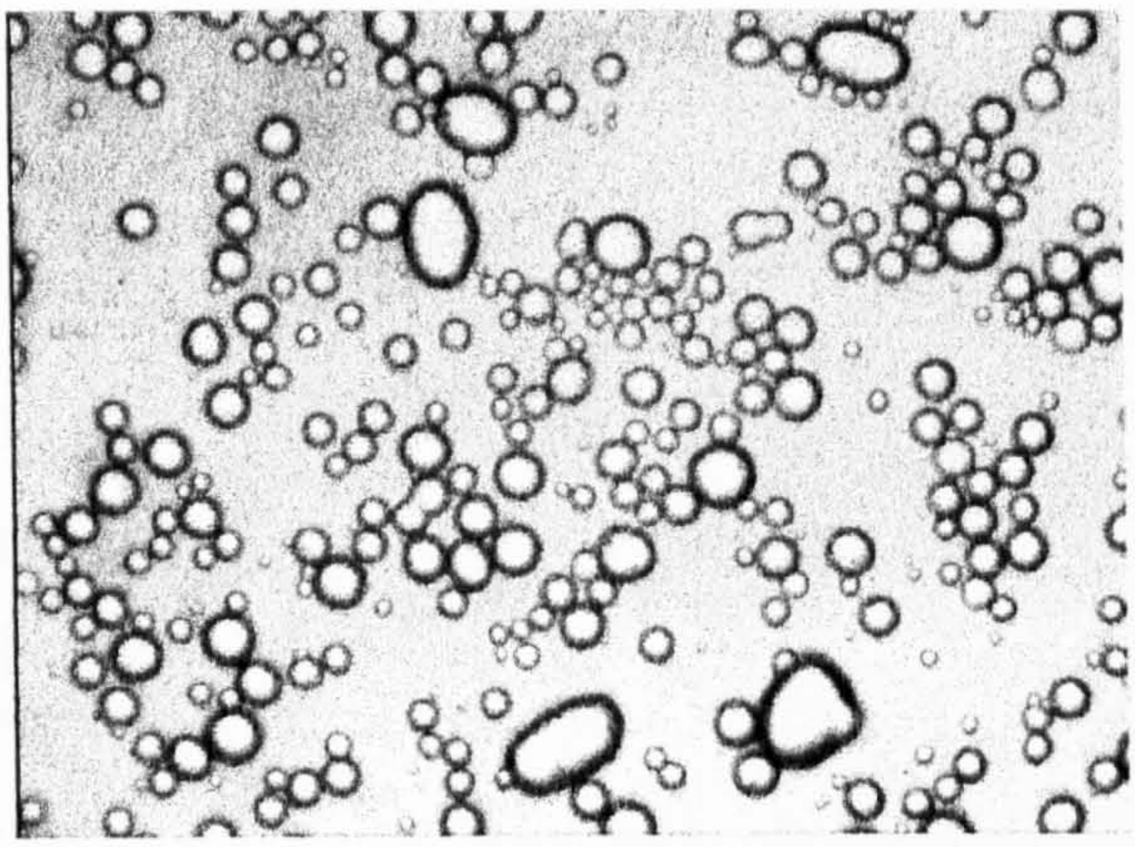

(b) sampled from bottom

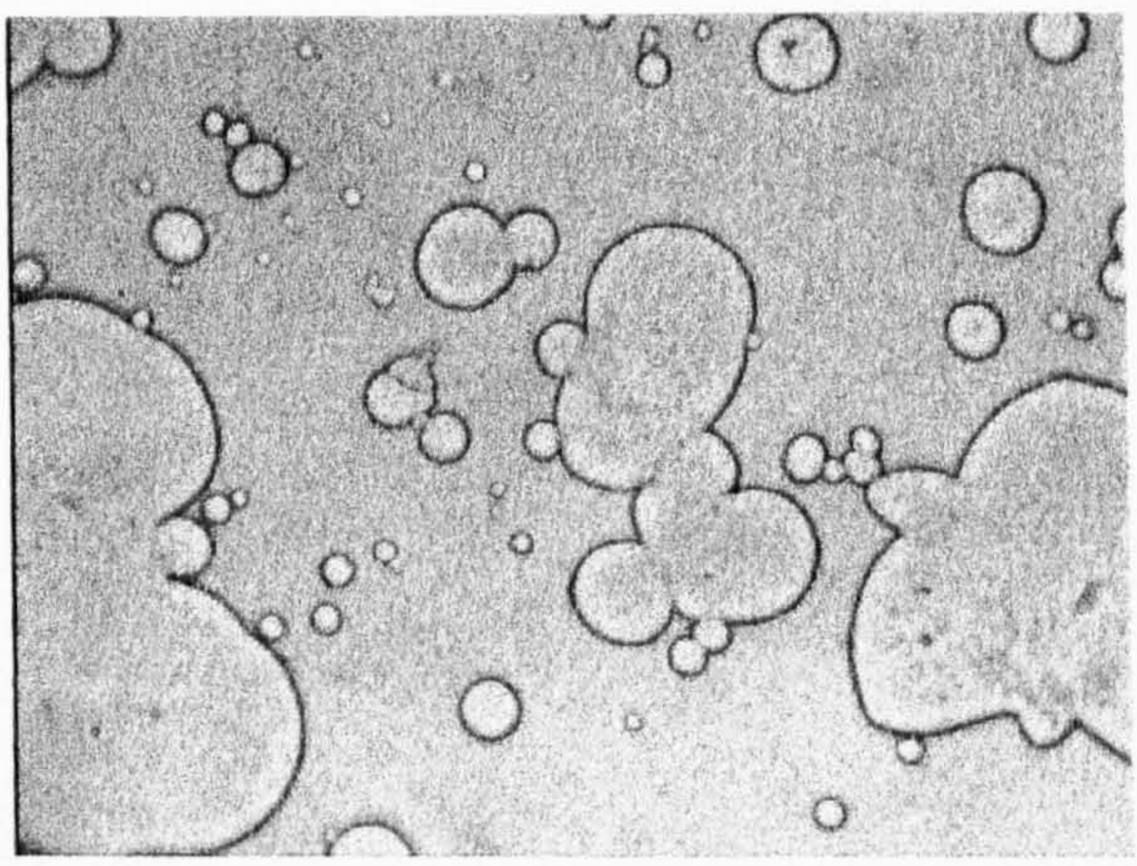

(c) sampled from top

Figure 4.18

In-situ conductivity of toluene-water emulsions stabilised by 10 wt.% N20 silica in water as a function of ϕ_w (homogenising at 24000 rpm for 1 minute between additions). Circles – oil added sequentially to water; squares – water added to oil.

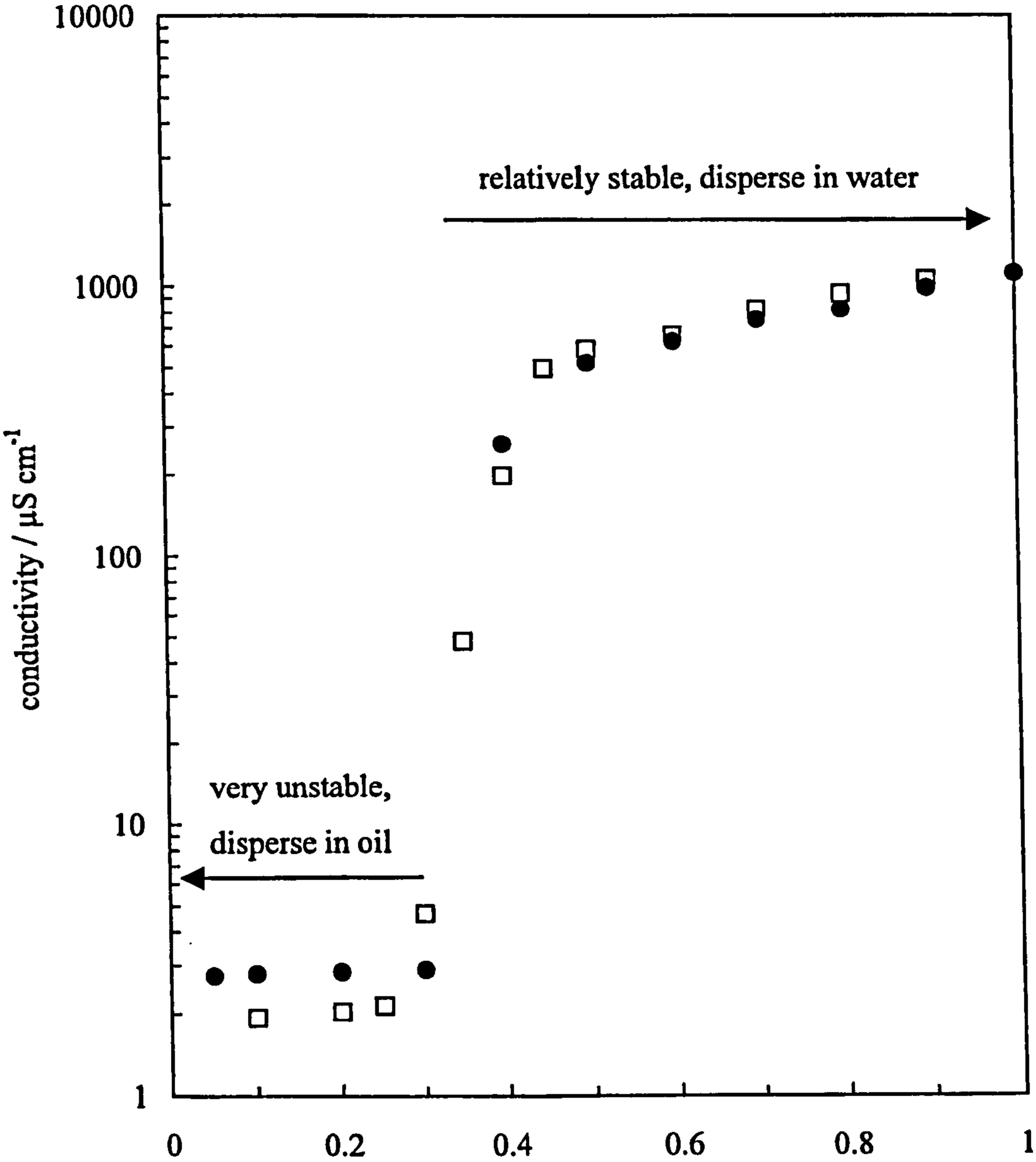

Figure 4.19

Drop diameter distribution of toluene-in-water emulsion at $\phi_w = 0.5$ stabilised by 5 wt.% N20 particles in water.

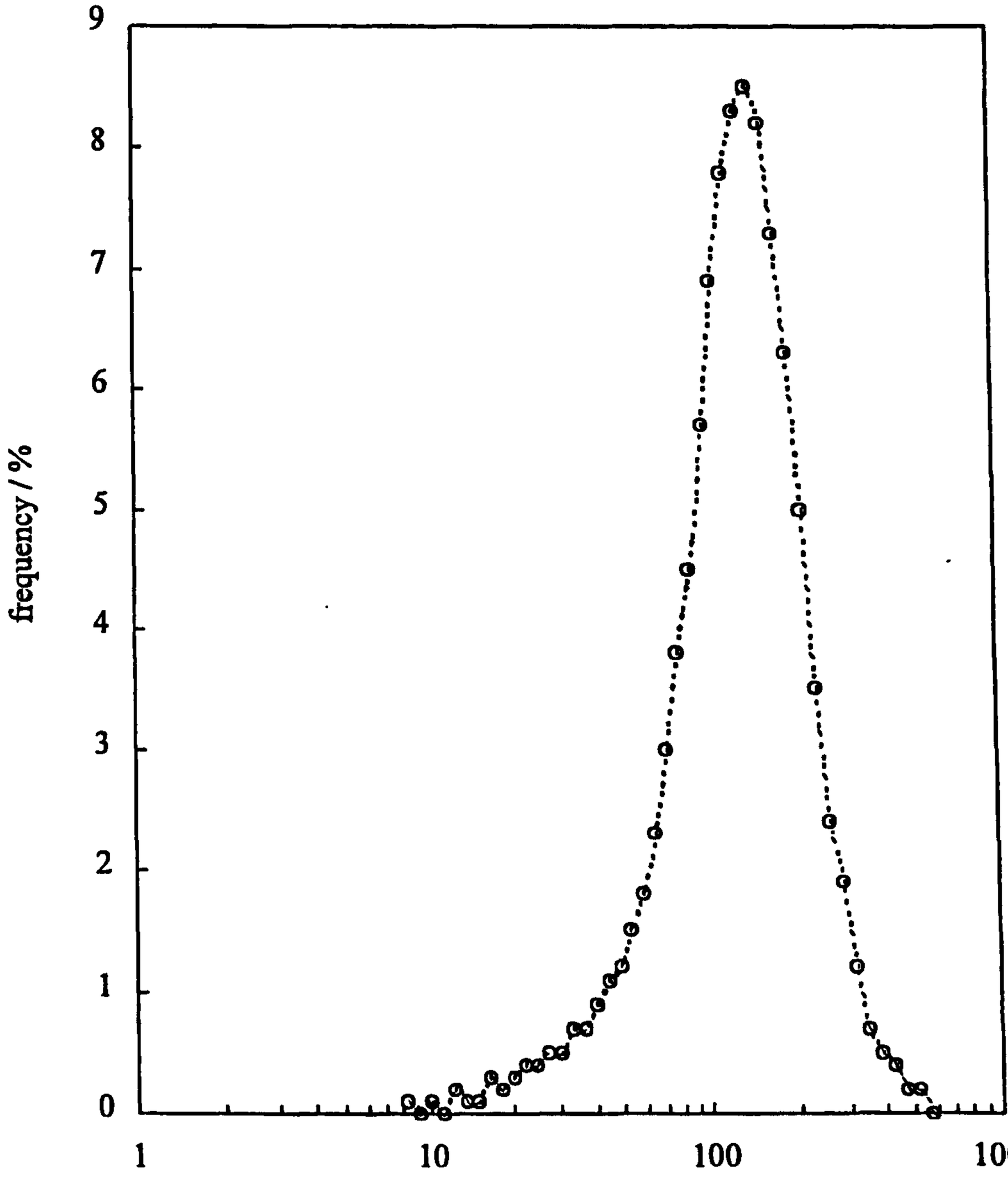

4.4 Effect of oil type and aqueous phase composition

In surfactant-stabilised emulsions the type of oil is important in dictating the emulsion type for equal volumes of oil and water. Short chain alkanes and aromatic oils favour w/o emulsions whereas long chain alkanes and polymeric silicone oils favour o/w emulsions.[130] The reasons for this difference are related to the extent of oil penetration into the surfactant chain region and hence to the preferred curvature of the oil-water interface. The effect of oil type has been investigated for solid-stabilised emulsions to see if it has any effect on the wettability of the particles. The conductivity of hydrophobic H30 silica stabilised emulsions as a function of ϕ_w has been investigated for a fluorinated oil, a linear alkane, a silicone oil and an iodine-containing oil. These oils were chosen so as to vary the cohesive energy density (c.e.d.), defined as the enthalpy required to vapourise a unit volume of liquid, from a low (fluorinated) to a high extreme (iodine-containing). The c.e.d. is reflected in, for example, the liquid-vapour surface tension, γ, and the contact angle the liquid makes with a hydrophobic solid surface in air, θ_a. A selection of values for γ and θ_a on a hydrophobic Teflon surface at 25 °C are given in Table 4.2. The cohesion between molecules in the pure liquid is lowest for fluorocarbons, is intermediate for hydrocarbons (silicone oils behaving similarly), and is highest for diiodomethane (due mainly to its high refractive index of 1.7425 and hence polarisability). The conductivity of emulsions containing the various oils is given in Figure 4.20 where it can be seen that inversion from w/o to o/w occurs for

Table 4.2 Surface tensions and contact angles on a hydrophobic Teflon surface under air for various oils

Oil	γ / mN m^{-1}	θ_a / °
perfluorohexane	11.4	0
toluene	27.9	50
Diiodomethane	51.3	102

Figure 4.20

Conductivity of oil-water emulsions stabilised by H30 particles versus ϕ_w. Oils are perfluorohexane (triangles, 2 wt.%), tetradecane (circles, 2 wt.%), PDMS (squares, 2 wt.%), and diiodomethane (crosses, 0.5 wt.%). Tetradecane and water at pH 1 (diamonds, 2 wt.%) also shown.

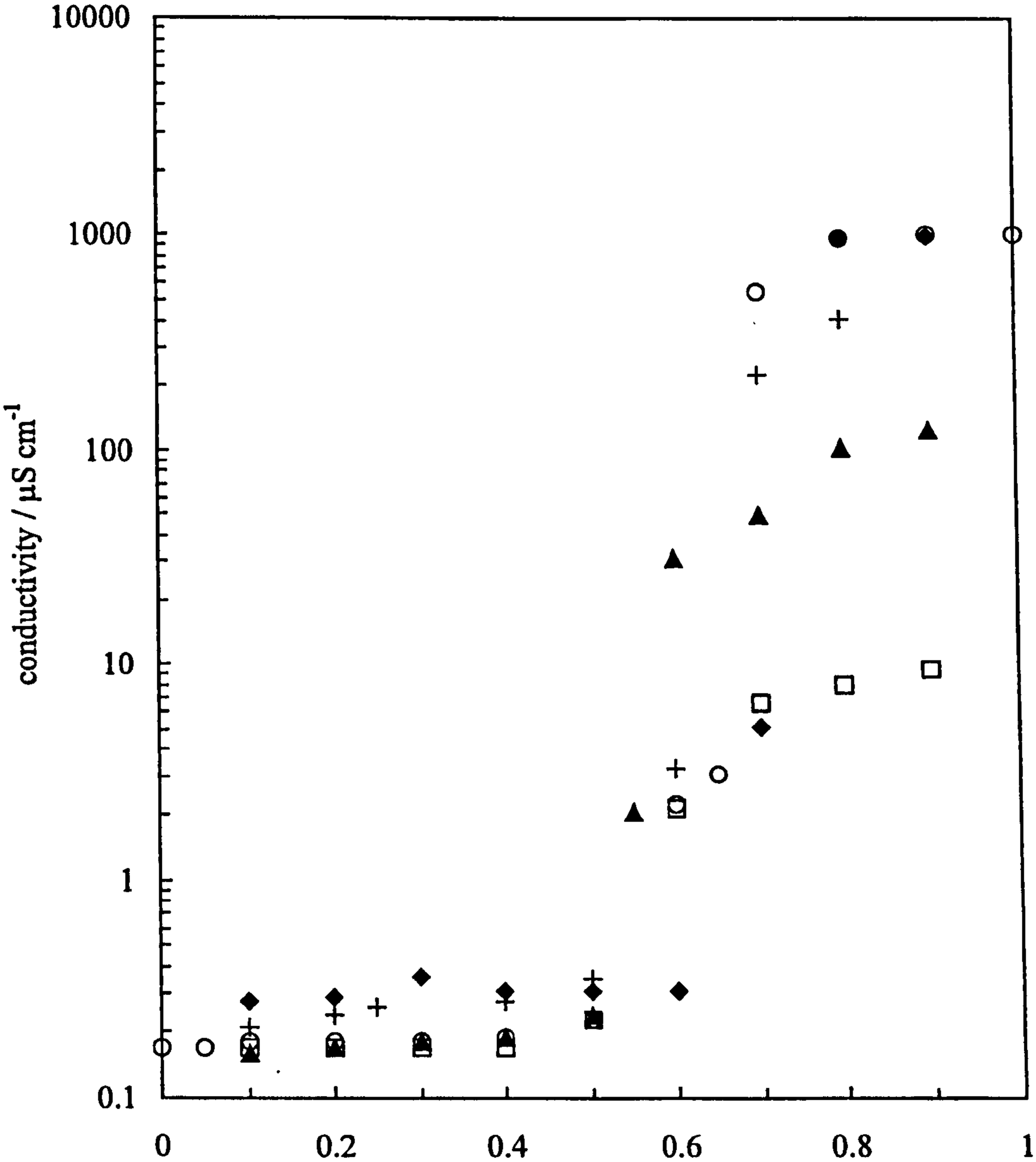

perfluorohexane, tetradecane and diiodomethane around ϕ_w equal to 0.65 similar to that for toluene. For PDMS, emulsions remained w/o up to $\phi_w = 0.9$ with only a slight increase in conductivity at high ϕ_w. It is known that PDMS adsorbs onto silylated silica[131] which may increase the hydrophobicity of the particles further so that the system will not invert to o/w emulsions even at high ϕ_w. From these results it can be concluded that the preferred emulsion type for this hydrophobic particle is w/o and that the type of oil has no influence on this.

The hydrophobic H30 particle is only partially hydrophobic and has approximately 50 % SiOH groups remaining on the surface. An increase in the pH of the aqueous phase in the emulsions described previously (where the pH $\approx$ 6) causes the SiOH groups to ionise and hence become more water-liking. This may cause the preferred emulsion type at $\phi_w = 0.5$ to be o/w instead of w/o at extremes of aqueous phase pH. As described in Chapter 3, the i.e.p. of untreated silica is around pH 2, with surfaces being positively charged below and negatively charged above this pH. Emulsions of tetradecane and water ($\phi_w = 0.5$) containing 2 wt.% particles were w/o at pH 1 (adding HCl) and pH 10 (adding NaOH), and those at pH 1 inverted in the usual way (Figure 4.20, diamonds) again indicating that the wettability of these particles is not changed sufficiently to invert the preferred emulsion type. The effect of oil and aqueous phase type is investigated further in Chapter 7 for a silica particle of intermediate hydrophobicity (67 % SiOH) where inversion is dependent on the properties of the bulk phases.

4.5 Conclusions

The following conclusions can be drawn concerning the properties of emulsions stabilised solely by solid silica particles.

- Hydrophobic silica particles (50 % SiOH) stabilise w/o emulsions at $\phi_w = 0.5$ with a drop diameter of approximately 0.6 μm. These emulsions are stable to coalescence indefinitely and the stability to sedimentation increases with an increase in particle concentration, which is due to an increase in the viscosity of the continuous oil phase.

- Catastrophic phase inversion of the emulsions from w/o to o/w occurs at a volume fraction of water close to 0.7, with no hysteresis as a result of mode of addition. Dramatic changes in the emulsion stability and drop diameter occur on inversion. The preferred emulsion type remains w/o for this hydrophobic particle irrespective of the oil type or the aqueous phase pH.
- Hydrophilic silica particles (100 % SiOH) stabilise o/w emulsions at $\phi_w = 0.5$ with a drop diameter of approximately 120 μm. The emulsions invert to w/o at oil volume fractions of around 0.7. The preferred emulsions are also very stable to coalescence despite the large drop size.

CHAPTER 5

CHAPTER 5

TRANSITIONAL PHASE INVERSION OF SOLID-STABILISED EMULSIONS USING PARTICLE MIXTURES

5.1 Introduction

In the previous chapter it was proposed that the system HLB which determines the preferred emulsion type is dependent on the wettability of the silica particles at the oil-water interface. At $\phi_w = 0.5$, hydrophobic particles, which are preferentially wetted by the oil, stabilise w/o emulsions and hydrophilic particles, which are preferentially wetted by water, stabilise o/w emulsions. In comparison to surfactant-stabilised emulsions hydrophobic particles give rise to low HLB systems and hydrophilic particles give high HLB systems. It was shown that emulsions stabilised by one particle type (hydrophobic or hydrophilic) catastrophically phase invert without hysteresis from o/w to w/o or vice versa by increasing the volume fraction of dispersed phase above a critical value. This corresponds to a horizontal transition in Figure 5.1 from B to A for low HLB systems and B^1 to A^1 in high HLB systems. The emulsion stability and drop size change dramatically around inversion.

The HLB in surfactant systems has been shown to be affected by temperature[132], oil type[133], electrolyte concentration[134] and addition of co-surfactant[135] at fixed volume fraction of oil and water. This may result in inversion of the preferred emulsion type, known as *transitional phase inversion*. This corresponds to the vertical transition from 1 to 2 (or vice versa) in Figure 5.1. In Chapter 3, the presence of various electrolytes in emulsions stabilised by Aerosil 200 silica particles did not affect the type of emulsion formed. However, this was thought to be due to the very hydrophilic nature (100 % SiOH) of these particles causing the emulsions to remain o/w in all cases. Raising the temperature of emulsions stabilised by nonionic surfactants often results in phase inversion;[132] however temperature has little effect on solid-stabilised emulsions as the particles are much less labile than surfactants. The effect of oil type on emulsion behaviour is investigated further in Chapter 7. In this Chapter, the HLB of the system is

Figure 5.1

Schematic representation of transitional phase inversion of emulsions. For solid-stabilised emulsions, paths 1 to 2 and 2 to 1 at $\phi_w = 0.5$ are followed using mixtures of hydrophobic and hydrophilic silica, e.g., starting at 1 with a w/o emulsion stabilised by H30 (hydrophobic) particles and progressing to 2 being an o/w emulsion by adding N20 (hydrophilic) particles.

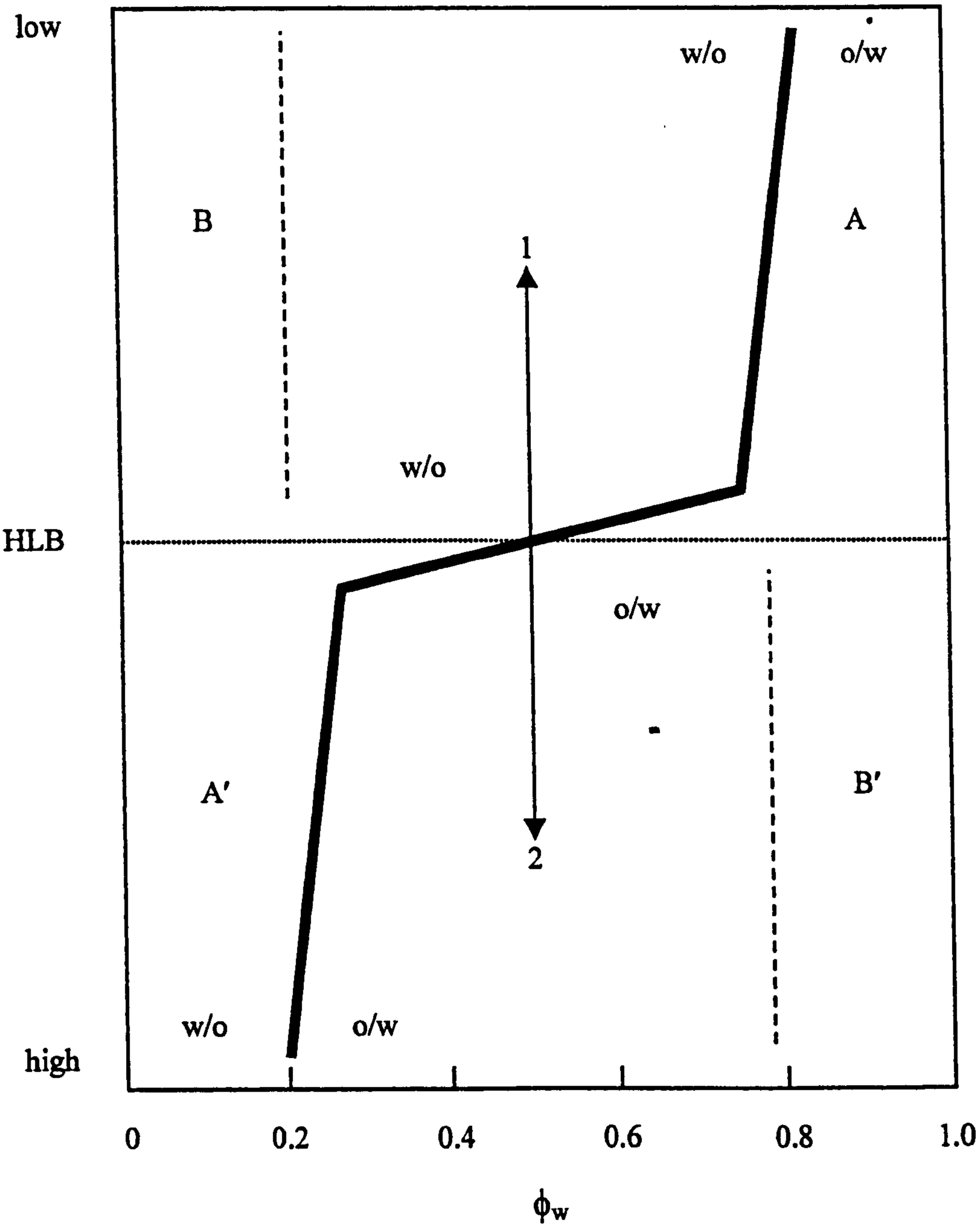

changed by using mixtures of two types of particles, one of which is hydrophobic and prefers w/o emulsions and the other, which is hydrophilic and prefers o/w emulsions. By varying the mass fraction of each the overall wettability of the system is altered causing the emulsion formed to invert from one type to the other. Water-in-oil emulsions stabilised by hydrophobic particles invert to oil-in-water emulsions on addition of hydrophilic particles (1 to 2 in Figure 5.1) and vice versa. The transition is akin to that observed in surfactant systems on addition of a second surfactant or a co-surfactant like an alcohol.[135] In contrast to catastrophic phase inversion, hysteresis is not observed during transitional inversion leading to the suggestion that it is not so much an inversion but a continuous change of the preferred emulsion type from o/w to w/o or vice versa.[112] The ball-in-hole analogy for transitional inversion is shown in Figure 5.2 for a surfactant system where inversion is thought to proceed via a microemulsion-oil-water phase (MOW). As the mole fraction of hydrophobic surfactant increases from A to E the initial two-state region (with the 'ball' in the o/w emulsion minimum) gradually forms a three-state region without the dramatic change in energy observed for catastrophic inversion. Eventually a two-state region is recovered with the 'ball' now in the opposite energy minimum (i.e. a w/o emulsion is formed). This inversion is reversible and proceeds without hysteresis. It is unlikely that transitional inversion of solid-stabilised emulsions proceeds via a microemulsion due to the comparatively large size of particles. The curvature of the oil-water interface is thought to be the important parameter in transitional inversion systems. The second surfactant or particle effects the curvature by co-adsorbing with the other stabilising material. The mode of preparation of the emulsions is investigated in this chapter in order to understand the importance of the initial location of particles in determining the preferred emulsion type. The two particle types used in this work are of the same primary size and only differ in their hydrophobicity.

5.2 Addition of hydrophilic silica (N20) to hydrophobic silica (H30)-stabilised w/o emulsions

It was shown in Chapter 4 that emulsions containing equal volumes of oil and water are w/o when stabilised by hydrophobic silica and o/w when stabilised by hydrophilic silica particles. The hydrophobic silica stabilises sub-micron diameter

Figure 5.2

The ball-in-hole analogy to depict transitional inversion of surfactant-stabilised emulsions. The mole fraction of hydrophobic surfactant increases from A to E. Redrawn from ref. 112.

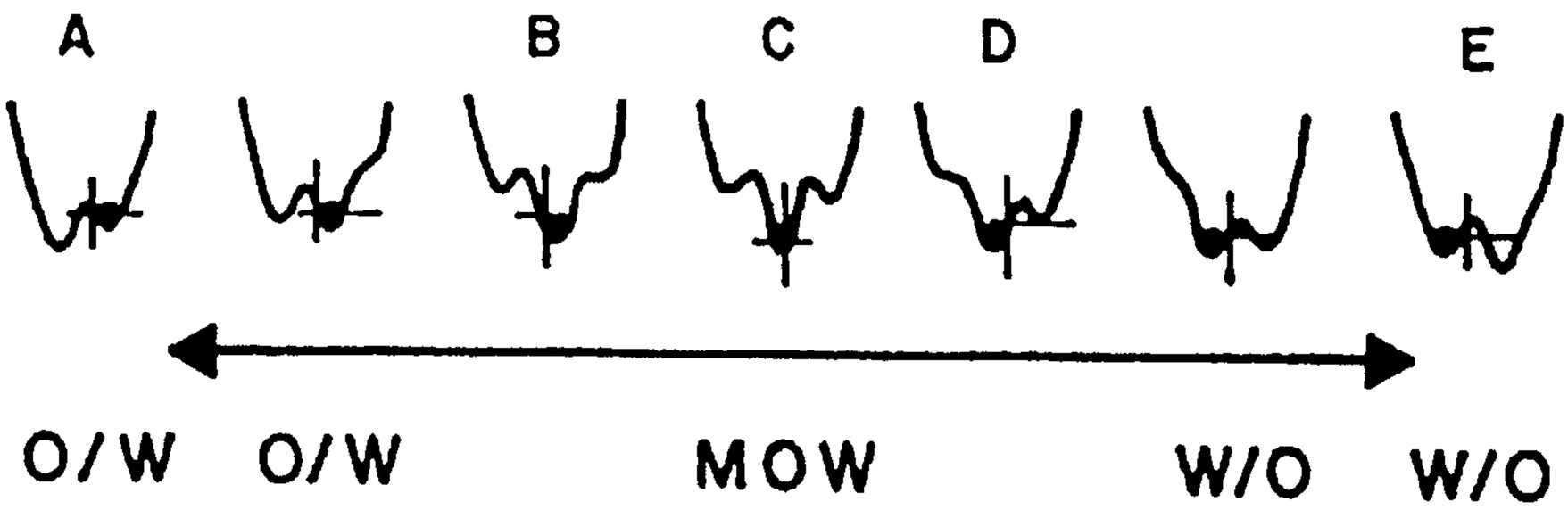

emulsion drops whereas the hydrophilic silica stabilises large drops of over 100 μm diameter. The difference in size is believed to be due to a difference in the strength of adsorption of the particles to the oil-water interface. Figure 5.3 shows how the emulsion conductivity varies in mixtures containing 2 wt.% H30 in oil and increasing amounts of N20 in water. In the absence of hydrophilic particles the conductivity is low (~ 0.2 μS cm^{-1}) indicative of w/o emulsions. The conductivity increases gradually up to 4.2 wt.% N20 whereupon it rises by three orders of magnitude as the emulsions invert to o/w. The onset of this phase inversion deduced via conductivity measurements occurs at the same concentration at which the emulsions transform from being able to disperse in oil to dispersing in water. It is seen that over twice the mass of hydrophilic silica (N20) compared with the mass of hydrophobic silica (H30) is required to invert the system, a fact which is probably related to differences in the extent of adsorption of the particles at the oil-water interface, as described above for emulsions stabilised by one particle type.

Figure 5.4 shows how the emulsion stability varies with the concentration of N20 in water 24 hours after preparation. Both types of emulsion are completely stable to coalescence (fraction of emulsion as oil phase) at all concentrations of N20. Stability to sedimentation (fraction of emulsion as aqueous phase) of w/o emulsions decreases progressively approaching phase inversion but remains reasonably high. Just after inversion, the o/w emulsions are unstable to creaming but the stability increases upon further addition of N20.

The drop size distributions of these emulsions immediately after preparation are shown in Figure 5.5. Distributions (a) to (c) are w/o emulsions and (d) to (f) are o/w emulsions. In the absence of N20 ((a)) and at low concentrations of added N20 ((b) and (c)) there are two populations of drops whose diameters are centred around 0.6 and 40 μm. However, over 80 vol% of the drops are in the range of diameters between 0.1 and 2 μm as seen for w/o emulsions in Figure 4.7. It was shown then that increasing the concentration of H30 particles causes the larger drop fraction to disappear and the two populations merge into one. The possibility exists that the larger size population represents a floc of the smaller size drops but the measurement is unable to distinguish between these possibilities. The distributions for the o/w emulsions ((d) to (f)) show a single population of drops of much larger diameters of between 5 and 150 μm. The variation in drop diameter through phase inversion is summarised in Figure 5.6 where both the arithmetic mean of the distribution (d(4,3)) and the diameter below which 50 % of the drops exist (d(v,0.5)) are plotted. The mean diameter, which is more

Figure 5.3

Conductivity of water-toluene emulsions (ϕ_w = 0.5) containing 2 wt.% H30 (hydrophobic) particles in toluene (fixed) as a function of added N20 (hydrophilic) particles in water.

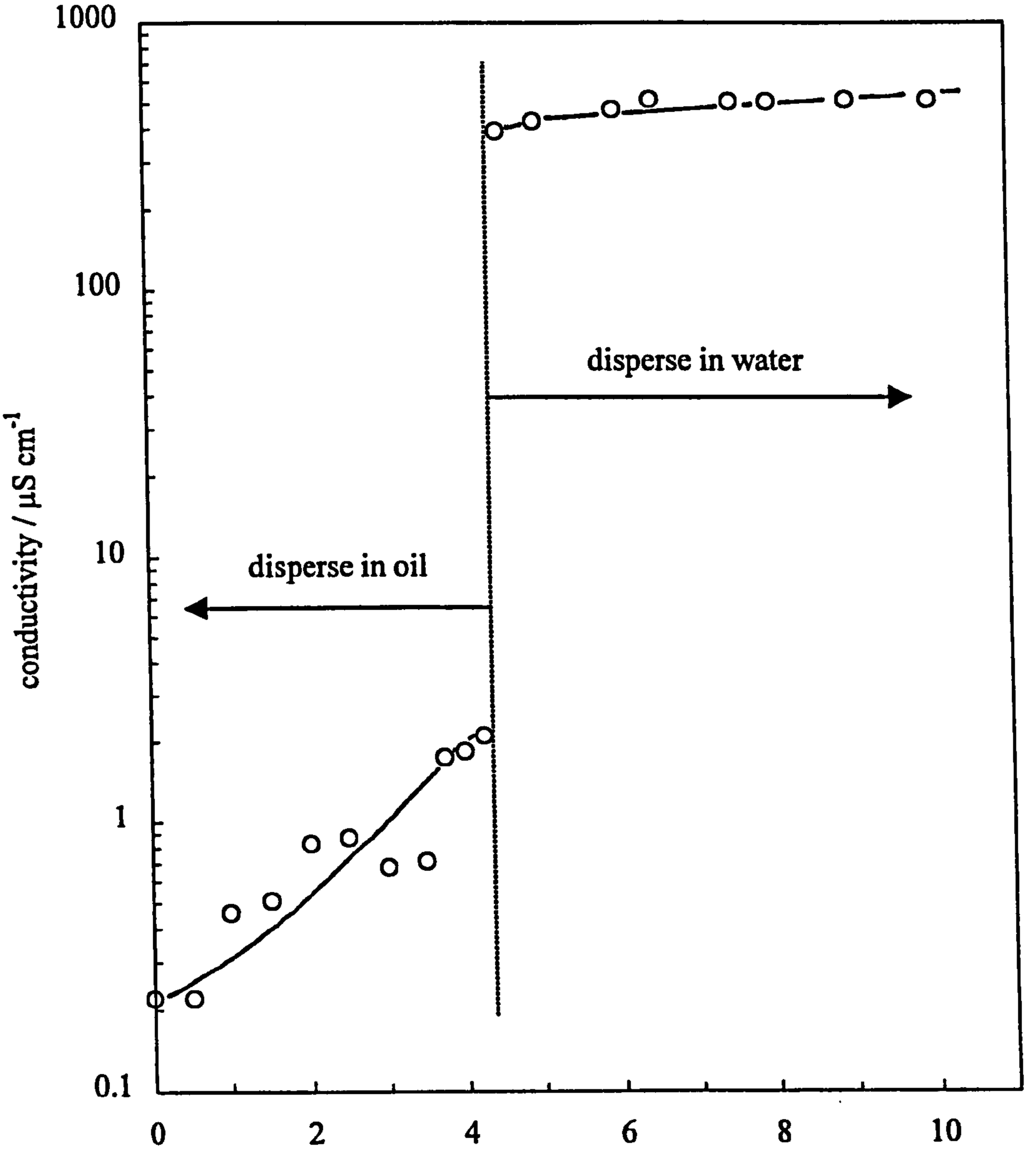

Figure 5.4

Stability after 24 hours of water-toluene emulsions ($\phi_w = 0.5$) stabilised by 2 wt.% H30 (hydrophobic) particles in toluene as a function of added N20 (hydrophilic) particles in water. For w/o emulsions, filled points refer to sedimentation and open points to coalescence. For o/w emulsions, open points refer to creaming and filled points to coalescence.

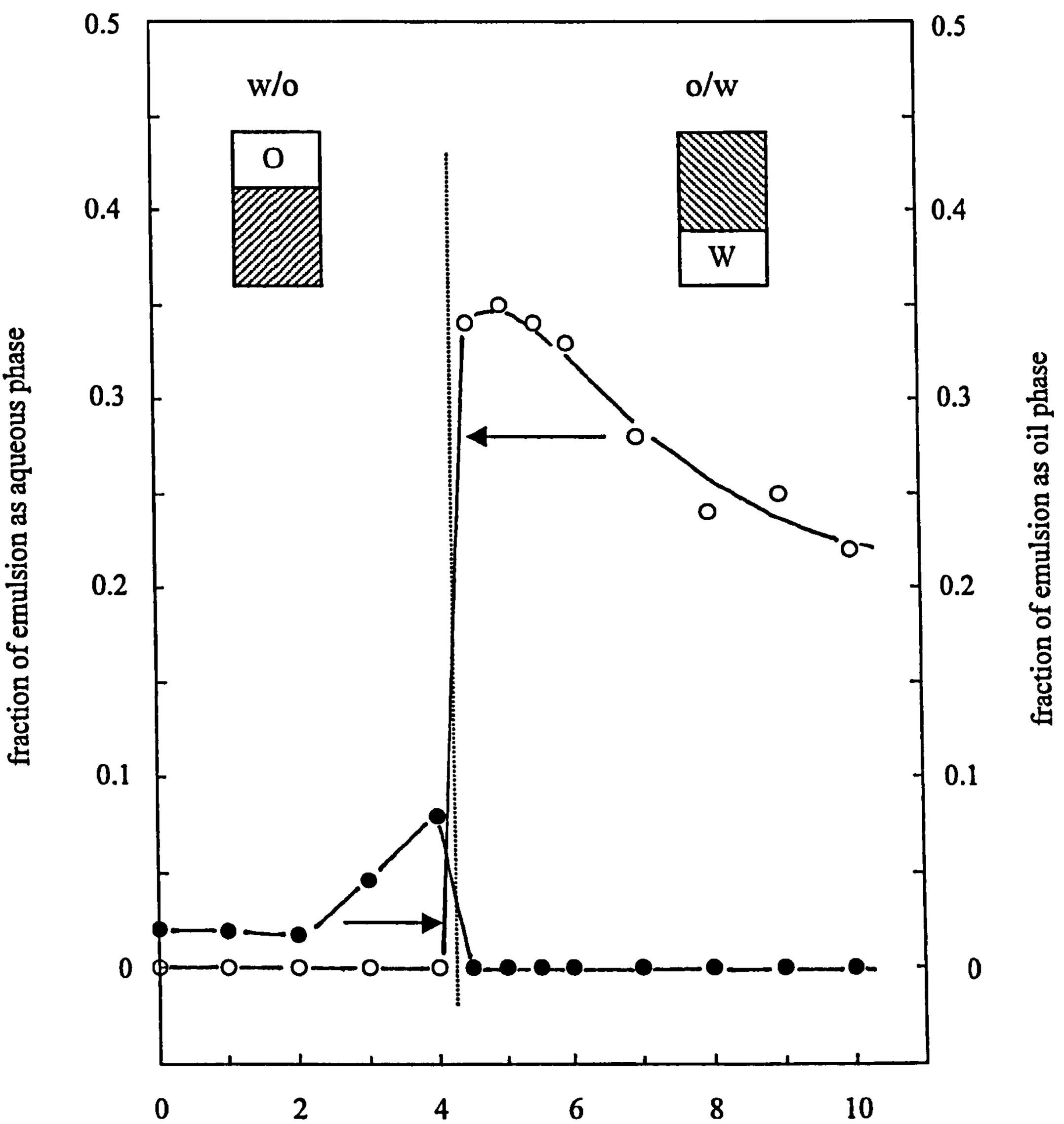

Figure 5.5

Drop diameter volume distributions (right-hand ordinate) for water-toluene emulsions ($\phi_w = 0.5$) stabilised by 2 wt.% H30 (hydrophobic) particles in toluene as a function of added N20 (hydrophilic) particles in water. The wt.% N20 are (a) 0, (b) 2, (c) 4, (d) 5, (e) 7, (f) 9 and emulsions are w/o for (a-c) and o/w for (d-f). Note the different abscissa scales between (a-c) and (d-f). The solid curves show the cumulative volume distributions (left-hand ordinate).

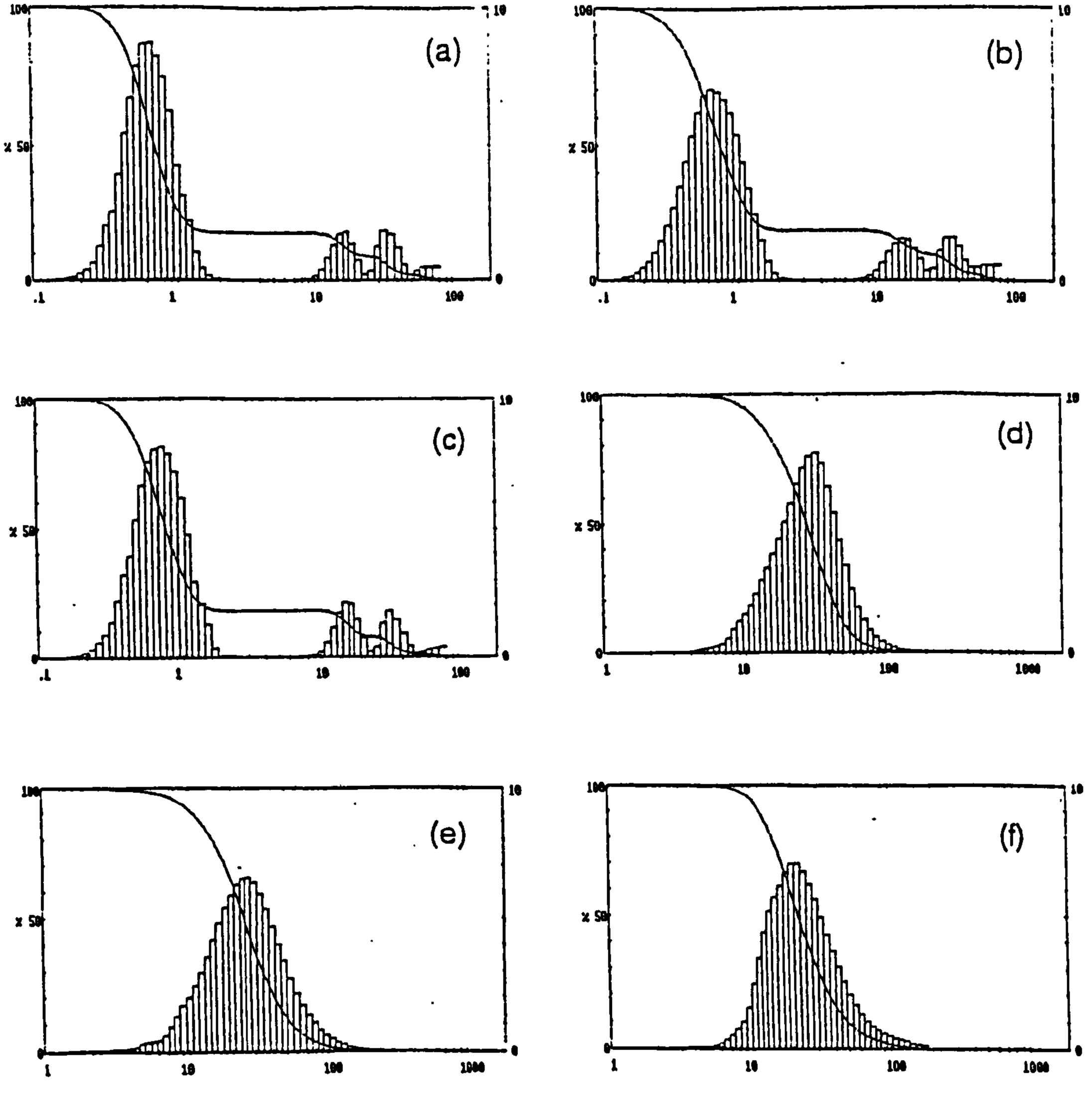

Figure 5.6

Drop diameters versus added N20 in water for water-toluene emulsions (ϕ_w = 0.5) stabilised by 2 wt.% H30 in toluene. d(4,3) is the arithmetic mean diameter (filled points), d(v,0.5) is the initial volume average diameter (open points).

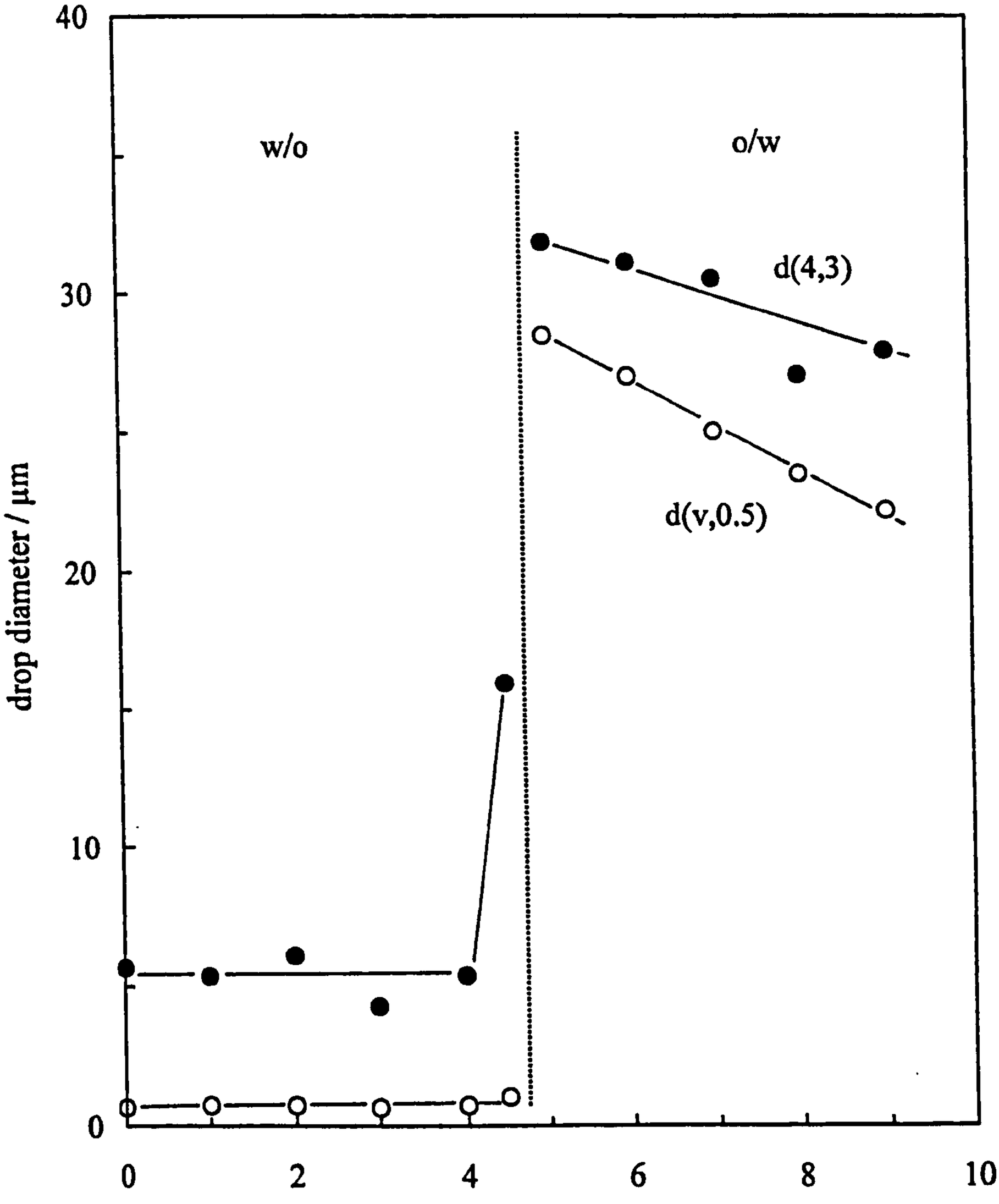

representative of the whole distribution for bimodal systems, remains around 5 μm for most of the w/o emulsions increasing to 15 μm just prior to inversion. The o/w emulsions above inversion have a diameter of approximately 30 μm which decreases slightly on increasing N20 concentration. The d(v,0.5) is more biased to the small size drop fraction resulting in a discontinuous change between w/o (0.7 μm) and o/w (> 20 μm) emulsions. These drops size distribution measurements agree with the stability trends observed in Figure 5.4. The w/o emulsions have small drops corresponding to stable emulsions and the o/w emulsions have larger drops which are less stable. In addition, the o/w emulsion drop diameter decreases above inversion as the stability to creaming increases, consistent with Stoke's law predictions (see § 1.2.3).

Optical microscopy images are given in Figure 5.7 for w/o emulsions (0 to 4 wt.% added N20) and o/w emulsions (≥ 6 wt.% added N20). In addition to confirming the maximum drop size around inversion, the images also suggest the drops are flocculated at low levels of N20, showing drop-containing and drop-free regions, which become deflocculated around inversion. The larger oil drops by contrast remain dispersed. An increase in the concentration of N20 particles in the system results in an increase in the mole fraction of N20 particles at the oil-water interface. The hydrophilic N20 particles have charged surfaces due to dissociation of silanol groups into SiO^- resulting in increased repulsion between drops which leads to deflocculation. This type of transition has been evidenced and theoretically described recently for nonionic surfactant-stabilised emulsions upon co-adsorption of low levels of ionic surfactant.[136] In this system dodecane-in-water emulsions stabilised by the nonionic surfactant n-decyl-β-D-glucoside are flocculated but do not coalesce or exhibit Ostwald ripening. The drops are deflocculated by the addition of a low mole fraction (with respect to the total surfactant) of a strongly adsorbing ionic surfactant (sodium n-octadecyl sulphate) which charges the drops resulting in a repulsion which is strong enough to overcome the flocculation. The concentration of ionic surfactant required for deflocculation depends on the concentration of electrolyte in the continuous aqueous phase.

In summary, it is possible to invert w/o emulsions, stabilised by hydrophobic silica, to o/w emulsions by addition of hydrophilic particles at fixed volume fraction of water. Inversion occurs when the mass of hydrophilic silica is approximately twice as much as that of hydrophobic silica. The w/o emulsion drops are flocculated in the

Figure 5.7

Optical microscope images of water-toluene emulsions ($\phi_w = 0.5$) stabilised by 2 wt.% H30 (hydrophobic) particles in toluene as a function of added N20 (hydrophilic) particles in water. Scale bar equals 100 μm.

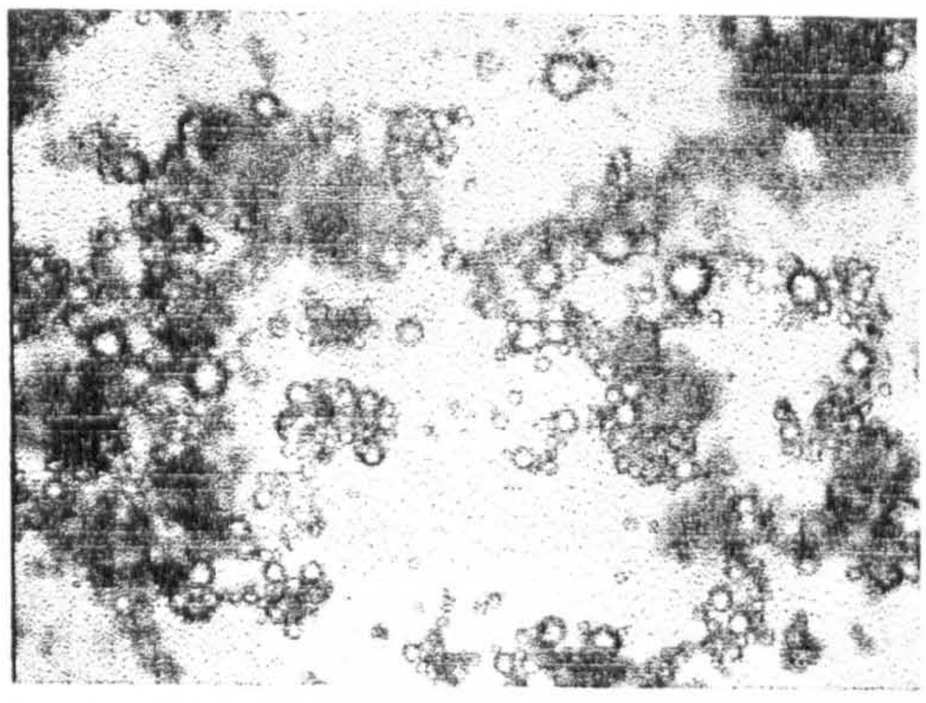

0 wt% N20

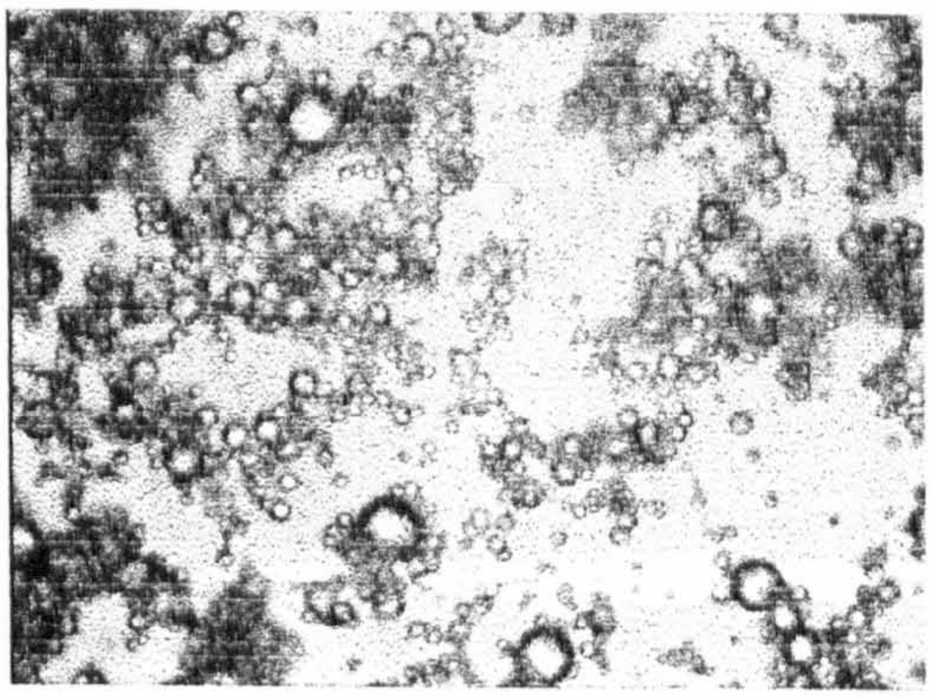

0.5 wt% N20

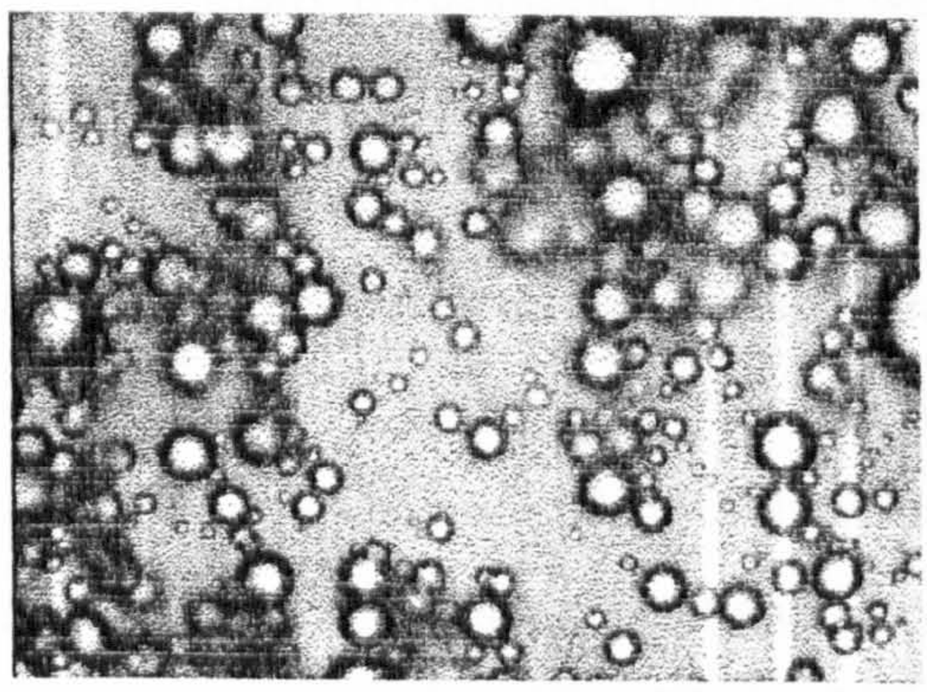

1 wt% N20

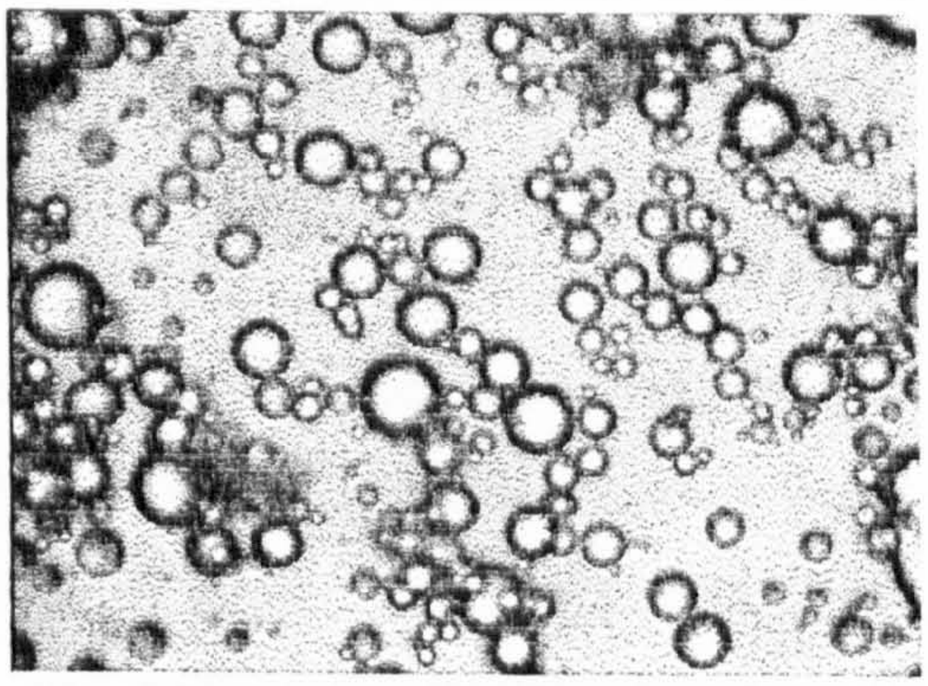

2 wt% N20

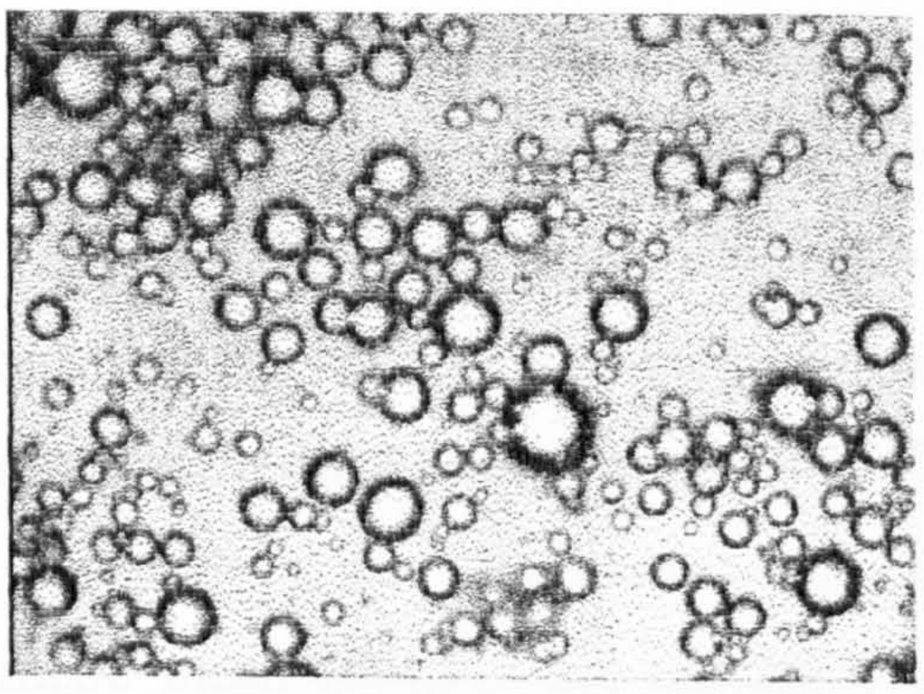

4 wt% N20

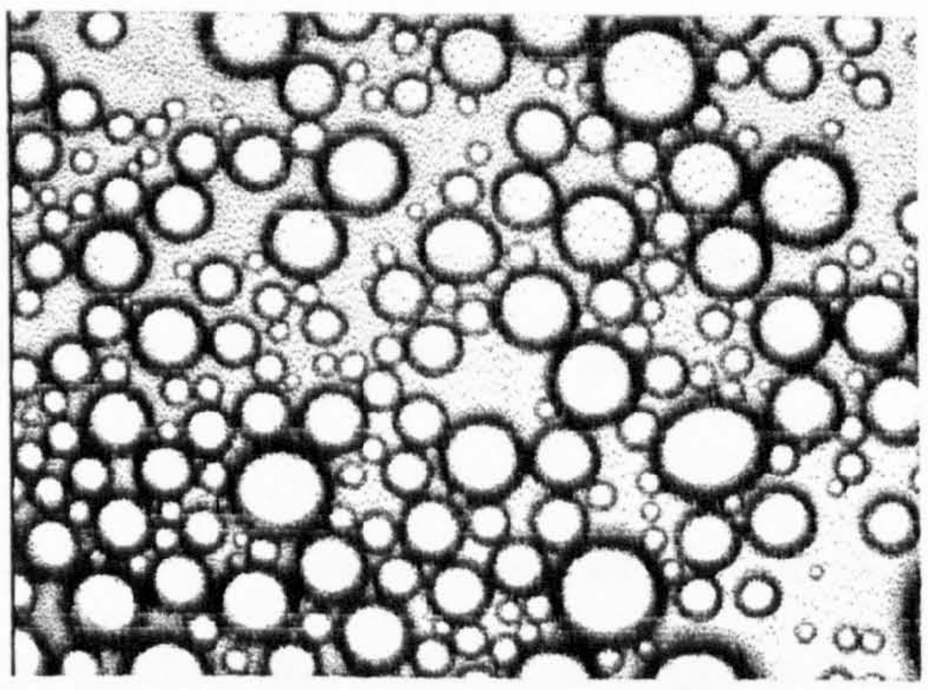

6wt% N20

8 wt% N20

10 wt% N20

absence of hydrophilic particles but deflocculate and eventually invert as the mass of hydrophilic particles is increased.

5.3 Addition of hydrophobic silica (H30) to hydrophilic silica (N20)-stabilised o/w emulsions

In the previous section, hydrophobic particles were shown to have a greater influence on the type of emulsion formed when investigating particle mixtures. This is most likely due to their stronger adsorption to the oil-water interface. It was shown that two times as many hydrophilic particles were required to invert the emulsion to o/w. In order to investigate the reverse transition, hydrophobic H30 particles in toluene have been added to a fixed amount of hydrophilic particles in water. Figure 5.8 shows the conductivity of water-toluene emulsions containing 2 wt.% N20 particles (fixed) in water plus 0 to 2 wt.% H30 particles in oil (varied). The emulsions invert from o/w to w/o at around 0.4 wt.% added H30. Below this value, emulsions dispersed in pure water and above it they dispersed in toluene. For 0.35 and 0.4 wt.% H30 a drop of emulsion sank to the bottom of a tube filled with toluene, and part of the sample was seen to disperse in water with some remaining undispersed. Clearly, around inversion the emulsions behave somewhere between the two extremes. The emulsion stabilities are plotted in Figure 5.9 as a function of added H30. The o/w emulsions were unstable with significant creaming and partial coalescence occurring, whereas w/o emulsions do not coalesce to any extent but sediment under gravity, the degree of sedimentation decreasing with increasing concentration of H30.

The drop size distributions of the emulsions have been measured and the arithmetic mean (d(4,3)) and median diameter (d(v,0.5)) are plotted in Figure 5.10 (upper). The o/w emulsions at low [H30] (< 0.4 wt.%) have large diameters (~ 120 μm) with a monomodal distribution of drops. The w/o emulsions exhibit bimodal drop distributions similar to that seen in Figure 5.5. The arithmetic mean and median diameter show a gradual decrease in the drop size above inversion consistent with an increase in the stability of the emulsion (Figure 5.9). The lower part of Figure 5.10 shows how the percentage of drops of diameter < 2 μm for w/o emulsions increases with increasing concentration of H30 as the emulsion size decreases. By 2 wt.% added H30,

Figure 5.8

Conductivity of water-toluene emulsions (ϕ_w = 0.5) containing 2 wt.% N20 (hydrophilic) particles in water (fixed) as a function of added H30 (hydrophobic) particles in toluene.

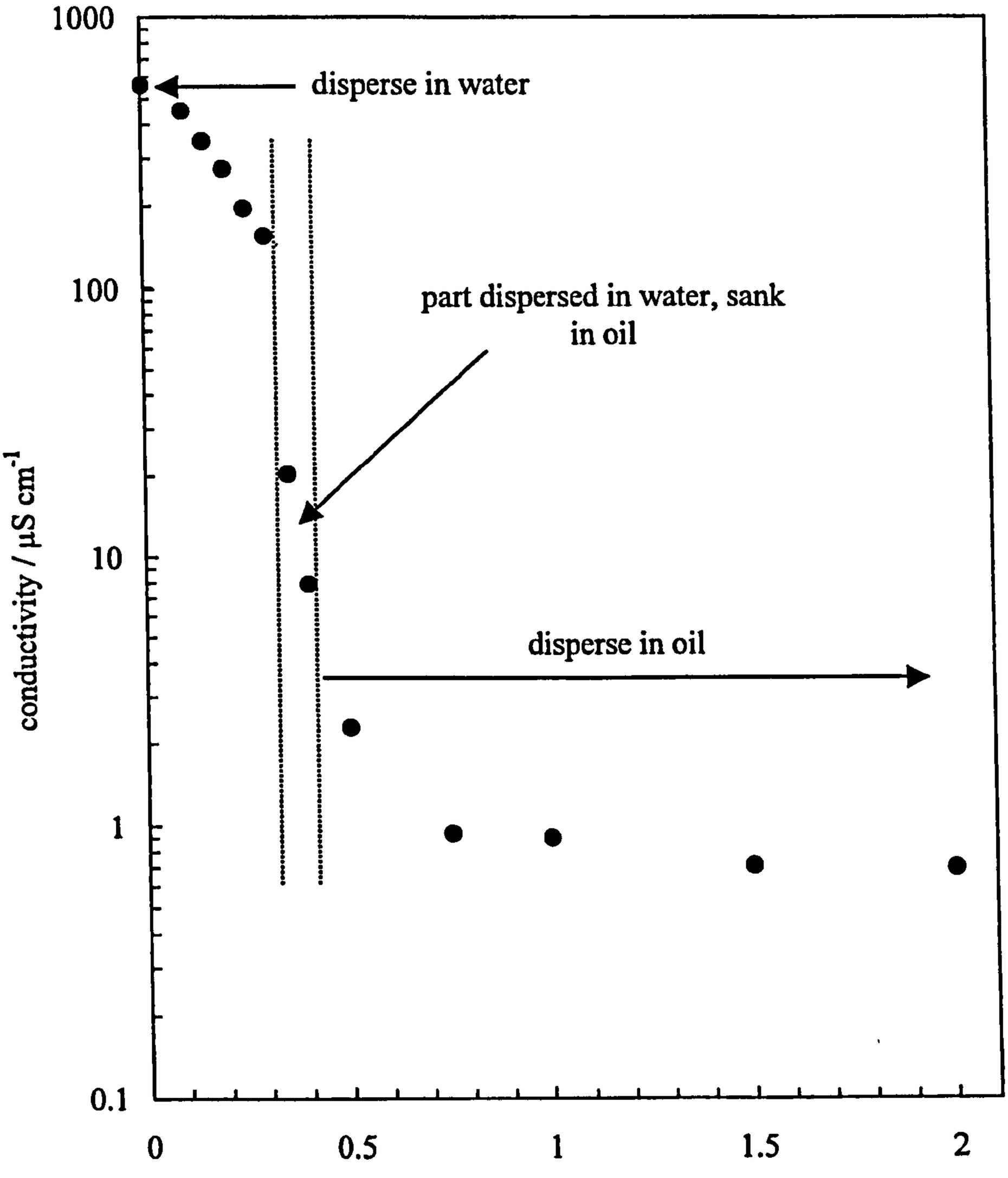

Figure 5.9

Stability after 24 hours of water-toluene emulsions ($\phi_w = 0.5$) stabilised by 2 wt.% N20 (hydrophilic) particles in water as a function of added H30 (hydrophobic) particles in oil. For w/o emulsions, filled points refer to sedimentation and open points to coalescence. For o/w emulsions, open points refer to creaming and filled points to coalescence.

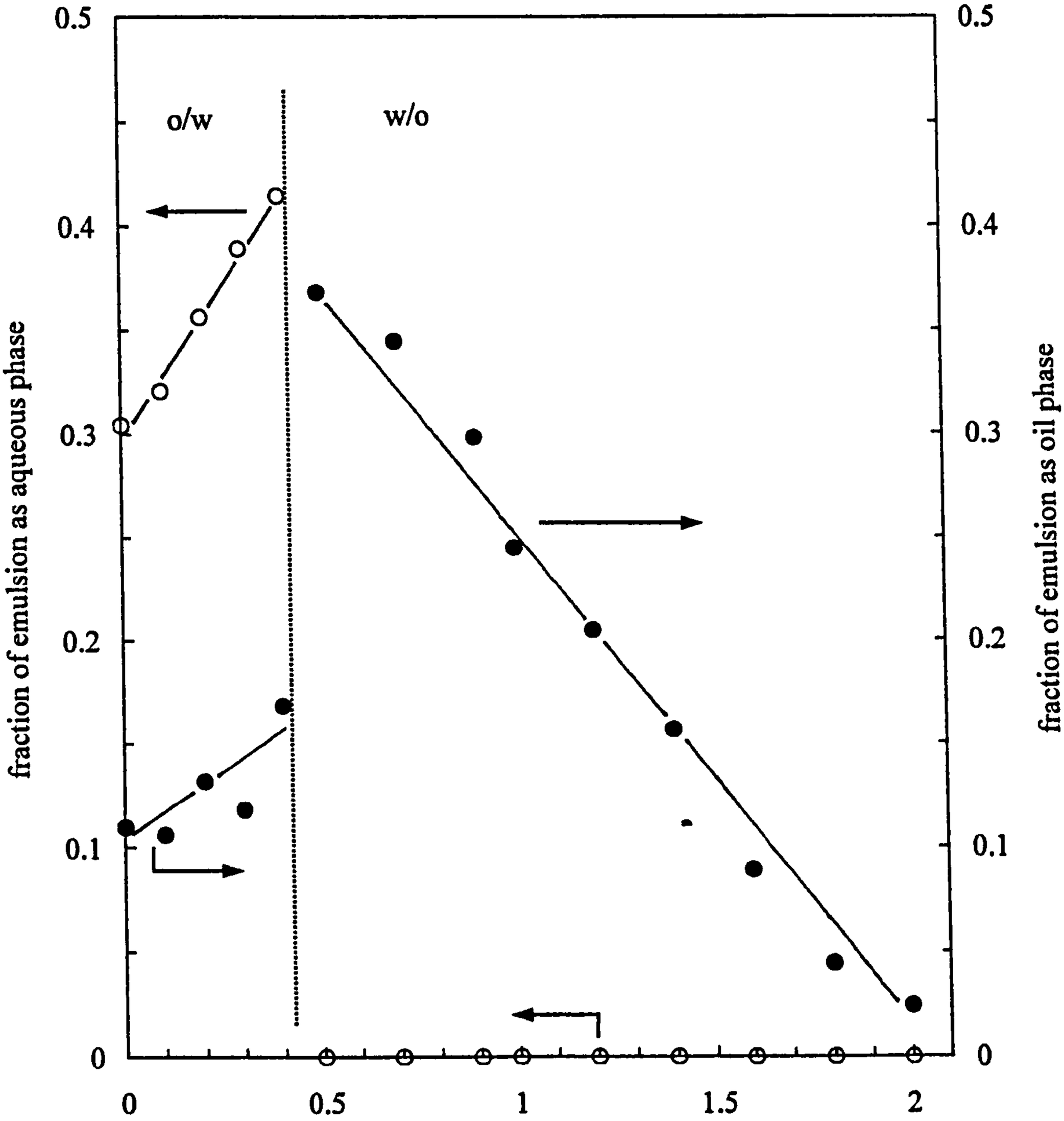

Figure 5.10

(*upper*) Drop diameters versus added H30 in toluene for water-toluene emulsions (ϕ_w = 0.5) stabilised by 2 wt.% N20 in water. d(4,3) is the arithmetic mean diameter (filled points). d(v,0.5) is the initial volume average diameter (open points). (*lower*) Percentage of drops of diameter less than 2 μm versus wt.% H30 in oil for w/o emulsions.

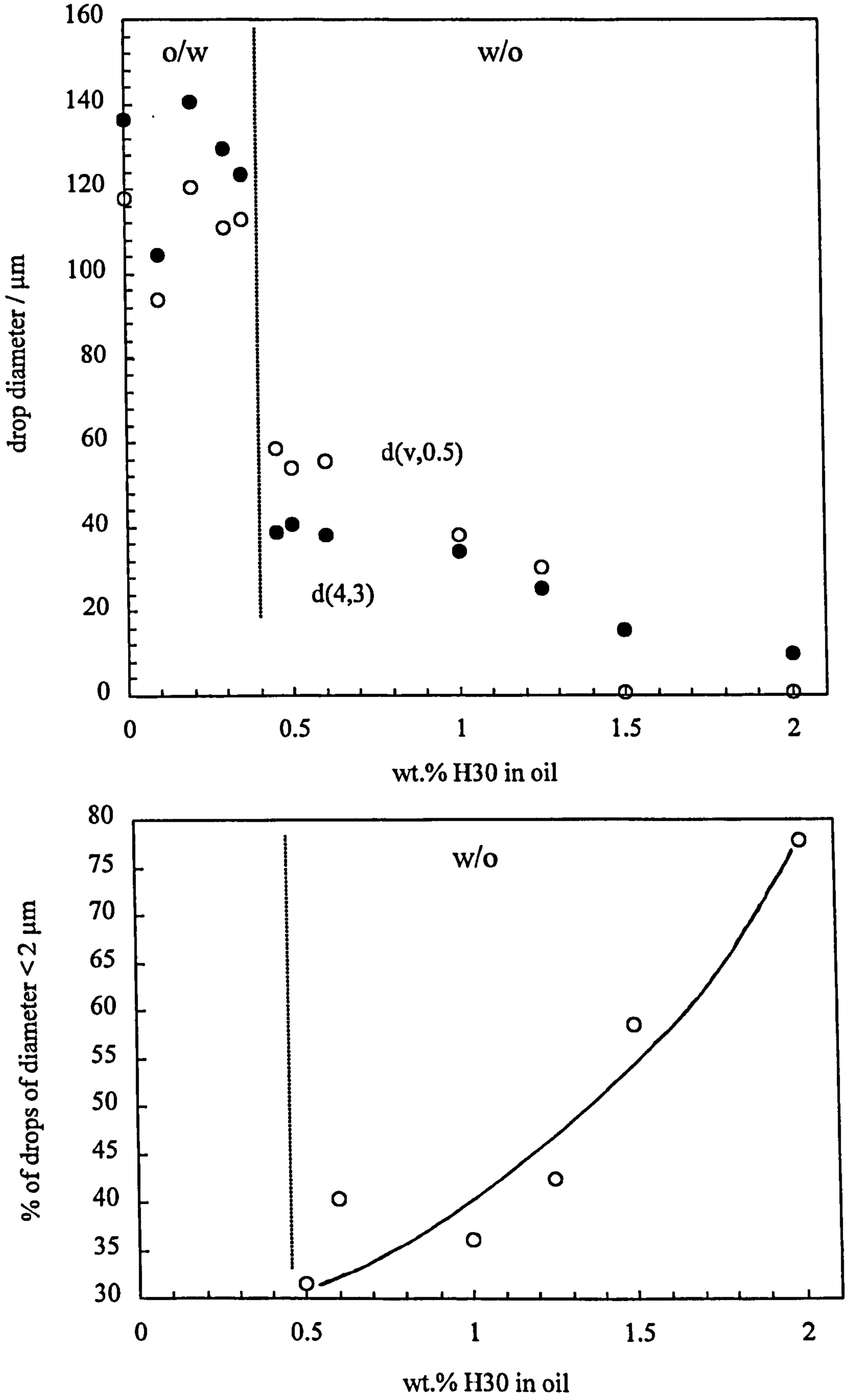

the distribution is indistinguishable from that for w/o emulsions stabilised by H30 particles alone at this concentration.

The hydrophobic particles are again shown to have the greatest influence on the type of emulsion formed. Oil-in-water emulsions in the absence of hydrophobic particles are relatively unstable and hence invert to w/o emulsions at a lower weight fraction (defined below) of H30 particles than the previous system where the H30 particle concentration was fixed.

5.4 Emulsions containing fixed concentration of particles

In the previous two sections, transitional phase inversion of silica-stabilised emulsions has been achieved by increasing the concentration of hydrophilic particles in systems containing a fixed concentration of hydrophobic particles and vice versa. The weight fraction of H30 particles (defined as weight H30/(weight H30 + weight N20)) required for inversion decreases with an increase in the total mass of particles in the system from 0.32 at constant H30 to 0.17 at constant N20. It is possible that inversion may be due to an increase in the overall particle concentration in the system, therefore this section investigates emulsions stabilised by a fixed overall concentration of silica equal to 2.5 wt.% with varying amounts of N20 in water and H30 in oil.

Figure 5.11 shows the emulsion conductivity as a function of the weight fraction of H30 in the system. The emulsion inverts from o/w (drop disperses in water) to w/o (drop disperses in oil) at a weight fraction H30 equal to 0.14. The time dependence of the sedimentation of w/o emulsions is given in Figure 5.12 for different weight fractions of H30. The stability of the emulsions decreases close to inversion and at a weight fraction equal to 0.2 sedimentation is instantaneous and extensive over 30 minutes. An increase in the weight fraction of H30 delays the onset of sedimentation and reduces its final extent. This is most likely due to the increase in the continuous oil phase viscosity with increasing H30 concentration as a network of particles is formed. At weight fractions of H30 greater than 0.5 the emulsions are completely stable to coalescence and sedimentation for up to 2 weeks. Figure 5.13 summarises the stability of both types of emulsion after 30 minutes for weight fractions of H30 below 0.5. The stability of o/w emulsions to creaming decreases towards inversion with stability to coalescence remaining constant at around 20 %. Stability of w/o emulsions to sedimentation

Figure 5.11

Conductivity of water-toluene emulsions (ϕ_w = 0.5) containing 2.5 wt.% total particles as a function of the weight fraction of H30. N20 particles (hydrophilic) are initially in water. H30 particles (hydrophobic) are initially in toluene.

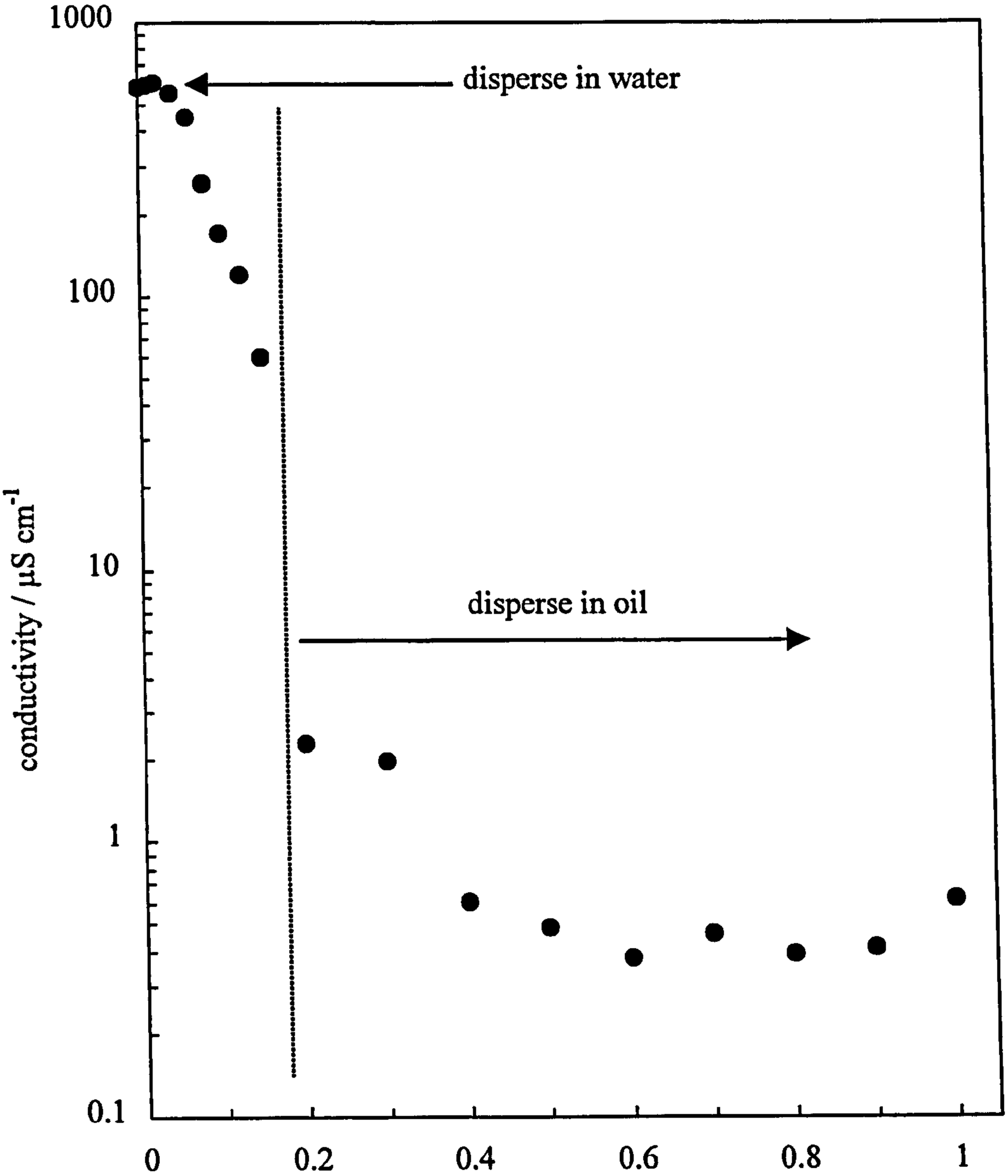

Figure 5.12

Fraction of emulsion as oil phase during sedimentation of w/o emulsions in system of Figure 5.11. Weight fractions of H30 are given.

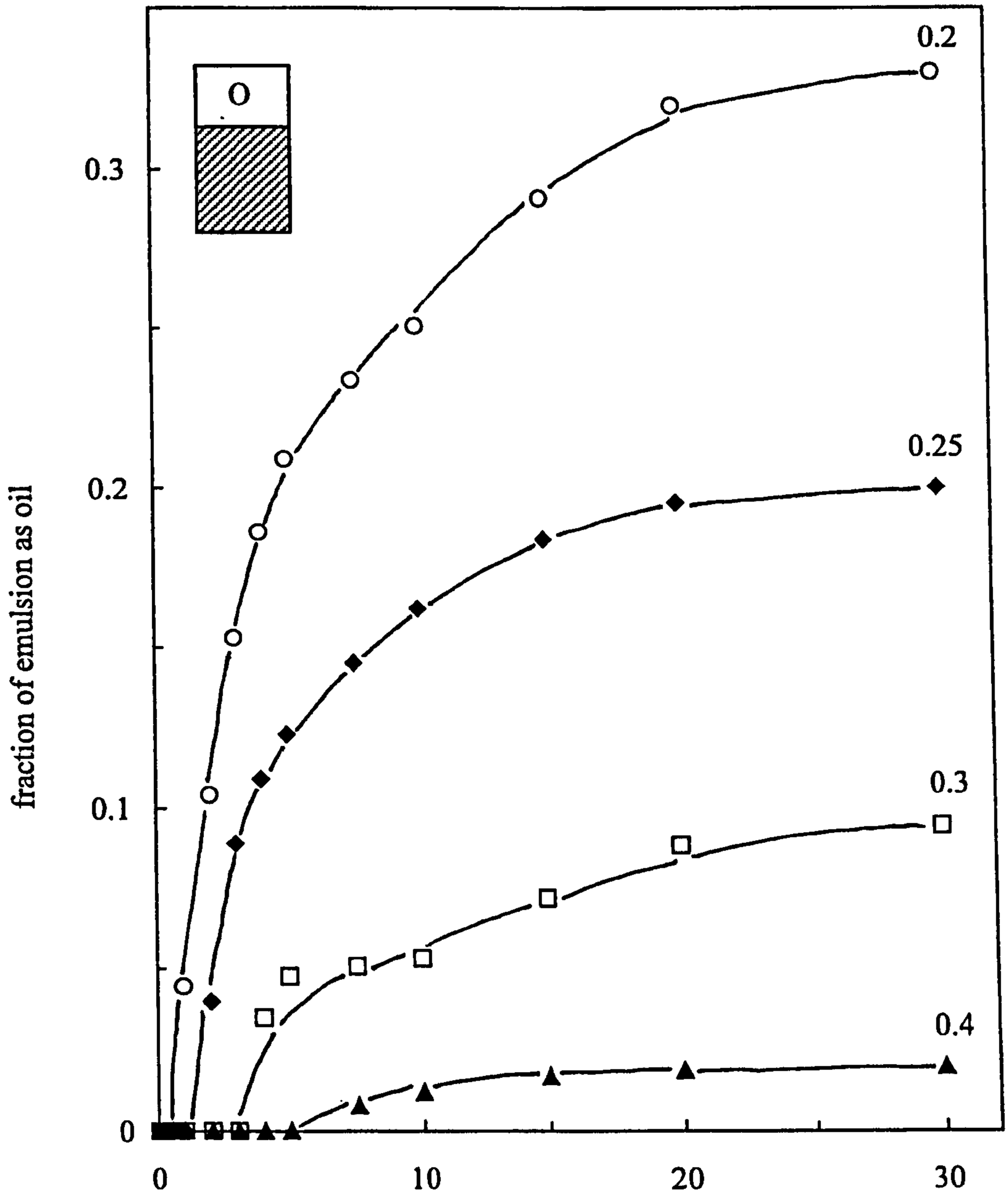

Figure 5.13

Stability after 30 minutes of water-toluene emulsions (ϕ_w=0.5) in the system of Figure 5.11. For o/w emulsions, open points refer to creaming and filled points to coalescence. For w/o emulsions, filled points refer to sedimentation and open points to coalescence.

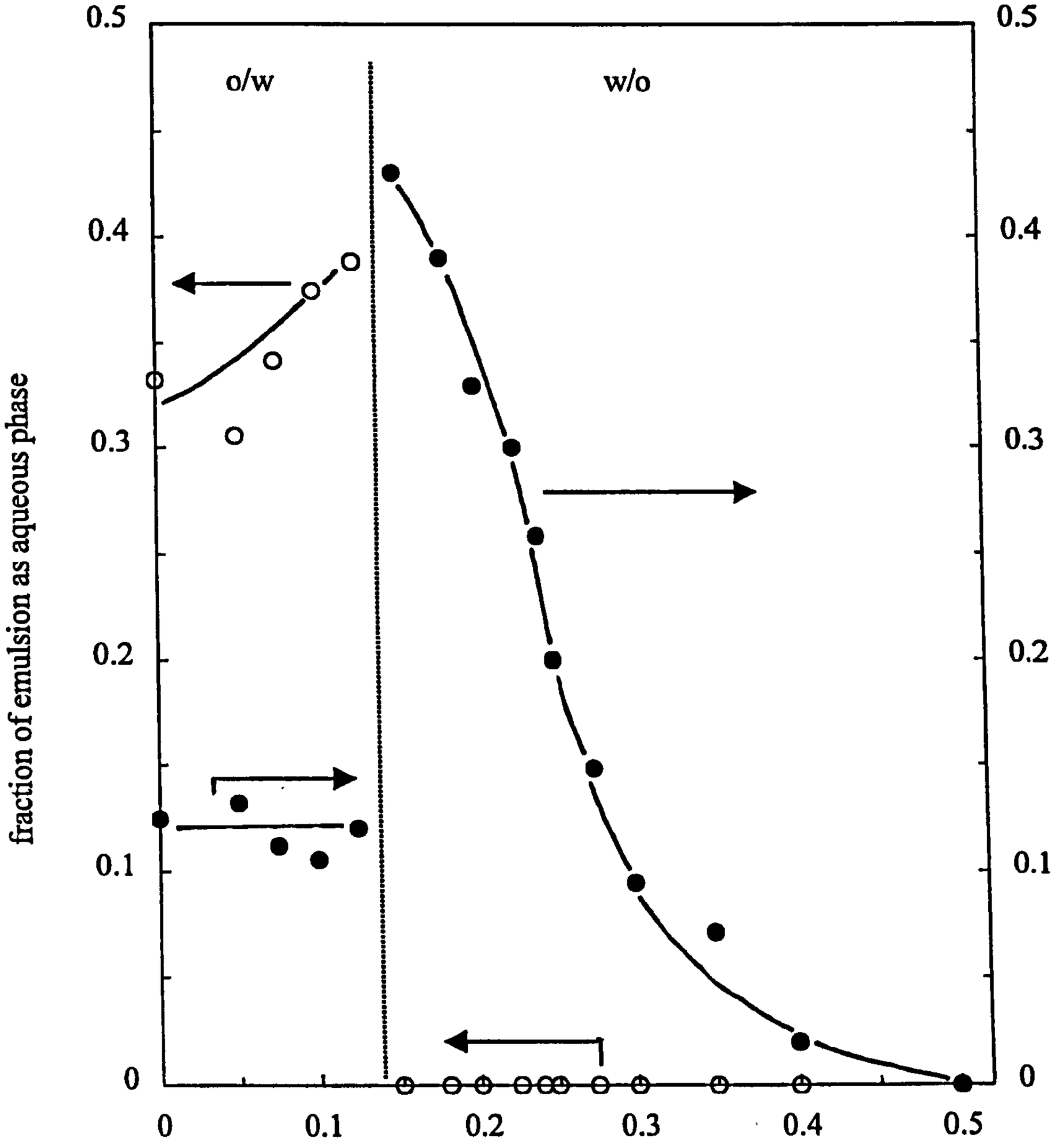

increases dramatically away from inversion with no coalescence occurring whatsoever. Thus, emulsions are most unstable to gravitational separation around inversion.

A selection of emulsion drop diameter distributions are shown in Figure 5.14. The o/w emulsions ((a) and (b)) show monomodal distributions centred around 120 μm. At conditions above inversion (d) a bimodal distribution appears in which the two populations are completely distinct. As the weight fraction of H30 particles increases the two populations begin to merge (e) and finally a single log normal distribution of small w/o drops is apparent at high H30 (f). The monomodal distributions at low and high weight fractions of H30 are similar in appearance to emulsions containing N20 and H30 particles alone (Chapter 4) which implies that the mass fraction of particles at interfaces of large drops are in favour of N20, while that at interfaces of small drops is in favour of H30. The arithmetic mean (d(4,3)) and median diameter (d(v,0.5)) of the emulsions are plotted in Figure 5.15 (upper) for weight fractions of H30 between 0 and 1. As before, the oil drops are centred around 120 μm but in this case the water drops formed immediately after inversion are also of large diameter but decrease progressively away from inversion. This decrease in size corresponds with an increase in the stability to sedimentation. Figure 5.15 (lower) shows how the percentage of small w/o drops increases reaching 90 % for a weight fraction of H30 of 0.5 and above where the distributions are virtually monomodal. In this system the average wettability of the particle mixtures at the oil-water interface is believed to change from mainly water wettable (hence stabilises o/w emulsions) to mainly oil wettable (stabilises w/o emulsions) as the weight fraction of H30 particles in the system increases. This is shown to be reasonable from the work of Diggins et al.[137] who measured the equilibrium capillary pressure in a packed bed of quartz particles (59 μm median diameter). The bed contained varying volume fractions of hydrophilic and fully methylated hydrophobic quartz particles. The macroscopic solid-water-air contact angle, θ, was obtained from the capillary pressure, ΔP, using

$$\Delta P = \frac{\gamma_{lv} \cos\theta \phi A}{(1-\phi)} \tag{5.1}$$

where γ_{lv} is the liquid-vapour surface tension, ϕ is the volume fraction of solid in the packed bed and A is the specific surface area per gram of the solid. The calculated

Figure 5.14

Drop diameter volume distributions (right-hand ordinate) for water-toluene emulsions (ϕ_w = 0.5) in the system of Figure 5.11. The weight fractions of H30 are (a) 0, (b) 0.09, (c) 0.15, (d) 0.25, (e) 0.4 and (f) 0.5 and emulsions are o/w for (a-b) and w/o for (c-f). The solid curves show the cumulative volume distribution (left-hand ordinate).

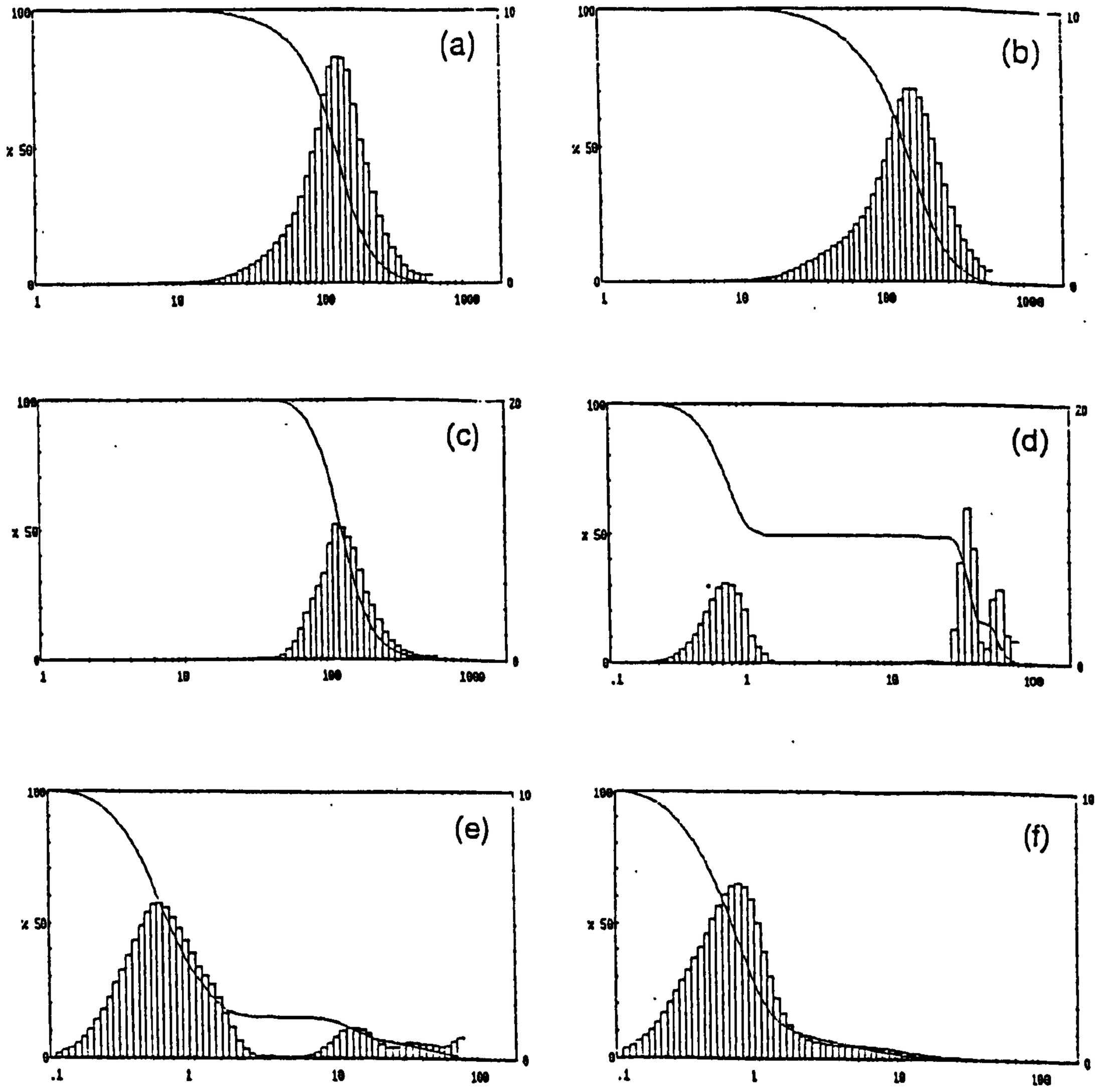

Figure 5.15

(upper) Drop diameters versus weight fraction of H30 for water-toluene emulsions (ϕ_w = 0.5) stabilised by 2.5 wt.% total particles. d(4,3) is the arithmetic mean diameter (filled points). d(v,0.5) is the initial volume average diameter (open points). (lower) Percentage of drops of diameter less than 2 μm versus weight fraction of H30 for w/o emulsions.

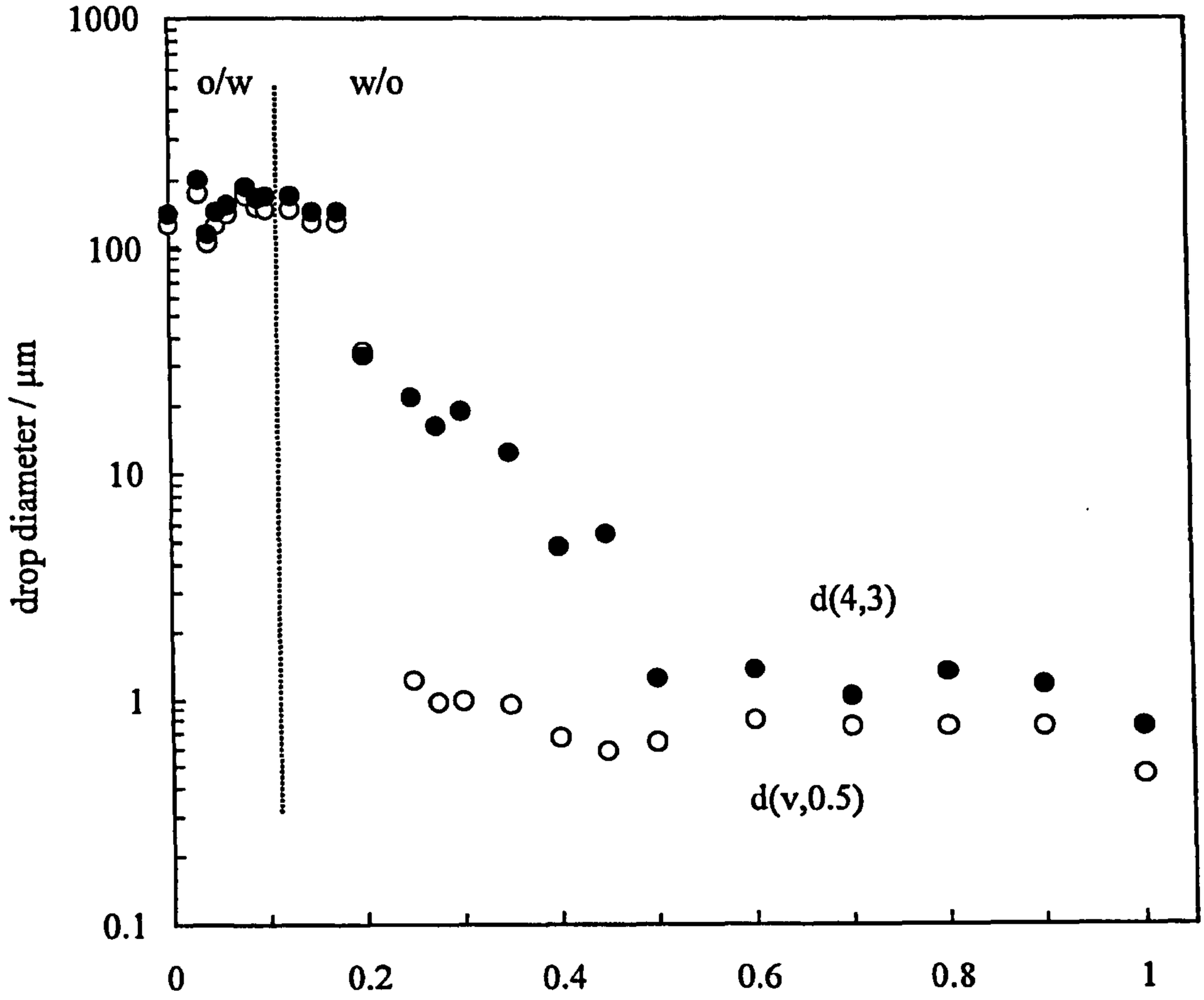

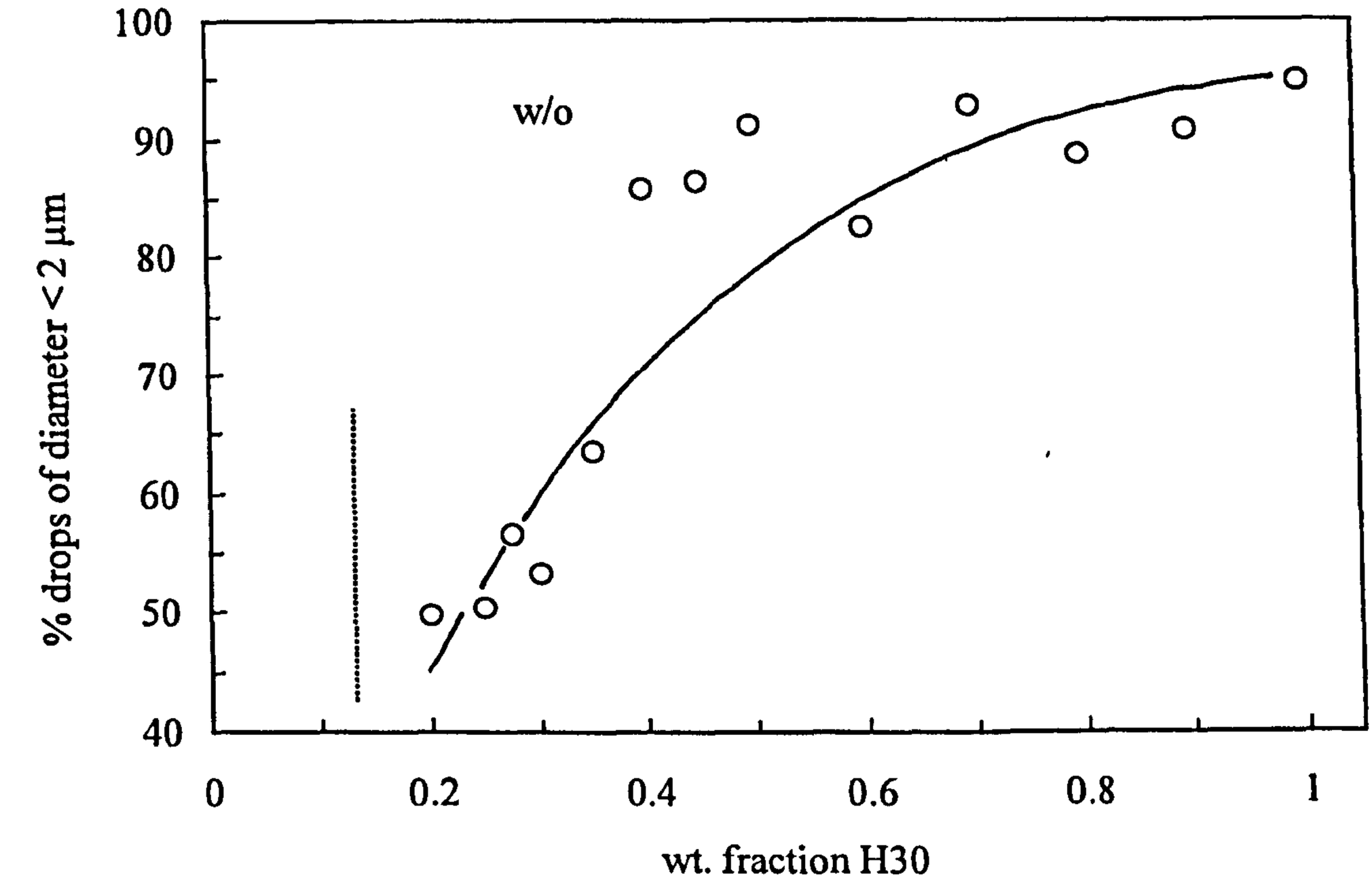

contact angle is plotted against the volume fraction of hydrophilic particles in the packed bed in Figure 5.16. θ decreases linearly from 100° for pure hydrophobic quartz to 0° for pure hydrophilic quartz. This is akin to increasing the weight fraction of hydrophilic silica particles in the emulsions described here.

5.5 Emulsions containing fixed particle concentration with N20 dispersed in oil

In surfactant-stabilised systems in which the oil and aqueous phases have not been pre-equilibrated before emulsification, it has been reported that the type and stability of emulsions prepared depend on the initial location of surfactant.[138, 139] If a hydrophilic surfactant is initially placed in the oil phase, a part of the aqueous phase added during emulsification is emulsified into oil forming a w/o emulsion. This primary emulsion inverts, sometimes through formation of a short-lived, multiple w/o/w emulsion, to the final o/w emulsion which is finer and more stable than that formed if the surfactant is initially dispersed in the aqueous phase.[139] In addition, it is expected that the effects are related to the differences in free energy of adsorption of surfactant from either oil or water to the oil-water interface. Although N20 particles are hydrophilic, they can be dispersed in toluene using ultrasound. Emulsions with a fixed overall [particle] of 2.5 wt.% have been prepared with both particle types initially dispersed in the oil phase. Figure 5.17 shows the inversion from o/w to w/o occurs at much lower weight fractions of H30 of around 0.015 (filled circles). The initial location of the particles is clearly important in dictating the final emulsion type and stability. The open squares in Figure 5.17 highlight this by showing the inversion of emulsions stabilised by hydrophilic particles in water and hydrophobic particles in oil occurs at a weight fraction equal to 0.14 (data of Figure 5.11). In the absence of rheological data for such phases, one can only speculate that the presence of N20 particles in H30-toluene mixtures either disrupts the particle network which forms or strengthens it by being incorporated within. Whichever happens, the emulsions end up closer to inversion as a result.

The drop diameter distributions of the emulsions at three weight fractions of H30 are shown in Figure 5.18. The o/w emulsion stabilised solely by N20 particles dispersed in oil (H30 = 0) is very similar to the distribution when N20 is dispersed in water (shown

Figure 5.16

Contact angles of water on quartz powders in air calculated from capillary pressure measurements using equation 5.1. Data replotted from ref. 137.

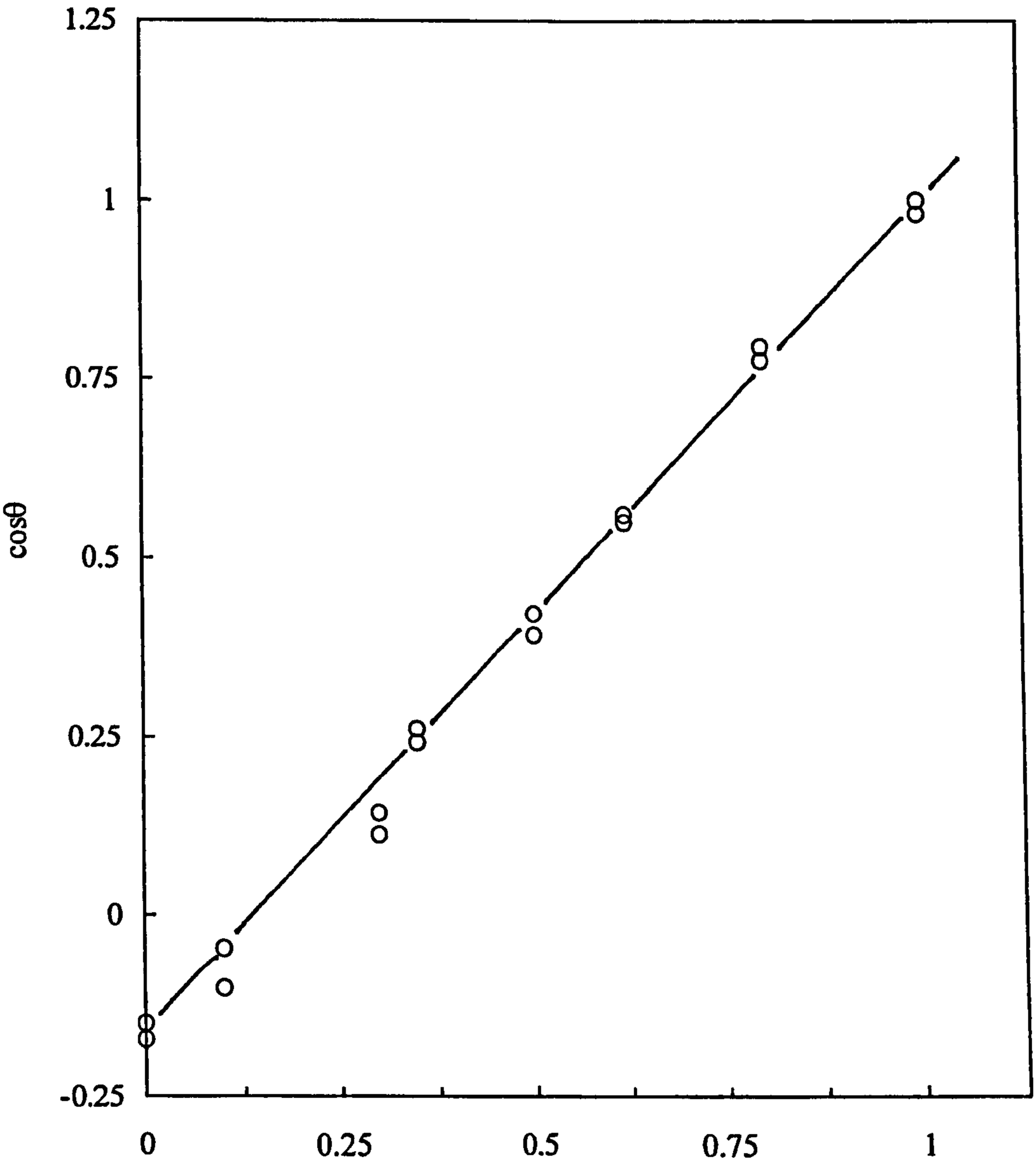

Figure 5.17

Conductivity of water-toluene emulsions (ϕ_w = 0.5) containing 2.5 wt.% total particles as a function of the weight fraction of H30. Squares – N20 dispersed in water, circles – N20 dispersed in oil.

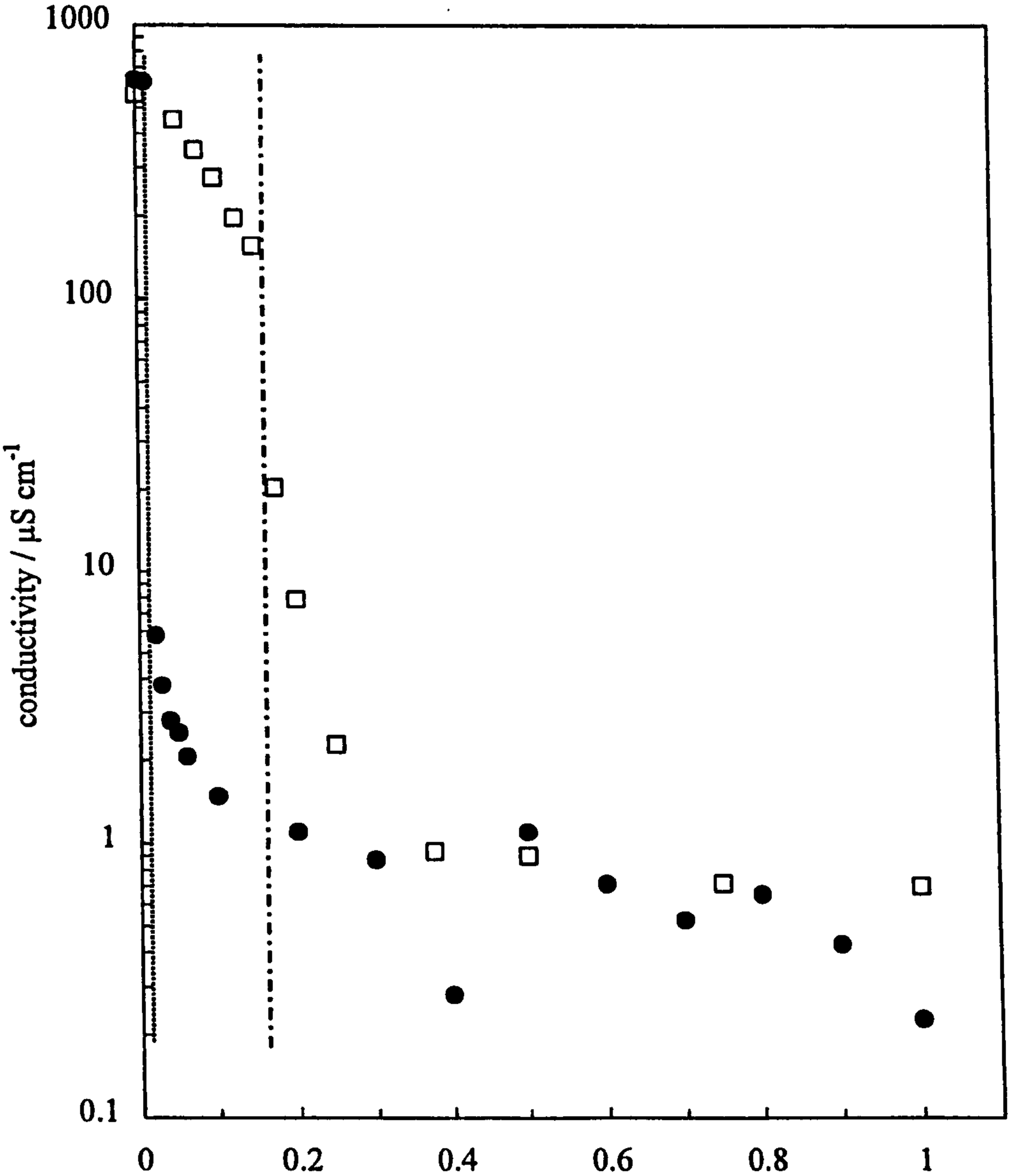

Figure 5.18

Drop diameter volume distributions (right-hand ordinate) for water-toluene emulsions ($\phi_w = 0.5$) containing 2.5 wt.% total particles both dispersed in oil as a function of the weight fraction of H30 (given). Emulsions are o/w for weight fraction H30 = 0 and w/o for weight fractions = 0.3 and 0.7. The solid curves show the cumulative volume distributions (left-hand ordinate).

earlier). The w/o emulsions above inversion are bimodal at intermediate H30 (= 0.3) but virtually monomodal at weight fraction H30 = 0.7. Both types of emulsion are completely stable to coalescence but the o/w emulsions are unstable to creaming. The w/o emulsions sediment up to a weight fraction of H30 = 0.5, after which no phase separation is visible. This behaviour is consistent with the variation in emulsion drop diameter as seen previously. The optical microscopy images in Figure 5.19 confirm the decrease in drop size from the o/w emulsion (H30 = 0) through to the high weight fraction H30 w/o emulsion (= 0.8). Also visible is the gradual transition from non-flocculated (H30 = 0.1) to flocculated water drops (H30 = 0.3 and 0.8) on increasing the weight fraction of H30 in the system. This is analogous to the reverse transition described in Figure 5.7 on reducing the proportion of H30 particles in the system.

5.6 Conclusions

The following conclusions can be drawn concerning the properties of emulsions containing equal volumes of water and toluene stabilised by mixtures of silica particles alone:

- Transitional inversion of emulsions occurs from w/o (o/w) to o/w (w/o) on addition of hydrophilic (hydrophobic) silica to systems stabilised by hydrophobic (hydrophilic) silica.
- Both types of emulsion are remarkably stable to coalescence. The stability to creaming of o/w emulsions and to sedimentation of w/o emulsions is least around phase inversion, exactly the opposite to that found for catastrophic inversion.
- For the majority of systems, the mean diameter of o/w drops is above 100 μm while that for w/o emulsions is below 10 μm. Inversion of one type to the other results in bimodal drop distributions.
- Emulsion drop sizes are maximum at inversion, consistent with the minimum in stability to gravity-induced separation.
- An increase in the proportion of hydrophilic silica in mixtures with hydrophobic silica results in deflocculation of water drops in the emulsion.
- The condition required for inversion depends on the initial location of the particles, although the characteristics of the emulsion remain unchanged.

Figure 5.19

Optical microscope images of water-toluene emulsions ($\phi_w = 0.5$) containing 2.5 wt.% total particles as a function of the weight fraction of H30. Emulsions are o/w for weight fraction H30 = 0 and w/o for weight fractions = 0.1, 0.3 and 0.8. Scale bar equals 100 μm.

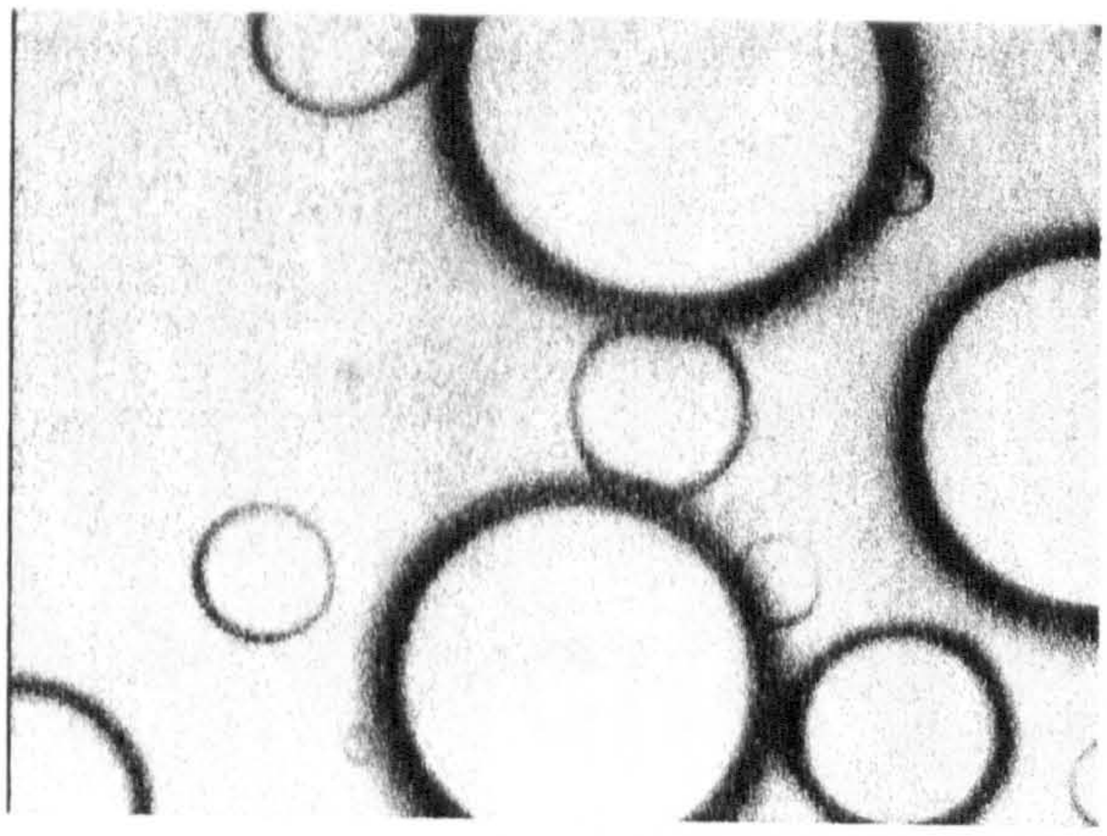

weight fraction H30 = 0

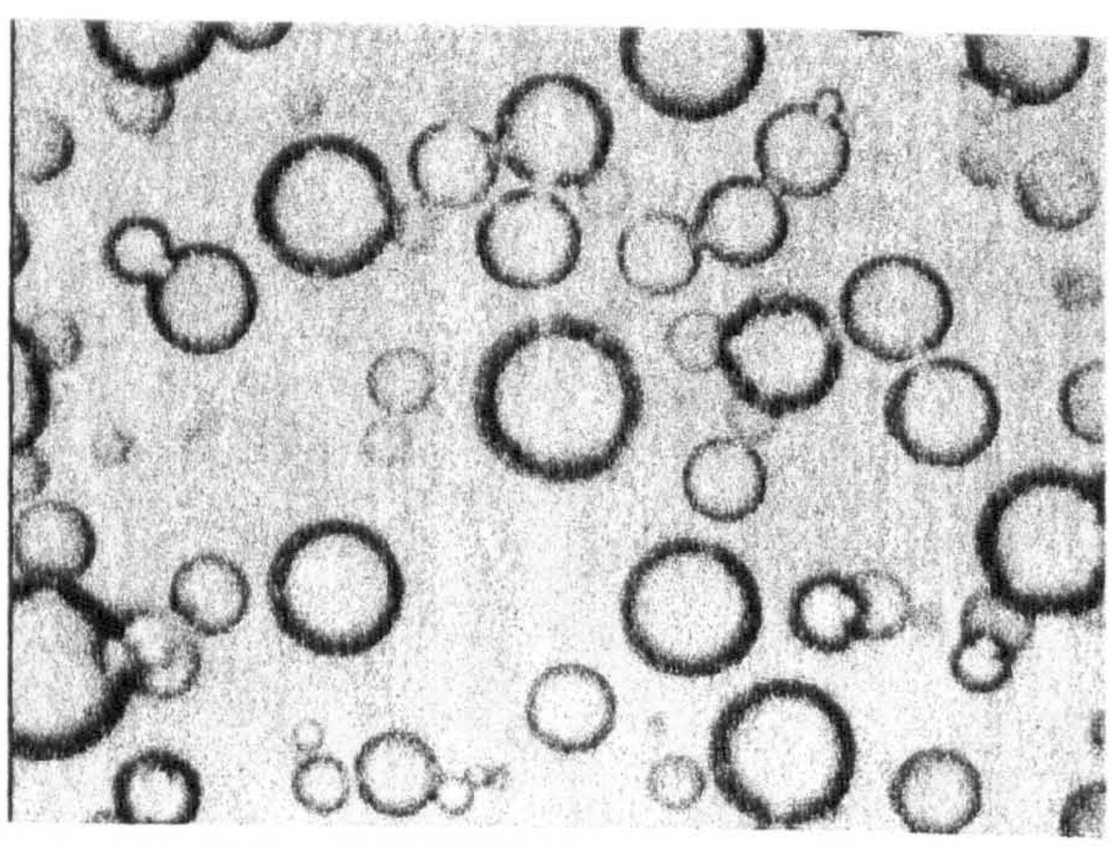

weight fraction H30 = 0.1

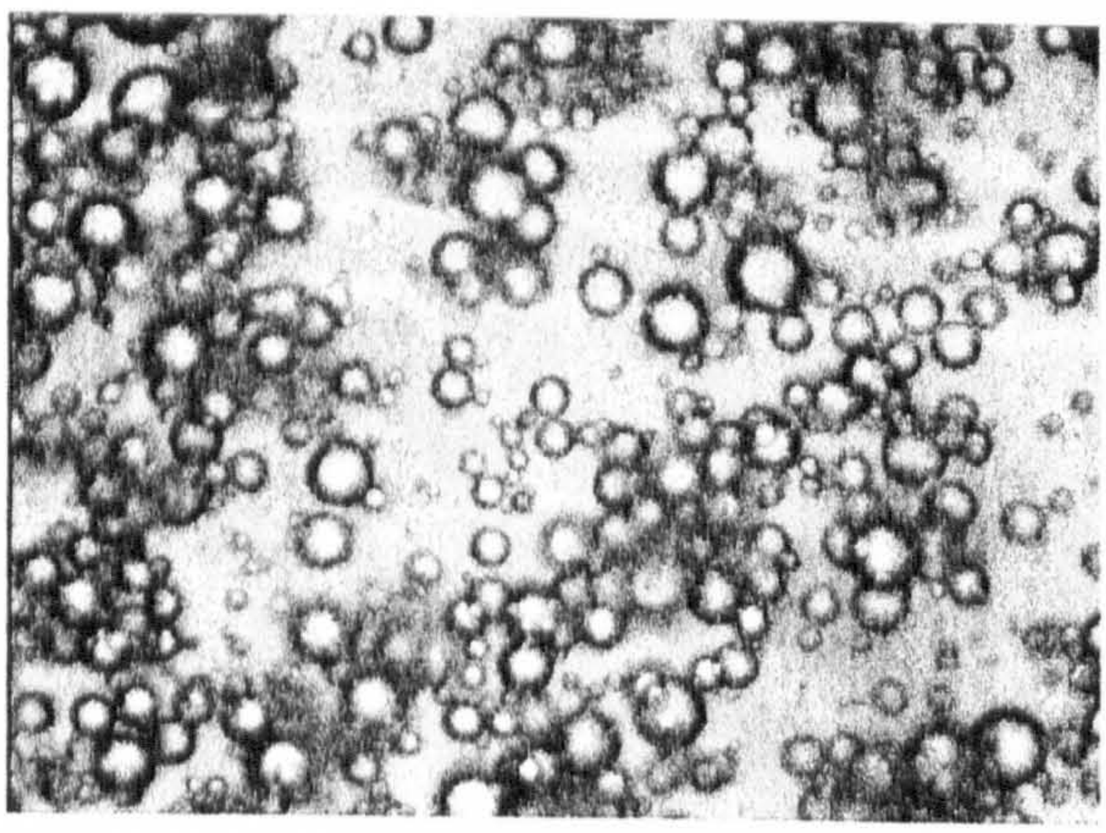

weight fraction H30 = 0.3

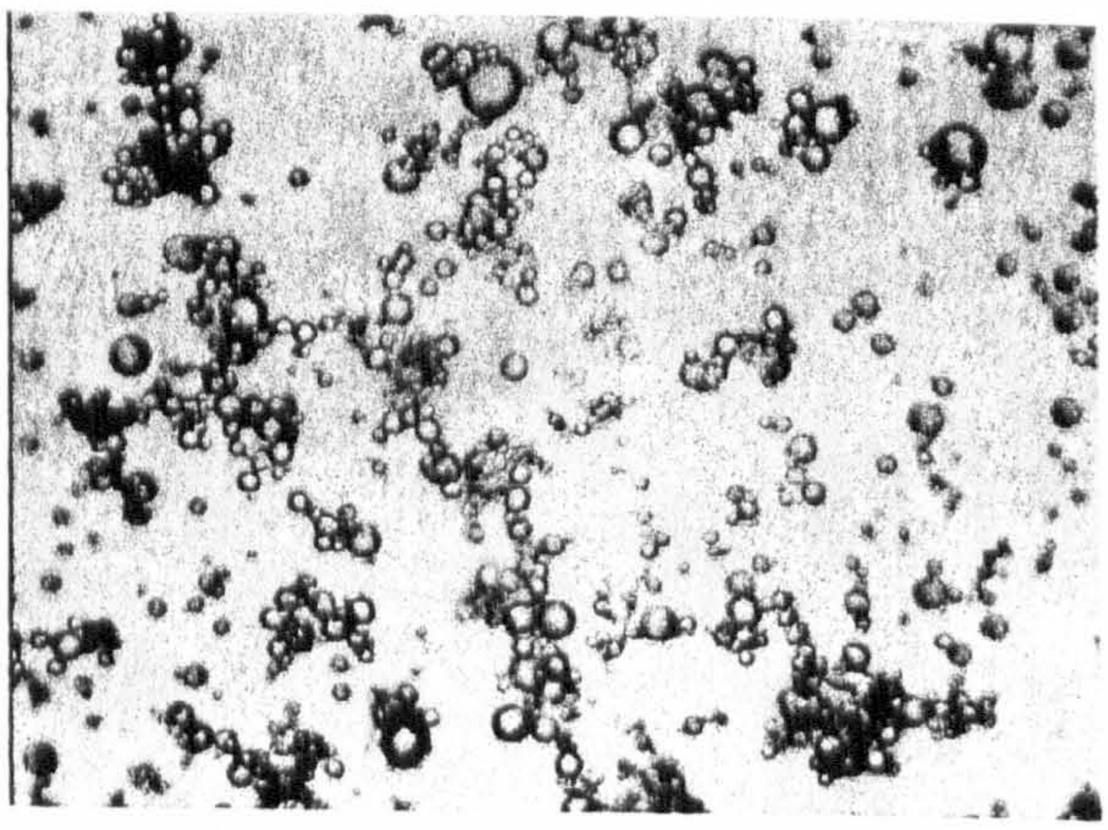

weight fraction H30 = 0.8

CHAPTER 6

CHAPTER 6

INFLUENCE OF PARTICLE WETTABILITY ON THE TYPE AND STABILITY OF SURFACTANT-FREE EMULSIONS

6.1 Introduction

The preferred type of emulsion stabilised by solid silica particles has been shown in previous chapters to depend on the wettability of the particle by the oil and water phases. In systems containing equal volumes of oil and water, hydrophobic particles are preferentially wetted by oil and stabilise w/o emulsions and hydrophilic particles are preferentially wetted by water and stabilise o/w emulsions. The particle wettability is quantified by the contact angle θ (measured through the aqueous phase) that the particle makes at the oil-water interface with the more poorly wetting liquid becoming the dispersed phase.[19] Hence, if $\theta < 90°$ the (hydrophilic) particle will prefer to stabilise o/w emulsions and if $\theta > 90°$ the (hydrophobic) particle will stabilise w/o emulsions. The strength with which a particle is held at an oil-water interface is related not only to θ but also to the tension of the interface,[27] γ_{ow}, and the radius of the particle, a. For a single spherical particle resting at an oil-water interface with a contact angle θ measured through the water phase (see Figure 6.1), the depth of immersion *h* into water is equal to $a(1+\cos\theta)$. The area of contact between the particle and water is $2\pi ah = 2\pi a^2(1+\cos\theta)$. The planar area of oil-water interface eliminated by the presence of the particle is

$$A_e = \pi a^2 \sin^2\theta = \pi a^2(1-\cos^2\theta) \qquad (6.1)$$

Assuming the particle is small enough so that the effect of gravity is negligible and the oil-water interface remains planar up to the contact line with the particle, the energy, E, required to remove the particle from the interface into the oil phase is given by

$$E = 2\pi a^2(1+\cos\theta)(\gamma_{so}-\gamma_{sw}) + \pi a^2(1-\cos^2\theta)\gamma_{ow} \qquad (6.2)$$

Figure 6.1

Variation of the energy of attachment, E (relative to kT), of a spherical particle radius a = 1 x 10^{-8} m at a planar oil-water interface of interfacial tension γ_{ow} = 36 x 10^{-3} N m^{-1} with the contact angle θ the particle makes with the interface (measured through the water phase) at 298 K, calculated using equation 6.4.

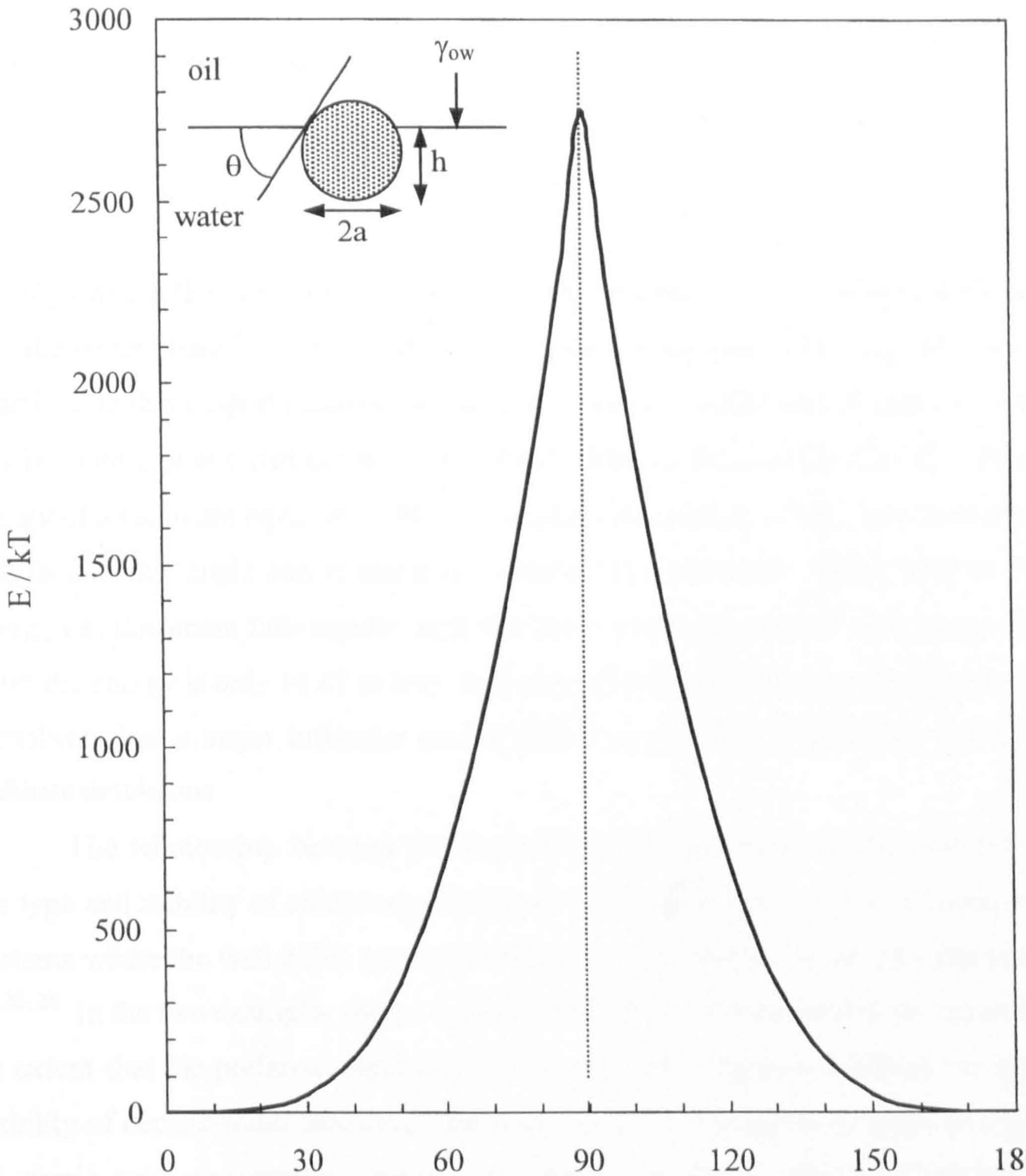

where γ refers to the appropriate interfacial tension and the subscripts s, o and w represent solid, oil and water, respectively. The tensions are related to the contact angle by Young's equation

$$\gamma_{so} - \gamma_{sw} = \gamma_{ow} \cos\theta \qquad (6.3)$$

Therefore equation 6.2 simplifies to

$$E = \pi a^2 \gamma_{ow} (1 + \cos\theta)^2 \qquad (6.4)$$

The sign within the bracket in equation 6.4 becomes negative for removal of the particle into the water phase.[140] The variation of E with θ, at constant a and γ_{ow}, for the system described in this chapter (toluene, water, silica particles) is shown in Figure 6.1, where it can be seen that the particle is most strongly held at the interface for θ = 90°. The energy of attachment equal to ~2800 kT suggests the particle is held very strongly at the interface at this angle and is unlikely to leave once adsorbed. Either side of 90° the energy of attachment falls rapidly such that for θ between 0 and 20° or between 160 and 180°, the energy is only 10 *kT* or less. It is proposed that this extreme variation of E with wettability has a major influence on the ability of particles of different wettability to stabilise emulsions.

The relationship between the contact angle θ, measured on flat substrates, and the type and stability of emulsions stabilised by solid particles has been investigated for systems where the wettability has been effected in situ by adsorption of surfactant.[20, 22-24, 26, 28] In the two examples shown in Figure 6.2 and 6.3 the wettability is varied to such an extent that the preferred emulsion type is changed. Figure 6.2 shows the type and stability of decane-water emulsions stabilised by 2.5 wt.% $CaCO_3$ in water as a function of stearic acid concentration, recast from data given in ref. 28. Also plotted versus stearic acid concentration is the contact angle of an aqueous drop on a calcite crystal under decane. It is clear that as the contact angle increases above 90° with increasing [stearic acid] the emulsion inverts from o/w to w/o, with the stability passing through a minimum around phase inversion, as in surfactant-stabilised emulsions. This appears to contradict the predictions of Figure 6.1 where the energy of attachment is maximum

Figure 6.2

Variation of contact angle (through water) of a water drop on a calcite crystal under decane (left-hand ordinate) and emulsion stability (right-hand ordinate) as a function of stearic acid concentration in decane. Emulsions contained equal volumes (15 cm^3) of oil (containing stearic acid) and water (containing calcium carbonate particles, 2.5 wt.%). Volume of emulsions remaining after 6 hours is plotted, with o/w emulsions shown above the zero level and w/o emulsions below it. Data from ref. 28.

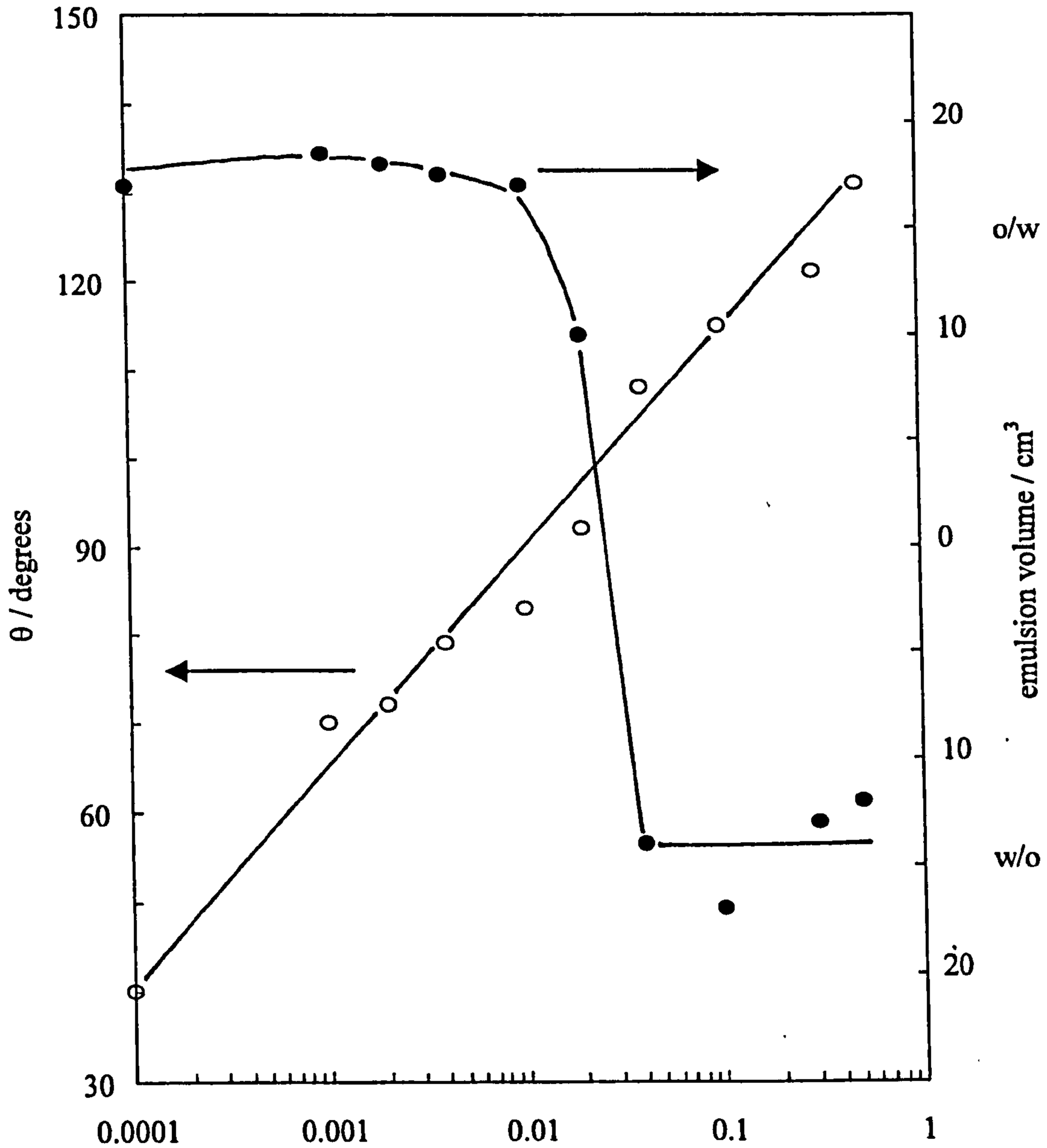

Figure 6.3

Variation of the contact angle (through water) of a benzene drop on a barium sulphate crystal under water as a function of pH. SDS (10^{-3} M in water) emulsions were w/o at all pH. Oleic acid (10^{-3} M in oil) emulsions were o/w at pH < 8 and w/o above this. Data from ref. 20.

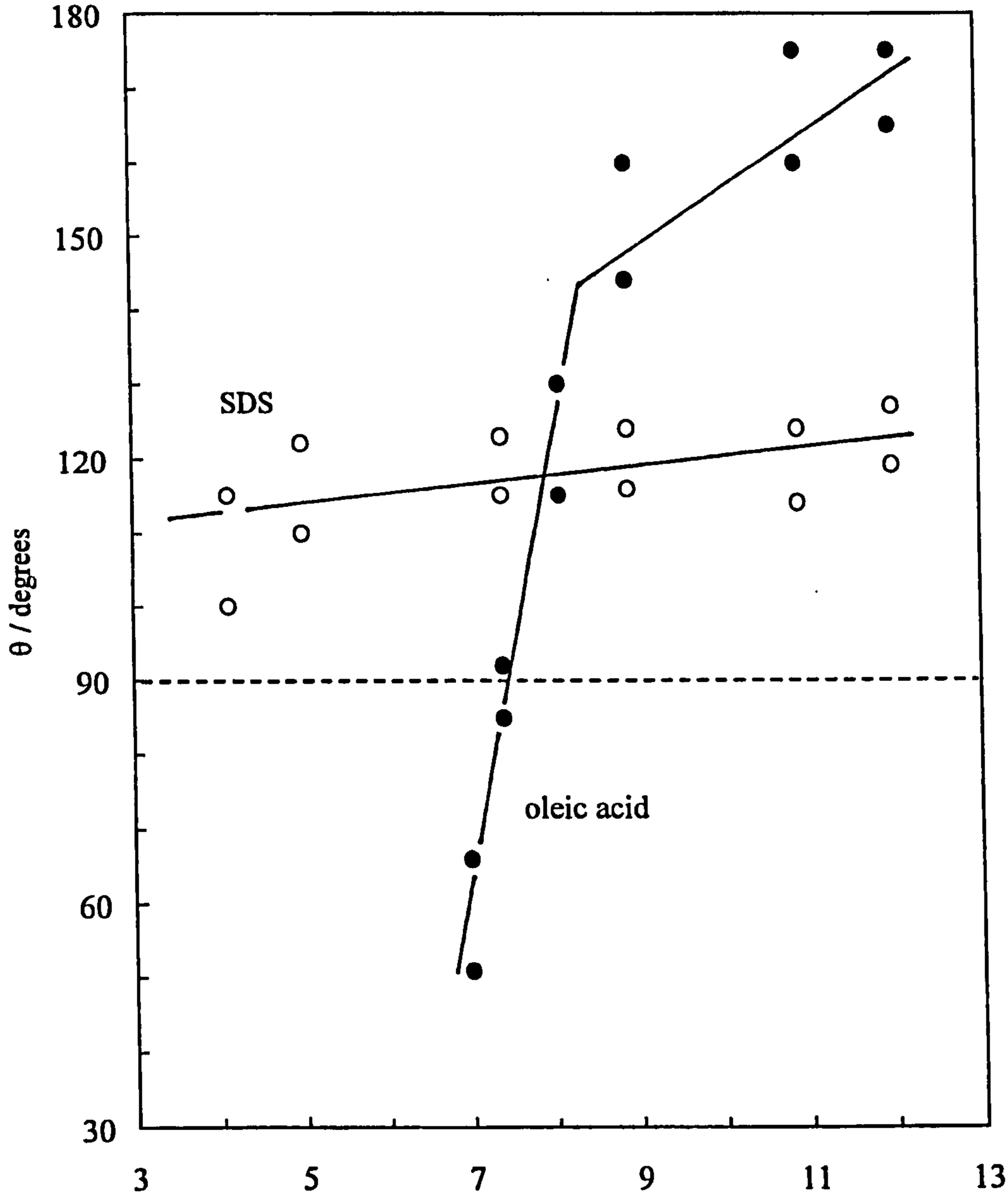

when the contact angle is 90°. However, one of the main factors affecting the stability of emulsions is the stability of the thin liquid film formed between two colliding drops. Denkov et al.[141] provide an explanation for the stability minimum by considering the capillary pressure arising from the deformation of liquid interfaces around an adsorbed particle as liquid is squeezed out of the film. The diagram below shows the model of a film stabilised by uniformly distributed microscopic spherical solid particles of equal size. In this theory the particles bridge the two surfaces of an emulsion film and are not located in the surface of two approaching drops. The model is described for an oil-in-water emulsion but works equally well for a water-in-oil emulsion.

Schematic of solid particles bridging two oil drops of an o/w emulsion

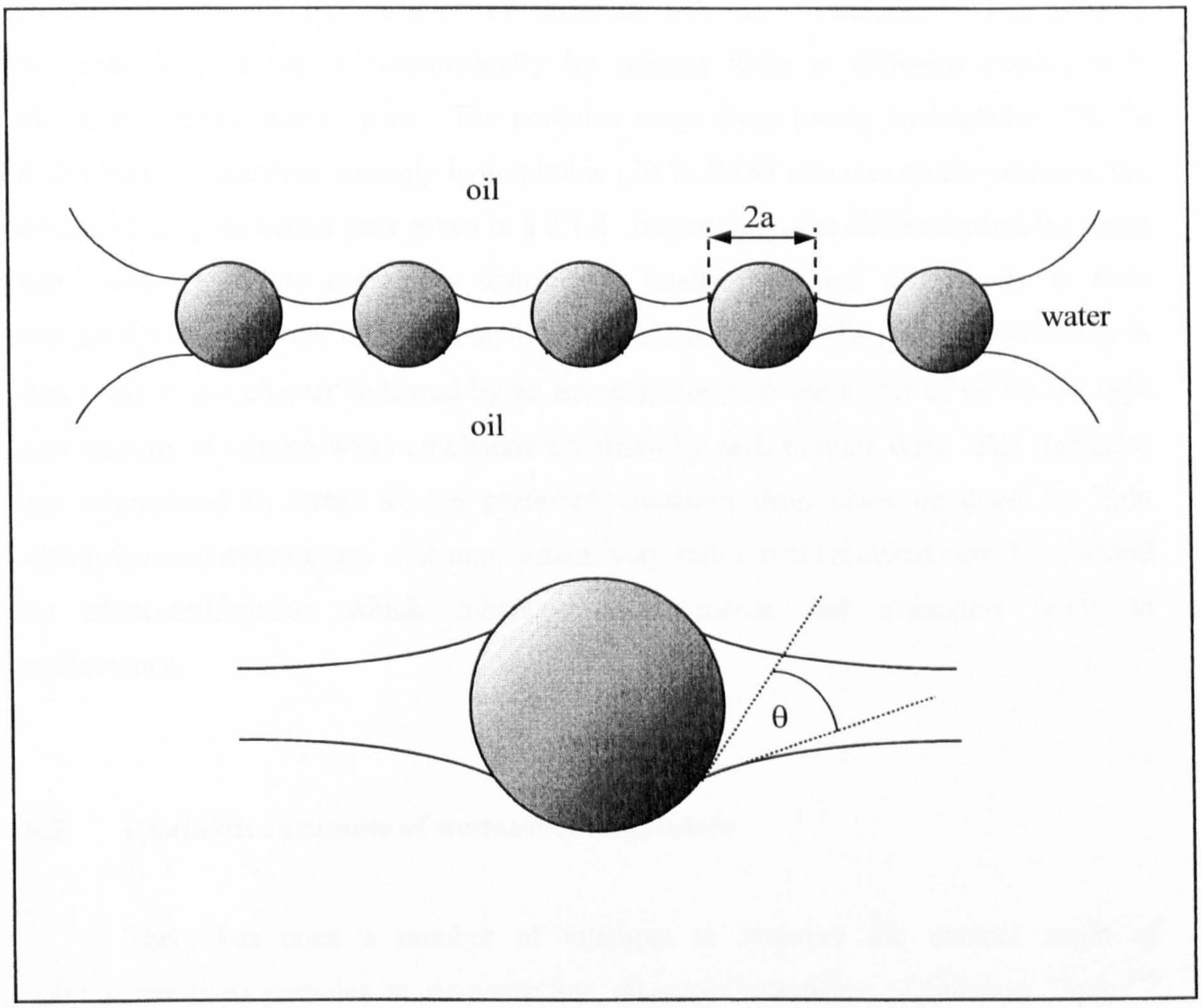

The maximum capillary pressure which can be resisted by liquid meniscuses formed between the adsorbed particles is least when $\theta = 90°$. The thin film is most stable when $\theta = 0$ or 180°.

In the second example (Figure 6.3), the variation in the contact angle (through water) of a benzene drop on a barium sulphate crystal under water as a function of pH is shown, taken from ref. 20. In the absence of solid particles, SDS forms o/w emulsions but these become w/o on adding $BaSO_4$. θ lies above 90° and is independent of pH as expected. On the contrary, oleic acid stabilises w/o emulsions without added solid but phase inverts at low pH in the presence of $BaSO_4$ with a concomitant reduction of θ to below 90°. It is believed that the surface density of oleic acid adsorbed on the particles increases with pH rendering them hydrophobic as a result of two dissociated carboxylate headgroups binding to each barium cation.

In contrast to these two examples where it is the surfactant that causes changes in wettability of the particles, this chapter describes the properties of toluene-water emulsions stabilised by particles of different *inherent* wettability. The particle hydrophobicity is varied systematically by coating them to different extents with dimethyldichlorosilane reagent. The particles range from purely hydrophilic (100 % SiOH on the surface) to strongly hydrophobic (20 % SiOH remains on the surface), the details of the preparation were given in § 2.1.4. Importantly, the different particles (once dispersed) are of the same size distribution (nanometer) and differ only in their wettability toward water or oil. A qualitative measurement of the particle wettability is described in this chapter followed by an investigation into the effect of ϕ_w on the type and stability of toluene-water emulsions stabilised by each particle type. The stabilities are rationalised in terms of the preferred emulsion drop sizes obtained by light diffraction and microscopy. For one system, very stable w/o emulsions are destabilised by ultracentrifugation which enhances sedimentation and ultimately leads to coalescence.

6.2 Qualitative estimate of wettability of powders

There has been a number of attempts to measure the contact angle of micrometer-sized particles at air-water and oil-water interfaces. Clint and Taylor[140] measured the contact angle of hydrophobic particles (500 nm) on water using a Langmuir film balance. The particles are compressed in the trough until they are assumed to be hexagonally close packed on the surface. Further compression causes the

particles to enter the water or air phases. The free energy per unit area to remove all the particles in the monolayer into air is

$$\Delta G = \pi\gamma_{lv}(1+\cos\theta)^2/\left[2(3)^{1/2}\right] \qquad (6.5)$$

and into bulk water is

$$\Delta G = \pi\gamma_{lv}(1-\cos\theta)^2/\left[2(3)^{1/2}\right] \qquad (6.6)$$

The surface area at hexagonal close packing of the particles corresponds to a critical surface pressure, π_c, denoted by a 'knee' in a plot of pressure versus area. Hence at this point

$$\pi_c = \pi\gamma_{lv}(1\pm\cos\theta)^2/\left[2(3)^{1/2}\right] \qquad (6.7)$$

This enables the calculation of the contact angle of water on hydrophobic particles from a pressure-area compression curve. This method assumes that the effect of gravity is zero and that interparticle interactions are negligible. Interparticle interactions are taken into account in an additional note[142] where it is shown that a simple linear approximation of the force-distance curve provides an adequate correction for this effect. In a similar investigation, Horvolgyi et al.[143] have studied the wetting behaviour of partially hydrophobic silanised glass microspheres (75 μm diameter) using a Wilhelmy film balance. The change in surface tension with area is measured using a platinum plate allowing the calculation of a surface pressure-area isotherm. The contact angle is then calculated using the equations above. These contact angles were in reasonable agreement with those measured from microscopy images where the particles reside at an air-water interface formed between two plane-parallel glass microscope slides (method described later). The Wilhelmy film balance is thought to be more sensitive than the Langmuir film balanced used previously[144] where the discrepancy between measured and calculated values of θ were more significant. Contact angle determinations of water on micrometer sized particles have also been carried out by measuring the capillary pressure in a packed bed of particles.[137] This method is described in detail in § 5.4. As mentioned previously, contact angle measurements at the oil-water interface have been

measured by optical microscopy.[143, 145] In these experiments the particles are spread on a curved meniscus formed between two vertical glass slides. The glass slides are separated by two spacer particles which were slightly larger than the ones being studied. The interfacial particles are then observed from the side using transmitted light from an optical microscope.

The majority of the previous work on contact angle determinations has been carried out on particles of greater than 10 microns. The silica particles used in the present study however are less than 30 nm in diameter when dispersed. As a result none of the methods developed previously were entirely satisfactory and in any case the wettability of powders composed of such particles is nontrivial.[146] However, in a recent study, Yan et al.[147] quote the contact angle of fumed silica nanospheres of varying hydrophobicity at the air-water, toluene-air and most importantly, the toluene-water interface. The contact angles were calculated from enthalpy of immersion data measured using heat flow microcalorimetry. Hydrophilic Aerosil 200 silica was coated with various silanising agents resulting in contact angles at the oil-water interface that varied from 0 (Aerosil 200) to 96°. Unfortunately, data for silica coated to varying extents with the same silanising agent have not been measured but it is encouraging that a reliable method has been described. In this work, a qualitative measure of the wettability was determined from powder immersion measurements. Fifty milligrams of powder was placed carefully and evenly on the surface of 20 cm^3 of a given water / methanol mixture contained in a tube of diameter 2.3 cm at room temperature. The time taken for all the powder to disappear from the liquid surface was measured and is equated with the immersion time.[75] The submersion of a powder involves three stages – adhesion, immersion and spreading – in which the solid-vapour surfaces disappear and are replaced by solid-liquid interfaces. The time for submersion depends on both the density difference between the powder and the liquid and the rate at which the liquid displaces air on the powder surfaces and in the voids between powder aggregates. For a powder of cube side length 1 cm, the total work for the overall dispersion process, W_d, is given by the sum of the three separate stages and is equal to;

$$W_d = -6\gamma_{lv}\cos\theta_{sl} \qquad (6.5)$$

where γ_{lv} is the tension of the liquid - vapour surface and θ_{sl} is the contact angle between the solid and liquid phases measured into the liquid. W_d is negative for powders with $\theta_{sl} < 90°$ and as a result the process is spontaneous. However, if the powder has $\theta_{sl} > 90°$, W_d is positive and work must be done to bring about complete immersion.

In such a test involving a range of powders of varying wettability, a liquid is chosen such that the most hydrophilic and the most hydrophobic powders can ultimately enter the liquid. A water / methanol mixture was chosen for these immersion measurements because their dielectric constants are sufficiently close (78.5 and 32.6 at 25 °C, respectively) for the above condition to apply. The immersion times of a fixed mass of powder on the surfaces of water-methanol mixtures of varying composition are given in Figure 6.4. The time *decreases* from 10 seconds in 10 vol% water to 3 seconds in 75 vol% water for the most hydrophilic particle (N20, filled circles) as expected. The time is very short (~ 8 seconds) in methanol-rich mixtures for the most hydrophobic particle (H18, open circles) but *increases* by over four orders of magnitude for 40 vol% water mixtures and above as the polarity of the liquid increases. Powders of intermediate wettability exhibit immersion times between these extremes in most cases. The immersion times of the powders in equal volumes of methanol and water increase progressively as the percentage silanol on the silica surface decreases. Although this qualitative trend in particle wettability does not apply to the toluene-water interface (which forms in emulsions), the silanol content is proportional to wettability and will be used in this chapter to describe it.

6.3 Effect of volume fraction of water on emulsion type for all particles

In Chapter 4, it was shown that hydrophilic N20 particles stabilise o/w emulsions and hydrophobic H30 particles stabilise w/o emulsions when $\phi_w = 0.5$. The emulsion type was shown to catastrophically invert at a particular volume fraction of dispersed phase which depended on the particle type. The volume fraction of oil, ϕ_o, was 0.65 for N20 whereas ϕ_w was 0.72 for H30. Figure 6.5 (upper) shows the conductivity of emulsions stabilised by particles of different wettabilities and wt.% given in the legend. The emulsions invert from low conducting w/o emulsions to high conducting o/w emulsions at particular values of ϕ_w. The value at inversion increases as the particles

Figure 6.4

Immersion time at 22 °C of six silica powders in methanol-water mixtures of different composition. Arrows indicate times > 24 hours. Filled circles – N20, crosses (+) – SLM 078, triangles – SLM 079, diamonds – SLM 081, crosses (X) – H30, open circles – H18.

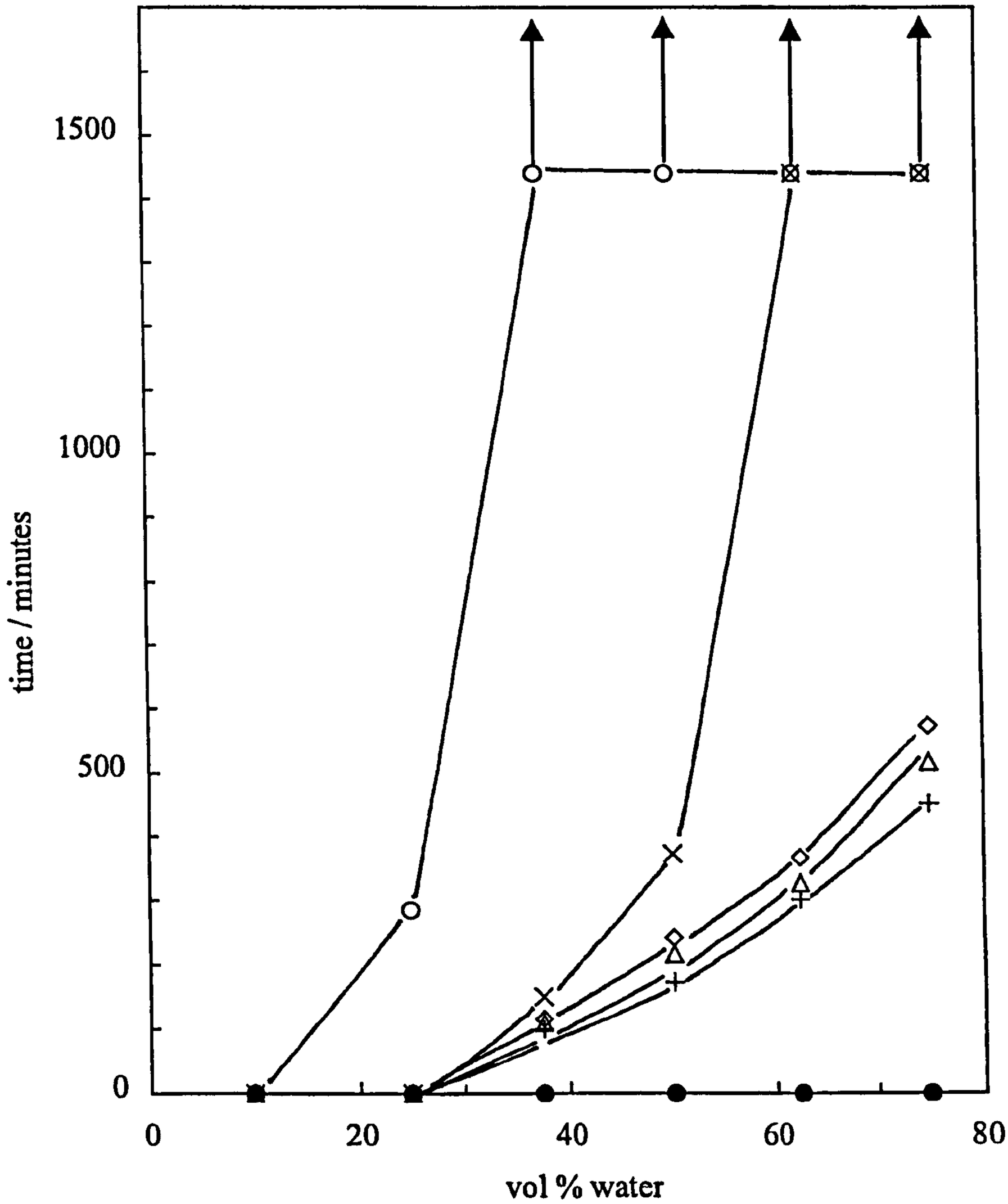

Figure 6.5

(*upper*) Conductivity of water-toluene emulsions stabilised by silica particles of varying hydrophobicity as a function of the volume fraction of water. The symbols and systems are: open circles - 10 wt.% N20 in water, filled triangles – 2 wt.% SLM 078 in oil, open squares – 2 wt.% SLM 079 in oil, filled circles – 2 wt.% SLM081 in oil, filled squares – 2 wt.% SLM 957, open triangles – 2 wt.% H30 in oil, stars – 2 wt.% SLM 091 and filled diamonds – 5 wt.% H18 in oil. (*lower*) Volume fraction of water at inversion of the above emulsions, ϕ_w^{inv}, versus the percentage of silanol groups on the silica particles.

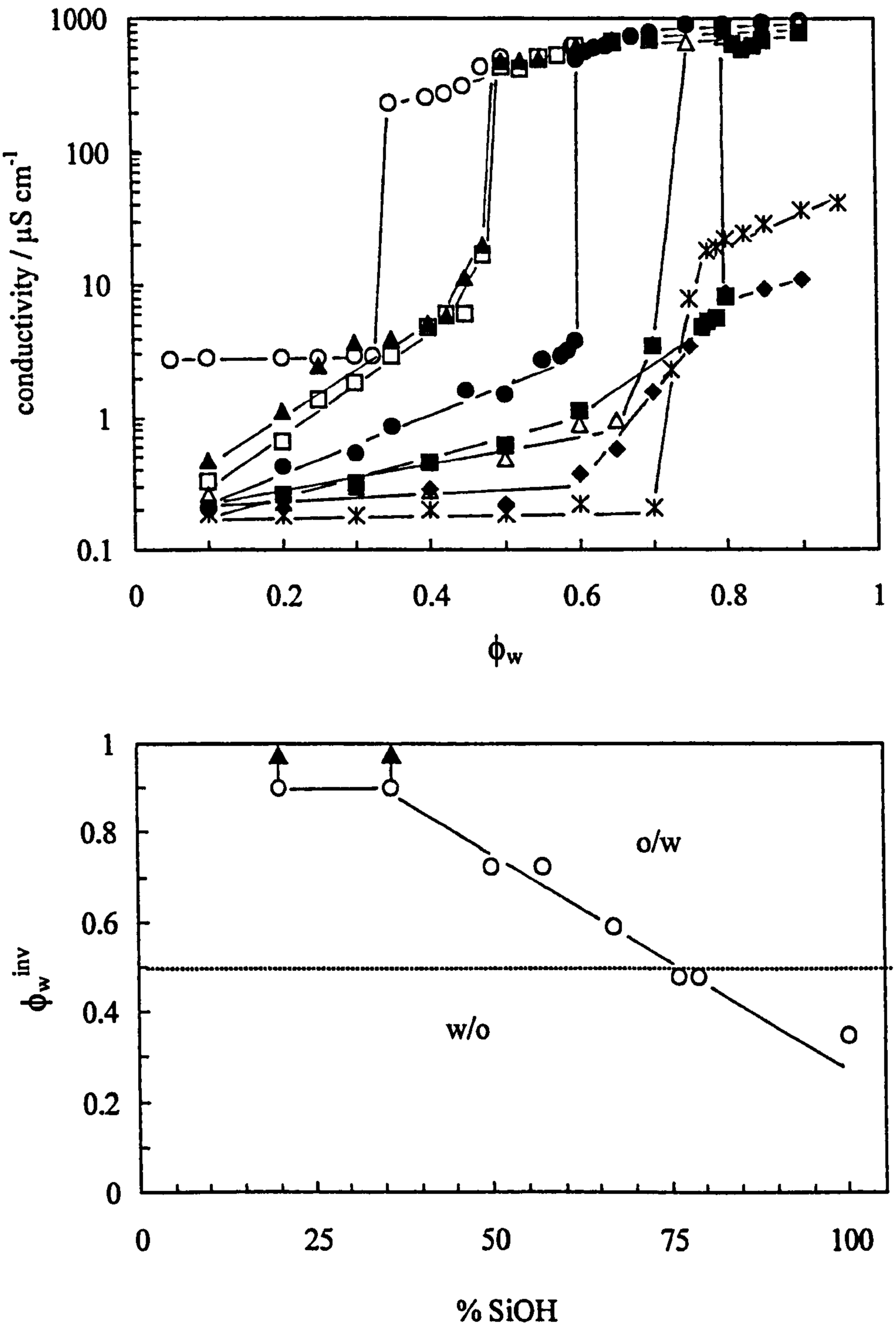

become more hydrophobic. Emulsion type was verified by continuous phase determination. The conductivity of the o/w emulsions increases with ϕ_w as the volume fraction of obstructing oil droplets decreases. The conductivity data is summarised in Figure 6.5 (lower) where ϕ_w at inversion is plotted as a function of the percentage SiOH on the particle surfaces. The more hydrophilic particles (high % SiOH) invert below or very close to $\phi_w = 0.5$ whereas the more hydrophobic particles invert above this value. The arrows for points at low silanol content indicate that the emulsions remained w/o up to ϕ_w of at least 0.9, and thus inversion is unlikely. It can be appreciated that expressing the results in this form is a quick and easy way of screening different types of particles and ranking them in terms of their hydrophobicity.

6.4 Effect of ϕ_w on emulsion stability for all particles

The stability of emulsions prepared at different values of ϕ_w ranging from 0.1 to 0.9, have been investigated for each of the particle types. The coalescence stability of water-toluene emulsions at $\phi_w = 0.5$, is shown to vary dramatically in Figure 6.6. The most hydrophilic (N20, 100 % SiOH) and the most hydrophobic silica (H18, 20 % SiOH)-stabilised emulsions are very unstable to coalescence immediately after emulsification even at high particle concentration. The instability is further enhanced when the particle concentration is lowered so that it is the same for all particle types. Emulsions stabilised by the silica particles of intermediate wettability show no sign of coalescence within at least 6 months, and for SLM 078 (79 % SiOH) limited coalescence occurs. A clear maximum in stability to coalescence is evident upon increasing the particle hydrophobicity for both series.

Unlike coalescence, which either happens or does not across the series, the stability to gravity induced separation, creaming for o/w and sedimentation for w/o emulsions, allows a distinction to be made for all the particles. Figures 6.7 – 6.9 show the stability of emulsions to gravity induced separation at $\phi_w = 0.2$, 0.5 and 0.8 respectively, as a function of time after emulsification. The ordinate denotes the fraction of oil or aqueous phase resolved, calculated using equation 3.28 without the volume fraction term so that the stability is independent of the initial ϕ_w. At $\phi_w = 0.2$ (Figure 6.7), the emulsions are all w/o and stability to sedimentation increases progressively

Figure 6.6

Fraction of emulsion coalesced for emulsions stabilised by the range of silica particles at $\phi_w = 0.5$, 10 minutes after emulsification. Particle concentration as in Figure 6.5 (diamonds) and 1 wt.% fixed particle concentration in emulsion (squares).

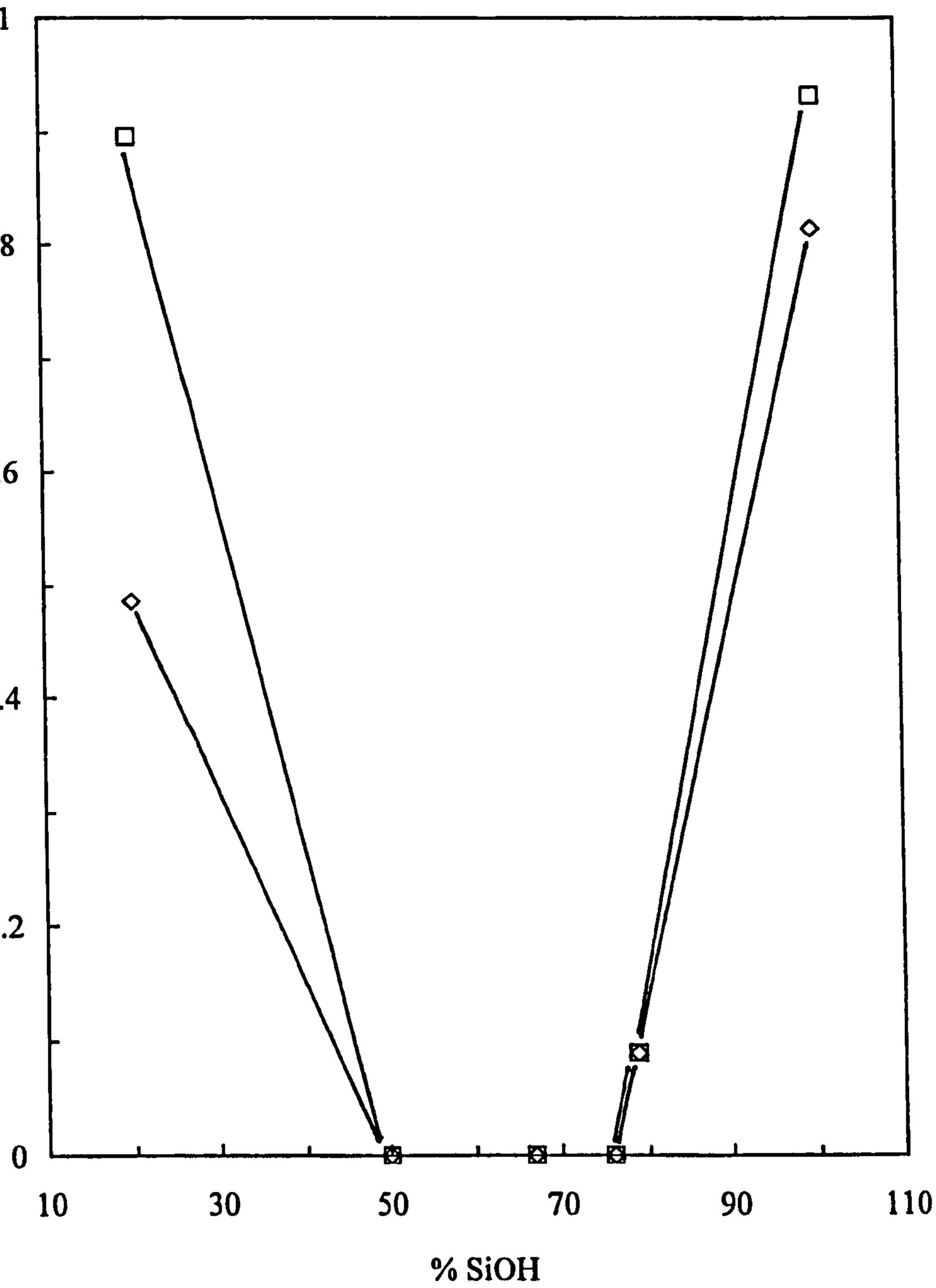

Figure 6.7

Fraction of emulsion as oil phase versus time for water-in-toluene emulsions stabilised by silica particles at $\phi_w = 0.2$. Concentrations of particles in the emulsions (wt.%) are 5 (N20), 1 (SLM 078), 1 (SLM 079), 0.5 (SLM 081), 0.5 (H30) and 2.5 (H18). All emulsions are w/o and the stability is thus to sedimentation.

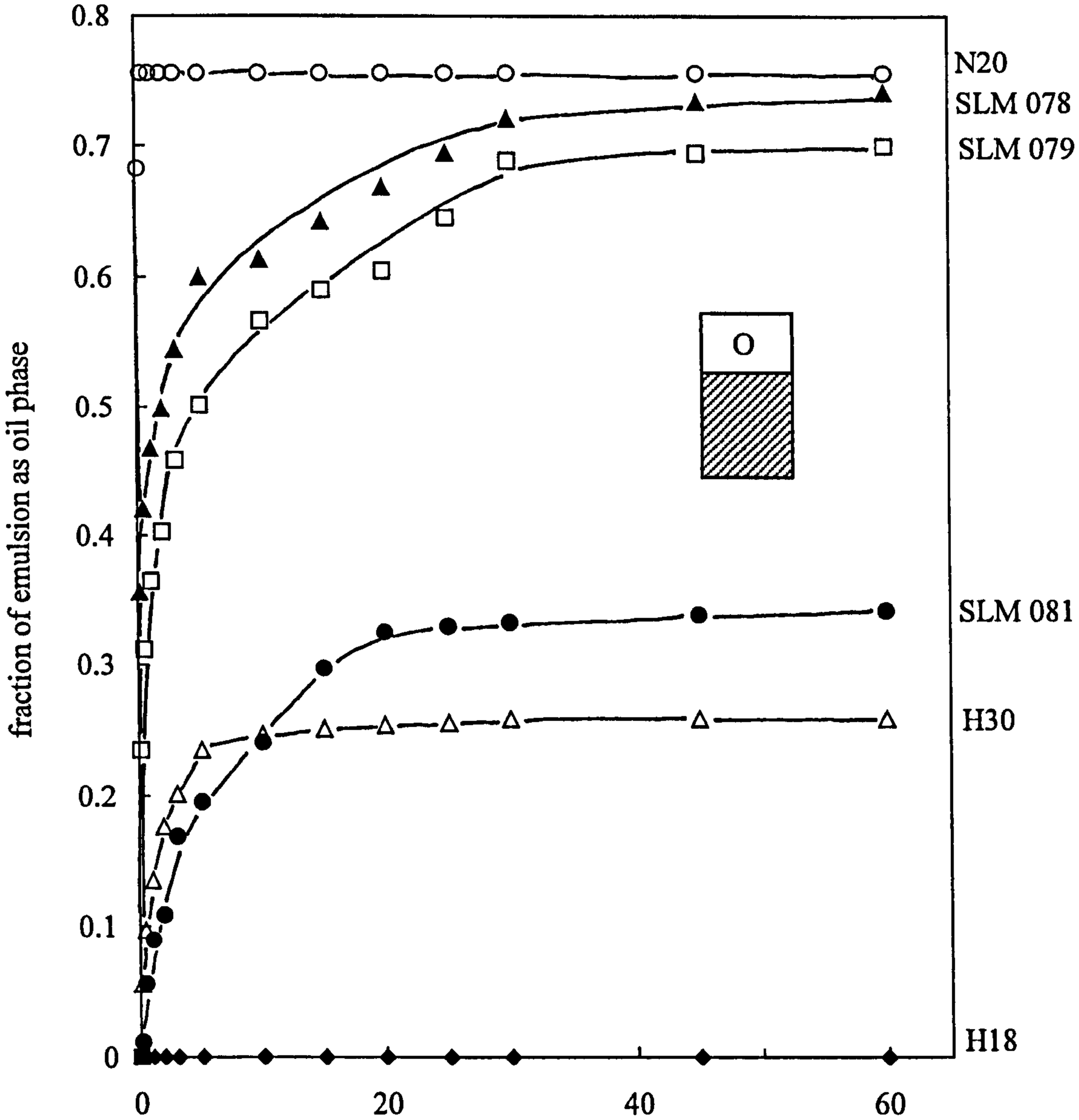

Figure 6.8

Fraction of emulsion as oil or aqueous phase versus time for toluene-water emulsions stabilised by silica particles at $\phi_w = 0.5$. Upper three emulsions are o/w (stability to creaming) and lower three are w/o (stability to sedimentation). Systems are as in Figure 6.7.

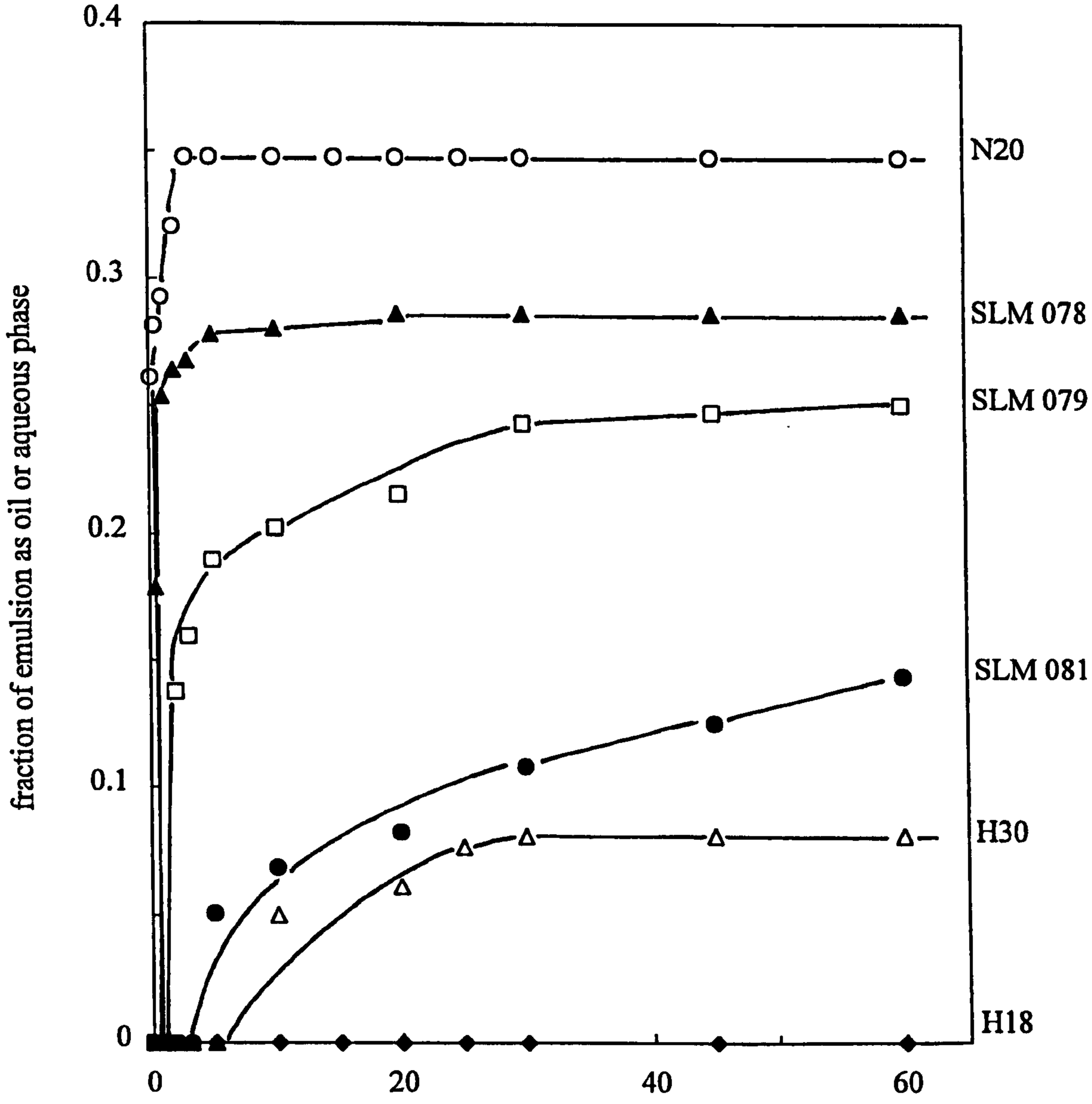

Figure 6.9

Fraction of emulsion as aqueous phase versus time for emulsions stabilised by silica particles at $\phi_w = 0.8$. Upper five emulsions are o/w and the stability is thus to creaming. Lowest emulsion (diamonds) is w/o and does not sediment but only coalesces. Systems are as in Figure 6.7.

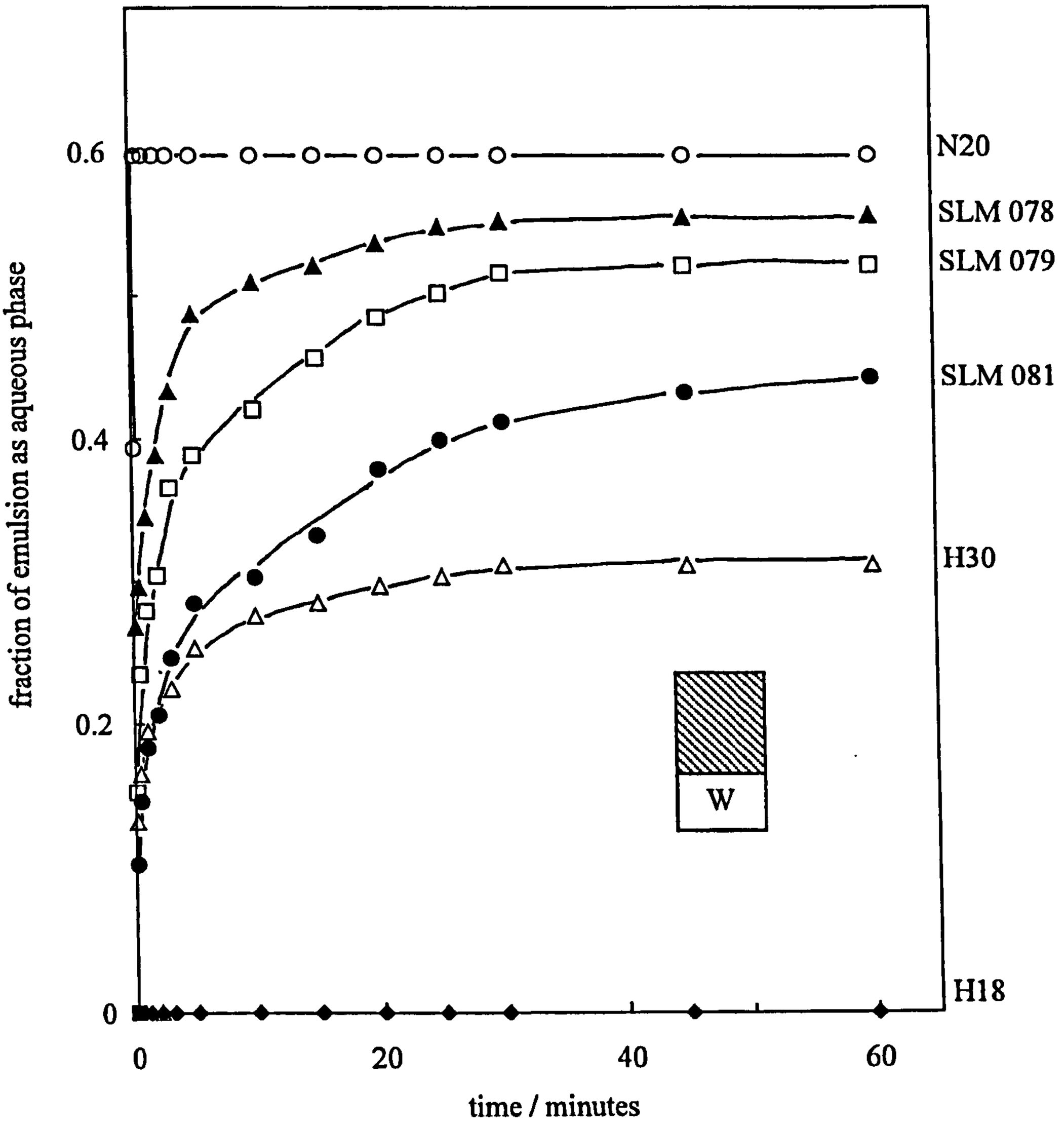

with increasing hydrophobicity. The time taken for sedimentation to plateau is rapid (1 minute) for hydrophilic particles (open circles), increases to around 1 hour for low degrees of hydrophobisation (filled triangles and open squares), and decreases to between 20 (filled circles) and 5 minutes (open triangles) for higher degrees. The resolved oil phase is colourless in all cases. Coalescence is so marked in emulsions stabilised by H18 silica (filled diamonds) that sedimentation does not have time to happen. At $\phi_w = 0.5$ (Figure 6.8), the preferred emulsion type is formed. The upper three curves show the stability to creaming of o/w emulsions and the lower three show the stability to sedimentation of w/o emulsions. The more hydrophilic particles are less efficient at stabilising o/w emulsions than the hydrophobic particles are at stabilising w/o emulsions. Figure 6.9 shows the stability to creaming of emulsions at $\phi_w = 0.8$ for all the particles except H18 (filled diamonds) which are w/o and do not sediment but only coalesce. Again the stability increases progressively as the particles become more hydrophobic.

The stability of emulsions to both creaming and coalescence as a function of ϕ_w are summarised in Figure 6.10 at times when the majority of emulsion breaking is complete. The particle hydrophobicity increases from left to right and from top to bottom. Open points refer to f_{aq} and filled points refer to f_{oil} in all cases. Hence points along the zero ordinate represent no coalescence of water or oil drops respectively. For all but the most hydrophobic particles, the stability to sedimentation of w/o emulsions and creaming of o/w emulsions increases to a maximum at phase inversion as discussed in Chapter 4. For H18 emulsions (20 % SiOH) which are w/o at all ϕ_w, coalescence increases with increasing ϕ_w, presumably due to an increase in the drop size.

Figure 6.11 compares the times for the emulsion breakdown to reach a plateau value of stability as a function of % SiOH on the silica surface. At each ϕ_w, the final extent of creaming or sedimentation (filled points) increases progressively with % SiOH or decreasing hydrophobicity. The plateau times (open points), however, pass through a very sharp maximum for intermediate values of wettability. The maximum always occurs for particles with 67 % SiOH on the surface even though the emulsion is at different positions relative to phase inversion.

In order to understand the emulsion stability measurements, the drop sizes of the emulsions have been measured for all particle types and values of ϕ_w. A selection of distribution plots measured immediately after preparation are given in Figure 6.12 for a

Figure 6.10

Stability of emulsions after a certain time, expressed as f_{aq} (fraction of aqueous phase resolved) and f_{oil} (fraction of oil phase resolved), versus volume fraction of water for all particles. The % SiOH on the particles and the time chosen respectively from left to right and top to bottom sequentially are (100, 30 min.), (79, 3 hr.), (76, 3 hr.), (67, 3 hr.), (50, 30 min.) and (20, 30 min.).

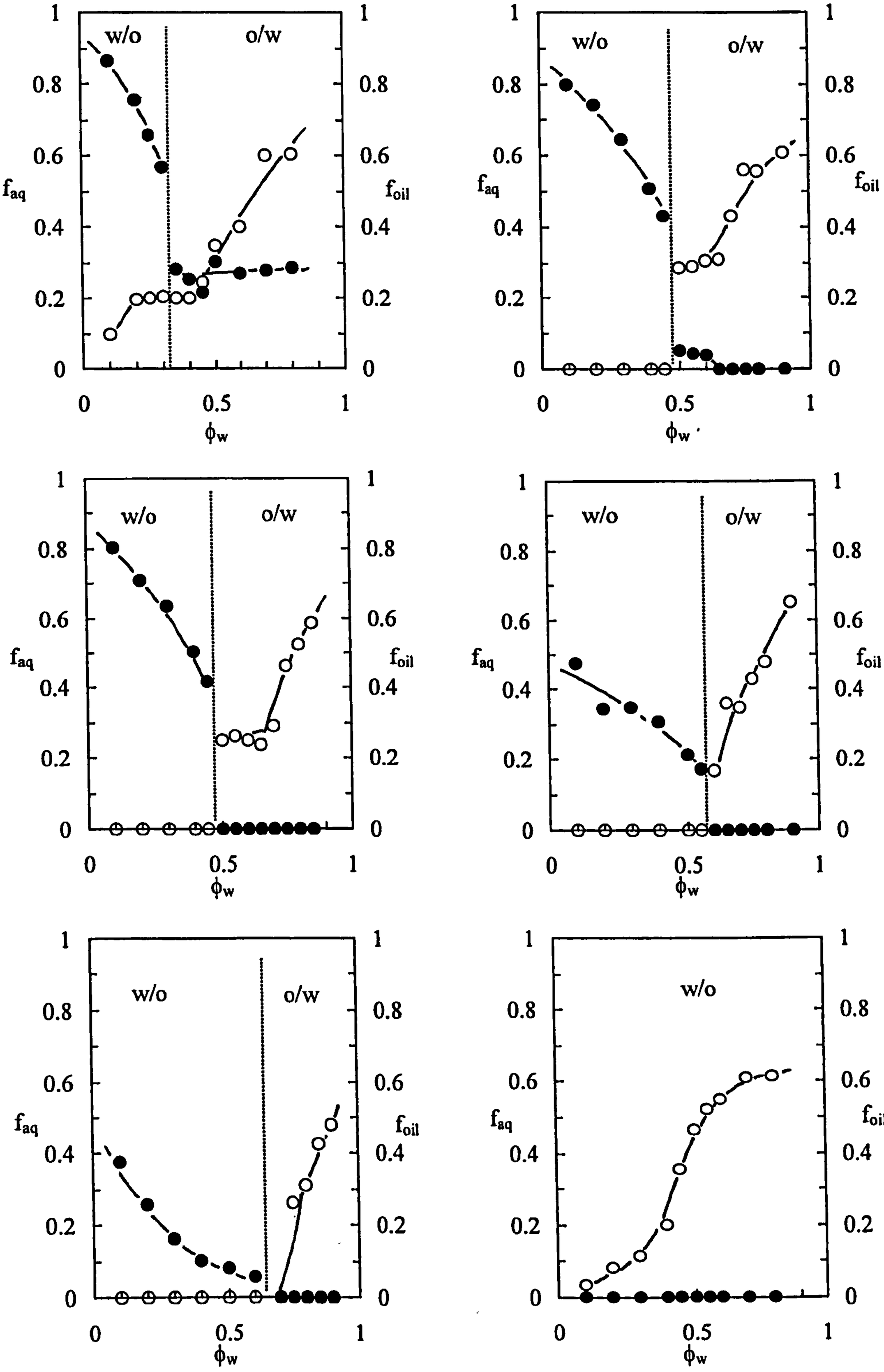

Figure 6.11

Variation of the time required to reach plateau value of emulsion stability (open points, left hand ordinate) and fraction of oil or aqueous phase resolved at that time (filled points, right hand ordinate) versus % SiOH on the particles for three volume fractions of water (given).

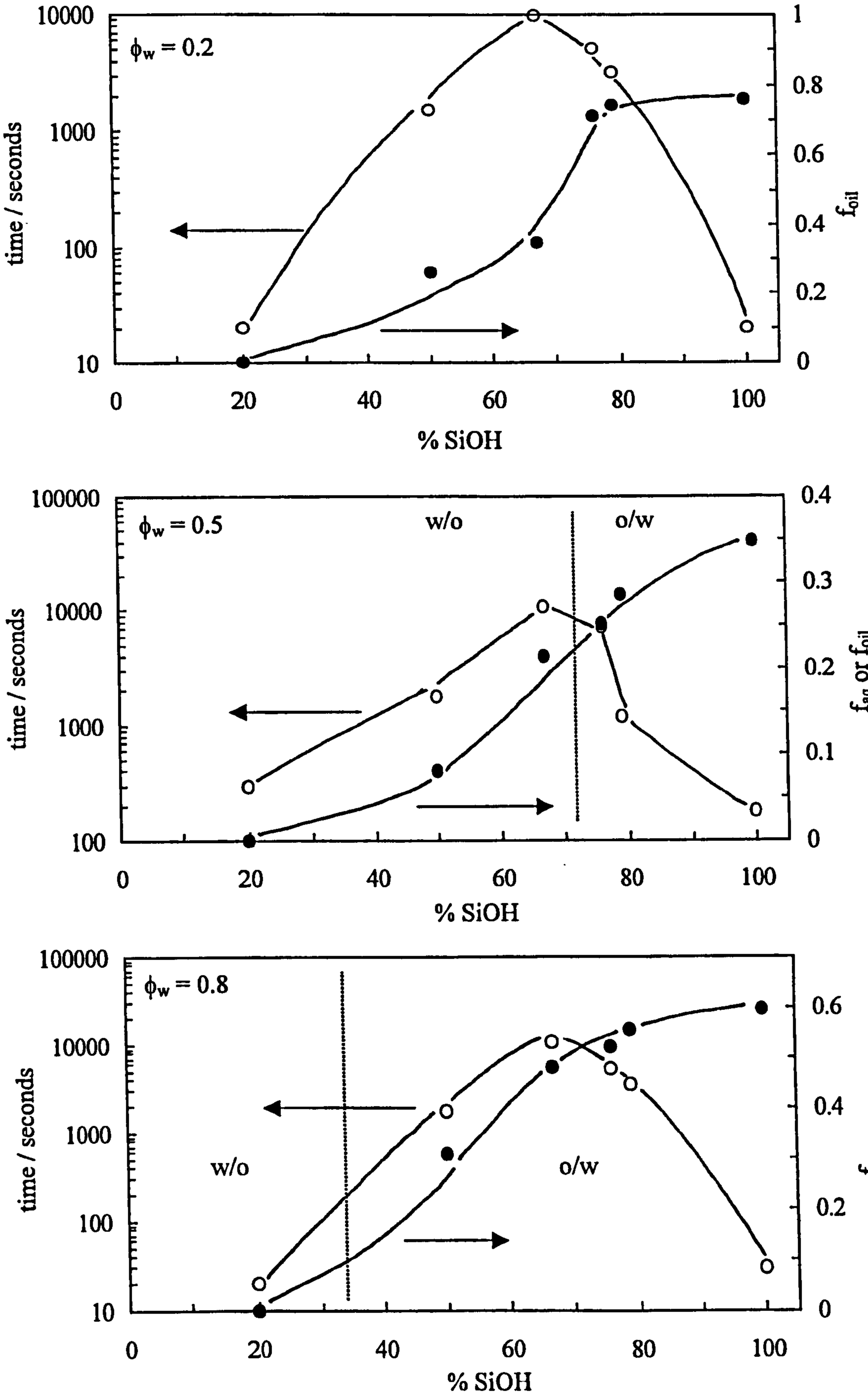

Figure 6.12

Initial drop diameter volume distributions (right-hand ordinate) for water-toluene emulsions ($\phi_w = 0.5$) stabilised by silica particles. The % SiOH on the particles are (a) 100, (b) 79, (c) 76, (d) 67, (e) 50, (f) 20 and emulsions are o/w for (a-c) and w/o for (d-f). Note the different abscissa scales. The solid curves show the cumulative volume distribution (left-hand ordinate). Systems are as in Figure 6.5.

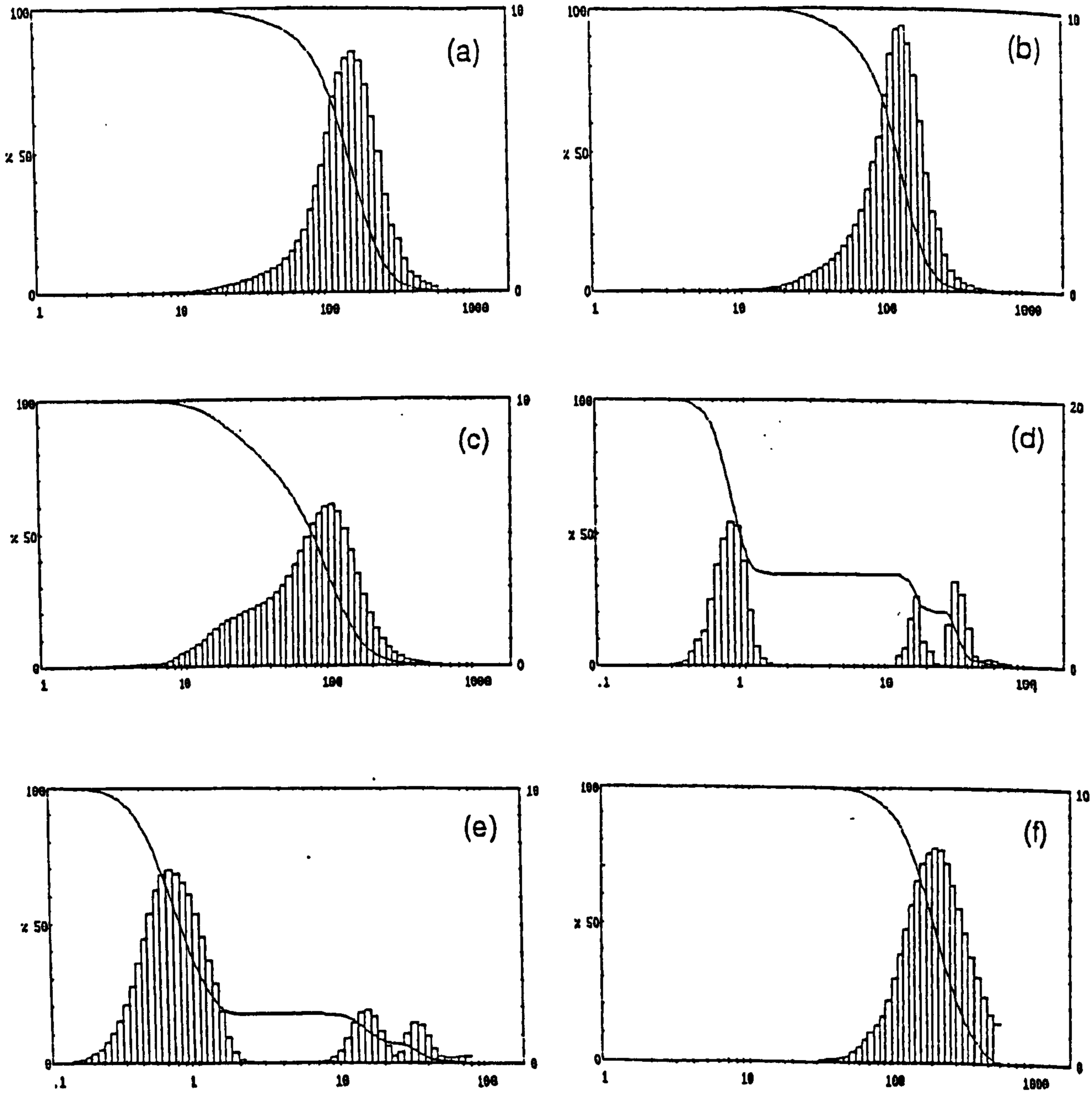

ϕ_w = 0.5 where the particle hydrophobicity increases from (a) to (f). Distributions (a)–(c) are o/w emulsions and (d)–(f) are w/o emulsions. The distributions at the extremes of wettability ((a) and (f)) are log-normal and centred around 200 μm corresponding to unstable emulsions. The distributions are skewed or slightly bimodal of much smaller size (around 10 μm) for emulsions stabilised by particles of intermediate wettability. Although creaming / sedimentation occurs with time for these emulsions, we have verified that the drop size distributions remain unaltered for over 3 hours, consistent with there being no coalescence in this time period. Coalescence was at least 80 % (Figure 6.6) complete after 3 hours for the hydrophilic particle-stabilised emulsion (a) meaning sampling of the millimetre sized drops proved to be difficult. The distribution for the very hydrophobic particle-stabilised emulsion (f) remained unchanged with time due to the coalescence being complete within 2 minutes, which is the minimum time required to determine the size distribution by light diffraction.

The time taken for the emulsion instability to plateau (Figure 6.11) and the initial arithmetic mean emulsion drop diameter are plotted as a function of % SiOH in Figure 6.13. The arithmetic mean is more representative of the overall distributions in this case due to the bimodality of the distributions. At each ϕ_w, the times pass through a maximum at the same % SiOH as the mean of the diameters passes through a minimum, i.e. the most stable emulsions contain the smallest drops. The phenomenon appears to be universal in that it occurs over a wide range of ϕ_w, independent of whether emulsions are o/w or w/o. As shown in Chapter 1, the rate of creaming of an isolated drop is proportional to the square of the radius[3] which explains this qualitative finding, although the overall width of the size distribution is also important. These results suggest that the stability of the emulsions is dependent on the wettability of the particles adsorbed at the oil-water interface and the proximity of a particular system to phase inversion has no important consequences on its stability. Very hydrophilic and very hydrophobic particles are poor at stabilising o/w and w/o emulsions respectively. However, particles of intermediate wettability (50 – 76% SiOH) stabilise o/w or w/o emulsions that are completely stable to coalescence and have a high stability to gravity-induced separation. This dependence relates directly to the energy of attachment predictions for a single particle at the oil-water interface, suggesting particles of intermediate wettability reside at the oil-water interface with a contact angle close to approximately 90°.

Figure 6.13

Comparison of the time required to reach plateau value of emulsion stability (open points, left hand ordinate) and initial arithmetic mean emulsion drop diameter (filled points, right hand ordinate) versus % SiOH on the particles for three volume fractions of water (given). Systems as in Figure 6.5.

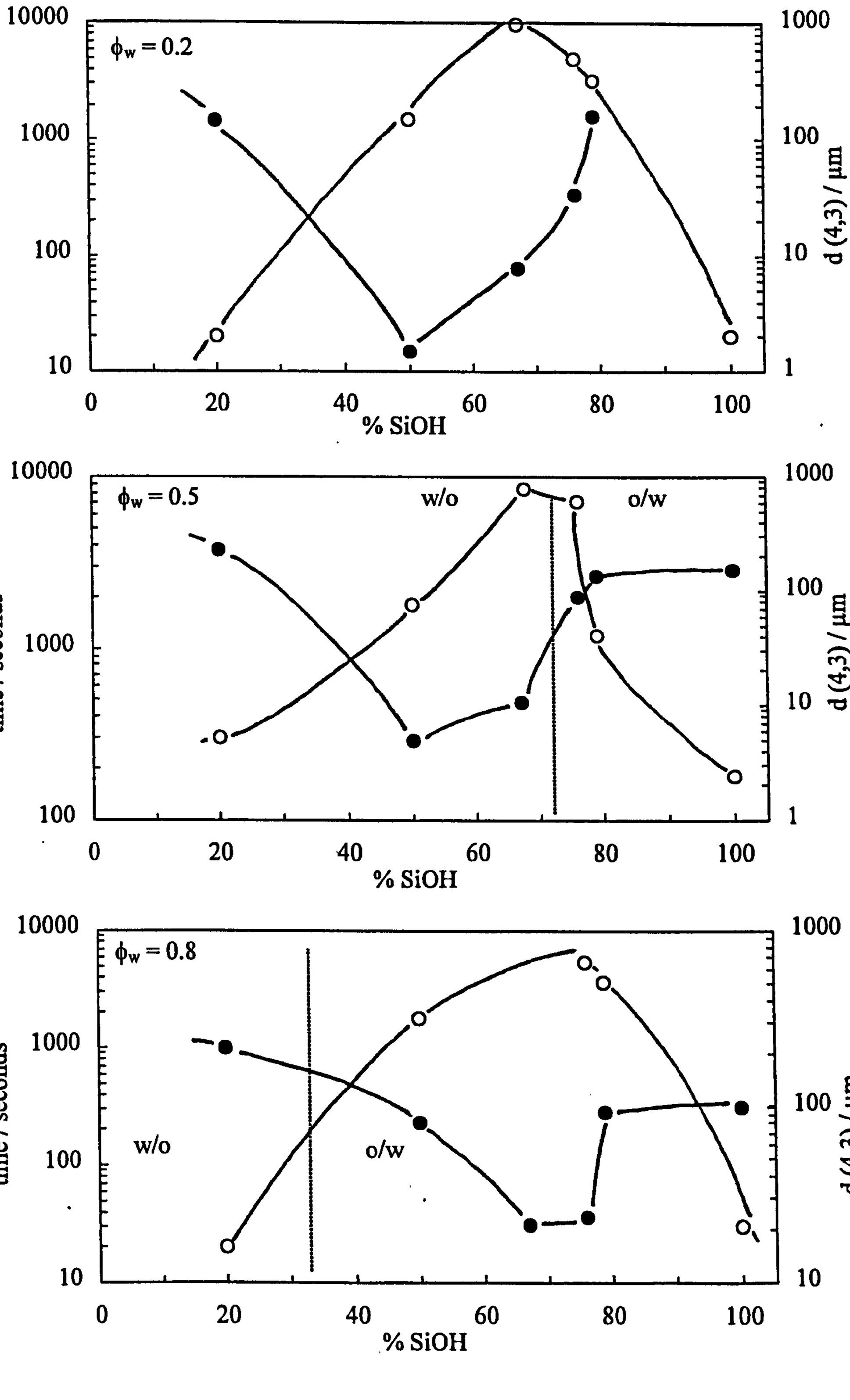

The drop size results were verified for preferred emulsions at $\phi_w = 0.5$ by taking optical microscopy images immediately after preparation. Figure 6.14 provides a visual confirmation of the drop size trends by clearly showing that, on decreasing the percentage SiOH on the particle surface, large oil drops first decrease progressively in size before inverting initially to small water drops which eventually increases in size. It is apparent that relatively small changes in the composition of the particle surfaces results in a large change in both the stability and type of these preferred emulsions.

6.5 Ultracentrifugation of w/o emulsions stabilised by H30 particles

Emulsions stabilised by particles of intermediate wettability (50 % SiOH) have been shown to be completely stable to coalescence indefinitely with a high stability to sedimentation and a mean drop size of less than 1 μm. In contrast to surfactant-stabilised systems where the surfactants are labile, such particles once adsorbed at the oil-water interface around drops resist being desorbed. In fact, the particles are attached by nearly 3000 kT at a contact angle (measured through the aqueous phase) of approximately 90° (Figure 6.1). In some applications involving emulsions the desire is to achieve maximum kinetic stability, however in some cases it is necessary to destabilise the emulsion in order to obtain the solvent phases. Ultracentrifugation of solid-stabilised emulsions has been attempted in order to enhance the destabilisation of the emulsion containing H30 particles. This technique has been used infrequently to destabilise surfactant-stabilised o/w emulsions[148, 149] where it was established that when spun at high speed the emulsions initially form a cream that is more or less equal to the volume of emulsified oil. The oil drops separated by thin films of water coalesce with time forming a clear layer above the cream which increases in volume at the expense of the cream layer, rapidly at first and then more slowly. In efficient systems the coalesced oil volume approaches a constant value corresponding to 100 % oil separation. The destabilisation process involves the formation of a concentrated emulsion (cream) in which oil drops become deformed into polyhedra separated by thin water films. This structure is called a bi-liquid foam. The appearance of coalesced oil is a result of rupture of the o-w-o films.

Figure 6.14

Optical microscopy images of toluene-water emulsions (ϕ_w = 0.5) stabilised by silica particles of varying hydrophobicity dispersed in water (N20) or oil (all others). Wt.% in dispersion is given. Scale bar equals 100 μm

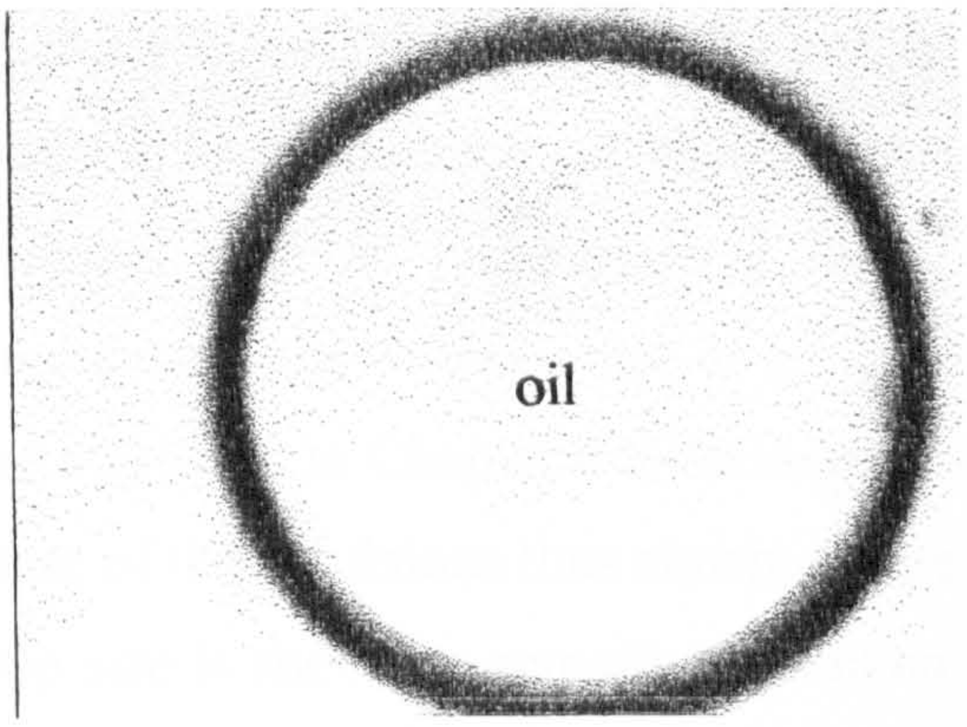

10 wt.% N20 in water

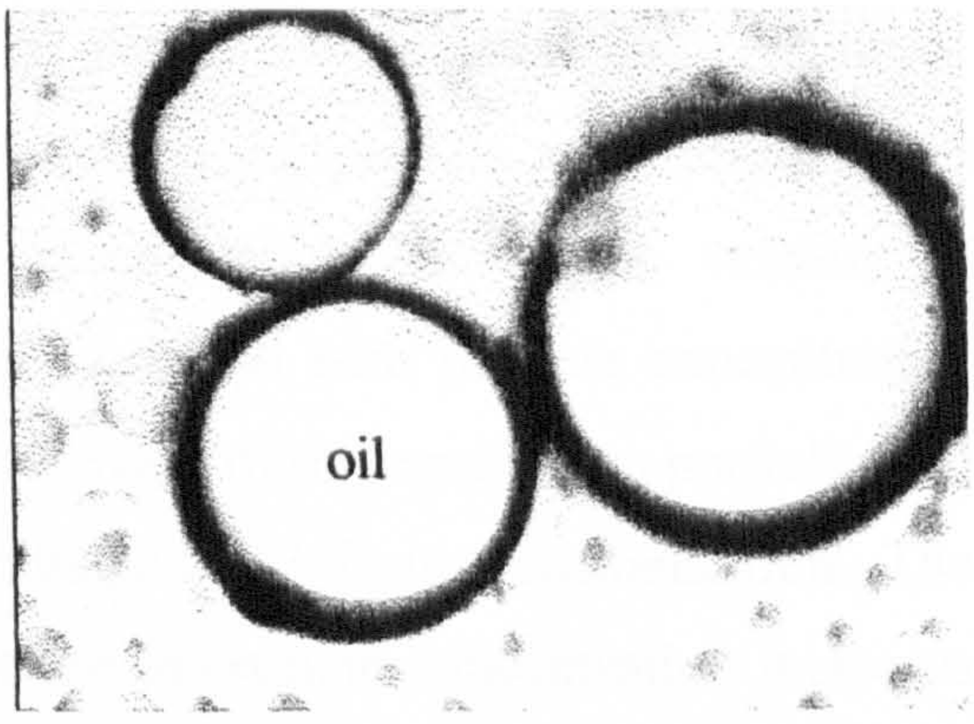

2 wt.% SLM 078 in toluene

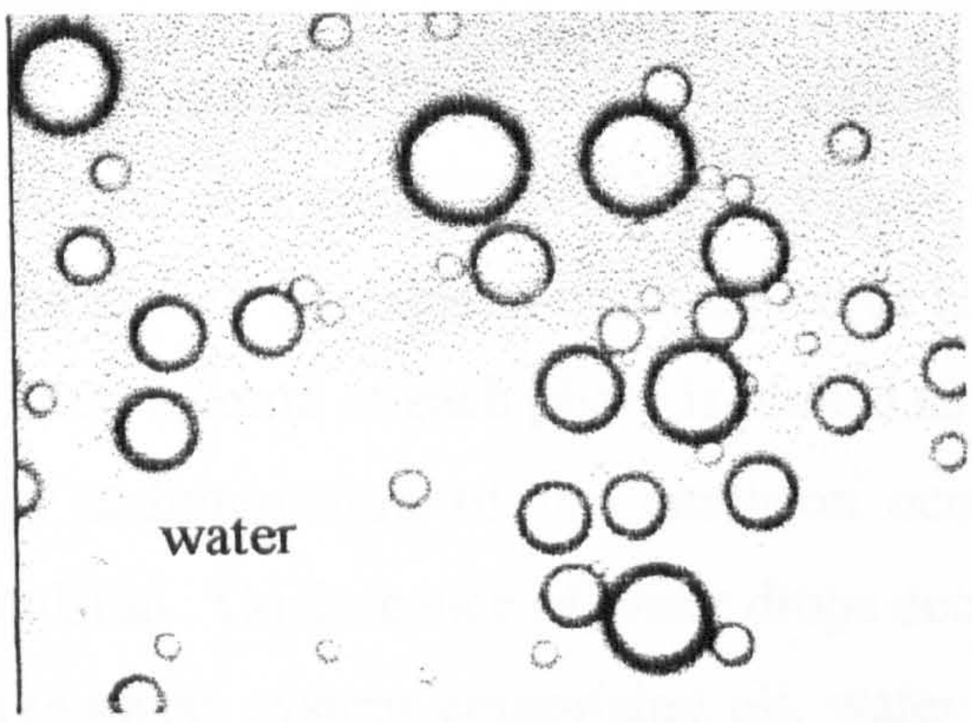

2 wt.% SLM 079 in toluene

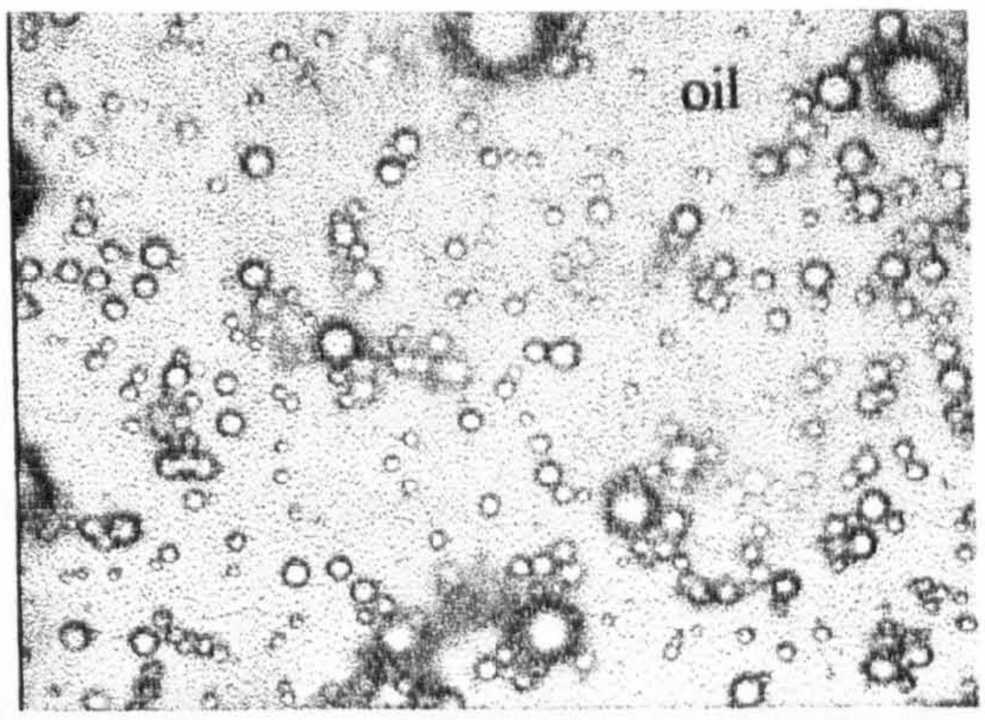

2 wt.% SLM 081 in toluene

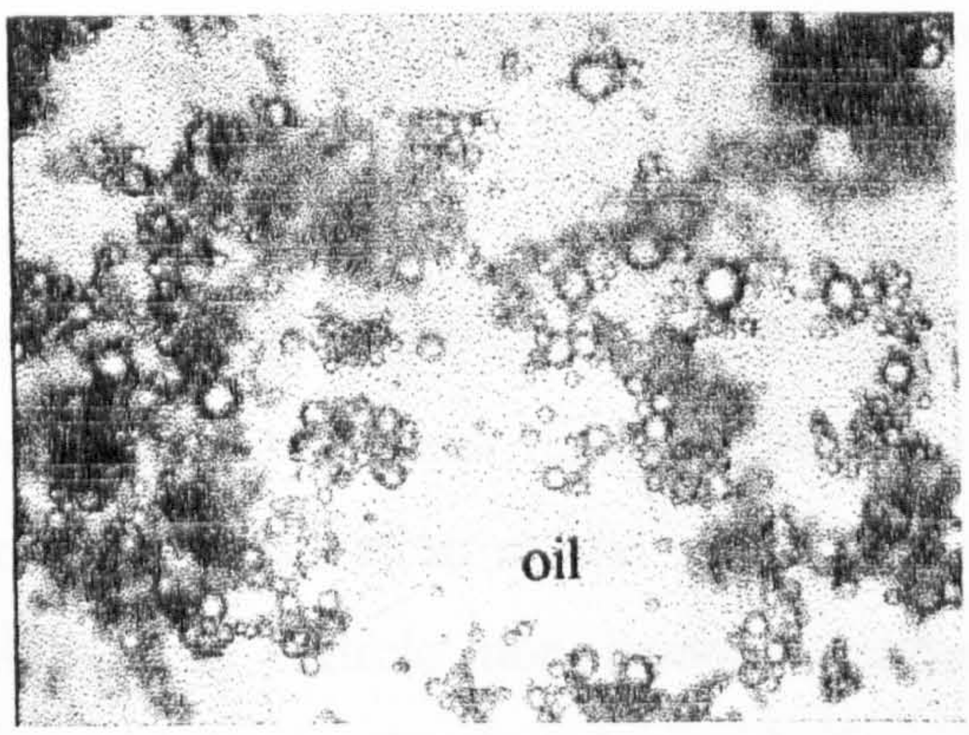

2 wt.% H30 in toluene

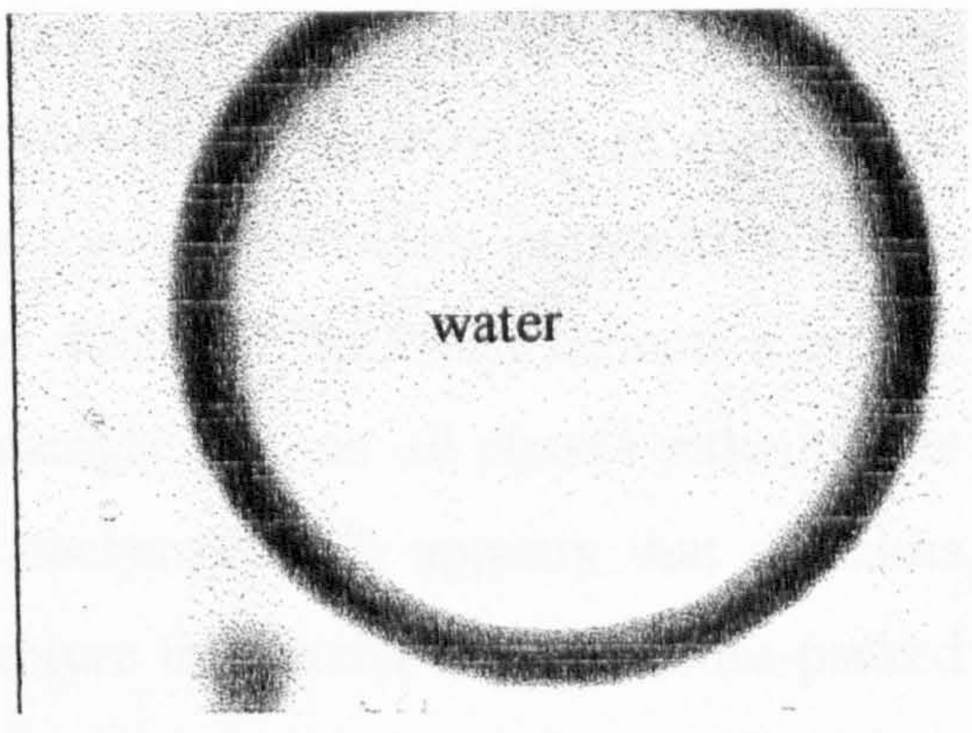

5 wt.% H18 in toluene

In this section ultracentrifugation has been used to observe the destabilisation of water-in-toluene emulsions stabilised by hydrophobic silica particles. Figure 6.15 shows the stability to sedimentation (f_{oil}) after 30 minutes of w/o emulsions prepared at ϕ_w = 0.5 stabilised by H30 particles, as a function of both the initial particle concentration in oil and the relative centrifugal field (RCF). To aid comparisons, the average drop diameter, d(v,0.5) = 0.57 ± 0.09 μm, is the same for all emulsions. The fraction of emulsion as sedimented oil phase decreases with increasing particle concentration and increases with an increase in g force. This is understandable as the velocity of sedimentation is proportional to g.[3] The stability increase with particle concentration was attributed in Chapter 4 to an increase in the viscosity of the continuous particle + oil phase of the emulsions thus slowing down the drainage of oil during sedimentation. The drop size is shown to remain constant so an increase in particle concentration increases the concentration of non-adsorbed particles in the continuous phase. At low particle concentration and high g force virtually all of the oil has sedimented from the emulsion phase.

Solid-stabilised emulsions can separate into a number of phases under the influence of a centrifugal field.[37] Figure 6.16 shows the appearance of w/o emulsions stabilised by different concentrations of H30 particles in toluene after 30 minutes. The relative volume of each phase is plotted as a function of the RCF, at low values of which only sedimentation of the emulsion occurs leaving a two-phase system of oil and emulsion. Coalescence of water drops occurs at critical values of the RCF resulting in a three-phase system comprising oil, water and sediment. The sediment, containing the remaining emulsion and the particles, is situated at the bottom of the vessel due to the density of the wet particles. At any concentration, an increase in the RCF induces coalescence even though the extent of sedimentation remains constant. The volume fraction of water in the sedimented emulsion reaches approximately 0.9 in most cases. The critical value of RCF required to initiate coalescence increases progressively with particle concentration from around 15000 to over 40000. This effect reflects a greater force required to break films formed from increasingly viscous oil phases although the particle concentration at the interface remains unchanged. It appears that oil films stabilised by particle monolayers are easier to rupture than water films of close-packed surfactant due to the fact that coalescence is initiated at higher values of RCF, around 70000, in the latter case.[149]

Figure 6.15

Ultracentrifugation stability after 30 minutes of w/o emulsions (ϕ_w = 0.5) stabilised by H30 particles. The fraction of oil phase resolved, f_{oil} (due to sedimentation), is plotted as a function of both the wt.% H30 in oil and the RCF.

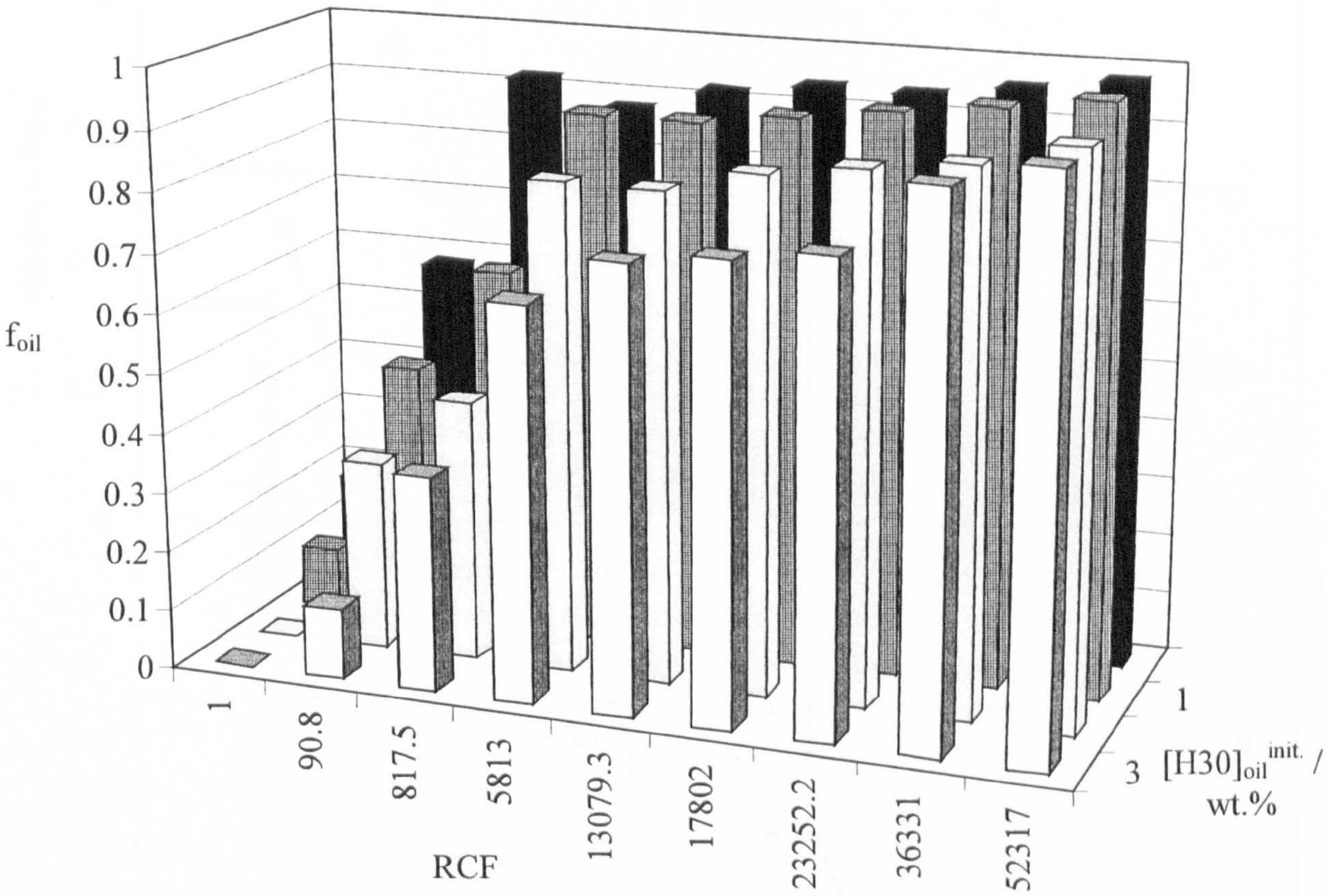

Figure 6.16

Representation of the different phases separating after ultracentrifugation for 30 minutes of w/o emulsions ($\phi_w = 0.5$) stabilised by H30 particles. The figures refer to initial wt.% H30 in oil of (a) 0.5, (b) 1.0, (c) 2.0, (d) 3.0. Dotted lines indicate the critical RCF required to induce coalescence (appearance of water).

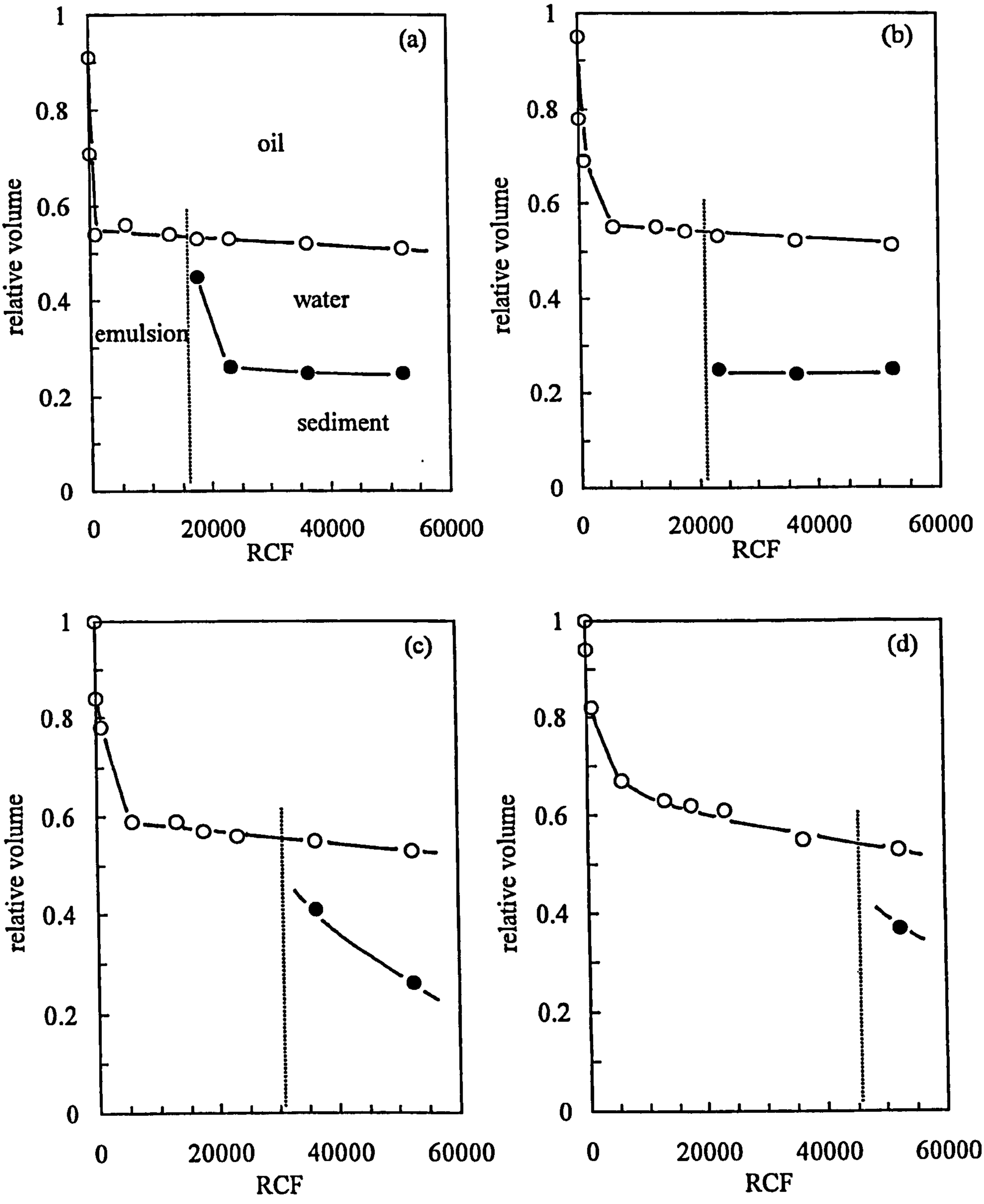

6.6 Conclusions

The following conclusions can be drawn following the systematic investigation into the influence of the wettability of spherical, nanometre-sized silica particles on the type and stability of water-toluene emulsions:

- The energy of attachment of a single particle at the oil-water interface is shown theoretically to depend on the contact angle it makes with it and is maximum for an angle of 90°. This energy consideration relates directly to the stability of emulsions stabilised by particles alone, whose surfaces are composed of silanol groups and dimethyldichlorosilane groups in different proportions.
- A qualitative estimate of the particle wettability was obtained via powder immersion measurements, allowing the silica to be ranked in terms of its hydrophobicity. The wettability is thus described in terms of the percentage SiOH on its surface.
- Emulsions catastrophically invert from w/o to o/w at a critical volume fraction of water, which increases as the particles become more hydrophobic.
- Emulsions stabilised by very hydrophilic (100 % SiOH) or very hydrophobic (20 % SiOH) silica particles have large drops (> 100 μm) which are unstable to coalescence at all ϕ_w. Those stabilised by particles of intermediate wettability are submicrometer in diameter and stable to coalescence indefinitely. The stability of w/o emulsions to sedimentation and o/w emulsions to creaming increases to a maximum at phase inversion, induced by changes in ϕ_w.
- For a fixed ϕ_w between 0.2 and 0.8, the stability of emulsions to gravity-induced separation passes through a sharp maximum upon increasing the particle hydrophobicity as the emulsion drop diameter passes through a minimum. This is universal and independent of the type of emulsion formed.
- Ultracentrifugation of very stable w/o emulsions containing particles of intermediate hydrophobicity enhances the extent of sedimentation at low g and induces coalescence at high g.

CHAPTER 7

CHAPTER 7

EFFECTS OF OIL TYPE AND REPLACEMENT OF WATER FOR EMULSIONS STABILISED BY PARTICLES OF INTERMEDIATE HYDROPHOBICITY

7.1 Introduction

The HLB of nonionic surfactants is dependent on the oil type in the system. Shinoda[132] has shown that, for a number of different oils, the HLB of a surfactant is a function of temperature. At a fixed temperature the HLB is lowered (more hydrophobic) as the alkane chain length decreases. Salager[112] agrees with this and highlights the nature of the oil phase as one of the key formulation variables which is capable of changing the surfactant HLB. It is therefore of interest to vary the nature of the bulk phases in solid-stabilised emulsions to investigate if the wettability of the particles and hence system HLB can be affected to such an extent that inversion of emulsion type occurs. It was shown in Chapter 4 that varying the oil and aqueous phase in systems stabilised by hydrophobic H30 silica particles with 50 % SiOH on the surface had no effect on the type of emulsion formed. The emulsions remained w/o in all cases suggesting this particle is too hydrophobic to stabilise o/w emulsions at $\phi_w = 0.5$. In this Chapter however, the emulsions are stabilised by SLM 081 particles which have 67 % SiOH on their surfaces. Being of intermediate hydrophobicity it could be imagined that systems incorporating these particles would be more sensitive to prevailing conditions, and it is this idea which is followed up here.

The energy of attachment of a single particle at the oil-water interface was shown in the previous chapter to depend on the particle radius, a, the oil-water interfacial tension, γ_{ow}, and the contact angle, θ, by the following equation:

$$E = \pi a^2 \gamma_{ow} (1 \pm \cos\theta)^2 \qquad (7.1)$$

In this chapter γ_{ow} and θ are varied systematically by varying the oil and aqueous phase type of emulsions stabilised by SLM 081 silica particles. In toluene-water systems this particle prefers to stabilise w/o emulsions at $\phi_w = 0.5$. The interfacial tension of toluene-water is 36.0 mN m^{-1}; oils with tensions above this are referred to as non-polar and those below are referred to as polar oils. The oils chosen ranged from non-polar hydrocarbons (of different structure) of relatively high γ_{ow} to polar alcohols or esters immiscible with water of relatively low γ_{ow}. Likewise, water is replaced by a number of non-aqueous solvents in an attempt to form emulsions with toluene. The emulsions are shown to catastrophically invert upon increasing the volume fraction of dispersed phase, the critical volume fraction depending on the work of adhesion existing between the two liquids. A qualitative estimate of θ is obtained from measurements of the contact angle at the liquid-liquid-solid interface for flat, partially hydrophobic glass substrates. Emulsions of undecanol-water were investigated further following the observation of an interesting breakdown phenomenon which is remarkably sensitive to temperature and similar to that seen for viscous crude oil emulsions.

This particular silica particle type is only partially hydrophobic (67 % SiOH), and it is possible to disperse it into oil and water. The type and stability of emulsions formed from particles dispersed in water were found to differ significantly from those that were dispersed in toluene. In contrast, the type and stability of emulsions stabilised by a pure non-ionic surfactant, $C_{12}E_5$, is shown to be independent of initial location.

7.2 Effect of oil and non-aqueous phase on the type and stability of emulsions

In Chapter 6 we saw that toluene-water emulsions stabilised by SLM 081 silica particles were w/o at $\phi_w = 0.5$ with a high stability to coalescence and sedimentation. The emulsions inverted from w/o to o/w at $\phi_w = 0.6$. The variation in emulsion conductivity and type with ϕ_w is shown in Figure 7.1 for a number of other oils. It is clear that inversion does not occur for the polar oils (e.g. undecanol, cineole and eugenol) and takes place at certain values of ϕ_w for the non-polar oils (e.g. linear alkanes, cyclohexane and the PDMS oils). Eugenol and cineole are oils used in the perfume industry, of density at 25 °C equal to 1.0628 and 0.9214 g cm^{-3} respectively. They are largely immiscible with water, with 0.6 and 3.6 vol% of water being the

Figure 7.1

Conductivity of water-oil emulsions stabilised by partially hydrophobic SLM 081 silica particles as a function of the volume fraction of water. Concentration of particles in all emulsions is 0.5 wt.%.

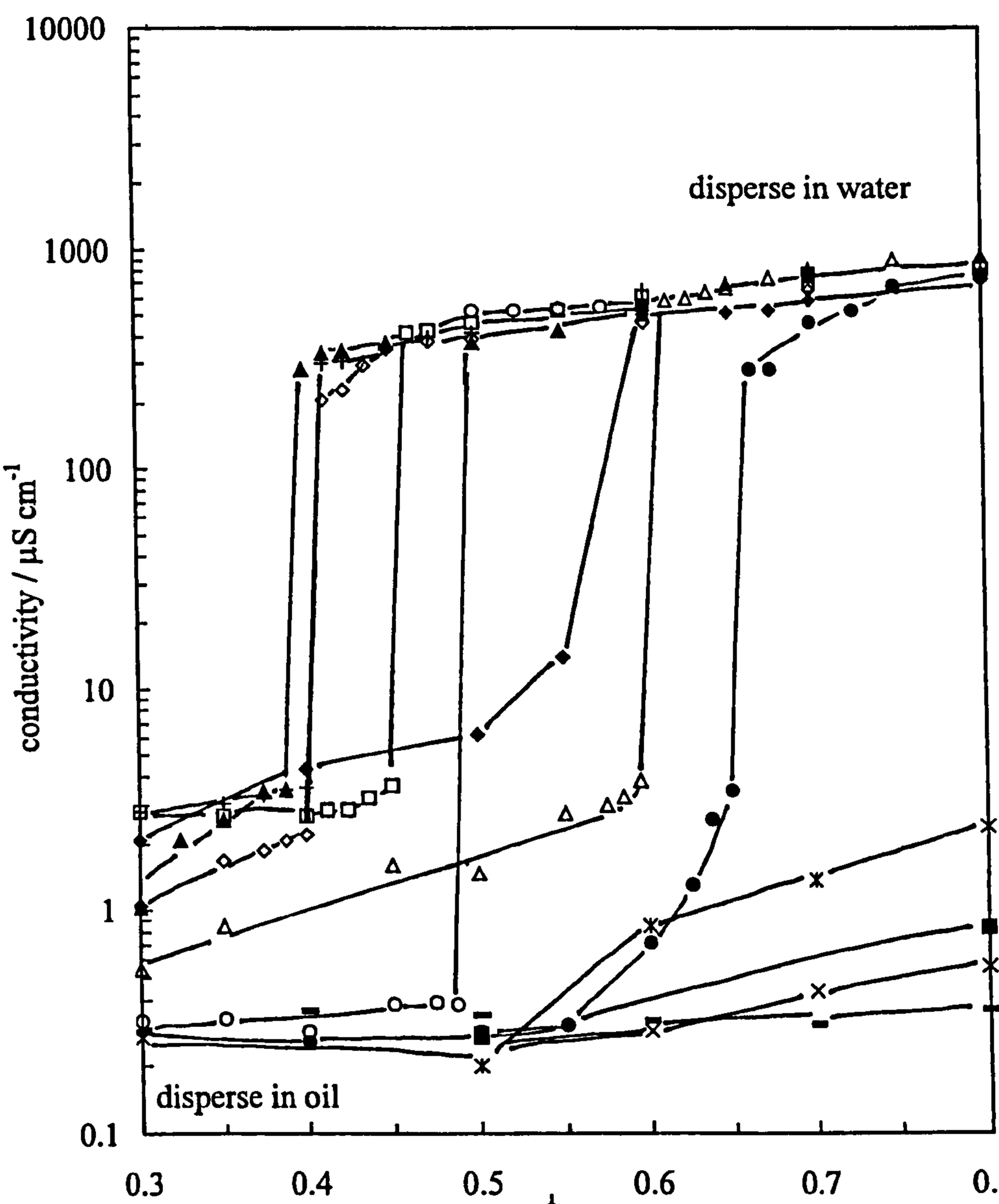

respective solubility limits. The extent of adsorption of the particles at the oil-water interface is expected to depend on the nature of the oil, although there is no systematic evidence of this in the literature. Polar oils are expected to interact more strongly with interfacial water than non-polar ones such as alkanes.[150] The strength of interaction can be quantified in terms of the work of adhesion, W_a, existing between the two liquids, given by the Dupré equation

$$W_a = \gamma_{oa} + \gamma_{aw} - \gamma_{ow} \qquad (7.2)$$

where γ is the interfacial tension and the subscripts oa, aw and ow refer to oil-air, air-water and oil-water respectively. W_a is defined as the reversible work required to part two columns of oil and water (see schematic in Figure 7.2). Table 7.1 shows the relevant surface and interfacial tensions required to calculate W_a for the oils used. W_a is seen to increase as the polarity of the oil increases (e.g. compare heptane with eugenol), due mainly to a continuous decrease in the value of the oil-water tension. Aveyard et al.[150] argued that values of W_a for hydrocarbons compared with methyl esters were consistent with a predominantly flat orientation of alkanes, and an essentially vertical orientation of esters, at the interface between these liquids and water. Since adsorption of particles at polar oil-water interfaces requires the displacement of oil from the interface, it is expected that an increased work of adhesion should lead to a decrease in the surface activity of the particles which will have consequences for the properties of the corresponding emulsions.

The volume fraction of water at inversion, ϕ_w^{inv}, is plotted as a function of W_a in Figure 7.2. With the exception of the perfluoroheptane system (point at lowest value of W_a), emulsion inversion occurs at higher ϕ_w as the W_a increases up to 72 mJ m^{-2} above which inversion does not occur and emulsions remain w/o at all ϕ_w. The preferred emulsion type at $\phi_w = 0.5$ is o/w for the non-polar oils such as alkanes and cyclohexane and w/o for aromatic oils and those containing alcohol or ester groups. The stability of the emulsions after 1 hour is shown in Figure 7.3. The alkanes and cyclohexane (a) form stable o/w emulsions (preferred) and unstable w/o emulsions (non-preferred), whereas the stability of w/o emulsions formed with polar oils (c) decreases with increasing ϕ_w and do not invert. Intermediate between these two extremes, emulsions formed with 50

Table 7.1

Values of the oil-air (γ_{oa}), oil-water (γ_{ow}), polar phase-air (γ_{pa}) and oil-polar phase (γ_{op}) tensions in mN m^{-1} at 25 °C alongwith calculated works of adhesion (W_a) in mJ m^{-2}. The contact angles (θ_{ow}, θ_{op}) refer to angles measured through the water or polar phase under oil on a modified glass substrate.[1]

Oil Phase[2]	γ_{oa}	γ_{ow}	W_a	**Ref.**	θ_{ow} / °
perfluoroheptane	12.8	56.7	28.0	151	92
heptane	19.8	50.7	41.0	150	105
dodecane	25.0	52.5	44.4	150	122
cyclohexane	24.1	50.9	45.1	Present	110
0.65 cS PDMS	16.0	38.7	49.2	152	105
50 cS PDMS	21.0	38.0	54.9	152	123
toluene	29.1	36.0	65.0	Present	125
isopropyl myristate	27.8	28.6	71.1	Present	155
methyl myristate	29.6	25.3	76.2	150	164
cineole	28.2	16.9	83.2	153	161
undecanol	28.5	9.5	90.9	150	160
eugenol	36.4	9.0	99.3	153	144
Polar phase[3]	γ_{pa}	γ_{op}	W_a	**Ref.**	θ_{op} / °
water	71.9	36.0	65.0	Present	125
ethylene glycol	46.2	8.8	66.5	Present	106
glycerol	61.9	20.1	70.9	Present	122
formamide	57.1	14.2	72.0	Present	118

[1] Hydrophilic glass coated with dimethyldichlorosilane reagent to give $\theta_{aw} = 64°$

[2] Systems with water where $\gamma_{aw} = 71.9$ mN m^{-1}

[3] Systems with toluene where $\gamma_{oa} = 29.1$ mN m^{-1}

Figure 7.2

Volume fraction of water at inversion of emulsions versus work of adhesion between oil and water for systems in Figure 7.1. Arrows indicate that emulsions remain w/o up to at least $\phi_w = 0.95$. Schematically shown is the process of parting two columns of oil and water of unit area of interface (γ_{ow}) to form unit surface areas of oil and water (γ_{oa} and γ_{aw}).

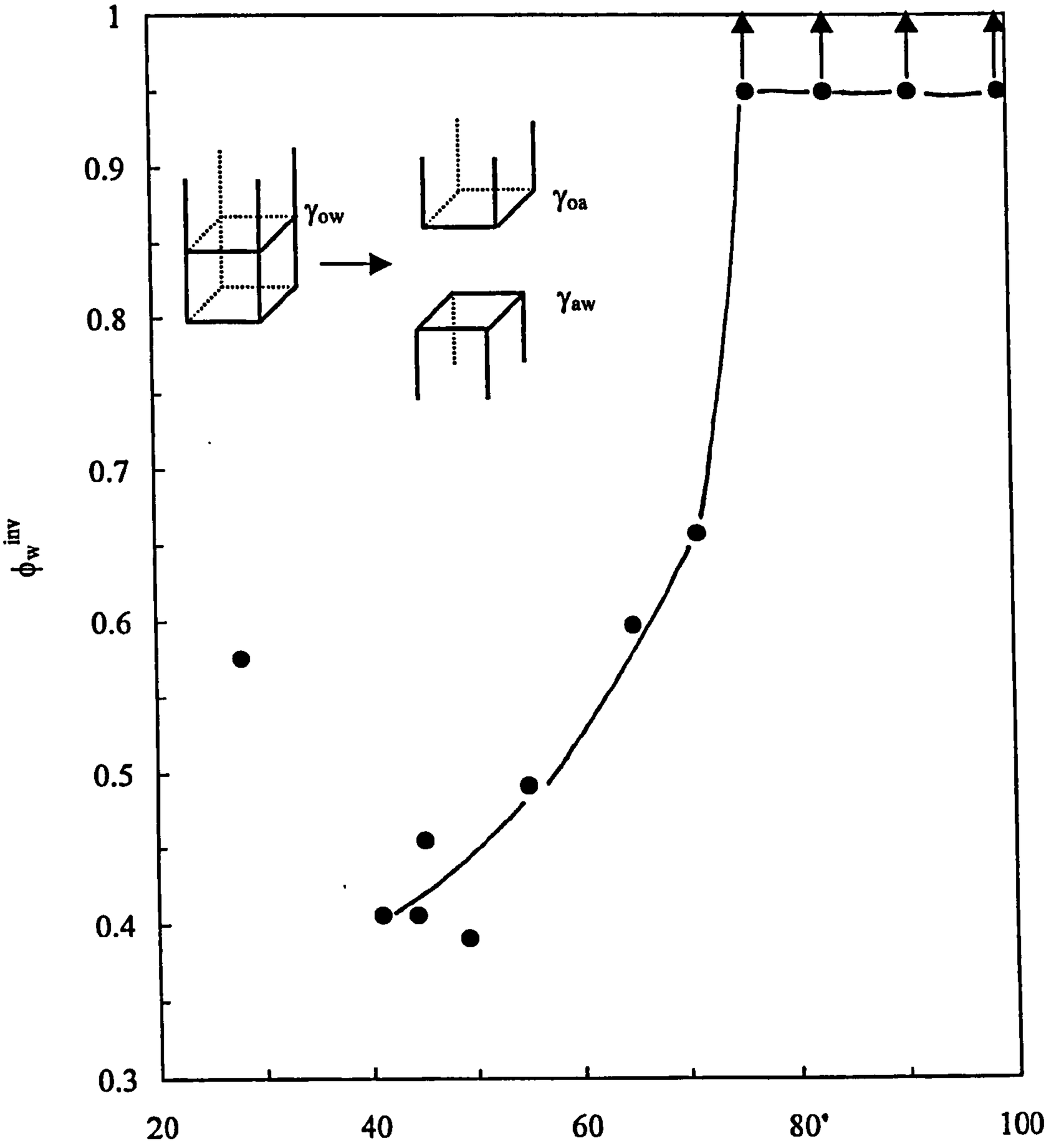

Figure 7.3

Stability after 1 hour of oil (given)-water emulsions stabilised by 0.5 wt.% SLM 081 silica particles as a function of ϕ_w. Open points – fraction of oil resolved (right-hand ordinate), filled points – fraction of water resolved (left-hand ordinate), 25 °C.

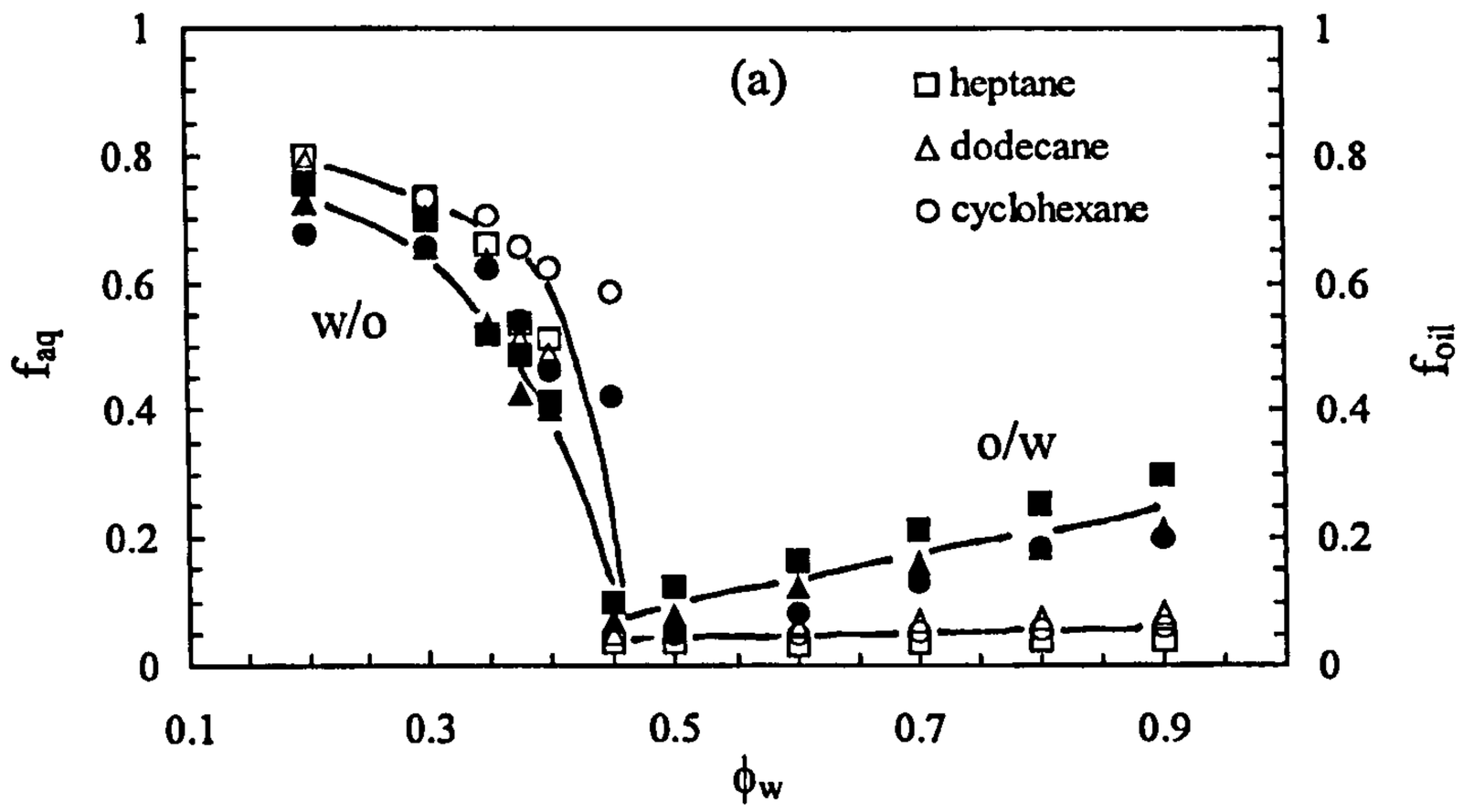

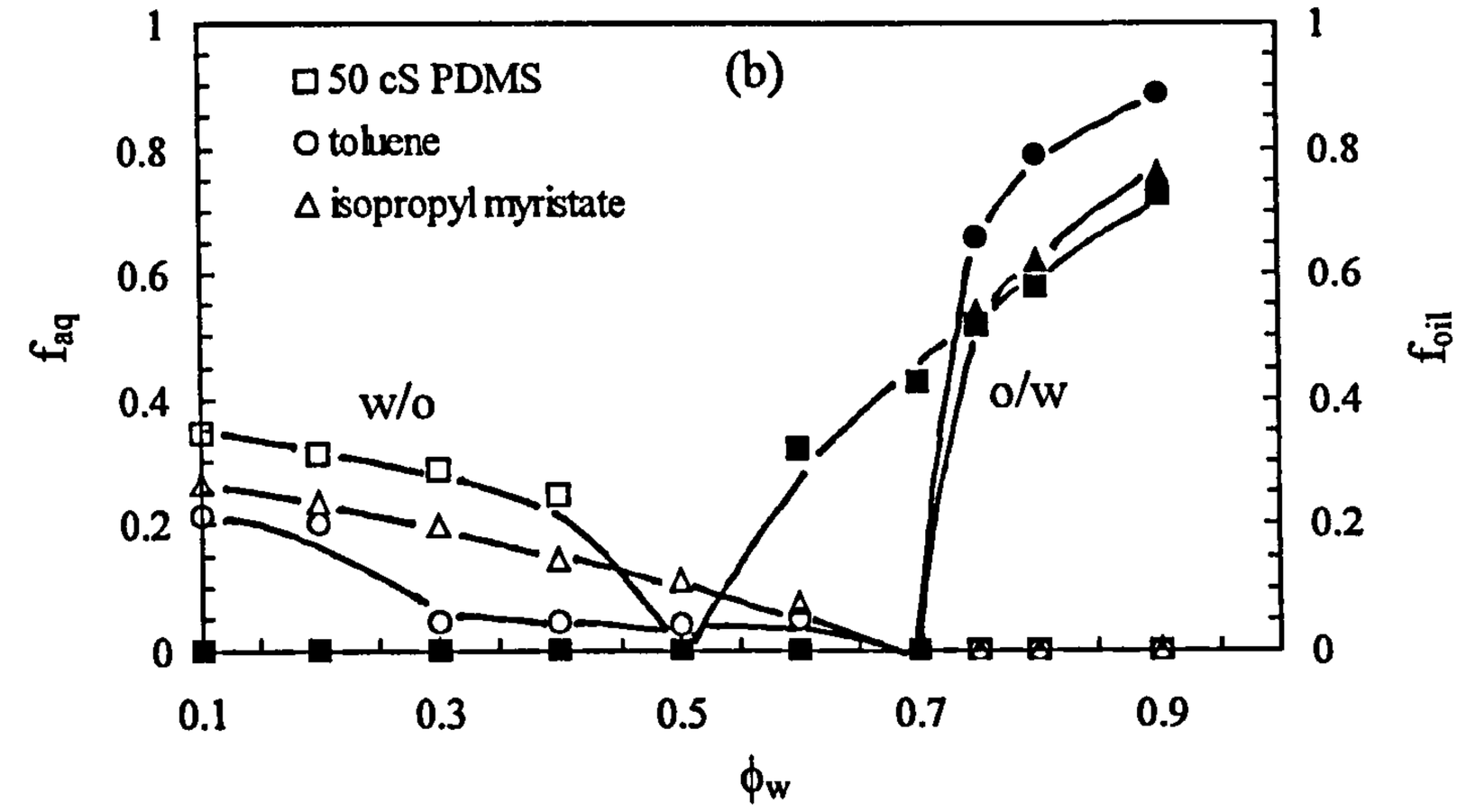

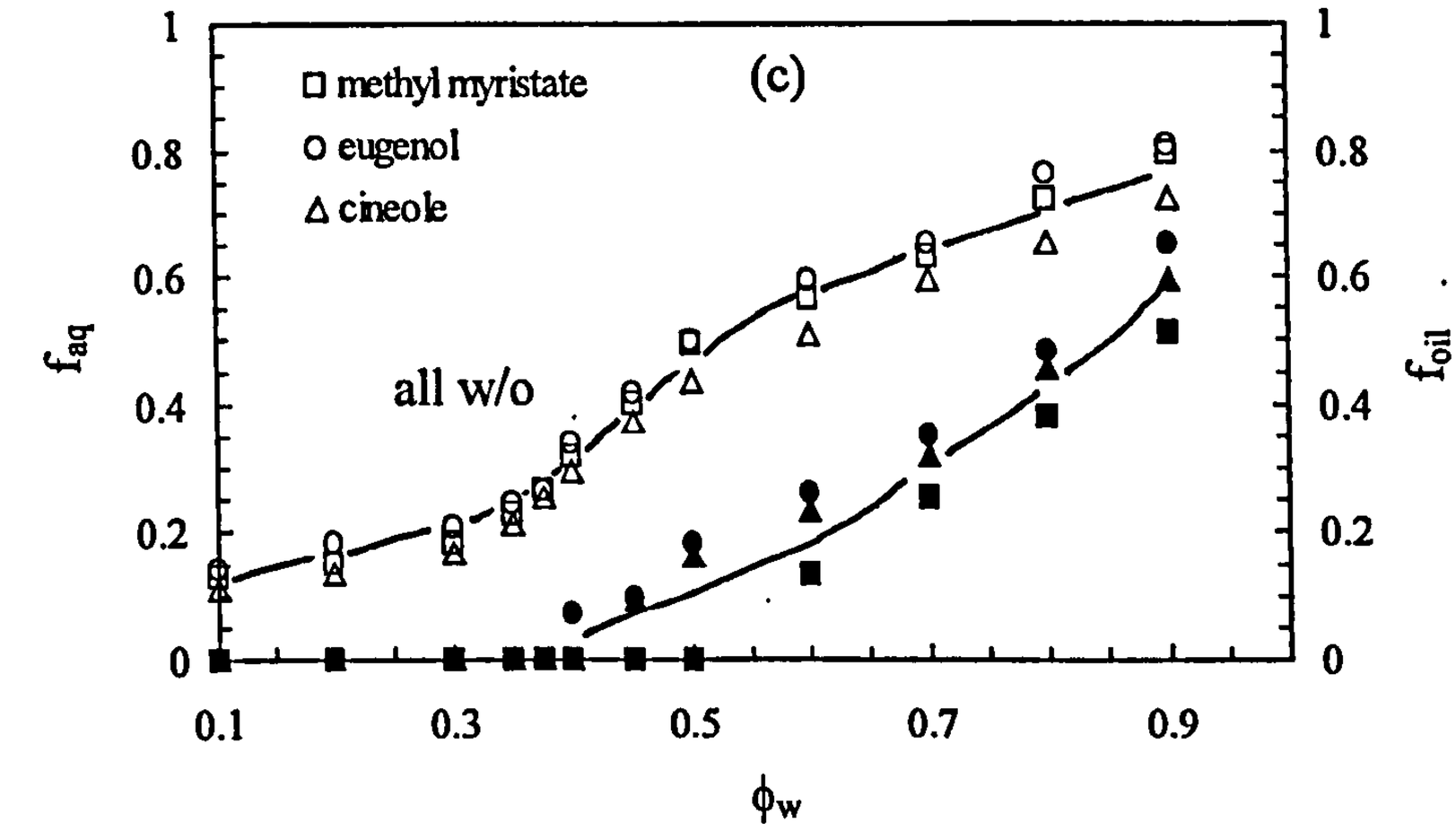

cS PDMS, toluene or isopropyl myristate (b) invert at $\phi_w \geq 0.5$ and form both stable w/o and reasonably stable o/w emulsions.

The contact angle θ that the particle makes at the oil-water interface was discussed in Chapter 6 where it was varied by changing the hydrophobicity of the silica surface. In the presence of the various oils the contact angle is thought to be dependent on the nature of the oil. As before the surface was modelled by coating flat glass plates with dimethyldichlorosilane reagent. Although the % SiOH on the surface of SLM 081 is known, the contact angle at the air-water surface this relates to is not. As a best approximation, the glass slides were coated with the hydrophobic reagent so that θ_{aw} equals 64° (cf. clean glass slide where $\theta_{aw} \leq 5°$). The contact angle of an aqueous drop on the modified surface under the various oils is given in Table 7.1. In general, the contact angle increases as the oil-water tension decreases, with a difference of over 70° between perfluoroheptane and methyl myristate. The particles are more hydrophobic (higher contact angles) at the polar oil-water interface than the non-polar one, which explains why w/o emulsions are preferred in the first case and o/w in the second. This relation between θ_{ow} and γ_{ow} provides an explanation for the major difference in emulsion stability observed between the various oils. For $\theta_{ow} > 90°$, the energy of attachment of the particles at the oil-water interface decreases as a result of a decrease in the interfacial tension. The magnitude of E for a particle in a perfluoroheptane system is over 1500 times greater than for an undecanol system, resulting in stable emulsions in the former system and very unstable ones in the latter (see later).

Water has been replaced by various non-aqueous solvents in systems containing toluene. Table 7.1 shows the variation in the polar phase-air tension (γ_{pa}) along with an almost equal variation in the oil-polar phase tension (γ_{op}) such that W_a remains more or less constant. The contact angle at the oil-polar phase-modified glass surface (θ_{op}) measured through the aqueous phase for the four liquids is virtually constant but decreases slightly as the liquid-liquid interfacial tension falls, as has been observed for a range of hydrophobic surfaces.[154] For a fixed particle concentration (0.5 wt.%) in emulsions at different ϕ_w, it was not possible to prepare emulsions in either ethylene glycol or glycerol systems. This is understandable because in surfactant systems replacement of water by ethylene glycol and glycerol leads to a reduced tendency for both surfactant aggregation, as evidenced by a large increase in the c.m.c., and adsorption.[155] The effects have been interpreted in terms of a reduced 'solvophobic'

interaction between the surfactant chains and the non-aqueous solvent. Presumably, particles distribute between bulk phases and the interface, and the inability of these two systems to stabilise emulsions may be associated with a similar reduction in the surface activity of the particles. Emulsions containing formamide however behave similarly to water-containing emulsions, phase inverting to o/w at the same value of ϕ_w (Figure 7.4). These emulsions were of poor quality with very unstable water drops at low ϕ_w and coarse o/w emulsions at high ϕ_w. It is noted that the relative permittivities at 25 °C of the diol (37.7) and triol (42.5) are lower than that of water (78.5), whereas that of formamide is higher (109.0). The values for ethylene glycol and glycerol confirm that emulsions containing these liquids have low repulsive interactions between drops resulting in increased coalescence.

7.3 Behaviour of undecanol-water systems

Water-in-undecanol emulsions have been investigated further following the observation of an interesting, highly reproducible phenomenon. The energy of attachment of a silica particle at the undecanol-water interface is low due to the relatively low interfacial tension (9.5 mN m^{-1}) and high undecanol-water contact angle (160°), which suggests these w/o emulsions are of low stability. The emulsions actually break completely to give the bulk phases in all cases, but the time for breaking is dependent on the volume fraction of water and interestingly the temperature of the system. Immediately after emulsification however, the emulsions can be gel-like of high viscosity which begin to break in an interesting and unusual manner. Figure 7.5 shows photographs of a water-in-undecanol ($\phi_w = 0.5$) emulsion at 18 °C at certain times after emulsification. The initial white emulsion which fills the glass vessel begins to break after 2 minutes. In contrast to emulsions formed with other oils where the emulsions break from the top and bottom of the vessel, this emulsion appears to shrink away from the walls of the vessel as it liberates first oil and then water due to coalescence. The emulsion appears to 'melt' as it maintains the shape of the cylindrical vessel. Within 4.5 minutes the emulsion has completely broken into the bulk phases. This mode of emulsion breakdown has been described as being akin to viscous sintering by Philip et al.[156] for coalescing o/w emulsions made from highly viscous oils. Coalescence consists

Figure 7.4

Conductivity of toluene-water emulsions versus the volume fraction of polar phase, with 0.5 wt.% SLM 081 particles in each emulsion. Open points – water (ϕ_w), filled points – formamide (ϕ_f).

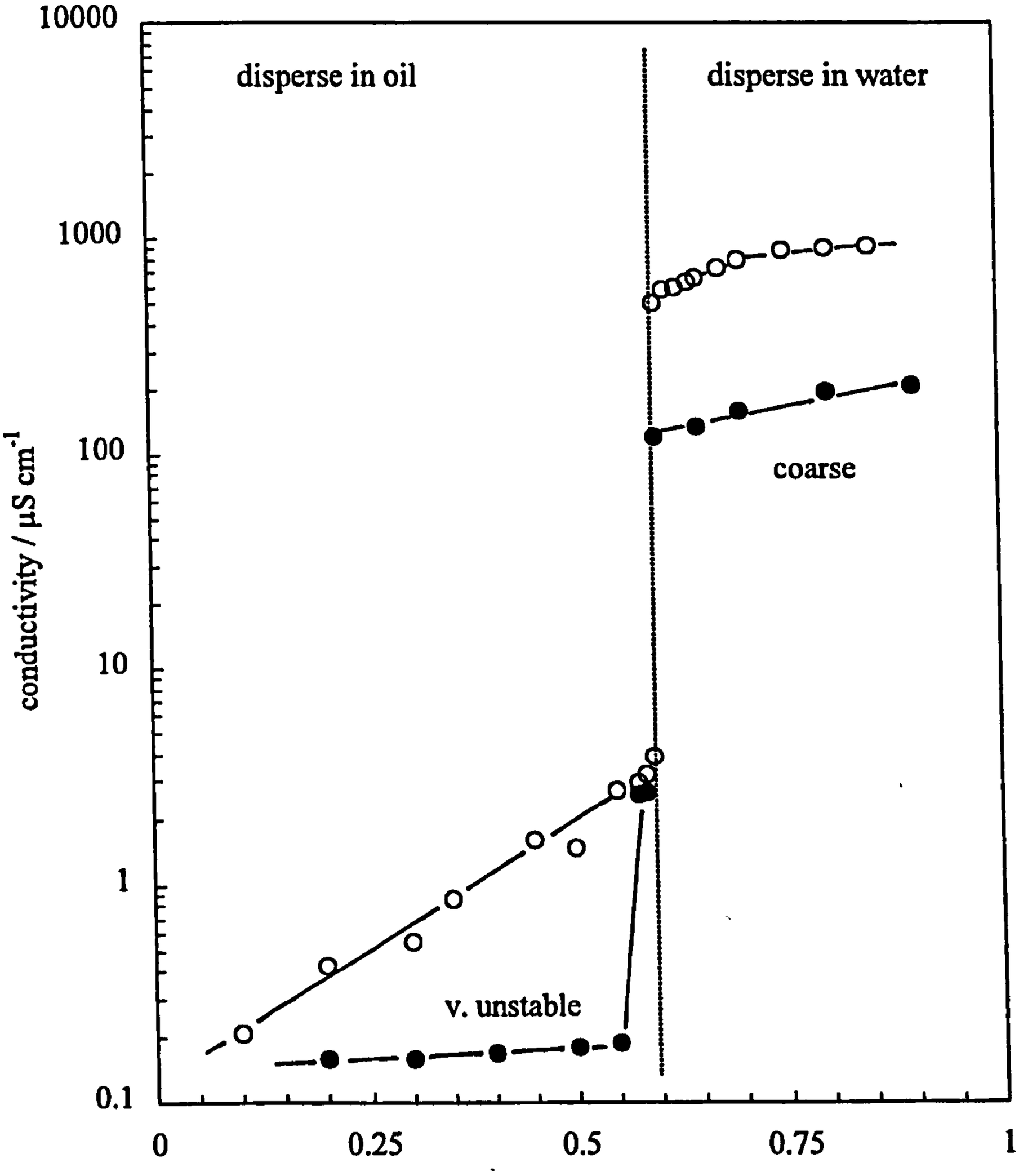

Figure 7.5

Photographs of the breakdown of a water-in-undecanol emulsion (ϕ_w = 0.5) stabilised by 0.5 wt.% SLM 081 particles at 18 °C. From left to right, the times in minutes since emulsion formation are 0, 2, 2.5, 3, 3.5, 4 and 4.5.

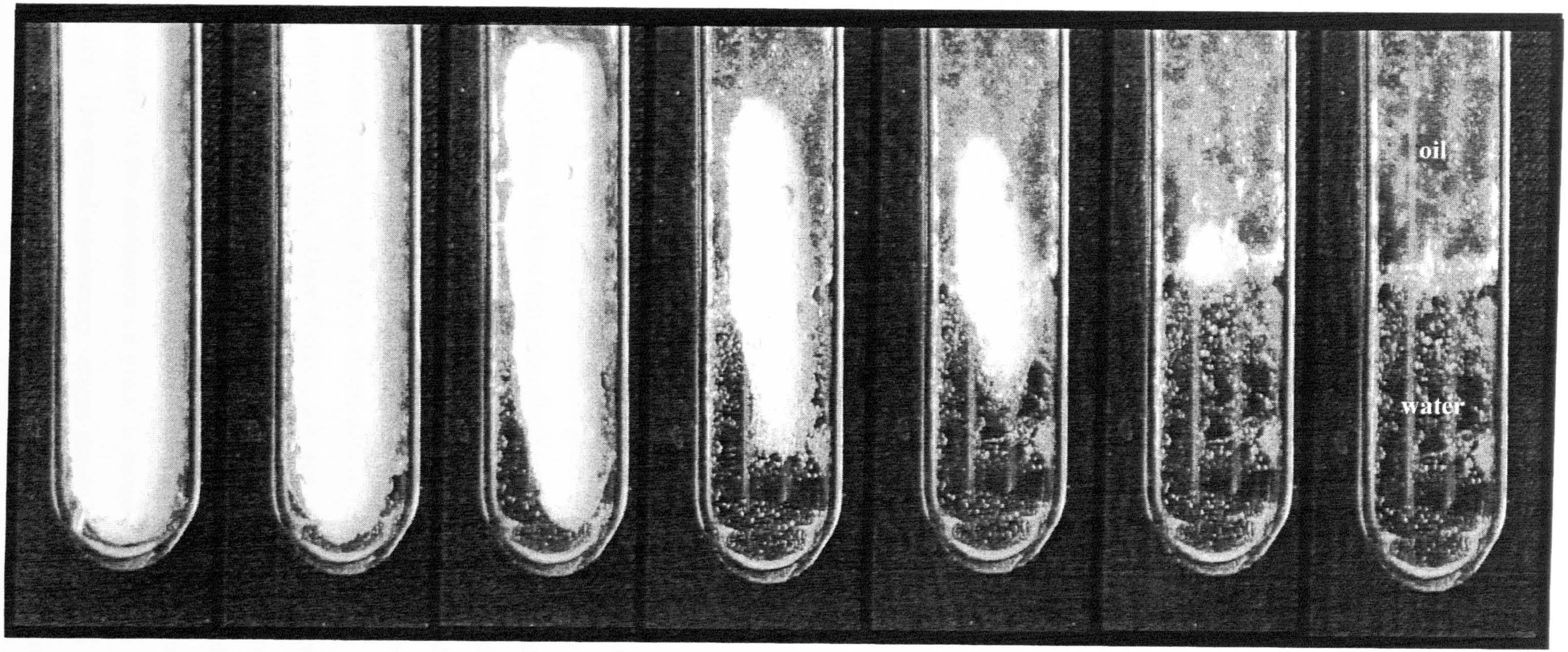

of the rupture of the thin liquid film between adjacent drops via the nucleation of a small channel. This is followed by a shape relaxation, driven by interfacial tension, causing two drops to fuse into one.

Model of drop coalescence redrawn from Bonakdar et al.[157]

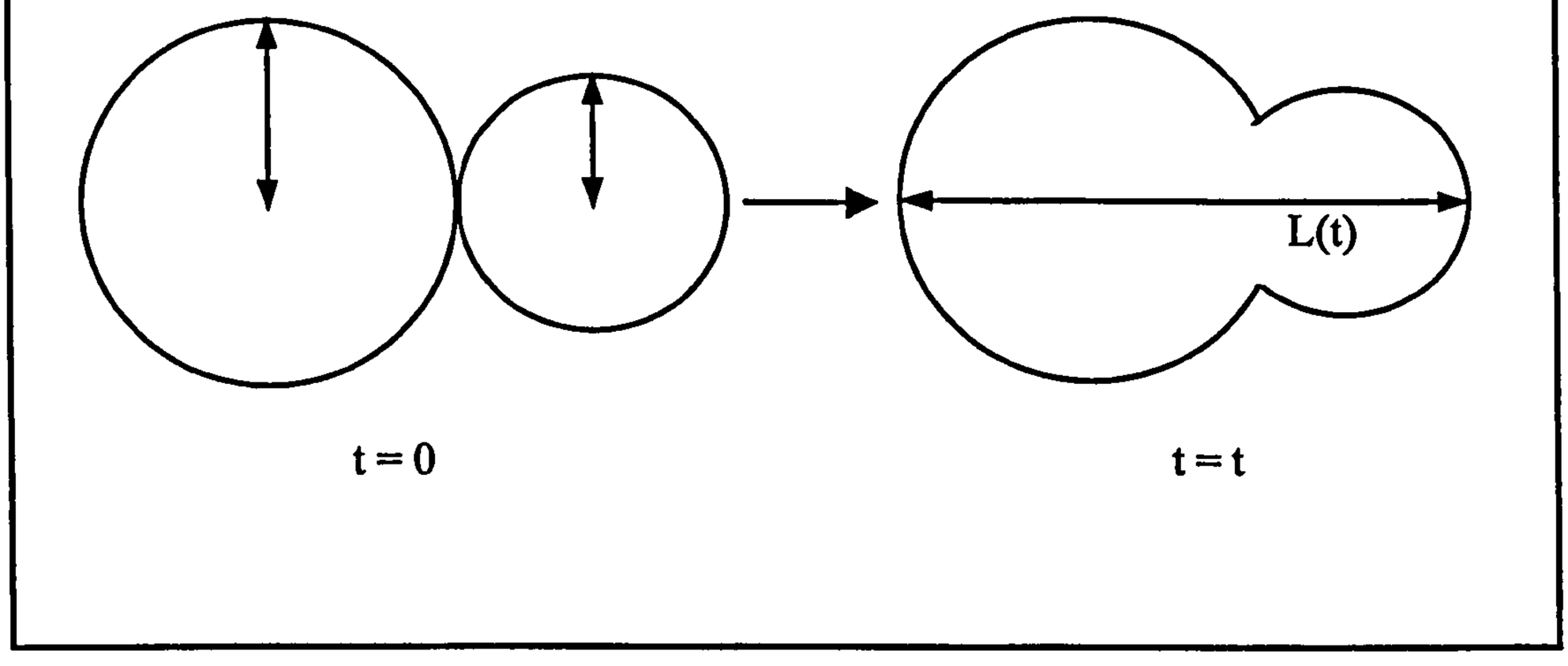

Under conditions where the characteristic time for shape relaxation, t_r, is much larger than the time between drop collisions, t_c, coalescence is limited by shape relaxation leading to different structures and kinetics than the more commonly encountered case in which $t_r < t_c$. The shape relaxation process induces a gradual decrease of the axial length L(t) along the line that joins the droplet centres. Emulsions of viscous bitumen oil-in-water stabilised by indigenous alkylcarboxylic acids and cationic surfactants studied by Philip et al.[156] are made to coalesce suddenly by addition of NaOH. The base causes dissociation of the acid groups, neutralising the interfaces. In the absence of electrostatic repulsion, emulsion drops adhere to each other and a three-dimensional gel network develops. Once formed, the gel starts to contract by reducing its interfacial area through coalescence, reminiscent of the sintering process which occurs during the densification of powders, eventually free oil is expelled from the emulsion. Although the undecanol-water system is different due to the presence of fluid water drops, the viscosity of the continuous oil phase is raised appreciably in the presence of silica particles. The optical microscopy images shown in Figure 7.6 are of the same emulsions photographed in Figure 7.5. The dark areas in the first four images

Figure 7.6

Optical microscopy images of a water-in-undecanol emulsion (ϕ_w = 0.5) stabilised by 0.5 wt.% SLM 081 particles at 18 °C. Note the network of drop-rich domains (dark) surrounded by large areas of drop-free continuous phase (light). Scale bar equals 500 μm. Time after emulsion formation is given.

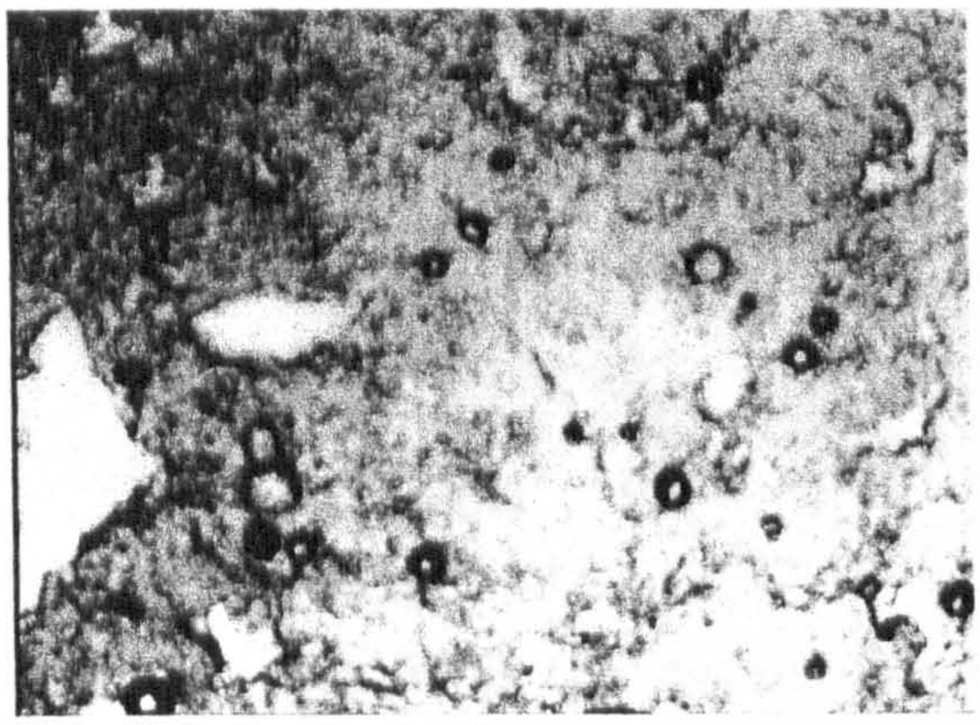

1 minute

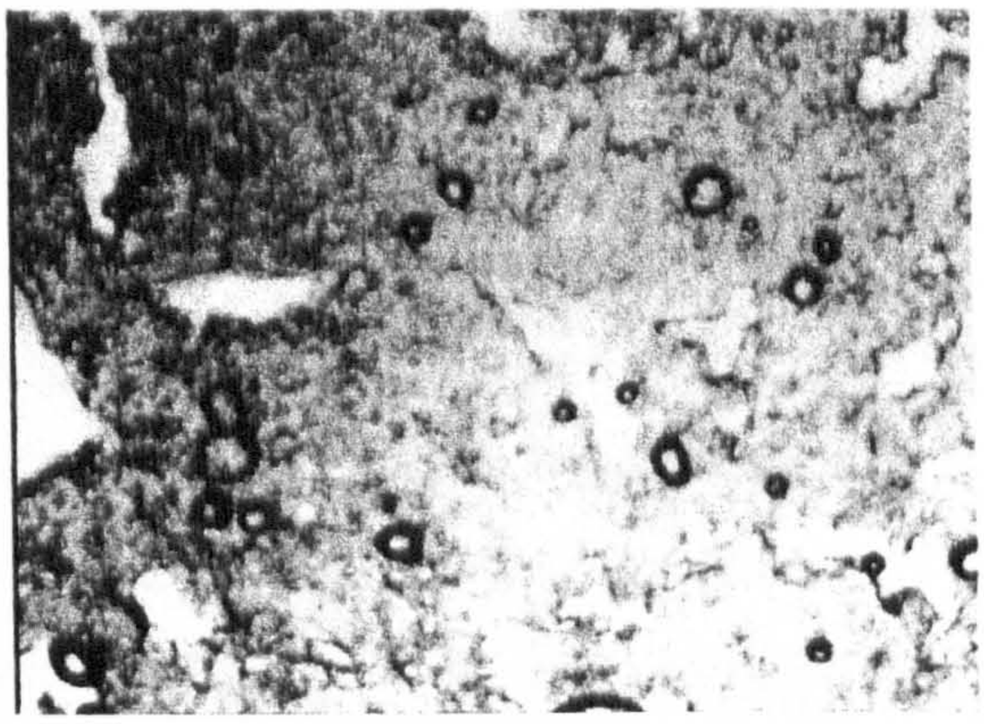

2 minutes

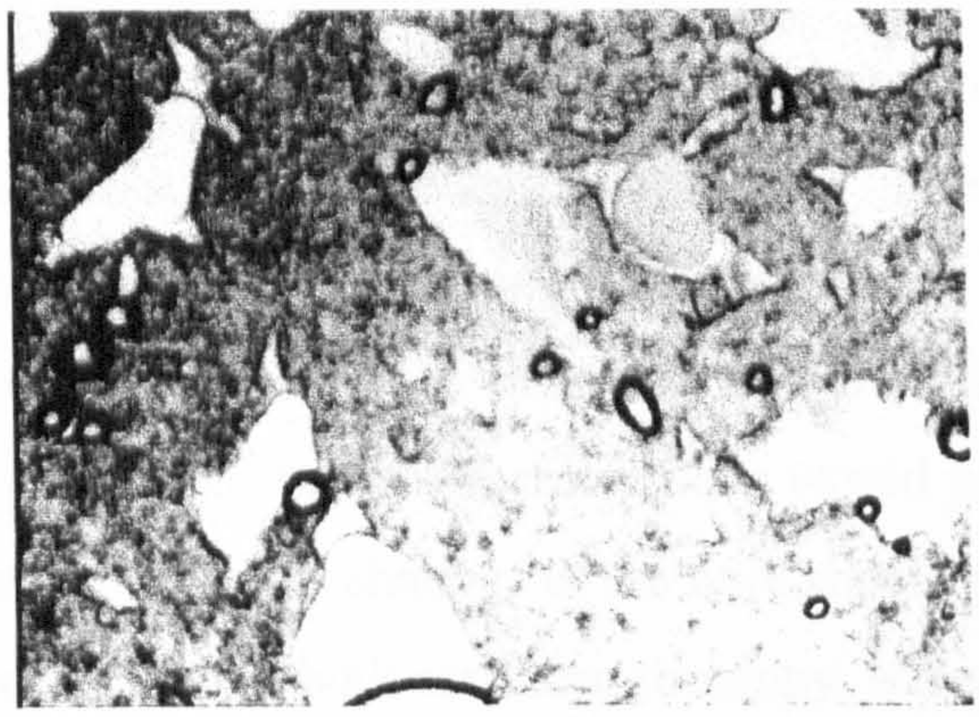

2.5 minutes

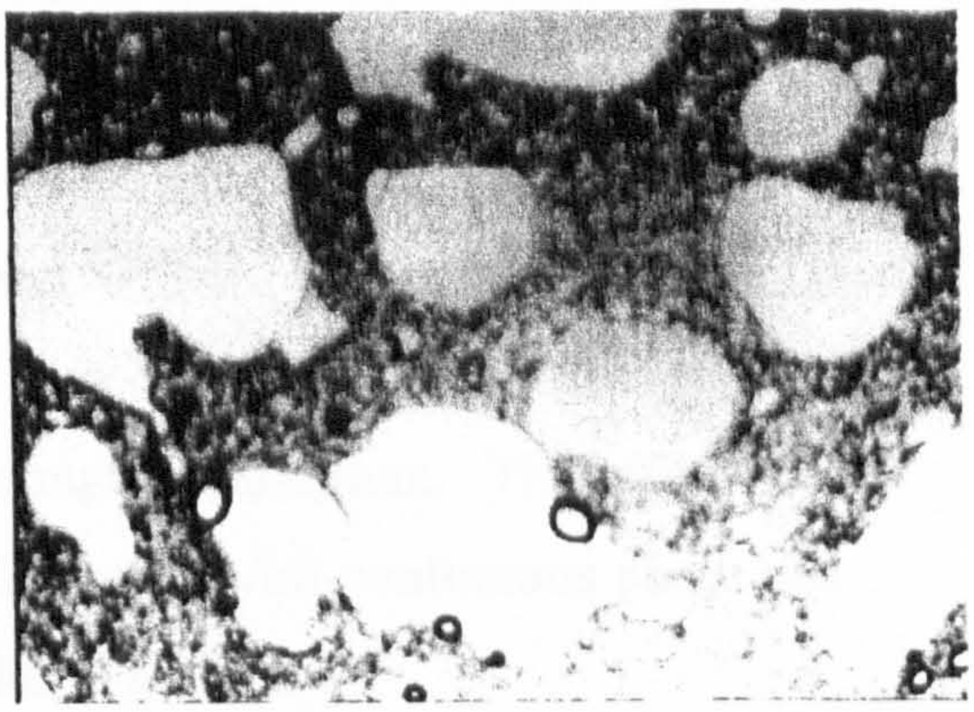

3 minutes

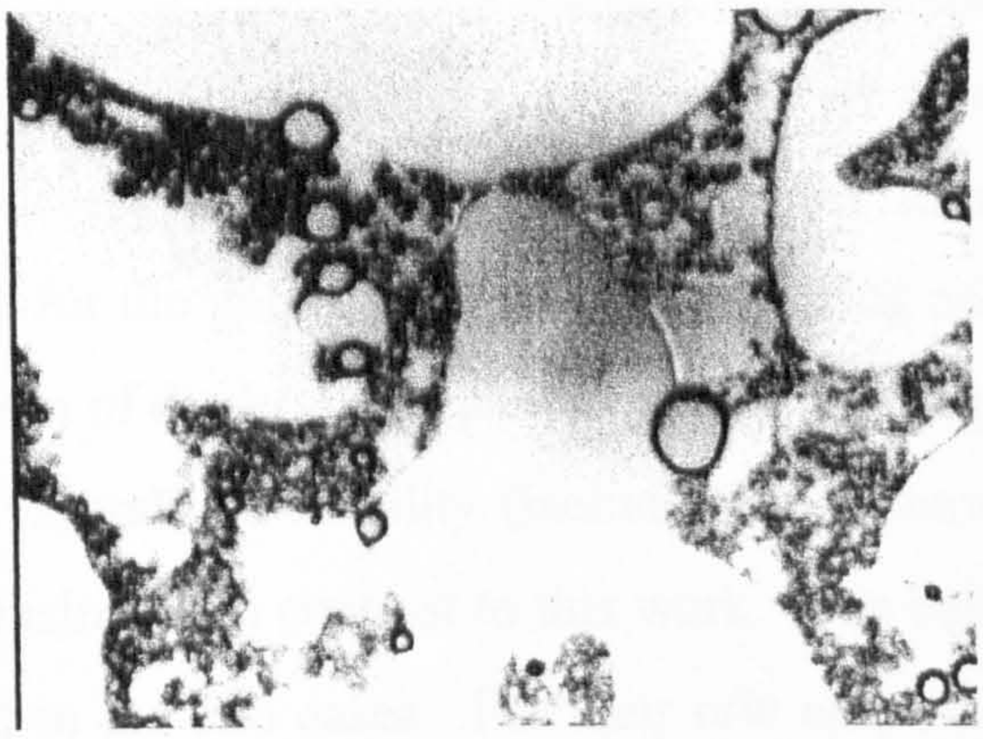

4 minutes

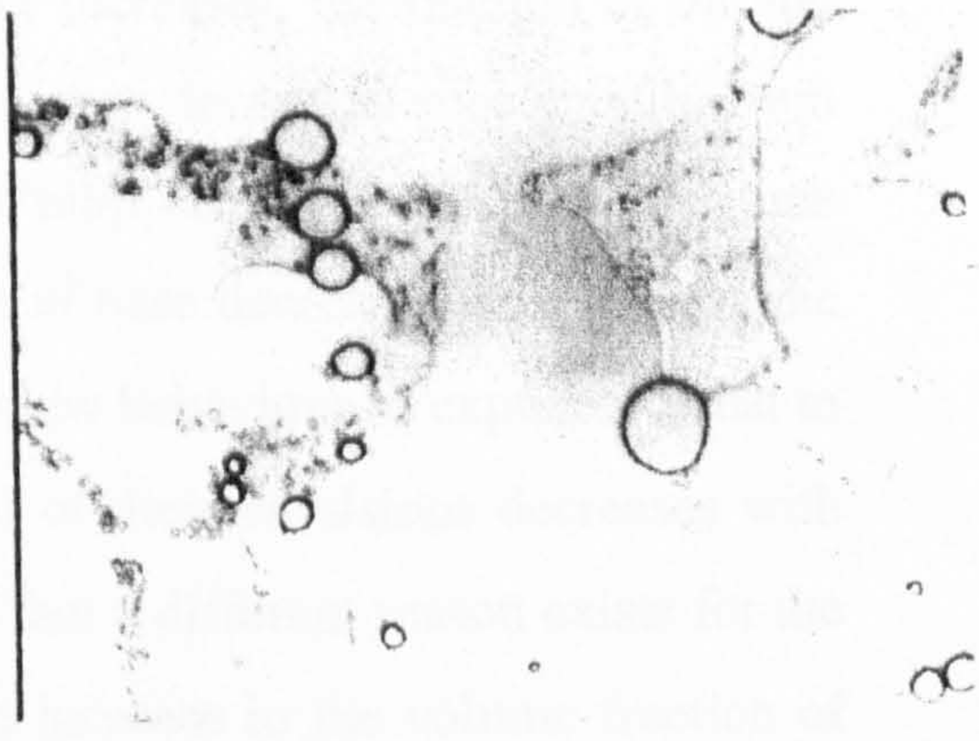

4.5 minutes

are drop rich domains which are surrounded by areas of drop-free continuous phase (light) As the drops coalesce the dark areas become lighter until eventually very few drops remain (4.5 minutes).

The timescale of the 'melting' destabilisation process for water-in-undecanol emulsions at five volume fractions of water is summarised in Figure 7.7. The stability is plotted as the time taken for 25 % of the oil phase to be resolved in each case. At a fixed ϕ_w, the emulsion stability passes through a sharp maximum with respect to temperature. At fixed temperature, emulsions become more stable with increasing ϕ_w. It was verified that emulsions were w/o for all specified conditions. The viscous sintering phenomenon was evident in all cases. The time course of the breakdown of the emulsions is shown in Figure 7.8 for three temperatures at fixed $\phi_w = 0.2$. The stability is plotted as the fraction of oil (f_{oil}) or water (f_{aq}) released, calculated using equations 3.28 and 3.29 without the volume fraction term. At temperatures $\leq$ 21 °C, oil and water were resolved almost simultaneously (e.g. see 18 °C) whereas at temperatures $\geq$ 22 °C oil was resolved much sooner than water (e.g. see 35 °C). In the latter case the volume fraction of water drops in the gel emulsion increases initially as oil is expelled, and it can be noted that the induction time for coalescence to become visible (via appearance of water) goes through a maximum with respect to temperature (note timescales on abscissa). Unfortunately, there is no ready explanation for this dramatic influence of temperature. The interfacial tension only increases gradually over this range and it is unlikely that the contact angle of a particle at the oil-water interface would pass through a maximum. The effect may be associated with changes in the bulk rheology of the particle/oil continuous phase and its impact on the bulk emulsion rheology, although this is not known.

Figure 7.9 shows the effect of ϕ_w on the emulsion stability at a fixed temperature of 35 °C. As the volume fraction of dispersed water increases, the fraction of oil and water liberated over a similar time period of 400 minutes decreases substantially from unity (very unstable) to below 0.2 (more stable). Philip et al.[156] report that the time taken for the gel network to form following addition of base decreases with the volume fraction of dispersed oil phase, ϕ_o, following a power law behaviour of exponent equal to –3. Overall the stability (including gel contraction) of their emulsions decreases with increasing ϕ_o in contrast to this work. It is believed that a different reason exists for the trend in the two cases. For their o/w emulsions, an increase in the volume fraction of (viscous) drops reduces the separation between them enhancing the possibility of

Figure 7.7

Stability of water-in-undecanol emulsions stabilised by 0.5 wt.% SLM 081 particles as a function of temperature and volume fraction of water (given). Ordinate is the time required for 25 % of oil to be resolved. Arrows indicate these times were >24 hours.

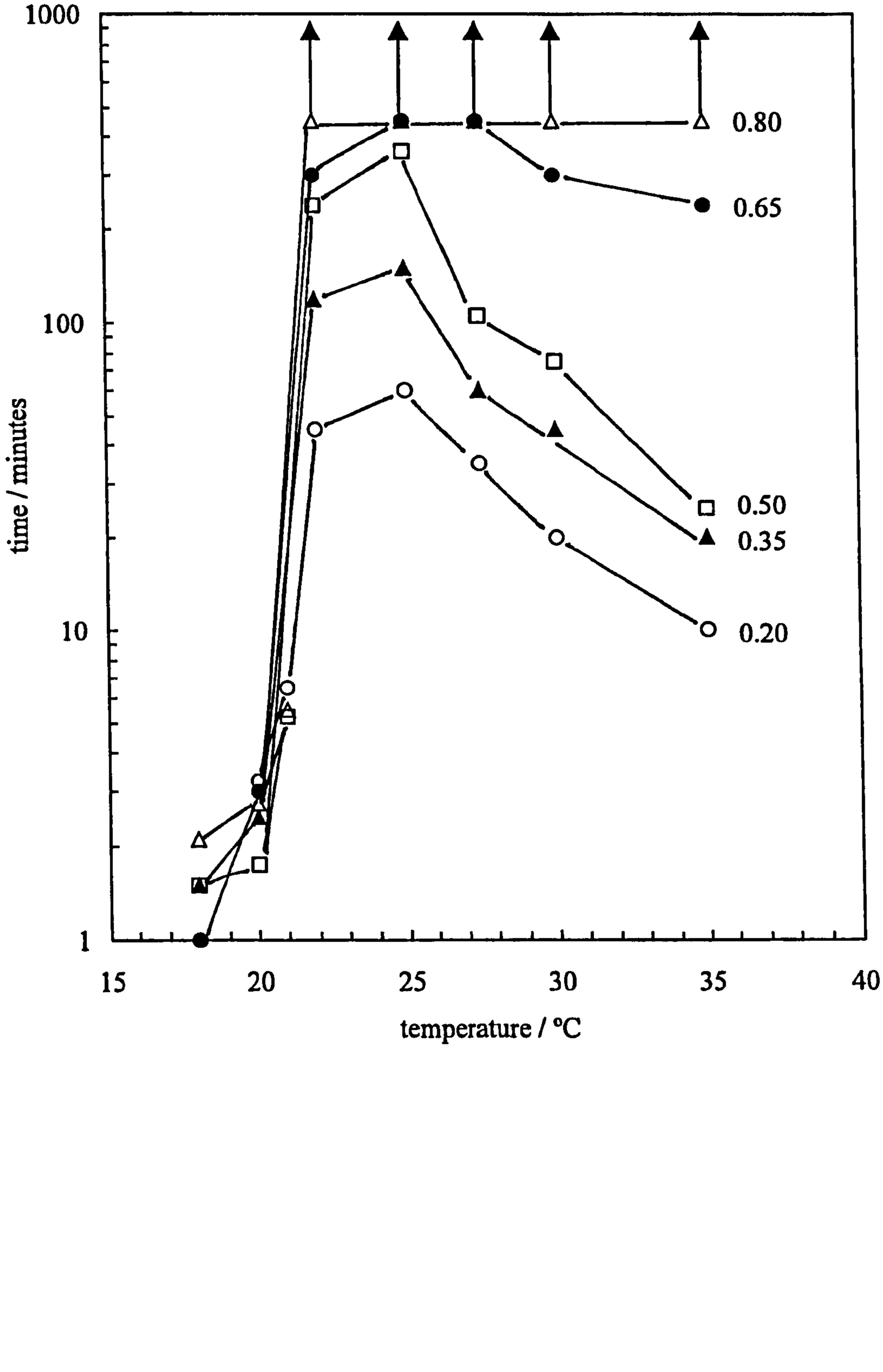

Figure 7.8

Fraction of oil (filled points, right hand ordinate) or water (open points, left hand ordinate) resolved versus time for water-in-undecanol emulsions stabilised by 0.5 wt.% SLM 081 particles in each emulsion at ϕ_w = 0.2 and 18 °C (upper), 25 °C (middle) and 35 °C (lower). Note the different scales.

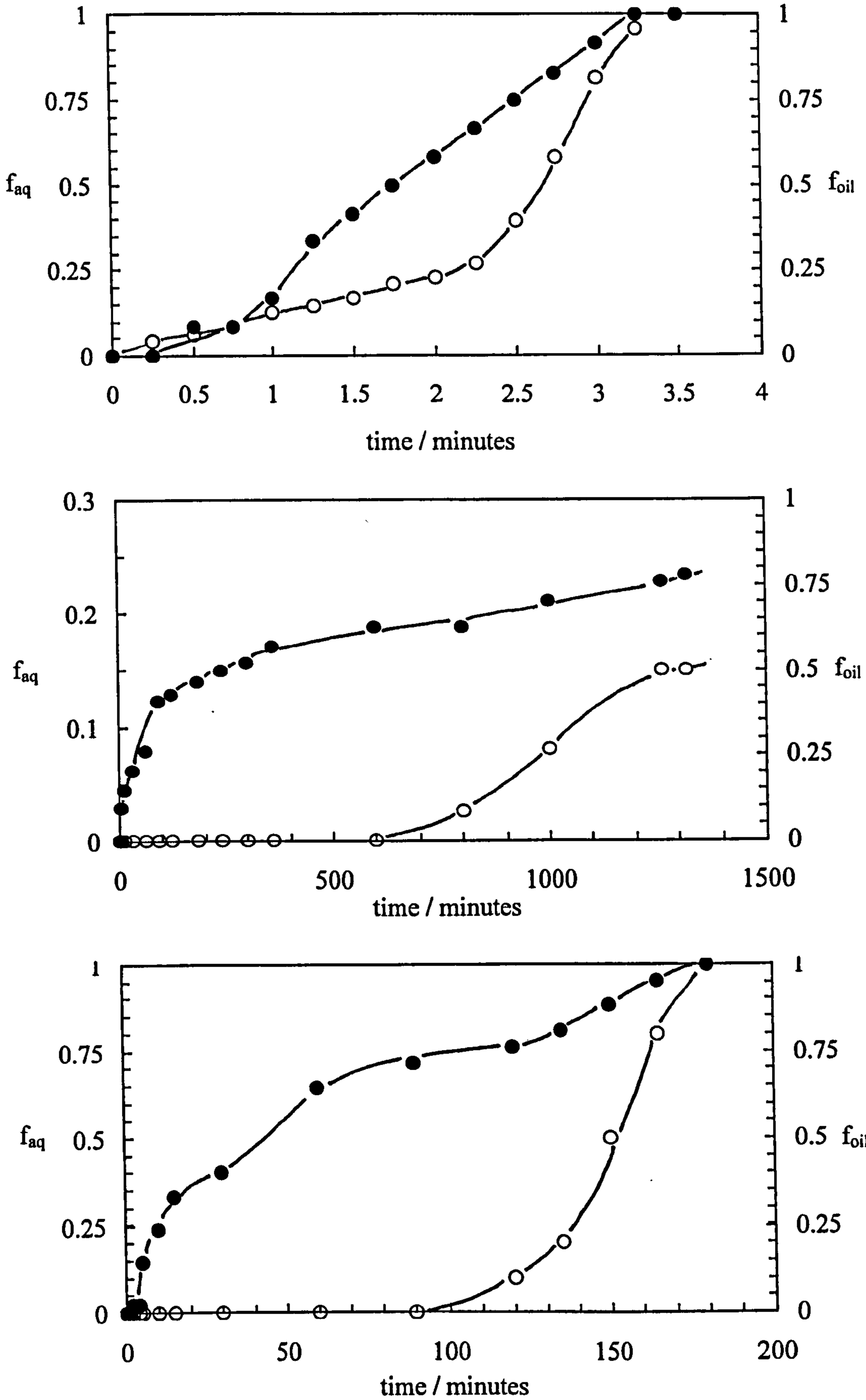

Figure 7.9

Fraction of oil (filled points, right hand ordinate) or water (open points, left hand ordinate) resolved versus time for water-in-undecanol emulsions stabilised by 0.5 wt.% SLM 081 particles in each emulsion at 35 °C and ϕ_w = 0.35 (upper), 0.65 (middle) and 0.80 (lower). Note the different scales.

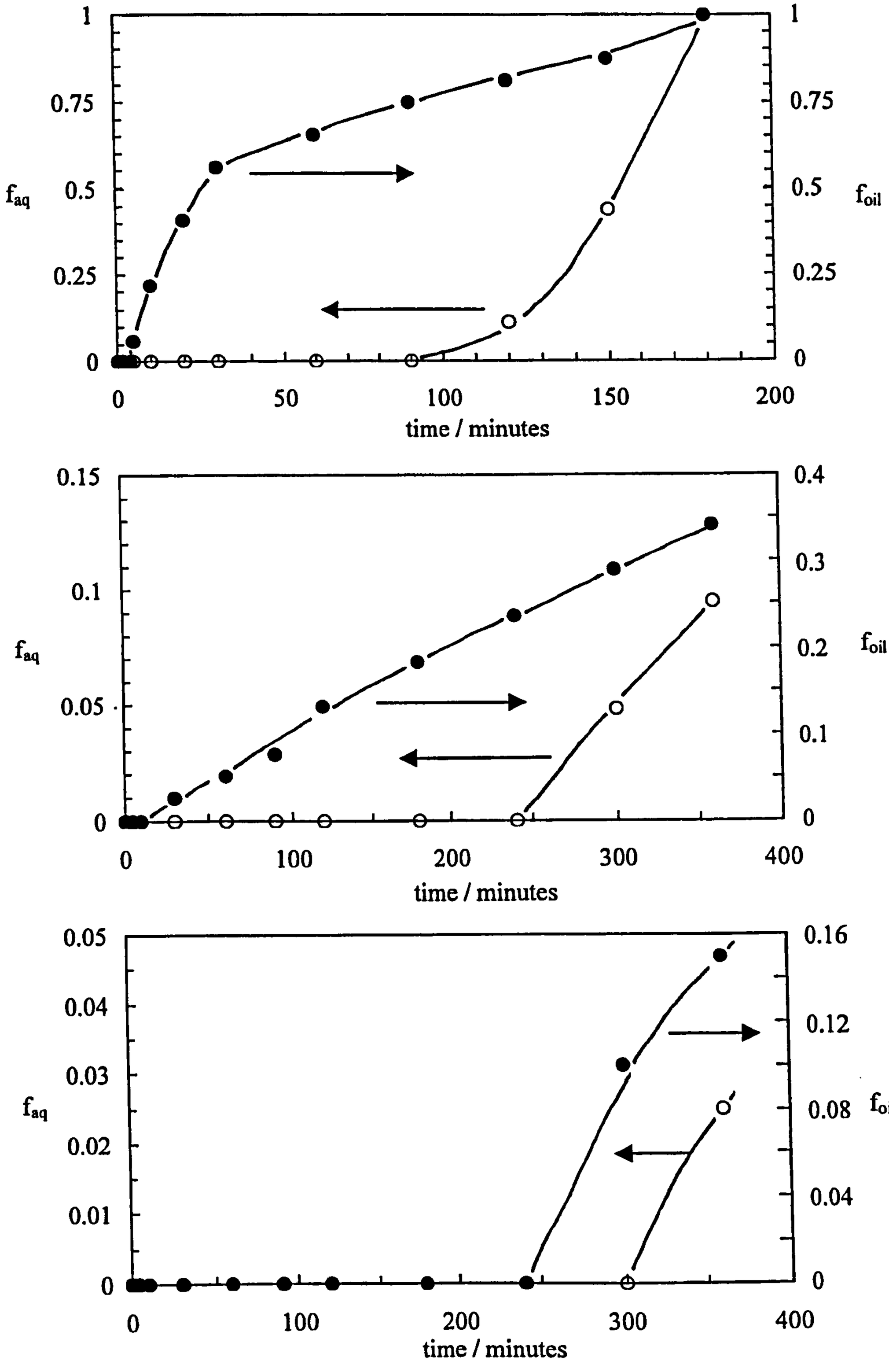

coalescence. For our w/o emulsions, the increase in the volume fraction of water drops causes a large increase in the initial viscosity of the emulsion such that it does not flow for ϕ_w = 0.5 and above. This is due mainly to an increase in the viscosity of the continuous oil phase containing an increasing concentration of particles in order to keep the overall concentration in the emulsion constant. Thus the viscosity of the continuous and not the dispersed phase governs the slow coalescence.

7.4 Effect of initial location of particles in the toluene-water system

It was shown in Chapter 5 that the initial location of hydrophilic particles in emulsions stabilised by mixtures of hydrophilic and hydrophobic particles was important in determining the type of emulsion formed. SLM 081 silica particles are of intermediate hydrophobicity (67 % SiOH) and hence can be dispersed in both water and oil using an ultrasonic probe. Consequently, it is of interest to investigate the effect of the initial location of particles on emulsion type and stability. Since the silica particles are significantly larger than small surfactant molecules such as $C_{12}E_5$, do they equilibrate between the bulk phases and interface to the same extent when dispersed in oil or water or is the behaviour dependent on which phase contacts the particles first? Figure 7.10 reveals that the phenomenon of catastrophic inversion is dependent on the initial location of the silica particles. For particles originally dispersed in toluene (triangles), ϕ_w at inversion is 0.60, compared with a value of 0.35 when starting in water (circles). When an equal mass of particles is dispersed in each phase prior to emulsification, an intermediate value of 0.45 is obtained. In conclusion, the continuous phase of the preferred emulsion is that in which particles are dispersed initially. The emulsion drop size distributions have been measured at three ϕ_w where the preferred type is w/o and three ϕ_w where the preferred type is o/w. The arithmetic mean (d(4,3)) and the median (d(v,0.5)) drop diameter are plotted as a function of ϕ_w in Figure 7.11 for emulsions where particles were initially dispersed in oil (triangles) and those initially dispersed in water (circles). The drop sizes are shown to increase towards inversion (dotted lines) and the preferred emulsions (w/o if starting in oil and o/w if starting in water) have the smallest sizes and are more stable than the non-preferred emulsions, for both emulsion

Figure 7.10

Conductivity and type of water-toluene emulsions stabilised by 0.5 wt.% SLM 081 particles versus the volume fraction of water. Triangles – particles initially dispersed in oil; circles – particles initially dispersed in water; squares – particles initially dispersed equally in oil and water.

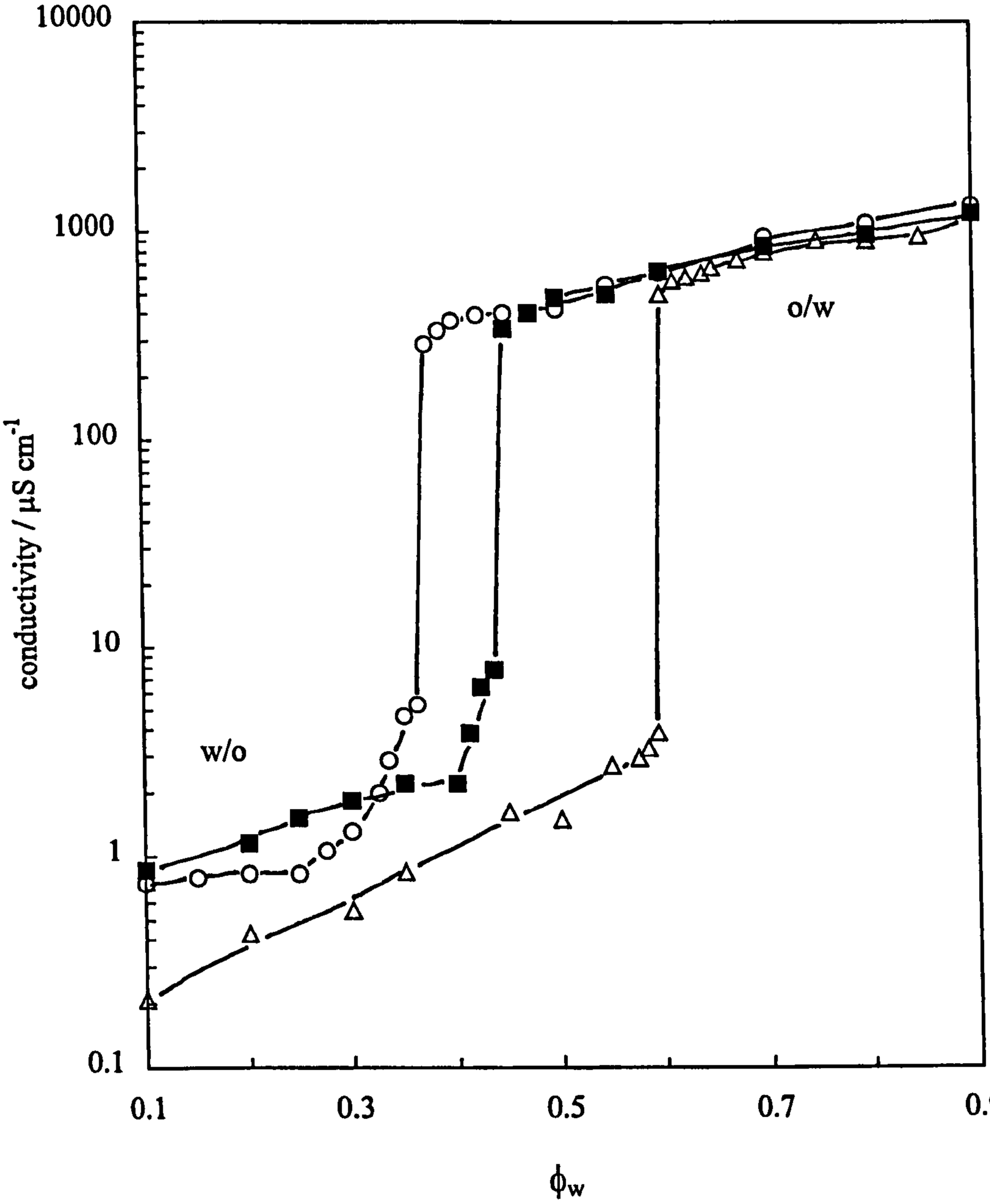

Figure 7.11

Initial emulsion drop diameters versus volume fraction of water for toluene-containing emulsions stabilised by 0.5 wt.% SLM 081. Filled points – d(4,3), open points – d(v,0.5); triangles – particles initially in oil, circles – particles initially in water.

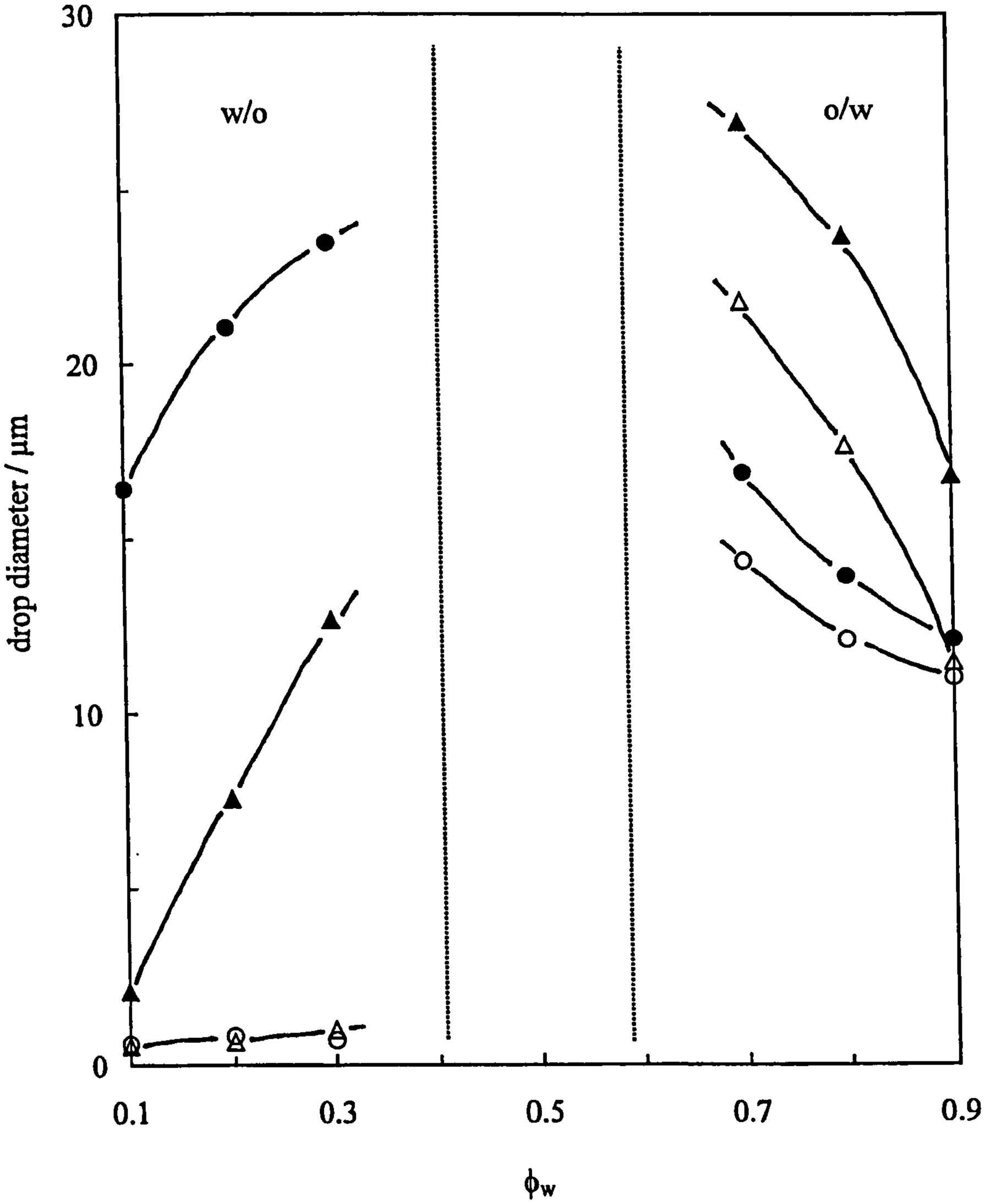

types. It is important to note that maximum stability can be obtained for either emulsion type by simply varying the initial particle location.

In order to make a comparison between solid-stabilised systems and surfactant systems, the behaviour of the pure non-ionic surfactant $C_{12}E_5$ has been investigated. Due to its smaller size $C_{12}E_5$ is expected to distribute faster between phases and will be more mobile laterally within interfaces. $C_{12}E_5$ was chosen as the surfactant in order to retain toluene as the oil phase and preferred emulsion type as w/o at 25 °C since the temperature at which these emulsions invert from w/o to o/w is predicted to be below 0 °C. As discussed previously,[8] a high concentration of monomeric $C_{12}E_5$ surfactant is present in the bulk oil phase and hence is unavailable for adsorption, therefore relatively large amounts of surfactant are required to yield stable emulsions comprising interfaces of close-packed surfactant monolayers. At 25 °C, the equilibrium system is Winsor II made up of a w/o microemulsion phase plus an excess water phase (see diagram in Figure 7.12). The microemulsion droplets are in equilibrium with monomeric surfactant in both oil (high concentration) and water (low concentration). Homogenisation of this two-phase system yields a w/o emulsion. Transfer of surfactant from the non-pre-equilibrated phases, where all the surfactant is present in either water or oil, to the Winsor II state occurs via two routes. Route 1 involves transfer of the majority of surfactant from water to oil and route 2 involves transfer of a low concentration of monomeric surfactant from oil to water. Emulsions prepared at different volume fractions of water are w/o (Figure 7.12) whether the same amount of surfactant is dissolved initially in water (open points) or oil (filled points). Unlike solid particles, $C_{12}E_5$ partitions readily during homogenisation and no initial location-induced preference for one or other type of emulsion is observed.

In further contrast to the solid-stabilised systems, the emulsions stabilised by $C_{12}E_5$ do not invert to o/w, even at high ϕ_w. Instead the formation of high internal phase w/o emulsion gels occurs.[158] The interfaces of these emulsions must be able to deform into a non-spherical shape because they remain w/o above the close packing volume fraction. Particle laden interfaces, on the other hand, are viscoelastic and resist deformation,[31] preferring to coalesce above the close packing condition.

Figure 7.12

Conductivity and type of water-toluene emulsions stabilised by $C_{12}E_5$ versus the volume fraction of water. Open points – 25 wt.% surfactant initially in water; filled points – 25 wt.% surfactant initially in oil. Shown schematically are the non-pre-equilibrated systems (left; shading indicates location of surfactant) and the equilibrated system (right; w/o microemulsion + excess water).

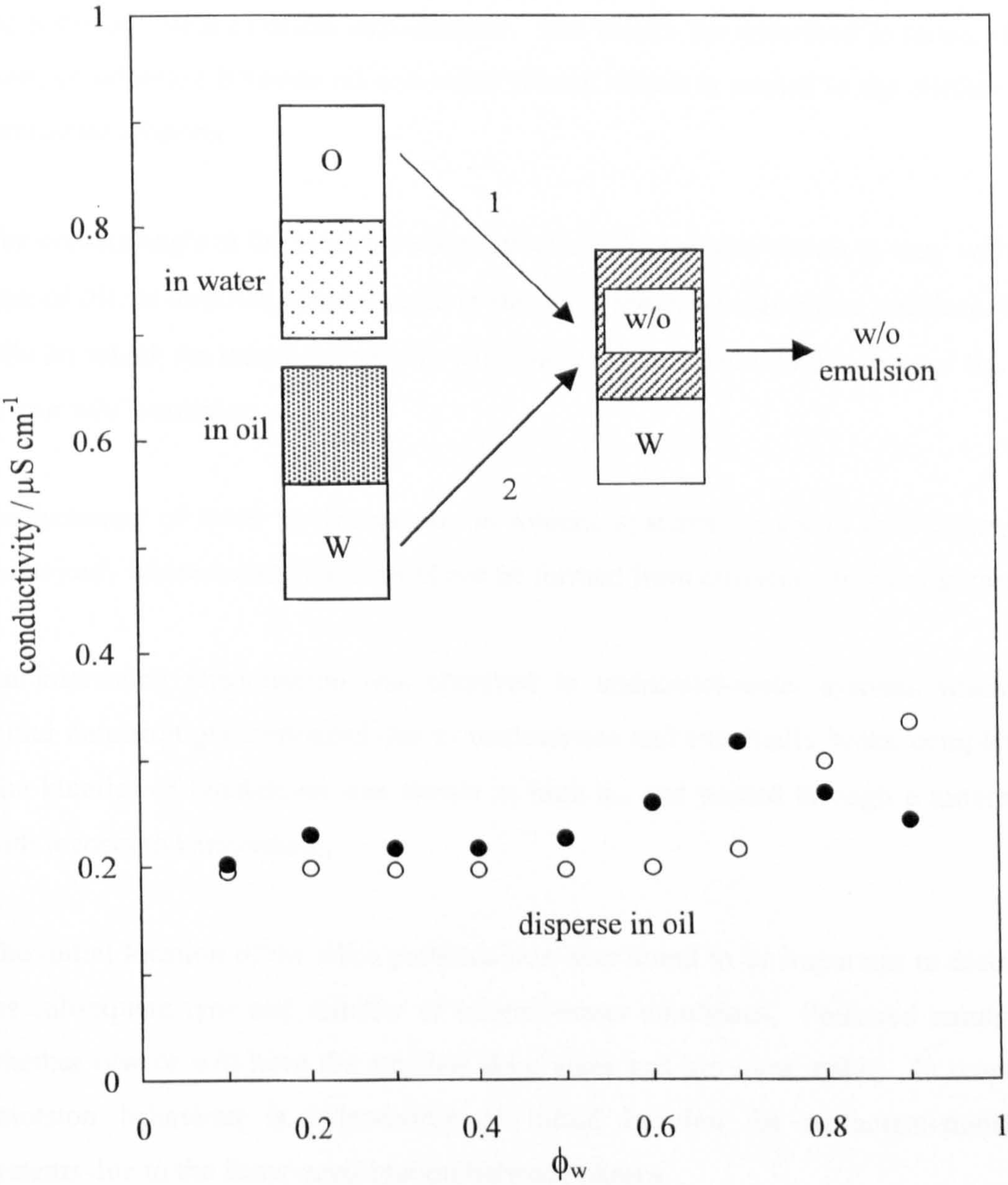

7.5 Conclusions

In this chapter the behaviour of oil-polar phase emulsions stabilised by silica particles of intermediate wettability have been investigated. The following conclusions can be drawn.

- The preferred emulsion type is o/w for non-polar oils such as hydrocarbons and w/o for polar oils such as esters and alcohols. The results are described in terms of the work of adhesion between oil and water phases which is related to the surface and interfacial tensions.

- The contact angle at the solid-oil-water interface (θ_{ow}) is also shown to vary with the type of oil, as does the contact angle at the solid-toluene-polar phase interface (θ_{op}). Oils for which the interfacial tension with water is low exhibit high values of θ_{ow} and favour w/o emulsions.

- Replacement of water by formamide in toluene systems results in little change in behaviour, whereas emulsions could not be formed from ethylene glycol or glycerol.

- An interesting phenomenon was observed in undecanol-water systems where an initial emulsion gel contracted due to coalescence and eventually broke completely. The kinetics of breakdown was slower at high ϕ_w and passed through a maximum with respect to temperature.

- The initial location of the silica particles was also found to be important in dictating the subsequent type and stability of toluene-water emulsions. Preferred emulsions whether o/w or w/o have the smallest drop sizes and are most stable. In contrast, emulsion behaviour is independent of initial location for surfactant-stabilised systems due to the faster equilibration between phases.

CHAPTER 8

CHAPTER 8

INFLUENCE OF pH AND ELECTROLYTE CONCENTRATION ON THE WETTABILITY OF SILICA SURFACES

8.1 Introduction

In Chapter 5 the system HLB was altered by changing the overall wettability of the system using particle mixtures. This was akin to addition of a co-surfactant to surfactant-stabilised emulsions. Another way of changing the HLB in zwitterionic surfactant systems is by affecting the charge of the headgroup by altering the pH.[112] The charge on the headgroup can also be screened by addition of electrolyte. In this chapter the influence of aqueous phase pH and electrolyte concentration on the wettability of silica particles is investigated by measuring the partitioning of the particles between toluene and water. It was shown by Healy[85] that a silica surface is negatively charged at high pH (see Figure 3.1) due to dissociation of silanol groups (SiOH) in to SiO^-. This will increase the particle affinity for the polar aqueous phase. The hydrophobic particles have varying percentages of SiOH groups remaining on their surface. If the particles become more hydrophilic on increasing the pH particle transfer from oil into the aqueous phase could conceivably occur. The type and stability of toluene-water emulsions stabilised by such silica particles as a function of pH is also reported. As mentioned earlier in Chapter 6, it is difficult to measure the contact angle (θ) of sub-micron particles at the oil-water interface. As an alternative, the silica particle surface has been modelled by coating flat glass plates with dimethyldichlorosilane (DMDCS) allowing the measurement of θ at the oil-water interface and air-water surface. A theoretical model is also proposed for the effect of pH and electrolyte concentration on the wettability of a silica surface. As a result of the findings in this chapter an alternative explanation is proposed for the behaviour of three diverse systems where particles are required to be hydrophobic.

8.2 Partitioning of silica particles between oil and water

The silica particles used in the previous experiments have varying percentages of SiOH groups on their surfaces. However, all but the most hydrophilic particles (100 % SiOH) are more readily dispersed in toluene than in water. At equilibrium, surfactant molecules partition between oil and aqueous phases and some remain at the oil-water interface. The partitioning of particles between the two phases is determined by drying the phases to constant weight after 30 minutes equilibration. If the SiOH groups do dissociate into SiO^- at high pH as suggested, the particles may prefer to be situated in the aqueous phase. This has been shown previously in water + coal-derived liquid systems containing micrometer-sized hydrophobic mineral particles obtained from coal.[159] Figure 8.1 shows the partitioning of the two most hydrophobic particles (H18 – 20 % SiOH and H30 – 50 % SiOH) between toluene and water as a function of the aqueous phase pH. After equilibration, the particles initially dispersed in toluene remain almost exclusively in the oil at all pH. The relatively low amount of SiOH groups on the surface of these particles is not enough to initiate transfer of the particles into the aqueous phase. Even at high pH the DMDCS groups still determine the preferred phase. The intermediate hydrophobicity particles, however, have more ionisable SiOH groups on their surface and the partitioning is shown in Figure 8.2 to be dependent on the pH of the aqueous phase. 2 wt.% SLM 078 (79 % SiOH), 079 (76 %) and 081 (67 %) particles initially dispersed in toluene remain in the slightly cloudy oil phase up to pH 10 whereupon they begin to leave the oil phase as the pH is increased further. The percentage of SLM 079 particles (triangles) in water starts to increase as soon as the percentage in oil begins to decrease until at pH 12 there are more particles in water than in toluene. By pH 13.75, ~ 100 % of the particles are situated in the aqueous phase. For SLM 078 and 081 the particles begin to leave the oil phase at pH 10 but do not appear in the aqueous phase until pH 11 and 12.5 respectively. In these cases approximately 45 % of the particles are situated in a third coarse emulsion phase composed of large millimetre-sized drops, which forms spontaneously at intermediate pH. At pH ≥ 13 the particles are almost entirely situated in the aqueous phase. The appearance of the phases is shown in the schematic below both before and after equilibration. It is clear that the particles transfer from oil to water with increasing pH.

Figure 8.1

Partitioning of 2 wt.% H18 (circles) and H30 (diamonds) particles initially dispersed in oil between toluene (open points) and water (filled points), (ϕ_w = 0.5) as a function of the pH of the aqueous phase.

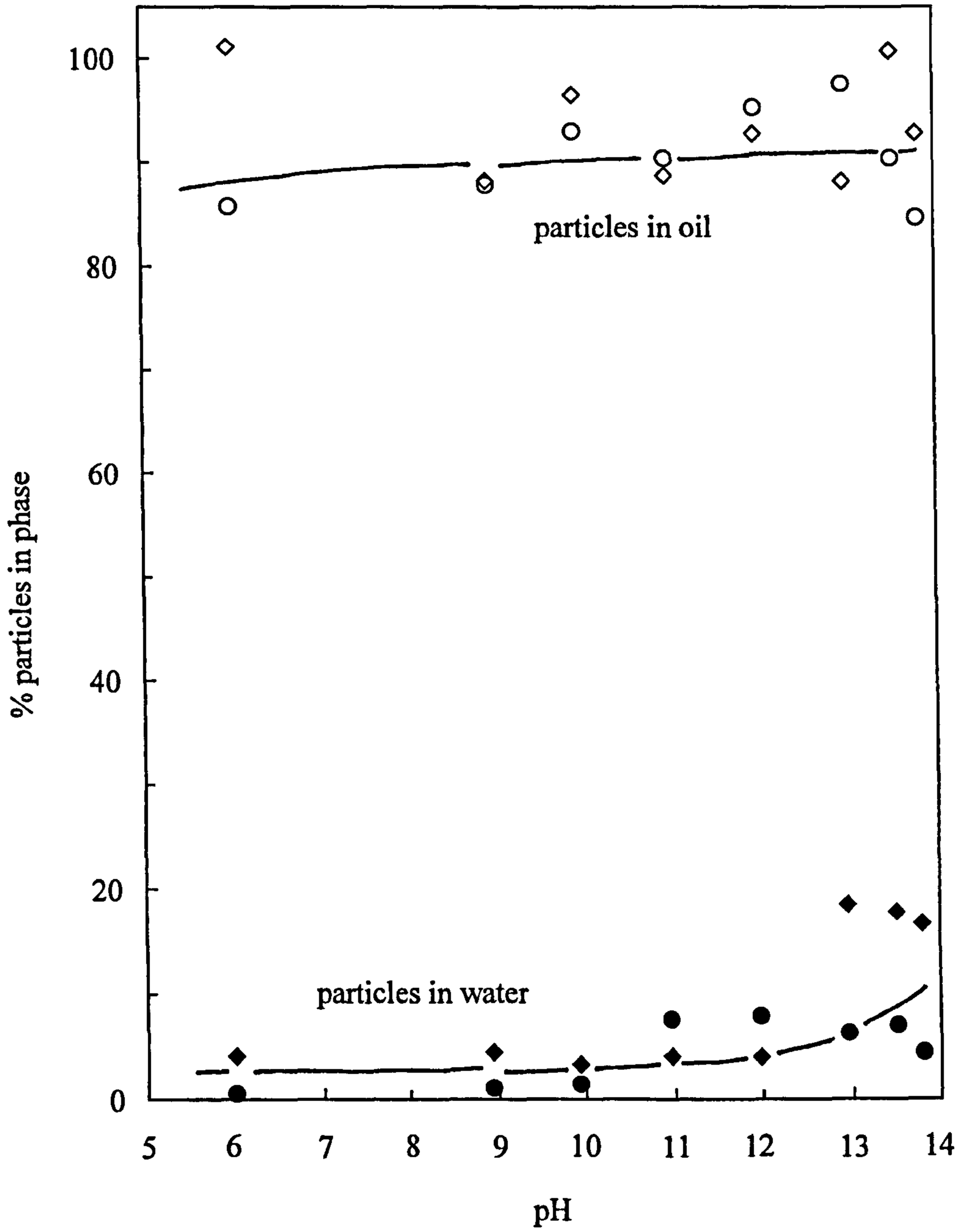

Figure 8.2

Partitioning of 2 wt.% SLM 078 (diamonds), 079 (triangles) and 081 (circles) particles initially dispersed in oil between toluene (open points) and water (filled points), ($\phi_w = 0.5$) as a function of the pH of the aqueous phase.

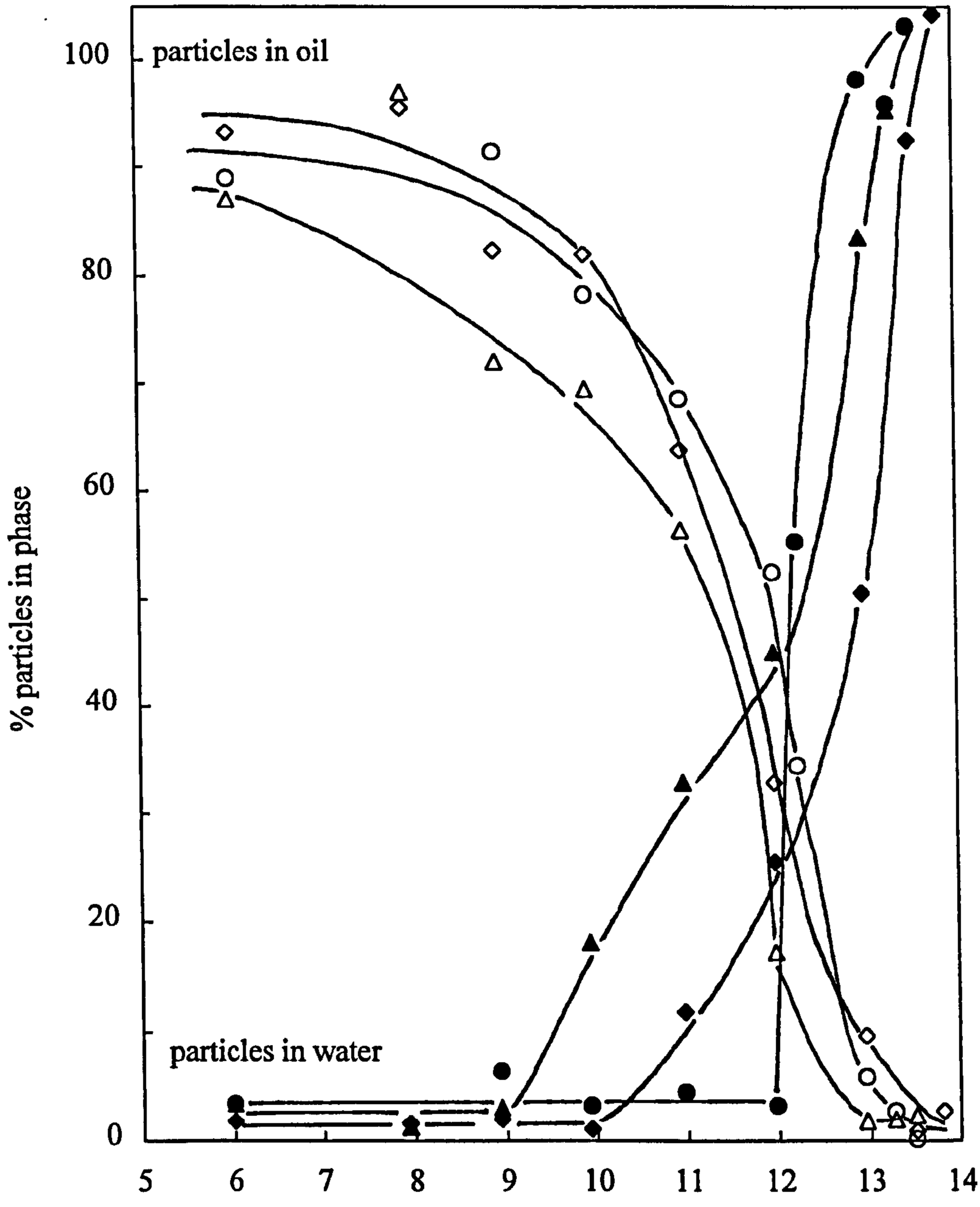

Appearance of liquid phases before and after equilibration

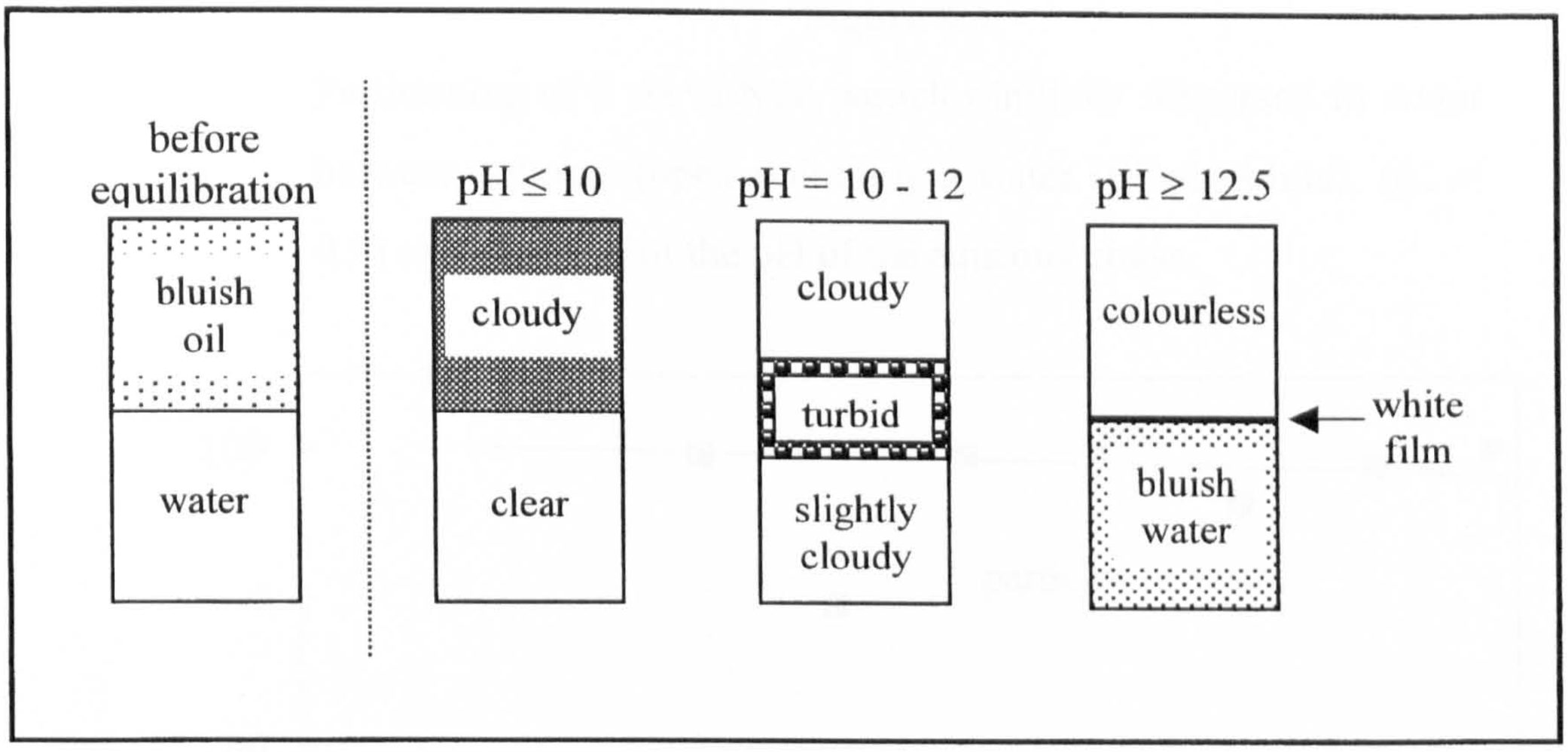

Figure 8.3 shows the partitioning of hydrophilic N20 silica particles (100 % SiOH), initially dispersed in water, between toluene and water as a function of pH. As expected, the particles remain in the aqueous phase at all pH. In all cases the mass of NaOH in the aqueous phase has been subtracted from the measured value after the drying process in order to obtain the mass of silica. In some cases the mass appeared to have reached a constant value but in fact some NaOH must have been present as a value of over 100 % was obtained. As a result, an error of ± 3 % is assumed for each point.

8.3 Effect of silica particle charge on the type and stability of emulsions

The partitioning experiments prove that it is possible to switch the preferred location of particles from oil to water in equilibrium systems on addition of NaOH. As a result, Bancroft's rule[7] would predict that emulsions should invert from w/o to o/w, as in surfactant systems. Figure 8.4 shows the conductivity and type of emulsions, prepared from the same equilibrated phases used for the partitioning experiments, as a function of the aqueous phase pH. Emulsions stabilised by H18 silica particles remain w/o of low conductivity at all pH, which is what would be expected knowing the partitioning where the particles remained in the oil phase at all pH. However, emulsions stabilised by H30

Figure 8.3

Partitioning of 2 wt.% N20 particles initially dispersed in water between toluene (open points) and water (filled points), (ϕ_w = 0.5) as a function of the pH of the aqueous phase.

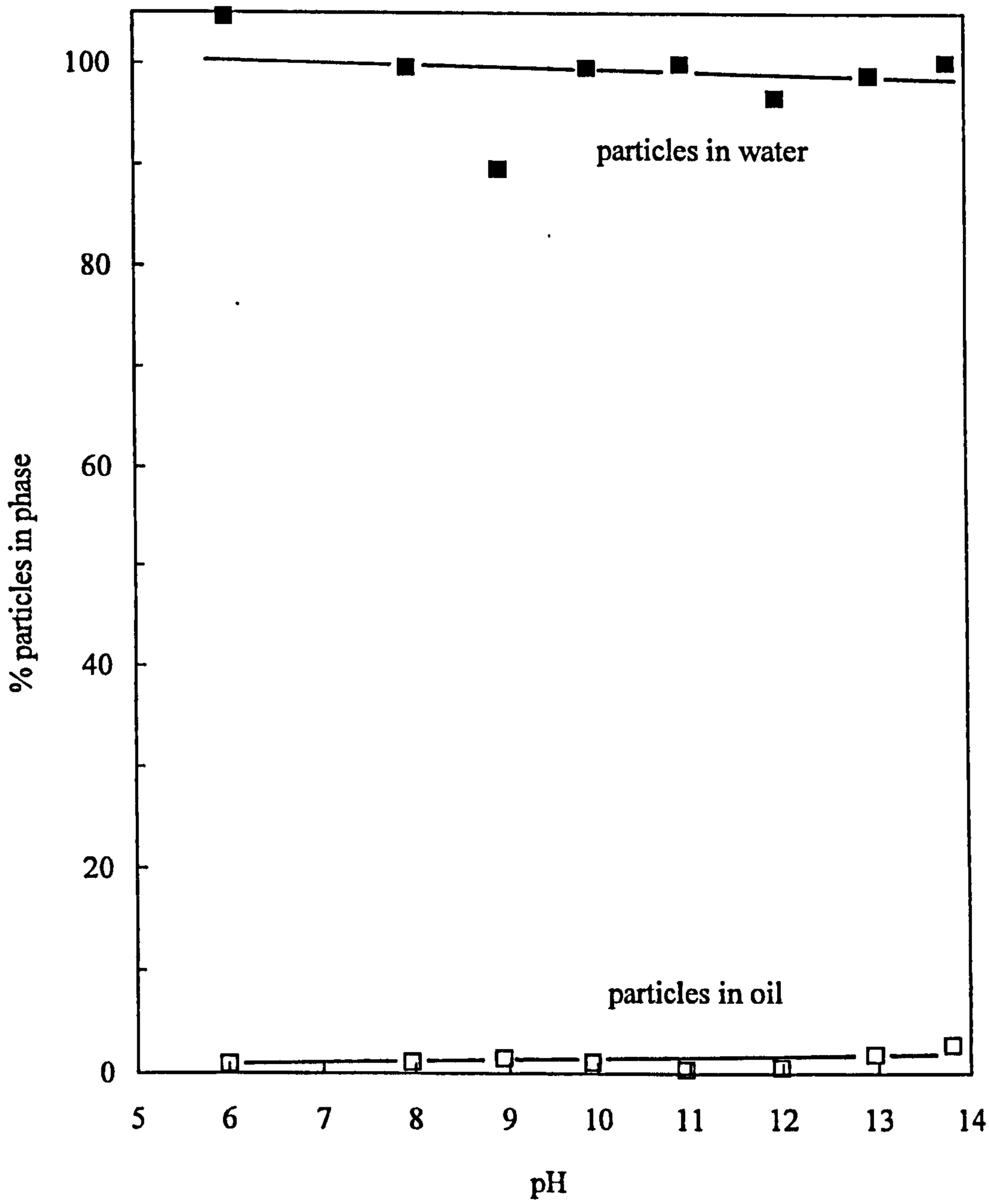

Figure 8.4

Effect of pH on the type and conductivity of toluene-water emulsions stabilised by 1 wt.% silica particles in emulsion immediately after homogenisation, 25 °C.

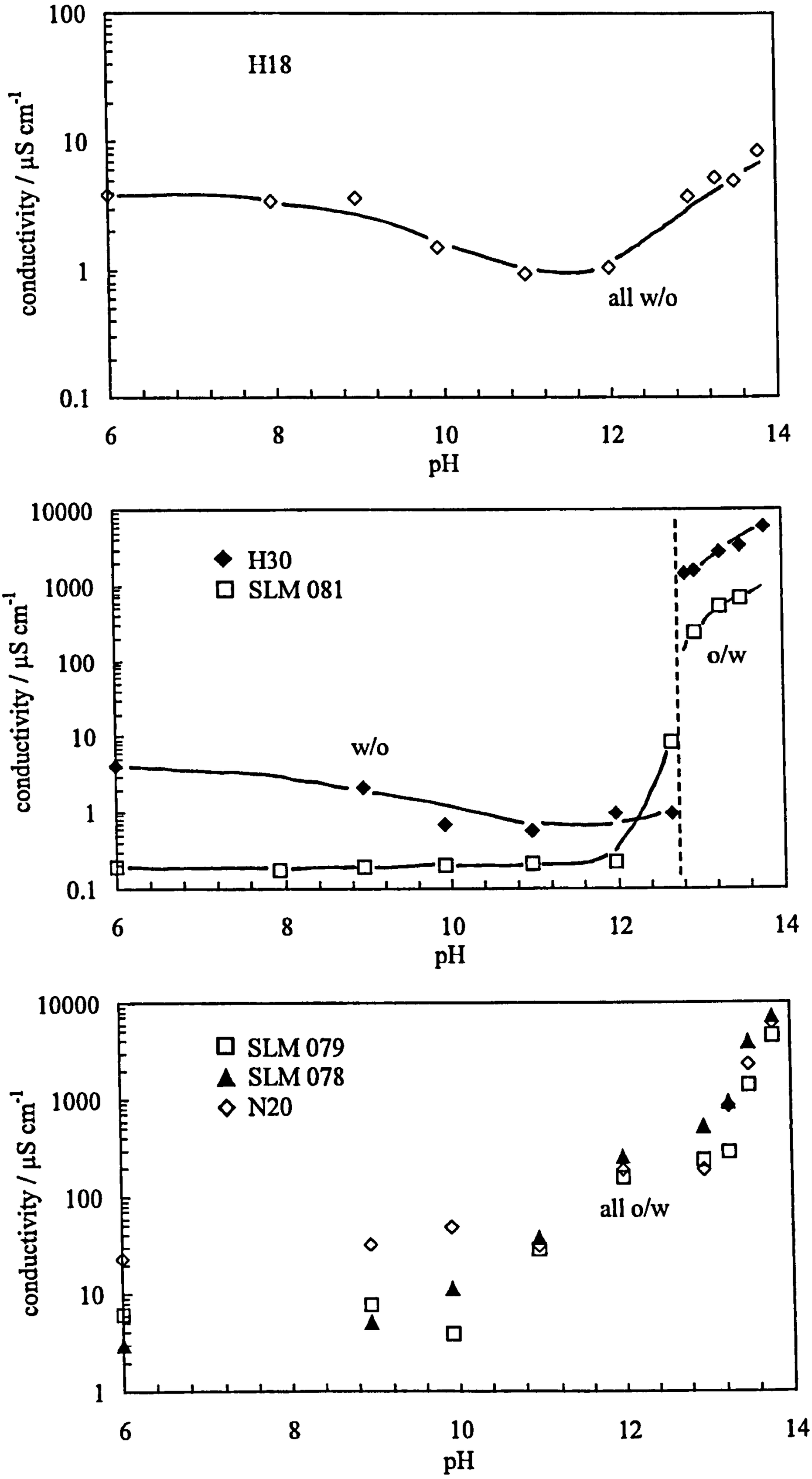

and SLM 081 silica particles are w/o at pH < 12.75 whereupon the conductivity increases as the emulsions invert to o/w. This can be understood for SLM 081 silica where the particles are shown to transfer from the oil to aqueous phase at pH ≈ 12.75 (Figure 8.2). H30 silica particles, however, remain in the oil at all pH so would be expected to stabilise w/o emulsions, but this is not the case at high pH. This suggests the partitioning of H30 had not reached equilibrium within 30 minutes of stirring whereas the high shear during emulsification presumably shortens the equilibration time. Emulsions stabilised by SLM 078, 079 and N20 remained o/w at all pH. The conductivity is low at pH < 10 due to the low concentration of hydroxyl ions in the aqueous phase but the emulsions are definitely o/w as proven by the drop test. This agrees with results in Chapter 6 where emulsions stabilised by these particles were o/w at $\phi_w = 0.5$. However it does not agree with the partition results where SLM 078 and 079 prefer to be in the oil phase at low pH. In Figure 6.5 emulsions stabilised by SLM 078 and 079 invert from w/o to o/w just below $\phi_w = 0.5$ suggesting the particles are held at the interface at a contact angle very close to 90°. As a result they are very sensitive to external conditions such as high shear during homogenisation. As expected, the very hydrophilic N20 silica particles stabilise o/w emulsions at all pH.

Phase inversion, when it occurs, is an example of transitional inversion, in which the system HLB is increased by pH. The stabilities of toluene-water emulsions stabilised by the intermediate wettability particles, SLM 081 (67 % SiOH) expressed as the fraction remaining after 30 minutes, are shown in Figure 8.5 as a function of aqueous phase pH. The w/o emulsions at low pH are stable to coalescence but sediment to an increasing extent approaching inversion. Above pH 12.5 the o/w emulsions exhibit coalescence and creaming, both of which increase moving away from inversion. In the presence of NaCl electrolyte the charge on the particles at high pH is screened thus the hydrophilicity of the particle is expected to diminish as seen by Kornil'ev et al.[160] Figure 8.6 shows the conductivity of emulsions stabilised by 2 wt.% H30 particles at various pH as a function of NaCl. Between pH 6 and 12.07 the emulsions remain w/o at all [NaCl] as expected. At pH 12.17 and 12.97 however the emulsions are o/w at all [NaCl] implying that it is not possible to re-invert the emulsions to w/o by screening the charge.

Figure 8.5

Stability of toluene-water emulsions stabilised by 2 wt.% SLM 081 particles dispersed in oil as a function of the pH of the aqueous phase.

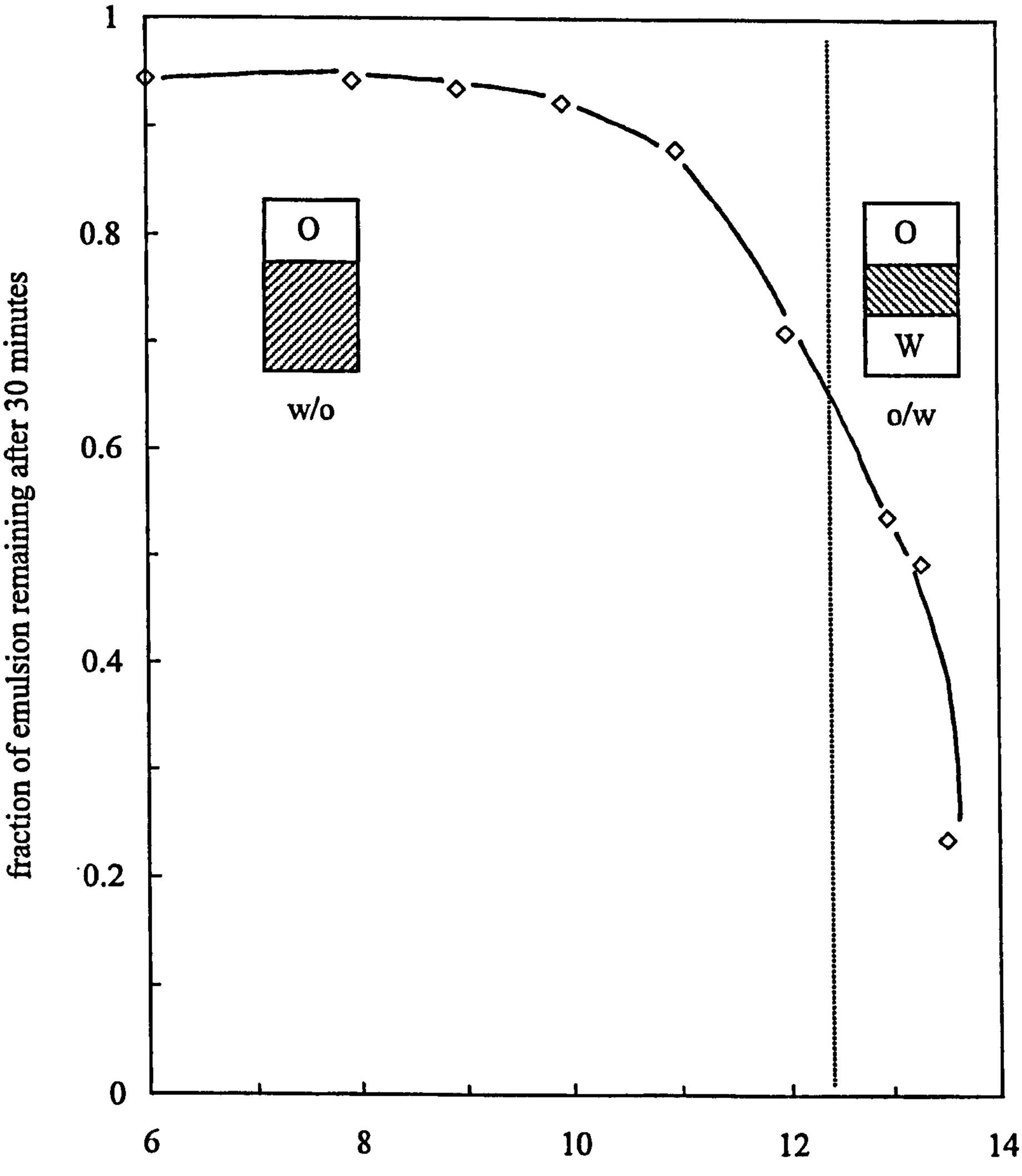

Figure 8.6

Conductivity of toluene-water emulsions stabilised by 2 wt.% H30 particles dispersed in oil as a function of NaCl concentration. The pH of the aqueous phase was 6 (diamonds), 9.97 (circles), 12.07 (stars), 12.17 (triangles) and 12.97 (squares).

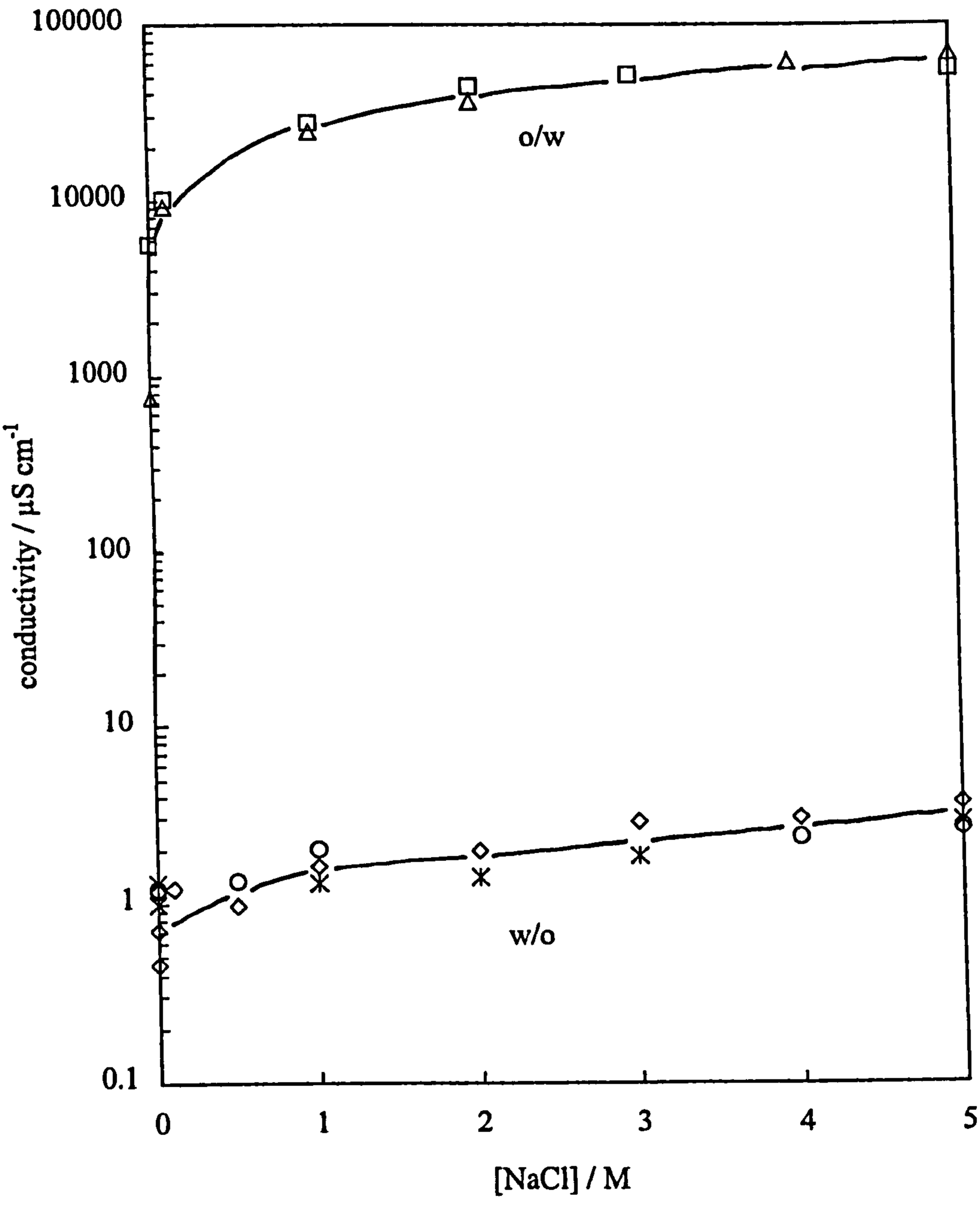

8.4 Wettability of planar silica surfaces under toluene

The surfaces of the silica particles used in all these experiments are coated to varying extents with dimethyldichlorosilane groups which impart some hydrophobic character. The contact angle θ that the particle makes at the oil-water interface is dependent on the wettability (extent of hydrophobisation) which is thought to determine the preferred emulsion type. If θ is < 90° the (hydrophilic) particle prefers to stabilise o/w emulsions and if θ is > 90° the (hydrophobic) particle prefers to stabilise w/o emulsions. An increase in the aqueous phase pH in solid-stabilised systems is believed to increase the hydrophilicity of the particle, hence cause a decrease in θ. It is shown in the previous section that an initially hydrophobic particle, which prefers to stabilise w/o emulsions, stabilises o/w emulsions at high pH. In order to obtain a qualitative measure of the contact angle at the air-water and oil-water interface it is necessary to model the silica surface by coating flat glass plates with dimethyldichlorosilane groups. It has been shown that measurements of θ on a flat plate are virtually the same as those measured for spherical particles.[68] It is not known what concentration of DMDCS corresponds to what contact angle but these measurements provide an illustration of how the silica surface is affected by pH. The Pyrex borosilicate glass slides were cleaned in a reproducible manner (see experimental) so that the uncoated slides had an advancing contact angle at the air-water surface θ_{aw}^{adv} of < 5° and at the toluene-water interface θ_{ow}^{adv} of 40°. Figure 8.7 shows the advancing contact angle of a water drop of varying pH in air (open points) and under toluene (filled points) as a function of the concentration of DMDCS used to coat the glass plate. θ_{aw}^{adv} is independent of pH at all [DMDCS] but increases progressively from approximately 35° at 1 x 10^{-5} M DMDCS to 95° at 0.05 M DMDCS. In contrast, θ_{ow}^{adv} does show some dependence on pH. At pH 6 (diamonds), the angle increases from 108° at 1 x 10^{-5} M DMDCS to 145° at 0.05 M DMDCS. However, as the pH is increased to 13.51 the contact angle decreases progressively to 87° at 1 x 10^{-5} M DMDCS and to 131° at 0.05 M DMDCS.

In order to investigate further the effect of pH on the wettability of the silica surface under toluene, the advancing (filled points) and receding angles (θ_{ow}^{rec} – open points) have been measured at three concentrations of DMDCS as a function of pH (Figure 8.8). The advancing and receding measurements are shown to remain constant

Figure 8.7

Advancing contact angle in air (open points) and under toluene (filled points) of a 20 μl water drop as a function of [DMDCS] used to coat the glass slides. The pH of the water drop was 6 (diamonds), 11.98 (triangles) and 13.51 (circles).

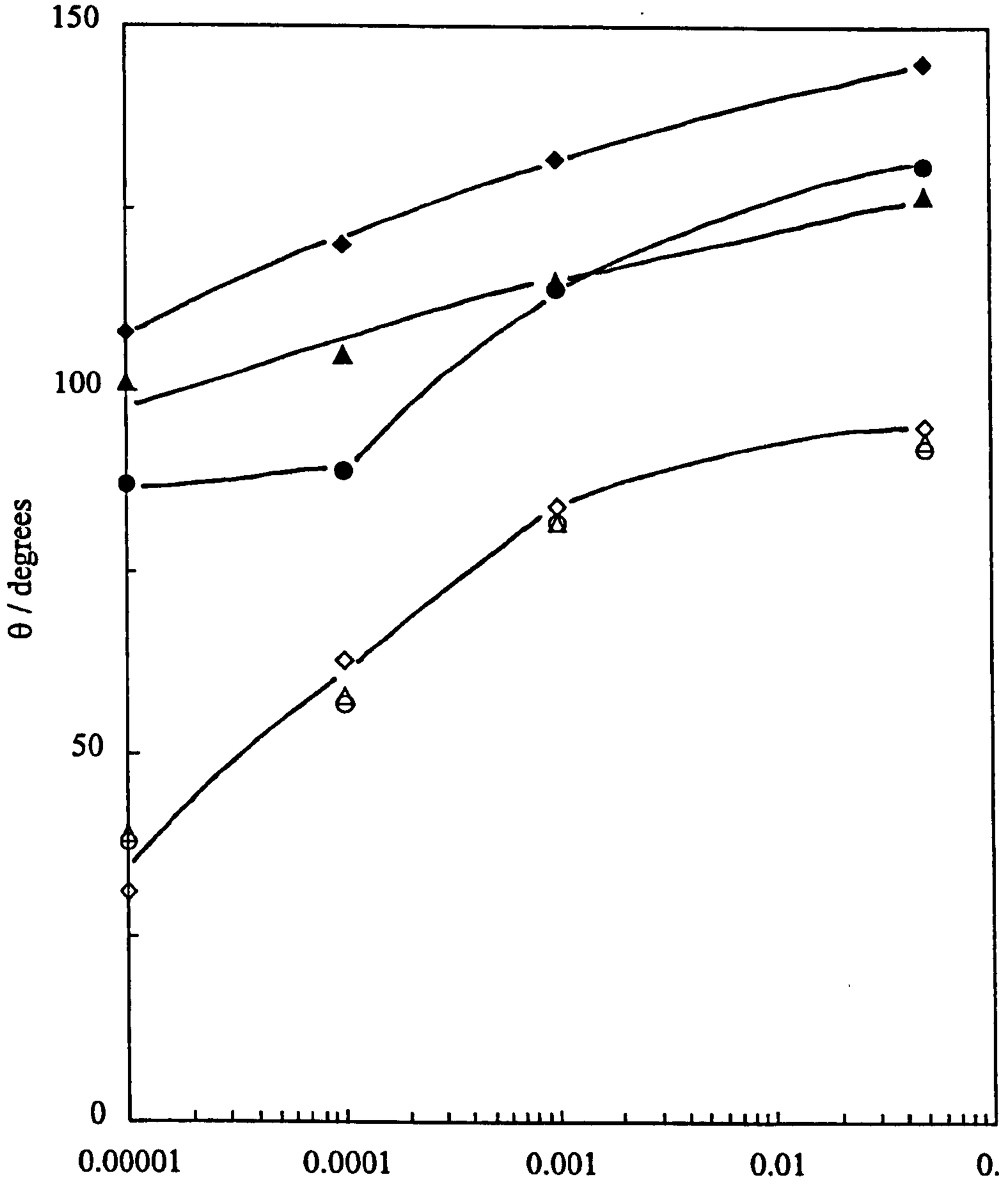

Figure 8.8

Advancing contact angle (filled points) and receding contact angle (open points) of a water drop under toluene as a function of pH. [DMDCS] used to coat glass slides was (a) 0.05 M, (b) 1 x 10^{-4} M, (c) 1x10^{-5} M and (d) 0 M.

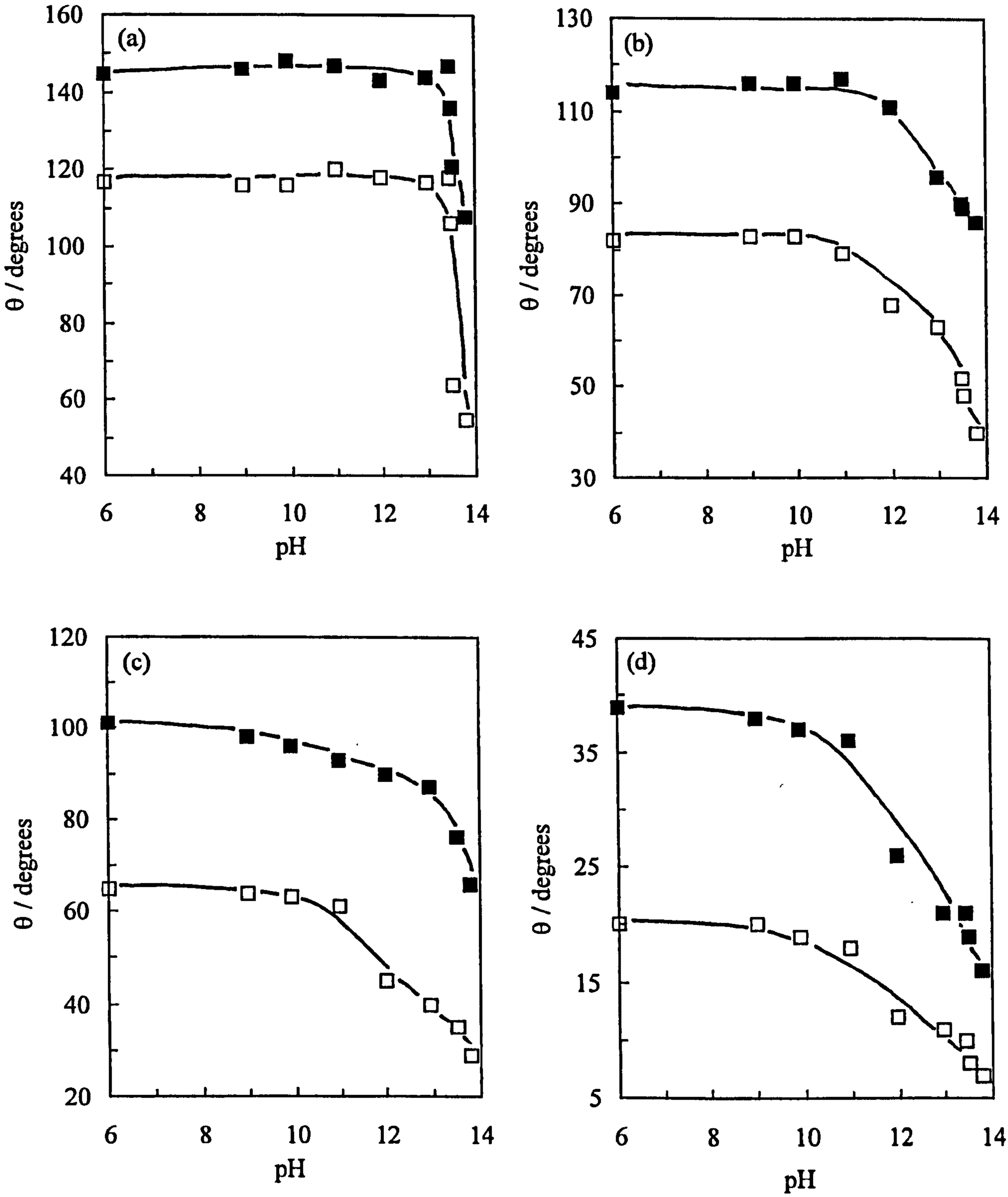

at ~ 145° and ~ 118° respectively below pH 13 at 0.05 M DMDCS (a), whereupon the angle falls rapidly to 108° and 55° by pH 13.8. Figure 8.8 (b), (c) and (d) show the dependence on pH of the advancing and receding angle at 1 x 10^{-4} M, 1 x 10^{-5} M and 0 M DMDCS respectively. In all cases both angles remain constant below pH 11 whereupon they decrease gradually up to pH 13.8. At any pH the angle decreases with decreasing concentration of DMDCS. The high concentration of DMDCS in (a) means there are fewer ionisable SiOH groups on the surface which is the reason why the contact angle is not affected until very high pH. Ideally the pH at which the contact angle begins to fall would decrease as the concentration of DMDCS on the surface decreases. However, it is not possible to distinguish between the lower concentrations apart from the fact that the contact angle is lower in low concentrations of DMDCS.

The difference between the advancing and receding angle at any pH is a measure of the hysteresis in the wettability of the solid surface which is discussed further in Chapter 9. The contact angle hysteresis ($\Delta\theta$) of a water drop on the glass slide is shown in Figure 8.9 to be dependent on both the concentration of DMDCS and pH. In the absence of hydrophobic modification (circles) the hysteresis is small (~ 20°) at low pH and decreases gradually to 10° as the pH increases. However, as the slides are coated with DMDCS to varying extents, the hysteresis increases from approximately 30° to 50° as the pH increases. For advancing angles, the drop spreads over uncharged silanol groups. For receding angles, the drop retracts over dissociated silanol groups, which make the surface more hydrophilic and hence lowers the contact angle. This results in considerable hysteresis between the two measurements. An increase in pH renders the surface more hydrophilic, which is highlighted in Figure 8.10 where $\Delta\theta_{max}$ is plotted as a function of [DMDCS]. $\Delta\theta_{max}$ is defined as θ_{ow}^{adv} (pH 6) – θ_{ow}^{rec} (pH 13.8) and hence indicates the maximum effect of pH on any surface. As the surface becomes more hydrophobic $\Delta\theta_{max}$ increases from 32° on an unmodified slide to over 90° at 0.05 M DMDCS. It was shown earlier that the contact angle at 0.05 M DMDCS is not affected until pH 13 but then falls dramatically, an effect that is further accentuated by measurement of the receding angle.

All of the above results refer to measurements where the water drop is injected onto the surface through the oil phase (Method 1). However, it is possible that the drop does not displace all of the oil present and a microscopic layer exists between the solid surface and the drop. In Method 2 the water drop is applied to the surface followed by

Figure 8.9

Hysteresis ($\Delta\theta$) of a water drop on clean or coated glass slides where $\Delta\theta = \theta_{ow}^{adv} - \theta_{ow}^{rec}$. [DMDCS] used for coating the glass slides was 0 M (circles), 1 x 10^{-5} M (triangles), 1 x 10^{-4} M (squares) and 0.05 M (diamonds).

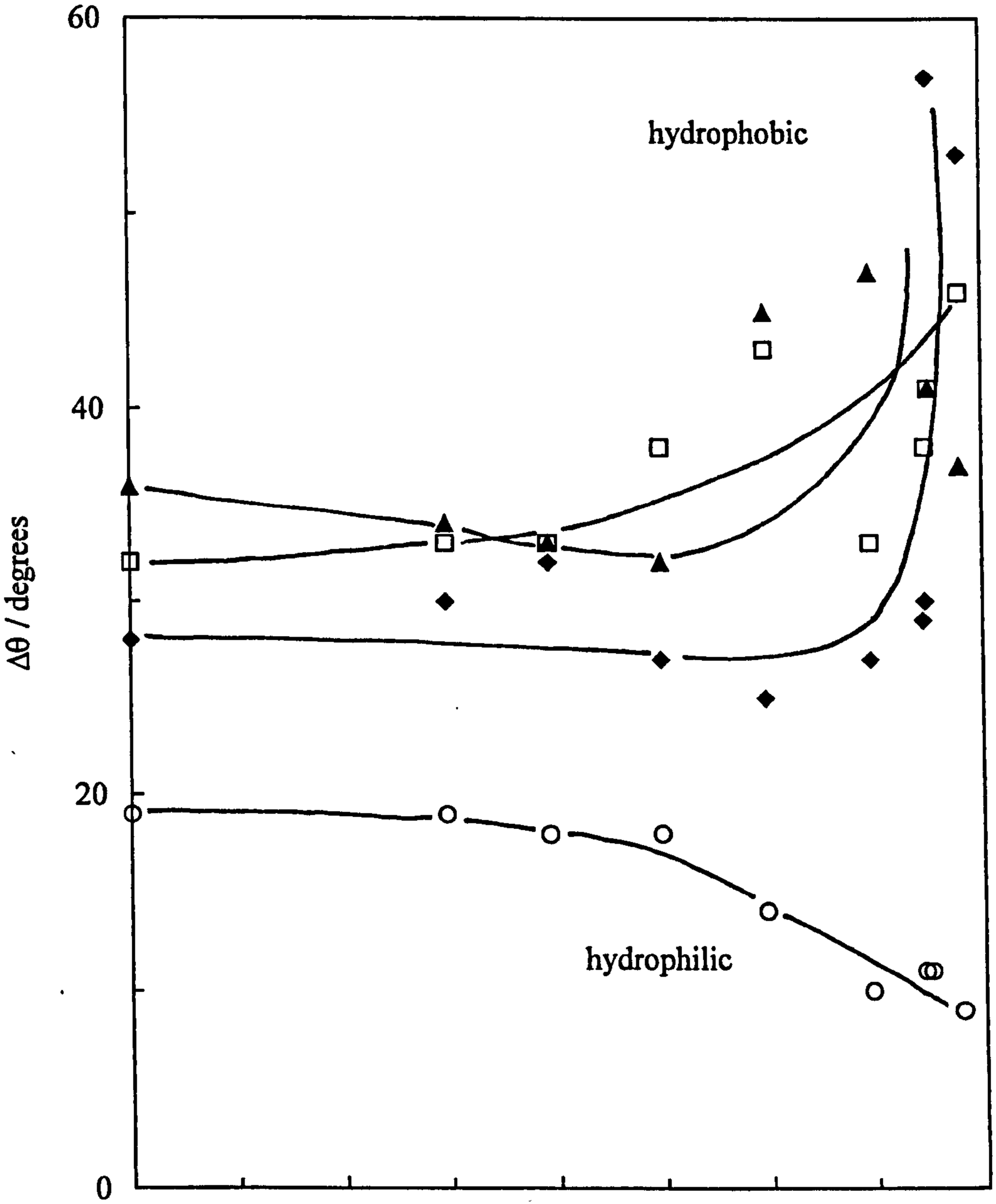

Figure 8.10

$\Delta\theta_{max}$ of a water drop on glass slides where $\Delta\theta_{max} = \theta_{ow}^{adv}$ (pH 6) – θ_{ow}^{rcc} (pH 13.8) as a function of [DMDCS] used to coat the surfaces.

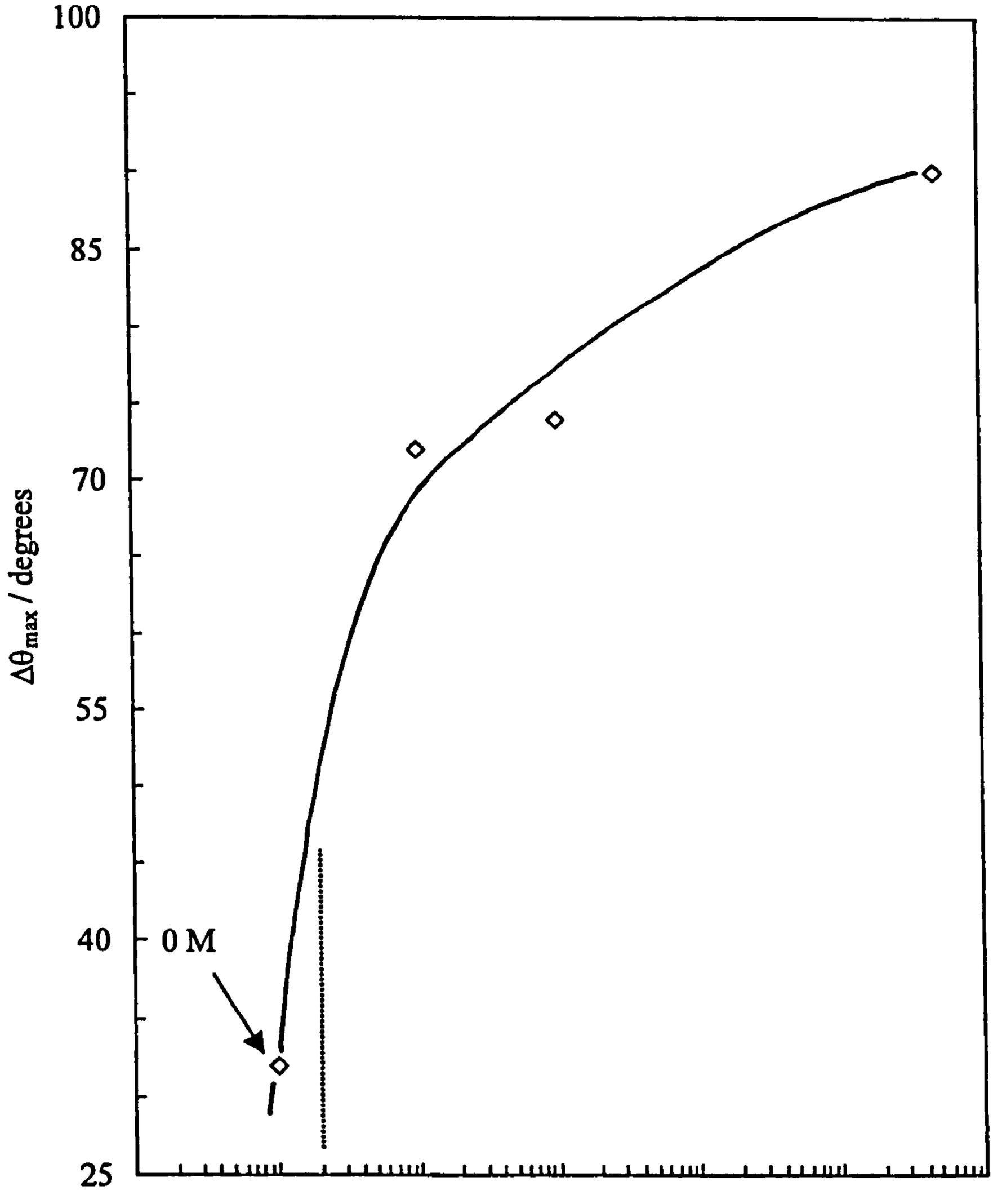

addition of oil. In Figure 8.11 the two methods are compared on a slide coated with 1 x 10^{-5} M DMDCS. The advancing and receding angles measured by Method 2 are equal and constant at ~60° within experimental error below pH 11, above which the advancing angle decreases to 40° by pH 13.8 and the receding angle falls to 20° at the same pH. There is less hysteresis by Method 2 because the drop has already wet the surface before addition of oil. In most cases the drop recedes back over a wetted surface on addition of oil so presumably the SiOH groups will have already dissociated. Reassuringly, the receding angles measured by both methods are virtually equal at all pH suggesting that either method can be used to determine the wettability of the surface.

Addition of electrolyte to the water drop is expected to influence the effect of pH on the wettability of a solid surface. Figure 8.12 shows the advancing and receding contact angles on a glass slide coated with 1 x 10^{-4} M DMDCS as a function of pH in the absence of NaCl (diamonds) and in 0.1 M NaCl (triangles). Within experimental error there is no effect of salt on the advancing or receding angle at all pH on glass slides of this hydrophobicity. However, when the concentration of DMDCS is lowered to 1 x 10^{-5} M the receding angle does show some dependence on [NaCl] although the advancing angle remains unaffected (Figure 8.13). For 0.1 M NaCl, θ_{ow}^{rec} goes through a maximum at intermediate pH before decreasing back in line with the angles measured in the absence of salt. This effect is highlighted in Figure 8.14 where the advancing and receding angles on a glass slide coated with 1 x 10^{-5} M DMDCS are plotted as a function of [NaCl] at pH 11. The advancing angle increases from 93° in the absence of salt to 105° in 1 M NaCl and the receding angle increases from 62° to 85° over the same salt concentration range, i.e. the surface becomes more hydrophobic on addition of salt.

8.5 Theory for effect of pH and [salt] on contact angles

A theoretical model to predict the contact angle of an aqueous drop under oil on a chargeable solid surface has been derived by Ettelaie.[161] The model estimates the contact angle of an aqueous drop on a solid surface as a function of pH in the presence of electrolyte by considering the three tensions in Young's equation

Figure 8.11

Advancing contact angle (diamonds) and receding angle (squares) of a water drop under toluene as a function of pH. [DMDCS] used for coating the glass was 1 x 10^{-5} M. Angles measured by Method 1 (oil first, then water) – filled points, or Method 2 (water first, then oil) – open points.

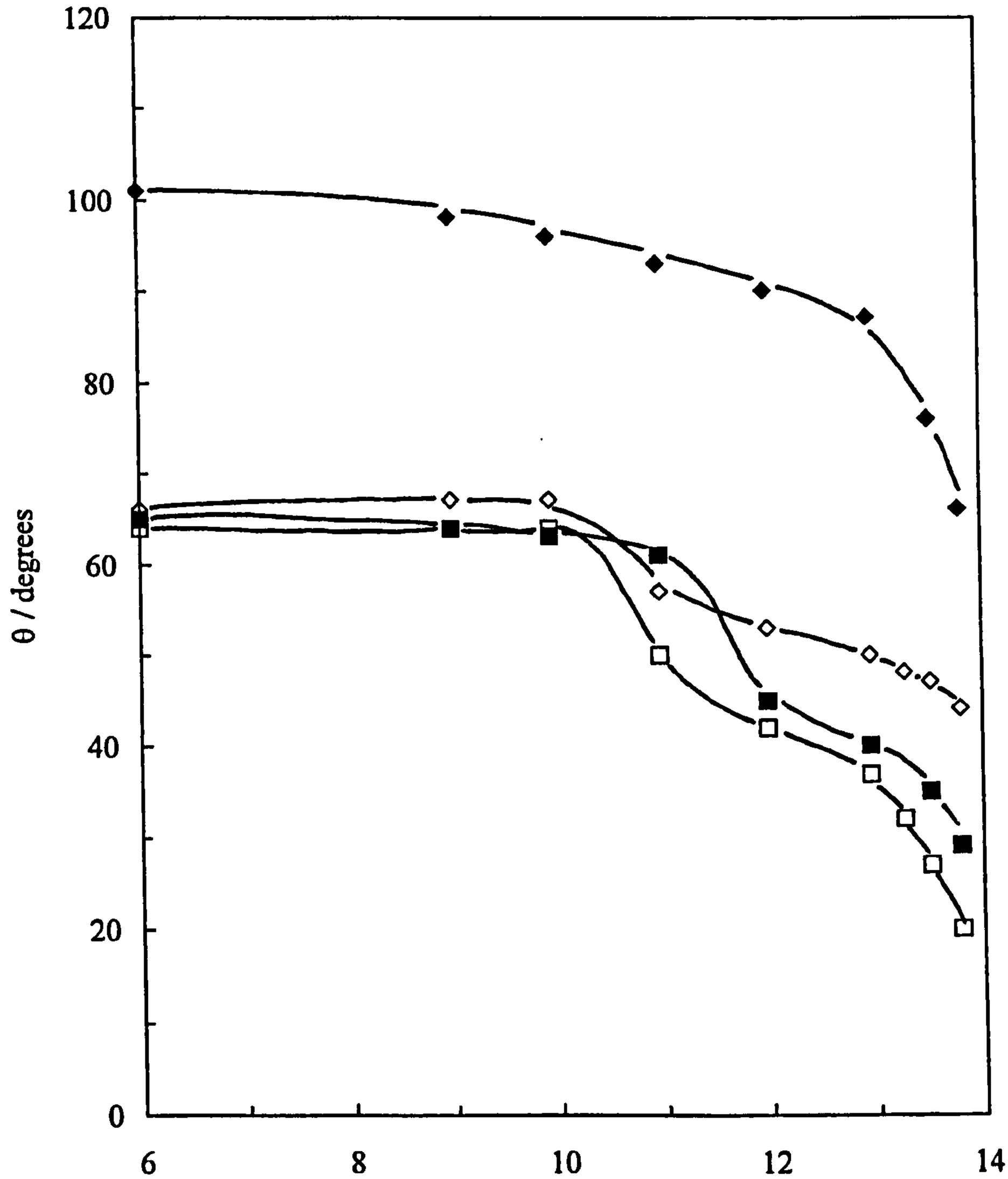

Figure 8.12

Advancing contact angle (open points) and receding angle (filled points) of an aqueous drop under toluene on a glass slide with 1 x 10^{-4} M DMDCS used as coating as a function of pH. Diamonds – 0 M NaCl, triangles – 0.1 M NaCl.

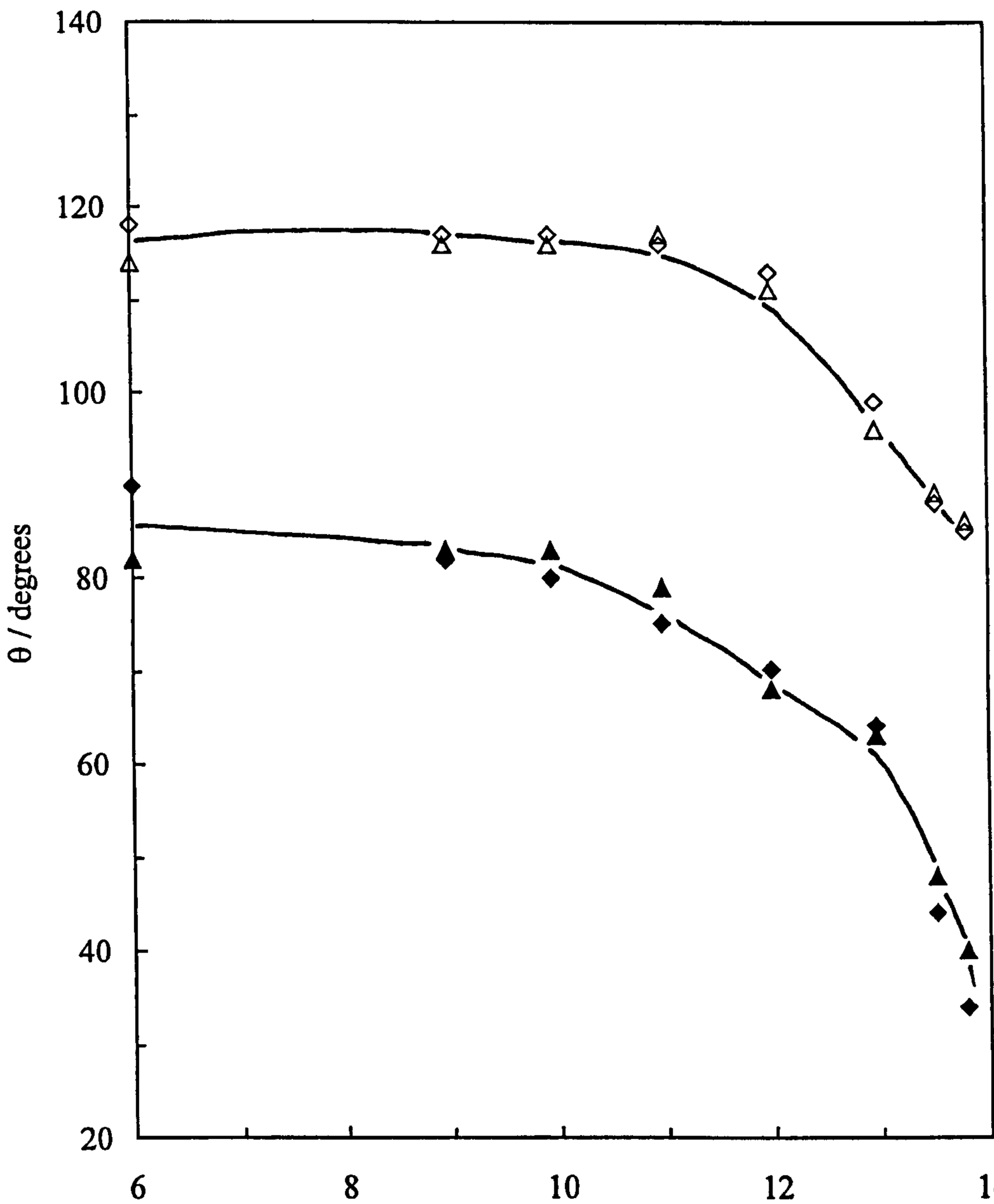

Figure 8.13

Advancing contact angle (open points) and receding angle (filled points) of an aqueous drop under toluene on a glass slide with 1 x 10^{-5} M DMDCS used as coating as a function of pH. Diamonds – 0 M NaCl, triangles – 0.1 M NaCl.

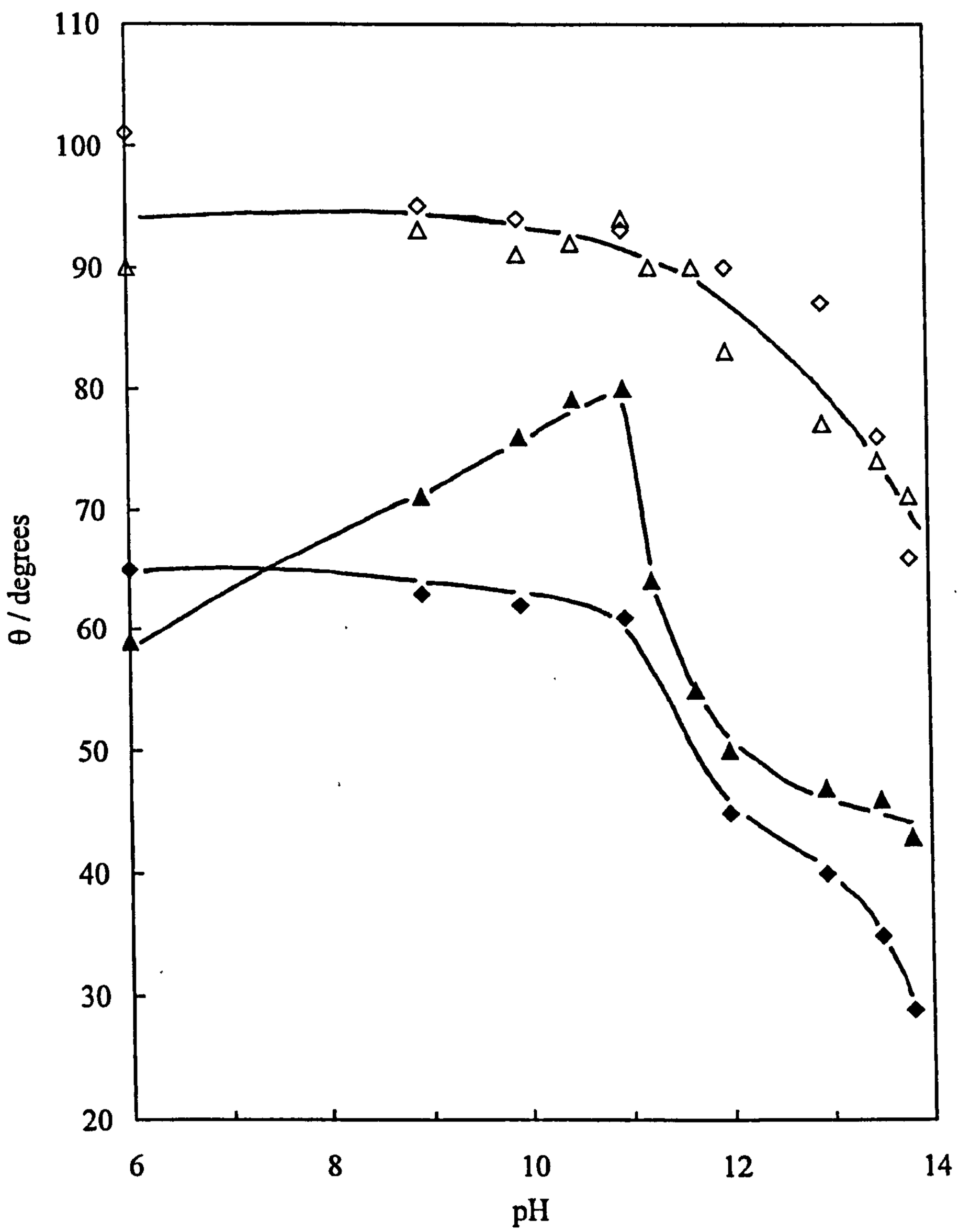

Figure 8.14

Advancing contact angle (open points) and receding angle (filled points) of an aqueous drop (pH 11) under toluene on a glass slide coated with 1 x 10^{-5} M DMDCS as a function of NaCl concentration.

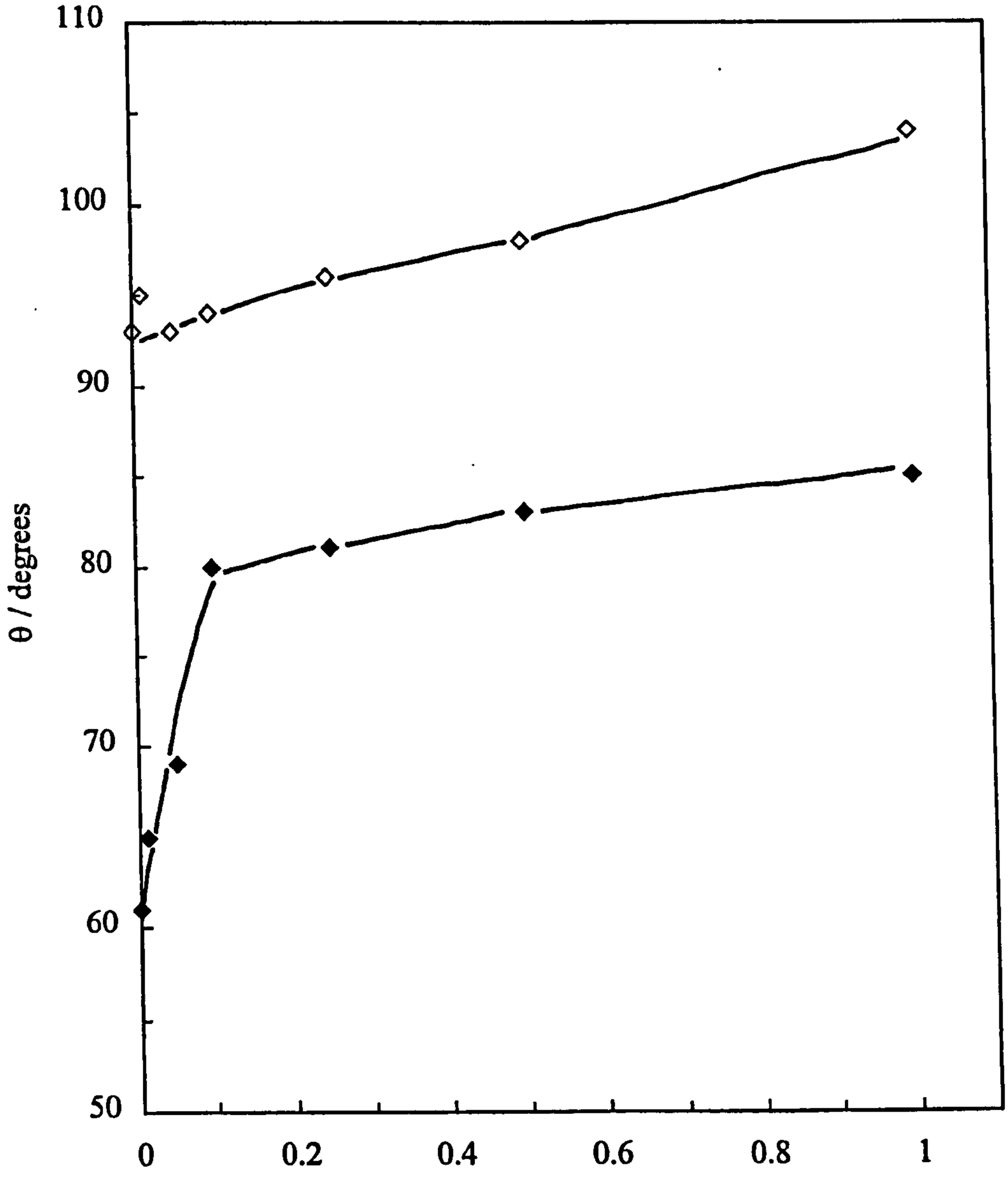

$$\cos\theta = \frac{\gamma_{os} - \gamma_{ws}}{\gamma_{ow}} \tag{8.1}$$

where the oil-water, oil-solid and water-solid interfacial energies are represented by γ_{ow}, γ_{os} and γ_{ws} respectively. The model assumes that there are no changes in the charge of the oil-water or oil-solid interface with pH or [salt]. The only interface responding to changes in pH or [salt] is the solid-water one, which leads to the formation of an electrostatic double layer at the interface. The free energy associated with the formation of this charge is accounted for by considering γ_{ws} as having two components. The first component is a short range interaction term (γ^{o}_{ws}), which is independent of charge and the second term is an electric double layer component (F_{el}) written

$$\gamma_{ws} = \gamma^{0}_{ws} + F_{el}(\psi_o) \tag{8.2}$$

where F_{el} depends on the surface potential ψ_o of the solid surface and in general is negative. Substituting equation 8.2 into 8.1 gives,

$$\cos\theta = \frac{\gamma_{os} - \gamma^{0}_{ws}}{\gamma_{ow}} - \frac{F_{el}}{\gamma_{ow}} = \cos\theta_0 - \frac{F_{el}}{\gamma_{ow}} \tag{8.3}$$

where θ_o represents the contact angle at conditions where the solid surface is uncharged (at the i.e.p.), where F_{el} is zero. The value of F_{el} depends on the nature of the surface as well as on the background electrolyte concentration and pH of the solution. For a constant potential surface F_{el} equals

$$F_{el} = -\frac{8n_o kT}{\kappa}\left[\cosh\left(\frac{e\psi_o}{2kT}\right) - 1\right] \tag{8.4}$$

where n_o is the bulk concentration of symmetric 1:1 electrolyte and κ is the inverse Debye length. Many oxide surfaces, however, are not constant potential surfaces and for these neither the surface charge nor the potential is fixed. Amphoteric surfaces can acquire charge through

$$OH_2^+ \leftrightarrow OH + H^+ \quad \text{below the i.e.p., dissociation constant } K_+$$

$$OH \leftrightarrow O^- + H^+ \quad \text{above the i.e.p., dissociation constant } K_-$$

For such surfaces Chan et al.[162, 163] have shown that the surface potential ψ_s and surface charge σ_s are related to each other by

$$\frac{\sigma_s}{eN_s} = \frac{\delta \sinh\left(\frac{e(\psi_N - \psi_o)}{kT}\right)}{1 + \delta \cosh\left(\frac{e(\psi_N - \psi_o)}{kT}\right)} \tag{8.5}$$

where ψ_N is the Nernst potential and N_s is the number of ionisable OH groups on the surface, and

$$\delta = 2\sqrt{\frac{K_-}{K_+}} = 2\left(10^{-\Delta pK/2}\right) \tag{8.6}$$

where ΔpK equals $pK_- - pK_+$. The Nernst potential for a bulk pH of pH_b and a surface with i.e.p. of pH_o is given by

$$\psi_N = 2.303\frac{kT}{e}(pH_o - pH_b) \tag{8.7}$$

Silica, for example, has $pH_o \sim 2$ and $\Delta pK \sim 6$, whereas alumina has $pH_o \sim 9$ and $\Delta pK \sim 4$. Equation 8.5 has two unknowns, σ_s and ψ_o, which can be solved using a second relation. The Poisson-Boltzmann equation for a single isolated surface is

$$\sigma_s = \frac{2kT\varepsilon}{e}\kappa \sinh\left(\frac{e\psi_o}{2kT}\right) \tag{8.8}$$

Equations 8.5 and 8.8 are simultaneous equations which can be solved numerically to obtain the surface charge and potential for any given electrolyte concentration and bulk

pH value. The free energy associated with the formation of the double layer (F_{el}) can then be determined using equation 8.4 for constant surface potential. For a charge regulating surface however, F_{el} has the form[164, 165]

$$F_{el} = -\frac{8n_o kT}{\kappa}\left[\cosh\left(\frac{e\psi_o}{2kT}\right)-1\right]+kTN_s \ln\left[\frac{1+\delta}{1+\delta\cosh\left(\frac{e\psi_N-\psi_o}{kT}\right)}\right] \qquad (8.9)$$

Thus F_{el} is calculated using equation 8.9 and the contact angle for any pH and electrolyte concentration is calculated using equation 8.3. Since F_{el} is invariably negative, it is predicted that the presence of a surface charge reduces the contact angle from its value at the i.e.p. (θ_o). In other words, particles at the oil-water interface will become more hydrophilic and prefer to reside in the aqueous phase as seen experimentally in § 8.2.

Figures 8.15 and 8.16 are plots of contact angle at the oil-water interface versus pH calculated using the above model. The hydrophobicity of the surface at the i.e.p. (θ_o at pH 2) is varied in Figure 8.15 which is akin to varying the number of silanol groups on silica surfaces (Figure 8.8). The contact angle remains virtually constant below pH 9 for $\theta_o \geq 50°$, whereupon it decreases continuously to pH 13.8 to a value dependent on the initial θ_o. The contact angle decreases to zero at pH 7, 11 and 13 for θ_o equal to 10, 50 and 90° respectively. The experimental contact angles shown in Figure 8.8 do not decrease to zero at any pH for similar initial contact angles however. The theoretical plots show ideal behaviour and in reality obtaining contact angles of zero is very difficult due to contaminated surfaces.

Figure 8.14 shows the experimental values of the contact angle increasing with salt concentration at pH 11. For a θ_o of 65° the theoretical plot in Figure 8.16 shows the effect of electrolyte concentration on the contact angle. The curves are shifted to lower pH as the concentration of NaCl is increased, i.e. at fixed pH, addition of salt is predicted to lower the contact angle, contrary to experiment. This suggests an inadequacy of the model which neglects charging of the oil-water interface, although this has been shown to be important when calculating the contact angle.[166] The theoretical model shows that the free energy is proportional to the surface potential (equation 8.2). On increasing the pH, ψ_s becomes increasingly negative[85] but on

Figure 8.15

Theoretical plot showing the effect of pH on the contact angle of an aqueous drop (1 x 10^{-5} M NaCl) under toluene (γ_{ow} = 36 mN m^{-1}) on a solid surface of varying hydrophobicity (θ_o, given).

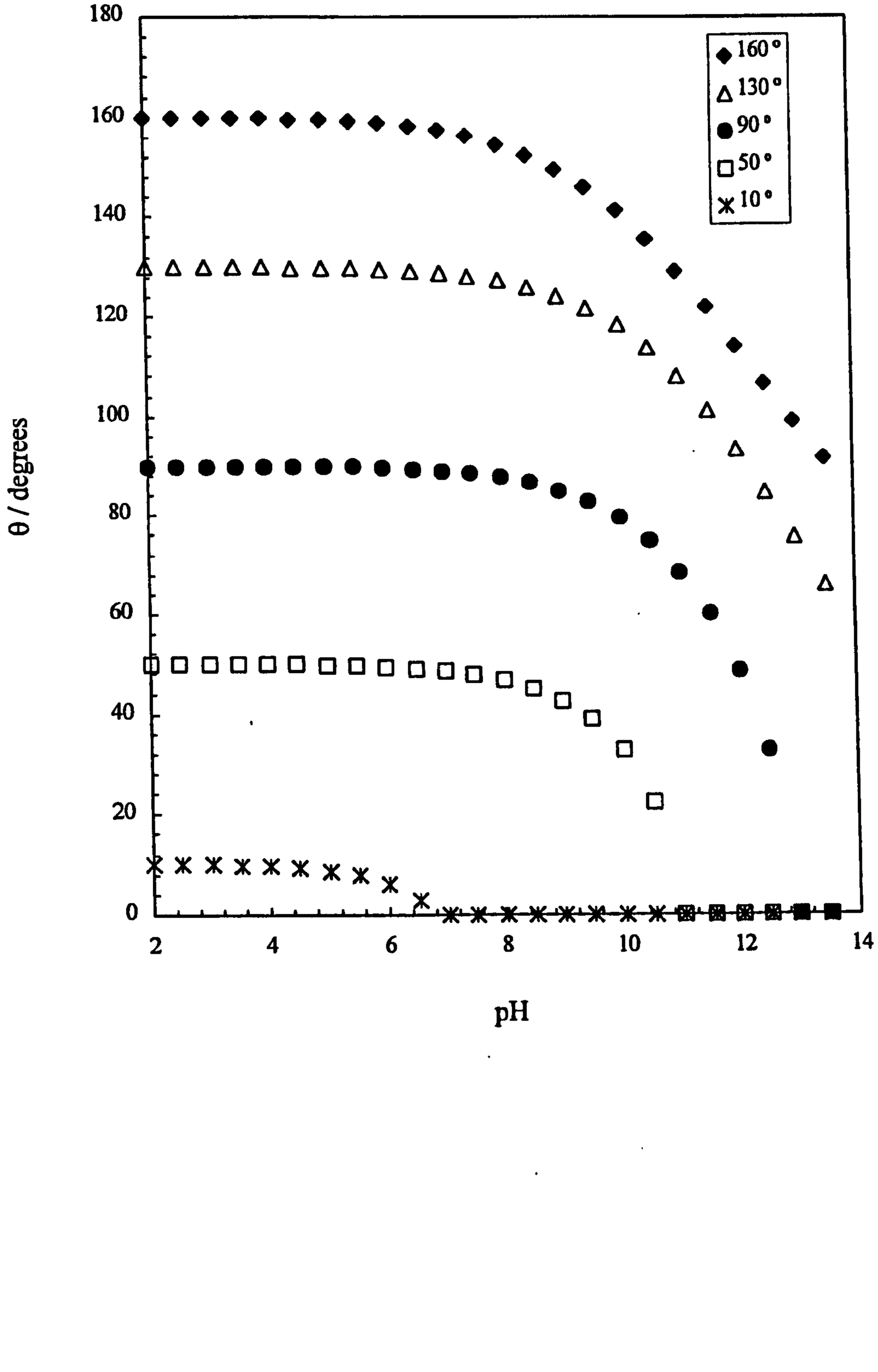

Figure 8.16

Theoretical plot showing the effect of NaCl concentration (given) on the contact angle of an aqueous drop under toluene (γ_{ow} = 36 mN m^{-1}) on a silica surface of θ_o = 65°.

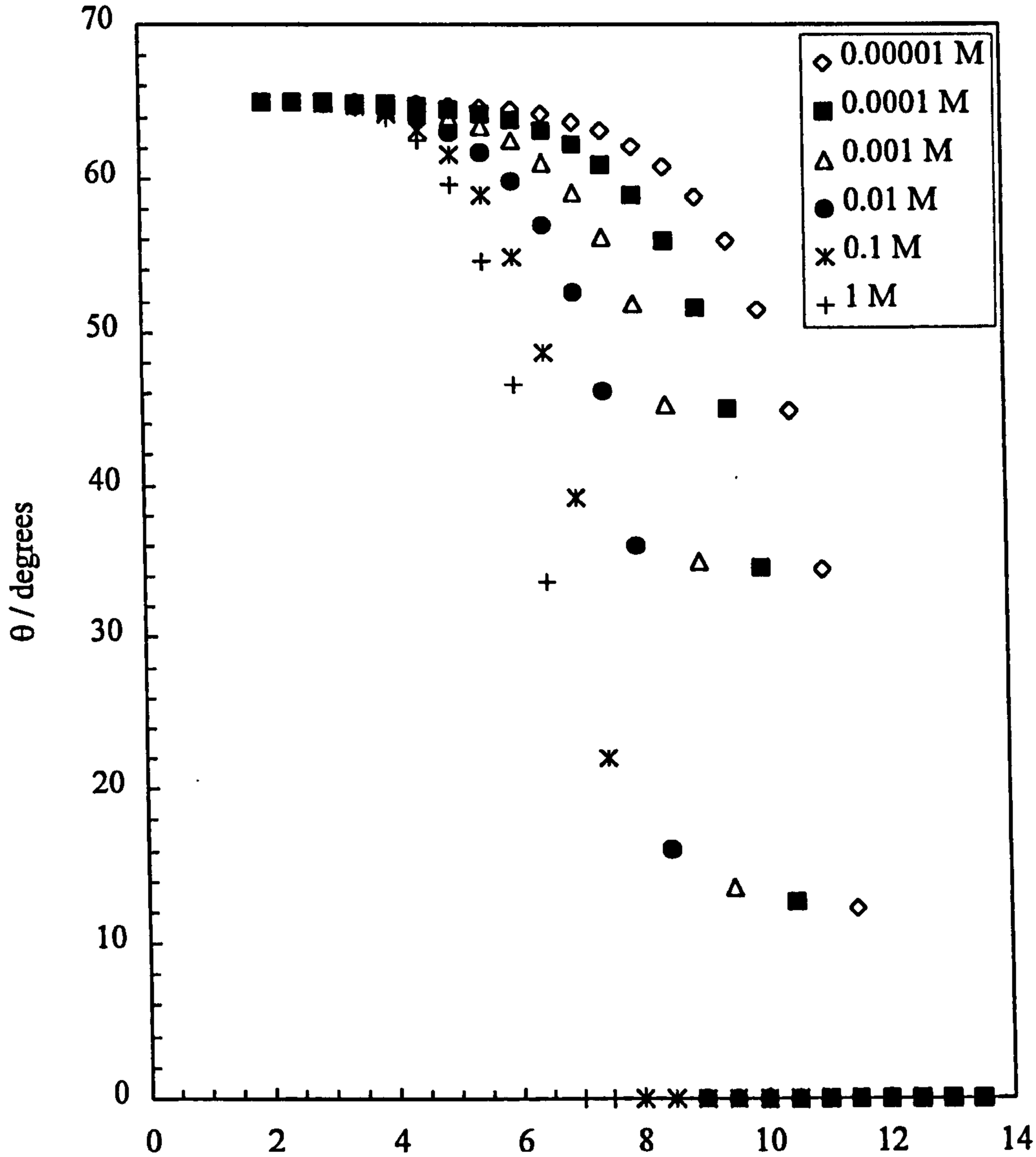

addition of electrolyte the charge is screened and ψ_s becomes more positive at fixed pH. Hence F_{el} becomes more positive with increasing electrolyte resulting in a decrease in $\cos\theta$ (equation 8.3) and an increase in θ at fixed pH. The model is currently being revised to include charging of the oil-water interface and will be described in a future publication.[167]

8.6 Other systems involving particles at interfaces

The effects of pH on the wettability of solid surfaces described in this chapter have important consequences for the behaviour of a whole range of systems involving particles which rely on them being hydrophobic at either air-water or oil-water interfaces. In this section three systems are described in which particles are thought to operate in different ways and a new explanation is offered for the observed effects. The three systems are the stability of water-in-crude-oil emulsions,[168] the flotation of solid particles[169] and the antifoam effect of particles in aqueous foams.[170] Figure 8.17 shows the stability after 24 hours of 80 wt.% water-in-Guanipa crude oil emulsions as a function of pH taken from ref. 168. Indigenous materials present in the crude oil were asphaltenes which acted as the emulsifier. Importantly, however, the presence of sand particles in oil was established from IR spectra since strong absorption bands from Si-OH and Si-O^- groups were present. These silica particles also adsorb at the oil-water interface of the emulsion drops. The emulsions are completely stable to coalescence below pH 10, above which the emulsions become completely unstable. The original authors proposed that the destabilisation at high pH was due to adsorption of hydroxyl anions onto the surfaces of silica particle flocs, resulting in their redispersion. In the light of the current work described in this chapter, it is suggested that the w/o emulsions formed at low pH are partially stabilised by the interfacially-active hydrophobic silica particles. As the pH is increased, the silanol groups dissociate into SiO^- rendering the particles more hydrophilic thus enhancing the possibility of coalescence of water drops. In other words, the charged particles are no longer effective at stabilising w/o emulsions due to their reduced strength of attachment to the interface and their preference to stabilise o/w emulsions.

Figure 8.17

Percentage coalescence after 24 hours at room temperature versus initial pH in water for 80 wt.% water-in-crude oil emulsions stabilised partly by silica particles. Redrawn from ref. 168.

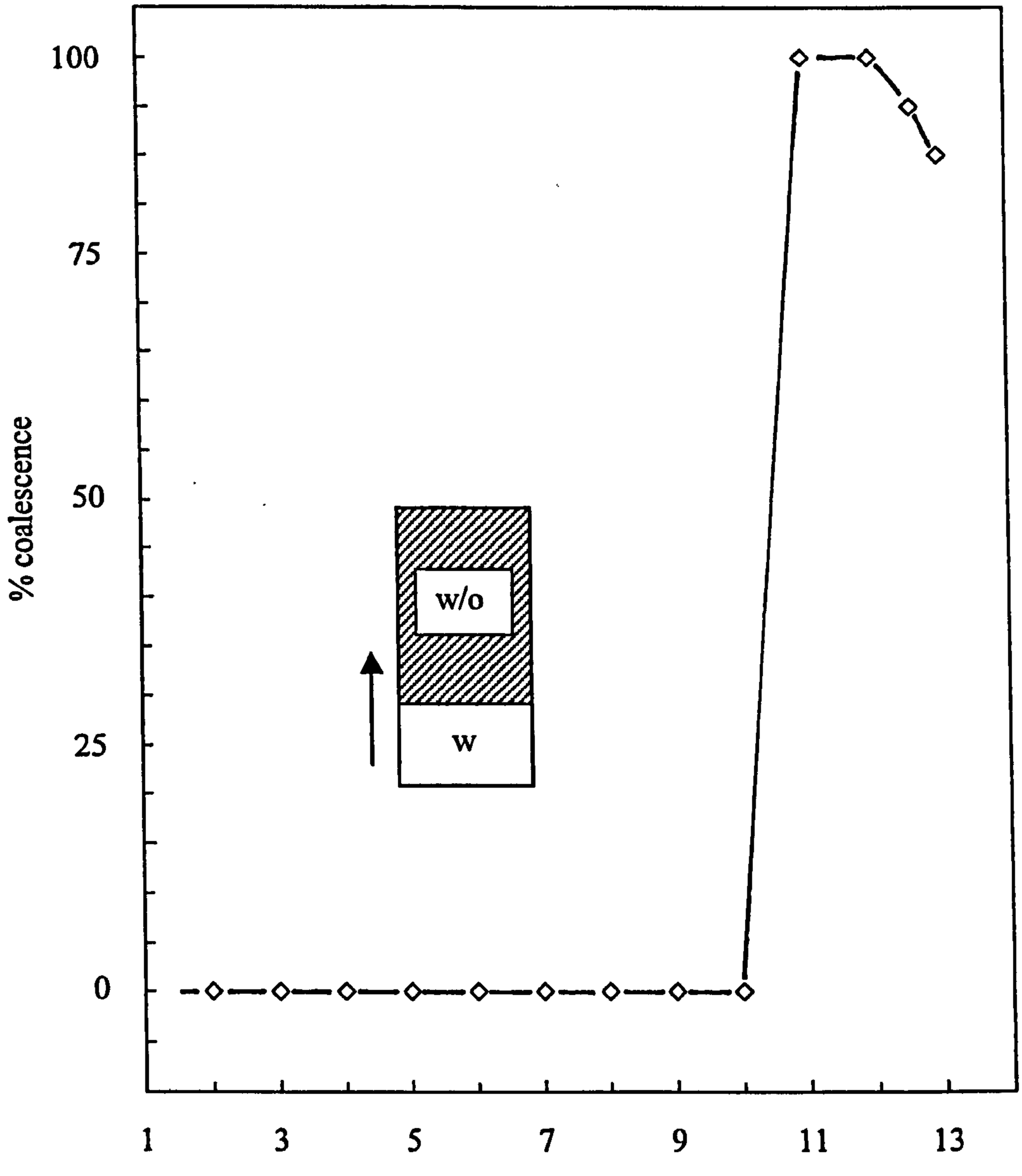

The second example is concerned with flotation. In this process, pulverised ore particles are rendered hydrophobic by addition of surface-active materials (collectors) so that, on aeration of an aqueous slurry of particles, the particles attach themselves to air bubbles and rise to the surface. Laskowski and Iskra[169] measured the flotation of ground quartz which had been partially hydrophobised using trimethylchlorosilane (Figure 8.18). At low pH the flotation was greater than 95 % but fell rapidly to less than 10 % at pH 11. The contact angle of a water drop in air on a partially hydrophobic vitreous silica plate decreased from around 75 to 25° between pH 4 and 12. Again, an increase in pH results in charging of the surface, making them more water wettable (lower θ) and reducing the probability of attachment of particles to non-polar air bubbles.

The third example concerns the effectiveness of antifoams. Commercial antifoams for aqueous foams stabilised by surfactants are either hydrophobic solid particles alone or similar particles dispersed in an oil.[171] In the first case, the so-called bridging-dewetting mechanism is thought to operate. Consider a spherical particle resting in one surface of an air-water-air foam film of thickness comparable to the particle diameter (inset of Fig. 8.19). As the film thins through drainage, the opposite surfaces of the film will ultimately engage the particle. If the contact angle through the water phase is > 90° (i.e. particles are hydrophobic), a curved meniscus is formed such that the Laplace pressure so generated will force liquid away from the particle, enhancing film drainage (arrow). The film ruptures when the two three-phase contact lines meet. Experiments using glass beads of various hydrophobicity showed that contact angles of around 93° were required to give effective breakdown of cationic surfactant-stabilised foams. Below this angle, particles either stabilised foams or had no effect.[170]

As shown earlier, SLM 081 particles become more wettable by water at high pH. Hence, if such particles are effective antifoams at low pH where they are hydrophobic, they should be ineffective at high pH where they are more hydrophilic. This is shown to be the case in Figure 8.19 for foams stabilised by the anionic surfactant SDS. This surfactant was chosen at a concentration above its c.m.c. so that no ambiguities arise from adsorption of surfactant onto the charged particle surfaces. In the absence of particles the foam volume is constant at approximately 105 cm^3 up to pH 13, after which it falls slightly to 95 cm^3. The decrease is likely to be due to an ionic strength effect screening the repulsions between surfactant anions thus destabilising the foam. In the

Figure 8.18

Percentage flotation (left-hand ordinate) of partially hydrophobic quartz powder in 0.5 N KCl as a function of initial pH in water. The right hand ordinate represents the contact angle of water drops in air resting on a partially hydrophobic vitreous silica substrate. Redrawn from ref. 169.

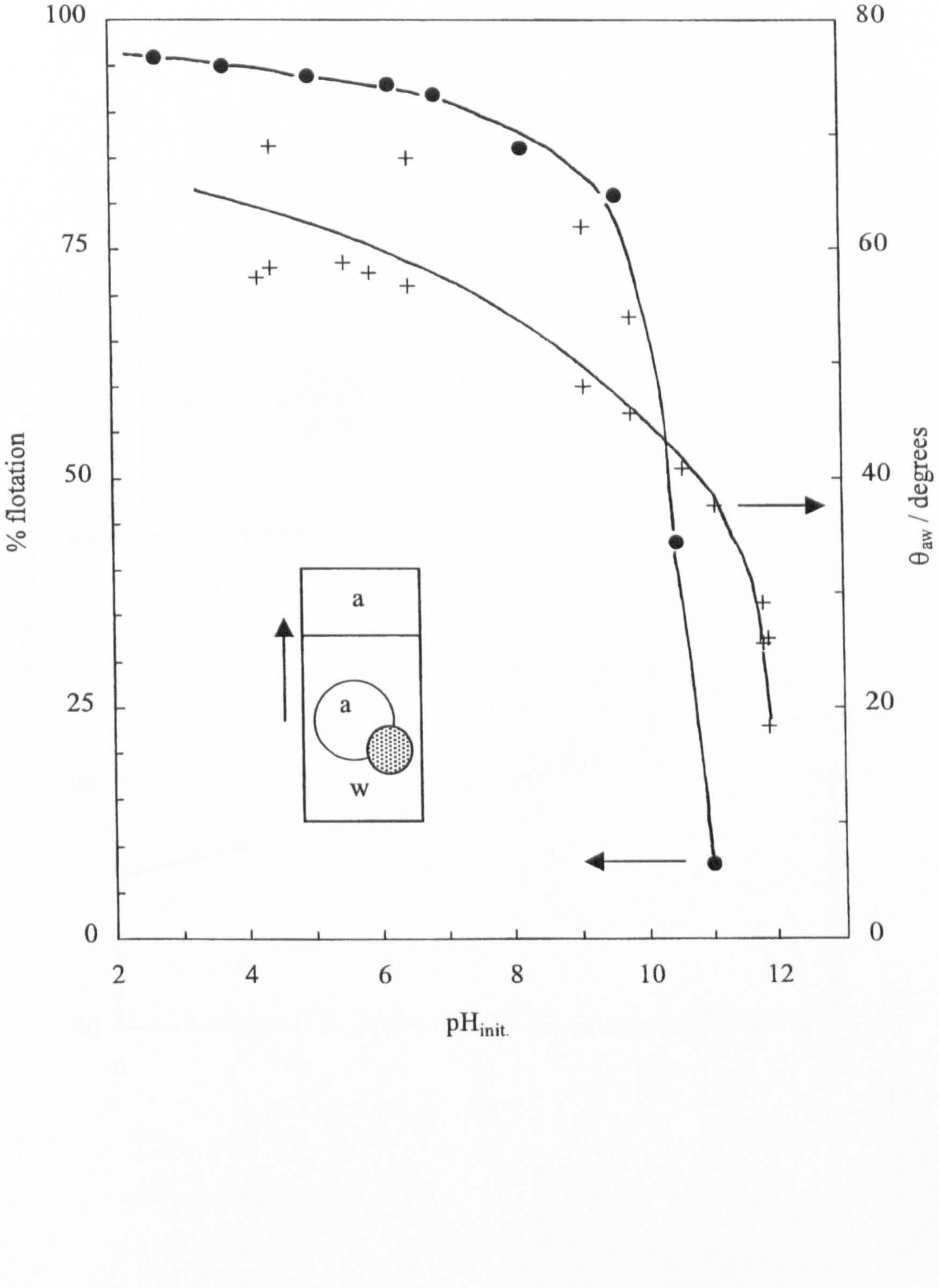

Figure 8.19

Initial foam volume of 10 cm^3 of 0.01 M SDS solutions versus initial pH in the absence (diamonds) and in the presence (squares) of antifoam. The antifoam was 30 mg of SLM 081 silica particles and was added prior to foam formation.

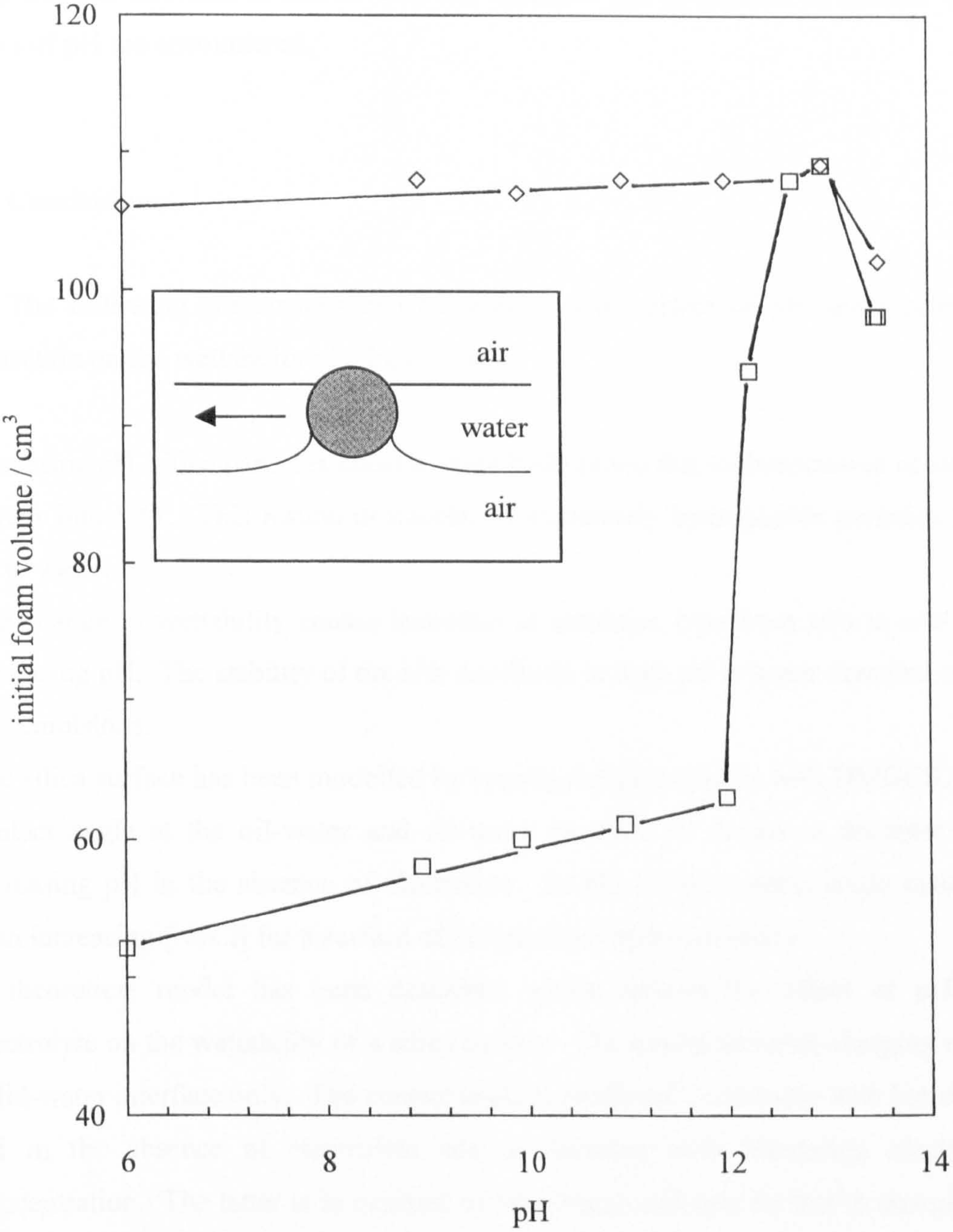

presence of particles, the powdered solid was added to the aqueous surfactant solution and gently swirled before foam formation. As a result the particle size in solution was expected to be large (~50 μm). In this case, the foam volume was reduced by over a factor of 2 to 50 cm^3 at low pH, but the original foam volume is gradually recovered by pH 12.6, above which it follows the curve without particles. The anti foaming effect of the initially hydrophobic particles is lost when the particles become charged, which is effected *in situ* here by an increase in pH. Such behaviour may be part of the reason why a particular antifoam is effective in one situation but ineffective in another when extremes of pH are encountered.

8.7 Conclusions

The following conclusions can be drawn on the effect of pH and electrolyte concentration on the wettability of silica surfaces:

- Increasing pH, silica particles become more hydrophilic due to dissociation of silanol groups into SiO^-. This results in transfer of moderately hydrophobic particles from oil to water.
- The change in wettability causes inversion of emulsion type from w/o to o/w with increasing pH. The stability of the o/w emulsions at high pH is lower than that of the w/o emulsions.
- The silica surface has been modelled by coating flat glass plates with DMDCS. The contact angle at the oil-water and air-water interface is shown to decrease with increasing pH in the absence of electrolyte. At pH 11 the contact angle increases with increasing [NaCl] for a surface of intermediate hydrophobicity.
- A theoretical model has been described which models the effect of pH and electrolyte on the wettability of a silica surface. The model assumes charging of the solid-water interface only. The contact angle is predicted to decrease with increasing pH in the absence of electrolyte and to decrease with increasing electrolyte concentration. The latter is in contrast to experiment and may be due to charging of the oil-water interface being neglected.
- As a result of the experimental findings a different explanation has been proposed for a number of diverse effects involving particle wettability with respect to pH.

CHAPTER 9

CHAPTER 9

SURFACTANT ADSORPTION AT PIGMENT-FLUID AND FLUID-FLUID INTERFACES

9.1 Introduction

The process of pigment flushing is described in detail in § 1.1.2. In short it involves the transfer of pigment particles, that have been precipitated in the aqueous phase, to a non-aqueous phase. The transfer of particles is often facilitated by the use of surfactants, which affect the wettability of the particles by both phases. In the previous chapter the wettability of silica particles was varied *in situ* by changing the pH of the aqueous phase. The initially hydrophobic surface became more hydrophilic at high pH due to dissociation of the silanol groups. The wettability of a solid surface can also be modified by adsorption of surfactant.[20, 22 – 24, 26, 28] The contact angle, θ, that a drop of surfactant solution makes on a flat solid surface provides information on the wettability of the pigment which can be used to improve the efficiency of the flushing process. In order to measure the contact angle on the micrometer-sized pigment particles the powder was compressed into discs using a Perkin Elmer KBr press, a technique that couldn't be used for the silica particles due to their light, fluffy nature. When a drop of surfactant solution is placed on a solid disc it will either spread or remain as a drop on the surface. The contact angle is a function of three tensions, γ, as shown by Young's equation[172] (for an oil-water system),

$$\cos\theta = \frac{\gamma_{so} - \gamma_{sw}}{\gamma_{ow}} \qquad (9.1)$$

where the subscripts s, o and w refer to solid, oil and water, respectively.

Interfacial tensions of an aqueous drop on a solid surface under oil

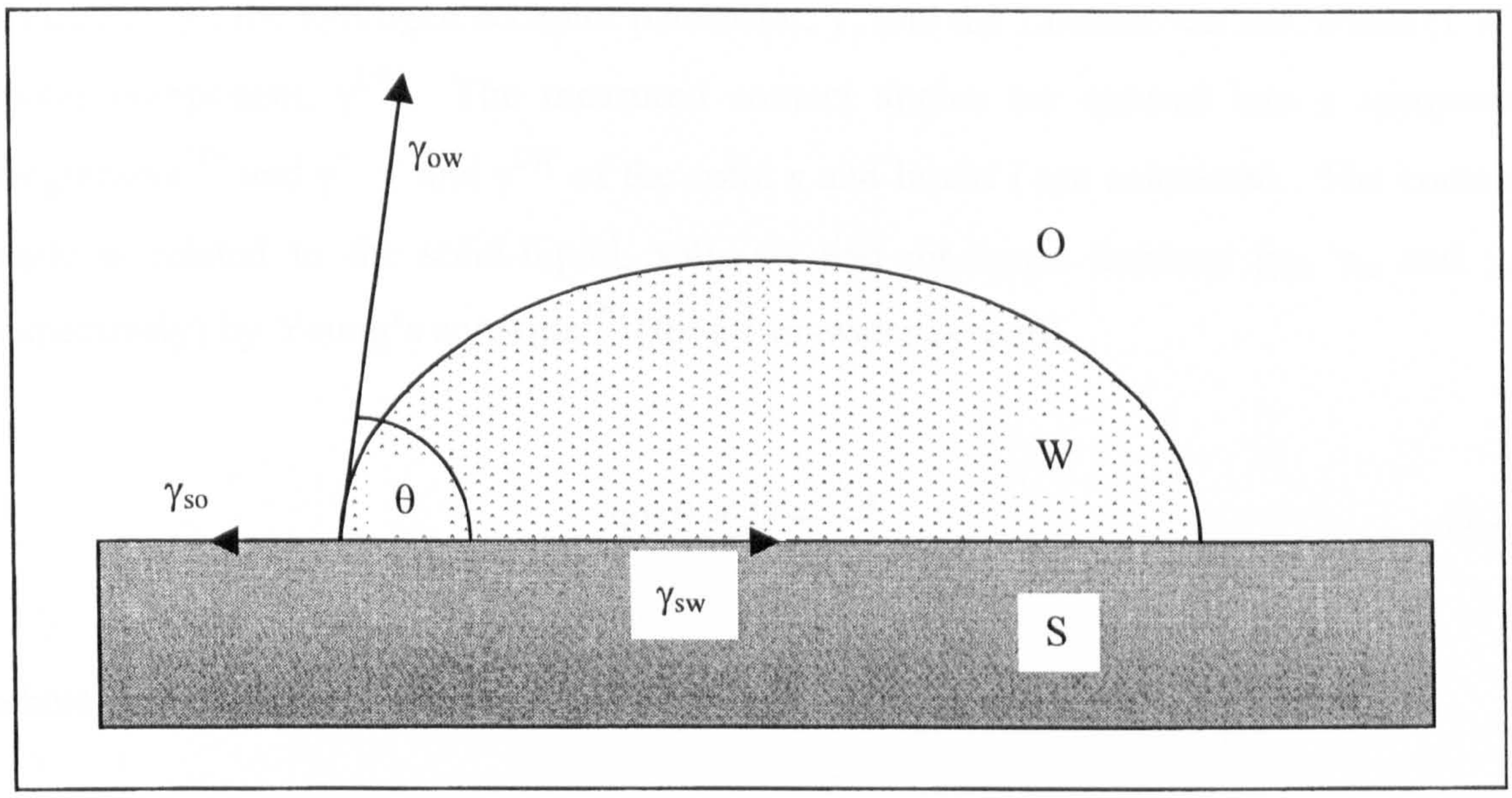

The tensions are affected by adsorption of surfactant at the various interfaces; the extent of adsorption at the three interfaces determines the wettability of the solid by the surfactant solution. Measurements of γ_{ow} (and γ_{aw}) have been carried out but γ_{so} and γ_{sw} cannot be measured directly. However, the concentration of surfactant at the solid-water interface is estimated in § 9.3 using an approach of Lucassen-Reynders[173] assuming no adsorption at the solid-oil (or solid-air) interface.

In this Chapter the wettability of two organic pigments by anionic, cationic and non-ionic surfactant solutions has been investigated at oil-water and air-water interfaces. The two pigments, Hansa yellow and phthalocyanine blue B, are often used in the paint industry due to their low cost and superior colouring ability. The wettability is shown to be dependent on the concentration and type of surfactant used. The surface energy of the pigments has been characterised using a treatment derived by van Oss et al.[174]

9.2 Characterisation of pigment surfaces by van Oss et al.[174] treatment

It is possible to estimate the surface energy of the pigments by applying a treatment developed by van Oss et al.[174] The polar and apolar parameters of the surface energy were described in Chapter 3.3 and can be estimated by measuring the contact angle of various probe liquids on the solid surface. The surface tension of the probe

liquids and the contact angle on the solid are used to determine the hydrogen donor parameter, γ^+, the hydrogen acceptor parameter, γ^-, and the Lifshitz-van der Waals (LW) apolar component, γ^{LW}. The measured contact angles are entered into a computer programme[175] and γ^+, γ^- and γ^{LW} of the solid *s* and liquid *l* are calculated. The contact angle is related to the solid-liquid, solid-air and air-liquid tensions (γ_{sl}, γ_{sa} and γ_{al} respectively) by Young's equation[172] (for an air-water system),

$$\cos\theta = \frac{\gamma_{sa} - \gamma_{sl}}{\gamma_{al}} \tag{9.2}$$

where the tensions are equal to

$$\gamma_{sa} = \gamma_s^{LW} + 2\sqrt{\gamma_s^+ \cdot \gamma_s^-} \tag{9.3}$$

$$\gamma_{sl} = \left(\sqrt{\gamma_s^{LW}} - \sqrt{\gamma_l^{LW}}\right)^2 + \left(2\sqrt{\gamma_s^+ \cdot \gamma_s^-}\right) + \left(\sqrt{\gamma_l^+ \cdot \gamma_l^-}\right) - \left(\sqrt{\gamma_s^+ \cdot \gamma_l^-}\right) - \left(\sqrt{\gamma_s^- \cdot \gamma_l^+}\right) \tag{9.4}$$

$$\gamma_{al} = \gamma_l^{LW} + 2\sqrt{\gamma_l^+ \cdot \gamma_l^-} \tag{9.5}$$

Two of the probe liquids were polar (water and ethylene glycol) and three of them were apolar (squalane, bromonaphthalene and diiodomethane). The measured contact angles on Hansa yellow and phthalocyanine blue B pigments are given in Table 9.1 along with the calculated components of the surface energy. The calculations indicate that neither pigment has a measurable hydrogen donor parameter but phthalocyanine blue B has greater apolar and hydrogen acceptor components than Hansa yellow. The goodness of fit for γ_s^+ and γ_s^- is given in Figures 9.1 and 9.2. The reasonably flat peak on both figures suggests the parameters are not very well defined. The use of additional probe liquids may have resulted in a higher resolution although the heterogeneity of the surface (see later) may prevent any improvement.

Figure 9.1

Goodness of fit plots for the hydrogen donor (γ_s^+) and hydrogen acceptor (γ_s^-) parameters for Hansa yellow pigment calculated from van Oss et al. treatment.[174]

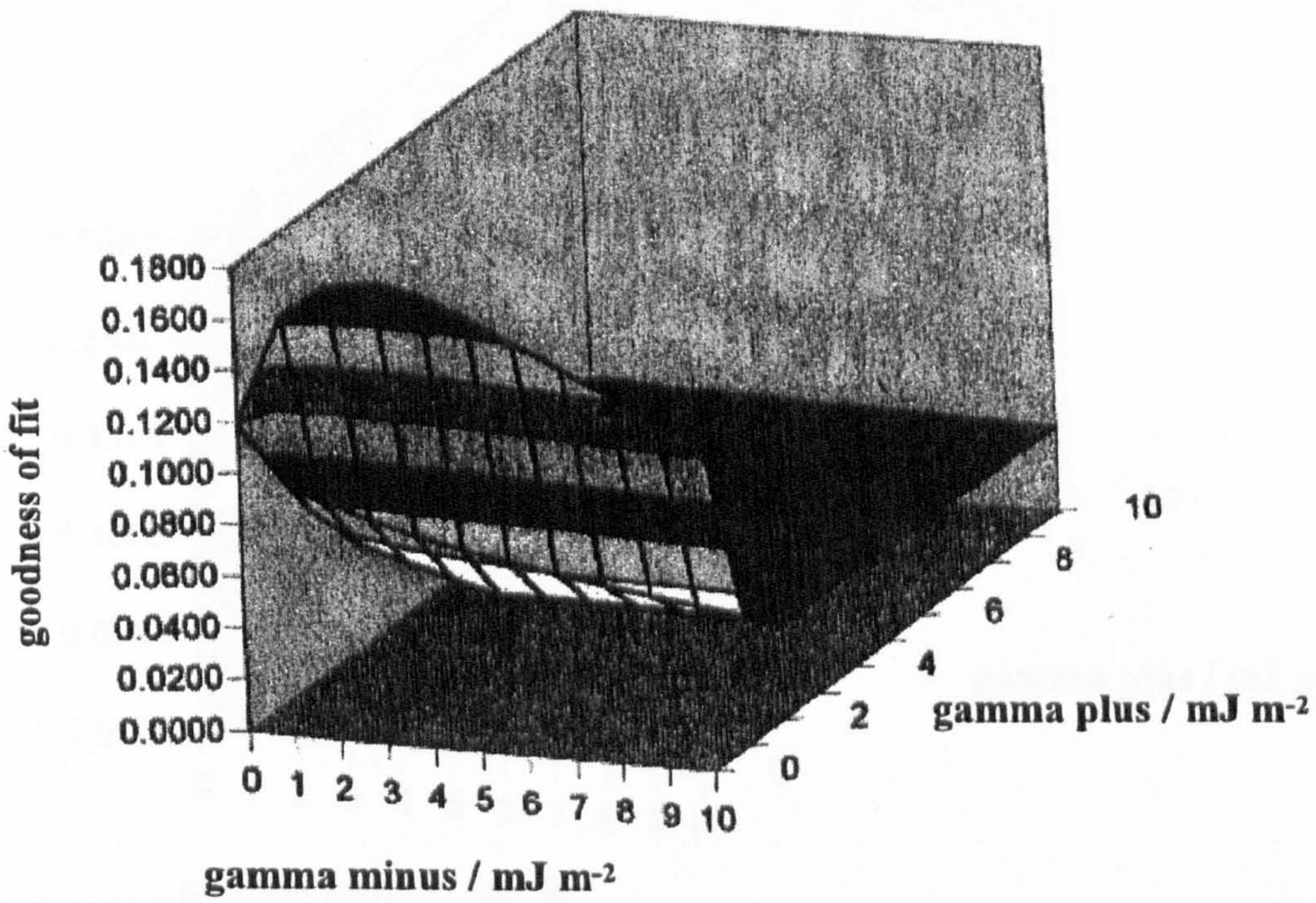

Figure 9.2

Goodness of fit plots for the hydrogen donor (γ_s^+) and hydrogen acceptor (γ_s^-) parameters for phthalocyanine blue B pigment calculated from van Oss et al. treatment.[174]

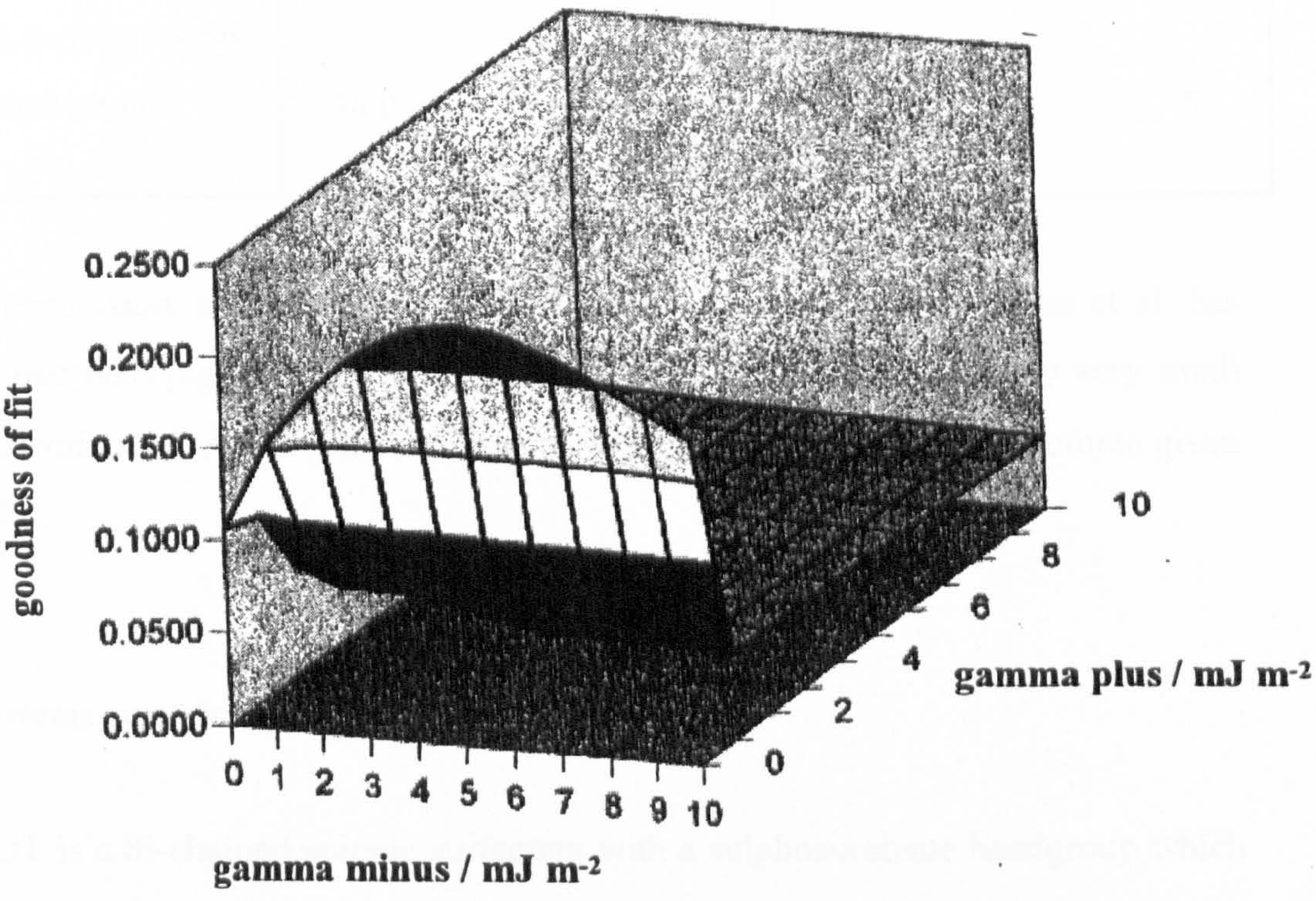

Table 9.1 Contact angles of probe liquids on pigment discs in air and calculated components of their surface energy (mJ m^{-2})

Probe Liquid	Hansa yellow			Phthalocyanine blue B		
	θ / °			θ / °		
water	81			75		
ethylene glycol	62			49		
squalane	4			3		
bromonaphthalene	9			9		
diiodomethane	21			12		
calculated surface energy components	γ_s^{LW}	γ_s^+	γ_s^-	γ_s^{LW}	γ_s^+	γ_s^-
	44.0	0	3	49.7	0	5

In conclusion, analysis of the surface using the treatment of van Oss et al. has confirmed that both pigments are largely hydrophobic (large γ_s^{LW}) with only very small polar characteristics (γ_s^+ and γ_s^-). This was to be expected knowing the structures given in Figure 2.3.

9.3 Systems containing AOT surfactant

AOT is a di-chained anionic surfactant with a sulphosuccinate headgroup which is readily dissolved in water. It is often used, alongside other surfactants, to improve the flushing efficiency of pigments from water to the oil phase. A greater understanding of the wettability of pigments in the presence of this surfactant will increase understanding of the flushing process. The three tensions in equation 9.1 are dependent on the extent of surfactant adsorption at the respective interfaces. Estimates of surfactant adsorption can be made using an approach of Lucassen-Reynders.[173] Differentiating equation 9.1 with respect to γ_{ow} gives,

$$\frac{d(\gamma_{ow}\cos\theta)}{d\gamma_{ow}} = \frac{d\gamma_{so}}{d\gamma_{ow}} - \frac{d\gamma_{sw}}{d\gamma_{ow}} \qquad (9.6)$$

The Gibbs equation gives the surface excess concentration, Γ, of surfactant (concentration c) at the various interfaces *i* in the system,

$$-\frac{d\gamma}{d\ln c} = \Gamma_i\, RT \qquad (9.7)$$

Combination of equations 9.6 and 9.7 gives,

$$\frac{d(\gamma_{ow}\cos\theta)}{d\gamma_{ow}} = \frac{(\Gamma_{so} - \Gamma_{sw})}{\Gamma_{ow}} \qquad (9.8)$$

Assuming that adsorption of surfactant at the planar solid-oil (or solid-air) interface is zero,

$$\frac{d(\gamma_{ow}\cos\theta)}{d\gamma_{ow}} = -\frac{\Gamma_{sw}}{\Gamma_{ow}} \qquad (9.9)$$

i.e. a plot of $\gamma_{ow}\cos\theta$ versus γ_{ow} gives the ratio of adsorption of surfactant at the solid-water and oil-water interfaces.

(a) Hansa yellow pigment

The structure of Hansa yellow is given in Figure 2.3. This pigment is widely used in the paint and printing inks industries due to its superior colouring in comparison to other monoazo dyes. Contact angles of aqueous solutions of the anionic surfactant AOT have been measured on Hansa yellow discs of dimension 16 mm x 5 mm. Figure 9.3 shows the advancing contact angles of AOT surfactant solutions in air and under squalane by Method 1 (oil first, then aqueous drop) and Method 2 (aqueous drop first, then oil). Toluene was not used as the oil for these measurements because it dissolved the disc. The value of θ_{aw} decreases with increasing [AOT] up to the c.m.c. and

Figure 9.3

Advancing contact angles of an aqueous drop on Hansa yellow pigment discs as a function of AOT concentration. θ_{aw} – squares, θ_{ow} Method 1 (squalane first, then aqueous drop) – diamonds and θ_{ow} Method 2 (aqueous drop first, then oil) – triangles.

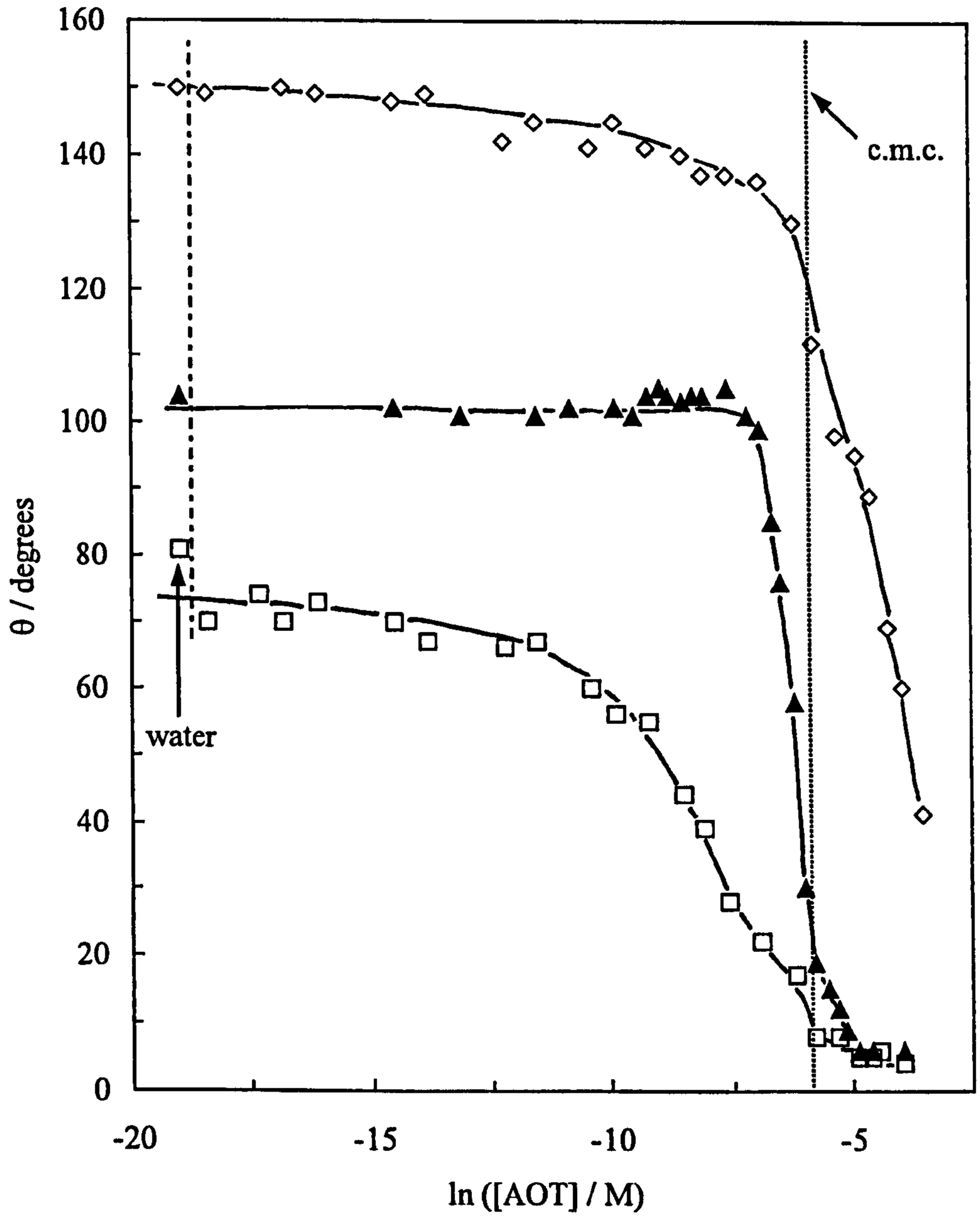

continues to fall above the c.m.c. In the presence of squalane, the value of θ becomes highly dependent on which method is used. The general trend is the same in both cases but the angle is approximately 40° higher when measured by Method 1 at all concentrations of AOT. The contact angle is independent of [AOT] below the c.m.c. but decreases dramatically above it. This is in contrast to the contact angle of an AOT drop under dodecane on a hydrophobic wax or teflon surface where θ remains at ~150° even above the c.m.c.[59] When silicone oil is used instead of squalane in the present study the dependence and magnitude of θ is the same. The difference between Methods 1 and 2 may be due to a microscopic layer of oil that is not displaced by the water drop in Method 1. Also, Method 1 is an advancing angle whereas when the oil is added to the system in Method 2 the aqueous drop recedes back across the surface that has already been in contact with the surfactant solution. Contact angle hysteresis is not an uncommon phenomenon, in fact it is to be expected. A major cause of hysteresis is surface roughness[176] which results when the solid is not molecularly smooth. Hysteresis even occurs on molecularly smooth surfaces where different microscopic regions of the solid have slightly different surface energies.[177] It is therefore critical to state which method is being used when carrying out contact angle measurements.

The tension of the squalane-water interface as a function of [AOT] is shown in Figure 9.4. It is important to note that the tension continues to fall above the c.m.c. These measurements enable the calculation of the surface excess concentration, Γ, of surfactant at the oil-water interface using the Gibbs equation for concentrations close to the c.m.c. for ionic surfactants in the absence of salt,

$$\Gamma_{ow} = \frac{-d\gamma_{ow}/d\ln c}{2RT} \qquad (9.10)$$

$$= 1.332 \times 10^{-6} \text{ mol m}^{-2}$$

The derived plot of $\gamma_{ow}\cos\theta$ versus γ_{ow} in Figure 9.5 (using θ measurements by Method 1) permits the calculation of the surface excess concentration at the solid-water interface using equation 9.9.

Figure 9.4

Interfacial tension measurements of squalane-water as a function of AOT concentration in water at 25 °C.

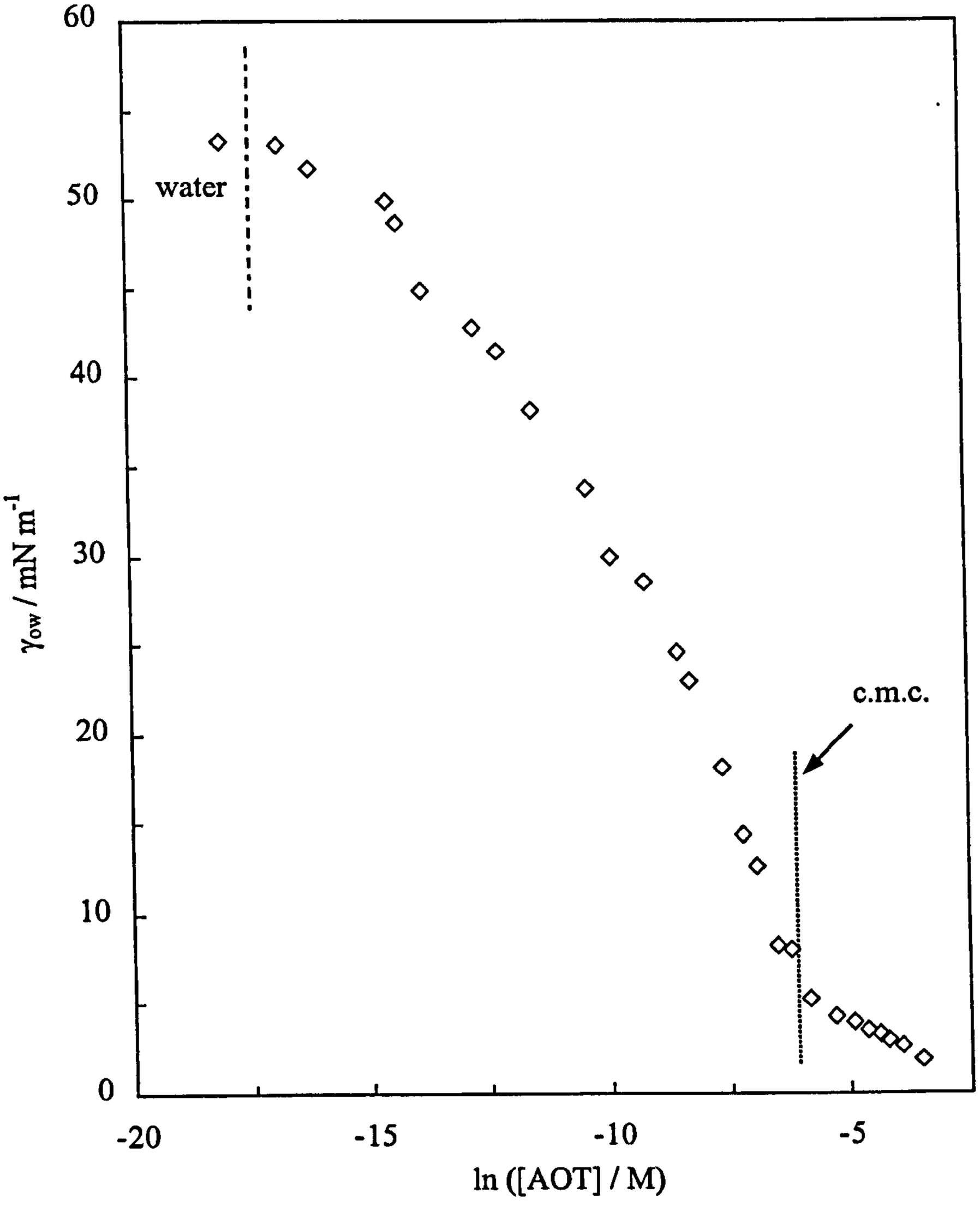

Figure 9.5

$\gamma_{ow}\cos\theta$ versus γ_{ow} for squalane-water systems on Hansa yellow discs in the presence of AOT surfactant. Contact angles measured by Method 1 (oil first, then aqueous drop); inset shows post c.m.c. values.

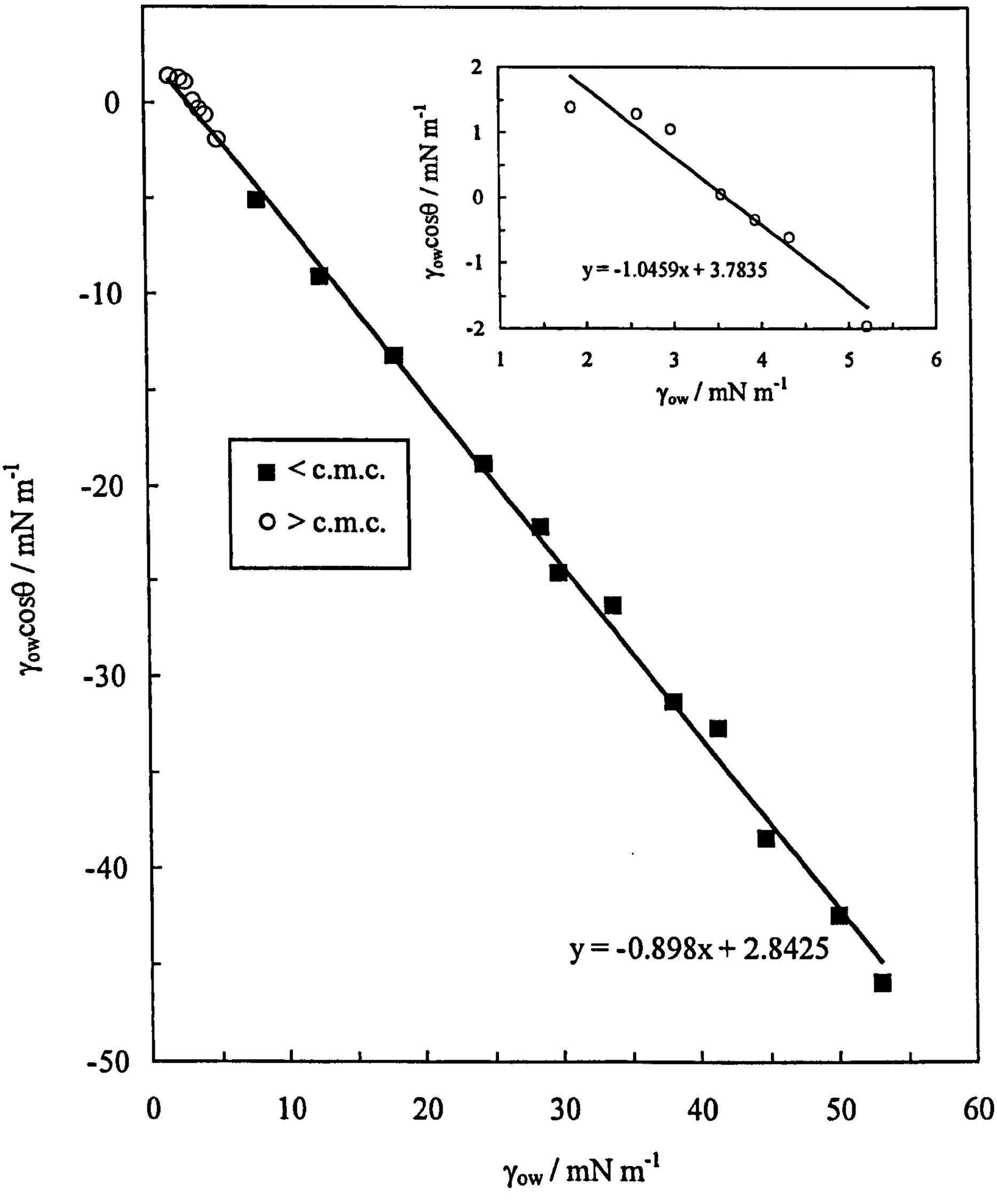

$$\frac{\Gamma_{sw}}{\Gamma_{ow}} = 0.898$$

Therefore,

$$\Gamma_{sw} = 1.20 \times 10^{-6} \text{ mol m}^{-2}$$

The ratio $\Gamma_{sw} / \Gamma_{ow}$ is close to unity, implying that there is nearly equal adsorption at both interfaces above and below the c.m.c. The inset in Figure 9.5 shows the plot for post c.m.c. values alone where the ratio of adsorption remains close to unity. Similarly, using the surface tensions in Figure 9.6, the extent of adsorption at the interfaces of an air-water system can be calculated (Figure 9.7). The surface excess concentration at the air-water interface (Γ_{aw}) was calculated using equation 9.10 just below the c.m.c. by drawing a tangent to the data points. Γ_{aw} was found to equal 1.433×10^{-6} mol m^{-2}. In this case the plot of $\gamma_{aw}\cos\theta$ versus γ_{aw} is linear below the c.m.c. but the sign of the slope changes above it. The ratio of adsorption below the c.m.c. is

$$\frac{\Gamma_{sw}}{\Gamma_{aw}} = 0.47$$

Therefore,

$$\Gamma_{sw} = 0.673 \times 10^{-6} \text{ mol m}^{-2}$$

The ratio implies that adsorption at the air-water surface is nearly twice as much as adsorption at the solid-water interface. Above the c.m.c. the gradient of the slope is positive which may be due to inaccurate contact angle measurements when θ is $< 10^{\circ}$. The surface excess concentration of surfactant at the solid-water interface in the air-water system is approximately half that in the oil-water system. This suggests that the hydrophobic tail prefers to be in air than in squalane which may be due to the high viscosity of squalane.

In the presence of NaCl, the c.m.c. of AOT decreases due to screening of the repulsion between charged headgroups.[178] Figure 9.8 shows the dependence of θ_{aw} on

Figure 9.6

Air-water tensions as a function of AOT concentration in water at 25 °C.

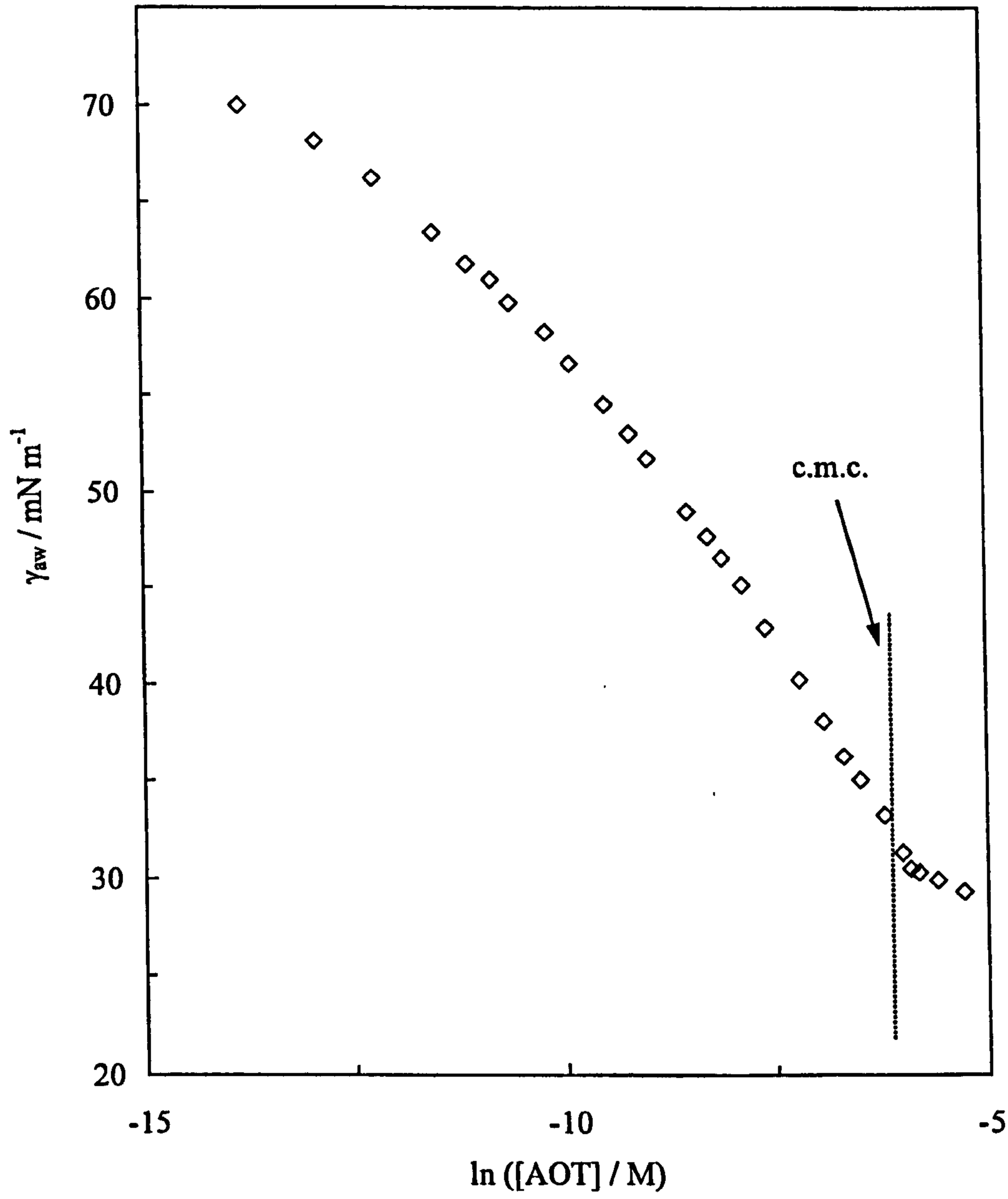

Figure 9.7

$\gamma_{aw}\cos\theta$ versus γ_{aw} in the presence of AOT in water on Hansa yellow discs.

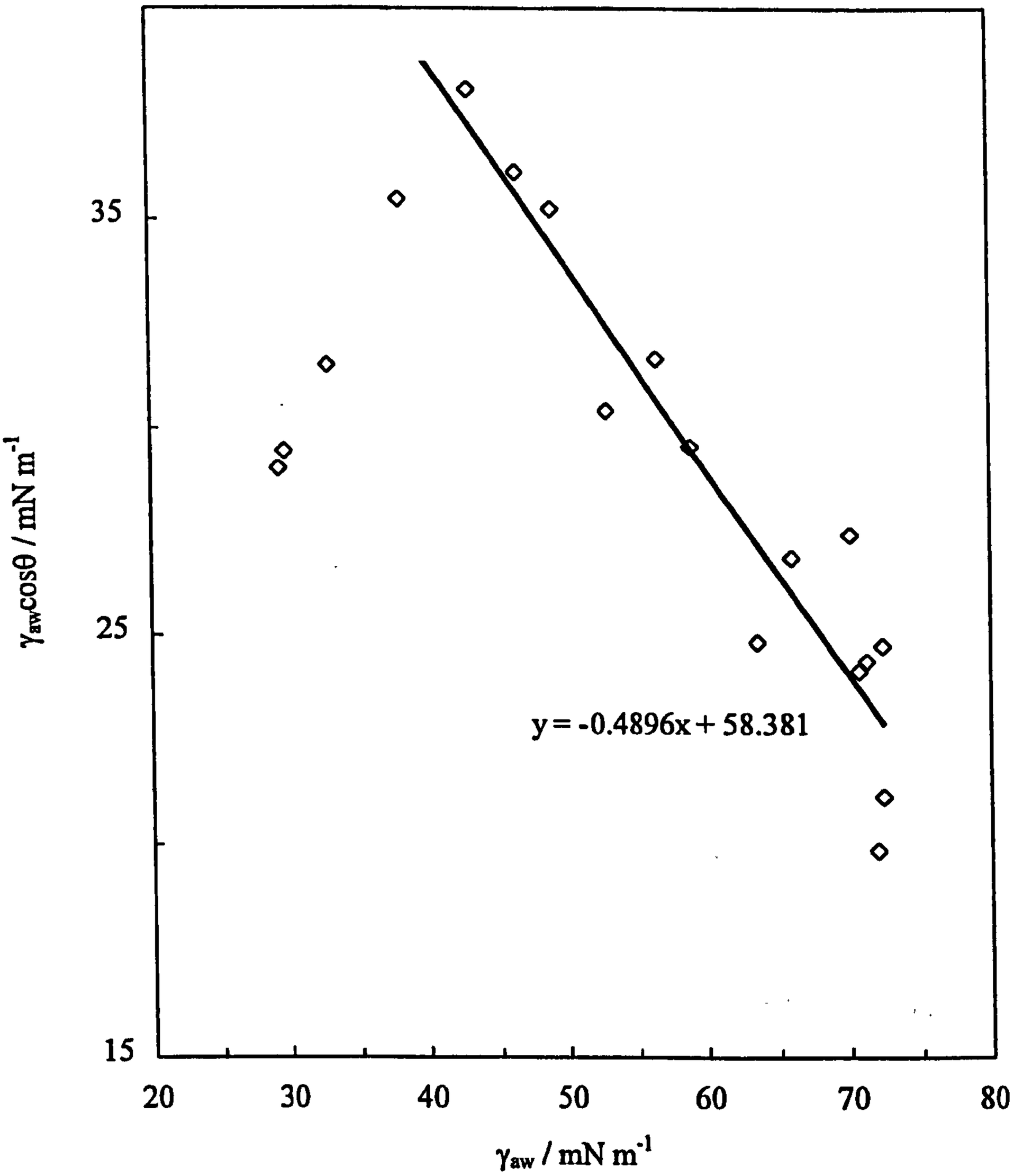

Figure 9.8

Advancing contact angles of an aqueous drop on Hansa yellow pigment discs in air as a function of AOT concentration. Drop contained 0 M NaCl (triangles), 0.1 M NaCl (diamonds) and 1.0 M NaCl (squares).

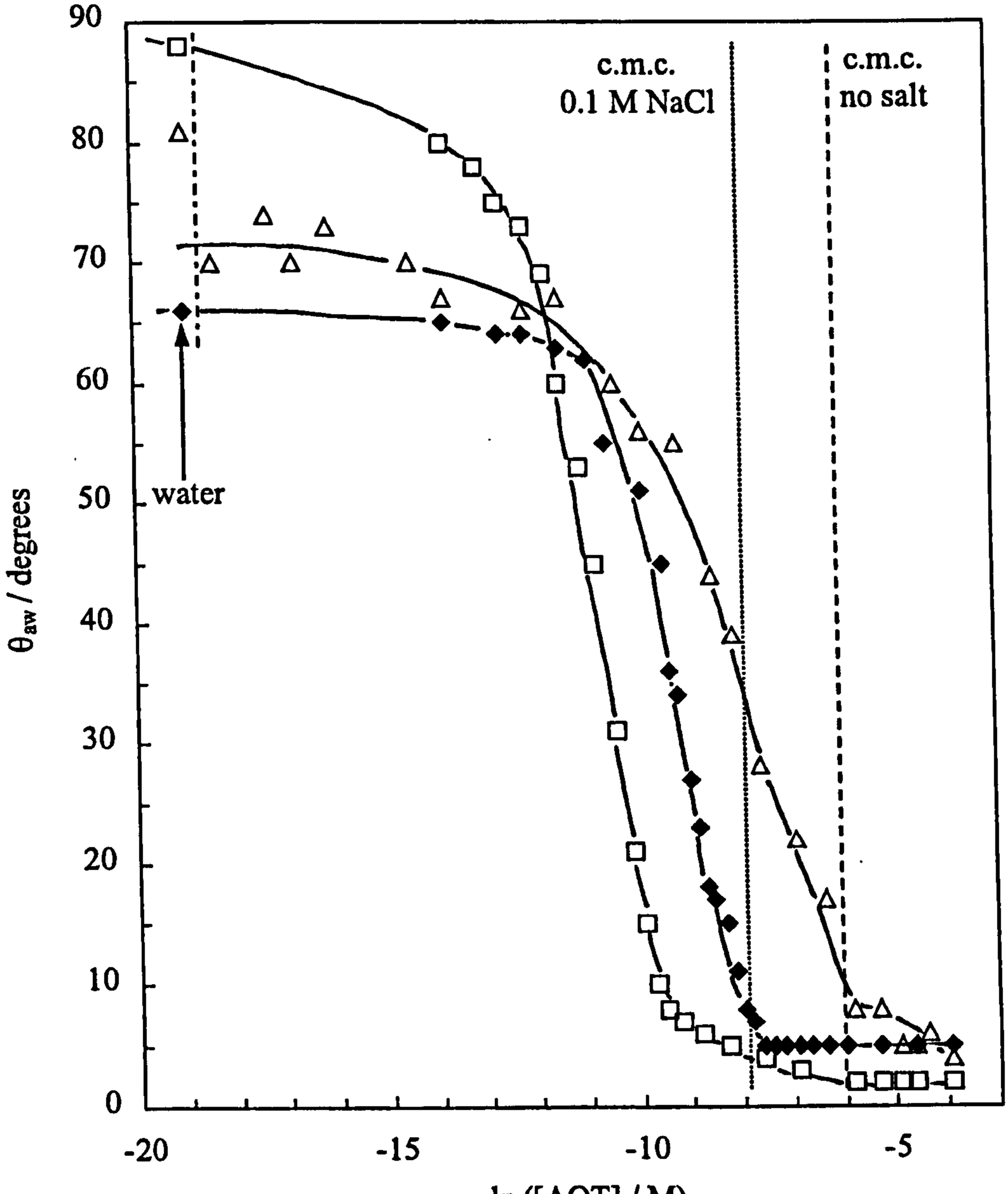

the concentration of AOT in the presence of 0.1 M and 1 M NaCl. The value of θ becomes constant (corresponding to complete wetting) at lower values of [AOT] as [NaCl] increases, consistent with the shift in the c.m.c. Figure 9.9 shows the dependence of θ_{ow} on the concentration of AOT in the presence of 0.1 and 1 M NaCl measured by Method 1. At 1 M NaCl, θ decreases at lower [AOT] than at 0.1 M NaCl but becomes constant at approximately 50°, whereas θ continues to fall to 20° in 0.1 M NaCl. The tension of the squalane-water interface decreases at lower [AOT] in the presence of 0.1 M NaCl than in the absence of NaCl and becomes constant at low tension (2-3 mN m^{-1}) above the c.m.c. (Figure 9.10). The surface excess concentration of surfactant in the presence of 0.1 M NaCl can be calculated by plotting $\gamma_{ow}\cos\theta$ versus γ_{ow} (Figure 9.11). The slope is close to unity (-0.86) below the c.m.c. Above the c.m.c., the data is somewhat scattered, possibly due to the difficulty of measuring low tensions (< 5 mN m^{-1}) using the du Noüy ring method. Figure 9.12 shows the effect of [NaCl] on the contact angle of a 10 mM AOT drop (which is above the c.m.c. at all salt concentrations) under squalane measured by Method 1. θ_{ow} changes from 87° in the absence of NaCl to a minimum of 20° in 0.1 M NaCl before increasing to 85° in 3 M NaCl.

In summary, Hansa yellow is a hydrophobic solid exhibiting a contact angle at the squalane-water interface of over 100°. In the absence of salt, addition of surfactant has little effect below the c.m.c. but decreases the contact angle above the c.m.c. and hence makes it more hydrophilic. This is due to the lower interfacial tension of AOT solutions at the c.m.c. (< 2 mN m^{-1}) in comparison to other surfactants such as SDS and CTAB (see § 9.4) which have a tension above 5 mN m^{-1}. Use of AOT above the c.m.c. would therefore be detrimental to flushing of the pigment from the aqueous to oil phase. In the presence of NaCl the contact angle is decreased at lower AOT as the salt concentration increases. It is known that systems with alkane and aqueous NaCl containing AOT above the c.m.c. can give ultralow tensions (~10^{-3} mN m^{-1}).[179] This fractional change in the oil-water tension causes a substantial change in the contact angle (equation 9.1).[180]

Figure 9.9

Advancing contact angles of an aqueous drop on Hansa yellow discs under squalane as a function of AOT. Drop contained 0 M NaCl (triangles), 0.1 M NaCl (diamonds) and 1.0 M NaCl (squares).

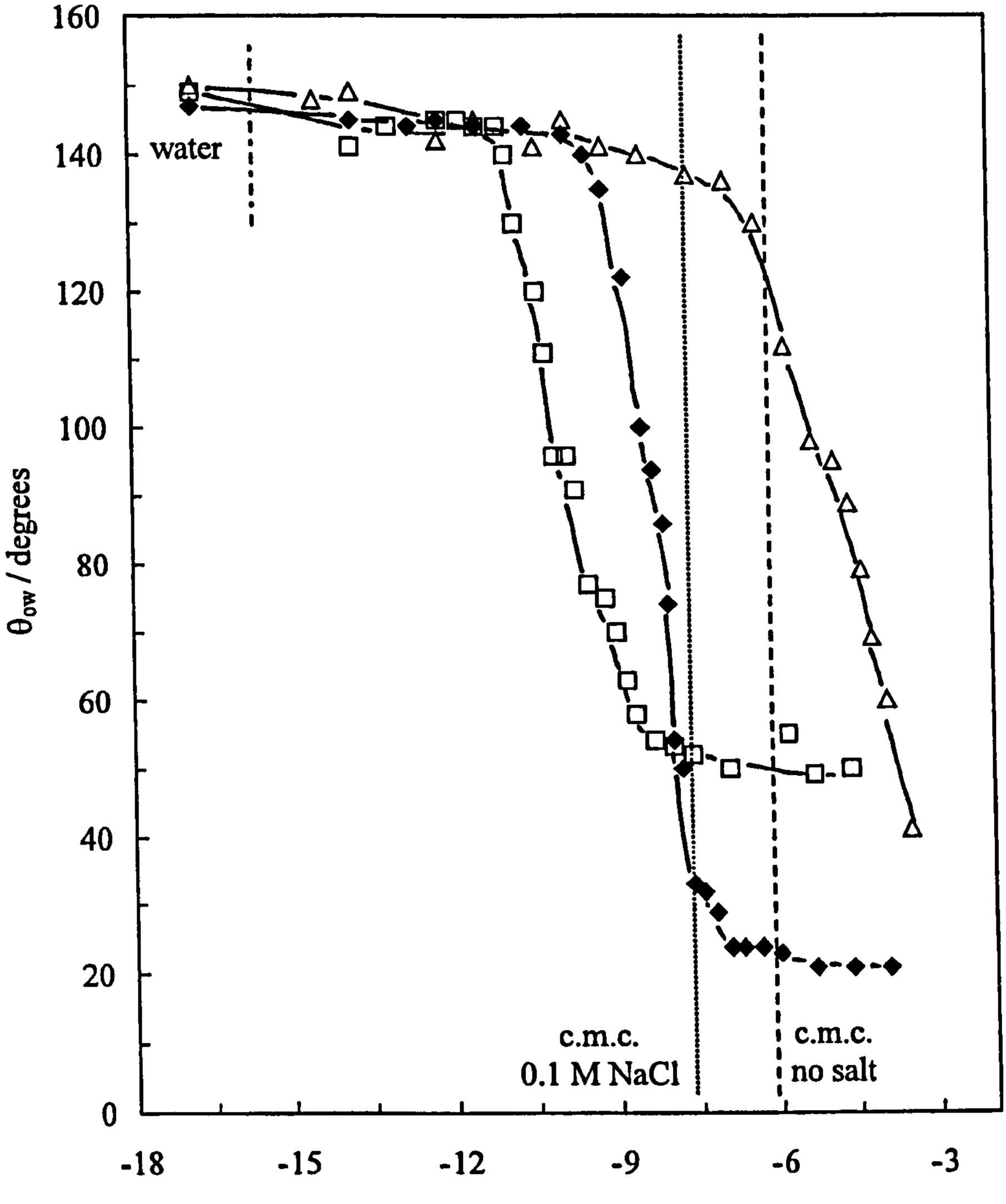

Figure 9.10

Interfacial tension measurements of squalane-water as a function of AOT in water at 25 °C. Water contained 0 M NaCl (squares) and 0.1 M NaCl (diamonds).

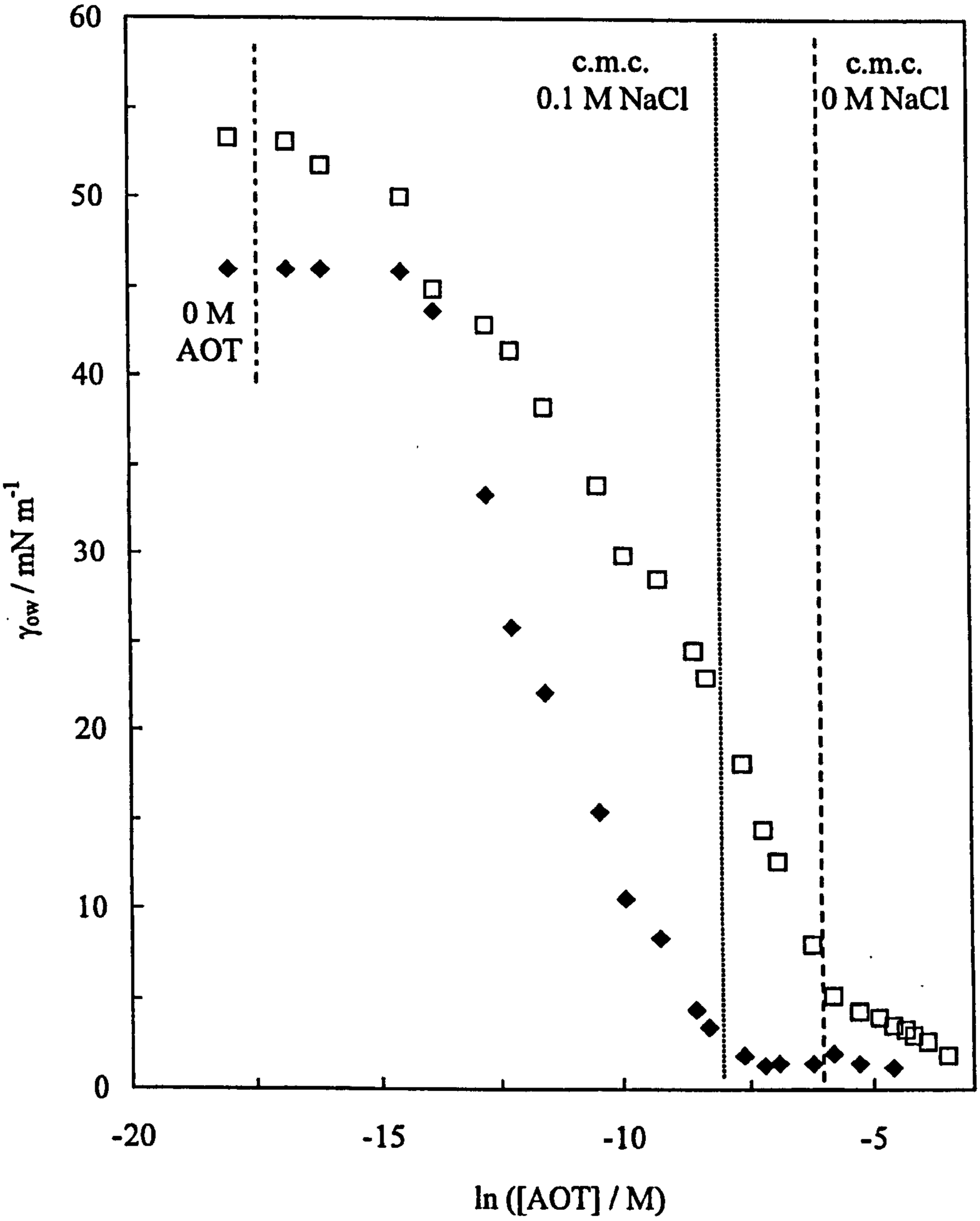

Figure 9.11

$\gamma_{ow}\cos\theta$ versus γ_{ow} for squalane-water systems on Hansa yellow discs in the presence of AOT surfactant and 0.1 M NaCl. Contact angles measured by Method 1 (oil first, then aqueous drop); inset shows post c.m.c. values.

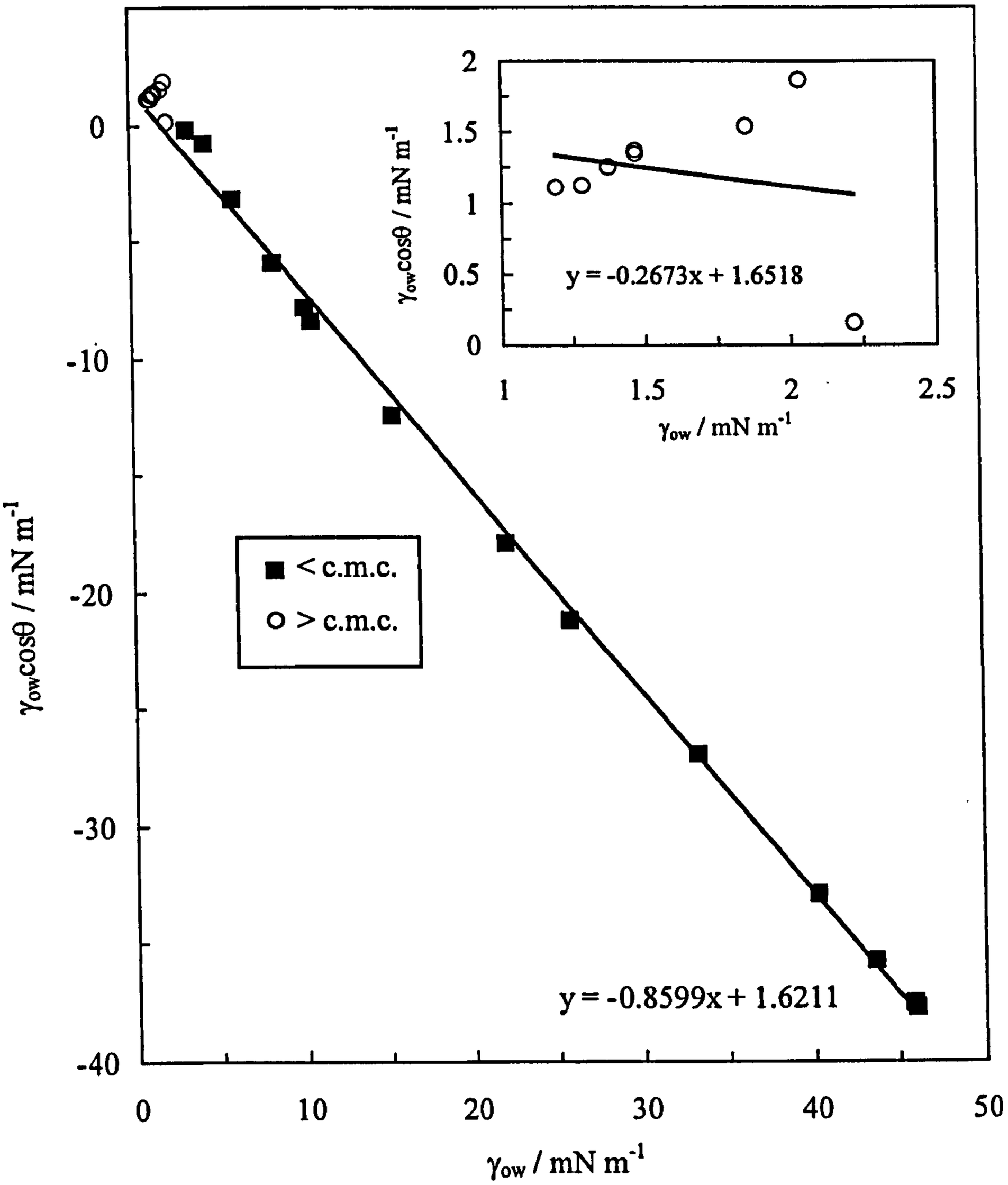

Figure 9.12

Advancing contact angle of 10 mM aqueous AOT drops on Hansa yellow discs under squalane as a function of NaCl. Angles measured by Method 1 (oil first, then aqueous drop).

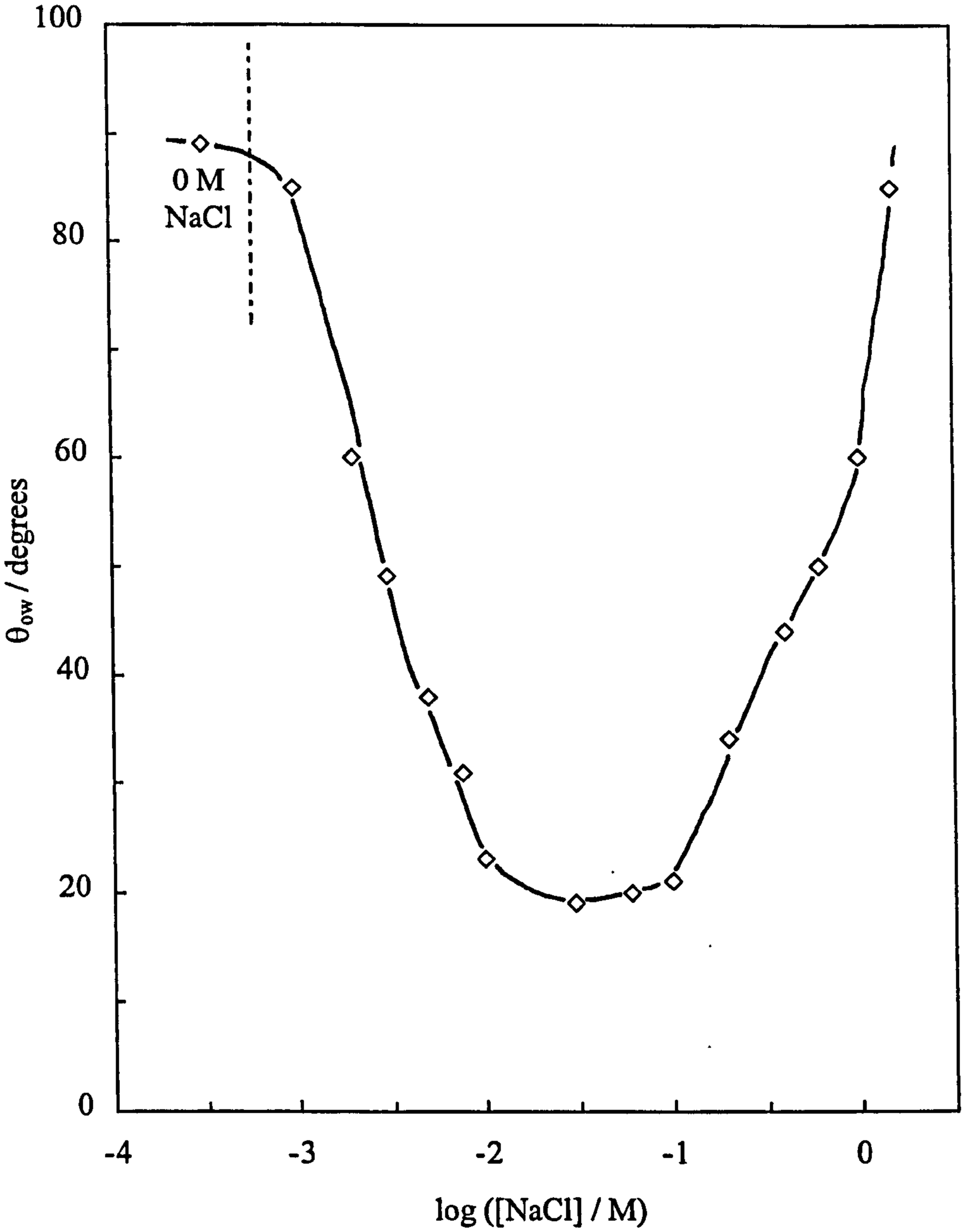

(b) Phthalocyanine blue B pigment

The structure of phthalocyanine blue B pigment is given in Figure 2.3. It is a widely used organic pigment formed by heating phthalic anhydride, urea and cupric acid. Figure 9.13 shows the contact angles of drops of aqueous AOT solution on solid phthalocyanine blue B discs in air and under squalane measured by Methods 1 and 2. The value of θ_{aw} is very similar to that measured on Hansa yellow but is slightly higher around and above the c.m.c. θ_{ow} measured by Method 1 is constant below the c.m.c. at approximately 155° but decreases to 80° above the c.m.c. in a similar way to that seen on Hansa yellow. However, θ_{ow} measured by Method 2 is approximately equal to θ_{aw} which is completely different to the behaviour seen on Hansa yellow. Figure 9.14 uses the tensions given in Figure 9.4 to plot $\gamma_{ow}\cos\theta$ versus γ_{ow} for phthalocyanine blue B discs measured by Method 1. The slope is approximately equal to unity (-0.93) which implies equal adsorption of surfactant at the solid-water and oil-water interfaces as seen for Hansa yellow. The equivalent plot for the air-water surface is shown in Figure 9.15 where again the sign of the slope changes above the c.m.c.

Phthalocyanine blue B is also a very hydrophobic pigment and addition of AOT makes it more hydrophilic. The large difference between Method 1 and Method 2 suggests the angles may not have been at equilibrium despite measurements being taken when a constant angle was obtained (~5 minutes after drop addition).

9.4 Systems containing CTAB surfactant

The effects of the cationic surfactant CTAB on the value of θ in air, under squalane and under silicone oil measured by Method 1 on Hansa yellow discs are shown in Figure 9.16. In air the dependence is similar to AOT although θ remains constant above the c.m.c. However, there is a significant difference between the two surfactants when the contact angle is measured under oil by Method 1. θ_{ow} remains constant and high above and below the c.m.c. under squalane and under silicone oil. This is due to the relatively high, constant value of γ_{ow} above the c.m.c. for this surfactant shown in Figure 9.17. This agrees with the behaviour of an aqueous drop of AOT under dodecane on teflon and hydrophobic wax measured by Aveyard et al.[59] However, it is in contrast

Figure 9.13

Advancing contact angles of an aqueous drop on phthalocyanine blue B pigment discs as a function of AOT. θ_{aw} – squares, θ_{ow} Method 1 (squalane first, then aqueous drop) – diamonds and θ_{ow} Method 2 (aqueous drop first, then squalane) – triangles.

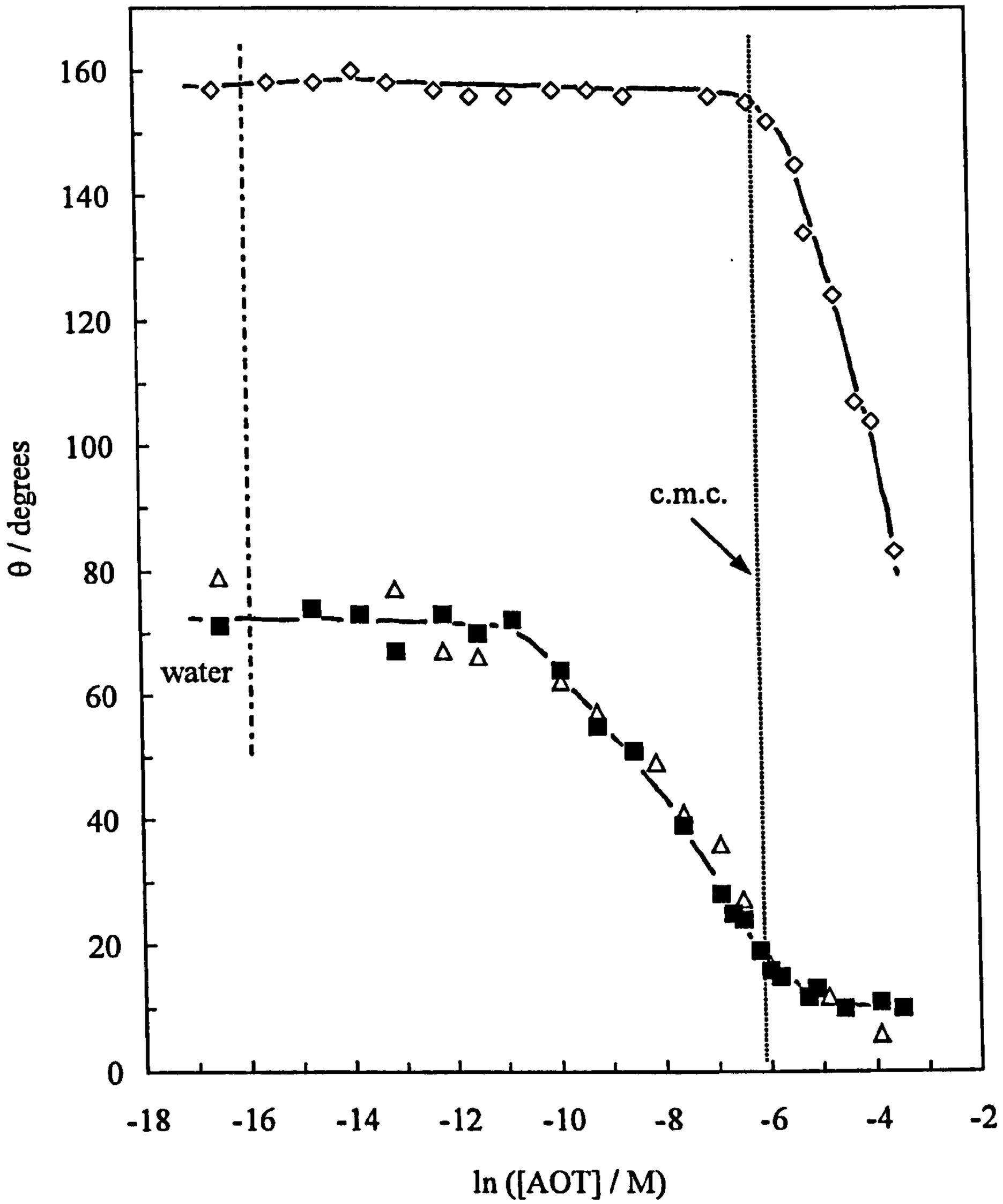

Figure 9.14

$\gamma_{ow}\cos\theta$ versus γ_{ow} for squalane-water systems on phthalocyanine blue B discs in the presence of AOT. Contact angles measured by Method 1 (oil first, then aqueous drop).

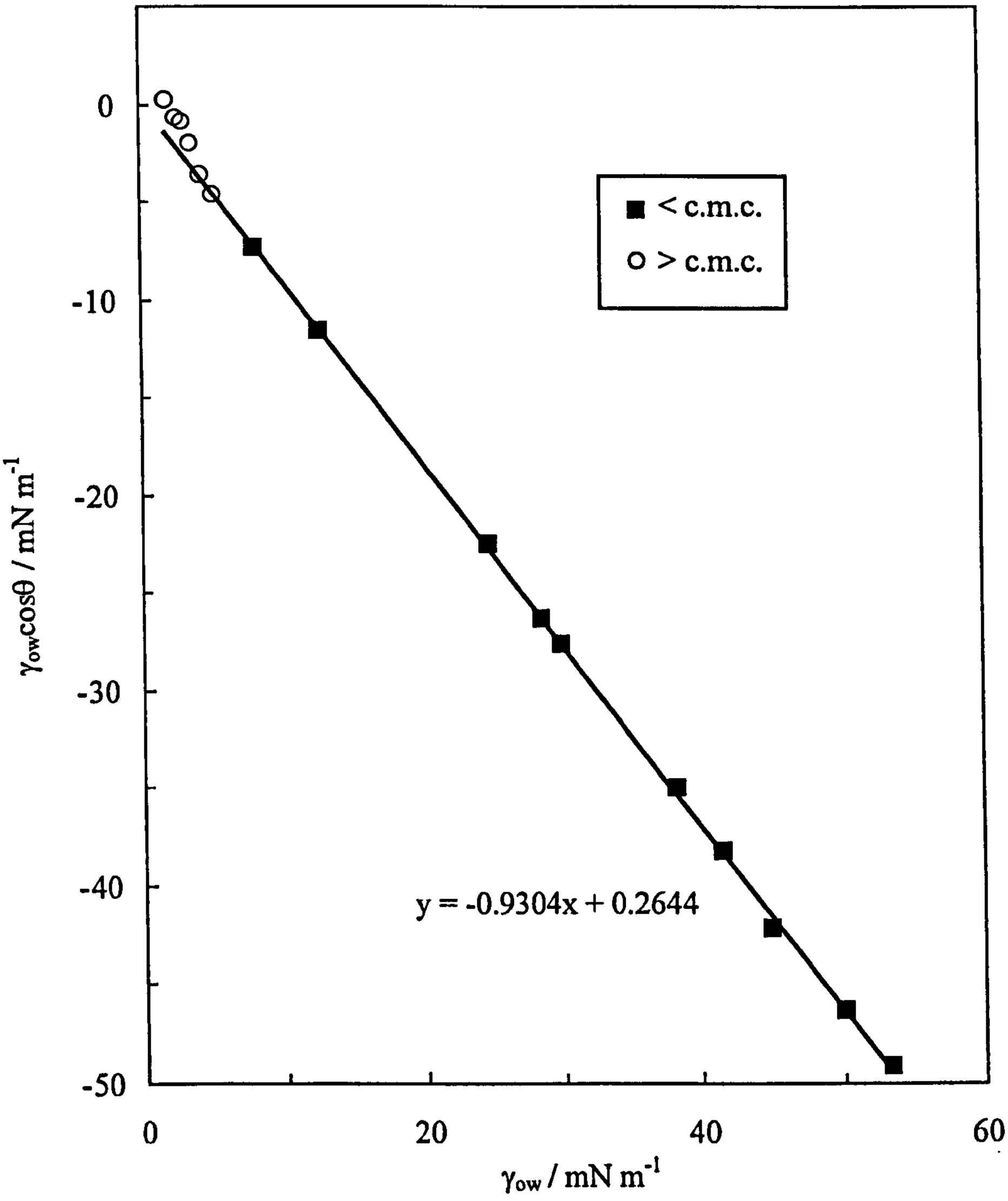

Figure 9.15

$\gamma_{aw}\cos\theta$ versus γ_{aw} in the presence of AOT in water on phthalocyanine blue B discs.

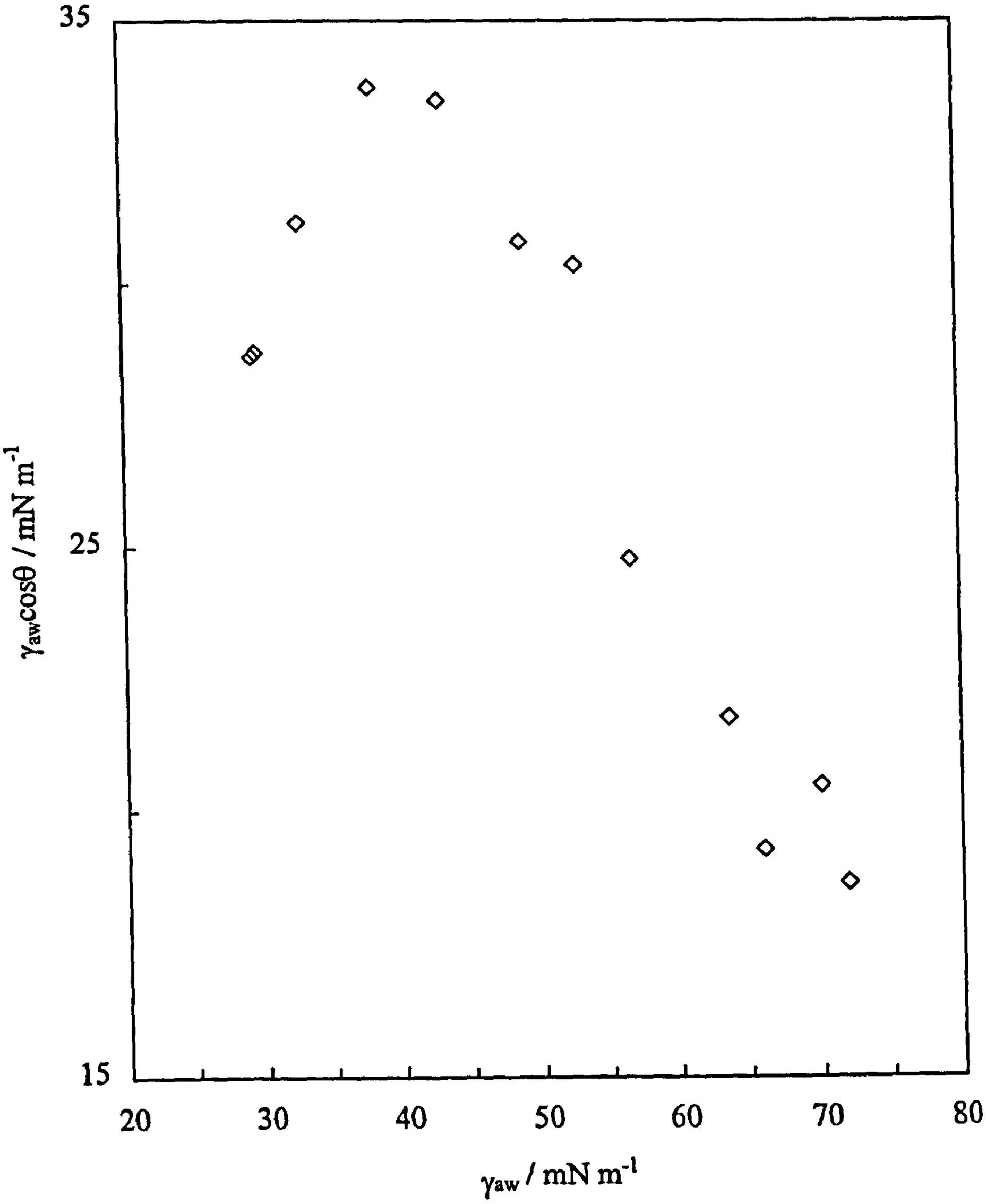

Figure 9.16

Advancing contact angles of an aqueous drop on Hansa yellow discs as a function of [CTAB]. θ_{aw} – squares, θ_{ow} Method 1 (squalane first, then aqueous drop) – triangles, θ_{ow} Method 1 (50 cS PDMS first, then aqueous drop) – diamonds.

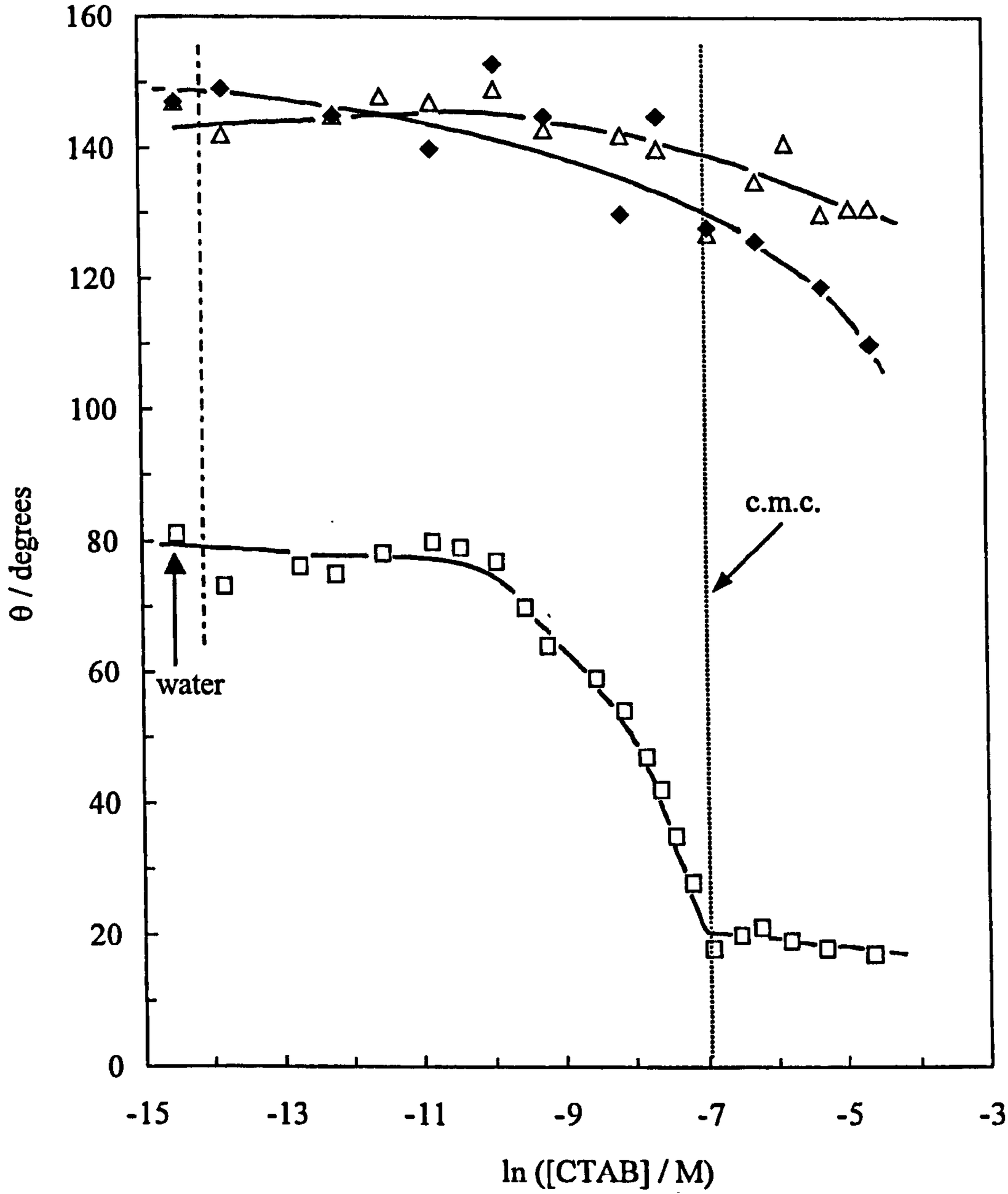

Figure 9.17

Interfacial tension measurements of squalane-water as a function of [CTAB] in water at 25 °C.

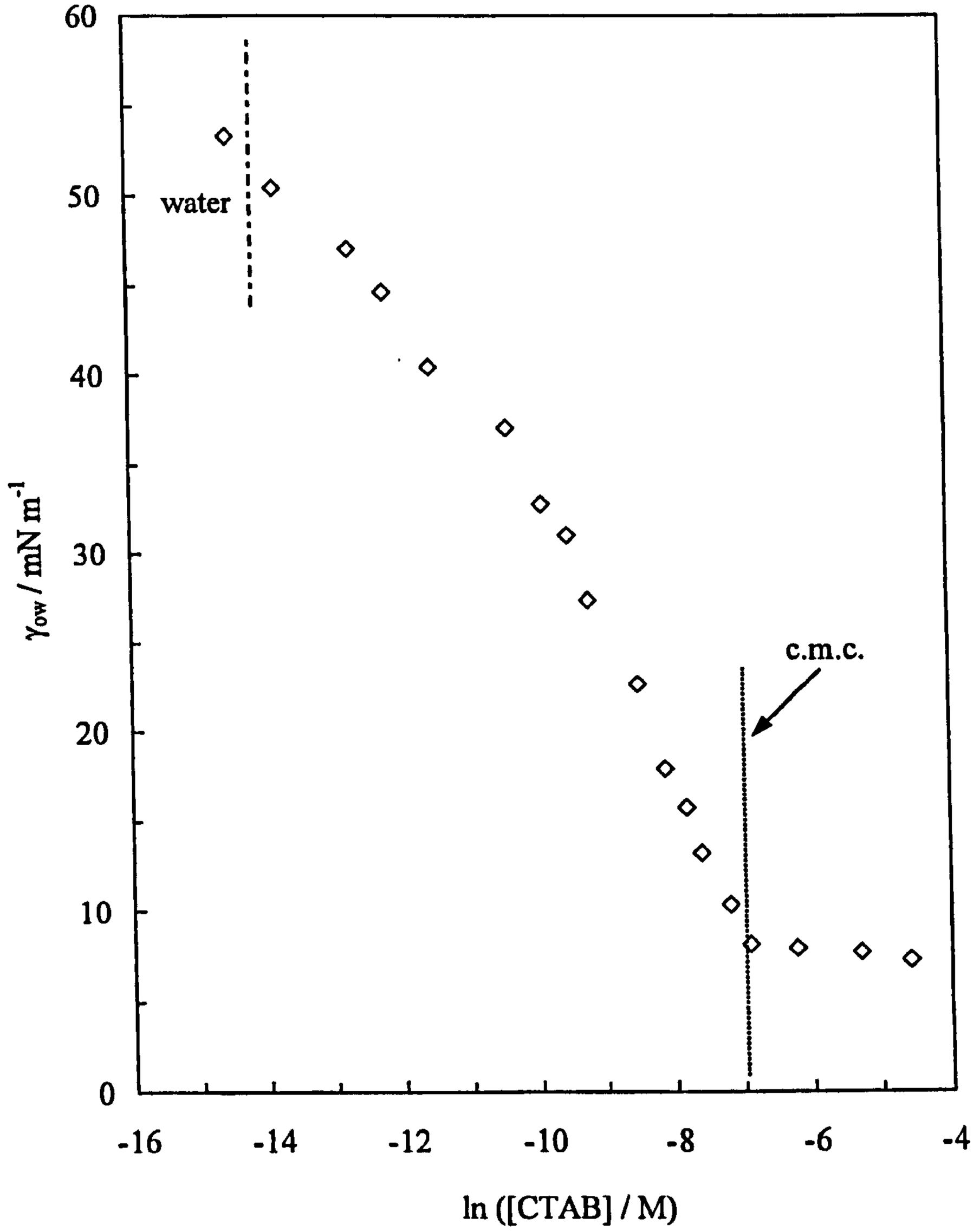

to the post c.m.c. values measured for the squalane-aqueous AOT interface where the tension continues to fall causing the decrease in θ_{ow} not seen for CTAB. The plot of $\gamma_{ow}\cos\theta$ versus γ_{ow} in Figure 9.18 indicates nearly equal adsorption at the oil-water and solid-water interfaces as seen for AOT. The slope of the $\gamma_{aw}\cos\theta$ versus γ_{aw} plot in Figure 9.19 is approximately –0.7 although the data is more scattered, suggesting adsorption at the air-water surface is greater than the solid-water interface.

9.5 Systems containing Silwet L-77 surfactant

The contact angle on Hansa yellow discs of AOT solutions in air in the presence of 1 M NaCl is very low (wetting) just below the c.m.c. (Figure 9.8). The surface tension of this solution is approximately 25 mN m^{-1}, which suggests that the critical wetting tension for Hansa yellow is of this order also. Interestingly, the c.m.c. tension of the non-ionic silicone surfactant L-77 is around 21 mN m^{-1}.[152] Therefore, it is predicted that wetting will occur below the c.m.c. for this surfactant in air, in contrast to the behaviour of AOT on Hansa yellow in the absence of NaCl where wetting only occurs above the c.m.c. Figure 9.20 shows the dependence of θ_{aw} on the concentration of L-77 on Hansa yellow discs. There is a dramatic fall in θ at 5×10^{-5} M L-77 which is below the c.m.c. of 1.2×10^{-4} M. The surface tension at 5×10^{-5} M L-77 is approximately 25 mN m^{-1} which is equal to the predicted wetting tension of Hansa yellow discs. Above the c.m.c. the contact angle is zero indicating complete wetting of the surface.

9.6 Bargeman consistency test

It has been shown by Bargeman[181] that combination of Young's equations for the systems studied can be used as a consistency test for the experimental results. At equilibrium, the contact angles of an aqueous drop on a solid in air and under oil can be used to predict the contact angle of an oil drop in air on that same surface. The Young's equations for these systems are,

$$\gamma_{sa} = \gamma_{aw}\cos\theta_{aw} + \gamma_{sw} \qquad (9.11)$$

Figure 9.18

$\gamma_{ow}\cos\theta$ versus γ_{ow} for squalane-water systems on Hansa yellow discs in the presence of CTAB surfactant. Contact angle measurements by Method 1 (oil first, then aqueous drop).

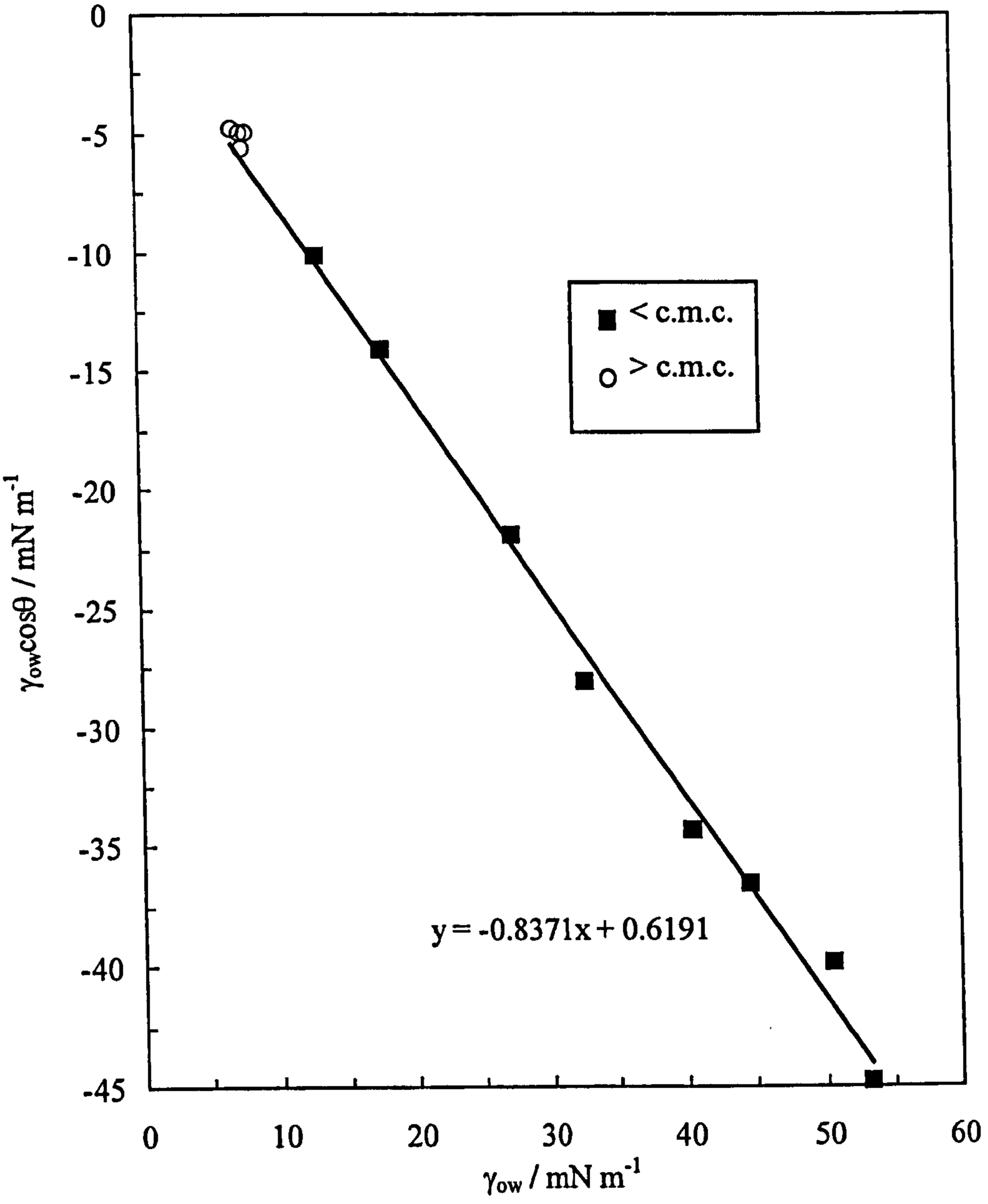

Figure 9.19

$\gamma_{aw}\cos\theta$ versus γ_{aw} in the presence of CTAB surfactant in water on Hansa yellow discs.

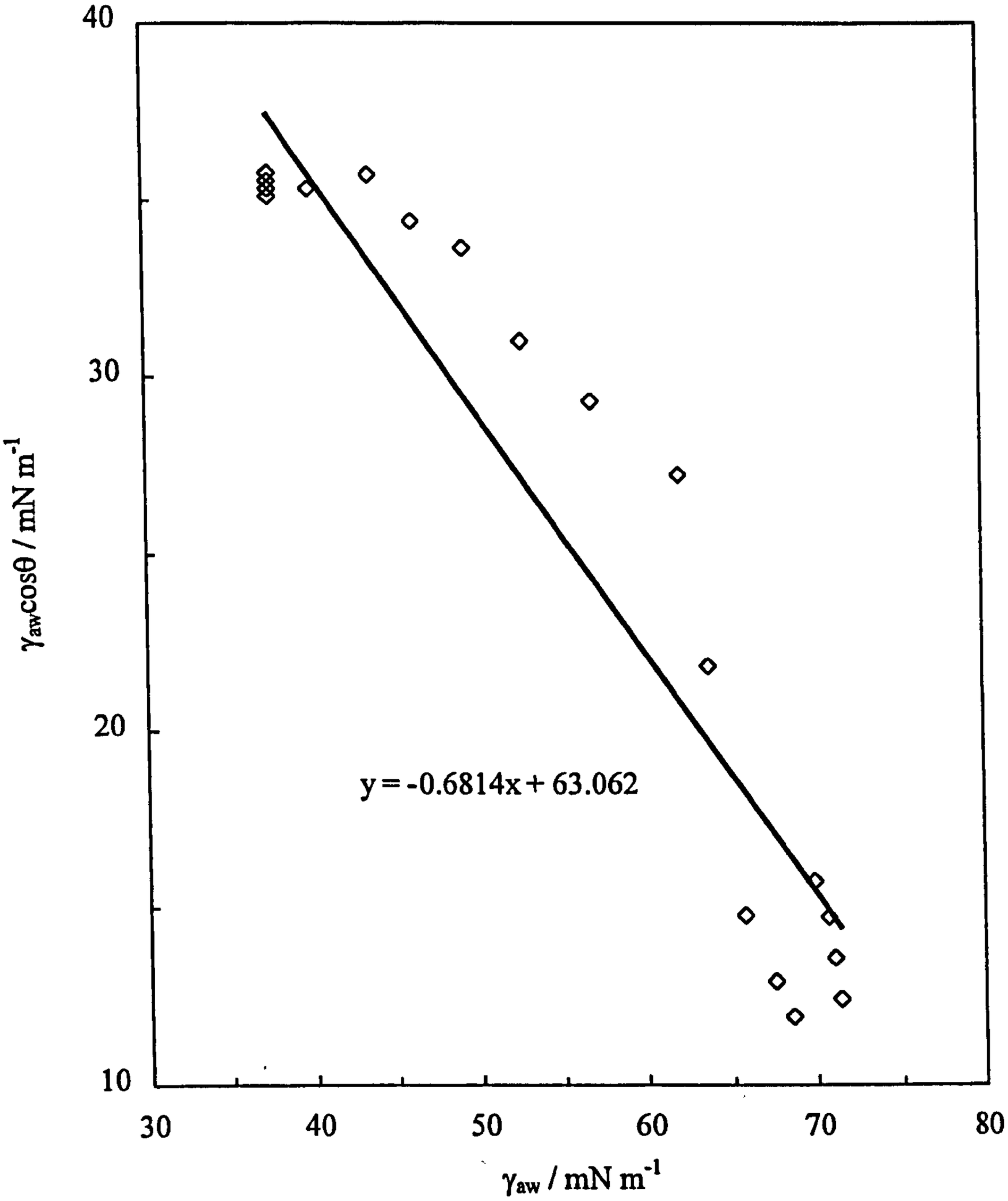

Figure 9.20

Advancing contact angle of an aqueous drop in air on Hansa yellow pigment discs as a function of L-77 concentration.

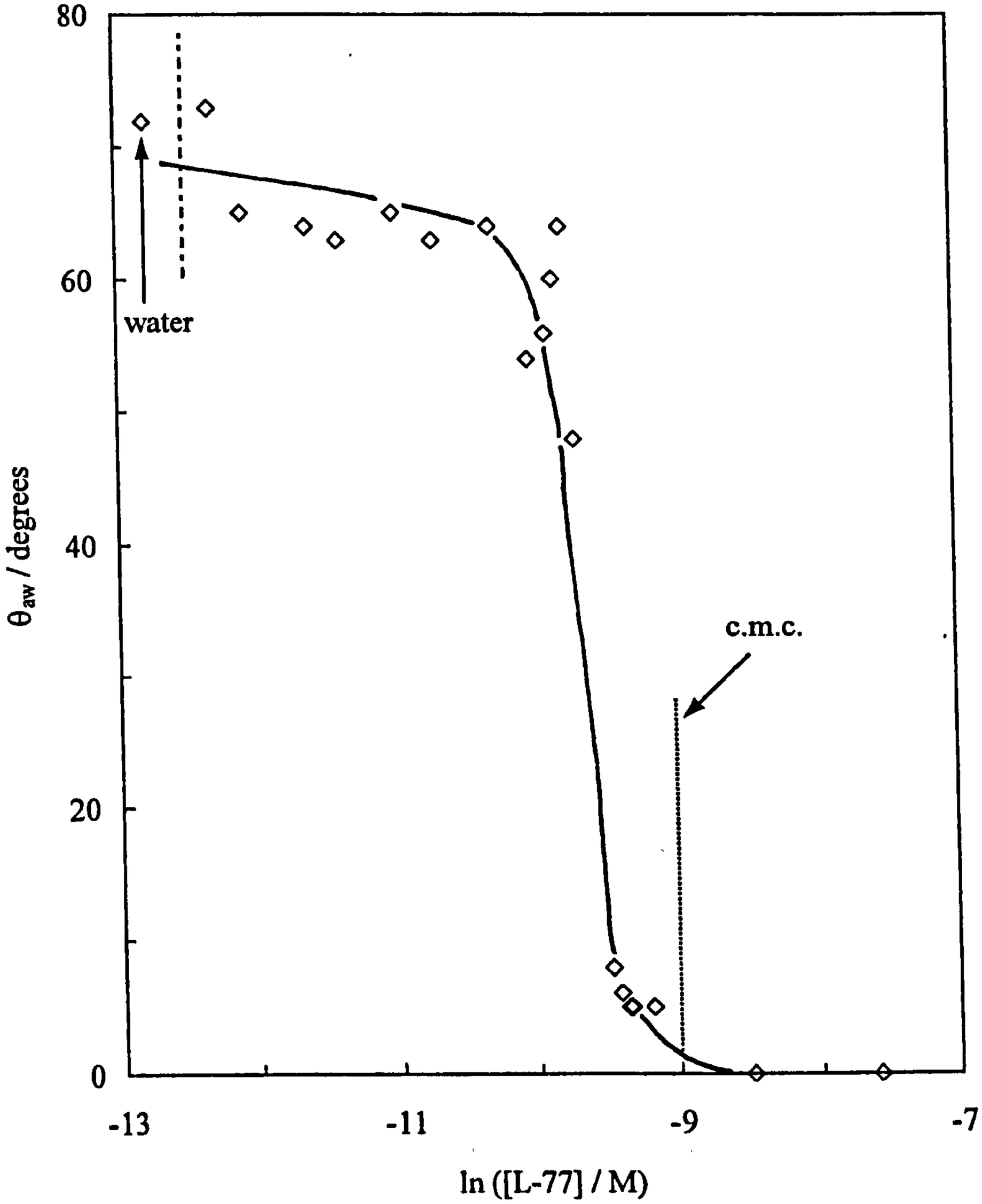

$$\gamma_{sa} = \gamma_{oa} \cos\theta_{oa} + \gamma_{so} \tag{9.12}$$

$$\gamma_{so} = \gamma_{ow} \cos\theta_{ow} + \gamma_{sw} \tag{9.13}$$

Combination of these equations gives,

$$\gamma_{ow} \cos\theta_{ow} + \gamma_{sw} = \gamma_{sa} - \gamma_{oa} \cos\theta_{oa}$$

$$\gamma_{ow} \cos\theta_{ow} + \gamma_{sa} - \gamma_{aw} \cos\theta_{aw} = \gamma_{sa} - \gamma_{oa} \cos\theta_{oa}$$

$$\gamma_{ow} \cos\theta_{ow} - \gamma_{aw} \cos\theta_{aw} = -\gamma_{oa} \cos\theta_{oa} \tag{9.14}$$

Equation 9.14 can be used to check the consistency of contact angles measured by Methods 1 and 2 for the Hansa yellow and phthalocyanine blue B systems studied earlier. The required contact angle and tension measurements are summarised in Table 9.2.

Table 9.2 θ and γ measurements for air or squalane / water / solid systems

Solid	θ_{aw} / degrees		θ_{oa} / degrees		θ_{ow} / degrees	
	Method 1	Method 2	Method 1	Method 2	Method 1	Method 2
Hansa yellow	77	77	4	4	147	101
Phthalocyanine blue B	75	75	3	3	157	79

γ_{aw} / mN m^{-1}	γ_{oa} / mN m^{-1}	γ_{ow} / mN m^{-1}
71.9	29	53

(a) Hansa yellow

Combination of Young's equations for measurements on Hansa yellow pigment using Method 1 gives

$$\gamma_{ow}\cos\theta_{ow} - \gamma_{aw}\cos\theta_{aw} = -\gamma_{oa}\cos\theta_{oa}$$

$$-44.5 - 16.2 = -28.9$$

$$-60.7 = -28.9 \qquad (\text{units} = \text{mN m}^{-1})$$

and by Method 2 gives

$$\gamma_{ow}\cos\theta_{ow} - \gamma_{aw}\cos\theta_{aw} = -\gamma_{oa}\cos\theta_{oa}$$

$$-10.1 - 16.2 = -28.9$$

$$-26.3 = -28.9 \qquad (\text{units} = \text{mN m}^{-1})$$

This suggests that contact angle measurements of water and squalane on Hansa yellow discs by Method 1 are not at equilibrium, possibly due to a microscopic layer of oil separating the solid and water for θ_{ow} measurements as suggested earlier.

(b) Phthalocyanine blue B

For phthalocyanine blue B measured by Method 1, combination of Young's equations gives,

$$\gamma_{ow}\cos\theta_{ow} - \gamma_{aw}\cos\theta_{aw} = -\gamma_{oa}\cos\theta_{oa}$$

$$-48.8 - 18.6 = -29.0$$

$$-67.4 = -29.0 \qquad (\text{units} = \text{mN m}^{-1})$$

and by Method 2 gives

$$\gamma_{ow}\cos\theta_{ow} - \gamma_{aw}\cos\theta_{aw} = -\gamma_{oa}\cos\theta_{oa}$$

$$10.1 - 18.6 = -29.0$$

$$-8.5 = -29.0 \qquad (\text{units mN m}^{-1})$$

Hence, neither method gives consistent results when the Young's equations are combined for measurements on phthalocyanine blue B discs. This may be due to the quality of the solid surface, especially under squalane, which becomes brittle after 10 minutes and is obviously imbibing some oil.

In summary, both methods of contact angle determination appear to have some frailties. However, these preliminary investigations have highlighted the importance of an understanding of pigment wettability in the presence of various surfactants. The general trends shown in this chapter provide information that could ultimately improve the efficiency of the flushing process.

9.7 Summary of other systems

The schematic below compares the effect of AOT on Hansa yellow under squalane with the behaviour of other systems involving surfactant adsorption on hydrophilic glass and calcite solid surfaces. There are three possible scenarios; θ remains constant, θ decreases or θ increases with increasing surfactant concentration. All three can be accounted for in terms of the ratio between the wetting tension and the oil-water tension. The wetting tension, γ^*, is defined as

$$\gamma^* = \gamma_{so} - \gamma_{sw} \tag{9.15}$$

which can be substituted in equation 9.1 to give a modified version of Young's equation

$$\cos\theta = \frac{\gamma^*}{\gamma_{ow}} \tag{9.16}$$

At concentrations of AOT above the c.m.c. (system 2) and for CTAB on a glass surface above the c.m.c. (system 1), θ decreases with increasing [surfactant]. This is due to an increase in the wetting tension due to a reduction in γ_{sw} (γ_{so} is not affected by increasing [surfactant]) and/or a reduction in γ_{ow}. The contact angle increases with increasing surfactant concentration for CTAB on glass at low concentrations (dashed-

dotted line) and for stearic acid on calcite at all concentrations (system 3, filled lines). This can be explained by a decrease in the wetting tension due to a decrease in γ_{so}. Stearic acid is dissolved in the oil and so has a minimal effect on the solid-water tension. In order for θ to increase, γ_{sw} and γ_{ow} would need to increase, which does not occur on addition of surfactant in either case. θ remains constant at low concentrations of AOT in the present work (dashed line) which must be due to a cancellation of any changes in the three tensions.

Effect of surfactant adsorption on the wettability of various solid surfaces

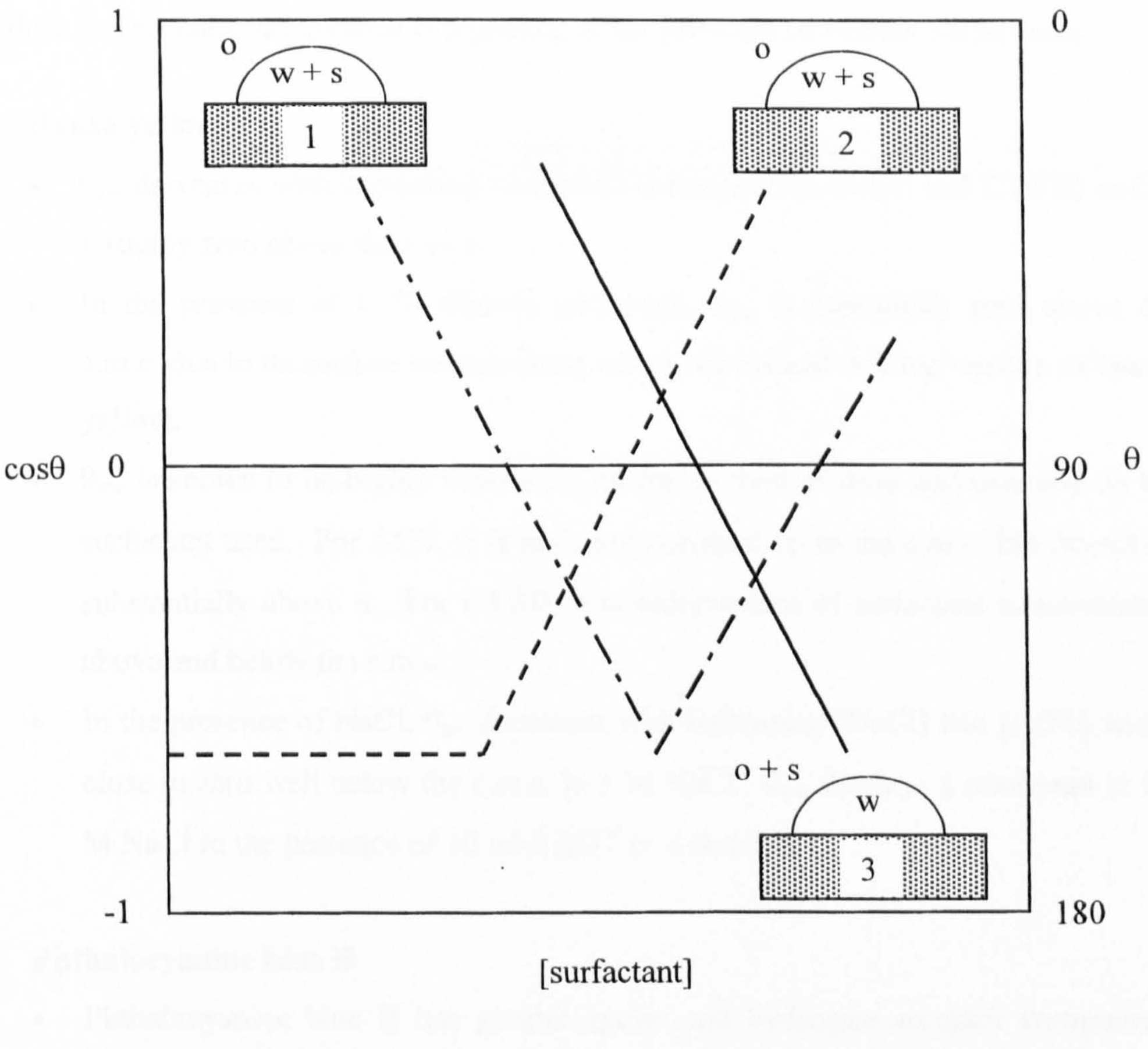

1. Solid: glass, surfactant: CTAB, oil: dodecane, ref. present, Figure 3.37.
2. Solid: Hansa yellow, surfactant: AOT, oil: squalane, ref. present, Figure 9.3.
3. Solid: calcite, surfactant: stearic acid, oil: decane, ref. 28.

It is shown in Figure 9.4 that γ_{ow} falls with increasing concentration so the wetting tension must fall in proportion. All cases relate to equilibrium and it is noted that contact angles are determined by tensions in the vicinity of the three phase contact line. Also, it is known that alkane molecules adsorb at the solid-water interface despite being completely insoluble in water, presumably by diffusion along the solid-water interface.

9.8 Conclusions

The following conclusions can be drawn regarding the wettability of Hansa yellow and phthalocyanine blue B pigments in the presence of various surfactants.

- **Hansa yellow**
  - θ_{aw} decreases with increasing surfactant concentration (AOT and CTAB) and is virtually zero above the c.m.c.
  - In the presence of L-77 silicone surfactant, θ_{aw} is essentially zero above the c.m.c. due to its surface tension being below the critical wetting tension of Hansa yellow.
  - θ_{ow} is shown to be highly dependent on the method of drop addition and on the surfactant used. For AOT, θ is high and constant up to the c.m.c. but decreases substantially above it. For CTAB, θ is independent of surfactant concentration above and below the c.m.c.
  - In the presence of NaCl, θ_{aw} decreases with increasing [NaCl] and [AOT] and is close to zero well below the c.m.c. in 1 M NaCl. θ_{ow} displays a minimum at 0.1 M NaCl in the presence of 10 mM AOT (> c.m.c.).

- **Phthalocyanine blue B**
  - Phthalocyanine blue B has greater apolar and hydrogen acceptor components than Hansa yellow.
  - θ_{aw} and θ_{ow} measured by Method 2 decrease with increasing [AOT] whereas θ_{ow} measured by Method 1 is constant below the c.m.c. and decreases above it.

- The Bargeman consistency test suggests some of the measurements are not at equilibrium. In spite of this it is proposed that the general trends observed provide important information on the wettability of the pigments in the presence of surfactant.

SUMMARY OF CONCLUSIONS AND SUGGESTIONS FOR FUTURE WORK

SUMMARY OF CONCLUSIONS

The following conclusions can be drawn from the work described in this thesis:

- Small solid particles can stabilise emulsions in the absence of any other adsorbing species.

- Oil-in-water emulsions stabilised by hydrophilic Aerosil 200 silica particles are very sensitive to the stability of the initial aqueous colloidal dispersion.

  In the presence of NaCl, the dispersions exhibit anomalous DLVO behaviour in that they are stable at the i.e.p. (pH 2) even at high salt concentrations but are unstable at high pH where the particles have a high negative charge. Emulsions are most stable at pH 4 where the particles have a low, negative zeta potential but are unstable at high pH when the particles are flocculated.

  In the presence of $LaCl_3$, emulsions are unstable at low pH where the silica is dispersed. At pH 10, the stability passes through a pronounced maximum between 2 and 5 mM salt corresponding to the onset of flocculation of the aqueous colloid. At higher [salt], extensive flocculation leads to destabilisation of the emulsion.

  In the presence of TEAB, emulsions are relatively unstable at high and low pH where the aqueous colloid is dispersed. At intermediate pH, emulsions exhibit maximum emulsion stability to creaming around salt concentrations corresponding to the onset of colloid flocculation.

- Catastrophic phase inversion of toluene-containing emulsions stabilised by hydrophobic silica particles (50 % SiOH) occurs at a volume fraction of water equal to 0.7. The w/o emulsions ($\phi_w \leq 0.7$) are stable to coalescence indefinitely and the stability to sedimentation increases with particle concentration. The o/w emulsions are also stable to coalescence but are less stable to creaming due to their larger drop size. Emulsions are most stable around inversion, which occurs with no hysteresis.

- Transitional phase inversion of emulsions occurs from w/o (o/w) to o/w (w/o) on addition of hydrophilic (hydrophobic) silica to systems stabilised by hydrophobic

(hydrophilic) silica at fixed oil:water ratio. Both types of emulsion are remarkably stable to coalescence with the stability to gravity-induced separation least around inversion, exactly the opposite to catastrophic inversion. The condition for inversion is shown to depend on the initial location of the particles although the characteristics of the emulsions remain unchanged.

- The energy of attachment of a single particle at the oil-water interface is shown theoretically to depend on the contact angle it makes with it and is maximum for an angle of 90°. The contact angle is related to the extent of hydrophobic modification on the silica surface. A range of particle types with varying concentrations of dimethyldichlorosilane groups on their surface has been investigated. A qualitative measurement of their wettability was obtained from powder immersion measurements allowing them to be ranked in terms of their hydrophobicity. Emulsions catastrophically invert from w/o to o/w at a critical volume fraction of water, which increases as the particles become more hydrophobic. Ultracentrifugation of very stable w/o emulsions containing particles of intermediate hydrophobicity enhances the extent of sedimentation at low g and induces coalescence at high g.

- The energy of attachment of a single particle at the oil-water interface is also dependent on the interfacial tension. This has been varied by changing the oil type and by replacement of water with other polar solvents. Oil-in-water emulsions are formed at $\phi_w = 0.5$ for non-polar oils such as hydrocarbons and w/o emulsions are formed with polar oils (low interfacial tension) such as esters and alcohols. Replacement of water by formamide in toluene systems result in little change in behaviour, whereas emulsions could not be formed with ethylene glycol or glycerol.

- An interesting phenomenon was observed in water-in-undecanol emulsions where the emulsion contracted initially to a gel followed by coalescence. The kinetics of complete breakdown was slower at high ϕ_w and passed through a maximum with respect to temperature.

- The wettability of a silica surface is shown to be dependent on the pH and electrolyte concentration of the aqueous phase. At high pH the silanol groups dissociate into SiO^- making them more hydrophilic which results in transfer of moderately hydrophobic particles from oil to the aqueous phase. The change in particle wettability causes inversion of emulsion type from w/o to o/w. As a result of the experimental findings a different explanation has been proposed for a number of previous situations involving particle wettability as a function of pH.

- The silica surface has been modelled by coating flat glass plates with dimethyldichlorosilane. The contact angle at the oil-water interface is shown to decrease with increasing pH (in the absence of electrolyte) but increases with increasing [electrolyte] at pH 11 on a surface of intermediate wettability. A theoretical model has also been advanced to describe these effects.

- The wettability of two pigment surfaces has been varied by adsorption of ionic, anionic or nonionic surfactants. The contact angle of an aqueous drop of CTAB or AOT in air on Hansa yellow pigment decreases with increasing [surfactant]. In the presence of the nonionic silicone surfactant L-77 the contact angle is essentially zero above the c.m.c. due to the surface tension being below the critical wetting tension. When the aqueous surfactant drop is under squalane the method of drop addition becomes important. For AOT, θ_{ow} is constant up to the c.m.c. but decreases substantially above it. For CTAB, θ_{ow} is independent of surfactant concentration above and below the c.m.c. In the presence of electrolyte, θ_{aw} decreases with increasing [NaCl] and [AOT] and is close to zero well below the c.m.c. at 1 M NaCl. θ_{ow} displays a minimum at 0.1 M NaCl in the presence of 10 mM AOT (above the c.m.c).

On phthalocyanine blue B pigment θ_{aw} and θ_{ow} measured by Method 2 decrease with increasing [AOT] whereas θ_{ow} measured by Method 1 is constant below the c.m.c. and decreases above it. Phthalocyanine blue is also shown to have greater apolar and hydrogen acceptor components than Hansa yellow.

SUGGESTIONS FOR FUTURE WORK

The area of solid-stabilised emulsions has not been widely investigated and the present work has opened up some interesting areas of future work.

- The majority of the current work has concentrated on emulsions stabilised by silica particles. Some work has already been started on emulsions stabilised by clay particles.[182] These particles have a disc-like shape (typical diameter 30 nm x 1 nm) and hence will align at the oil-water interface differently to spherical silica particles. Organoclays can also be prepared.

- The effect of particle size on emulsion type and stability has not been investigated in the current work where the silica particles all have a diameter between 5 and 30 nm. Monodisperse polystyrene sulphate-latex particles (purchased from IDC, Oregon) of diameter between 0.21 and 2.7 μm have been used to stabilise cyclohexane-water emulsions.[183] The particles are supplied as aqueous dispersions but, interestingly, prefer to stabilise w/o emulsions at all ϕ_w. The effect of particle concentration and flocculation by electrolyte on the stability of emulsions is investigated. Attempts to prepare monodisperse using a shear cell emulsifier with a fixed gap between rotor and stator is one of the aims of the future work.

- The pigment flushing process involves particles and surfactants. As described earlier, the process is believed to involve water-in-oil emulsification. It would be of interest to investigate emulsions stabilised by particles in the presence of surfactant to see whether the surfactant enhances or diminishes emulsion stability.

- The viscosity of emulsions described in Chapters 4 and 6 appear to go through a maximum upon catastrophic phase inversion. A greater understanding of the inversion process could be obtained by measuring the rheology of the emulsions as a function of ϕ_w. This has been attempted using a CarriMed cone and plate rheometer but evaporation of toluene resulted in irreproducible results. It should be possible to measure the rheology using the concentric cylinder geometry where less of the emulsion is exposed. Measuring the rheology of the aqueous or non-aqueous

dispersion prior to emulsification would be required in order to correctly treat the emulsion data.

- The kinetics of solid-stabilised emulsion drop coalescence could also be investigated. The coalescence of two drops can be modelled on a macroscopic scale by looking at a large drop coalescing with a planar interface.

- It would also be of interest to investigate the ability of solid particles to stabilise aqueous foams. The particles are now situated at the air-water surface as opposed to the oil-water interface of emulsion drops. It is anticipated that the particles would have to be larger than those used to stabilise emulsion drops following investigations by Wilson.[184] Are conditions which result in solid-stabilised emulsions similar to those which result in solid-stabilised foams?

REFERENCES

REFERENCES

1. T. A. Langstroth, in *The Pigment Handbook*, Volume 3, Characterisation and Physical Relationships, ed. C. Patton, Wiley and Sons, 1973, p. 447.

2. A. S. Gomm, G. Hull and J. L. Moilliet, *J. Oil Col. Chem. Assoc.*, **51**, 143 (1968).

3. B. P. Binks, in *Modern Aspects of Emulsion Science*, ed. B. P. Binks, The Royal Society of Chemistry, Cambridge, 1998, pp. 1-55.

4. J. H. Clint, *Surfactant Aggregation*, Blackie, Glasgow, 1992.

5. C. Tanford, *The hydrophobic effect: Formation of micelles and biological membranes*, 2nd edition, Wiley, New York, 1980.

6. J. W. Gibbs, *Collected works*, 1, Longmans Green, New York, 1931.

7. W. D. Bancroft, *J. Phys. Chem.*, **91**, 4528 (1913).

8. B. P. Binks, *Langmuir*, **9**, 25 (1993).

9. W. C. Griffin, *J. Soc. Cosmet. Chem.*, **1**, 311 (1949).

10. R. Aveyard, B. P. Binks and P. D. I. Fletcher, in *The Structure, Dynamics and Equilibrium Properties of Colloidal Systems*, eds. D. M. Bloor and E. Wyn-Jones, Kluwer, Dordrecht, 1990, p.557.

11. A. Graciaa, J. Lachaise, G. Marion and R. S. Schechter, *Langmuir*, **5**, 1315 (1989).

12. H. T. Davis, *Colloids Surf. A*, **91**, 9 (1994).

13. G. G. Stokes, *Philos. Mag.*, **1**, 337 (1851).

14. W. Thomson (Lord Kelvin), *Proc. Roy. Soc. Edinburgh*, **7**, 63 (1871).

15. See chapters in *Modern Aspects of Emulsion Science*, ed. B.P. Binks, Royal Society of Chemistry, Cambridge, 1998.

16. S. U. Pickering, *J. Chem. Soc.*, **91**, 2001 (1907).

17. W. C. Moore, *J. Am. Chem. Soc.*, **41**, 940 (1919).

18. T. R. Briggs, *J. Ind. Eng. Chem.*, **13**, 1008 (1921).

19. P. Finkle, H. D. Draper and J. H. Hildebrand, *J. Am. Chem. Soc.*, **45**, 2780 (1923).

20. J. H. Schulman and J. Leja, *Trans. Faraday Soc.*, **50**, 598 (1954).

21. E. H. Lucassen-Reynders and M. van den Tempel, *J. Phys. Chem.*, **67**, 731 (1963).

22. P. M. Kruglyakov and A. F. Koretskii, *Izv. Sib. Otd. AN SSSR, Ser. Khim. Nauk*, **9**, 16 (1971).

23. A. Tsugita, S. Takemoto, K. Mori, T. Yoneya and Y. Otani, *J. Colloid Interface Sci.*, **95**, 551 (1983).

24. A. Gelot, W. Friesen and H. A. Hamza, *Colloids Surf.*, **12**, 271 (1984).

25. S. Levine and E. Sanford, *Can. J. Chem. Eng.*, **62**, 258 (1985).

26. H. Hassander, B. Johansson and B. Tornell, *Colloids Surf.*, **40**, 93 (1989).

27. S. Levine, B. D. Bowen and S. J. Partridge, *Colloids Surf.*, **38**, 325 (1989).

28. D. E. Tambe and M. M. Sharma, *J. Colloid Interface Sci.*, **157**, 244 (1993).

29. D. E. Tambe and M. M. Sharma, *J. Colloid Interface Sci.*, **162**, 1 (1994).

30. D. E. Tambe and M. M. Sharma, *Adv. Colloid Interface Sci.*, **52**, 1 (1994).

31. D. E. Tambe and M. M. Sharma, *J. Colloid Interface Sci.*, **171**, 456 (1995).

32. D. E. Tambe, J. Paulis and M. M. Sharma, *J. Colloid Interface Sci.*, **171**, 463 (1995).

33. Y. H. Yan and J. H. Masliyah, *Ind. & Eng. Chem. Res.*, **36**, 1122 (1997).

34. S. Abend, N. Bonnke, U. Gutschner and G. Lagaly, *Colloid Polym. Sci.*, **276**, 730 (1998).

35. B. R. Midmore, *Colloids Surf. A*, **132**, 257 (1998).

36. B. R. Midmore, *J. Colloid Interface Sci.*, **213**, 352 (1999).

37. G. Lagaly, M. Reese and S. Abend, *Appl. Clay Sci.*, **14**, 83 (1999).

38. G. Gouy, *J. Phys. Radium*, **9**, 457 (1910).

39. D. L. Chapman, *Phil. Mag.*, **25**, 475 (1913).

40. O. Stern, *Z. Elektrochem.*, **30**, 508 (1924).

41. D. J. Shaw, *Introduction to colloid and surface chemistry*, 4th edition, Butterworth-Heinemann Ltd., London, 1991, p.174.

42. B. V. Derjaguin and L. Landau, *Acta Physicochim. URSS*, **14**, 633 (1941).

43. E. J. W. Verwey and J. Th. G. Overbeek, *Theory of Stability of Lyophobic Colloids*, Elsevier, Amsterdam, 1948.

44. J. W. Jansen, C. G. de Kruif and A. Vrij, *J. Colloid Interface Sci.*, **114**, 492 (1986).

45. J. W. Jansen, C. G. de Kruif and A. Vrij, *J. Colloid Interface Sci.*, **114**, 481 (1986).

46. J. Edwards, D. H. Everett, T. O'Sullivan, I. Pangalou and B. Vincent, *J. Chem. Soc. Faraday Trans. 1*, **80**, 2599 (1984).

47. J. Clarke and B. Vincent, *J. Colloid Interface Sci.*, **82**, 208 (1981).

48. B. Vincent, J. Edwards, S. Emmett and A. Jones, *Colloids Surf.*, **18**, 261 (1986).

49. A. Jones and B. Vincent, *Colloids Surf.*, **42**, 113 (1989).

50. Handbook of Chemistry and Physics, C.R.C. Press, Boca Raton, Florida, 65th edn., 1984.

51. J. Timmermans, *Physico-Chemical Constants of Pure Organic Compounds*, Vol.2, Elsevier, Amsterdam (1965).

52. R. K. Iler, *The Chemistry of Silica*, Wiley, New York, (1979).

53. Wacker HDK Fumed Silica brochure Nr. 4955e., Wacker-Chemie GmbH, München, (December 1998).

54. M. Fuji, K. Machida, T. Takei, T. Watanabe and M. Chikazawa, *Langmuir*, **16**, 3281 (2000).

55. H. Balard, E. Papirer, A. Khalfi and H. Barthel, *Composite Interfaces*, **6**, 19 (1999).

56. J. J. Kirkland, J. L. Glajch and R. D. Farlee, *Anal. Chem.*, **61**, 2 (1989).

57. M. L. Hair, *J. Colloid Interface Sci.*, **60**, 154 (1977).

58. Pigments, Dyestuffs and Lakes, Oil and Colour Chemists Association, Kluwer Academic Press, Amsterdam, (1983).

59. R. Aveyard, P. Cooper, P. D. I. Fletcher and C. E. Rutherford, *Langmuir*, **9**, 604 (1993).

60. E. K. Mann and D. Langevin, *Langmuir*, **7**, 1112 (1991).

61. B. P. Binks, Ph.D Thesis, University of Hull (1986).

62. J. Weiss, G. Zografi and A. P. Simonelli, *J. Pharm. Sci.*, **63**, 381 (1974).

63. R. Aveyard, B. P. Binks, S. Clark and P. D. I. Fletcher, *J. Chem. Soc. Faraday Trans.*, **86**, 3111 (1990).

64. B. P. Binks and J. Dong, *Colloids Surf. A*, **132**, 289 (1998).

65 J. Eisenlauer and E. Killmann, *J. Colloid Interface Sci.*, **74**, 108 (1980).

66. M. W. Rutland and R. M. Pashley, *J. Colloid Interface Sci.*, **130**, 448 (1989).

67. Malvern Mastersizer User Manual – IM 100, Issue 2 (1990).

68. R. Aveyard, B. P. Binks, P. D. I. Fletcher and C. E. Rutherford, *Colloids Surf. A*, **83**, 89 (1994).

69. G. Newcombe and J. Ralston, *Langmuir*, **8**, 190 (1992).

70. W. D. Harkins and H. F. Jordan, *J. Am. Chem. Soc.*, **52**, 1751 (1930).

71. B. B. Freud and H. Z. Freud, *J. Am. Chem. Soc.*, **52**, 1772 (1930).

72. H. H. Zuidema and G. W. Waters, *Ind. Eng. Chem.*, **13**, 312 (1941).

73. L. Wilhelmy, *Ann. Phys.*, **119**, 177 (1863).

74. A. Dognon and M. Abribat, *Compt. Rend. Acad. Sci.*, (Paris), **208**, 1881 (1939).

75. R. Benitez, S. Contreras and J. Goldfarb, *J. Colloid Interface Sci.*, **36**, 146 (1971).

76. L. H. Allen and E. Matijevic, *J. Colloid Interface Sci.*, **31**, 287 (1969).

77. L. H. Allen and E. Matijevic, *J. Colloid Interface Sci*, **33**, 420 (1970).

78. J. Depasse and A. Watillon, *J. Colloid Interface Sci.*, **33**, 430 (1970).

79. J. Rubio and J. Goldfarb, *J. Colloid Interface Sci.*, **36**, 289 (1971).

80. R. D. Harding, *J. Colloid Interface Sci.*, **35**, 172 (1971).

81. H. Freundlich and H. Cohn, *Kol. Zeit.*, **34**, 28 (1926).

82. A. Watillon and P. Gérard, *Proc. Int. Congr. Surface Activity*, 4th, 1261 (1964).

83. J. Eisenlauer, E. Killman and M. Korn, *J. Colloid Interface Sci.*, **74**, 120 (1980).

84. D. Heath and TH. F. Tadros, *J. Colloid Interface Sci.*, **93**, 320 (1983).

85. P. J. Scales, F. Grieser, T. W. Healy, L. R. White and D. Y. C. Chan, *Langmuir*, **8**, 965 (1992).

86. R. J. Hunter, *Zeta potential in Colloid Science*, Academic Press, London, 1981.

87. J. Visser, *Adv. Colloid Interface Sci.*, **3**, 331 (1972).

88. J. Depasse, *J. Colloid Interface Sci.*, **194**, 260 (1997).

89. T. W. Healy, in *The Colloid Chemistry of Silica*, ed. H. E. Bergna, Advances in Chemistry Series 234, ACS, Washington DC, 1994, p. 147.

90. H. Yotsumoto and R-H. Yoon, *J. Colloid Interface Sci.*, **157**, 426 (1993).

91. J. S. Clunie, J. F. Goodman and P. C. Symons, *Nature*, **216**, 1203 (1967).

92. J. N. Israelachvilli, *Surf. Sci. Rep.*, **14**, 111 (1992).

93. Ya. I. Rabinovich, B. V. Derjaguin and N. V. Churaev, *Adv. Colloid Interface Sci.*, **16**, 63 (1982).

94. R. G. Horn, D. T. Smith and W. Haller, *Chem. Phys. Lett.*, **162**, 404 (1989).

95. H. Yotsumoto and R-H. Yoon, *J. Colloid Interface Sci.*, **157**, 434 (1993).

96. J. A. Molina-Bolivar, F. Galisteo-Gonzalez and R. Hidalgo-Alvarez, *Phys. Rev. E*, **55**, 4522 (1997).

97. M. Kerker, *The Scattering of Light and other Electromagnetic Radiation*, Academic Press, London, 1969.

98. A. S. Kabalnov, A. V. Pertzov and E. D. Shchukin, *J. Colloid Interface Sci.*, **118**, 590 (1987).

99. *Solubilities of Inorganic and Organic Compounds*, Ed. H. Stephen and T. Stephen, Vol. 1, Part 1, Pergamon Press, Oxford, 1963.

100. P. Taylor, *Adv. Colloid Interface Sci.*, **75**, 107 (1998).

101. H. Schulze, *J. Prakt. Chem.*, **25**, 431 (1882).

102. W. B. Hardy, *Proc. Roy. Soc. London*, **66**, 110 (1900).

103. J. Th.G. Overbeek, in *Colloid Science*, ed. H. R. Kruyt, Vol.1, Elsevier, Amsterdam, 1952.

104. C. J. van Oss, R. F. Giese and P. M. Costanzo, *Clays Clay Miner.*, **2**, 151 (1990).

105. W. Wu, R. F. Giese, Jr. and C. J. van Oss, *Colloids Surf. A*, **89**, 241 (1994).

106. J. C. J. van der Donck, G. E. J. Vaessen and H. N. Stein, *Langmuir*, **9**, 3553 (1993).

107. P. Claesson, R. G. Horn and R. M. Pashley, *J. Colloid Interface Sci.*, **100**, 250 (1984).

108. J. Bibette, *J. Colloid Interface Sci.*, **147**, 474 (1991).

109. E. S. Pagac, D. C. Prieve and R. D. Tilton, *Langmuir*, **14**, 2333 (1998).

110. R. Aveyard, B. P. Binks, P. D. I. Fletcher, C. E. Rutherford, P. J. Dowding and B. Vincent, *Phys. Chem. Chem. Phys.*, **1**, 1971 (1999).

111. R. Aveyard, J. H. Clint and D. Nees, *Colloid Polymer Sci.*, **278**, 155 (2000).

112. J. L. Salager, in *Encyclopedia of Emulsion Technology*, ed. P. Becher, Marcel Dekker: New York, vol.3, 1988, p. 79.

113. B. W. Brooks, H. N. Richmonds and M. Zerfa, in *Modern Aspects of Emulsion Science*, ed. B. P. Binks, Royal Society of Chemistry, Cambridge, 1998, p. 175.

114. R. Thom, *Stabilité structurelle et morphogénèse*, Benjamin, London, 1972; English translation: *Structural Stability and Morphogenesis* (D. H. Fowler, Transl.), Addison-Wesley, California, 1989.

115. G. E. J. Vaessen and H. N. Stein, *J. Colloid Interface Sci.*, **176**, 378 (1995).

116. E. Dickinson, *J. Colloid Interface Sci.*, **84**, 284 (1981).

117. E. C. Zeeman, '*Catastrophe Theory*', Addison-Wesley, Reading, MA, 1977.

118. E. Dickinson, *J. Colloid Interface Sci.*, **87**, 416 (1982).

119. W. Ostwald, *Kolloid Z.*, **7**, 64 (1910).

120. P. Jarry, M. Miñana-Pérez and J. L. Salager, in *Surfactants in Solution*, vol.6, ed. K. Mittal, Plenum, New York, 1987, p. 1689.

121. J. L. Salager, M. Minana-Perez and F. Silva, *J. Disp. Sci. Technol.*, **3**, 279 (1982).

122. B. W. Brooks and H. N. Richmond, *Chem. Eng. Sci.*, **49**, 1065 (1994).

123. P. Walstra and P. E. A. Smulders in *Modern Aspects of Emulsion Science*, ed. B. P. Binks, Royal Society of Chemistry, Cambridge, 1998, pp. 56-99.

124. P. Becher, in *Emulsion: Theory and Practice*, 2nd edn., Reinhold, New York, 1966.

125. B. W. Brooks and H. N. Richmond, *Colloids Surf.*, **58**, 131 (1991).

126. B. W. Brooks and H. N. Richmond, *Chem. Eng. Sci.*, **49**, 1053 (1994).

127. S. I. Clarke and H. Sawistowski, *Trans. Inst. Chem. Eng.*, **56**, 50 (1978).

128. A. H. Selker and C. A. Sleicher, *Can. J. Chem. Eng.*, **43**, 298 (1965).

129. B. P. Binks, W-G. Cho, P. D. I. Fletcher and D. N. Petsev, *Langmuir*, **16**, 1025 (2000).

130. R. Aveyard, B. P. Binks and J. Mead, *J. Chem. Soc., Faraday Trans. 1*, **82**, 1755 (1986).

131. H. Barthel, L. Rösch, J. Weis, A. Khalfi, H. Balard and E. Papirer, *Composite Interfaces*, **6**, 27 (1999).

132. K. Shinoda, *Bull. Chem. Soc. Jpn.*, **89**, 435 (1968).

133. S. Friberg, I. Lapczynska and G. Gillberg, *J. Colloid Interface Sci.*, **56**, 19 (1976).

134. K. Shinoda and H. Takeda, *J. Colloid Interface Sci.*, **41**, 328 (1970).

135. B. W. Brooks, S. Sajjadi and M. Zerfa, *Colloids Surf. A*, **155**, 323 (1999).

136. R. Aveyard, B. P. Binks, J. Esquena, P. D. I. Fletcher, R. Buscall and S. Davies, *Langmuir*, **15**, 970 (1999).

137. D. Diggins, L. G. J. Fokkink and J. Ralston, *Colloids Surf.*, **44**, 299 (1990).

138. T. J. Lin and J. C. Lambrechts, *J. Soc. Cosmet. Chem.*, **20**, 185 (1969).

139. T. J. Lin, H. Kurihara and H. Ohta, *J. Soc. Cosmet. Chem.*, **26**, 121 (1975).

140. J. H. Clint and S. E. Taylor, *Colloids Surf.*, **65**, 61 (1992).

141. N. D. Denkov, I. B. Ivanov, P. A. Kralchevsky and D. T. Wasan, *J. Colloid Interface Sci.*, **150**, 589 (1992).

142. J. H. Clint and N. Quirke, *Colloids Surf. A*, **78**, 277 (1993).

143. Z. Horvolgyi, M. Mate, A. Daniel and J. Szalma, *Colloids Surf. A*, **156**, 501 (1999).

144. Z. Horvolgyi, S. Nemeth and J. P. Fendler, *Langmuir*, **12**, 997 (1996).

145. R. Aveyard, J. H. Clint, D. Nees and V. N. Paunov, *Langmuir*, **16**, 1969 (2000).

146. E. Kissa, *Dispersions; Surfactant Science Series*; Marcel Dekker: New York, vol. 84, 1999, Chapter 5.

147. N. Yan, Y. Maham, J. H. Masliyah, M. R. Gray and A. E. Mather, *J. Colloid Interface Sci.*, **228**, 1 (2000).

148. S. J. Rehfeld, *J. Phys. Chem.*, **66**, 1966 (1962).

149. R. D. Vold and R. C. Groot, *J. Phys. Chem.*, **66**, 1969 (1962).

150. R. Aveyard, B. J. Briscoe and J. Chapman, *J. Chem. Soc., Faraday Trans. 1*, **68**, 10 (1972).

151. T. Handa and P. Mukerjee, *J. Phys. Chem.*, **85**, 3916 (1981).

152. B. P. Binks and J. Dong, *J. Chem. Soc., Faraday Trans.*, **94**, 401 (1998).

153. J. R. MacNab, Ph.D Thesis, University of Hull, 1996.

154. D. Y. Kwok and A. W. Neumann, *Colloids Surf. A*, **161**, 31 (2000).

155. R. Aveyard, B. P. Binks, P. D. I. Fletcher, A. J. Kirk and P. Swansbury, *Langmuir*, **9**, 523 (1993).

156. J. Philip, L. Bonakdar, P. Poulin, J. Bibette and F. Leal-Calderon, *Phys. Rev. Lett.*, **84**, 2018 (2000).

157. L. Bonakdar, J. Philip, P. Bardusco, J. Petkov, J. J. Potti, P. Méléard and F. Leal-Calderon, *Colloids Surf. A*, in press.

158. H. Kunieda, Y. Fukui, H. Uchiyama and C. Solans, *Langmuir*, **12**, 2136 (1996).

159. J. D. Henry, Jr., M. E. Prudich and C. Lau, *Colloids Surf.*, **1**, 335 (1980).

160. I. N. Kornil'ev, Z. M. Zorin and N. V. Churaev, *Colloid J. USSR*, **46**, 783 (1984).

161. R. Ettelaie, ICI Wilton, 2000.

162. D. Y. C. Chan, J. W. Perram, L. R. White and T. W. Healy, *J. Chem. Soc., Faraday Trans. 1*, **71**, 1046 (1975).

163. D. Y. C. Chan, L.R. White and T. W. Healy, *J. Chem. Soc., Faraday Trans. 1*, **72**, 2845 (1976).

164. D. Y. C. Chan, in *Geochemical processes at mineral interfaces*, eds. J. A. Davis and K. F. Hayes, ACS symposium series No. 323, Washington, 1986, p. 99.

165. R. Ettelaie and R. Buscall, *Adv. Colloid Interface Sci.*, **61**, 131 (1995).

166. N.V. Churaev and V. D. Sobolev, *Colloid J.*, **57**, 843 (1995).

167. B. P. Binks, R. Ettelaie and S. O. Lumsdon, in preparation.

168. J. J. Oren and G. D. M. Mackay, *Fuel*, **56**, 382 (1977).

169. J. Laskowski and J. Iskra, *J.I.M.M. Trans.*,**79**, C6 (1970).

170. R. Aveyard, B. P. Binks, P. D. I. Fletcher and C. E. Rutherford, *J. Disp. Sci. Technol.*, **15**, 251 (1994).

171. P. R. Garrett, in *Defoaming: Theory and Industrial Applications*, ed. P. R. Garrett, Surfactant Science Series Vol. 45, Marcel Dekker, New York, 1993, p. 1.

172. T. Young, *Phil. Trans. Roy. Soc. London*, **95**, 65 (1805).

173. E. H. Lucassen-Reynders, *J. Phys. Chem.*, **67**, 969 (1963).

174. C. J. van Oss, L. Ju, M. K. Chaudhury and R. J. Good, *J. Colloid Interface Sci.*, **128**, 313 (1989).

175. J. H. Clint, University of Hull (1997).

176. R. J. Good, in *Surface and colloid science*, ed. R. J. Good and R. R. Stromberg, Vol. 11, Plenum, New York, 1979, pp. 1-30.

177. L. R. Fisher, *J. Colloid Interface Sci.*, **72**, 200 (1979).

178. C. Tanford, in *The hydrophobic effect and formation of micelles and biological membranes*, Wiley, New York, 2nd Edition, 1980.

179. R. Aveyard, B. P. Binks and J. Mead, *J. Chem. Soc., Faraday Trans. 1*, **81**, 2169 (1985).

180. R. Aveyard, B. P. Binks and P. D. I. Fletcher, in *Micelles, Microemulsions and Monolayers*, ed. D. O. Shah, Marcel Dekker, New York, 1998, p. 395.

181. D. Bargeman, *J. Colloid Interface Sci.*, **40**, 344 (1972).

182. N. P. Ashby and B. P. Binks, *Phys. Chem. Chem. Phys.*, in press.

183. B. P. Binks and S. O. Lumsdon, *Phys. Chem. Chem. Phys.*, submitted.

184. J. C. Wilson, Ph.D Thesis, University of Bristol, 1980.

APPENDIX

Figure 3.3 Turbidity of 0.5 wt.% Aerosil 200 dispersions in water at pH 2 as a function of [NaCl].

[NaCl] / M	turbidity / NTU	
	0 hours	24 hours
0	320	310
0.01	315	305
0.1	310	300
0.5	300	290
1	275	260
1.5	250	245
2	225	220
2.5	200	200
3	180	180
3.5	165	160
4	150	150
4.5	145	145
5	140	135

Figure 3.4 Turbidity of 0.5 wt.% Aerosil 200 dispersions in water at pH 10 as a function of [NaCl].

[NaCl] / M	turbidity / NTU	
	0 hours	24 hours
0	325	305
0.01	330	308
0.1	325	310
0.2	315	305
0.25	310	305
0.3	305	300
0.4	300	295
0.45	300	
0.5	300	450
0.6	295	
0.7	290	390
0.85	285	345
1	280	360
1.25	270	340
1.5	250	355
2	230	345

Figure 3.5 Change in turbidity with time of 0.5 wt.% Aerosil 200 dispersions in water at pH 10 in the presence of NaCl.

time / hours	turbidity / NTU	
	1.5 M NaCl	2 M NaCl
0	250	230
0.5	250	230
1	250	225
2	270	245
3	295	260
4	310	280
5	330	290
6	335	300
7	350	320
8	350	340
16	355	340
24	355	345

Figure 3.6 Turbidity of 0.5 wt.% Aerosil 200 dispersions in water 24 hours after adding NaCl.

[NaCl] / M	turbidity / NTU					
	pH 2	pH 4	pH 5	pH 6	pH 7	pH 10
0	310	310	300	295	305	305
0.01	305	305	290	290	300	308
0.1	300	300	290	285	300	310
0.3		295	270	270	295	300
0.5	290	285	255	255	280	450
0.75		260	250	235	255	390
1	260	250	240	230	300	360
1.25		245	230	220	315	340
1.5	245	235	215	225	340	355
2	220	210	195	230	300	345
2.5	200	195	180	240	250	
3	180	180	155	205	245	
3.5	160	155	155	195	210	
4	150	145	145	150	190	
4.5	145	135	140	145	175	
5	135	125	155	135	155	

Figure 3.7 Critical coagulation concentration of NaCl for silica dispersions in water as a function of pH, 24 hours after mixing.

pH	critical coagulation concentration of NaCl / M		
	allen & matijevic	present data	rubio & goldfarb
2			
4			
5			
6		2.5	
6.4	1.4		
7	0.95	1.5	2.3
7.3	0.8		
7.5			1.8
7.7	0.68		1.6
8		1	1.25
8.4	0.5		
8.5	0.4		
8.6			1
9		0.7	0.8
9.1			0.75
10		0.6	
10.2	0.2		

Figure 3.8 Surface tensions of Aerosil 200 dispersions in water at pH 2 and 10 at 25 °C as a function of particle concentration measured using the Wilhelmy plate.

particle concentration / wt%	surface tension mN m^{-1}	
	pH 2	pH 10
0	72	72
0		
0.5		71.6
1	72.5	71.7
2	72.3	71.9
3	72.2	71.9
4	72	71.7
5	71.9	71

Figure 3.9 Stability to creaming and coalescence of 20 vol% toluene-in-water emulsions stabilised by Aerosil 200 at pH 4.

time / mins	fraction of emulsion as aqueous phase			fraction of emulsion as oil phase		
	0.2 wt.%	0.5 wt.%	1 wt.%	0.2 wt.%	0.5 wt.%	1 wt.%
0	0	0	0	0	0	0
0.5	0.710	0	0	0.092	0	0
1	0.715	0	0	0.092	0	0
2	0.715	0	0	0.092	0	0
3	0.715	0	0	0.092	0	0
4	0.715	0.730	0	0.092	0.123	0
5	0.715	0.730	0	0.092	0.123	0
7.5	0.715	0.730	0	0.092	0.123	0
10	0.715	0.730	0.698	0.092	0.123	0.092
12.5	0.715	0.730	0.698	0.092	0.123	0.092
15	0.715	0.730	0.698	0.092	0.123	0.092
20	0.715	0.730	0.698	0.092	0.123	0.092

Figure 3.10 Stability to creaming and coalescence of 20 vol% toluene-in-water emulsions stabilised by Aerosil 200 at pH 10.

time / mins	fraction of emulsion as aqueous phase			fraction of emulsion as oil phase		
	0.2 wt.%	0.5 wt.%	1 wt.%	0.2 wt.%	0.5 wt.%	1 wt.%
0	0	0	0	0	0	0
0.5	0.261	0.435	0.324	0.071	0.043	0.059
1	0.522	0.661	0.598	0.071	0.043	0.059
2	0.730	0.730	0.730	0.071	0.043	0.059
3	0.730	0.730	0.730	0.071	0.043	0.059
4	0.730	0.730	0.730	0.071	0.043	0.059
5	0.730	0.730	0.730	0.071	0.043	0.059
7.5	0.730	0.730	0.730	0.071	0.043	0.059
10	0.730	0.730	0.730	0.071	0.043	0.059
15	0.730	0.730	0.730	0.071	0.043	0.059
20	0.730	0.730	0.730	0.071	0.043	0.059

Figure 3.11 Stability to coalescence after 30 minutes of 20 vol% toluene-in-water emulsions stabilised by 0.5 wt.% Aerosil 200 as a function of NaCl.

[NaCl] / M	fraction of emulsion as oil phase		
	pH 2	pH 4	pH 10
0	0.057	0	0.071
0.01	0.071	0	0.071
0.1	0.062	0	0.181
0.5	0.06	0	0.183
1	0.036	0	0.183
1.5	0.015	0	0.185
2	0	0	0.185

Figure 3.12 Stability to coalescence after 30 minutes of 20 vol% toluene-in-water emulsions stabilised by 0.5 wt.% Aerosil 200 as a function of pH

pH	fraction of emulsion as oil phase	
	0 M NaCl	1 M NaCl
2	0.054	0.036
3	0.045	0.025
4	0.008	0
5	0.023	0.066
6	0.035	0.105
7	0.049	0.122
8	0.065	0.183
9	0.067	0.2
10	0.105	0.2

Figure 3.13 Conductivity of toluene-in-water emulsions stabilised by 0.5 wt.% Aerosil 200 as a function of [NaCl] at pH given.

[NaCl] / M	log(conductivity / μS cm-1)		
	pH 2	pH 5	pH 10
0	2.08	0.79	1.68
0.01	2.53	2.2	2.32
0.03	2.7	2.74	2.8
0.05	2.74	2.93	2.86
0.1	3.04	3.14	3.42
0.15	3.06	3.32	3.44
0.2	3.18	3.31	3.63
0.3	3.14	3.54	3.73
0.5	3.28	3.83	3.83
0.7	3.32	3.86	4.01
0.9	3.58	4.05	4.06

Figure 3.14 Stability to creaming and coalescence of 20 vol% toluene-in-water emulsions stabilised by Ludox HS-40 at pH 2

time / mins	fraction of emulsion as aqueous phase		fraction of emulsion as oil phase	
	0.5 wt.%	3.5 wt.%	0.5 wt.%	3.5 wt.%
0	0	0	0	0
0.5	0.745	0	0.015	0.04
1	0.745	0	0.015	0.04
2	0.745	0	0.031	0.04
3	0.745	0	0.046	0.04
4	0.745	0.800	0.046	0.04
5	0.745	0.800	0.046	0.04
10	0.745	0.800	0.046	0.04
20	0.745	0.800	0.046	0.04
30	0.745	0.800	0.046	0.04

Figure 3.15 Stability to creaming and coalescence of 20 vol% toluene-in-water emulsions stabilised by Ludox HS-40 at pH 10.

time / mins	fraction of emulsion as aqueous phase			fraction of emulsion as oil phase		
	1 wt.%	2 wt.%	5 wt.%	1 wt.%	2 wt.%	5 wt.%
0	0	0	0	0	0	0
0.5	0	0	0	0.057	0.018	0.036
1	0	0.245	0	0.071	0.018	0.055
2	0	0.408	0.033	0.071	0.055	0.055
3	0.267	0.735	0.717	0.071	0.055	0.073
4	0.782	0.735	0.717	0.071	0.055	0.073
5	0.782	0.735	0.733	0.071	0.055	0.091
10	0.782	0.735	0.750	0.071	0.091	0.091
20	0.782	0.767	0.750	0.200	0.091	0.145
30	0.782	0.767	0.750	0.200	0.164	0.182

Figure 3.16 Stability to creaming and coalescence of 20 vol% toluene/CCl_4 emulsions stabilised by 0.5 wt.% Ludox HS-40.

time / mins	fraction of emulsion as aqueous phase		fraction of emulsion as oil phase	
	pH 2	pH 10	pH 2	pH 10
0	0	0	0	0
0.5	0	0	0	0
1	0	0	0	0
5	0	0	0	0
10	0	0.144	0	0
15	0	0.32	0	0
20	0	0.456	0	0
30	0	0.672	0	0
40	0	0.696	0	0
50	0	0.712	0	0
60	0	0.712	0	0
75	0.4	0.728	0	0
90	0.62	0.744	0	0
120	0.65	0.744	0	0
150	0.65	0.744	0	0.056
180	0.67	0.768	0	0.057
210	0.67	0.784	0	0.057
240	0.67	0.784	0	0.057

Figure 3.17 Stability to creaming and coalescence of 20 vol% toluene-in-water emulsions stabilised by 0.5 wt.% Ludox HS-40 at pH 2.

time / mins	fraction of emulsion as a queous phase			fraction of emulsion as oil phase		
	0.1 M	0.3 M	1.0 M	0.1 M	0.3 M	1.0 M
0	0	0	0	0	0	0
0.5	0	0	0	0.031	0.025	0.014
1	0	0	0	0.031	0.025	0.029
2	0.763	0	0	0.031	0.025	0.029
3	0.763	0	0	0.046	0.038	0.029
4	0.763	0	0	0.046	0.038	0.029
5	0.763	0.8	0	0.046	0.038	0.029
10	0.763	0.8	0	0.046	0.050	0.029
15	0.763	0.8	0.6	0.046	0.064	0.029
20	0.763	0.8	0.743	0.046	0.075	0.029

Figure 3.18 Stability to creaming and coalescence of 20 vol% toluene-in-water emulsions stabilised by 0.5 wt.% Ludox HS-40 at pH 9.

time / mins	fraction of emulsion as aqueous phase			fraction of emulsion as oil phase		
	0.1 M	0.3 M	0.7 M	0.1 M	0.3 M	0.7 M
0	0	0	0	0	0	0
0.5	0.782	0.8	0.782	0.114	0.138	0.114
1	0.764	0.8	0.782	0.114	0.138	0.114
2	0.764	0.8	0.782	0.129	0.138	0.114
3	0.764	0.8	0.782	0.129	0.138	0.114
4	0.764	0.8	0.782	0.129	0.138	0.114
5	0.764	0.8	0.782	0.129	0.138	0.114
10	0.764	0.8	0.782	0.129	0.138	0.114
20	0.764	0.8	0.782	0.129	0.138	0.114

Figure 3.19 Turbidity of 0.5 wt.% Aerosil 200 dispersions in water at two pH values as a function of [$LaCl_3$].

[$LaCl_3$] / mM	turbidity / NTU 0 hours		turbidity / NTU 24 hours	
	pH 2	pH 10	pH 2	pH 10
0	330	330	330	330
0.25	330	340	310	290
0.5	330	340	320	305
0.75	325	340	320	330
1	325	340	320	340
2	330	370	320	390
3	330	400	330	420
4	330	440	350	475
5	330	475	320	520
6	330	520	320	540
7	330		325	650
8	330	605	325	680
9	345		330	720
10	345	650	330	730
15		705		785
20	340	860	340	

Figure 3.20 Turbidity of 0.5 wt.% Aerosil 200 dispersions in water 24 hours after adding $LaCl_3$ at pH given.

$LaCl_3$ / mM	turbidity / NTU						
	pH 2	pH 4	pH 4.5	pH 5	pH 6	pH 8	pH 10
0	330	330	330	340	330	330	330
0.25	310	330	330	330		325	290
0.5	320	330	330	345		380	305
0.75	320	320	330	345		345	330
1	320	320	350	350	350	390	340
2	320	340	355	355	380	415	390
3	330	315	345	380	385	450	420
4	350	330	350	360	395	525	475
5	320	320	350	370	395	555	520
6	320				375		540
7	325	330	325	390	395	580	650
8	325				395		695
9	330	325	350	355	390	660	720
10	330	340	345	395	400	730	730
15		325	350	390	480	755	745
20	340	330	355	395	450	790	860

Figure 3.21 Stability to creaming and coalescence after 30 minutes of 20 vol% toluene-in-water emulsions stabilised by 0.5 wt.% Aerosil 200 as a function of [$LaCl_3$] at pH 2.

[$LaCl_3$] / mM	fraction of emulsion as aqueous phase	fraction of emulsion as oil phase
0	0.795	0.085
1	0.77	0.1
2	0.74	0.12
3	0.77	0.092
4	0.795	0.092
6	0.7	0.1
7.5	0.73	0.115
10	0.73	0.122
12.5	0.7	0.13
15	0.75	0.092
17.5	0.76	0.135
20	0.75	0.1

Figure 3.22 Stability to creaming and coalescence after 30 minutes of 20 vol% toluene-in-water emulsions stabilised by 0.5 wt.% Aerosil 200 as a function of [$LaCl_3$] at pH 10.

[$LaCl_3$] / mM	fraction of emulsion as aqueous phase	fraction of emulsion as oil phase
0	0.765	0.114
0.25	0.783	
0.5	0.78	0.1
1	0.728	0.071
1.5		0.086
1.75	0.4	0.067
2	0.053	0
3	0.088	0
4	0.16	
4.5	0.153	0
5	0.195	0.067
6	0.689	0.092
8	0.722	0.108
10	0.754	0.114

Figure 3.23 Stability to creaming and coalescence after 30 minutes of 20 vol% toluene-in-water emulsions stabilised by 0.5 wt.% Aerosil 200 in 5 mM $LaCl_3$.

pH	fraction of emulsion as aqueous phase	fraction of emulsion as oil phase
2	0.8	0.186
3	0.8	0.157
4	0.766	0.086
5	0.7	0.107
6	0.261	0.018
7	0.139	0.042
8	0.32	0
9	0.266	0.028
10	0.178	0.06

Figure 3.24 Stability to creaming and coalescence after 30 minutes of 20 vol% toluene-in-water emulsions stabilised by 0.5 wt.% Aerosil 200 in 10 mM $LaCl_3$.

pH	fraction of emulsion as aqueous phase	fraction of emulsion as oil phase
2	0.8	0.18
3	0.78	0.2
4	0.79	0.175
5	0.8	0.169
5.5	0.373	0.043
6	0.28	0
6.5	0.223	0.067
6.75	0.693	0.067
7.5	0.767	0.107
8	0.74	0.173
8.5	0.8	0.12
9	0.79	0.146
9.5	0.731	0.12
10	0.7	0.163

Figure 3.25 Effect of [$LaCl_3$] on the initial volume average diameter of 20 vol% toluene-in-water emulsions stabilised by 0.5 wt.% Aerosil 200 at pH 2 and 10.

[$LaCl_3$] / mM	d(v,0.5) / μm	
	pH 2	pH 10
1	78.5	50.3
0	77.6	53.8
1.5		48.9
2		46.8
2.5		42.4
3	78.3	49.6
4		56.8
4.5		63.4
5	78.9	70.65
6		79.3
6.5		78.5
7.5	77.3	78.2
9		78.7
10	77.5	74.55

Figure 3.27 Effect of [$LaCl_3$] on the initial volume average diameter and stability to creaming of 20 vol% toluene-in-water emulsions stabilised by 0.5 wt.% Aerosil 200 at pH 10.

[$LaCl_3$] / mM	d(v,0.5) / μm	fraction of emulsion as aqueous phase
0	53.8	0.765
0.25		0.783
0.5		0.78
1	50.3	0.728
1.5	48.9	
1.75		0.4
2	49	0.053
2.5	42.4	
3	49.6	0.088
4	56.8	0.16
4.5	63.4	0.153
5	70.65	0.195
6	79.3	0.689
6.5	78.5	
7.5	78.2	
8		0.722
9	78.7	
10	74.55	0.754

Figure 3.28 Conductivity of 0.5 wt.% Aerosil 200 dispersions in water and 50 vol% toluene-in-water emulsions stabilised by 0.5 wt.% Aerosil 200 at pH 6 as a function of [$LaCl_3$].

[$LaCl_3$] / mM	log (conductivity / μS cm^{-1})	
	emulsion	colloid
1	2.6	2.975
2	2.5	2.95
3	2.55	3.15
4	2.85	3.25
5	2.875	3.215
6	2.925	3.275
7	2.9	3.3
8	3.25	3.4
10	3.35	3.5
15	3.5	3.65
20	3.6	3.75

Figure 3.29 Turbidity of 0.5 wt.% Aerosil 200 dispersions in water 24 hours after adding TEAB.

log[TEAB] / M	turbidity / NTU	
	pH 2	pH 10
-3	305	310
-2.52	310	320
-2.3	305	330
-2	305	335
-1.52	310	335
-1.3	305	
-1.12	305	340
-1.1		330
-1	300	340
-0.7		310
-0.6	300	
-0.52	300	305
-0.3	275	295
-0.12	245	
0	215	205

Figure 3.30 Stability to creaming after 30 minutes of 20 vol% toluene-in-water emulsions stabilised by 0.5 wt.% Aerosil 200 as a function of [TEAB].

log([TEAB] / M)	fraction of emulsion as aqueous phase	
	pH 2	pH 10
-3		0.783
-2.3		0.765
-2	0.7	0.782
-1.3	0.747	0.8
-1	0.711	0.8
-0.6	0.698	
-0.46	0.715	
-0.3	0.747	0.8
-0.12	0.722	
0	0.732	0.783
0.18		0.8

Figure 3.32 Turbidity of 0.5 wt.% Aerosil 200 dispersions in water 24 hours after adding TEAB at pH 6.

log[TEAB] / M	turbidity / NTU
-3	305
-2.7	290
-2.52	460
-2.3	440
-2	450
-1.52	440
-1.3	430
-1.12	450
-1.1	455
-1	380
-0.7	385
-0.6	375
-0.52	325
-0.3	255
-0.22	240
-0.15	225
-0.12	225
0	200

Figure 3.33 Turbidity and height of resolved aqueous phase of 0.5 wt.% Aerosil 200 dispersions in water 24 hours after adding TEAB at pH 6.

log [TEAB] / M	turbidity / NTU	height of colourless aqueous phase / cm
-3	305	0
-2.7	290	0
-2.52	460	2.5
-2.3	440	2.2
-2	450	2.2
-1.52	440	2.1
-1.3	430	2.1
-1.12	450	2.6
-1.1	455	2
-1	380	2.1
-0.7	385	
-0.6	375	0.7
-0.52	325	0.6
-0.3	255	1.1
-0.22	240	0.4
-0.15	225	0
-0.12	225	0
0	200	0

Figure 3.34 Stability to creaming after 30 minutes of 20 vol% toluene-in-water emulsions stabilised by 0.5 wt.% Aerosil 200 at pH 6.

log [TEAB] / M	fraction of emulsion as aqueous phase
-3	0.749
-2.52	0.348
-2.12	0.106
-2.3	0.327
-2.7	0.45
-2	0.112
-1.7	0.104
-1.5	0.119
-1.3	0.156
-1.1	0.33
-1	0.47
-0.9	0.516
-0.76	0.452
-0.7	0.391
-0.6	0.4
-0.52	0.678
-0.4	0.676
-0.3	0.681
0	0.713

Figure 3.35 Turbidity of 0.5 wt.% Aerosil 200 in water 24 hours after addition of TEAB and stability to creaming after 30 minutes of 20 vol% toluene emulsions stabilised by 0.5 wt.% Aerosil 200 at pH 6.

log [TEAB] / M	turbidity / NTU	fraction of emulsion as aqueous phase
-3	305	0.749
-2.7	290	0.348
-2.52	460	0.327
-2.3	440	0.106
-2	450	0.112
-1.52	440	0.104
-1.3	430	0.119
-1.12	450	0.156
-1.1	455	0.33
-1	380	0.47
-0.7	385	0.516
-0.6	375	0.452

Figure 3.35 continued

log [TEAB] / M	turbidity / NTU	fraction of emulsion as aqueous phase
-0.52	325	0.391
-0.3	255	0.4
-0.22	240	0.678
-0.15	225	0.676
-0.12	225	0.681
0	200	0.713

Figure 3.36 Initial volume average diameter of 20vol% toluene-in-water emulsions stabilised by 0.5 wt.% Aerosil 200 as a function of [TEAB].

log [TEAB] / M	d (v,0.5) / μm
-3	77
-2.5	76.2
-2.3	76.9
-2.1	75.2
-1.75	64.9
-1.65	62.3
-1.46	58.1
-1.4	49.7
-1.34	64
-1.3	45.8
-1.2	48.9
-1.15	45.1
-1.1	42.5
-0.94	42.7
-0.8	41.1
-0.78	39.9
-0.73	41.5
-0.7	45.4
-0.65	43.1
-0.6	61.5
-0.52	72.5
-0.46	77
-0.35	77.1
-0.3	77.7
-0.12	77.5
0	77.4

Figure 3.38 Conductivity of 0.5 wt.% Aerosil 200 dispersions in water and 50 vol% toluene-in-water emulsions stabilised by 0.5 wt.% Aerosil 200 at pH 6.

[TEAB] / M	conductivity / μS cm^{-1}	
	colloid	emulsion
0.005	555	210
0.0075	780	250
0.01	1020	380
0.05	4220	1620
0.075	6500	2540
0.085	6620	2490
0.1	7300	2810
0.11	8200	3150
0.12	8820	3350
0.125	9250	3490
0.13	9300	3520
0.2	13100	4000
0.5	25000	6000
0.75	28000	6500
1	31200	7500
0.25	15280	5780

Figure 3.39 Static advancing contact angle of a drop of aqueous CTAB solution (pH 6) on a hydrophilic glass plate under dodecane measured 30 minutes after addition of oil.

log [CTAB] / M	Advancing contact angle / °
-6	25
-5	54
-4.3	68
-4	85
-3.8	90
-3.3	116
-3.15	127
-3	132
-2.82	125
-2.7	113
-2.52	105
-2	90

Figure 3.40 Stability to creaming and coalescence of 20 vol% dodecane-in-water emulsions stabilised by 0.5 wt.% Aerosil 200 as a function of [CTAB].

log [CTAB] / M	fraction of emulsion as aqueous			fraction of emulsion as oil		
	pH 2	pH 6	pH 10	pH 2	pH 6	pH 10
-6.5	0.76	0.67	0.71	0.02	0.02	0.15
-6	0.76	0.77	0.78	0.04	0.02	0.14
-5.52	0.71	0.73	0.78	0.03	0.02	0.12
-5.15	0.7	0.75	0.72	0.03	0.02	0.09
-5	0.77	0.71	0.69	0.05	0.02	0.05
-4.52	0.74	0.75	0.66	0.03	0	0
-4.15	0.69	0.57	0.56	0.03	0	0
-4	0.69	0.54	0.53	0	0	0
-3.52	0.56	0.39	0.41	0	0	0
-3.3	0.61	0.37	0.4	0	0	0
-3.15	0.53	0.36	0.37	0	0	0
-3.05	0.47	0.39	0.36	0	0	0
-3	0.4	0.38	0.29	0	0	0
-2.52	0.25	0.42	0.39	0	0	0
-2.3	0.09	0.44	0.51	0	0	0
-2	0.2	0.5		0	0	

Figure 3.41 Conductivity of 0.5 wt.% Aerosil 200 dispersions in water and 50 vol% dodecane-water emulsions stabilised by 0.5 wt.% Aerosil 200.

log [CTAB] / M	conductivity / $\mu S\ cm^{-1}$					
	pH 2		pH 6		pH 10	
	colloid	emulsion	colloid	emulsion	colloid	emulsion
-6	10500	3800	20	16	200	50
-5.3	10700	4200	21	9	220	65
-5	9600	3600	17	10	207	40
-4.3	9500	3200	17	9	210	50
-4	10800	4100	19	10	222	95
-3.3	10800	4400	33	16	203	95
-3.2	9500	3900	69	21	230	100
-3.1	8900	3200	95	21	405	105
-3	10000	3900	94	22	402	110
-2.3	10000	1900	203	67	480	125
-2	9500	1800	243	74	800	260

Figure 4.5 Stability to coalescence and sedimentation after 30 minutes of 50 vol% water-in-toluene emulsions stabilised by H30 particles as a function of initial concentration of particles in oil.

wt.% particles in oil	fraction of emulsion as aqueous phase	fraction of emulsion as oil phase
0.01	0.333	0.495
0.05	0.154	0.481
0.1	0.03	0.388
0.25	0	0.258
0.5	0	0.162
0.75	0	0.134
1	0	0.132
1.25	0	0.1
1.5	0	0.054
2	0	0.043
2.5	0	0.02
3	0	0
4	0	0
5	0	0

Figure 4.9 Effect of homogenisation speed for 2 minutes on the various volume drop diameters for water-in-toluene emulsions stabilised by 2 wt.% H30.

r.p.m.	d(v,0.1) / μm	d(v,0.5) / μm	d(v,0.9) / μm
8000	0.22	0.55	1.82
9500	0.22	0.57	1.6
13500	0.25	0.65	1.94
20500	0.24	0.63	1.76
24000	0.27	0.72	2.05

Figure 4.10 Conductivity of water-toluene emulsions stabilised by 2 wt.% H30 particles in oil as a function of the volume fraction of water.

ϕ_w	conductivity / μS cm^{-1}	
	water to oil	oil to water
0.05	0.2	
0.1	0.28	
0.15	0.4	
0.2	0.41	0.21
0.25	0.43	
0.3	0.43	0.21
0.35	0.44	
0.4	0.43	0.23
0.45	0.44	0.52
0.5	0.45	0.71
0.55	1.7	1.87
0.6	3.48	2.5
0.625	7.6	
0.65	85	305
0.675	205	
0.7	625	650
0.75	895	790
0.8	1040	805
0.9		890
0.95		960

Figure 4.11 Conductivity of water-toluene emulsions stabilised by H30 silica particles as a function of the volume fraction of water. Emulsions prepared at each ϕ_w by direct mixing of components.

ϕ_w	conductivity / μS cm^{-1}	
	2 wt.% in oil	1 wt.% in emulsion
0.05		0.18
0		0.16
0.1	0.26	
0.2	0.23	0.22
0.3	0.3	0.18
0.4	0.28	0.19
0.5	0.49	0.19
0.6	0.89	1.81
0.65	0.95	

Figure 4.11 continued

ϕ_w	conductivity / $\mu S\ cm^{-1}$	
	2 wt.% in oil	1 wt.% in emulsion
0.7	3.59	4.65
0.75	680	16.75
0.775		235
0.8	750	685
0.85	870	932
0.9	960	1052
1		1100

Figure 4.12 Fraction of oil phase resolved versus time for water-in-toluene emulsions stabilised by 2 wt.% H30 particles in oil.

time / mins	fraction of oil resolved				
	$\phi_w = 0.01$	$\phi_w = 0.05$	$\phi_w = 0.1, 0.2$	$\phi_w = 0.3 - 0.6$	$\phi_w = 0.7$
0	0	0	0	0	0
0.1	0	0	0	0	0
0.5	0	0	0	0	0
1	0	0	0	0	0
2	0.102	0	0	0	0
5	0.186	0.105	0	0	0
10	0.205	0.175	0.108	0	0
30	0.265	0.204	0.187	0.012	0
45	0.28	0.236	0.205	0.028	0
60	0.286	0.266	0.212	0.043	0

Figure 4.13 Fraction of aqueous phase resolved versus time for toluene-in-water emulsions stabilised by 2 wt.% H30 particles in oil.

time / mins	fraction of water resolved		
	$\phi_w = 0.75$	$\phi_w = 0.8$	$\phi_w = 0.9$
0	0	0	0
0.1	0	0	0
0.5	0	0	0.11
1	0	0.09	0.41
2	0.12	0.38	0.61
5	0.32	0.59	0.73
10	0.5	0.7	0.85
30	0.56	0.75	0.87
60	0.66	0.79	0.91

Figure 4.14 Stability after 1 hour of toluene-water emulsions stabilised by 2 wt.% H30 particles in oil.

ϕ_w	fraction of aqueous phase resolved	fraction of oil phase resolved
0.01	0	0.286
0.05	0	0.266
0.1	0	0.212
0.2	0	0.202
0.3	0	0.045
0.4	0	0.045
0.5	0	0.043
0.6	0	0.05
0.7	0	0
0.75	0	0.66
0.8	0	0.79
0.9	0	0.91

Figure 4.16 Drop diameter versus ϕ_w for toluene-water emulsions stabilised by 2 wt.% H30 particles.

ϕ_w	sequential addition		direct addition	
	D(v,0.5) / μm	D(4,3) / μm	D(v,0.5) / μm	D(4,3) / μm
0.1	0.64	0.97	0.73	1.05
0.2	0.55	0.85	0.82	1.24
0.3	0.57	1.02	0.58	0.91
0.4	0.93	2.79	0.48	1.29
0.5	0.54	2.53	0.74	3.79
0.6	0.87	5.47	0.75	8.23
0.65			0.92	15.58
0.7	108.09	135.04	116.55	150.05
0.8	65.86	89.09	77.48	105.17
0.9	81.43	109.17	67.44	101

Figure 4.17 Volume fraction of oil in creamed emulsion versus initial volume fraction of water for toluene-in-water emulsions stabilised by H30 particles.

initial ϕ_w	ϕ_o cream
0.75	0.58
0.8	0.63
0.85	0.665
0.9	0.71
0.95	0.73

Figure 4.18 In-situ conductivity of toluene-water emulsions stabilised by 10 wt.% N20 silica in water as a function of ϕ_w.

ϕ_w	conductivity / μS cm^{-1}	
	oil to water	water to oil
1	1100	
0.9	980	1050
0.8	816	930
0.7	756	820
0.6	625	660
0.5	515	580
0.45		495
0.4	258	198
0.35		47.23
0.3	2.89	4.63
0.25		2.16
0.2	2.84	2.03
0.1	2.8	1.95
0.05	2.74	

Figure 4.20 Conductivity of oil-water emulsions stabilised by H30 particles versus ϕ_w.

ϕ_w	conductivity / μS cm^{-1}				
	tetradecane	PDMS 20 cS	perfluorohexane	diiodomethane	tetradecane and water (pH 1)
0	0.17				
0.05	0.17				
0.1	0.18	0.17	0.16	0.21	0.28
0.2	0.18	0.17	0.17	0.24	0.29
0.25				0.26	
0.3	0.18	0.17	0.18		0.36
0.4	0.19	0.17	0.19	0.28	0.31
0.5	0.23	0.23	0.24	0.35	0.31
0.55			2.06		
0.6	2.23	2.13	31.2	3.23	0.31
0.65	3.08				
0.7	540	6.5	49.6	222	5.1
0.8	960	8	102	405	970
0.9	1010	9.5	124	1005	990
1	1015				

Figure 5.3 Conductivity of water-toluene emulsions containing 2 wt.% H30 particles in toluene (fixed) as a function of added N20 particles in water.

wt.% N20 in water	conductivity / μS cm^{-1}
0.5	0.22
0	0.22
1	0.46
1.5	0.51
2	0.83
2.5	0.87
3	0.67
3.5	0.71
3.75	1.73
4	1.83
4.25	2.09
4.5	392
5	430
6	475
6.5	517
7.5	510
8	507
9	513
10	515

Figure 5.4 Stability after 24 hours of water-toluene emulsions stabilised by 2 wt.% H30 particles in toluene as a function of added N20 particles in water.

wt.% N20 in water	fraction of emulsion as aqueous phase	fraction of emulsion as oil phase
0	0	0.02
1	0	0.019
2	0	0.018
3	0	0.046
4	0	0.079
4.5	0.34	0
5	0.35	0
5.5	0.34	0
6	0.33	0
7	0.28	0
8	0.24	0
9	0.25	0
10	0.22	0

Figure 5.6 Drop diameters versus added N20 in water for water-in-toluene emulsions ($\phi_w = 0.5$) stabilised by 2 wt.% H30 in toluene.

wt.% N20 in water	d(v,0.5) / μm	d(4,3) / μm
0	0.68	5.68
1	0.72	5.33
2	0.75	6.07
3	0.67	4.25
4	0.76	5.37
4.5	1.06	15.87
5	28.51	31.87
6	27.02	31.13
7	25.01	30.51
8	23.51	27.09
9	22.2	27.96

Figure 5.8 Conductivity of water-toluene emulsions ($\phi_w = 0.5$) containing 2 wt.% N20 particles in water as a function of added H30 particles in toluene.

wt.% H30 in oil	conductivity / μS cm^{-1}
0	560
0.1	456
0.15	350
0.2	276
0.25	198
0.3	156
0.35	20.3
0.4	7.92
0.5	2.3
0.75	0.92
1	0.9
1.5	0.71
2	0.69

Figure 5.9 Stability after 24 hours of water-toluene emulsions ($\phi_w = 0.5$) stabilised by 2 wt.% N20 particles in water as a function of added H30 particles in oil.

wt.% H30 in oil	o/w		w/o	
	fraction of emulsion as oil	fraction of emulsion as aqueous	fraction of emulsion as oil	fraction of emulsion as aqueous
0	0.11	0.305		
0.1	0.106	0.321		
0.2	0.132	0.356		
0.3	0.118	0.389		
0.4	0.168	0.415		
0.5			0	0.368
0.7			0	0.345
0.9			0	0.298
1			0	0.245
1.2			0	0.205
1.4			0	0.156
1.6			0	0.089
1.8			0	0.045
2			0	0.025

Figure 5.10 (upper) Drop diameters versus added H30 in toluene for water-toluene emulsions ($\phi_w = 0.5$) stabilised by 2 wt.% N20 in water.

wt.% H30 in oil	d(v,0.5) / μm	d(4,3) / μm
0	117.88	136.5
0.1	93.78	104.39
0.2	120.6	140.64
0.3	111.03	129.56
0.35	112.98	123.69
0.45	58.59	38.65
0.5	53.99	40.7
0.6	55.34	38.1
1	38.04	34.28
1.25	30.37	25.62
1.5	0.89	15.57
2	0.75	9.88

Figure 5.10 (lower) Percentage of drops of diameter less than 2 μm versus wt.% H30 in oil for w/o emulsions.

wt.% H30 in oil	% of drops of diameter < 2μm
0.5	31.5
0.6	40.4
1	36.1
1.25	42.4
1.5	58.4
2	77.8

Figure 5.11 Conductivity of water-toluene emulsions ($\phi_w = 0.5$) containing 2.5 wt.% total particles as a function of the weight fraction of H30. N20 particles are initially in water, H30 particles are initially in oil.

wt. fraction H30	conductivity / μS cm^{-1}
1	0.62
0.9	0.41
0.8	0.39
0.7	0.46
0.6	0.38
0.5	0.49
0.4	0.61
0.3	1.98
0.2	2.3
0.15	60
0.125	120
0.1	171
0.08	260
0.06	450
0.04	556
0.02	605
0.01	595
0	580

Figure 5.12 Fraction of emulsion as oil phase during sedimentation of w/o emulsions in system of Figure 5.11

time / mins	fraction of emulsion as oil phase			
	wt. frac. H30 = 0.2	wt. frac. H30 = 0.25	wt. frac. H30 = 0.3	wt. frac. H30 = 0.4
0	0	0	0	0
0.5	0	0	0	0
1	0.045	0	0	0
2	0.104	0.04	0	0
3	0.153	0.089	0	0
4	0.186	0.109	0.035	0
5	0.209	0.123	0.048	0
7.5	0.234	0.145	0.051	0.008
10	0.251	0.162	0.053	0.012
15	0.291	0.184	0.072	0.017
20	0.32	0.195	0.088	0.019
30	0.33	0.2	0.094	0.02

Figure 5.13 Stability after 30 minutes of water-toluene emulsions ($\phi_w = 0.5$) in the system of Figure 5.11.

wt. fraction H30	o/w		w/o	
	fraction of emulsion as oil	fraction of emulsion as aqueous	fraction of emulsion as oil	fraction of emulsion as aqueous
0	0.125	0.332		
0.05	0.132	0.306		
0.075	0.112	0.342		
0.1	0.105	0.375		
0.125	0.12	0.388		
0.15			0.43	0
0.18			0.39	0
0.2			0.33	0
0.225			0.3	0
0.24			0.258	0
0.25			0.2	0
0.275			0.148	0
0.3			0.094	0
0.35			0.071	0
0.4			0.02	0
0.5			0	0

Figure 5.15 (upper) Drop diameters versus weight fraction of H30 for water-toluene emulsions ($\phi_w = 0.5$) stabilised by 2.5 wt.% total particles.

wt. fraction H30	d[v,0.5] / μm	d[4,3] / μm
0	127.77	141.48
0.03	173.98	199.81
0.04	104.81	114.77
0.05	125.83	144.61
0.06	140.31	154.92
0.08	169.29	186.37
0.09	150.85	167.13
0.1	148.08	170.75
0.125	149.07	168.04
0.15	129.32	144.27
0.175	130.19	143.47
0.2	34.88	33.75
0.25	1.2	22.08
0.275	0.97	16.39
0.3	1	19.16
0.35	0.95	12.5
0.4	0.67	4.79
0.45	0.59	5.4
0.5	0.64	1.25
0.6	0.81	1.35
0.7	0.75	1.04
0.8	0.75	1.32
0.9	0.76	1.15
1	0.46	0.75

Figure 5.15 (lower) Percentage of drops of diameter less than 2 μm versus weight fraction of H30 for w/o emulsions.

wt. fraction H30	% drops of diameter < 2μm
0.2	49.9
0.25	50.5
0.275	56.7
0.3	53.4
0.35	63.6
0.4	85.9
0.45	86.4

Figure 5.15 (lower) continued

wt. fraction H30	% drops of diameter < 2μm
0.5	91.2
0.6	82.5
0.7	92.9
0.8	88.8
0.9	90.7
1	94.8

Figure 5.17 Conductivity of water-toluene emulsions ($\phi_w = 0.5$) containing 2.5 wt.% total particles as a function of the weight fraction of H30.

wt. fraction H30	conductivity / μS cm^{-1}	
	N20 in oil	N20 in water
0	630	560
0.01	626	
0.02	5.86	
0.03	3.81	
0.04	2.81	
0.05	2.56	456
0.06	2.09	
0.075		350
0.1	1.49	276
0.125		198
0.15		156
0.175		20.3
0.2	1.09	7.92
0.25		2.3
0.3	0.87	
0.375		0.92
0.4	0.28	
0.5	1.09	0.9
0.6	0.71	
0.7	0.52	
0.75		0.71
0.8	0.65	
0.9	0.43	
1	0.23	0.69

Figure 6.4 Immersion time at 22 °C of six silica powders in methanol-water mixtures of different composition.

vol.% water	time taken for all particles to leave the surface / minutes					
	HDK H18	HDK H30	SLM 081	SLM 079	SLM 078	HDK N20
10	0.1333	0.2	0.133	0.083	0.083	0.166
25	283	0.266	0.217	0.183	0.166	0.15
37.5	1440	150	115	110	100	0.133
50	1440	370	240	215	170	0.083
62.5	1440	1440	365	325	300	0.083
75	1440	1440	570	515	450	0.05

Figure 6.5 (upper) Conductivity of water-toluene emulsions stabilised by silica particles of varying hydrophobicity as a function of the volume fraction of water.

ϕ_w	conductivity / $\mu S\ cm^{-1}$							
	HDK N20	SLM 078	SLM 079	SLM 081	HDK H30	HDK H18	SLM 091	SLM 957
0.05	2.74							
0.1	2.8	0.48	0.33	0.21	0.26		0.19	
0.2	2.84	1.12	0.66	0.43	0.23	0.21	0.18	0.26
0.25	2.85	2.46	1.35					
0.3	2.89	3.71	1.86	0.55	0.3	0.3	0.18	0.32
0.325	2.95							
0.35	235	3.98	2.89	0.85				
0.4	258	5.08	4.79		0.28	0.29	0.2	0.46
0.425	279	5.79	6.05					
0.45	312	11.56	6.09	1.61				
0.475	437	20.16	16.75					
0.5	515	475	435	1.49	0.49	0.22	0.19	0.61
0.525		490	420					
0.55		492	520	2.71				
0.575			536	2.95				
0.585				3.25				
0.595	625			3.86				
0.6		601	635	503	0.89	0.38	0.22	1.11
0.613				578				
0.625				601				
0.64				631				
0.65		694	662	665	0.95	0.58		
0.675				730				
0.7	756	738	701	795	3.59	1.56	0.21	3.48

Figure 6.5 (upper) continued

ϕ_w	conductivity / μS cm^{-1}							
	HDK N20	SLM 078	SLM 079	SLM 081	HDK H30	HDK H18	SLM 091	SLM 957
0.725							2.31	
0.75				894	680	3.51	7.8	625
0.768								4.83
0.775							18	5.25
0.788							19.23	5.64
0.8	816	842	864	905	750	8.72	22.1	655
0.813								8.09
0.825							24.68	592
0.838								623
0.85				934	870	9.21	28.6	685
0.9	980				960	11.2	36	780
0.95							41.2	

Figure 6.5 (lower) Volume fraction of water at inversion of the above emulsions versus the percentage of silanol groups on the silica particles.

% SiOH	$\phi_w^{(inv)}$
100	0.35
79	0.48
76	0.48
67	0.59
57	0.725
50	0.725
36	0.9
20	0.9

Figure 6.6 Fraction of emulsion coalesced for emulsions stabilised by the range of particles at $\phi_w = 0.5$, 10 minutes after emulsification.

% SiOH	fraction of emulsion coalesced	
	variable []	fixed []
20	0.486	0.895
50	0	0
67	0	0
76	0	0
79	0.089	0.089
100	0.814	0.932

Figure 6.7 Fraction of emulsion as oil phase versus time for water-in-toluene emulsions stabilised by silica particles at $\phi_w = 0.2$.

time / mins	fraction of emulsion as oil phase					
	HDK N20	SLM 078	SLM 079	SLM 081	HDK H30	HDK H18
0	0	0	0	0	0	0
0.1	0.683	0.356	0.235	0.012	0.056	0
0.5	0.756	0.42	0.312	0.056	0.096	0
1	0.756	0.467	0.365	0.089	0.135	0
2	0.756	0.498	0.403	0.109	0.176	0
3	0.756	0.543	0.458	0.168	0.201	0
5	0.756	0.599	0.501	0.195	0.235	0
10	0.756	0.613	0.566	0.241	0.246	0
15	0.756	0.642	0.589	0.298	0.25	0
20	0.756	0.668	0.603	0.325	0.253	0
25	0.756	0.694	0.645	0.329	0.255	0
30	0.756	0.721	0.689	0.333	0.258	0
45	0.756	0.734	0.695	0.338	0.258	0
60	0.756	0.742	0.7	0.342	0.258	0
120	0.756	0.742	0.707	0.344	0.258	0
180	0.756	0.742	0.707	0.345	0.258	0

Figure 6.8 Fraction of emulsion as oil or aqueous phase versus time for toluene-water emulsions stabilised by silica particles at $\phi_w = 0.5$.

time / mins	fraction of emulsion as oil or aqueous phase					
	HDK N20	SLM 078	SLM 079	SLM 081	HDK H30	HDK H18
0	0	0	0	0	0	0
0.1	0.261					0
0.5	0.282	0.178	0	0	0	0
1	0.293	0.254	0	0	0	0
2	0.321	0.264	0.137	0	0	0
3	0.348	0.268	0.159	0	0	0
5	0.348	0.278	0.189	0.051	0	0
10	0.348	0.28	0.202	0.068	0.05	0
15	0.348					0
20	0.348	0.286	0.215	0.082	0.061	0
25	0.348				0.076	0
30	0.348	0.286	0.243	0.108	0.081	0
45	0.348	0.286	0.247	0.125	0.081	0
60	0.348	0.286	0.25	0.143	0.081	0
90	0.348	0.286	0.252	0.164	0.081	0
120	0.348	0.286	0.252	0.18	0.081	0
180	0.348	0.286	0.252	0.213	0.081	0

Figure 6.9 Fraction of emulsion as aqueous phase versus time for emulsions stabilised by silica particles at $\phi_w = 0.8$.

time / mins	fraction of emulsion as aqueous phase					
	HDK N20	SLM 078	SLM 079	SLM 081	HDK H30	HDK H18
0	0	0	0	0	0	0
0.1	0.394	0.268	0.153	0.103	0.132	0
0.5	0.598	0.296	0.234	0.146	0.165	0
1	0.598	0.345	0.279	0.183	0.195	0
2	0.598	0.389	0.304	0.206	0	0
3	0.598	0.433	0.365	0.246	0.224	0
5	0.598	0.487	0.389	0.284	0.253	0
10	0.598	0.509	0.421	0.302	0.276	0
15	0.598	0.521	0.456	0.332	0.284	0
20	0.598	0.536	0.485	0.378	0.296	0
25	0.598	0.548	0.501	0.399	0.302	0
30	0.598	0.551	0.516	0.412	0.31	0
45	0.598	0.554	0.52	0.432	0.31	0
60	0.598	0.555	0.521	0.442	0.31	0
120	0.598	0.555	0.523	0.456	0.31	0
180	0.598	0.555	0.523	0.48	0.31	0

Figure 6.10 Stability of emulsions after a certain time versus volume fraction of water for all particles.

ϕ_w	N20		SLM 078		SLM 079	
	fraction of emulsion as aqueous	fraction of emulsion as oil	fraction of emulsion as aqueous	fraction of emulsion as oil	fraction of emulsion as aqueous	fraction of emulsion as oil
0.1	0.098	0.867	0	0.798	0	0.802
0.2	0.197	0.756	0	0.742	0	0.707
0.25	0.201	0.658				
0.3	0.205	0.568	0	0.645	0	0.635
0.35	0.201	0.283				
0.4	0.198	0.253	0	0.508	0	0.503
0.45	0.243	0.215	0	0.432	0	0.42
0.5	0.348	0.302	0.286	0.051	0.252	0
0.55			0.289	0.045	0.262	0
0.6	0.398	0.268	0.305	0.04	0.248	0
0.65			0.31	0	0.239	0
0.7	0.598	0.278	0.432	0	0.293	0
0.75			0.5625	0	0.465	0
0.8	0.603	0.284	0.555	0	0.523	0
0.85					0.587	0
0.9			0.608	0		

Figure 6.10 continued

ϕ_w	SLM 081		H30		H18	
	fraction of emulsion as aqueous	fraction of emulsion as oil	fraction of emulsion as aqueous	fraction of emulsion as oil	fraction of emulsion as aqueous	fraction of emulsion as oil
0.1	0	0.476	0	0.377	0.033	0
0.2	0	0.345	0	0.258	0.08	0
0.25						
0.3	0	0.35	0	0.164	0.113	0
0.35						
0.4	0	0.309	0	0.104	0.199	0
0.45					0.352	0
0.5	0	0.213	0	0.081	0.465	0
0.55	0	0.173			0.52	0
0.6	0.167	0	0	0.057	0.55	0
0.65	0.361	0				
0.7	0.35	0	0	0	0.61	0
0.75	0.43	0	0.261	0		
0.8	0.48	0	0.31	0	0.613	0
0.85			0.425	0		
0.9	0.65	0	0.48	0		

Figure 6.11 Variation of the time required to reach plateau value of emulsion stability and fraction of oil or aqueous phase resolved at that time versus % SiOH on the particles for three volume fractions of water.

% SiOH	$\phi_w = 0.2$		$\phi_w = 0.5$		$\phi_w = 0.8$	
	time / seconds	f_{oil}	time / seconds	f_{aq} or f_{oil}	time / seconds	f_{aq}
20	20	0	300	0	20	0
50	1500	0.258	1800	0.081	1800	0.31
67	9600	0.345	10800	0.213	10800	0.48
76	5000	0.707	7200	0.252	5400	0.523
79	3200	0.742	1200	0.286	3600	0.555
100	20	0.756	180	0.348	30	0.598

Figure 6.13 Comparison of the time required to reach plateau value of emulsion stability and initial arithmetic mean emulsion drop diameter versus % SiOH on the particles for three volume fractions of water.

% SiOH	$\phi_w = 0.2$		ϕ_w=0.5		$\phi_w = 0.8$	
	time / seconds	d(4,3) / μm	time / seconds	d(4,3) / μm	time / seconds	d(4,3) / μm
20	20	146.69	300	229.62	20	217.55
50	1500	1.47	1800	4.96	1800	80.11
67	9600	7.76	10800	10.63	10800	21.28
76	5000	33.91	7200	87.93	5400	23.46
79	3200	158.31	1200	136.07	3600	93.73
100	20		180	155.16	30	98.66

Figure 6.15 Ultracentrifugation stability after 30 minutes of w/o emulsions ($\phi_w = 0.5$) stabilised by H30 particles

	RCF								
wt.% H30	1	90.8	817.5	5813	13079	17802	23252	36331	52317
3	0	0.12	0.36	0.66	0.74	0.76	0.78	0.9	0.94
2	0	0.32	0.44	0.82	0.82	0.86	0.88	0.9	0.94
1	0.1	0.44	0.62	0.9	0.9	0.92	0.94	0.96	0.98
0.5	0.18	0.58	0.92	0.88	0.92	0.94	0.94	0.96	0.98

Figure 6.16 Representation of the different phases separating after ultracentrifugation for 30 minutes of w/o emulsions ($\phi_w = 0.5$) stabilised by H30 particles.

RCF	0.5 wt% H30		1.0 wt% H30		2.0 wt% H30		3.0 wt% H30	
	$(1-f_o)$	f_{sed}	$(1-f_o)$	f_{sed}	$(1-f_o)$	f_{sed}	$(1-f_o)$	f_{sed}
1	0.91		0.95		1		1	
90.8	0.71		0.78		0.84		0.94	
817.5	0.54		0.69		0.78		0.82	
5813	0.56		0.55		0.59		0.67	
13079.3	0.54		0.55		0.59		0.63	
17802	0.53	0.45	0.54		0.57		0.62	
23252.2	0.53	0.26	0.53	0.25	0.56		0.61	
36331	0.52	0.25	0.52	0.24	0.55	0.41	0.55	
52317.4	0.51	0.25	0.51	0.25	0.53	0.26	0.53	0.37

CHAPTER 7
EFFECTS OF OIL TYPE AND REPLACEMENT OF WATER FOR EMULSIONS STABILISED BY PARTICLES OF INTERMEDIATE HYDROPHOBICITY

Figure 7.1 Conductivity of water-oil emulsions stabilised by partially hydrophobic SLM 081 silica particles (0.5 wt.% in emulsion) as a function of the volume fraction of water.

ϕ_w	conductivity / μS cm^{-1}					
	PDMS (0.65 cS)	heptane	dodecane	cyclohexane	PDMS (50 cS)	perflouroheptane
0.1		0.22	1.86	1.56	0.25	
0.2	0.98	0.44	2.43	1.9	0.28	
0.25		0.78				
0.3	1.04	1.06	2.8	2.8	0.32	2.06
0.325	2.08					
0.35	2.58	1.69	3.05	2.65	0.33	
0.375	3.48	1.87	3.34			
0.388	3.51	2.08	3.56			
0.4	285	2.21	3.63	2.65	0.29	4.38
0.413	333	205	305	2.84		
0.425	343	230	312	2.86		
0.438		296		3.23		
0.45	375	352	356	3.69	0.38	
0.463				420		
0.475		382	395	427	0.39	
0.488					0.38	
0.5	373	389	420	465	520	6.21
0.525					520	
0.55	425			530	532	14.1
0.575					551	
0.585						
0.595						
0.6	560	458	650	606	560	498
0.613						
0.625						
0.638						
0.65	689					513
0.663						
0.675						528

Figure 7.1 continued

ϕ_w	conductivity / μS cm^{-1}					
	PDMS (0.65 cS)	heptane	dodecane	cyclohexane	PDMS (50 cS)	perflouroheptane
0.7	760	652	791	762	682	589
0.725						
0.75						
0.8		761	850	802	831	720
0.85						
0.9		996	999	993	1010	869

Figure 7.1 continued

ϕ_w	conductivity / μS cm^{-1}					
	toluene	isopropyl myristate	cineole	eugenol	methyl myristate	undecanol
0.1	0.21					0.21
0.2	0.43		0.16		0.27	
0.3	0.55				0.27	0.29
0.35	0.85					
0.4		0.26				0.36
0.45	1.61					
0.5	1.49	0.29	0.2	0.27	0.28	0.34
0.55	2.71	0.31				
0.575	2.95					
0.585	3.25					
0.595	3.86					
0.6	503	0.72	0.86		0.29	0.32
0.613	578					
0.625	601	1.29				
0.638	631	2.58				
0.65	665	3.46				
0.663		282				
0.675	730	285				
0.7	795	462	1.36		0.43	0.31
0.725		530				
0.75	894	680				
0.8	905	750	2.36	0.83	0.56	0.36
0.85	934		2.89			
0.95					0.83	2.86
0.9		909	3.63	1.36	0.68	0.45

Figure 7.2 Volume fraction of water at inversion of emulsions versus work of adhesion between oil and water for systems in Figure 7.1.

W_a / mJ m^{-2}	ϕ_w^{inv}
28	0.575
41	0.40625
44.4	0.40625
45.1	0.45625
49.2	0.39125
54.9	0.49125
65	0.5975
71.1	0.65825
76.2	0.95
83.2	0.95
90.9	0.95
99.3	0.95

Figure 7.3 (upper) Stability after 1 hour of oil-water emulsions stabilised by 0.5 wt.% SLM 081 silica particles as a function of ϕ_w.

ϕ_w	heptane		dodecane		cyclohexane	
	f_{aq}	f_{oil}	f_{aq}	f_{oil}	f_{aq}	f_{oil}
0.2	0.754	0.8	0.724	0.789	0.678	0.754
0.3	0.698	0.735	0.654	0.705	0.654	0.735
0.35	0.521	0.658	0.534	0.634	0.623	0.705
0.375	0.487	0.536	0.426	0.512	0.543	0.654
0.4	0.412	0.513	0.401	0.487	0.465	0.621
0.45	0.098	0.035	0.068	0.051	0.421	0.587
0.5	0.125	0.037	0.078	0.061	0.053	0.048
0.6	0.164	0.034	0.125	0.06	0.084	0.051
0.7	0.213	0.038	0.158	0.068	0.132	0.054
0.8	0.256	0.041	0.186	0.073	0.185	0.058
0.9	0.298	0.039	0.214	0.084	0.199	0.06

Figure 7.3 (middle) As upper.

ϕ_w	50 cS PDMS		toluene		isopropyl myristate	
	f_{aq}	f_{oil}	f_{aq}	f_{oil}	f_{aq}	f_{oil}
0.01	0	0.398	0	0.286	0	0.345
0.05	0	0.368	0	0.266	0	0.298
0.1	0	0.345	0	0.212	0	0.264
0.2	0	0.312	0	0.202	0	0.235
0.3	0	0.289	0	0.045	0	0.197
0.4	0	0.246	0	0.045	0	0.145
0.5	0	0	0	0.043	0	0.111
0.6	0.32	0	0	0.05	0	0.076
0.7	0.43	0	0	0	0	0
0.75	0.52	0	0.66	0	0.54	0
0.8	0.58	0	0.79	0	0.62	0
0.9	0.73	0	0.89	0	0.76	0

Figure 7.3 (lower) As upper.

ϕ_w	methyl myristate		cineole		eugenol	
	f_{aq}	f_{oil}	f_{aq}	f_{oil}	f_{aq}	f_{oil}
0.1	0	0.132	0	0.112	0	0.142
0.2	0	0.154	0	0.134	0	0.187
0.3	0	0.186	0	0.167	0	0.211
0.35	0	0.232	0	0.212	0	0.245
0.375	0	0.268	0	0.256	0	0.269
0.4	0	0.321	0	0.298	0.076	0.342
0.45	0	0.405	0.095	0.375	0.099	0.421
0.5	0	0.498	0.165	0.435	0.184	0.501
0.6	0.135	0.568	0.234	0.511	0.264	0.598
0.7	0.256	0.632	0.321	0.598	0.354	0.654
0.8	0.384	0.723	0.456	0.654	0.486	0.765
0.9	0.513	0.798	0.598	0.723	0.654	0.812

Figure 7.4 Conductivity of toluene-water emulsions versus the volume fraction of polar phase, with 0.5 wt.% SLM 081 particles in each emulsion.

ϕ_w or ϕ_f	conductivity / $\mu S\ cm^{-1}$	
	toluene / water	toluene / formamide
0.1	0.21	
0.2	0.43	0.16
0.3	0.55	0.16
0.35	0.85	
0.4		0.17
0.45	1.61	
0.5	1.49	0.18
0.55	2.71	0.19
0.575	2.95	2.62
0.585	3.25	2.69
0.595	3.86	
0.6	503	120
0.6125	578	
0.625	601	
0.64	631	
0.65	665	135
0.675	730	
0.7	795	158
0.75	894	
0.8	905	195
0.85	934	
0.9		209

Figure 7.7 Stability of water-in-undecanol emulsions stabilised by 0.5 wt.% SLM 081 particles as a function of temperature and ϕ_w. Ordinate is time taken for 25 % of oil to be resolved.

temp. / °C	time / minutes			
	$\phi_w = 0.2$	$\phi_w = 0.35$	$\phi_w = 0.5$	$\phi_w = 0.8$
18	1	1.5	1.5	2.1
20	3.25	2.5	1.75	2.75
21	6.5		5.25	5.5
22	45	120	240	450
25	60	150	360	450
27.5	35	60	105	450
30	20	45	75	450
35	10	20	25	450

Figure 7.8 (upper) Fraction of oil or water resolved versus time for water-in-undecanol emulsions stabilised by 0.5 wt.% SLM 081 particles in each emulsion.

time / mins	18 °C, $\phi_w = 0.2$	
	f_{aq}	f_{oil}
0	0	0
0.25	0	0.0416
0.5	0.083	0.0625
0.75	0.083	0.083
1	0.166	0.125
1.25	0.333	0.145
1.5	0.416	0.166
1.75	0.5	0.208
2	0.583	0.229
2.25	0.666	0.271
2.5	0.75	0.396
2.75	0.83	0.583
3	0.917	0.8125
3.25	1	0.958
3.5	1	1

Figure 7.8 (middle) As upper.

time / mins	25 °C, $\phi_w = 0.2$	
	f_{aq}	f_{oil}
0.5	0	0
1	0	0
5	0	0.093
10	0	0.148
30	0	0.203
60	0	0.259
90	0	0.407
120	0	0.426
180	0	0.463
240	0	0.5
300	0	0.519
360	0	0.57
600	0	0.625
800	0.025	0.625
1000	0.08	0.7
1260	0.15	0.757
1320	0.15	0.777

Figure 7.8 (lower) As upper

time / mins	35 °C, $\phi_w = 0.2$	
	f_{aq}	f_{oil}
0	0	0
0.5	0	0
1	0	0
2	0	0.024
4	0	0.024
5	0	0.143
10	0	0.238
15	0	0.333
30	0	0.404
60	0	0.643
90	0	0.714
120	0.1	0.761
135	0.2	0.809
150	0.5	0.881
165	0.8	0.952
180	1	1

Figure 7.9 Fraction of oil or water resolved versus time for water-in-undecanol emulsions stabilised by 0.5 wt.% SLM 081 particles in each emulsion at 35 °C.

time / mins	$\phi_w = 0.35$		$\phi_w = 0.65$		$\phi_w = 0.8$	
	f_{aq}	f_{oil}	f_{aq}	f_{oil}	f_{aq}	f_{oil}
0	0	0	0	0	0	0
0.5	0	0	0	0	0	0
1	0	0	0	0	0	0
2	0	0				
4	0	0				
5	0	0.059	0	0	0	0
10	0	0.219	0	0	0	0
20	0	0.406				
30	0	0.562	0	0.026	0	0
60	0	0.656	0	0.051	0	0
90	0	0.75	0	0.077	0	0
120	0.11	0.813	0	0.132	0	0
150	0.44	0.875				
180	1	1	0	0.184	0	0
240			0	0.236	0	0
300			0.048	0.289	0	0.1
360			0.095	0.342	0.025	0.15

Figure 7.10 Conductivity and type of water-toluene emulsions stabilised by 0.5 wt.% SLM 081 particles versus the volume fraction of water.

ϕ_w	conductivity / μS cm^{-1}		
	particles in water	particles in oil	particles in water and oil
0.1	0.75	0.21	0.86
0.15	0.8		
0.2	0.83	0.43	1.16
0.25	0.82		1.54
0.275	1.06		
0.3	1.31	0.55	1.83
0.325	1.99		
0.335	2.86		
0.35	4.68	0.85	2.21
0.3625	5.36		
0.375	288		
0.3875	336		
0.4	371		2.25
0.4125			3.89
0.425	391		6.4
0.4375			7.68
0.45	402	1.61	343
0.475			406
0.5	420	1.49	474
0.55	556	2.71	498
0.575		2.95	
0.585		3.25	
0.595		3.86	
0.6	631	503	635
0.6125		578	
0.625		601	
0.64		631	
0.65		665	
0.675		730	
0.7	942	795	836
0.75		894	
0.8	1080	905	954
0.85		934	
0.9	1310		1220

Figure 7.11 Initial emulsion drop diameters versus volume fraction of water for toluene-containing emulsions stabilised by 0.5 wt.% SLM 081.

ϕ_w	drop diameter / mm			
	particles in oil		particles in water	
	d(v,0.5) / μm	d(4,3) / μm	d(v,0.5) / μm	d(4,3) / μm
0.1	0.53	2.08	0.61	16.43
0.2	0.64	7.58	0.81	21.05
0.3	1.02	12.71	0.73	23.51
0.7	21.76	26.91	14.32	16.86
0.8	17.63	23.64	12.08	13.89
0.9	11.4	16.78	11	12.06

Figure 7.12 Conductivity and type of water-in-toluene emulsions stabilised by $C_{12}E_5$ versus the volume fraction of water.

ϕ_w	conductivity / μS cm^{-1}	
	in water	in oil
0.1	0.195	0.201
0.2	0.198	0.229
0.3	0.197	0.216
0.4	0.197	0.216
0.5	0.197	0.225
0.6	0.199	0.259
0.7	0.215	0.316
0.8	0.298	0.268
0.9	0.334	0.243

CHAPTER 8
EFFECT OF ELECTROLYTE CONCENTRATION ON THE WETTABILITY OF SILICA PARTICLES

Figure 8.1 Partitioning of 2 wt.% H18 and H30 particles initially dispersed in oil between toluene and water, ($\phi_w = 0.5$) as a function of pH of the aqueous phase.

pH	H30		H18	
	% in oil	% in water	% in oil	% in water
6.00	101.17	4.00	85.67	0.60
8.94	88.13	4.47	87.73	1.20
9.93	96.57	3.27	92.97	1.43
10.97	88.73	4.00	90.33	7.67
11.98	92.80	4.13	95.33	8.00
12.96	88.13	18.60	97.67	6.33
13.51	100.70	17.73	90.33	7.00
13.80	92.80	16.60	84.67	4.40

Figure 8.2 Partitioning of 2 wt.% SLM 078, 079, and 081 particles initially dispersed in oil between toluene and water, ($\phi_w = 0.5$) as a function of the pH of the aqueous phase.

pH	SLM 078		SLM 079		SLM 081	
	% in oil	% in water	% in oil	% in water	% in oil	% in water
6.00	93.30	1.77	87.03	3.40	89.00	3.30
7.93	95.67	1.63	97.00	1.17		
8.94	82.33	1.87	71.87	2.97	91.50	6.42
9.93	81.90	1.13	69.40	18.03	78.20	3.12
10.97	63.77	11.80	56.23	32.90	68.66	4.46
11.98	32.87	25.53	17.27	45.00	52.33	3.19
12.23					34.46	55.23
12.96	9.57	50.47	1.77	83.57	5.93	98.32
13.27			1.97	95.47	2.63	96.01
13.51	0.97	92.60	2.23	105.73	0.17	103.22
13.80	2.73	104.33				

Figure 8.3 Partitioning of 2 wt.% N20 particles initially dispersed in water between toluene and water, ($\phi_w = 0.5$) as a function of the pH of the aqueous phase.

pH	N20	
	% in oil	% in water
6.00	0.93	104.56
7.96	1.03	99.56
8.94	1.50	89.57
9.93	1.07	99.53
10.97	0.44	100.07
11.98	0.53	96.63
12.96	1.80	98.80
13.80	2.87	100.10

Figure 8.4 Effect of pH on the type and conductivity of toluene-water emulsions stabilised by 1 wt.% silica particles in emulsion immediately after homogenisation, 25 °C.

pH	conductivity / μS cm^{-1}					
	N20	H30	H18	SLM 081	SLM 079	SLM 078
6	23.2	4.13	3.86	0.19	6.15	3.02
7.93			3.42	0.18		
8.94	32.4	2.1	3.66	0.19	7.64	5.12
9.93	48.8	0.68	1.53	0.2	3.9	11
10.97	31.4	0.58	0.94	0.21	28.8	38
11.98	193.3	0.95	1.04	0.22	156	257
12.65		0.96		8.56		
12.85		1476.6				
12.96	193	1562	3.73	236	236	520
13.27	873	2800	5.26	536	293	926
13.51	2253	3440	5	689	1410	3913
13.8	6050	5946	8.41		4466	7066

Figure 8.5 Stability of toluene-water emulsions stabilised by 2 wt.% SLM 081 particles dispersed in oil as a function of the pH of the aqueous phase.

pH	fraction of emulsion remaining
6	0.95
7.93	0.94
8.94	0.93
9.93	0.91
10.97	0.88
11.98	0.72
12.96	0.55
13.27	0.51
13.51	0.27

Figure 8.6 Conductivity of toluene-water emulsions stabilised by 2 wt.% H30 particles in oil as a function of NaCl.

[NaCl] / M	conductivity / μS cm^{-1}				
	pH 6	pH 9.97	pH 12.07	pH 12.17	pH 12.97
0	0.46	1.18	1.31	761	5700
0.001	0.71	1.23			
0.1	1.21			9300	10100
0.5	0.97	1.36			
1	1.63	2.06	1.31	24600	28000
2	2.01		1.43	37000	45000
3	2.86		1.86		51000
4	3.02	2.36		61000	
5	3.65	2.68	2.86	68000	56000

Figure 8.7 Advancing contact angle under air and under toluene of a 20 μl aqueous drop as a function of DMDCS coating on glass slides.

[DMDCS] / M	pH 6		pH 11.98		pH 13.51	
	θ_{aw}	θ_{ow}	θ_{aw}	θ_{ow}	θ_{aw}	θ_{ow}
0	4					
0.00001	31	108	39	101	38	87
0.0001	63	120	58	105	57	89
0.001	84	132	82	115	82	114
0.05	95	145	93	127	92	131

Figure 8.8 Advancing and receding contact angle of an aqueous drop under toluene as a function of pH.

pH	0.05 M DMDCS		1 x 10^{-4} M DMDCS		1 x 10^{-5} M DMDCS		0 M DMDCS	
	θ_{ow}^{adv} / °	θ_{ow}^{rec} / °	θ_{ow}^{adv} / °	θ_{ow}^{rec} / °	θ_{ow}^{adv} / °	θ_{ow}^{rec} / °	θ_{ow}^{adv} / °	θ_{ow}^{rec} / °
6	145	117	114	82	101	65	39	20
8.96	146	116	116	83	98	64	38	20
9.93	148	116	116	83	96	63	37	19
10.97	147	120	117	79	93	61	36	18
11.98	143	118	111	68	90	45	26	12
12.96	144	117	96	63	87	40	21	11
13.46	147	118					21	10
13.48	136	106	90	52				
13.51	121	64	89	48	76	35	19	8
13.8	108	55	86	40	66	29	16	7

Figure8.9 Hysteresis ($\Delta\theta$) of an aqueous drop on a clean glass slide where $\Delta\theta$ is defined as $\theta_{ow}^{adv} - \theta_{ow}^{rec}$ at each pH.

pH	$\Delta\theta$ / degrees			
	0.05 M	1×10^{-4} M	1×10^{-5} M	0 M
6	28	32	36	19
8.97	30	33	34	19
9.93	32	33	33	18
10.97	27	38	32	18
11.98	25	43	45	14
12.96	27	33	47	10
13.46	29			11
13.48	30	38		
13.51	57	41	41	11
13.8	53	46	37	9

Figure 8.10 $\Delta\theta_{max}$ of an aqueous drop on a clean glass slide where $\Delta\theta_{max}$ is defined as θ_{ow}^{adv} (pH 6) – θ_{ow}^{rec} (pH 13.8) as a function of the DMDCS coating on a clean glass slide.

[DMDCS] / M	$\Delta\theta_{max}$ / °
0	32
1×10^{-5}	72
1×10^{-4}	74
0.05	90

Figure 8.11 Advancing and receding contact angle of an aqueous drop under toluene as a function of pH.

pH	Method 1		Method 2	
	θ_{ow}^{adv} / °	θ_{ow}^{rec} / °	θ_{ow}^{adv} / °	θ_{ow}^{rec} / °
6	101	65	66	64
8.97	98	64	67	64
9.93	96	63	67	64
10.97	93	61	57	50
11.98	90	45	53	42
12.96	87	40	50	37
13.27			48	32
13.51	76	35	47	27
13.8	66	29	44	20

Figure 8.12 Advancing and receding contact angle of an aqueous drop on a glass slide coated with 1 x 10^{-4} M DMDCS as a function of pH.

pH	0.1 M NaCl		0 M NaCl	
	θ_{ow}^{adv} / °	θ_{ow}^{rec} / °	θ_{ow}^{adv} / °	θ_{ow}^{rec} / °
6	118	90	114	82
8.94	117	82	116	83
9.93	117	80	116	83
10.97	116	75	117	79
11.98	113	70	111	68
12.96	99	64	96	63
13.51	88	44	89	48
13.8	85	34	86	40

Figure 8.13 Advancing and receding contact angle of an aqueous drop on a glass slide coated with 1 x 10^{-5} M DMDCS as a function of pH.

pH	0.1 M NaCl		0 M NaCl	
	θ_{ow}^{adv} / °	θ_{ow}^{rec} / °	θ_{ow}^{adv} / °	θ_{ow}^{rec} / °
6	90	59	101	65
8.94	93	71	95	63
9.93	91	76	94	62
10.46	92	79		
10.97	94	80	93	61
11.23	90	64		
11.65	90	55		
11.98	83	50	90	45
12.96	77	47	87	40
13.51	74	46	76	35
13.8	71	43	66	29

Figure 8.14 Advancing and receding contact angle of an aqueous drop on a glass slide coated with 1 x 10^{-5} M DMDCS as a function of NaCl.

[NaCl] / M	θ_{ow}^{adv} / °	θ_{ow}^{rec} / °
0	93	61
0.01	95	65
0.05	93	69
0.1	94	80
0.25	96	81
0.5	98	83
1	104	85

Figure 8.15 Theoretical plot showing the effect of pH on the contact angle of an aqueous drop (1 x 10^{-5} M NaCl) under oil (γ_{ow} = 36 mN m^{-1}) on a solid surface of varying hydrophobicity.

pH	160 °	130 °	90 °	50 °	10 °
2	160	130	90	50	10
2.5	159.991	129.996	89.9964	49.995	9.97722
3	159.961	129.981	89.9849	49.9793	9.90472
3.5	159.907	129.956	89.9638	49.9503	9.76948
4	159.82	129.914	89.93	49.9037	9.5473
4.5	159.689	129.851	89.8784	49.8324	9.19684
5	159.494	129.758	89.8013	49.7258	8.64633
5.5	159.21	129.619	89.6874	49.5677	7.76091
6	158.799	129.417	89.5199	49.3345	6.23432
6.5	158.21	129.12	89.2742	48.9908	2.74761
7	157.375	128.689	88.9146	48.4842	0
7.5	156.206	128.064	88.3891	47.7366	0
8	154.599	127.164	87.6235	46.6305	0
8.5	152.429	125.88	86.5118	44.9864	0
9	149.564	124.066	84.9052	42.5221	0
9.5	145.873	121.547	82.5996	38.768	0
10	141.244	118.121	79.3222	32.8378	0
10.5	135.616	113.593	74.725	22.4012	0
11	129.039	107.835	68.3901	0	0
11.5	121.726	100.875	59.8462	0	0
12	114.041	92.9559	48.4921	0	0
12.5	106.315	84.4088	32.7445	0	0
13	98.6912	75.4157	0	0	0
13.5	91.1519	65.9109	0	0	0

Figure 8.16 Theoretical plot showing the effect of electrolyte concentration on the contact angle of an aqueous drop under toluene on a silica surface

pH	θ / degrees					
	0.00001 M	0.0001 M	0.001 M	0.01 M	0.1 M	1 M
2	65	65	65	65	65	65
2.5	64.9957	64.9912	64.9862	64.983	64.9816	64.9811
3	64.9823	64.9629	64.9383	64.9166	64.9038	64.8982
3.5	64.9576	64.9104	64.8397	64.757	64.6872	64.6467
4	64.9177	64.8252	64.669	64.4436	64.1861	63.9748
4.5	64.8568	64.6945	64.3974	63.9054	63.2103	62.4498
5	64.7657	64.4986	63.983	63.051	61.54	59.5225
5.5	64.6308	64.2083	63.3638	61.7485	58.8892	54.5453

Figure 8.16 continued

pH	θ / degrees					
	0.00001 M	0.0001 M	0.001 M	0.01 M	0.1 M	1 M
6	64.4319	63.7804	62.4471	59.8005	54.8336	46.575
6.5	64.1396	63.1511	61.0956	56.9089	48.6844	33.5679
7	63.7101	62.2265	59.1056	52.6125	39.131	0
7.5	63.0796	60.8679	56.171	46.1472	22.0398	0
8	62.1537	58.8703	51.8186	35.9814	0	0
8.5	60.7937	55.9258	45.2596	16.0542	0	0
9	58.7943	51.5579	34.8765	0	0	0
9.5	55.847	44.9698	13.5327	0	0	0
10	51.4745	34.5148	0	0	0	0
10.5	44.8772	12.6212	0	0	0	0
11	34.3991	0	0	0	0	0
11.5	12.3179	0	0	0	0	0
12	0	0	0	0	0	0
12.5	0	0	0	0	0	0
13	0	0	0	0	0	0
13.5	0	0	0	0	0	0

Figure 8.19 Initial foam volume of 10 cm^3 of 0.01 M SDS solutions versus initial pH in the absence and the presence of antifoam. The antifoam was 30 mg of SLM 081 silica particles and was added prior to foam formation.

pH	Initial foam volume / cm3	
	No solid	0.03g 081
6	106	52
8.94	108	58
9.93	107	60
10.97	108	61
11.98	108	63
12.23		94
12.64		108
12.96	109	109
13.46		98
13.51	102	98

Figure 9.3 Advancing contact angles of an aqueous drop on Hansa yellow pigment discs as a function of AOT concentration.

ln [AOT] / M	Method 1		Method 2
	θ_{ow} / °	θ_{aw} / °	θ_{ow} / °
-19	150	81	104
-18.4206807	149	70	
-17.3220685		74	
-16.8112428	150	70	
-16.1180957	149	73	
-14.5086577	148	70	102
-13.8155106	149	67	
-13.1223634			101
-12.2060726	142	66	
-11.5129255	145	67	101
-10.8197783			102
-10.4143132	141	60	
-9.90348755	145	56	102
-9.49802244			101
-9.21034037	141	55	104
-8.98719682			105
-8.80487526			104
-8.51719319	140	44	103
-8.29404964			104
-8.11172808	137	39	104
-7.60090246	137	28	105
-7.19543735			101
-6.90775528	136	22	99
-6.68461173			85
-6.50229017			76
-6.2146081	130	17	58
-5.99146455			30
-5.80914299	112	8	19
-5.52146092			15
-5.29831737	98	8	12
-5.11599581			9
-4.89285226	95	5	6
-4.60517019	89	5	6
-4.42284863		6	
-4.19970508	69		
-3.91202301	60	4	6
-3.5065579	41		

Figure 9.4 Interfacial tension measurements of squalane-water as a function of [AOT] in water at 25 °C.

ln [AOT] / M	γ_{ow} / mN m^{-1}
-16.118	51.752
-18.000	53.328
-16.811	53.040
-14.286	48.682
-14.509	49.959
-13.816	44.829
-12.717	42.826
-12.206	41.417
-11.513	38.211
-10.414	33.813
-9.903	29.926
-9.210	28.556
-8.517	24.560
-8.294	22.956
-7.601	18.093
-7.195	14.360
-6.908	12.659
-6.502	8.238
-6.215	8.034
-5.809	5.216
-5.298	4.330
-4.893	3.941
-3.507	1.839
-3.912	2.593
-4.200	2.979
-4.382	3.263
-4.605	3.554

Figure 9.5 $\gamma_{ow}\cos\theta$ versus γ_{ow} for squalane-water systems on Hansa yellow discs in the presence of AOT surfactant. Contact angles measured by Method 1.

γ_{ow} / mN m^{-1}	$\gamma_{ow}\cos\theta$ / mN m^{-1}
53.04	-45.9327
49.959	-42.3652
44.829	-38.4185
41.417	-32.6367
38.211	-31.2946
33.813	-26.2727
29.926	-24.5094
28.556	-22.1883
24.56	-18.8128

Figure 9.5 continued

γ_{ow} / mN m^{-1}	$\gamma_{ow}\cos\theta$ / mN m^{-1}
18.093	-13.2261
12.659	-9.10204
8.0342	-5.16599
5.2158	-1.95594
4.3298	-0.60184
3.941	-0.34287
3.5544	0.060424
2.9785	1.066313
2.593	1.296506
1.8391	1.388508

Figure 9.6 Air-water tensions as a function of AOT concentration in water at 25 °C.

ln AOT / mol dm^{-3}	γ_{aw} / mN m^{-1}
-5.295	29.3
-5.583	29.9
-5.806	30.3
-5.893	30.5
-5.988	31.3
-6.212	33.2
-6.499	35
-6.682	36.2
-6.905	38.1
-7.192	40.2
-7.598	42.9
-7.886	45.1
-8.109	46.5
-8.291	47.7
-8.514	49
-8.984	51.7
-9.207	53
-9.495	54.5
-9.9	56.6
-10.188	58.2
-10.594	59.8
-10.817	61
-11.104	61.8
-11.51	63.4
-12.203	66.2
-12.9	68.1
-13.812	70

Figure 9.7 $\gamma_{aw}\cos\theta$ versus γ_{aw} in the presence of AOT in water on Hansa yellow discs.

γ_{aw} / mN m^{-1}	$\gamma_{aw}\cos\theta$ / mN m^{-1}
70.650	24.164
72.020	19.851
72.336	24.741
72.440	21.179
71.234	24.363
70.092	27.387
65.993	26.842
63.604	24.852
59.051	29.525
56.613	31.657
52.979	30.387
48.970	35.226
46.450	36.099
43.094	38.050
38.214	35.432
32.959	31.519
29.711	29.422
29.300	29.015

Figure 9.8 Advancing contact angles of an aqueous drop on Hansa yellow pigment discs in air as a function of AOT concentration.

ln [AOT] / M	θ_{aw} / °		
	0.1 M	1.0 M	0 M NaCl
-19.000	66	88	81
-18.421			70
-17.322			74
-16.811			70
-16.118			73
-14.509			70
-13.816	65	80	67
-13.122		78	
-12.717	64	75	
-12.206	64	73	66
-11.801		69	
-11.513	63	60	67
-11.107		53	
-10.953	62		
-10.820		45	
-10.597	55		
-10.414		31	60

Figure 9.8 continued

ln [AOT] / M	θ_{aw} / °		
	0.1 M	1.0 M	0 M NaCl
-10.260			
-10.127		21	
-9.903	51	15	56
-9.721		10	
-9.498	45	8	
-9.373	36		
-9.210	34	7	55
-8.987	27		
-8.805	23	6	
-8.651	18		
-8.517	17		44
-8.294	15	5	
-8.112	11		39
-8.032			
-7.958	8		
-7.824	7		
-7.601	5	4	28
-7.419	5		
-7.195	5		
-6.908	5	3	22
-6.685	5		
-6.348	5		17
-5.991	5		
-5.809		2	8
-5.298	5	2	8
-4.893		2	5
-4.605	5	2	5
-4.382			6
-3.912	5	2	4

Figure 9.9 Advancing contact angles of an aqueous drop on Hansa yellow discs under squalane as a function of AOT.

ln ([AOT] / M)	θ_{ow}^{adv} / °		
	0.1 M NaCl	1.0 M NaCl	0 M NaCl
-16.811	147	149	150
-14.508			148
-13.815	145	141	149
-13.122		144	
-12.716	144		

Figure 9.9 continued

ln ([AOT] / M)	θ_{ow}^{adv} / °		
	0.1 M NaCl	1.0 M NaCl	0 M NaCl
-12.206	145	145	142
-11.800		145	
-11.512	144	144	145
-11.107		144	
-10.953		140	
-10.819		130	
-10.596	144		
-10.414		120	141
-10.260		111	
-10.126		96	
-9.903	143	96	145
-9.721		91	
-9.498	140	77	
-9.372			
-9.210	135	75	141
-8.987		70	
-8.804	122	63	
-8.650		58	
-8.517	100		140
-8.294	94	54	
-8.111	86		
-8.031	74		
-7.957	54	53	
-7.824	50		
-7.600	33	52	137
-7.418	32		
-7.195	29		
-6.907	24	50	136
-6.684	24		
-6.348	24		130
-5.991	23		
-5.809		55	112
-5.298	21	49	98
-4.892			95
-4.605	21	50	89
-4.382			79
-4.199			69
-3.912	21		60
-3.506			41

Figure 9.10 Interfacial tension measurements of squalane-water as a function of AOT in water at 25 °C.

ln [AOT] / M	γ_{ow} / mN m^{-1}	
	0 M	0.1 M NaCl
-18.00	53.33	45.98
-16.81	53.04	45.98
-16.12	51.75	45.98
-14.51	49.96	45.86
-13.82	44.83	43.58
-12.72	42.83	33.33
-12.21	41.42	25.84
-11.51	38.21	22.05
-10.41	33.81	15.34
-9.90	29.93	10.52
-9.21	28.56	8.35
-8.52	24.56	4.43
-8.29	22.96	3.39
-7.60	18.09	1.85
-7.20	14.36	1.28
-6.91	12.66	1.47
-6.21	8.03	1.37
-5.81	5.22	2.03
-5.30	4.33	1.47
-4.89	3.94	
-4.61	3.55	1.19
-4.38	3.26	
-4.20	2.98	
-3.91	2.59	
-3.51	1.84	

Figure 9.11 $\gamma_{ow}\cos\theta$ versus γ_{ow} for squalane-water systems on Hansa yellow discs in the presence of AOT surfactant and 0.1 M NaCl. Contact angles measured by Method 1.

γ_{ow} / mN m^{-1}	$\gamma_{ow}\cos\theta$ / mN m^{-1}
45.976	-37.654
45.976	-37.654
45.864	-37.563
43.575	-35.688
40.213	-32.934
33.332	-26.966
25.840	-21.163

Figure 9.11 continued

γ_{ow} / mN m^{-1}	$\gamma_{ow}\cos\theta$ / mN m^{-1}
22.045	-17.835
15.342	-12.412
10.523	-8.408
10.204	-7.816
8.346	-5.900
6.017	-3.189
4.431	-0.771
3.394	-0.231
2.215	0.155
2.030	1.870
1.846	1.549
1.280	1.120
1.469	1.342
1.374	1.256
1.189	1.110

Figure 9.12 Advancing contact angle of 10 mM aqueous AOT drops on Hansa yellow discs under squalane as a function of NaCl, angles measured by Method 1.

log [NaCl] / M	θ_{ow} / °
-3.500	89
-3.000	85
-2.699	60
-2.523	49
-2.301	38
-2.125	31
-2.000	23
-1.523	19
-1.222	20
-1.000	21
-0.699	34
-0.398	44
-0.222	50
0.000	60
0.176	85

Figure 9.13 Advancing contact angles of an aqueous drop on phthalocyanine blue B pigment discs as a function of AOT.

ln [AOT] / M	Method 1		Method 2
	θ_{ow} / °	θ_{aw} / °	θ_{ow} / °
-16.500	157	71	79
-15.425	158		
-14.732		74	
-14.509	158		
-13.816	160	73	
-13.122	158	67	77
-12.206	157	73	67
-11.513	156	70	66
-10.820	156	72	
-9.903	157	64	62
-9.210	157	55	57
-8.517	156	51	
-8.112			49
-7.601		39	41
-6.908	156	28	36
-6.685		25	
-6.502		24	27
-6.215	155	19	
-5.991		16	17
-5.809	152	15	
-5.298	145	12	
-5.116	134	13	
-4.893			12
-4.605	124	10	
-4.200	107		
-3.912	104	11	6
-3.507	83	10	

Figure 9.14 $\gamma_{ow}\cos\theta$ versus γ_{ow} for squalane-water systems on phthalocyanine blue B discs in the presence of AOT, angles measured by Method 1.

γ_{ow} / mN m^{-1}	$\gamma_{ow}\cos\theta_{ow}$ / mN m^{-1}
53.328	-49.116
49.959	-46.312
44.829	-42.095
41.417	-38.145
38.211	-34.925
29.926	-27.562
28.556	-26.300
24.560	-22.448

Figure 9.14 continued

γ_{ow} / mN m^{-1}	$\gamma_{ow}\cos\theta_{ow}$ / mN m^{-1}
12.659	-11.571
8.034	-7.279
5.216	-4.606
4.330	-3.546
3.554	-1.987
2.979	-0.870
2.593	-0.628
1.839	0.224

Figure 9.15 $\gamma_{aw}\cos\theta$ versus γ_{aw} in the presence of AOT in water on phthalocyanine blue B discs.

γ_{aw} / mN m^{-1}	$\gamma_{aw}\cos\theta_{aw}$ / mN m^{-1}
71.900	18.622
70.092	20.467
65.993	19.270
63.604	21.753
56.613	24.796
52.929	30.381
48.970	30.802
43.094	33.484
38.214	33.743
32.959	31.179
29.711	28.701
29.300	28.655

Figure 9.16 Advancing contact angles of an aqueous drop on Hansa yellow discs as a function of [CTAB] measured by Method 1.

ln [CTAB] / M	θ_{aw} / °	θ_{ow} / ° (silicone oil)	θ_{ow} / ° (squalane)
-13.816	73	149	142
-14.500	81	147	147
-12.717	76		
-12.206	75	145	145
-11.513	78		148
-10.820	80	140	147
-10.414	79		
-9.903	77	153	149
-9.498	70		
-9.210	64	145	143
-8.517	59		
-8.112	54	130	142

Figure 9.16 continued

ln [CTAB] / M	θ_{aw} / °	θ_{ow} / ° (silicone oil)	θ_{ow} / ° (squalane)
-7.824	47		
-7.601	42	145	140
-7.419	35		
-7.195	28		
-6.908	18	128	127
-6.502	20		
-6.215	21	126	135
-5.809	19		141
-5.298	18	119	130
-4.893			131
-4.605	17	110	131

Figure 9.17 Interfacial tension measurements of squalane-water as a function of [CTAB] in water at 25 °C.

ln [CTAB] / M	γ_{ow} / mN m^{-1}
-14.500	53.298
-13.816	50.492
-12.717	46.984
-12.206	44.588
-11.513	40.435
-10.414	36.988
-9.903	32.721
-9.498	31.027
-9.210	27.363
-8.517	22.604
-8.112	17.872
-7.824	15.661
-7.601	13.172
-7.195	10.374
-6.908	8.141
-6.215	7.937
-5.298	7.734
-4.605	7.222

Figure 9.18 $\gamma_{ow}\cos\theta$ versus γ_{ow} for squalane-water systems on Hansa yellow discs in the presence of CTAB surfactant, angles measured by Method 1.

γ_{ow} / mN m^{-1}	$\gamma_{ow}\cos\theta_{ow}$ / mN m^{-1}
53.298	-44.717
50.492	-39.788
44.588	-36.517
40.435	-34.289
32.721	-28.041
27.363	-21.863
17.872	-14.083
13.172	-10.090
8.141	-4.901
7.937	-5.612
7.734	-4.973
7.222	-4.738

Figure 9.19 $\gamma_{aw}\cos\theta$ versus γ_{aw} in the presence of CTAB surfactant in water on Hansa yellow discs.

γ_{aw} / mN m^{-1}	$\gamma_{aw}\cos\theta_{aw}$ / mN m^{-1}
71.381	12.395
71.095	13.566
70.721	14.704
69.912	15.727
68.608	11.914
67.520	12.883
65.688	14.777
63.773	21.812
62.112	27.228
56.847	29.278
52.762	31.013
49.327	33.641
46.321	34.423
43.624	35.735
40.008	35.325
37.600	35.760
37.600	35.332
37.600	35.103
37.600	35.551
37.600	35.760
37.600	35.570

Figure 9.20 Advancing contact angle of an aqueous drop in air on Hansa yellow pigment discs as a function of L-77 concentration.

ln [L-77] / M	θ_{aw} / °
-13.5	80
-12.79	72
-12.32	73
-12.09	65
-11.62	64
-11.4	63
-10.99	65
-10.71	63
-10.3	64
-10.03	54
-9.9	56
-9.84	60
-9.79	64
-9.7	48
-9.48	8
-9.42	6
-9.36	5
-9.34	5
-9.19	5
-8.5	0
-7.58	0